

CARDIFF
UNIVERSITY

PRIFYSGOL
CAERDYDD

ROLE OF CAVEOLIN-1 IN
MICROGLIAL PHENOTYPE:
IMPACT ON GLIOBLASTOMA

Role of Caveolin-1 in microglial phenotype:
impact on Glioblastoma

A thesis submitted in accordance with the conditions
governing candidates for the degree
of
Philosophiae Doctor in Cardiff University

by

Cátia Neto

May 2021
Cardiff School of Pharmacy and Pharmaceutical Sciences
Cardiff University

ABSTRACT

Glioblastoma multiform (GBM) is a lethal brain tumour composed by many distinct cell types that are closely connected and dependent on their surrounding environment. Microglia are the brain immune cells, which are highly abundant in GBM and create an immunosuppressive microenvironment that promotes tumour progression. Caveolin-1 (Cav1) is the most important protein of caveolae and it is involved in cell signalling activity. In the GBM, Cav1 promotes the tumour invasion and it is correlated with a poor prognosis. In immune cells, its role is not well explored, however it can be involved in immune response. Our hypothesis was that Cav1 could have an impact in the response of human microglia to the environment, influencing tumour progression.

To test our hypothesis, a human microglia cell line and an iPSC cell line were used to generate Cav1 knockout clones using CRISPR-Cas9 technology. The iPSC was used to generate human microglia cells.

Primary human microglia expressed low levels of Cav1, which could be regulated upon activation. The viral immortalized human microglia cells expressed strong Cav1 protein levels, possibly correlated with the immortalization procedure with SV40 large T antigen. This infection in combination with the culture conditions might lead to a constitutive pro-inflammatory phenotype, impacting the ability of microglia to react to other stimulus and to do phagocytosis. A slightly modified protocol to generate microglia from iPSC allowed the differentiated cells to be polarized towards pro-inflammatory and anti-inflammatory phenotype and to perform phagocytosis.

In microglia, Cav1 was involved in the regulation of the inflammatory response, cell migration, phagocytosis, and sensitivity to temozolomide. The microglia cell line did not impact the tumour behaviour, likely due to the profile presented by the cells. However, the deletion of Cav1 in microglia derived from iPSC promoted the tumour invasion.

ACKNOWLEDGEMENTS

First, I would like to thank my supervisor, Professor Mark Gumbleton, without whom none of this work would have been possible. I sincerely thank him for all the opportunities that he gave me to grow as a researcher and as a person over these years, for all the discussions, thoughts and feedback that enabled me to complete this project and this thesis.

I would also like to thank Professor Geoff Pilkington for all the valuable discussions and knowledge. Similarly, I am deeply grateful to Professor Nick Allen and his team that welcomed me to his laboratory, gifted precious cell lines, and shared his protocols for microglia and astrocytes differentiation from iPSC, contributing to the value of this project. I would also like to thank to my advisor, Dr. Stephen Hiscox, for his advice and guidance. I am also grateful to my colleges for sharing the knowledge and creating a good work environment.

I am thankful to my mother and father for their love and for continuing to support me during this journey, even from abroad. I am particularly grateful to my husband, Rafael, for his unconditional support and encouragement, and for changing his life to make Cardiff our home. This adventure was much easier thanks to him.

Finally, this project would not have been possible without the funding provided by Brain Tumour Research, Thorne Mason Trust, and Cardiff University School of Pharmacy and Pharmaceutical Sciences. Thank you.

*"I hate brain cancer because it steals away memories,
personalities, and abilities before finally stealing life"*

- Amanda Haddock

To all brain tumour worriers and their families.

LIST OF ABBREVIATIONS

AAVS1	Adeno-Associated Virus Integration Site 1
ADF	Astrocytes Differentiated cells
APC	iPSC-derived astrocyte precursors cells
BBB	Blood Brain Barrier
BDNF	Brain-Derived Neurotrophic Factor
bFGF	Basic Fibroblast Growth Factor
BMDM	bone marrow-derived macrophages
BMP4	Bone Morphogenetic Protein 4
Cas9	CRISPR-associated protein 9
Cav1	Caveolin-1
CCL22	Chemokine (C-C motif) ligand 22
CD	Cluster of Differentiation
cDNA	Complementary DNA
CNS	Central Nervous System
CNTF	Ciliary Neurotrophic Factor
CRISPR	Clustered Regularly Interspaced Short Palindromic Repeats
CXCL10	(C-X-C motif) chemokine ligand 10
DAPI	4',6-diamidino-2-phenylindole
DE	Differential expression
DDR	DNA damage repair
DMEM	Dulbecco's Modified Eagle Media
DMSO	Dimethyl Sulfoxide
DNA	Deoxyribonucleic Acid
EB	Embryonic Body
ECM	Extracellular matrix
ESC	Embryonic Stem cell
EGF	Epidermal Growth Factor
EMT	Epithelial mesenchymal transition
FBS	Foetal Bovine Serum

FDR	False Discovery Rate
FITC	Fluorescein Isothiocyanate
FN	Fibronectin
GAM	Glioma associated microglia and macrophages
GBM	Glioblastoma
GM-CSF	Granulocyte Macrophage Colony Stimulating Factor
gRNA	guide RNA
GSEA	Gene Set Enrichment Analysis
GO	Gene Ontology
HSC	Hematopoietic stem cells
IBA1	Ionised Calcium-Binding Adapter Molecule 1
IDH	Isocitrate Dehydrogenases
IFN-γ	Interferon gamma
IL	Interleukin
iPSC	Induced Pluripotent Stem Cells
iPSC-MG	iPSC-derived microglia
KO	Knock-out
LPS	Lipopolysaccharide
M-CSF	Macrophage Colony Stimulating Factor
ME	Mercaptoethanol
MGMT	Methyl Guanine Methyl Transferase
mRNA	Messenger Ribonucleic Acid
NT	Non-target control
NF-κB	Nuclear Factor kappa-light-chain-enhancer of Activated B Cells
ORA	Over-representation analysis
PBS	Phosphate Buffer Saline
PCR	Polymerase Chain Reaction
PE	Phycoerythrin
PVA	Polyvinyl alcohol
qRT-PCR	quantitative Reverse Transcription-PCR
Ri	Rho kinase inhibitor
RISC	RNA-Interfering Silencing Complex

RNP	Ribonucleoprotein
RPM	Revolutions per minute
STAT	Signal Transducer and Activator of Transcription
TGF-β	Transforming Growth Factor β
TLR	Toll Like Receptor
TME	Tumour microenvironment
TMEM119	Transmembrane protein 119
TMZ	Temozolomide
TNFα	Tumour Necrosis Factor Alpha
TP53	Tumour Protein 53
TREM2	Triggering Receptor Expressed on Myeloid cells 2
VEGF	Vascular Endothelial Growth Factor
VTN	Vitronectin
WHO	World Health Organization
WT	Wild Type

CONTENTS

Chapter 1 – General Introduction

1.1	Glioblastoma: Clinical and Molecular Features	2
1.1.1	Glioma.....	2
1.1.2	Glioblastoma Multiforme (GBM).....	3
1.1.3	Molecular Classification of GBMs.....	4
1.1.4	Glioblastoma Therapy	7
1.2	Tumour Microenvironment and Immune System	9
1.2.1	Microglia	11
1.2.2	GAM and GBM	15
1.3	Induced pluripotent stem cells-derived microglia	18
1.4	Caveolae	20
1.4.1	Caveolin-1 and Cancer.....	22
1.4.2	Caveolin-1 and immune cells	24
1.5	Aims of the Project.....	26

Chapter 2 – General Material and Methods

2.1	Material.....	29
2.1.1	Cell lines	29
2.1.2	Cell culture mediums	29
2.1.3	Other Cytokines, Growth Factors, and Inhibitors	31
2.1.4	Other Cell Culture Reagents	31
2.1.5	Antibodies for FACS.....	32
2.1.6	Antibodies for Western Blot.....	32
2.1.7	Antibodies for Immunofluorescence	33
2.1.8	Kits	33
2.1.9	Plastics and others	34
2.2	Cell culture maintenance.....	36
2.2.1	Standard culture and freezing.....	36
2.3	Microglia progenitor’s characterization by FACS	40
2.4	Immunofluorescence Staining.....	41

2.5	Microglia and Macrophages polarization	41
2.6	Co-culture System of GBM cell lines with CHME3	43
2.7	qRT-PCR.....	43
2.8	Western Blot	46
2.9	Phagocytosis assay	47
2.10	Cytokine array.....	48
2.11	Transwell migration and invasion assay.....	49
2.12	Cellular co-cultures – Vybrant™ dyes.....	49
2.13	Spheroid invasion assay.....	50
2.14	Statistics.....	51
 Chapter 3 – Genetic knockout of Caveolin-1		
3.1	Introduction	53
3.1.1	RNAi	53
3.1.2	CRISPR-Cas9	54
3.2	Aim	57
3.3	Methods	58
3.3.1	Cav1 knockout by CRISPR-Cas9	58
3.3.2	Genomic Cleavage Detection – Editing Efficiency Analysis.....	62
3.3.3	Cellular proliferation by MTT Assay.....	64
3.3.4	Screening CRISPR-Cas9 clones for predicted deletions	64
3.4	Results.....	66
3.4.1	Efficiency of transfection and editing.....	66
3.4.2	CRISPR-Cas9 clone characterization	69
3.5	Discussion.....	76
 Chapter 4 – Impact of Caveolin-1 knockout upon CHME3 phenotype		
4.1	Introduction	81
4.2	Aim	82
4.3	Methods	83
4.3.1	General methods.....	83
4.3.2	TMZ chemosensitivity	83
4.4	Results.....	84
4.4.1	CHME3 cells expressed pan-microglial markers after Cav1 KO	84

4.4.2	CHME3 cells lack phagocytic ability irrespective of status	85
4.4.3	Cav1 important for microglial CHME3 Transwell migration	86
4.4.4	Cav1 promotes microglia CHME3 sensitivity to TMZ.....	87
4.4.5	Impact of Cav1 upon CHME3 phenotype in response to pro-/anti-inflammatory stimuli.....	88
4.4.6	Impact of activation and Cav1 status upon CHME3 secretome.....	92
4.5	Discussion.....	99
Chapter 5 – GBM environment and CHME3 Cav1 knockout		
5.1	Introduction	110
5.2	Aim	111
5.3	Methods	111
5.3.1	General Methods	111
5.4	Results	113
5.4.1	Co-culture of CHME3 cells with GBM: impact on microglial proliferation and migration.....	113
5.4.2	Co-culture of CHME3 cells with GBM: impact on microglial phenotype	115
5.4.3	Co-culture of CHME3 cells with GBM: impact on secretome	118
5.4.4	Effect of CHME3 Cav1 phenotype on GBM proliferation.....	122
5.4.5	Effect of CHME3 Cav1 phenotype on GBM migration.	123
5.4.6	Effect of CHME3 Cav1 phenotype on GBM invasion	124
5.5	Discussion.....	131
Chapter 6 –iPSC-derived microglia and the impact of Caveolin-1 knockout		
6.1	Introduction	137
6.2	Aim	138
6.3	Methods	138
6.3.1	General methods.....	138
6.3.2	RNA-seq	139
6.4	Results	142
6.4.1	Characterization of the microglial progenitors by FACS	142
6.4.2	Study of Cav1 in iPSC-derived microglial cells	144
6.4.3	iPSC-MG expressed pan-microglial markers after Cav1 KO	146
6.4.4	Impact of the differentiation process on iPSC-MG	146

6.4.5	Impact of Cav1 on pro-inflammatory and anti-inflammatory gene expression by qRT-PCR.....	151
6.4.6	Impact of Cav1 on microglia activation by cytokine array.....	154
6.4.7	Transcriptomic profile of activated microglia - RNA-seq.....	159
6.4.8	Impact of Cav1 upon the transcriptomic profile – RNA-seq.....	169
6.4.9	Phagocytic ability on iPSC-derived microglia activation: the impact of Cav1.....	174
6.5	Discussion.....	177
Chapter 7 – GBM and iPSC-derived microglia environment: The role of Cav1		
7.1	Introduction.....	187
7.2	Aim.....	188
7.3	Methods.....	188
7.3.1	General methods.....	188
7.3.2	TaqMan Gene Expression Array.....	189
7.3.3	Darmanis et al. scRNA-seq database.....	190
7.4	Results.....	190
7.4.1	Impact of iPSC-MG upon spheroid U87 invasion: Role of Cav1 status ..	190
7.4.2	Effect of the GBM cell on microglia responsiveness.....	192
7.4.3	Effect of microglia on the GBM cell responsiveness.....	197
7.4.4	Co-cultures of iPSC-MG cells with GBM: impact on secretome.....	201
7.4.5	Immune population in GBM tumours: scRNA-Seq database.....	207
7.5	Discussion.....	211
Chapter 8 – Summary Discussion and Future Directions		
8.1	Summary discussion.....	220
8.2	Future Directions.....	227
Appendices		
	APPENDIX I - CRISPR-Cas9 vector approach.....	231
	APPENDIX II - CRISPR-Cas9 RNP approach optimization.....	238
	APPENDIX III – THP1-derived macrophages.....	240
	APPENDIX IV – shRNA Cav1 knockdown in GBM cells.....	249
	APPENDIX V – Vybrant™ dyes optimization.....	264
	APPENDIX VI – Human XL Cytokine Array.....	267

APPENDIX VII – RNA-seq	272
APPENDIX VIII – TaqMan Gene expression Array plate.....	275
APPENDIX IX – Other GBM databases.....	292
APPENDIX X– Copyright Permissions	300
Bibliography.....	301

INDEX OF FIGURES

Figure 1.1 – Genetic classification of GBM	5
Figure 1.2 – The microenvironment of GBM	10
Figure 1.3 – Impact of GAMs on tumour environment.....	11
Figure 1.4 – Microglia states in human brain.....	13
Figure 1.5 – Microglia activation	14
Figure 1.6 – Caveolae and Caveolin-1	21
Figure 1.7 – Dual role of Cav1 in Cancer	23
Figure 2.1 – Astrocytes differentiation from APC.	37
Figure 2.2 – CHME3 and iPSC-derived microglia polarization protocol.....	42
Figure 2.3 – THP1 differentiation and macrophages polarization protocol.	42
Figure 2.4 – Transwell® system.....	43
Figure 2.5 – pHRodo phagocytosis Assay.....	48
Figure 2.6 – Invasion assay diagram	51
Figure 3.1 – siRNA and shRNA mechanisms for gene knockdown.	54
Figure 3.2 – The principle of CRISPR-Cas9.	56
Figure 3.3 – crRNA guide 1 design	58
Figure 3.4 – crRNA guide 2 design	59
Figure 3.5 – Example of a dot blot.	61
Figure 3.6 – Schematic representation of sgRNA 1 and 2 deletions.	65
Figure 3.7 – Gel image from U87 sorted cells, 72 hours after transfection.	67
Figure 3.8 - Gel image from UP007 sorted cells, 72 hours after transfection	67
Figure 3.9 – Gel image from UP029 sorted cells, 72 hours after transfection	67
Figure 3.10 – Gel image from CHME3 sorted cells, 72 hours after transfection.	68
Figure 3.11 – Gel image from THP1 sorted cells, 72 hours after transfection.....	68
Figure 3.12 – Representative Cav1 protein levels of NT and KO clones.....	70
Figure 3.13 – PCR products of THP1 clones.	71
Figure 3.14 - PCR amplification products of U87 Cav1 NT C1 and C2, U87 Cav1 KO C6 and KO C8.	71
Figure 3.15 - PCR amplification products of UP007 Cav1 NT C1 and Cav1 KO C1, C5, KO C3 and KO C11. Note: UP007 Cav1 KO C3 and C11 were run in different gels.	72

Figure 3.16 - PCR amplification products of UP029 Cav1 NT C1, UP029 Cav1 KO C5 and KO C7.	72
Figure 3.17 – PCR amplification products of CHME3 Cav1 NT C1, CHME3 Cav1 KO C4, KO C6, KO C9 and KO C17. Note: C17 was run in a different gel.....	73
Figure 3.18 - PCR amplification products of THP1 Cav1 NT C1, THP1 Cav1 KO C1, KO C2 and KO C3.	74
Figure 3.19 - PCR amplification products of iPSC-Kolf2 Cav1 NT C1, C2, C3, C4 and Kolf2 Cav1 KO C1, C2, C6 and C8.....	74
Figure 3.20 – Proliferation of U87, UP007, UP029, CHME3 and THP1.	75
Figure 4.1 – Microglial TMEM119 and IBA1 markers and Cav1 expression	84
Figure 4.2 – CHME3 phagocytosis assay.	85
Figure 4.3 – Impact of Cav1 upon Transwell CHME3 migration.....	86
Figure 4.4 – Impact of Cav1 in microglia sensitivity to TMZ.....	87
Figure 4.5 – Role of Cav1 in protein expression.....	88
Figure 4.6 – Basal expression of the pro-inflammatory and anti-inflammatory related genes by CHME3 Cav1 NT (black) and CHME3 Cav1 KO (grey) cells.....	89
Figure 4.7 – Pro-inflammatory related marker analysis by qRT-PCR.....	90
Figure 4.8 – Anti-inflammatory related markers analysis by qRT-PCR.....	91
Figure 4.9 – Cytokine array of CHME3 Cav1 NT under a pro-inflammatory phenotype.	93
Figure 4.10 – Cytokine array of CHME3 Cav1 NT under an anti-inflammatory phenotype	94
Figure 4.11 – Cytokine array of CHME3 Cav1 KO under a pro-inflammatory phenotype.	95
Figure 4.12 – Cytokine array of CHME3 Cav1 KO under an anti-inflammatory phenotype.	96
Figure 4.13 – Comparison of CHME3 Cav1 NT and CHME3 Cav1 KO	97
Figure 5.1 – Impact of GBM CC on microglial proliferation.....	113
Figure 5.3 – Impact of GBM CC on microglia cell migration.....	114
Figure 5.4 – Relative protein expression after CC.....	115
Figure 5.5 – Impact of GBM environment on CHME3 cells – Pro-inflammatory-related genes	116

Figure 5.6 – Impact of GBM environment on CHME3 cells – Anti-inflammatory-related genes	117
Figure 5.7 – Secretome of CHME3 Cav1 NT under GBM co-culture.....	119
Figure 5.8 – Secretome of CHME3 Cav1 KO under GBM co-culture	120
Figure 5.9 – Comparison of CHME3 Cav1 NT and CHME3 Cav1 KO under GBM co-culture	121
Figure 5.10 – Impact of CHME3 CC on tumour proliferation	122
Figure 5.11 – Impact of CHME3 CC on tumour migration.....	123
Figure 5.12 – Impact of Cav1 upon GBM spheroid invasion.	124
Figure 5.13 – Impact of microglia upon U87 invasion.....	126
Figure 5.14 – Spheroid invasion analysis of U87 cell in CC with Astrocytes and CHME3..	127
Figure 5.15 – Impact of microglia upon U87 invasion at day 3	128
Figure 5.16 – Impact of CHME3 upon U87 invasion.....	129
Figure 5.17 – Impact of CHME3 upon U87 invasion (Green) into Astrocyte only spheroids (RED).....	130
Figure 6.1 – Differentiation protocol of iPSC-derived microglia	138
Figure 6.2 – RNA-seq workflow.	140
Figure 6.3 – CD34, CD45 and CD11b iPSC-derived microglial progenitors Cav1 NT population.	142
Figure 6.4 – CD34, CD45 and CD11b iPSC-derived microglial progenitors Cav1 KO population	143
Figure 6.5 – Cav1 expression in iPSC-derived microglia cells.	145
Figure 6.6 – Microglial markers and Cav1 expression.....	146
Figure 6.7 – Effect of the resting period on microglial morphology.....	147
Figure 6.8 – Effect of the microglial differentiation process upon gene expression on unstimulated cells.....	148
Figure 6.9 – Effect of the microglial differentiation process upon gene expression on stimulated cells.....	149
Figure 6.10 – Basal expression of the pro-inflammatory and anti-inflammatory related genes by iPSC-MG Cav1 NT (dark grey) and iPSC-MG Cav1 KO cells (light grey).	151

Figure 6.11 – Pro-inflammatory related genes by iPSC-MG Cav1 NT (dark grey) and iPSC-MG Cav1 KO cells (light grey).....	152
Figure 6.12 – Anti-inflammatory related genes by iPSC-MG Cav1 NT (dark grey) and iPSC-MG Cav1 KO cells (light grey).....	153
Figure 6.13 – Representative membranes from the human cytokine array	154
Figure 6.14 – Secreted products upon pro-inflammatory activation of iPSC-MG Cav1 NT cells.....	155
Figure 6.15 – Secreted products upon anti-inflammatory activation of iPSC-MG Cav1 NT cells.....	156
Figure 6.16 – Canonical microglial genes expressed by iPSC-MG Cav1 NT.	159
Figure 6.17 – Heatmap demonstrating the differential clustering of iPSC-MG Cav1 NT	160
Figure 6.18 – GSEA biological process of pro-inflammatory iPSC-MG Cav1 NT.	161
Figure 6.19 – Functional analysis of the iPSC-derived microglia under pro-inflammatory phenotype.	163
Figure 6.20 – GSEA biological process of anti-inflammatory iPSC-MG Cav1 NT.....	164
Figure 6.21 – Functional analysis of the iPSC-derived microglia under anti-inflammatory phenotype	165
Figure 6.22 – Microglial key genes involved in activation and homeostasis	166
Figure 6.23 – ORA of biological processes of the common genes upregulated in pro-inflammatory and anti-inflammatory microglial phenotype.....	167
Figure 6.24 – ORA of biological process of the common genes downregulated in pro-inflammatory and anti-inflammatory microglial phenotype.....	168
Figure 6.25 – ORA of biological process of the common genes upregulated in pro-inflammatory and downregulated in anti-inflammatory microglial phenotype.....	168
Figure 6.26 – ORA of biological process of the common genes downregulated in pro-inflammatory and upregulated in anti-inflammatory microglial phenotype.....	169
Figure 6.27 – PCA analysis of iPSC-MG Cav1 NT (Cav1 +ve) and iPSC-MG Cav1 KO. ...	170
Figure 6.28 – Heatmap demonstrating the impact of Cav1 status on microglial basal phenotype.	171
Figure 6.29 – Heatmap demonstrating the impact of Cav1 status on microglial pro-inflammatory phenotype	172

Figure 6.30 – Heatmap demonstrating the impact of Cav1 status on microglial anti-inflammatory phenotype.....	173
Figure 6.31 – Phagocytic ability of iPSC-MG Cav1 NT and iPSC-MG Cav1 KO.....	175
Figure 6.32 – Impact of Cav1 upon Phagocytic ability of microglia cells.....	176
Figure 6.33 – Impact of Cav1 on microglia activation.....	185
Figure 7.1 – Experimental design.....	189
Figure 7.2 – Impact of iPSC-MG on U87 invasion.....	191
Figure 7.3 – impact of the iPSC-MG on the U87 area of invasion.....	192
Figure 7.4 – Impact of tumour cells on the microglial immune response.....	194
Figure 7.5 – Impact of tumour cells on the microglial immune response.....	196
Figure 7.6 – Impact of iPSC-MG on tumour gene expression.....	197
Figure 7.7 – Impact of iPSC-MG on tumour gene expression.....	198
Figure 7.8 – Impact of iPSC-MG on tumour gene expression.....	200
Figure 7.9 – Impact of tumour immune environment upon the secretome.....	202
Figure 7.10 – Impact of tumour immune environment upon the secretome.....	203
Figure 7.11 – Impact of Cav1 in microglia cell on the tumour immune secretome. ...	205
Figure 7.12 – Impact of Cav1 status in microglia cells in tumour immune environment upon the secretome.....	206
Figure 7.13 – t-SNE representation of single cells collected from four GBM samples.	208
Figure 7.14 – Tumour cell distribution.....	209
Figure 7.15 – Cav1 expression based on localization and cell type.....	210
Figure 8.1 – Impact of the virus in the immortalization process on Cav1.....	222
Figure 8.2 – Tumour inflammatory environment: impact of Cav1 KO in microglia cells.....	226
Figure 8.3 – Cerebral organoid model.....	229

INDEX OF TABLES

Table 1.1 – Microglia and Macrophages characterization	12
Table 2.1 – Primers for qRT-PCR	45
Table 3.1 – crRNA sequences.....	59
Table 3.2 – Nucleofection program and conditions.....	60
Table 3.3 – PCR primers for PCR amplification to DNA cleavage study.....	63
Table 3.4 – Primers for screening the predicted deletion zones.....	65
Table 3.5 – Editing Efficiency according with each cell line.	66
Table 3.6 – Summary of editing efficiency of 5 cell lines.	68
Table 3.7 – Number of transfected clones analysed by Dot Blot and WB.....	69
Table 6.1 – CD11b and CD45 positive population of iPSC-derived microglial progenitors of Cav1 NT and Cav1 KO cells.....	144
Table 6.2 – The impact of Cav1 on secretome of iPSC-MG	157

CHAPTER 1 –
GENERAL INTRODUCTION

1.1 Glioblastoma: Clinical and Molecular Features

Tumours of the Central Nervous System (CNS) represent a distinct and heterogeneous group of both benign and malignant characteristics affecting children as well as adults. These tumours are relatively rare but associated with a high morbidity and death rate. Although in recent years there has been a substantial increase in the understanding of the molecular basis of the malignant phenotype, this is not translated in longer quality-adjusted survival.

CNS tumours are considered primary when the tumour initiates originally in the CNS and secondary when tumours begin elsewhere in the body and spread to the brain, i.e. brain metastasis. The classification of these tumours, according to the 2016 World Health Organization (WHO), is based on their cell of origin, primary location within the CNS, their level of differentiation, as well as their molecular features (Louis et al. 2016).

1.1.1 Glioma

Gliomas are the most common form of primary malignant brain tumours, and are classified into astrocytic tumours, oligodendroglial tumours and not otherwise specified/NOS tumours (group of tumours that do not match into these two narrowly defined entities). The histopathological classification of gliomas relies on morphological resemblance of tumour cells to normal cell types in the brain. Tumours with astrocytic features arising from astrocytes are classified as astrocytomas, while those with oligodendroglial features are termed oligodendrogliomas and are believed to originate from the oligodendrocytes or from a glial precursor cell (Louis et al. 2016).

The WHO classifies gliomas into 4 distinct grades based on histopathological features, nuclear morphology, mitotic activity or growth index, necrosis, margins, infiltration ability and vascular proliferation (D. M. Park and Rich 2009). A higher histological grade corresponds to a less differentiated phenotype and to an increased malignancy (Chiu, Peng, and Wang 2011; Louis et al. 2016):

- **Grade I** — the tumour grows slowly (low-grade), has cells that look like normal cells, and rarely spreads into nearby tissues. Grade I brain tumours can usually be cured by surgical resection and they are frequently associated with long-term survival.

They constitute the most common glioma found in children, i.e. pilocytic astrocytoma.

- **Grade II** — are also low-grade tumours with a slow growth rate but have a diffusely infiltrative nature and spread into nearby tissue, which renders them incurable by surgery. Recurrence after resection usually leads toward a higher-grade tumour.
- **Grade III** — includes anaplastic gliomas, which usually arise from low grade diffuse astrocytomas or *de novo* without evidence of a less malignant precursor. This grade is rapidly growing in malignant tumours exhibiting increased anaplasia (loss of morphology characteristic of the differentiated cell type) and proliferation over grade II tumours, and increased ability to spread into normal brain tissue. They require aggressive adjuvant treatment with radiotherapy and/or chemotherapy in addition to surgery.
- **Grade IV** — is a fast-growing tumour that grows and spreads very quickly, shows features of malignancy including vascular proliferation and necrotic areas. It is assigned to glioblastomas which are the most common and most malignant type of glioma in patients over 55 years old. Around 70% of patients die within 12 months despite multimodal aggressive treatments (Brodgelt et al. 2015).

In general, grades I and II tumours are considered low-grade, while grades III and IV are high-grade tumours.

1.1.2 Glioblastoma Multiforme (GBM)

GBM, or WHO Grade IV malignant glioma, accounts for 70-75% of all diffuse gliomas (Molinaro et al. 2019). They are highly invasive, infiltrating the surrounding brain parenchyma, yet they are typically confined to the CNS and rarely metastasize (Omuro and DeAngelis 2013).

In adults, its prevalence increases with age with the peak age range incidence after 55 years. GBM patients have a poor prognosis with a median survival of 15 months and only 3.4% patients surviving more than five years (Brodgelt et al. 2015). Some characteristics associated with a better prognosis include: age at the time of diagnosis (younger patients have better prognosis), total surgical resection of the tumour,

tolerance to complete adjuvant treatments, an epithelioid, giant-cell and gliosarcoma subtype and oligodendroglial differentiation characteristics (Crocetti et al. 2012; Thakkar et al. 2014; Louis et al. 2016). The high morbidity and mortality are associated with the invasive character and inability to undertake repeated surgical resections which can include only limited normal margins. Moreover, the chemotherapy is relatively ineffective due to an inherent chemoresistance of the tumour and/or the presence of the blood brain barrier (BBB) also limiting access of agents to brain (Ostrom et al. 2019).

1.1.3 Molecular Classification of GBMs

GBMs are characterized histologically by a significant cellularity and mitotic activity, vascular proliferation, and necrosis. The cells in these tumours are pleomorphic (varying in shape and size), thus the basis of the tumours naming, glioblastoma multiforme.

GBMs can be classified into three subtypes: Primary GBM, or **IDH-wild type** (90% of cases) that develops without the presence of any precursor neoplastic lesion; the secondary GBM or **IDH-mutant** (10% of cases) that develops from lower grade tumours, such as diffuse or anaplastic astrocytomas, and arises in younger patients (between 20 and 29 years); and **GBM-NOS** (i.e., not otherwise specified), where complete IDH evaluation cannot be performed (Louis et al. 2016). Histologically these subtypes are indistinguishable but have different response to therapy and prognosis.

Using global transcriptomic profile, in 2008 the Cancer Genome Atlas Project, Verhaak *et al.* divided GBM into four distinct subtypes: **classical**, **mesenchymal**, **proneural** and **neural**, as illustrated in **Figure 1.1**. Microarray techniques on DNA, RNA and protein level allowed the establishment of new classifications that have shown the vast heterogeneity of GBMs (Verhaak et al. 2010). These types differ by gene expression, clinical characteristics, response to therapy and outcomes (Meir et al. 2010; Mauerer-saccà, Martino, and Maria 2013).

The existence of GBM subtypes and different molecular and biological mechanisms, suggests that each should be approached as a distinct disease and that a universal therapy for all GBMs does not exist. The diversity of tumour characteristics is the result of hereditary or somatic alterations that control critical biological processes. This normally includes the activation of the oncogenes and/or the silencing of tumour

suppressor genes. These genetic alterations disrupt the cell cycle arrest pathways and/or activate various signal transduction pathways.

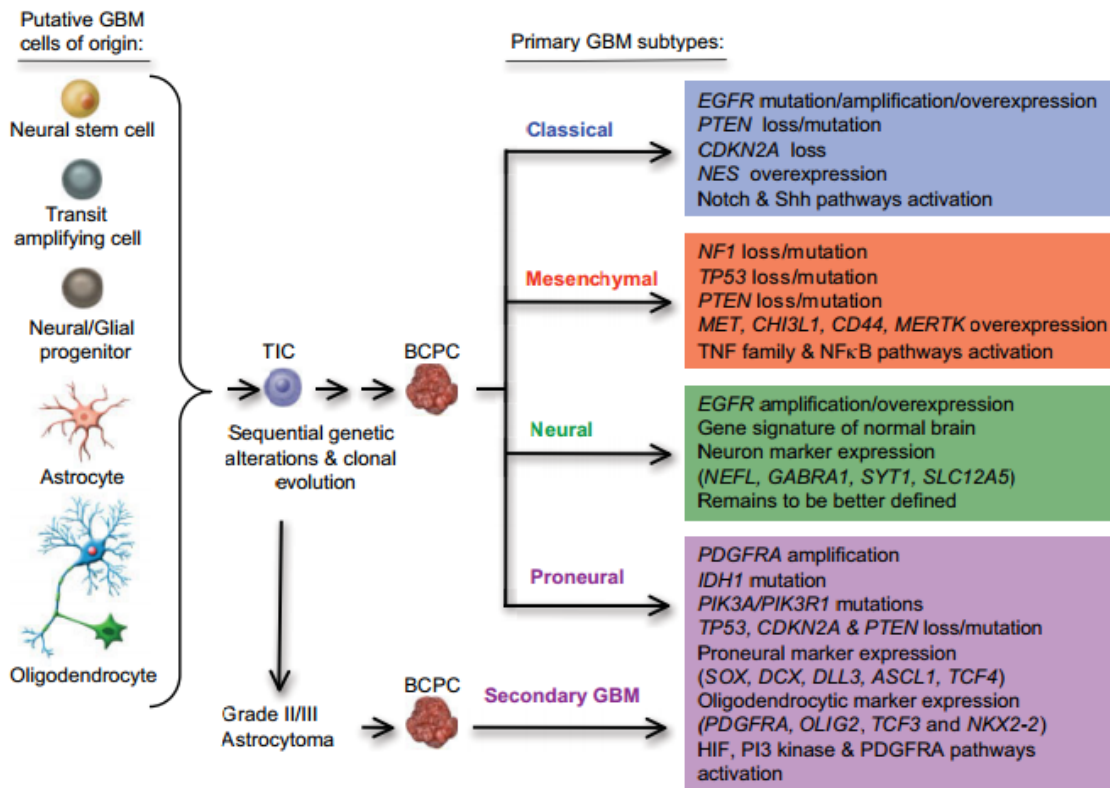


Figure 1.1 – Genetic classification of GBM. TIC - tumour-initiating cells, BCPC - brain cancer-propagating cells, EGFR, epidermal growth factor receptor; PTEN, phosphatase and tensin homolog; CDKN2A, Cyclin Dependent Kinase Inhibitor 2A; NES, Nestin; Shh, Sonic hedgehog; NF1, Neurofibromatosis type 1; TP53, Tumour Protein P53; PTEN, Phosphatase And Tensin Homolog; MET, MET Proto-Oncogene, Receptor Tyrosine Kinase; CHI3L1, Chitinase 3 Like 1; MERTK, MER Proto-Oncogene, Tyrosine Kinase; TNF, tumour necrosis factor; NF-κB, Nuclear Factor-kappa B; EGFR, Epidermal Growth Factor Receptor; NEFL, Neurofilament, Light Polypeptide; GABRA1, Gamma-Aminobutyric Acid Type A Receptor Alpha1 Subunit; SYT1, Synaptotagmin 1; SLC12A5, Solute Carrier Family 12 Member 5; PDGFRA, platelet-derived growth factor receptor-A; IDH, isocitrate dehydrogenase; PIK3, phosphoinositol 3-kinase; PIK3R1, PIK3 – 1-receptor; SOX, Sry-related HMG box; OLIG2, Oligodendrocyte Lineage Transcription Factor 2; TCF3, Transcription Factor 3; NKX2-2, NK2 Homeobox; HIF, hypoxia-inducible factor (Meir et al. 2010).

The **classical** subtype has a characteristic profile of highly proliferative cells. These are characterized by frequent gains in chromosome 7 and losses in chromosome 10, that result in amplifications or mutations of the epidermal growth factor receptor (EGFR) gene that encodes the receptor for the epidermal growth factor (EGF), and loss or mutation in the phosphatase and tensin homolog (PTEN) tumour suppressor gene. Patients with tumours classified with classical GBM subtype demonstrate

responsiveness to classical therapies (radiotherapy and chemotherapy), mainly because the p53 DNA damage response is intact in this group (Meir et al. 2010).

The **mesenchymal** subtype is characterized by frequent mutations or losses in the neurofibromatosis type 1 gene (NF-1), TP53, PTEN genes and high expression of CHI3L1, MET, and genes involved in the tumour necrosis factor (TNF) and nuclear factor- κ B (NF- κ B) pathways. These tumours demonstrate response to aggressive chemoradiotherapy, phosphoinositide 3-kinase (PI3K) inhibitors and angiogenesis inhibitors, because this subtype is associated with a high angiogenesis (Meir et al. 2010).

The **proneural** subtype has an expression profile reminiscent of gene activation in neuronal development, with high levels of expression of oligodendrocytic and proneural development genes. These tumours exhibit frequent mutations in p53, platelet-derived growth factor receptor- α (PDGFRA) and isocitrate dehydrogenase (IDH) 1 or 2. The IDH1/2 were originally discovered in 2009 and patients that present mutations in this gene have a better outcome than those with wild type IDH genes. Furthermore IDH1/2 mutations have been defined as a reliable genetic marker for secondary GBM, which develops from lower-grade gliomas. Amplification of chromosome 7 and losses on chromosome 10 are significant, but less frequent than in the classical subtype. In terms of prognosis, proneural GBM is associated with an increased overall survival rate relative to other molecular subtypes (Meir et al. 2010).

The **neural** subtype is less defined and has gene expression signatures that are most like those found in normal brain tissues and neuronal marker expression. Many molecular abnormalities and mutations overlap across the other transcriptional subclasses, like EGFR (Omuro and DeAngelis 2013).

Teo *et al.* incorporating different databases, including Caucasian, Korean and Chinese populations, demonstrated that the original proneural and neural subgroups defined by Verhaak formed a single cluster (proneural/neural subtype) (Teo et al. 2019).

1.1.4 Glioblastoma Therapy

The current treatment of GBM follows the Stupp's protocol which includes maximal safe surgical removal followed by radiation and chemotherapy (Stupp 2005). These tumours rarely metastasize outside the brain, but infiltrate extensively into surrounding normal brain which makes for difficult surgical removal without damaging adjacent normal brain (Soeda et al. 2009; Province et al. 2010; Stupp 2005).

Surgery

Generally, the first step in the treatment of GBM is surgery. The surgery improves the patient's survival and life quality, by reducing the symptoms caused by the presence of the tumour, like seizures, headache, nausea, or vomiting. The resected tissue will also assist the full molecular diagnosis and treatment planning. In the absence of complete resection, partial surgical resection provides a temporary reduction in tumour volume and pressure, however the residual GBM cells will later contribute to tumour regrowth unless they are effectively killed by adjunctive radiotherapy and/or chemotherapy.

Radiotherapy

In adults, radiotherapy is the standard treatment after tumour resection or biopsy. Different treatments of radiation may be given using various doses and schedules. Conventional fractionated external beam radiation is the standard radiation approach, usually the radiotherapy dose is 60 Gy divided in 30 fractions, i.e. five days a week for six weeks. The use of intensity modulated radiotherapy has been progressively preferred because of better targeting capability and dose deposition. Because GBM is a diffusely infiltrative disease, there is currently no defined role for stereotactic radiosurgery (highly precise radiation techniques that allow the use of ablative radiation doses to the tumour while minimizing dose to the adjacent normal structures) or brachytherapy (radioactive seed implanted inside or near to the tumour) as part of first-line treatment (Omuro and DeAngelis 2013; Redmond and Mehta 2015).

Radiation sensitizing drugs, chemotherapy during radiation therapy and drugs that increase oxygen levels in the brain are being studied as tactics of making tumour cells more sensitive to radiation or enhancing the effects of radiation (Palumbo et al. 2012; Van Nifterik et al. 2012).

Chemotherapy

The actual role of the BBB in limiting access of chemotherapeutics to GBM is not fully determined, however, chemotherapeutic drugs used to treat GBM have certain physicochemical properties considered important to cross the BBB, namely: low molecular weight and hydrophobic character. The main two chemotherapeutic compounds mostly used to treat GBMs, in combination with surgery and radiotherapy, are carmustine (BCNU) and temozolomide (TMZ) (Zulch 1986). BCNU and TMZ are examples of cytotoxic drugs that are toxic for cells, preventing cellular growth and replication. In contrast, cytostatic agents are used to alter the behaviour of a tumour, for example, angiogenesis inhibitors (anti-VEGF therapies) that stop the growth of new blood vessels. In some cases, cytotoxic and cytostatic chemotherapy drugs may be combined to increase their effectiveness (Omuro 2013).

BCNU and TMZ are alkylating agents that react with the nitrogen and oxygen atoms of DNA bases to form covalent alkyl lesions causing DNA damage in the form of intrastrand and interstrand cross-links. The resultant alkylated bases and mismatched bases will trigger activation of the mismatch repair (MMR) system. Lesions caused by methylation of the O⁶ position of Guanine (O⁶-meG), which is considered the most toxic lesion induced by these chemotherapeutic agents, cannot be repaired by MMR mechanisms. The unrepaired O⁶-meG lesion will eventually lead to DNA breaks and cell death as a result of apoptosis or autophagy (Ohgaki and Kleihues 2013). However, the O⁶-methylguanine-DNA methyltransferase (MGMT) is an important DNA repair enzyme that contributes to resistance of GBM to TMZ, a major determinant in patients' response to this therapy. MGMT reverses the alkylation caused by TMZ by removing the methyl group from guanine and transferring it to an internal cysteine residue (Cys145), preventing DNA damage-induced apoptosis. MGMT is considered a "suicide repair protein" because once MGMT transfers the methyl group to itself, it gets degraded and new MGMT must be synthesized in order to continue DNA repair. Patients are often screened for overexpression of this gene after tumour resection to determine the likelihood of TMZ success (Piperi et al. 2010).

Methylation of cytosine-phosphate-guanine (CpG) regions is the epigenetic event that is well characterized in these tumours. These regions are characterized by a high

percentage of guanine and cytosine, and they are typically located in the promoter regions of the genes, which in normal cells are typically unmethylated, allowing the transcription of the genes. The CpG regions that lie outside the promoter are commonly methylated and are responsible for transcriptional repression, *e.g.*, repetitive sequences. MGMT gene activity can also be silenced by promoter methylation. Epigenetic silencing of the MGMT gene by promoter methylation is associated with reduced DNA-repair activity, favourable outcome in patients and long-term survival (Heddleston et al. 2013; Sze et al. 2013).

1.2 Tumour Microenvironment and Immune System

The tumour is a complex system constituted by many distinct types of cell that are closely connected and dependent on their surrounding cellular and tissue environment. Tumour cells can adapt to the local environment and change it to their own advantage, this mechanism requires complex multilevel communication and interaction between themselves and with non-malignant cells in their microenvironment (Shao et al. 2015). The tumour environment (**Figure 1.2**), which is composed by tumour cells, surrounding stroma, blood vessels, immune cells (microglia and macrophages) and extracellular matrix, has an important role in the neoplastic progression, proliferation, survival and migration (Sotgia et al. 2012; Godlewski et al. 2015). It is the tumour microenvironment that is likely a major contributor to tumour heterogeneity, *i.e.* variation of cell morphology, gene expression, metabolism, motility, proliferation, invasion, drug resistance etc. (Wu, Zhuo, and Wang 2016).

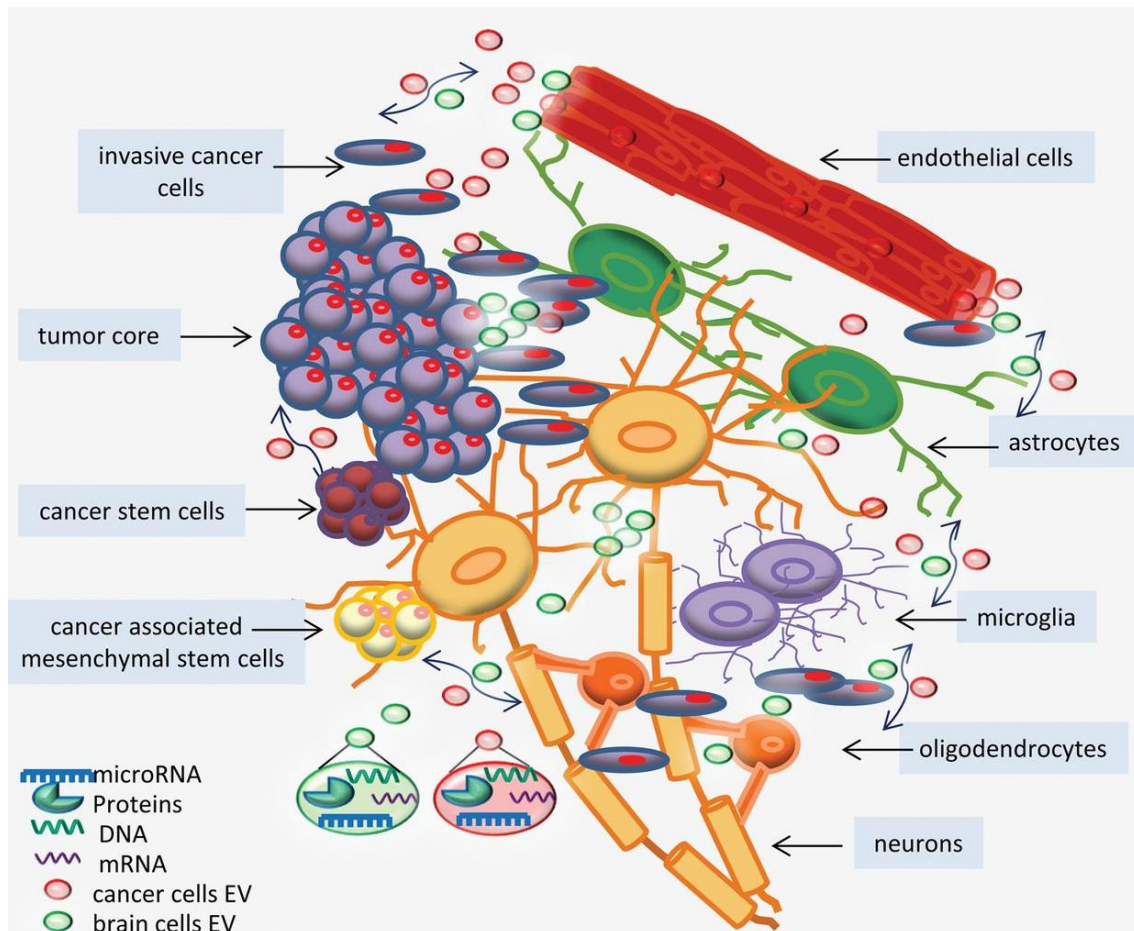


Figure 1.2 – The microenvironment of GBM is composed by numerous specialized cell types, which may contribute to tumour progression. Different cell types from the tumour microenvironment communicate via direct cell-cell contact and/or the release and uptake of soluble factors (Godlewski et al. 2015).

Tumour initiation and progression is a complex process involving genomic mutations, epigenetic alterations, microenvironmental factors and inflammatory mediators which generate an inflammatory microenvironment (Landskron et al. 2014). In many cancers, inflammation plays a major role in the pathogenesis. For example, helicobacter pylori infections are correlated with gastric cancer, hepatitis B or C infections associated with hepatocellular carcinoma and inflammatory bowel disease is connected with colorectal cancer (Crusz and Balkwill 2015). The main function of the immune system is to recognize and protect the organism from infections and damage, contributing for the homeostasis. However, the environment created by glioma associated macrophages/microglia (**GAM**) can be responsible for cell proliferation, tumour invasion, angiogenesis, metastasis and suppression of some immune functions (**Figure 1.3**) (Albulescu et al. 2013; Korkaya, Liu, and Wicha 2011; Filatova, Acker, and Garvalov 2013).

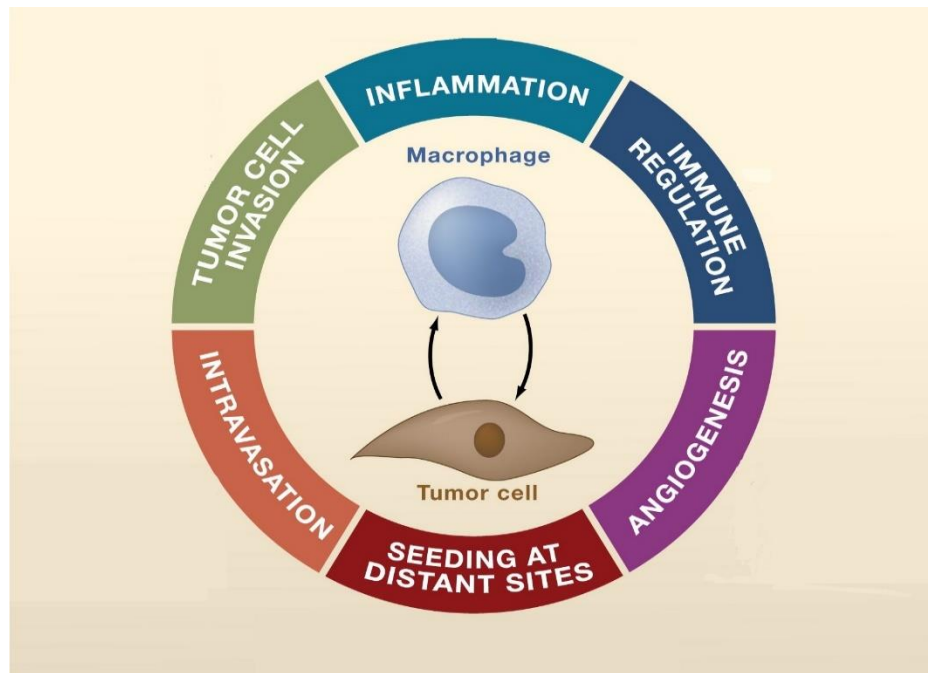


Figure 1.3 – Impact of GAMs on tumour environment (adapted from Qian and Pollard 2010).

The immune system should recognise the tumour cells as a threat. However, the neoplastic cells can manipulate the immune cells, promoting immunosuppressive mechanisms that usually promote the self-tolerance. This immunosuppressive environment downregulates mechanisms that were able to combat the tumour cells and control the disease and promotes the production of soluble factors to the microenvironment that will contribute to the tumour progression and therapy resistance. Immunotherapies are an appealing treatment for GBM, not only because they can control the tumoral microenvironment, but also because it will allow tumour specificity, minimizing the damage of normal brain tissue.

1.2.1 Microglia

Microglia is the name of the resident myeloid cells of the brain comprising between 10 to 12% of total brain population. The microglia population was first identified in the late 1800's and named as "rod-cells" by Nicolás Achúcarro (Sierra, Paolicelli, and Kettenmann 2019). However, in 1919, Pio del Río-Hortega described it as "mesoglia" or "third element", acknowledging the mesodermal origin of these cells, unlike the other brain cells. He used silver carbonate staining to visualize the microglia and he drew it in

under different pathological conditions, suggesting varied functions as the activation and phagocytic capacity (Río-Hortega 1919c, 1919d, 1919b, 1919a).

Microglia cells migrate into the CNS from the yolk sac during early embryogenesis, presenting a mesodermal origin. During the development, microglia is critical for the maintenance of brain homeostasis doing phagocytosis of apoptotic cells, supporting the neurogenesis, refining synaptic and axonal growth. Through the adulthood, microglia is tightly regulated and acts as a sentinel, detecting non-healthy conditions and phagocytosing pathogenic agents, damage tissue, protein aggregates and even tumour cells. In contrast, macrophages present in brain are originated from brain-infiltrating bone marrow-derived macrophages (BMDM) that have as the progenitor cell the hematopoietic stem cell. Only under pathological conditions, the inflammatory response can modify the BBB integrity and allow the BMDM to infiltrate the CNS (Ajami et al. 2011; Ginhoux and Garel 2018).

Both microglia and macrophages represent two distinct myeloid cell populations with similar immune regulatory functions. The consensus phenotypic profile to distinguish microglia from macrophages is described on next table:

Table 1.1 – Microglia and Macrophages characterization (Guillemin 2003; Bennett et al. 2016; Dubbelaar et al. 2018; A. M. Young et al. 2019) .

	Microglia	Macrophage
CD68	+	+
CD45	Low	High
CD11b	+	+
CD11c	High	High
MHC II	+	+
CD14	-	High
TMEM119	+	-
P2RY12	+	-

In the adult brain, microglia as well as macrophages can switch between two major states: resting, or surveying, and activated. In the resting state they present a ramified

morphology. When there is brain damage or injury, like viral or bacterial infections, microglia cells rapidly enlarge their bodies, a morphological change characteristic of activated microglia assuming an amoeboid morphology (**Figure 1.4**). With activation, microglia shows increased proliferation, migration, phagocytic activity and release of soluble factors (Crews and Vetreno 2016). Moreover, the released soluble factors are able to attract other immune cells to the inflammatory site.

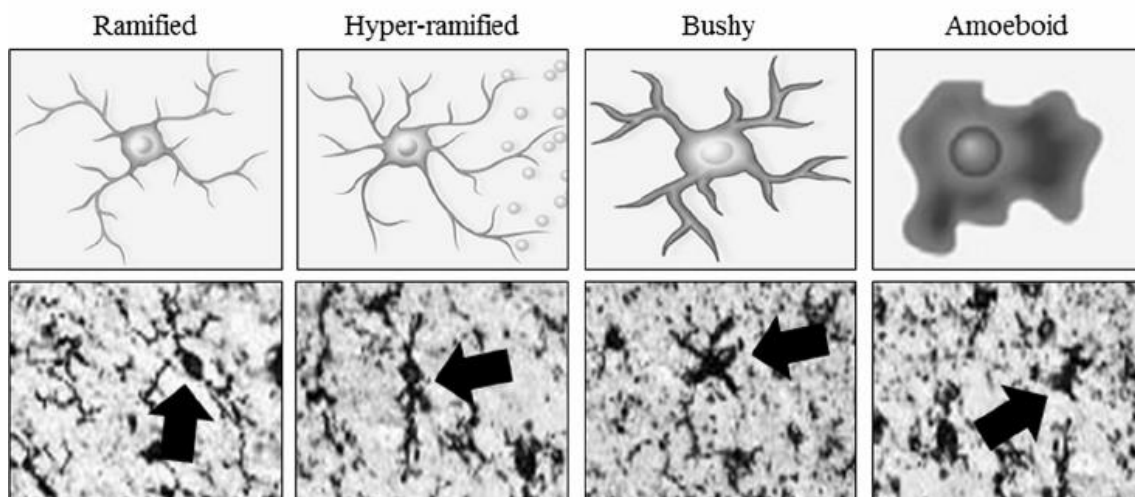


Figure 1.4 – Microglia states in human brain. Representative schematics and photomicrographs of human brain microglia (*Iba1* immunohistochemistry) representing morphological stages of microglial activation (Crews and Vetreno 2016).

Microglia and macrophages are mononuclear cell types characterized by considerable diversity and plasticity. Their activation can represent different stages of activation depending upon the stimulus (**Figure 1.5**).

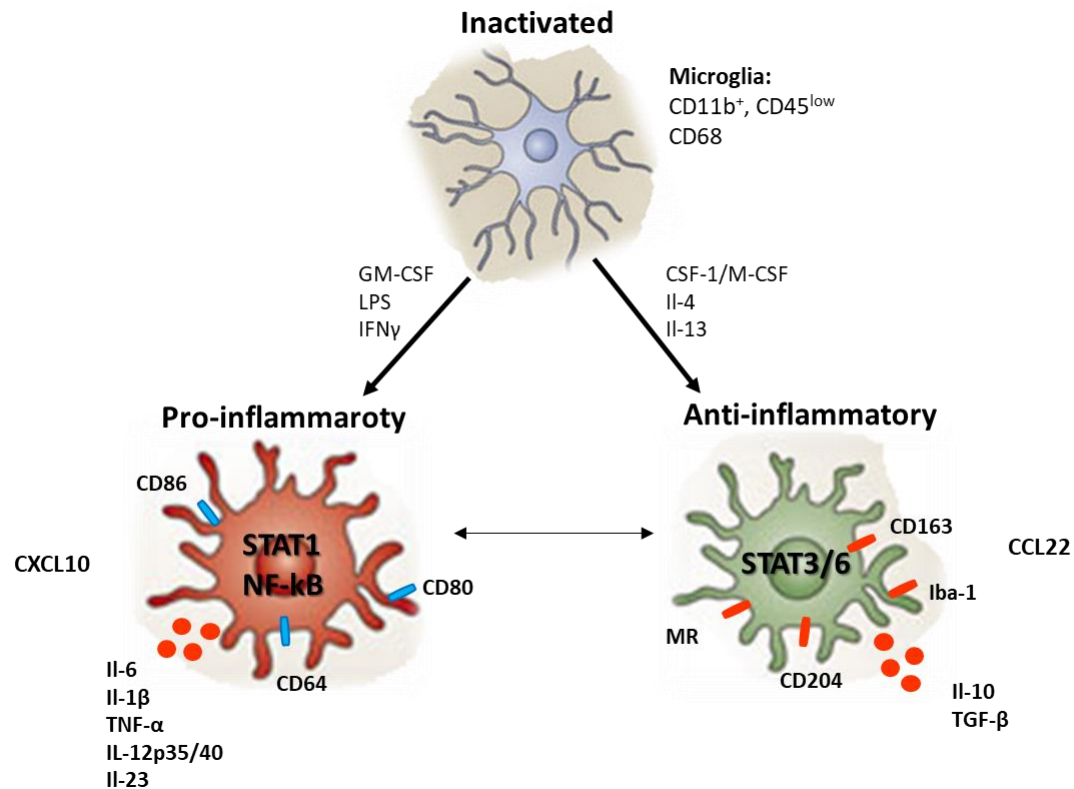


Figure 1.5 – Microglia activation. Inactivated microglia in the presence of GM-CSG, LPS and/or IFN- γ becomes activated into pro-inflammatory phenotype. On the other hand, in the presence of m-CSF, IL-4 and/or IL-13, the microglia assumes an anti-inflammatory phenotype (adapted from Wei et al. 2013).

The pro-inflammatory **M1**, classical or “**anti-tumoral**” **phenotype**, is typically acquired after stimulation with toll-like receptor 4 (TLR4) ligands and IFN- γ . Briefly, TLR4 stimulation leads to activation of nuclear factor- κ B (NF- κ B) and signal transducer and transcription (STAT)1 signalling and the activated pro-inflammatory cells display: IL-12^{high}, IL-23^{high}, IL-10^{low} phenotype and produce nitrogen intermediates and inflammatory cytokines such as IL-1 β , TNF- α , and IL-6, with high receptor expression for CD80, CD86, Fc-gamma receptors 1 and 2 (CD64 and CD32), CXCL10 and CCR7.

The anti-inflammatory **M2**, alternative or “**pro-tumoral**” **phenotype**, is typically acquired after stimulation with IL-4, IL-10 and/or IL-13. IL-4 can signal through either the type I (IL-4R α / γ c) or the type II (IL-4R α /-13R α 1), whereas IL-13 signals exclusively via the type II IL-13 receptor and IL-10 signals via IL-10R (Junttila et al. 2008). The M2 activation can be further subdivided into different activation states: M2a (Th2 responses, type II inflammation, killing of pathogens, allergy); M2b (Th2 activation, immunoregulation) and M2c (immunoregulation, matrix deposition, tissue remodelling). These

subpopulations differ with respect to receptor expression, effector function, and cytokine and chemokine production (Hambardzumyan, Gutmann, and Kettenmann 2015; Lisi et al. 2014). In contrast, IL-4R and IL-10R stimulation leads to activation of STAT6 and STAT3 signalling, respectively, and the activated anti-inflammatory cells display: IL-12^{low}, IL-23^{low}, IL-10^{high} phenotype and have high expression of several receptors such as class A scavenger receptor (SR-A, CD204), mannose receptor (CD206), CD163, CD200R, transglutaminase 2 (TGM2), CCL22, and DC-SIGN (CD209) (Komohara et al. 2008).

1.2.2 GAM and GBM

Between 30–50% of the cells in GBM are microglia or macrophages. The possibility has been raised that targeting microglia and macrophages might emerge as an adjuvant therapy for cancer treatment (Ransohoff and Cardona 2010). Several studies have demonstrated significant interaction between glioma cells and microglia and macrophages. They are attracted to the tumour milieu, and their activation and modulation is enhanced by GBM secreted factors.

Studies performed by Hao *et al.* (Hao et al. 2002) about the expression of cytokines and cytokine receptors in human gliomas and glioma cell lines indicate that a strongly immunosuppressive cytokine response greatly predominates. For instance, the cytokines IL-6, leukemia-inhibitory-factor (LIF), TGF- β and their respective receptors were strongly expressed in approximately all GBM and cell lines tested, whereas pro-inflammatory cytokines IFN- γ , TNF- α , IL-2 and IL-12 family members and their receptors were virtually absent in both tumours and cell lines. Others have documented similar expression patterns of immunosuppressive cytokines in gliomas. TGF- β , for example, inhibits the proliferation of microglia and the production of other cytokines *in vitro*, whereas the cytokines IL-6 and IL-10 have been postulated to promote glioma cell proliferation (Suzumura et al. 1993). The immunosuppressive cytokine IL-10 not only promotes glioma cell proliferation, but also enhances their ability to migrate *in vitro* (De Vleeschouwer et al. 2007).

On the other hand, components of extracellular matrix (ECM) are required during the process of tissue morphogenesis and development and contribute to the normal homeostasis. Matrix metalloproteinases (MMP) contain endopeptidases that participate in the ECM degradation and are important for tumour invasion and metastasis of cancers (Sahai 2005). The impact of microglia on GBM cell migration also correlates to the production of membrane type 1-matrix metalloprotease (MT1-MMP) released by microglia in response to soluble factors secreted by tumour cells. MT1-MMP promotes cell migration and invasion by degrading the ECM niche (Itoh 2006). Glioma cells also release matrix metalloproteases 2 (MMP-2) that are fully activated by MT1-MMP released from microglia, complementing the pathway. The consequent degradation of the ECM enhances the invasion of glioma cells into the brain parenchyma (H. Lee and Tsygankov 2010). Markovic *et al.* used mouse cell lines to show that, under basal conditions, microglia do not produce MT1-MMP, but, when exposed to glioma cells, they induce the upregulation of MT1-MMP. In human glioma samples, MT1-MMP expression positively correlates with an increased glioma malignancy grade (Markovic *et al.* 2009).

In the tumour microenvironment there are several examples of productive GAM - glioma cell interactions ultimately promoting glioma proliferation, migration, and invasion.

Microglial cells:

- release stress-inducible protein 1 (STI1), a cellular prion protein ligand (PrP^C) that increases the proliferation and migration of glioblastomas *in vitro* and *in vivo*, by modulation of MMP-9 (Carvalho da Fonseca *et al.* 2014).
- release EGF, which also stimulates GBM cell invasion.

Glioma cells:

- promote the activity of microglia via CSF-1, which is constitutively released by the tumour cells. CSF-1 or M-CSF is a chemoattractant for microglia and, at the same time, converts microglia into a pro-tumorigenic (M2) phenotype (Coniglio *et al.* 2012).
- CCL22 released from human glioma cells acts on the CCL22 receptor (CCR4) expressed on microglia (J. Zhang *et al.* 2012). CCL22 can trigger the release of IL-

6 from microglia, which in turn, promotes the invasiveness of glioma cells (Hambardzumyan, Gutmann, and Kettenmann 2015). CCL22 can also facilitate the recruitment and retention of T regulatory cells (Tregs) in the tumour environment (Z. Chen and Hambardzumyan 2018).

Several approaches have been used to ablate GAM, inhibit their tumour-promoting functions, or enhance the anti-tumoral roles. Pyonteck *et al.* investigated CSF-1R inhibition, which decreased the anti-inflammatory population and reduced tumour volume in several xenograft models (Pyonteck et al. 2013). On the other hand, TGF- β increased the migration of glioma cells through processes that likely involve increased integrin expression and function. Wesolowska *et al.* concluded that TGF- β is predominantly released from microglia in co-culture systems and blocking TGF- β signalling impairs the proliferation, migration and invasion of GBM cells (Wesolowska et al. 2008). In addition, TGF- β 2 induces the expression of MMP2 and suppresses the expression of tissue inhibitor of metalloproteinases (TIMP)-2, which together promote the glioma invasion (Wick, Platten, and Weller 2001). Antagonizing TGF- β function was already considered as a potential anti-tumour therapy, however it has severe side effects. The systemic inhibition of TGF- β signalling results in acute inflammation and disruption of the immune system homeostasis (Wesolowska et al. 2008).

In other tumours the T-cell population can be a crucial element for an adequate immune surveillance and production of an anti-tumoral immune response. However in GBM context the absence of anti-tumour response by T-cells is commonly observed and for the first time reported by Brooks *et al* in 1976 (Brooks, Roszman, and Rogers 1976). Together with the immunosuppressive environment, the low levels of T-cell infiltration are characteristic shared between GBM patients.

One mechanism identified and responsible for this lack of T-cells is correlated with the loss of surface sphingosine-1-phosphate receptor 1 (S1P1). S1P1 normally regulates T-cell trafficking out of the bone marrow, spleen, thymus, and lymph node, caused by sphingosine-1-phosphate (S1P) activation. The concentration of S1P is higher in blood and lymph, which establishes a chemotactic gradient for the migration of T-cells from the lymphoid organs into the circulation. Chongsathidkiet *et al* noticed that patients with

brain tumours showed a low number of T-cells in the peripheral blood, spleen and thymus, contrasting with the high number of these cells in the bone marrow (Chongsathidkiet et al. 2018). This phenomenon was noticed not only in brain tumours, but in other tumour that metastasized into the brain. How the brain triggers the dysfunction of this receptor on T-cell is still an unknown, however, the stabilization of S1P1-S1P axis in mice increased the levels of T-cells into the blood (Chongsathidkiet et al. 2018).

The few cells that reach the tumour milieu are dysfunctional, showing exhaustion, energy, senescence and/or tolerance. There is still a long way ahead to understand all the mechanisms behind this behaviour (K. I. Woroniecka et al. 2018; K. Woroniecka et al. 2018).

The activation of T-cells is coordinated by antigens presenting cells (APC), which are mandatory to the initiation phase in the lymphoid organs and to the effector phase at the site of action. APC should express MHCII, such as dendritic cells (DC), B cells and microglia. Due to the privileged immune environment of the brain, neurological diseases rely only on microglia cells to coordinate the T-cell activation. However, since the microglia cannot leave the brain environment to drain the antigens to the lymph nodes, it is believed that monocyte-derived DCs located at neighbouring sites around the brain can capture these antigens and present them to the naïve T-cells for complete activation (Schetters et al. 2018). A better knowledge about microglia cells in the tumour environment will provide fundamental insights about the T-cell activation for further therapies.

1.3 Induced pluripotent stem cells-derived microglia

The study of microglia has mainly relied on non-human models or rodent models, due to the easy access to the source. Primary human microglia cannot be propagated and the availability to fresh tissue is very limited. Even more, studies of Butovsky et al. showed that primary fresh isolated microglia quickly loses their identity when cultured in mono-culture *in vitro*, highlighting the importance of the brain environment for the

microglial phenotype (Butovsky et al. 2014). The human immortalized microglial cells usually present highly proliferative rate, and since they are cultured *in vitro* without the interference of the brain environment, perhaps these cells are not representative of a non-proliferating and a differentiated cell type. There is therefore a need for a model which can represent closely the human microglia. To overcome this gap, different protocols to generate microglia cells from induced pluripotent stem cells (iPSC) were published in 2016 and 2017 (Muffat et al. 2016; Abud et al. 2017; Douvaras et al. 2017; Haenseler et al. 2017; Pandya et al. 2017; Takata et al. 2017).

The iPSC are cells that are reprogrammed to a stem phenotype from differentiated or adult cells and can be maintained in a self-sustaining pluripotent state equivalent to the embryonic stem cells (ESC). Like ESC, the iPSC are able to self-renewal and, upon appropriate stimulation, differentiate into three germ layers: endoderm, mesoderm and ectoderm. Moreover, after being differentiated into the respective germ layer, these cells can be further fully differentiated in any cell type of the human body. In 2006, Takahashi and Yamanaka demonstrated for the first time that murine embryonic fibroblasts can be reprogrammed into iPSC through overexpression of four transcription factors using a retroviral approach. From a list of 24 transcription factors, Oct3/4, Sox2, KLF4 and c-myc (OSKM factors) were carefully selected showing the best results for the reprogramming process (Takahashi et al. 2006). One year later, the same group dedifferentiated human fibroblasts into iPSC using the same cocktail of transcription factors (Takahashi et al. 2007). Since then other groups are using the same concept to reprogram not only skin fibroblasts, but also other human somatic cells as peripheral blood mononuclear cells (PBMCs) (Chou et al. 2011), CD34+ cells (Mack et al. 2011) and renal epithelial cells from urine samples (Zhou et al. 2012).

The current protocols to differentiate microglia from iPSC use chemically defined conditions that mimic the embryonic development. iPSC-derived microglia (iPSC-MG) is similar by morphology, transcription, cytokine release and phagocytic capacity to the human primary microglia. Furthermore, iPSC-MG is distinct from other macrophages showing a different transcriptional profile (Muffat et al. 2016; Haenseler et al. 2017; Abud et al. 2017). Microglia derived from the mesodermal primitive yolk sac progenitors, by Myb-independent and RUNX1-, Pu.1- and Irf8-dependent pathways

(Ginhoux et al. 2010; Schulz et al. 2012; Kierdorf et al. 2013). The RUNX1, Pu.1 and Irf8 are transcriptional factors involved in haematopoiesis and myeloid differentiation. However, the transcriptional factor Myb is critical for development of HSC, but dispensable for yolk sac haematopoiesis, confirming the different origin of monocytes-derived macrophages and microglia (Schulz et al. 2012; Buchrieser, James, and Moore 2017). Furthermore, yolk sac-derived microglia, as well as other yolk sac-derived resident macrophages self-renew locally, independently of the hematopoietic stem cells (HSC) and circulating monocytes, in healthy conditions.

The iPSC-MG resembles the human foetal and adult microglia and presents a transcriptomic profile distinct from macrophages, monocytes and dendritic cells, expressing microglial specific signature, i.e. P2RY12, GPR34, CABLES1, BHLHE41, TREM2, OLFML3, APOE, among others (Haenseler et al. 2017; Abud et al. 2017). The differentiated cells are functional, able to migrate, do phagocytosis and increase the pro-inflammatory genes, like TNF- α , IL-8 and CCL4 in response to IFN- γ , IL-1 β or LPS (Abud et al. 2017).

1.4 Caveolae

Caveolae are plasma membrane 50–100 nm invaginations that function as specialized membrane microdomains (Palade 1953), which develop as a result of a localized enrichment of cholesterol, glycosphingolipids, sphingomyelin, and the caveolin proteins (**Figure 1.6**) (Razani, Woodman, and Lisanti 2002).

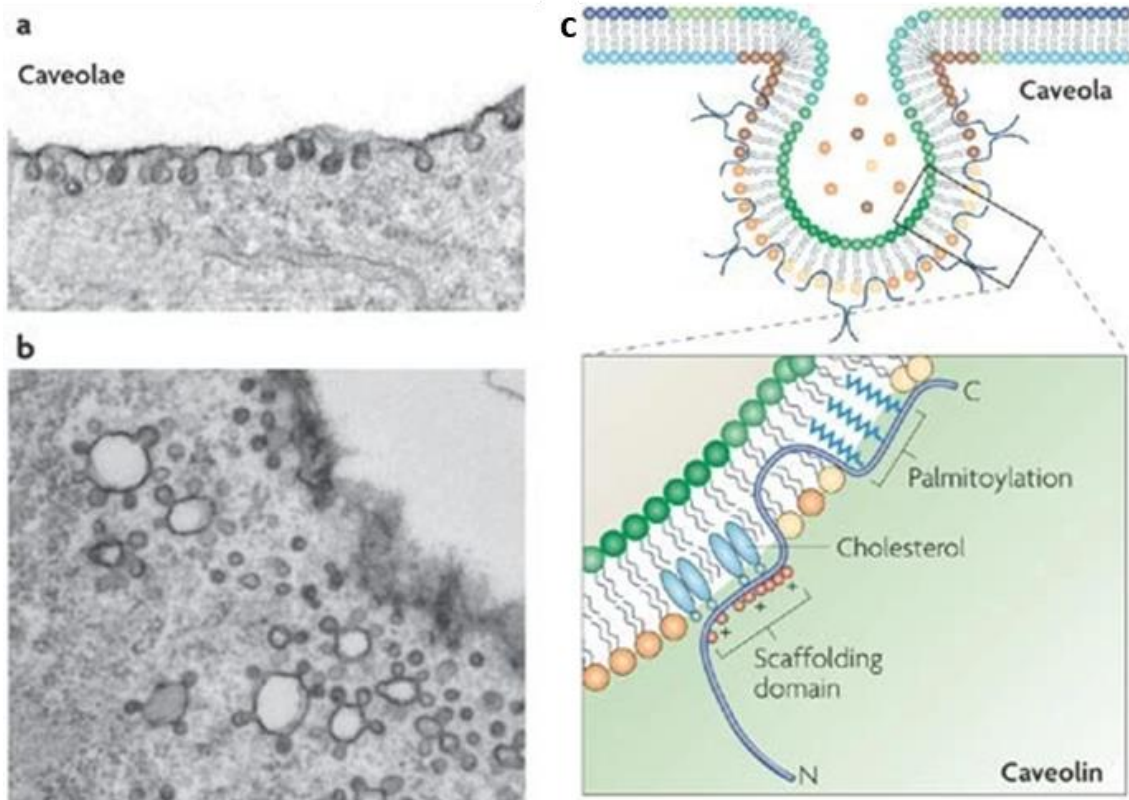


Figure 1.6 – Caveolae and Caveolin-1. Electron micrographs showing the ultrastructure of caveolae in adipocytes (**a** and **b**). **c** – diagram showing how caveolin-1 is inserted into the caveolar membrane, with the C and N terminal facing the cytoplasm and a putative hairpin intramembrane (adapted from Parton and Simons 2007).

Generally, caveolae emerges in a variety of shapes, including flat, vesicular, and U shape. Three small coat proteins have been identified in caveolae, caveolin-1 (Cav1), caveolin-2 (Cav2) and caveolin-3 (Cav3). Cav1 and Cav2 are universally co-expressed on epithelial and endothelial cells, fibroblasts, smooth muscle cells, adipocytes and pneumocytes. Cav3 expression is mainly restricted to striated (skeletal and cardiac), smooth muscle and glia cells (Fridolfsson et al. 2014). In the human cerebral cortex, Cav1 immunoreactivity is detected on all the cortex microvessels and also on bodies of astrocyte-like cells that extend fine processes ending on the microvessel wall (Virgintino et al. 2002). Using western blot, Ramirez *et al.* identified the Cav1 in plasmatic membrane of cortex and hippocampus as well (Ramírez et al. 2009). All three caveolins show a topology with N and C terminal in the cytoplasm and a long putative hairpin intramembrane domain embedded into the membrane. The scaffolding domain is a highly conserved region of caveolin, that might have a role in cholesterol interactions.

Cav1 binds to cholesterol molecules (Murata et al. 1995) and is also palmitoylated in the C-terminus region (Dietzen, Hastings, and Lublin 1995). Cholesterol is essential for caveola formation, and the depletion disturbs its structure (Parton and Simons 2007).

Cav1 gene is located close to Cav2 in the chromosome 7q31.1 and is composed by three exons, with respective sizes of 30, 165 and 342 bp, spaced by two introns with approximate size of 1.5 and 32 kbp (Razani, Woodman, and Lisanti 2002; Engelman et al. 1998). There are four transcript variants which encode the protein. Cav1 protein occurs in two isoforms: Cav1 α and Cav1 β , 24 kDa and 21 kDa, respectively. These two isoforms differ in their N-terminus truncated by 31 amino acids, presenting an overlapping but a slightly different distribution in mammalian cells (Scherer et al. 1995; Nohe et al. 2005). Cav1 is synthesized in the endoplasmic reticulum in a signal recognition particle-dependent manner (Monier et al. 1995). The newly synthesized protein suffers a first stage of oligomerization and then is transported into the Golgi complex (Monier et al. 1996; Pol et al. 2005). In the Golgi complex, Cav1 is further oligomerized and associated with cholesterol and glycosphingolipid-rich lipid raft domains to form a mature caveola-like configuration (Parton and Simons 2007). Mature Cav1 is then transported to the plasma membrane mainly regulated by syntaxin 6 (Choudhury et al. 2006).

Caveolae regulate signal transduction within the cell, as well as numerous other cellular processes including vesicular transport (transcytosis, endocytosis), cholesterol homeostasis to nitric oxide production, cell migration and adhesion, and cell cycle (Senetta et al. 2013).

1.4.1 Caveolin-1 and Cancer

The capability of Cav1 to modulate intracellular signalling has important implications in biological and pathological conditions, including cancer processes, such as cell transformation, tumour growth, cell migration and invasion, drug resistance and angiogenesis (Senetta et al. 2013). The loss of Cav1 was frequently observed in various types of malignancies during the earlier stages, such as breast and colon cancers and ovarian carcinomas. However, other studies also indicate that Cav1 is positively correlated with cancer drug resistance and metastasis, such as colon, breast and lung

cancer (Z. Wang et al. 2015). Moreover, cancer patients with high Cav1 expression had a worse chemotherapeutic response and progression, which translated into a poor prognosis (Senetta et al. 2013). Therefore, Cav1 can have a dual role and may be a tumour suppressor gene or a tumour promotor gene (**Figure 1.7**), depending on tumour microenvironment and temporal context.

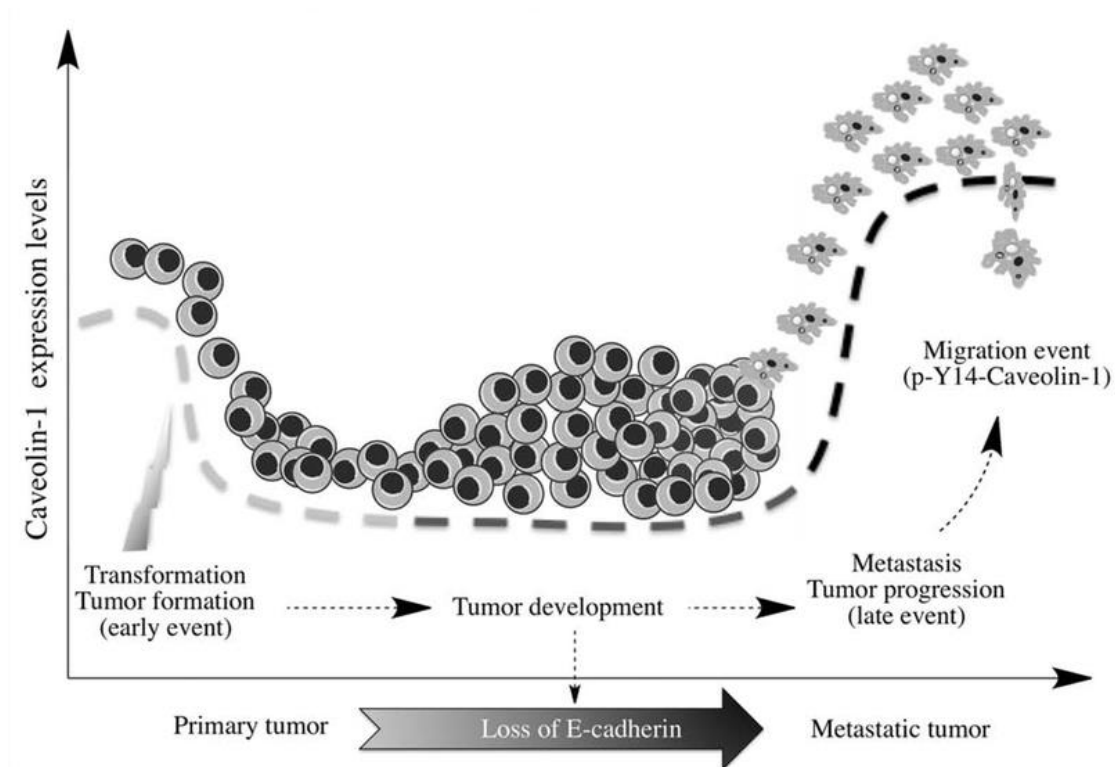


Figure 1.7 – Dual role of Cav1 in Cancer. Cav1 can act as a tumour suppressor or as a tumour promotor, depending on tumour context, stage of tumour development and progression. In some tumours, like breast, lung, and colon, Cav1 acts as a tumour suppressor, and in the early stages of cell transformation and tumour development is correlated with Cav1 reduction (light grey dashed line). However, as tumour progresses and proliferates, some alterations like epithelial-mesenchymal transition that leads to loss of E-cadherin is observed. Upon re-expression of Cav1 (black dashed line), for example, triggered by hypoxia, the protein may contribute to development of characteristics associated with enhanced malignancy (multidrug resistance and metastasis), usually associated with phosphorylation of Cav1 on Tyrosine-14. In other tissues, where Cav1 is not expressed, like prostate and pancreatic cancer or gliomas, Cav1 is associated with enhanced tumour cell malignancy and a more aggressive phenotype, represented in the late event on the model above (G. Quest et al. 2013)

The contribution of Cav1 to tumour progression seems to be complex (Quest, Gutierrez-Pajares, and Torres 2008). To explain Cav1's role during the cancer development, Wang et al. proposed that the early stages of tumour formation and malignant transformation may be promoted by Cav1 loss and this would sensitize normal cells to an oncogenic

event, suggesting Cav1 as a tumour suppressor. On the other hand, Cav1 is commonly upregulated in several advanced epithelial tumours, including prostate, kidney, breast, and bladder carcinomas. Whereas, in cancer progression Cav1 re-/over-expression will contribute to tumour cell resistance and metastasis, suggesting Cav1 as a tumour promotor (Z. Wang et al. 2015).

The role of Cav1 in GBM is still poorly understood and controversial as well. *In vitro* studies of Cosset *et al.* with U87MG, a GBM cell line, have demonstrated that Cav1 acts as a tumour suppressor by downregulating $\alpha 5\beta 1$ integrin expression, following with the decrease of TGF β /SMAD activity, which increased the proliferation, invasion and clonogenicity when Cav1 was downregulated (Cosset et al. 2012; Martin et al. 2009). Quann and collaborators demonstrated that Cav1 has a negative correlation with tumour growth, and when Cav1 was upregulated in U87 cells these cells showed a decrease of proliferation and invasion, associated with an increase of chemosensitivity and apoptosis (Quann et al. 2013). In contrast other groups found a positive correlation between Cav1 expression and tumour grade with tumour samples (Cassoni et al. 2007; Barresi et al. 2009; Pu et al. 2019; Moriconi 2019). Annabi *et al.* demonstrated a positive correlation of CD44 and Cav1, and that CD44 was highly expressed in highly invasive gliomas (Annabi et al. 2004). Studies of Abulrob *et al.* proposes that low phosphorylation states of EGFR or EGFRVIII are accompanied by increased localization of the receptor in caveolae and attenuation of the transformed glioblastoma cell phenotype, suggesting that caveolae may be beneficial in suppressing aberrant signalling through the receptor in glioblastoma cells and tumours, decreasing the tumoral aggressive features (Abulrob et al. 2004).

1.4.2 Caveolin-1 and immune cells

The role of Cav1 in immune cells is not completely understood, however Cav1 seems to be expressed in all immune cells (Harris et al. 2002). Regarding the Cav1 expression in microglia cells, this has not been thoroughly investigated. In 2013, Niesman *et al.* detected the Cav1 expression in murine microglial BV-2 cells, and Cav1 protein was significantly reduced in inactivated microglial, while the activated state showed an increase of Cav1 expression (Niesman et al. 2013). On the other hand, Portugal *et al.* showed that Cav1 is involved in the inflammatory phenotype by internalization of the

sodium-vitamin C cotransporter 2 (SVCT2) in human microglia cell line, CHME3 (Portugal et al. 2017).

In immune cells, caveolae have been suggested to play a role on the regulation of cell activation in response to external stimulus, release of soluble factors, cell migration, phagocytosis and endocytosis of pathogens and necrotic cells, however, the function of this protein might be dependent on the cell type studied, and their expression can fluctuate reflecting the activation and/or maturation stage of the cell (Feng et al. 2013). The uptake of virus, as SV40, and bacteria, like *Pseudomonas aeruginosa*, is mainly coordinated by Cav1 (Norkin 1999; Gadjeva et al. 2010). Moreover, the exacerbated inflammatory response leading to chronic inflammation was observed in Cav1 knockout (KO) models, increasing the plasma levels of inflammatory mediators as IL-6, TNF- α , IL-12p70, CXCL13/BLC, G-CSF, IL-3, and CXCL10/IP-10 (Codrici et al. 2018a). In sepsis context, Cav1 seem to exert a protective function, modulating the inflammatory response by inhibition of LPS-TLR4 signalling, relieving the bacterial burdens, and suppressing thymocyte apoptosis. Cav1 inhibits the LPS-TLR4 pathway by directly binding to TLR4, which prevents the TLR4 association with MyD88 and TRIF, and by suppressing the activation of ERK1/2/MAPK, JNK/MAPK, and PI3K (Feng et al. 2010).

Cav1 is involved in inflammation, adhesion, and phagocytosis of the monocyte/macrophage. Furthermore, higher expression of phosphorylated Cav1 (pCav1) was found in activated macrophages and microglia in mouse experiments (Shin 2007; Bucci et al. 2000). On the other hand, Tsai *et al.* showed that deletion of Cav1 in macrophages suppresses their phagocytic activity with downregulation of CD14 and CD36 (anti-inflammatory related markers). They also reported that NF- κ B activation is inhibited in Cav1 KO macrophages through downregulation of TLR4 and MyD88 (Tsai et al. 2011), showing contradictory results published by Feng and collaborators (Feng et al. 2010). This emphasises again that the Cav1 role is dependent of cell type and/or pathologic environment. Moreover, Cav1 is associated with the nuclear translocation of transcription factors and integrin signals, the major regulators in monocyte differentiation (Y. Fu et al. 2012). Shimato *et al.* observed a significantly upregulated of Cav1 in monocytes in the presence of GBMs. They demonstrated that siRNA inhibition of Cav-1 restores myeloid cell function, as measured by TNF- α secretion in the presence

of GBMs (Shimato et al. 2013). Studies of Wang *et al.* demonstrated that Cav1 can have a potent immunomodulatory effector molecule in murine alveolar and peritoneal macrophages. They also showed that Cav1 has a protective role for inflammation by suppression of pro-inflammatory cytokine production (TNF- α and IL-6) and increase of the IL-10 production, related with a M2 phenotype (X. M. Wang et al. 2006).

1.5 Aims of the Project

Cav1 in GBM contributes to tumour invasion and it is associated to a shorter survival rate (Pu et al. 2019; Moriconi 2019). In immune cells, particularly in human microglia cells, the function of Cav1 is not well understood, but Portugal *et al.* suggests that the protein is involved in the inflammatory response (Portugal et al. 2017). On the other hand, Shimato and colleges demonstrated that the inhibition of Cav1 could restore the myeloid function in human GBM (Shimato et al. 2013).

Taking this into consideration, the hypothesis of this work is that Cav1 is a modulator of microglia immune response and it regulates the tumour-microglia interaction in order to promote the development and progression of GBM.

To investigate how the Cav1 status in microglia may modulate immune response, cell-cell communication, and cell invasion within the GBM microglial environment, the project was defined by 4 objectives:

Objective 1: Create stable Cav1 KO of three established GBM cell lines, one human microglia cell line and one iPSC cell line. Design a CRISPR-Cas9 system to target the Cav1 gene. Upon electroporation, clones prevent from single cells are generated, characterized, and deposited in a cell bank for further experiments and projects (Chapter 3).

Objective 2: Study how Cav1 status in microglia influences its pro-inflammatory and anti-inflammatory biochemical and functional phenotype. Study the microglial biochemical phenotype with regards to responsiveness to standard microglia activation treatments (e.g. cytokines) using two different human microglia, a established cell line

and iPSC-derived microglia, taking into consideration the Cav1 status (Cav1 NT and Cav1 KO). Investigate the impact in the chemosensitivity to TMZ, migration and phagocytic competence based on the Cav1 status in microglia (Chapter 4 and 6).

Objective 3: Investigate how the Cav1 status in microglia impacts the microglia responsiveness to GBM immune tumour environment. Upon co-culture with three GBM cell lines, study the impact on microglial proliferation, migration, transcriptome, and molecular mechanisms correlated with human immune response, contemplating the Cav1 status in microglia. Investigate the expression of Cav1 in myeloid cells using online databases from single cell analysis of healthy donors and GBM tumour samples (Chapter 5 and 7).

Objective 4: Explore how tumour immune environments created by microglia Cav1 NT and microglia Cav1 KO impact the GBM behaviour. Using a 2D co-culture model, evaluate the impact of microglia (Cav1 status dependent) on tumour proliferation, invasion, and on transcriptomic profile of genes involved in tumour invasion. Study the impact of microglia (Cav1 status dependent) on tumour invasion upon establishment of a 3D co-culture model (Chapter 5 and 7).

CHAPTER 2 – GENERAL MATERIAL AND METHODS

2.1 Material

2.1.1 Cell lines

Name	Type	Source
U87MG	GBM	ECACC (#89081402)
UP007	GBM	SEBTA
UP029	GBM	SEBTA
CHME3	Microglia	Brian Bigger, Manchester University
THP1	Monocytes	ECACC (#88081201)
KOLF2	iPSC (HPSI0114i-kolf_2)	Nick Allen, Cardiff University
34D6*	Astrocytes precursors cells	Nick Allen, Cardiff University
HEK-blue2	Engineered HEK293 cells to test mycoplasma contamination	InvivoGen (#rep-pt1)

*34D6 – iPSC-derived astrocytes progenitor cells (APC), from fibroblasts of normal female (40 y old; CRL-2524; ATCC)

2.1.2 Cell culture mediums

- **GBM and CHME3 media**

Components	Concentration	Company (Cat#)
DMEM high glucose		Gibco (42430025)
FBS	10%	Gibco (10500064)
Penicillin/Streptomycin	1%	Gibco (15140122)

- **THP1 media**

Components	Concentration	Company (Cat#)
RPMI 1640		Gibco (61870010)
FBS	10%	Gibco (10500064)
Penicillin/Streptomycin	1%	Gibco (15140122)

- **iPSC media**

Components	Concentration	Company (Cat#)
Essential 8 Flex basal medium		Gibco (A28583-01)
Essential 8 Flex supplement	1X	Gibco (A28584-01)

- **EB 3G media**

Components	Concentration	Company (Cat#)
mTeSR 1 Basal Medium		StemCell (85851)
mTeSR 1 5X Supplement	1X	StemCell (85852)
BMP-4	50 ng/ml	Peprotech (120-05ET)
Human VEGF 165	50 ng/ml	Peprotech (100-20)
Human SCF	20 ng/ml	Miltenyi (130-096-692)

- **X-VIVO Factory Media**

Components	Concentration	Company (Cat#)
X-VIVO 15		Lonza (LZBE02-060F)
Penicillin/Streptomycin	1%	Gibco (15140122)
Glutamax	1X	Gibco (35050038)
2-ME	55 μ M	Gibco (21985023)
IL-3	25 ng/ml	BioLegend (578006)
M-CSF	100 ng/ml	BioLegend (574806)

- **X-VIVO Microglia Differentiation Media**

Components	Concentration	Company (Cat#)
X-VIVO 15		Lonza (LZBE02-060F)
Penicillin/Streptomycin	1%	Gibco (15140122)
Glutamax	1X	Gibco (35050038)
2-ME	55 μ M	Gibco (21985023)
IL-34	100 ng/ml	BioLegend (577904)
GM-CSF	10 ng/ml	BioLegend (572903)

- **Microglia Resting Media**

Components	Concentration	Company (Cat#)
X-VIVO 15		Lonza (LZBE02-060F)
Penicillin/Streptomycin	1%	Gibco (15140122)
Glutamax	1X	Gibco (35050038)
2-ME	55 μ M	Gibco (21985023)
N2	1:100	Gibco (17502048)

- **EF20 – APC media**

Components	Concentration	Company (Cat#)
Advance DMEM/F12		Gibco (12634010)
Penicillin/Streptomycin	1%	Gibco (15140122)
Glutamax	1X	Gibco (35050038)
N2	1:100	Gibco (17502048)
B27	1:1000	Gibco (17504044)
Human EGF	20 ng/ml	R&D Systems (236-EG)

FGF-2	20 ng/ml	Peprtech (450-33)
Heparin	20 ng/ml	Sigma (H3149-10KU)

- **CNTF – ADF media**

Components	Concentration	Company (Cat#)
Neurobasal		Gibco (21103049)
Penicillin/Streptomycin	1%	Gibco (15140122)
NEAA	1X	Gibco (11140050)
Glutamax	1X	Gibco (35050038)
B27	1:500	Gibco (17504044)
CNTF	10 ng/ml	R&D Systems (257-NT)

- **HEK-Blue-2 media**

Components	Concentration	Company (Cat#)
DMEM high glucose		Gibco (42430025)
FBS	10%	Gibco (10500064)
Penicillin/Streptomycin	1%	Gibco (15140122)
HEK-blue selection	1X	InvivoGen (hb-sel)
Normocin	100 µg/ml	InvivoGen (ant-nr-1)

2.1.3 Other Cytokines, Growth Factors, and Inhibitors

Components	Concentration	Company (Cat#)
LPS	1 µg/ml or 100 ng/ml	Sigma (L2630)
IFN-γ	20 ng/ml	PeprTech (300-02)
IL-4	20 ng/ml	PeprTech (200-04)
IL-13	20 ng/ml	PeprTech (210-13)
PMA	150 µM	Sigma (P8139)
Y-27632 Rho Kinase Inhibitor	10 µM	Abcam (ab120129)

2.1.4 Other Cell Culture Reagents

Components	Company (Cat#)
Alt-R S.p. Cas9 Nuclease 3NLS	IDT (1074181)
Alt-R® CRISPR-Cas9 tracrRNA, ATTO™ 550	IDT (1075927)
Alt-R® Cas9 Electroporation Enhancer	IDT (1075915)
Stem-CellBanker - GMP Grade	AMSBIO (11890)

DMSO	Sigma (D2650)
VTN	Gibco (A14700)
FN	Millipore (FC010)
Geltrex	Gibco (A1413301)
Matrigel - Growth factor reduced	Corning (354230)
StemPro Accutase	Gibco (A1110501)
ReLeSR Enzyme-free	StemCell (5873)
KnockOut DMEM medium	Gibco (10829018)
Cell Dissociation Buffer	Gibco (11530456)
PBS pH 7.4	Gibco (10010023)
Live Cell Imaging Solution	Gibco (A14291DJ)
Calcein AM	Invitrogen (C1430)
PI	Sigma (P4864)
DAPI	Invitrogen (D1306)
Hoescht	Thermo Sci (62249)

2.1.5 Antibodies for FACs

Components	Company (Cat#)
CD45 (2D1) – FITC	eBioscience (11-9459)
CD34 (4H11) – PE-Cyanine7	eBioscience (25-0349)
CD11b (ICRF44) – APC	eBioscience (17-0118)
FITC Mouse IgG1, κ Isotype Ctrl	Biologend (400109)
PE/Cy7 Mouse IgG1, κ Isotype Ctrl	Biologend (400109)
APC Mouse IgG1, κ Isotype Ctrl	Biologend (400109)

2.1.6 Antibodies for Western Blot

Components	Dilution	Company (Cat#)
Phospho-Cav1 (Tyr14)	1:1000	Cell Signaling (3251)
Cav1	1:1000	Cell Signaling (3238)
Phospho-STAT1 (Tyr701) (58D6)	1:1000	Cell Signaling (9164)
STAT1 (D1K9Y)	1:1000	Cell Signaling (4994)

Phospho-NF- κ B p65 (Ser536) (93H1)	1:1000	Cell Signaling (3033)
NF- κ B p65 (D14E12)	1:1000	Cell Signaling (8242)
Phospho-STAT3 (Tyr705) (D3A7)	1:1000	Cell Signaling (9145)
STAT3	1:1000	Cell Signaling (9132)
Phospho-STAT6 (Tyr641)	1:1000	Cell Signaling (9361)
STAT6	1:1000	Cell Signaling (9362)
Anti-rabbit IgG, HRP-linked 2 ^o antibody	1:10000	Cell Signaling (7074)

2.1.7 Antibodies for Immunofluorescence

Components	Dilution	Company (Cat#)
IBA-1	1:100	Abcam (ab5076)
TMEM119	1:100	Abcam (ab185337)
Cav1	1:500	Cell Signaling (3238)
Goat anti-rabbit IgG Alexa Fluor 488	1:400	Invitrogen (A11034)
Donkey anti-goat IgG Alexa Fluor 488	1:400	Invitrogen (A11055)

2.1.8 Kits

Name	Company (Cat#)
SE Cell Line 4D-Nucleofector X Kit S	Lonza (V4XC-1032)
P3 Primary Cell 4D-Nucleofector Kit S	Lonza (V4XP-3032)
PureLink Genomic DNA Kit	Invitrogen (K182001)
RNeasy Mini Kit	Qiagen (74104)
AllPrep RNA/Protein Mini Kit	Qiagen (80404)
High-Capacity cDNA Reverse Transcription Kit	AB (4368814)
Vybrant Multicolor Cell-Labeling Kit	Invitrogen (V22889)
Cell Proliferation Kit I (MTT)	Roche (11465007001)
CyQUANT Direct Cell Proliferation Assay Kit	Invitrogen (C35011)
Pierce™ Coomassie Plus (Bradford) Assay Kit	Thermo Sci (23236)
SuperSignal West Dura substrate	Thermo Sci (34075)
SuperSignal West Femto substrate	Thermo Sci (34094)

Proteome Profiler Human XL Cytokine Array Kit	R&D Sys (ARY022B)
TaqMan Array, Human Tumor Metastasis	AB (4418743)
TaqMan Array, Human Immune	AB (4418718)
pHrodo Red E. coli BioParticles Conjugate - Phagocytosis	Invitrogen (P35361)
pHrodo Green E. coli BioParticles Conjugate - Phagocytosis	Invitrogen (P35366)

2.1.9 Plastics and others

Name	Company (Cat#)
Countess chamber slides	Invitrogen (C10312)
Slide glasstic 10	Kova (U87144E)
ecoSHIELD Gloves PF 250	Shield Sci (625122)
Nunc™ cell culture treated flasks T80 cm ²	Thermo Sci (178905)
Nunc™ cell culture treated flasks T25 cm ²	Thermo Sci (136196)
Cell culture not-treated flasks T75 cm ²	Corning (431464)
Cell culture not-treated flasks T25 cm ²	Corning (431463)
Cryogenic tubes	Thermo Sci (363401)
50 ml tubes	Fisherbrand (431176)
15 ml tubes	Fisherbrand (430885)
1.5 ml tubes	Fisherbrand (FB74031)
0.5 ml tubes	Thermo Sci (AB0350)
0.2 ml PCR tubes	Fisherbrand (14230225)
Filtered 1250 µl tips	SLS (SLS5160)
Filtered 300 µl tips	SLS (SLS5156)
Filtered 20 µl tips	SLS (SLS5150)
Filtered 10 µl tips	SLS (SLS5148)
5 ml Stripette Serological pipets	Costar (4487)
10 ml Stripette Serological pipets	Costar (4488)
25 ml Stripette Serological pipets	Costar (4489)
Flat bottom 6-well treated plates	Costar (3516)
Flat bottom 12-well treated plates	Costar (3513)
Flat bottom 24-well treated plates	Costar (3524)
Flat bottom 48-well treated plates	Costar (3548)

Flat bottom 96-well treated plates	Costar (3596)
Round Bottom Ultra Low Attachment 96-well plates	Costar (7007)
Transwell with 0.4 µm Pore Polyester Membrane Insert	Corning (3459)
HTS Transwell®-96 with 8.0 µm Pore Polyester Membrane	Corning (3374)
HTS Transwell®-96 Receiver Plate	Corning (3583)
17 mm petri dish	Thermo Sci (150350)
Round-bottom polystyrene test tubes	Falcon (352058)
Skim Milk Powder	Serva (42590)
96-Well Semi-Skirted PCR Plate for Roche Lightcycle	Starlab (1402-9909)
MicroAmp Fast Optical 96-Well Reaction Plate, 0.1 ml	Thermo Sci (4346907)
Clear Polypropylene Seal (PCR)	Starlab (E2796-0793)
Mini-PROTEAN TGX Gels	Bio Rad (4561046)
Precision Plus Protein Kaleidoscope Standards	Bio Rad (150350)
MagicMark™ XP Western Protein Standard	Invitrogen (LC5602)
NuPAGE Sample Reducing Agent	Invitrogen (NP0004)
NuPAGE™ LDS Sample Buffer	Invitrogen (NP008)
Gel Loading Tip 1-200µl	Fisherbrand (11937734)
PowerUp SYBR Green Master Mix	Applied Bio (A25918)
TaqMan™ Fast Advanced Master Mix	Applied Bio (4444556)
RNase Inhibitor	Applied Bio (N8080119)
Hyclone RNase/DNase/ Protease free water	GE (SH30538.03)
Ethidium Bromide Solution	Invitrogen (15585-011)
UltraPure TBE 10x buffer	Invitrogen (15581-044)
Agarose Genetic Analysis Grade	Fisher (BP1356)
ProLong Glass Antifade Mountant-5 x 2 mL	Invitrogen (P36980)

2.2 Cell culture maintenance

2.2.1 Standard culture and freezing

Three human GBM cell lines (U87MG, UP007 and UP029) and the human microglia cell line (CHME3) grow attached in a monolayer and were maintained in culture with GBM and CHME3 media described in section **2.1.2**, in a humidified atmosphere with 5% CO₂, at 37°C. The cells were passaged when they reached the 70-80% confluence. For passaging, the growth medium was removed, and cells were gently washed in PBS. In order to detach the cells, 1 ml of trypsin solution was added, and the flask was returned to the incubator for 3 to 5 minutes, then 5 ml of standard culture media was added in order to inactivate the trypsin activity. Cells were collected and centrifuged at 1200 RPM, for 5 minutes. The supernatant was discarded, and cellular pellet was re-suspended in fresh media. Cell density was first measured using a discarded haemocytometer (KOVA) or with Countess II FL Automated Cell Counter (Life Technologies). Around 4,000 cells/cm² were added to 10 ml of pre-warmed growth media in a fresh 75 cm² treated culture flask, and then returned to the incubator.

THP1 cells grow in suspension and were maintained in culture in not-treated flasks with THP1 media described in section **2.1.2**, at the same cell culture conditions, a humidified atmosphere with 5% CO₂, at 37°C. THP1 was seeded at 400,000 cell/ml in non-treated flasks and maintained in culture until it reached the maximum of 2x10⁶ cell/ml. After collecting the cells, they were centrifuged, the supernatant was discarded, and the cell density was determined as the other cells.

For long-term storage, GBM and microglia cells were kept in freezing medium (FBS plus 10% DMSO) in liquid nitrogen. THP1's freezing medium was constituted with only 5% DMSO to prevent the monocytes differentiation into macrophages (high concentration of DMSO is able to induce the monocyte differentiation (Taetle et al. 1991)). Cells chosen for storage were passaged as few times as possible. Cells were detached, collected, and counted as described above. After the centrifugation, the pellet was re-suspended in freezing medium at the density of 1 x 10⁶ cells/ml. The cell suspension was then added to cryovials, 1 ml per vial, and stored into Mr. Frosty™ Freezing Container, at -80°C. After 24 hours, the cryovials with cells were transferred to a liquid nitrogen storage unit.

Since GBM cell lines were cultured in DMEM, THP1 cells were gradually cultured in DMEM for future co-cultures (CC). To avoid drastic alterations and to improve their adaptation, THP1 cells were cultured in 100% RPMI, then switched every two days to 75% RPMI:25%DMEM, 50% RPMI:50% DMEM, 25% RPMI:75% DMEM and finally to 100% DMEM. Monocytes cells were maintained in culture in DMEM one week to create new freezing stocks and for phenotype characterization.

THP1-derived macrophages

Macrophages were obtained after THP1 treatment with 150 nM of phorbol 12-myristate 13-acetate (PMA) for 72 hours, followed by a recovery period of 24 hours in culture in the absence of PMA. After PMA treatment, monocytes (that grow in suspension) differentiate into macrophages and become adherent resembling the phenotype and functional characteristics of primary human macrophages (Y. Y. Fu et al. 2012; Lund et al. 2016).

Astrocytes progenitors' cells and astrocytes differentiation

Astrocytes were used as a control of non-tumour cell for CC with microglia, invasion, and confrontation studies. 34D6 astrocyte progenitor cells (APC) were derived from iPSC 34D6 cell line, a healthy 40-year-old female, reprogrammed by retrovirus, a kind gift of Prof. Nick Allen, Cardiff University.

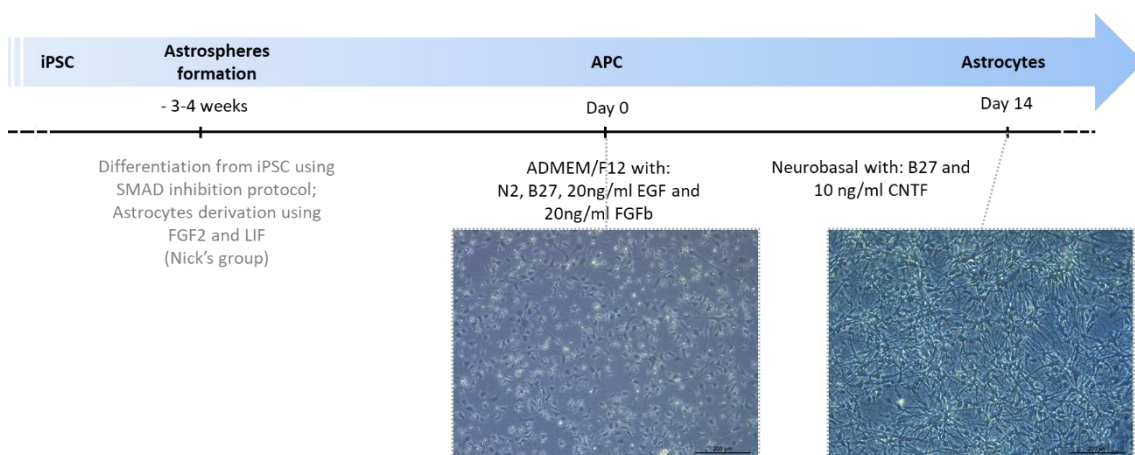


Figure 2.1 – Astrocytes differentiation from APC. The APC were previously produced by Nick Allen's group and maintained in culture in EF20 medium, supplemented with EGF, FGfb, N2 and B27. The astrocytes were differentiated from APC in neurobasal medium supplemented with CNTF and B27 for 14 days. Scale bar: 200 μM.

The monolayer APC cultures were propagated in EF20 medium (see section 2.1.2), in Matrigel-coated flasks (1:80) and passaged when confluent by using Stem Pro Accutase

(Sigma) (split ratio 1:2–1:3). Astrocyte populations were obtained by differentiating 8×10^6 APCs for 14 days with CNTF medium (*see section 2.1.2*) in Matrigel-coated tissue culture flasks (Serio et al. 2013; Bilican et al. 2012; Krencik and Zhang 2011). The mediums were renewed every 2-3 days.

iPSC-derived microglia

Prof Nick Allen, from Cardiff University, generously gifted the induced pluripotent cell (iPSC) cell line KOLF2 (HPSI0114i-kolf_2) that was used to generate the human microglia. KOLF2 was established from a healthy white British male, age between 55-59, where a fibroblast was reprogrammed using CytoTune™ 1-iPS Reprogramming Kit which contains four SeV-based reprogramming vectors or Yamanaka factors (i.e., Oct4, Sox2, Klf4, and c-Myc). The wild type (WT), as well as, mCherry tag inserted into the safe harbour AAVS1 locus, KOLF2-AAVS1-mCherry (generated by Prof. Nick Allen group) were used in this project.

iPSC cell maintenance

iPSC cells were cultured in feeder-free conditions and maintained in Essential E8 Flex medium (Gibco) on vitronectin (Gibco) coated plates ($0.5 \mu\text{g}/\text{cm}^2$). The medium was renewed every other day. To passage the cells, iPSC colonies were washed with PBS and incubated with ReleSR (StemCell) at 37°C for 2 minutes. ReleSR was aspirated, the colonies with stem cell characteristics were detached with KO-DMEM medium (Gibco) and centrifugated at 1,000 RPM for 3 minutes at RT. The supernatant was aspirated, the remaining pellet was resuspended in Essential E8 Flex medium and iPSC colonies were plated on to vitronectin-coated plates in a ratio of 1:4 to 1:6. To freeze down iPSC, the colonies were resuspended in STEM-CELLBANKER (amsbio) medium and stored into Mr. Frosty™ Freezing Container, at -80°C . After 24 hours, the cryovials with cells were transferred to liquid nitrogen storage unit.

Microglia-progenitor cells differentiation

Microglia-progenitor cells were obtained by embryonic bodies (EB) formation, followed by factory differentiation. iPSC colonies were previously treated with $10 \mu\text{M}$ of Y-27632 dihydrochloride a selective Rho kinase inhibitor (Ri – abcam) for 1 hour. After the Ri treatment to improve the cell survival as a single cell, the colonies were washed with

PBS and detached with StemPro Accutase Cell Dissociation Reagent (Gibco) for 5 minutes at 37 °C, KO-DMEM medium was used to stop the reaction and the iPSC centrifuged at 1,000 RPM for 3 minutes at RT. The supernatant was aspirated, and the remaining pellet was resuspended in 500 µl of KO-DMEM. Cell density was calculated using Countess II FL Automated Cell Counter. In order to form 20 EB, around 360,000 cells were resuspended in 400 µl of 4 mg/ml of Poly(Vinyl Alcohol) (PVA – Sigma) dissolved in Essential E8 flex medium, previously filtrated, with 10 µM of Ri, and seeded as 20 µl drop on a petri dish where the EBs were left to form for 24 hours by hanging drop technique, in a humidified atmosphere with 5% CO₂, at 37°C.

The next day, EBs were carefully transferred to a 1.5 ml tube and allowed to settle by gravity. The supernatant medium was removed and replaced with mTeSR™1 medium (StemCell) supplemented with 50 ng/ml BMP-4 (Miltenyi Biotec), 50 ng/ml VEGF (Peprotech) and 20 ng/ml SCF (Miltenyi Biotec). EBs were cultured for 7 days, with a 50% media change every 2 days.

Factory Differentiation

7 days post EB formation, the EBs were plated in a T25 Matrigel-coated flask (1:80) with 5 ml of XVIVO-15 medium (Lonza), with 2 mM Glutamax, 100 U/ml penicillin and 100 µg/ml streptomycin, 0.055 mM 2-ME, supplemented with 25 ng/ml of IL-3 (Biolegend) and 100 ng/ml M-CSF (Biolegend). Around 60% of the medium was renewed every 5th day, being careful not to disturb the progenitors.

Non-adherent microglia progenitors began to appear from 2 weeks onwards. During media renewals, around 60% of the media was collected and centrifuged at 1,000 RPM for 3 minutes at RT. The supernatant was aspirated, and the progenitors were re-suspended in 1 ml of medium. 10 ul of cell suspension was mixed with 10 ul of trypan blue exclusion dye to carry out a cell count using Countess II FL Automated Cell Counter. Cells were periodically tested for their surface antigens by flow cytometry, to ensure the correct lineage CD45⁺/CD11b⁺/CD34⁻.

Microglia differentiation

When the non-adherent cells were confirmed to express markers for the microglia lineage, they were harvested as mentioned above and counted. The microglia

progenitors' cells were plated at 200,000 cell/well of a 6-well vitronectin-coated plate in X-VIVO Microglia Differentiation Media (XVIVO-15 medium, with 2 mM Glutamax, 100 U/ml penicillin and 100 µg/ml streptomycin, 0.055 mM 2-ME, supplemented with 100 ng/ml of IL-34 and 10 ng/ml GM-CSF). The microglia was differentiated for 14 days and the medium was renewed every 3 days.

Microglia resting stage

Once microglia was differentiated with X-VIVO Microglia Differentiation Media, which contains GM-CSF (pro-inflammatory cytokine), the differentiated cells were allowed to rest for an additional 5 days in Microglia Resting Media (*see section 2.1.2*), in a humidified atmosphere with 5% CO₂, at 37°C.

2.3 Microglia progenitor's characterization by FACs

Non-adherent microglia progenitors were collected after 14 days of differentiation and centrifuged at 1,500 RPM for 5 minutes. The supernatant was discarded, the pellet was washed in 0.1% BSA/PBS and split into 3 FACs tubes for another cycle of centrifugation using the same parameters. Pelleted cells were resuspended in 200 µl of 0.1% BSA/PBS and 2.5 µl of CD45 Monoclonal Antibody (2D1), FITC, CD34 Monoclonal Antibody (4H11), PE-Cyanine7, and CD11b Monoclonal Antibody (ICRF44), APC, (all from eBioscience) were added. In another tube was added 2.5 µl of each isotype control, FITC Mouse IgG1, κ Isotype Ctrl (FC) Antibody [Clone: MOPC-21], APC Mouse IgG1, κ Isotype Ctrl (FC) Antibody [Clone: MOPC-21], PE/Cy7 Mouse IgG1, κ Isotype Ctrl Antibody [Clone: MOPC-21] (all from Biolegend). Unlabelled samples were used as a negative control. The antibodies were incubated at RT in the dark for 1 hour. After incubation cells were washed 3 times in 0.1% BSA/PBS and resuspended in 200 µl of the same buffer. The samples were then run using a BD Bioscience FACS Verse machine and analysed using FlowJo (version v10.5).

2.4 Immunofluorescence Staining

CHME3 and differentiated iPSC-derived microglia was fixed with 4% paraformaldehyde (PFA) for 10 minutes at RT. Fixed cells were washed 3 times with PBS for 5 minutes at RT. In order to permeabilize the cells, the samples were incubated with 0.3% Triton-X (Promega) in PBS for 10 minutes at RT. Permeabilized cells were washed 3 times with PBS for 5 minutes at RT and then blocked with 1% BSA (Sigma) in PBS plus 0.1% Tween 20 (Fisher Scientific), for an additional 60 minutes at RT. After blocking, cells were incubated with an adequate primary antibody, TMEM119 (abcam), IBA1 (abcam), Cav1 (Cell Signalling) (1:100 or 1:500 dilution in blocking buffer) overnight at 4°C. After that, primary antibodies were washed 3 times with PBS for 5 minutes at RT. The respective secondary antibody was diluted (1:400) in blocking buffer and incubated protected from the light, at RT for 1 hour. The secondary antibody was decanted and washed 3 times with PBS for 5 minutes at RT, protected from the light. The counter staining was performed with DAPI (0.5 µg/ml) for 5 minutes, followed by an additional 3 washes with PBS for 5 minutes. The coverslips were mounted with ProLong Gold (Life Technologies) mounting medium. The mounted samples were allowed to cure for 24 hours on a flat and dry surface, at RT and protected from the light. On the following day, the samples were imaged using the Confocal Leica TCS SP5 microscope and images were created using ImageJ.

2.5 Microglia and Macrophages polarization

Microglia (CHME3 and iPSC-derived microglia) and macrophages (THP1-derived macrophages) were activated towards a classical pro-inflammatory phenotype or alternative anti-inflammatory phenotype, following the protocols in **Figure 2.2** and **Figure 2.3**. Cells in standard conditions culture (inactivated) were used as control.

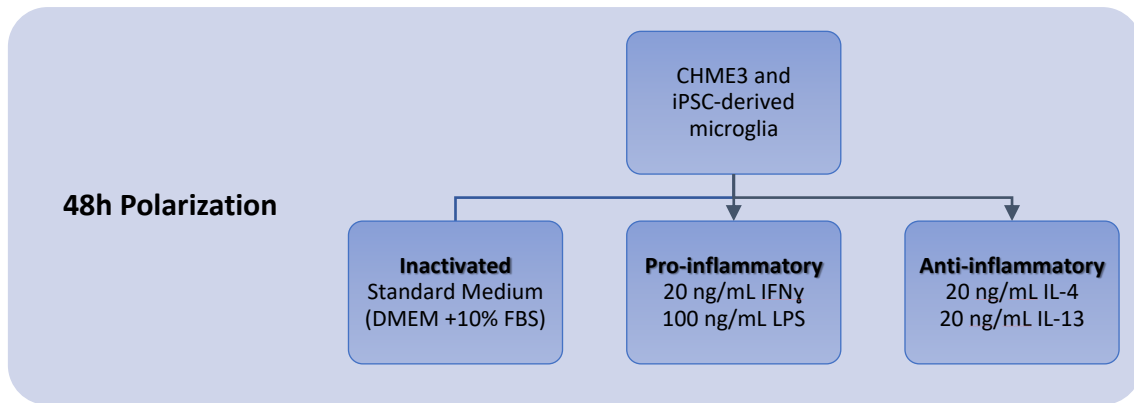


Figure 2.2 – CHME3 and iPSC-derived microglia polarization protocol.

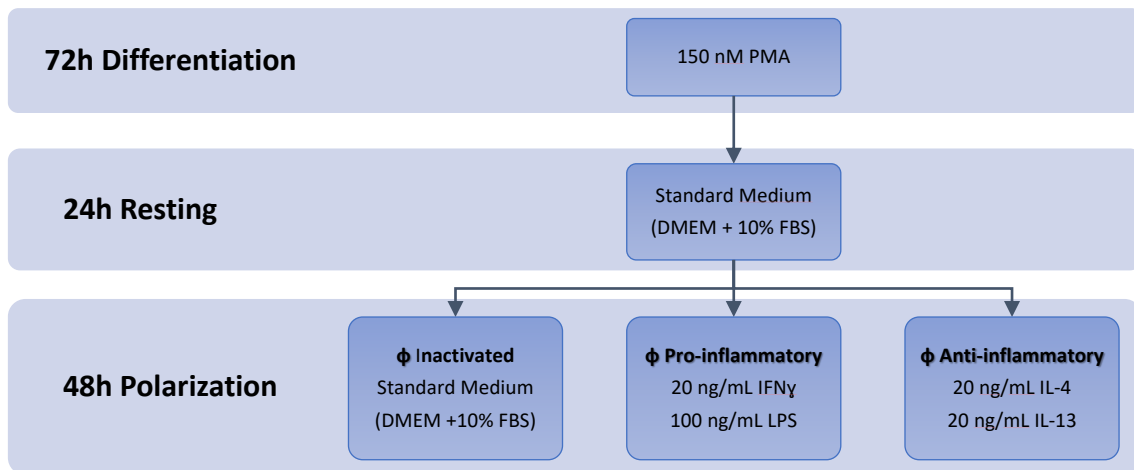


Figure 2.3 – THP1 differentiation and macrophages polarization protocol.

Macrophages were previously differentiated from monocytes THP1 cells for 72 hours, following the protocol described in 2.2.1 - *THP1-derived macrophages*, and let to rest for 24 hours. iPSC-derived microglia was differentiated from KOFL2 cells for 40 days following the protocol described in 2.2.1 – *iPSC-derived microglia*. CHME3, iPSC-derived microglia and THP1-derived macrophages were polarized towards a pro-inflammatory phenotype with 20 ng/ml of IFN- γ plus 100 ng/ml of LPS, or an anti-inflammatory phenotype with 20 ng/ml of IL-4 and IL-13, for 48 hours. Inactivated cells were cultured in standard culture conditions for the same period and were used as a control.

2.6 Co-culture System of GBM cell lines with CHME3

The co-culture (CC) of U87, UP007, UP029 or 34D6 cells with microglia CHME3 cells or iPSC-derived microglia was performed using a 6-well Transwell system (Corning). 34D6 astrocytes were used as a control of non-tumour cells. The system is composed by inserts with microporous membranes of 0.4 μm pore size that allow the exchange of soluble factors released by the cells located in the upper and lower compartment.

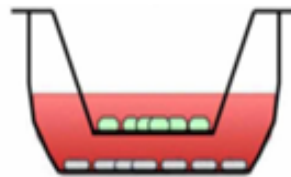


Figure 2.4 - Transwell® system.

Microglial cells (CHME3) were plated in the lower compartment at a density of 10,500 cells/cm². iPSC-derived microglia was differentiated into 6-well plates previously to the CC, following the same conditions described in section 2.2.1 – Microglia differentiation. GBM or astrocytes cells were seeded at the bottom of the insert at 10,500 cells/cm² (1:1 proportion) in separate wells, not containing microglial cells on the lower compartment. After 24 hours of equilibration, the culture medium in both compartments was refreshed and the inserts containing GBM cells were transferred to the plates with microglial cells. The co-culture system was maintained in a 5% CO₂ incubator at 37°C for an additional 48 hours.

2.7 qRT-PCR

Gene expression of pro-inflammatory (IL-6, IL-1 β , TNF, IL-12p40 and CXCL12) and anti-inflammatory (IL-10, TGF- β , CCL22, CD200R, CD206 and CD163) related markers, as well as Cav1 were analysed by real-time quantitative reverse transcription-polymerase chain reaction (qRT-PCR).

RNA isolation

Total RNA was isolated using a TRIzol reagent (Sigma). Cells with 60-70% of confluent were pelleted and then lysed with 1 mL of TRIzol. The samples were incubated at RT for

5 minutes and then 200 µl chloroform was added and mixed vigorously for 15 seconds. The cells were then centrifuged at 13,000 RPM at 4°C for 10 minutes. The upper aqueous phase was transferred to a clean tube containing 500 µL of isopropanol. After centrifugation, the pelleted RNA was washed with 500 µl of 75% ethanol and centrifuged once again at 13,000 RPM at 4°C for 5 minutes. The supernatant was discarded, and the pellet was dissolved in 40-60 µL of pure water.

RNA from iPSC-derived microglia and from GBM cell lines was isolated using AllPrep DNA/RNA/Protein Mini Kit (Qiagen) and RNeasy mini Kit (Qiagen), respectively, following the instructions on the respective kits. The RNA was eluted in 30 µL of DNA/RNA free water.

The quantification and integrity of the extracted mRNA was performed by spectrophotometry, by measuring the absorbance at 260 and 280 nm wavelengths in NanoDrop One Spectrophotometer (Thermo Fisher).

Synthesis of complementary DNA (cDNA)

The first strand of complementary DNA (cDNA) was synthesized using 1 µg of RNA by reverse transcription using the High-Capacity cDNA Reverse Transcription Kit (ABI Applied Biosystems) according to the manufacturer's instructions, in a reaction volume of 20 µL. Obtained cDNA samples were stored at -20°C.

qRT-PCR

All primers designed for reference and target genes were based on sequences published on National Centre for Biotechnology Information (NCBI). BLAST® searches were performed to confirm the total gene specificity of the primer sequences. Primer sequences are listed in **Table 2.1** and were purchased from Invitrogen.

Table 2.1 – Primers for qRT-PCR. Size: bp

Gene	Forward	Reverse	Size
Pro-inflammatory			
IL-6	CTCAATATTAGAGTCTCAACC CCCA	GAAGGCGCTTGTGGAGAAGG	146
IL-1β	CTCTTCGAGGCACAAGGCAC A	ATTTCACTGGCGAGCTCAGGT	112
TNF	CAGGTCCTCTTCAAGGGCCA A	GGGGCTCTTGATGGCAGAGA	120
IL-12 p40	CAAGACCTCAGCCACGGTCA	GCACAGATGCCCATTCGCTC	101
CXCL10	GAACCTCCAGTCTCAGCACC A	TGCTGATGCAGGTACAGCGT	123
Anti-inflammatory			
IL-10	AAGGCGCATGTGAACTCCCT	CCACGGCCTTGCTCTTGTTTT	103
TGF-β	CAGCATCTGCAAAGCTCCCG	CGAGGTCCTTGCGGAAGTCA	145
CCL22	GAGATCTGTGCCGATCCAG	AGGGAATGCAGAGAGTTGGC	178
CD200R1	GGTGCTGCTCAACCAAACAA	AGCCATCTTTACAGGCCATGA	156
CD206/ MRC1	ACACTCGGTCATCTAGTACCT CA	AAGGACAGACCAGTACAATTCAG TA	135
CD163	GAGACAGCGGCTTGCAGTT	ATCAGCTGACTCATGGGAATTTTC T	136
Agr1	GGGTTGACTGACTGGAGAGC	CGTGGCTGTCCCTTTGAGAA	111
Macrophages differentiation			
CD14	ACACAGAACCCTAGATGCC	CCTCTGTGAACCCTGATCACC	141
CD68	CCTAGCTGGACTTTGGGTGA G	GAAGGATGGCAGCAAAGTAGC	140
Others			
Cav1	GAGCAGAACAACCTTTGGC G	CGTGGCTGGATGAAAAGTGTG	159
HKG			
GAPDH	CGCTGAGTACGTCGTGGAGT	GGGGGCAGAGATGATGACCC	100
HPRT1	AGCCCTGGCGTCGTGATTAG	TCGAGCAAGACGTTTCAGTCCT	141

The qRT-PCR was performed in duplicate using PowerUP™ SYBR™ Green master mix (Applied Biosystems), using a LightCycler 96 system (Roche) or QuantStudio 5 (ThermoFisher), in a final volume of 12 μ L, containing 0.5 μ L of cDNA, according to the following protocol: initial incubation at 50°C for 2 minutes plus 95°C for 2 minutes, followed by 45 cycles of 15 seconds at 95°C, 15 seconds at 60°C and 60 seconds at 72°C, followed by a melting curve increasing from 55°C to 95°C.

One gene with stable expression in both cell lines (GAPDH) was selected as housekeeping gene (HKG) for a reliable normalization of qRT-PCR experiments. Water and non-transcript template (mRNA) were used as a negative control. Target gene

expression levels were normalized to the HKG using the Δ Ct method. After qRT-PCR, the PCR products were analysed in a 2% agarose gel, by electrophoresis.

2.8 Western Blot

Total protein and the phosphorylated protein levels of pro-inflammatory (STAT1 and NF- κ B p65) and anti-inflammatory (STAT6 and STAT3) related pathways, as well as the total form of Cav1, were analysed by Western Blot (WB), following the cell lysis and protein quantification protocol.

Cell lysis and protein quantification

The cells were harvested and centrifuged, the pellet was transferred to the centrifuge tubes and lysed in RIPA buffer (RIPA, Radioimmunoprecipitation assay, Thermo Scientific) with 1% of protease inhibitors cocktail (Thermo Scientific) and 1% 0.5M EDTA (Thermo Scientific). The samples were kept on ice for 30 minutes, and vortexed every 5 minutes. The lysed cells were then centrifuged at 13,000 RPM at 4°C for 7 minutes, and the supernatant collected and stored at -20°C until required.

The total protein in the cell lysates was quantified using Coomassie Plus Reagent (Thermo Scientific) following the manufacturer's protocol. All samples were measured at 595 nm using a LT5000MS ELISA reader. Protein concentrations were calculated using diluted albumin standards.

Gel Electrophoresis

Gel electrophoresis was performed with 12% Mini-PROTEAN® TGX™ Precast Protein Gels (BIORAD). 20 to 50 μ g of protein was pre-mixed with LDS Sample Buffer (4x, Life Technologies) plus Sample Reducing Agent (10x, Life Technologies), warmed at 95°C for 5 minutes. Gel was placed in the apparatus submerged in running buffer (0.025M Tris base, 0.192 M Glycine, pH 8.3) and samples were loaded, as well as the marker. Electrophoresis was performed at 80V for 15 minutes and then at 150V for 2 hours or until a good separation between bands.

Blotting

The blotting was done using a wet blotting approach (BioRad Blotting system). The filters and nitrocellulose membrane were submerged in blotting buffer (0.025 M Tris base, 0.192 M Glycine, 20% Methanol) and positioned into the chamber in contact with the gel. The blotting was performed at 100 V for 60 minutes, with an ice pack in the cassette to prevent overheating.

Immunodetection

The nitrocellulose membrane was removed and washed in a washing buffer (pH 7.5, NaCl 100 mM, Tris 100 mM, 0.1% Tween 20), and the proteins were stained with 0.1% (w/v) Ponceau S (Sigma) in 5% acetic acid to confirm the consistent transfer of protein across the membrane. Membranes were washed 3 times for 10 minutes in a washing buffer and then blocked in blocking buffer (5% milk in wash buffer), on a rocking platform for 1 hour at RT. The membrane was then washed 3 times for 10 minutes in a washing buffer and incubated with primary antibody Cav1 (Cell Signalling), at a dilution of 1:1000, under roller, overnight, at 4°C. After incubation with primary antibody, the membrane was washed 3 times for 10 minutes at RT, and then incubated with the HRP-linked anti-rabbit IgG secondary antibody (Cell Signalling), at a dilution of 1:10000 in blocking buffer, for 1 hour, at RT. After this step, the membrane was washed 3 times for 10 minutes each and the signal detected using SuperSignal™ West Dura Extended Duration Substrate (Life Technologies) on a ChemiDoc XRS+ (BIORAD, Hertfordshire, UK). GAPDH (Cell Signalling) has been used as housekeeping to normalize the protein expression. The density of the bands was measured using ImageJ.

2.9 Phagocytosis assay

Microglial phagocytic ability was evaluated using pHrodo™ Red or Green *E. coli* BioParticles™ Conjugate (life technologies). This kit measures the cellular phagocytic activity relying on acidification of the particles as they are ingested. At pH 7.4 the particles that are not fluorescent start to increase the fluorescence level with the pH decreasing. During the phagocytosis, the vesicles are processed in the phagosome, where the pH decrease until 4, as demonstrated in **Figure 2.5**.

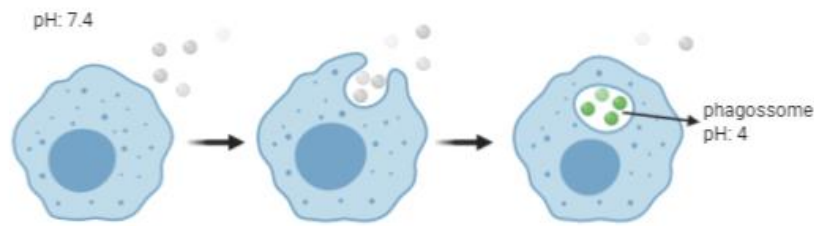


Figure 2.5 – pHrodo phagocytosis Assay. *E. Coli* bioparticles labelled with pHrodo™ dye are added to cells. The phagocyte bioparticles are then processed, and the pH decreases to 4 and the pHrodo -labelled bioparticles fluoresce brightly.

CHME3 and iPSC-derived microglial Cav1 NT and Cav1 KO were plated into a 96-well plate at 10,000 cells/well. Cells were stimulated towards a pro-inflammatory or anti-inflammatory phenotype. Untreated cells were used as a control. The phagocytosis was assessed according to the manufacturer's instructions. Briefly, pHrodo bioparticles were resuspended in live imaging solution at 0.5 mg/ml and sonicated for 5 minutes. After stimulation, media was exchanged by 90 μ l of live imaging solution and 10 μ l of the resuspended bioparticles and incubating from 4 to 20 hours at 37°C. Cells without bioparticles and bioparticles treated with a pH 4 solution were used and a negative and positive control, respectively. Images every 15 minutes were taken using the IncuCyte® S3 Live Cell Analysis System (Essenbioscience).

2.10 Cytokine array

The cytokine profile of CHME3 and iPSC-derived microglia Cav1 NT and Cav1 KO cells were performed with a Human XL Cytokine Array kit (R&D Systems). CHME3 and iPSC-derived microglia Cav1 NT and KO were seeded into a 6-well plate and polarized towards pro-inflammatory or anti-inflammatory status for 48 hours, using the protocol described in section 2.5. Microglia cells were co-cultured with different GBM cell lines using a transwell system (described in section 2.6). Non-treated cells and cells cultured without interference of cytokines or GBM were used as a control. After 48 hours of incubation, for each condition the supernatant was collected, centrifugated at 1,500 RPM for 5 minutes and incubated with the respective membrane, following the manufacturer's

instructions. Final membrane images were taken with ChemiDoc XRS+ with the same exposure time. The analysis was performed using ImageJ. The Human XL Cytokine Array Coordinates are described in **Appendix IV – Human XL Cytokine Array Coordinates**.

2.11 Transwell migration and invasion assay

The single-cell migration and invasion assay was carried out using HTS 96 transwell permeable supports with 8 µm pores (Corning). For the invasion assay, transwells were previously coated with 21 µl of Matrigel at a concentration of 0.4 mg/ml. After CC, the cells were plated in the transwell (upper chamber) with a concentration of 600,000 cells/ml, in FBS free medium. DMEM with 20% FBS was added in the lower chamber as chemoattractant. The transwell system was incubated at 37°C and 5% CO₂ for 16 hours. At least one well per experiment was used as a blank (no cells) and other as an internal control without FBS on the bottom. After this period, calcein-AM (5 µM; Sigma) was diluted in a cell dissociation buffer (Gibco) and added to the lower chamber to stain and detach the migrated or invaded cells, at 37°C for 1 hour. Samples were transferred into HTS Transwell-96 Receiver Plate Black (Corning) and fluorescence was measured in a fluorescence microplate reader (SynergyTM HT, Biotek Instruments) with an excitation wavelength of 485 nm and an emission wavelength of 528 nm and expressed as relative fluorescence units (RFU).

A standard curve with known cell numbers was performed for each cell line to convert the RFU to cell number. The total number of cells that passed through the membrane of each well was expressed as percentage of the initial number of cells seeded.

2.12 Cellular co-cultures – VybrantTM dyes

During the invasion assay with a mix population of cells, cell-label dyes were used to distinguish different cell types. The lipophilic carbocyanines DiI, DiO and DiD (VybrantTM multicolour cell-labelling kit – Molecular Probes) are weakly fluorescent in water but highly fluorescent and photostable when incorporated into membranes. The dyes diffuse laterally within plasma membranes, resulting in staining of the entire cell. They

are low cytotoxic dyes, which are retained in living cells through several generations, transferred to daughter cells, but not adjacent cells.

Following the manufacturer's instructions, 1,000,000 cells were incubated with 5 µl/ml of DIO or DID dye cell solution for 15 minutes, protected from light, at 37°C in a 5% CO₂-humidified atmosphere, followed by three PBS washing steps. The optimization of labelling process is described in the **Appendix V**. After the labelling procedure, cells were seeded using a 6-well plate, and incubated overnight to prevent cross-contamination with dye from one cell line to the other, that could be attached outside the cellular membrane. After that, cells were collected and used for sphere formations to the invasion assay.

2.13 Spheroid invasion assay

For the invasion assay and previous to the sphere formation (**Figure 2.6**), GBM, CHME3 and astrocytes cells were pre-labelled with DiL, DiO or DID dyes (*described in 2.12*). The labelled cells were mixed in a 1:1 ratio, GBM:Microglia or GBM:Astrocytes and seeded in a 96-well plate, round-bottomed with ultra-low adherence conditions (ULA) (COSTAR), at a concentration of 1,000 cells/well for the U87 and 5,000 cells/well for the UP007 and UP029. For the co-culture, half the number of cells were seed in order to keep the same total number of cells and sphere size. After seeding, cells were gently centrifuged (300 g, for 1 min) and incubated for four days, at 37°C with 5% of CO₂. After the sphere formation, at day 0 of invasion, around half of the medium was replaced with Matrigel™ to make 4 mg/ml in a total of 200 µl (growth factors reduced, Corning). After the matrix was added, the plate was kept on ice for an additional 30 minutes to allow for an homogeneous mixture of Matrigel™ with the reminiscent medium, and incubated again at 37°C with 5% of CO₂ to allow the polymerization of the matrix around the spheres. After two hours, 100 µl of medium was added to the wells and pictures were taken immediately after and every 24 hours for the following 3 days. For the mix cultures, the pre-labelled GBM, and the microglial cells with different dyes, additional pictures were taken in an epifluorescence or Evos M7000 microscope.

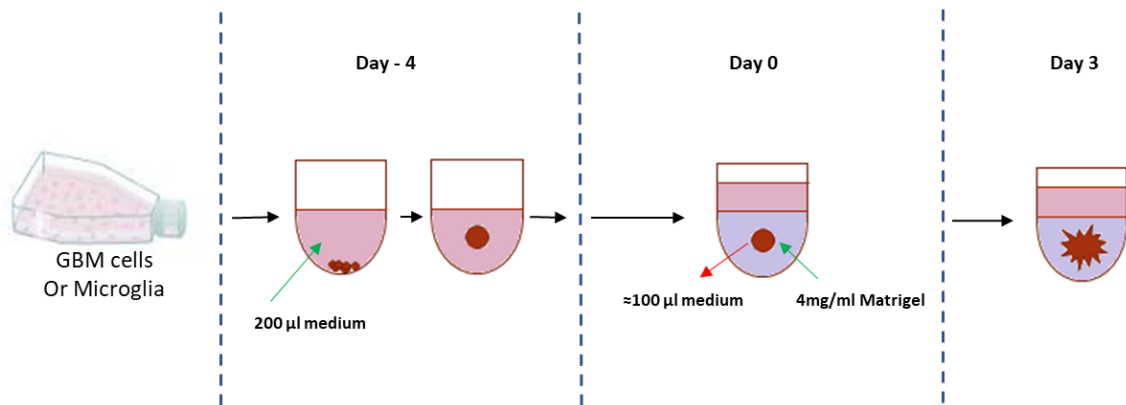


Figure 2.6 – Invasion assay diagram. Tested cells were seeded into a 96-well plates, ULA and round bottom, and left to adhere for 4 days in standard culture media and culture conditions. After the sphere formation, half of the media was removed and Matrigel was added to produce a final concentration of 4 mg/ml, returned to the incubator, and left to invade for an additional 3 days.

The spheroid analysis was performed using INSIDIA macro run into ImageJ (Moriconi et al. 2017).

2.14 Statistics

Statistical analysis was performed using GraphPad Prism 6.0 software. Data was presented as the mean \pm standard error of the mean (SEM) of the indicated number of independent experiments (n).

The normality of data was tested using the Shapiro-Wilk test. Kruskal-Wallis (non-parametric) with Dunn's correction or ANOVA (parametric) test with Tukey correction was performed for multiple comparisons. A p-value < 0.05 was set as statistically significant.

**CHAPTER 3 –
GENETIC KNOCKOUT OF CAVEOLIN-1**

3.1 Introduction

The Human Genome Project sequencing, carried on by Lander and colleagues in 2001 (Lander et al. 2001), offered new horizons to understand human biology and disease, including cancer. During more than 15 years of research, they have found thousands of genes with unknown functions. Based on their work, other researchers are trying to understand the function of each gene and how genes work together, in a balanced environment or during pathological conditions.

The most widely used approach for deciphering the gene function is to reduce or completely disrupt its normal expression and study the phenotypes that result from that. At first, RNA interference (RNAi) offered a technique to disrupt gene expression in many organisms. However, new biotechnological tools, specifically Clustered Regularly Interspaced Short Palindromic Repeats (CRISPR)-based technologies, have become available and dominant into mammalian cell studies.

3.1.1 RNAi

The RNAi method involves the introduction of small synthetic RNAs into the cells that are complementary to the desired mRNA, degrading the target sequence. The gene suppression by RNAi can be mediated through the introduction of chemically synthesized small interfering RNAs (siRNAs) or by vector based short-hairpin RNAs (shRNAs). While siRNA is directly delivered into the cytosol (based on lipotransfection, for example), shRNA is capable of integrating the DNA. The shRNA method uses plasmid systems with DNA vectors, providing selectable markers for stable shRNA expression, which can be used to create stable knockdown or knock-in cell lines who express the shRNA for several generations. On the other hand, silencing a gene with shRNA relies on the concentration of cytoplasmic siRNA. High concentration of siRNA can increase the off-target effects and transfection of high proliferative cells. However, when the siRNA concentration becomes diluted, so much so that the desired target gene knockdown is unachievable (Kumar and Clarke 2007; D. D. Rao et al. 2009).

After transfection with shRNA plasmids or shRNA lentiviral particles for transient or stable gene silencing, the transcription of the shRNAs is undertaken into the nucleus,

originating a pre-shRNAs (**Figure 3.1**). These initial precursors are processed by Drosha and DGCR8, resulting in the shRNA that will be exported to the cytoplasm by Exportin 5. The shRNA is then cleaved by Dicer, removing the hairpin, and creating a 20-25 nt double-stranded siRNA. This active siRNA is then loaded onto the RISC complex. The siRNA is recognized by RISC, which mediates cleavage of the target mRNA for gene silencing and downregulation of the target protein. In contrast, siRNA can be directly transfected into the cell, joining the RNAi pathway when it assembles with RISC in the cytoplasm (Boettcher and McManus 2015).

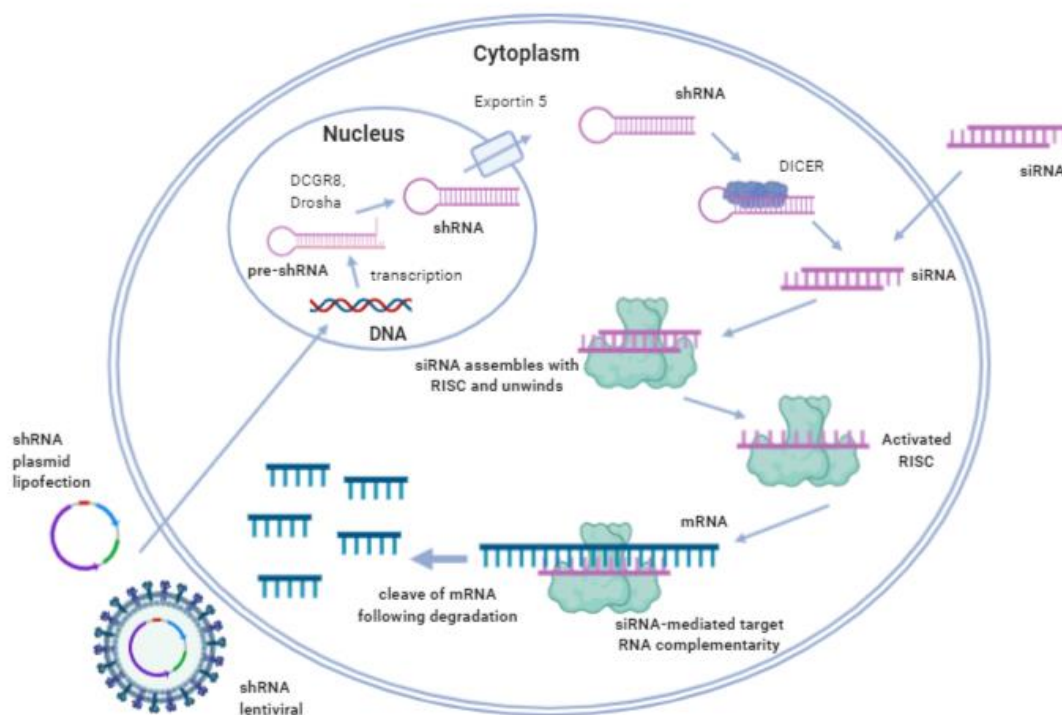


Figure 3.1 – siRNA and shRNA mechanisms for gene knockdown.

3.1.2 CRISPR-Cas9

The first available genetic complete loss-of-function or knockout (KO) approaches involved zinc-finger nucleases (ZFNs) followed by the transcription activator-like effector nucleases (TALENs). These techniques use customizable DNA-binding domains (DBDs) that are designed and engineered to recognize a specific target in DNA sequences. Associated with nucleases, DBDs are used to induce double-strand breaks (DSBs) and

consequent frameshift mutations into the genes, leading to a transcriptional repression or KO (Gaj et al. 2013). However, these technologies require new protein designs and validations for each experiment, restricting their wide adoption and requiring a long-term experiments (Barrangou and Doudna 2016).

Alternatively, over the last decade the CRIPSR approach using RNA-guided CRISPR-associated protein 9 (Cas9) has emerged as a method of choice to study individual gene function, perform genome-wide screens, create disease models, and/or evaluate experimental therapy strategies. Though, like the ZFNs and TALENs approach, to achieve a complete KO of the gene with CRISPR-Cas9, every functional copy of the target gene needs to be edited and disrupted.

The genome editing toolbox CRISPR-Cas9 is an efficient adaptive system that uses single guide RNA (gRNA) to guide the toolbox and cleave target regions of DNA (Cong and Zhang 2015). The Cas9 enzyme is a nuclease that when guided by small RNA through base pairing with a target DNA, generates a double-strand break (DSB) within the exact target region. The DSB is repaired either by non-homologous end joining (NHEJ) or homology-directed repair (HDR). The error-prone NHEJ pathway typically generates small insertions or deletions (indels) that are unpredictable, however, it frequently causes mutations in the targeted sequence that are usually inactivating mutations. The HDR pathway is useful for precise insertion of donor DNA into the targeted site (Ran et al. 2013). The use of donor DNA allows the creation of a precise type of mutation or gene correction is the objective.

Briefly, as described in **Figure 3.2 (1)**, the single guide RNA (sgRNA) is composed by a guide RNA (gRNA), also known by crispr RNA (crRNA), connected by an artificial tetraloop to the transactivate crRNA (tracrRNA) promoter site. The crRNA is a fragment with 19-20 base pairs (bp), designed specifically to generate site-specific DNA breaks. The tracrRNA is an essential component of the Cas9 target recognition and cleavage complex. The sgRNA can be synthetically generated, produced by *in vitro* transcription (IVT) or *in vivo* from a DNA template that is inserted into a vector for synthesis by the organism. The sgRNA can be synthetically generated by chemical processes or generated by IVT, requiring a DNA template that is transcribed using commercial kits. As for the plasmid approach (*in vivo*), the protospacer (complementary to crRNA) is cloned into a

plasmid vector which is then introduced into the bacterial or cell genome, transcribed and processed to produce the target crRNA. The IVT and plasmid techniques require additional purification steps before they can be used in CRISPR experiments.

The sgRNA hybridizes to form a complex with the Cas9 nuclease, which is guided to a target DNA sequence by the protospacer portion of the crRNA (**Figure 3.2 - 2-3**). Nevertheless the target DNA is only cleaved if the 20 bp target sequence is directly adjacent to a short protospacer adjacent motif (PAM), 5'-NGG, which is recognized by the Cas9 protein itself (Deltcheva et al. 2011; Ran et al. 2013). The generated DSB by the Cas9 protein can be repaired by NHEJ recombination, which may disrupt the gene function (**Figure 3.2 - 4**).

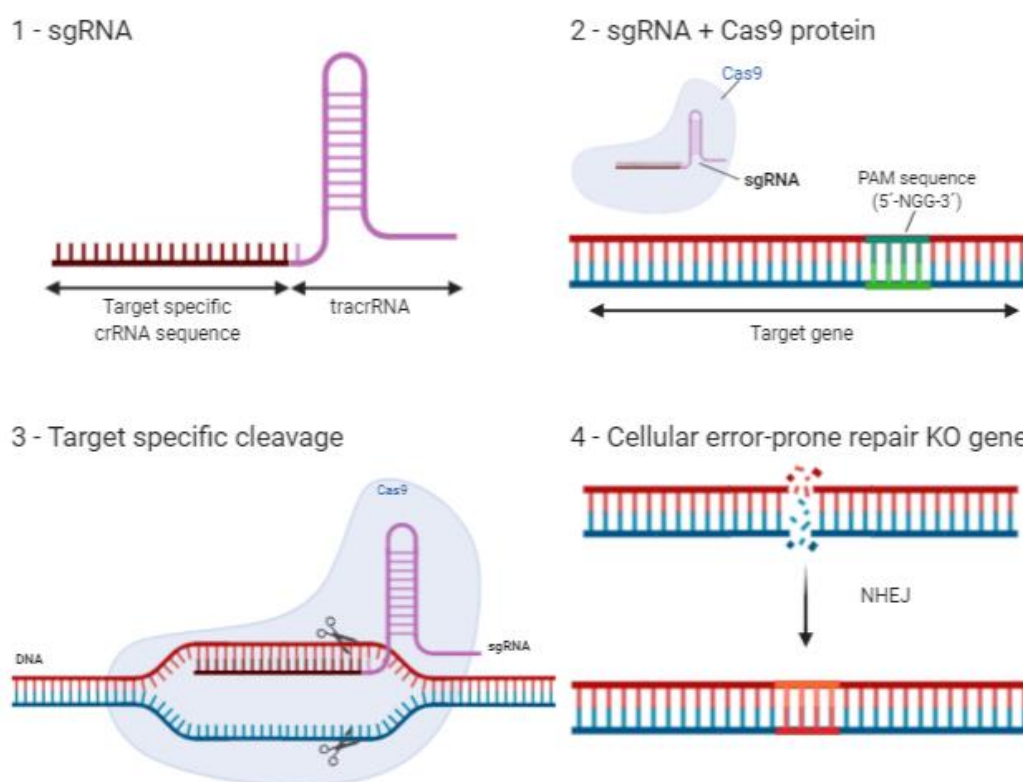


Figure 3.2 - The principle of CRISPR-Cas9. A single guide RNA (sgRNA), consisting of a crRNA sequence, that is specific to the DNA target, and a tracrRNA sequence, that interacts with the Cas9 protein (1), binds to a recombinant form of Cas9 protein that has DNA endonuclease activity (2). The resulting complex will produce target-specific double-stranded DNA cleavage (3). The cleavage site will be repaired by the non-homologous end joining (NHEJ), an error-prone process that may result in insertions and/or deletions and may disrupt gene function (4).

3.2 Aim

In order to understand the function of Cav1 in GBM and microglia cells the aim of this Chapter is to generate and characterize CRISPR-Cas9 Cav1 KO clones and the respective controls (CRISPR-Cas9 Cav1 NT) for all cell lines used in the project. First, the CRISPR-Cas9 system was designed using *in silico* tools. Followed by the electroporation of the targeted cell lines with the CRISPR-Cas9 system and clone isolation. the protein expression on the generated clones was evaluated by WB, the cellular proliferation was investigated by MTT and the generated indels analysed by PCR.

3.3 Methods

3.3.1 Cav1 knockout by CRISPR-Cas9

crRNA design

Two crRNA guides were designed using the online DESKGEN Library (<https://www.deskgen.com/landing/disrupt.html>) and confirmed using MIT programme (<http://crispr.mit.edu/>). Throughout the design it was taken into consideration that crRNA guides should target the genomic DNA in the codifying DNA regions (blue regions - **Figure 3.3** and **Figure 3.4**), localized in first exons of the target gene (Cav1), in order to have a successful gene disruption, and next to a PAM region, to allow the DNA cut by the Cas9 protein (Ran et al. 2013; Hough et al. 2016; F. Zhang, Wen, and Guo 2014). Moreover, the guides were chosen taking into consideration high predicted on-target (activity) and off-target scores. As seen in **Figure 3.3** and **Figure 3.4**, both guides presented a high off-target score, and should display low off-target effects, only predicted for non-coding regions and when two or more mismatches occur.



Figure 3.3 – crRNA guide 1 design. CDS – Coding DNA sequences.

μM , followed by heating the oligos to 95°C for 5 minutes and slowly cooling them down to room temperature on the bench top.

The ribonucleoprotein (RNP) complex was formed by dilution of $1.2\ \mu\text{L}$ crRNA:tracrRNA duplex ($100\ \mu\text{M}$) (two guides - $0.6\ \mu\text{L}$ of each) and $1.7\ \mu\text{L}$ of Cas9 protein ($61\ \mu\text{M}$) in $2.1\ \mu\text{L}$ of PBS, to reach the final volume of $5\ \mu\text{L}$, per reaction. As control, non-target (NT) complex, tracrRNA was complexed with Cas9 protein without crRNA guide. RNP complex was incubated at RT for 20 minutes.

The cells were trypsinized, collected and washed twice in PBS to remove the remaining trypsin, media and FBS, which may contain RNase activity and can quickly degrade the critical CRISPR RNA components. Per reaction, 100,000 to 200,000 cells were resuspended into $20\ \mu\text{L}$ of Nucleofection Solution SE (Lonza) or P3 Primary Cell Solution (Lonza - iPSC) together with $5\ \mu\text{L}$ of RNP complex and $1\ \mu\text{L}$ of Alt-R™ Cas9 Electroporation Enhancer ($100\ \mu\text{M}$, IDT). The cells were electroporated using a Nucleofection Module into the Amaxa 4D-Nucleofector X unit, using the respective protocol (**Table 3.2**). The electroporation protocols are cell-type dependent. Protocols for THP1, U87 and iPSC are available in the Lonza nucleofection library, however, the optimization (transfected efficiency and viability) was performed for CHME3 and UP029 with GFP, positive control provided with the kit (**APPENDIX II - CRISPR-Cas9 RNP approach optimization**). Since UP029 and U87 were sharing the same optimal conditions to perform the transfection, the same protocol was used to electroporate the UP007 cell line as well.

Table 3.2 – Nucleofection program and conditions.

Cell line	Program	Cell Number
CHME3	FF-100	200 000
THP1	FF-100	200 000
UP029	DS-126	100 000
UP007	DS-126	100 000
U87	DS-126	100 000
KOLF2 AAVS1-mCherry	DC-100	200 000

The electroporated cells were transferred into a 6-well plate with pre-warmed medium and incubated, using standard conditions (37°C, 5% CO₂), for 24 hours before FACS sorting.

Since RNP complex is composed by tracrRNA-ATTO 550, the successfully transfected cells can be selected by FACS sorting. ATTO 550 displayed an excitation of 554 nm and emission of 575 nm. The cells were collected and sorted 24 hours after the transfection, and the transfection efficiency was calculated by FACS. The positive ATTO 550 cells were sorted and allowed to recuperate in standard conditions for an additional 48 hours.

ATTO 550 iPSC-positive cells were seeded at low density (100 cell/dish) in a vitronectin-coated 60 mm petri dish in essential E8 flex medium with 10 µM of Ri. The Ri was removed when cell divisions were observed under the microscope. After a few days, colonies were formed, picked under a dissecting microscope, and plated for further expansion and analysis.

For the other cell lines, the positive transfected cells were then seeded at low density (30 cells/96-well plate) for clone isolation and expansion. The remaining cells were kept in culture in order to determine the editing efficiency and to create a frozen stock to re-seed in case of any viable KO was obtained from the first clone selection. 24 hours after the cells were seeded, the plates were inspected using a microscope to identify wells with a single cell. Wells with more than one cell were discarded. The medium was renewed twice a week. When a well reached the confluency, one third of the total cells were lysed and used to perform a dot blot. The remaining cells were kept in culture. The dot blot was performed in duplicate to check the Cav1 **(a.)** and GAPDH **(b.)** expression (**Figure 3.5**), as described by Estep *et al.* (Estep et al. 2016). Only clones with the Cav1 negative protein expression were expanded for further analysis by WB.

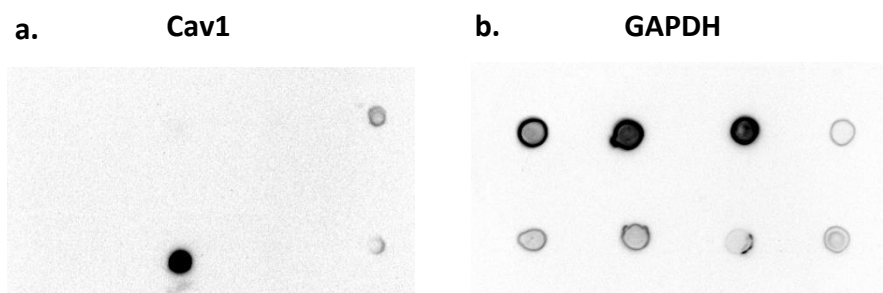


Figure 3.5 – Example of a dot blot.

3.3.2 Genomic Cleavage Detection – Editing Efficiency Analysis

The detection of locus specific cleavage was performed using the GeneArt® Genomic Cleavage Detection Kit (Life Technologies) following the manufacturer's instructions. Briefly, the first step involves cellular lysis and DNA extraction, subsequently a PCR amplification, followed by enzyme digestion.

The primers for PCR were designed according to the potential cleavage site (**Table 3.3**). The pair of primers for the region of guide 1 was designed to amplify the region where Cas9 will potentially cut the DNA guided by crRNA guide 1. After the amplification, it is expected a product size with 512 bp. Using an enzyme T7 Endonuclease I (T7EI), that recognizes mismatches from 1 bp, cutting the amplified DNA will produce two additional bands (190 bp plus 322 bp) corresponding to DNA from edited cells. The pair of primers for region 2 was designed following the same rules, amplifying the region where Cas9 will potentially cut the DNA guided by crRNA guide 2. In this case, it is expected a product with 539 bp, and after enzymatic digestion with T7EI, it is predicted other two additional bands (366 bp plus 173 bp). Guide 1 is localized 1,600 bp in distance from guide 2. Since, both guides were transfected simultaneously, there is the possibility that both sgRNA guides are cutting the DNA in the same cell, creating the opportunity to produce cells with deletion around 1,600 bp. For this specific case, a pair of primers was designed that will amplify the region before guide 1 until the region after guide 2. Since it is a large region (2,400 bp), it will only be efficiently amplified if the 1,600 bp deletion happens, creating a product size dependent on the piece of DNA that was cut.

Table 3.3 – PCR primers for PCR amplification to DNA cleavage study.

Potential cleavage site	Forward	Reverse	Product size
Region Guide1	GAGCAGAACAAACCTTTGGC	GGGAGCATCCTAGACCCATC	512 (190+322)
Region Guide 2	TGTCCTCTGCGAGATCCTCTTA	GCTCCACACATCAAACCC	539 (366+173)
Region 3	GTGGATTGTTTCTGCCGCC	GTCTGTTGCTGAGGTCAATA GGC	-

The DNA extraction was performed 72 hours after the nucleofection process, using GeneArt® Genomic Cleavage Detection Kit (Life Technologies), following the manufacturer's instructions. Briefly, for each cell line and condition (NT and KO), around 200,000 cells were collected and re-suspended in 25 µL of cell lysis buffer with 1 µL of protein degradation in a PCR tube, and incubated at 68°C for 15 minutes followed by an additional 10 minutes at 96°C, in a PTC-100 Programmable Thermal Controller thermocycler (MJ Research). Each region was amplified using AmpliTaq Gold®360 master mix in a final volume of 50 µL containing 2 µL of genomic DNA, according to the following protocol: initial incubation at 95°C for 10 minutes, followed by 42 cycles of 30 seconds at 95°C, 30 seconds at 55°C and 30 seconds at 72°C, finishing with a final extension at 72°C for 7 minutes.

After PCR amplification, PCR products were analysed in 2% agarose gel by electrophoresis to confirm the amplification. Subsequently, around 2 µL of PCR product was run in a re-annealing reaction, where PCR fragments were randomly annealed with and without indels to form heterogeneous DNA duplexes containing the deletion, following the protocol: initial incubation at 95°C for 5 minutes followed by a ramp from 95°C to 85°C, where the temperature decreases 2°C every second, and finishing with another ramp from 55°C to 25°C, where the temperature decreases 0.1°C every second. Later, the detection enzyme was added in order to cleave the DNA, incubating at 37°C

for 1 hour. The final product was analysed in 2% agarose gel, by electrophoresis and the efficiency of cleavage was calculated using the following equation:

$$\text{Cleavage Efficiency} = 1 - [(1 - \text{fraction cleaved})^{1/2}],$$

where, fraction cleaved = sum of cleaved band intensities/(sum of the cleaved and parental band intensities).

3.3.3 Cellular proliferation by MTT Assay

Growth curves were determined to ensure that the clones obtained display a similar proliferation behaviour compared to wild type (WT) cells. Cell proliferation was assessed by Cell Proliferation Kit I (Roche) that monitors the conversion of MTT to formazan by mitochondrial dehydrogenase enzymes. Briefly, WT cell lines and generated clones, NT and KO, were seeded at seeding densities of 1×10^5 cell/ml, into 96-well plates (100 μ l/well) and allowed to adhere for 24 hours. The cell viability was assessed daily for 10 days by adding 10 μ l of MTT, followed by a 4 hours of incubation period at 37°C with 5% of CO₂. After the formation of the purple formazan crystals, they were dissolved using 100 μ l of solubilization solution and incubated at 37°C with 5% of CO₂ overnight. The absorbance at 550 nm and 690 nm was measured with a plate reader (BMG LABTECH Ltd). The growth curve was constructed by plotting absorbance ($A_{550 \text{ nm}} - A_{690 \text{ nm}}$).

3.3.4 Screening CRISPR-Cas9 clones for predicted deletions

For each successful generated clone, deletion by sgRNA 1 and sgRNA 2, or combination of both, was screened by PCR. Four pairs of primers were designed in order to cover the three different events that were likely to occur (**Figure 3.6** and **Table 3.4**).

The sets of primers for region 1 and 2 were designed to cover each region, respectively, and the forward or reverse primer is complementary to the predicted cut size. If any indel mutation is present in these regions, the set of primer will not amplify efficiently the region. It should be taken into consideration that small indels (around 1 bp) can be amplified.

The pair of primers internal to the sequence to be deleted (non-deletion band (ND)- red arrows) and another pair of primers upstream and downstream of the sgRNA cleavage sites (deletion band (D) - blue arrows) were designed. In the absence of deletion, the

“deletion band” is too large to be efficiently amplified and the nondeletion band is amplified (Bauer, Canver, and Orkin 2015; Canver et al. 2014).

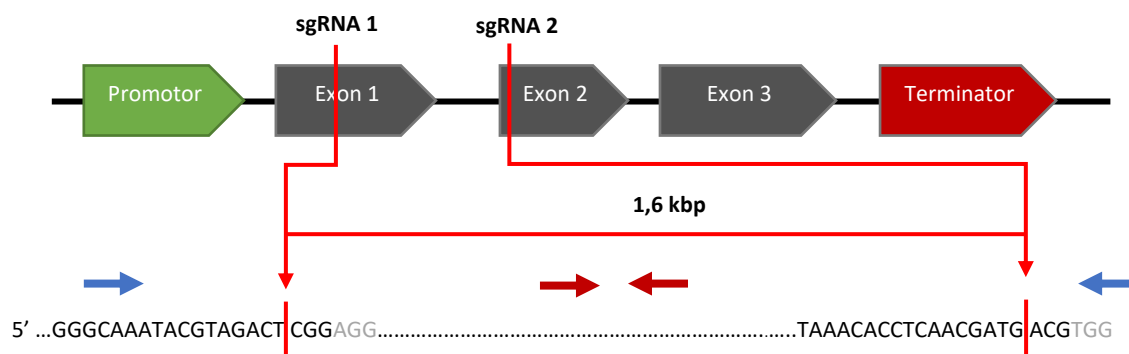


Figure 3.6 – Schematic representation of sgRNA 1 and 2 deletions. Blue arrows indicate primers to detect the deletion band amplicon (**D**), and the red arrows indicate the primers to detect nondeletions (**ND**) band amplicon.

Table 3.4 – Primers for screening the predicted deletion zones. ND: Non-deletion; D-Deletion.

Potential cleavage site	Forward	Reverse	Product size
Region Guide1	CAAATACGTAGACTCGGAGG	CTAGAACTCAGTCTCACCTGC	749
Region Guide 2	ACACCTCAACGATGACGTGG	CCTCAGCACAAGACCTGACA	460
ND	TGGGGACTTTTCGGGATTGTG	CTTCACCTGTTTCGCGTTCC	247
D	GTGGATTGTTTCTGCCGCC	GTCTGTTGCTGAGGTCAATAGGC	2400

The genomic DNA was extracted using PureLink® Genomic DNA Kit (Life Technologies). Each region was amplified separately using Taq DNA polymerase kit (Qiagen), combined with dNTPs (10 mM, ThermoFisher), forward and reverse primers (10 μM) and genomic DNA (2 μl), in a total volume of 20 μl, following the PCR condition: initial incubation at 95°C for 10 minutes, followed by 42 cycles of 30 seconds at 94°C, 30 seconds at 55°C and 90 seconds at 72°C, followed by a final extension at 72°C for 10 minutes. After PCR amplification, PCR products were analysed in 2% agarose gel, by electrophoresis.

3.4 Results

3.4.1 Efficiency of transfection and editing

The efficiency of transfections was assessed 24 hours after the transfections by FACS sorting, using the 10% fluorescent top of ATTO 550 positive cells. Kolf2 AAVS1-mCherry were not sorted due the overlap of absorbance and emission from the tracrRNA and mCherry. For this cell line, cells were directly seeded at low density to pick single colonies. As seen in **Table 3.5**, all sorted cell lines displayed a high transfection efficiency of more than 90%. Transfections of tracrRNA-Cas9 protein (NT) compared with crRNA-tracrRNA-Cas9 protein (KO) were slightly less efficient.

Table 3.5 – Editing Efficiency according with each cell line.

	CHME3	THP1	UP007	UP029	U87
Cav1 NT	92%	92%	95%	90%	99%
Cav1 KO	95%	93%	96%	94%	99%

Regarding the editing efficiency, this was calculated 48 hours after the FACS sorting and 72 hours after the CRISPR RNP transfection, in the sorted populations, using the commercial kit GeneArt® Genomic Cleavage Detection Assay. The kit has an internal control for the reaction - Control PCR templates, where after enzymatic treatment it shows a less intense primary band when compared with non-enzymatic digestion, and two cleaved band, as seen on **Figure 3.10**. The set of primers for guide 1 (g1) and guide 2 (g2) were designed to amplify regions crRNA guide 1 and guide 2, respectively. Guide 3 (g3) is only amplified when both guides cut the DNA in the same cell and delete around 1,600 bp (distance between two guides).

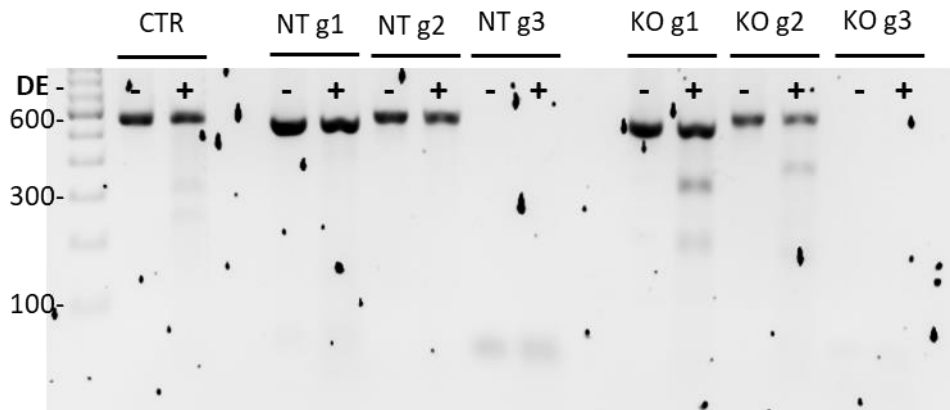


Figure 3.7 – Gel image from **U87** sorted cells, 72 hours after transfection. CTR: positive control, NT: Non-target, KO: knockout, DE: Digestion enzyme treatment.

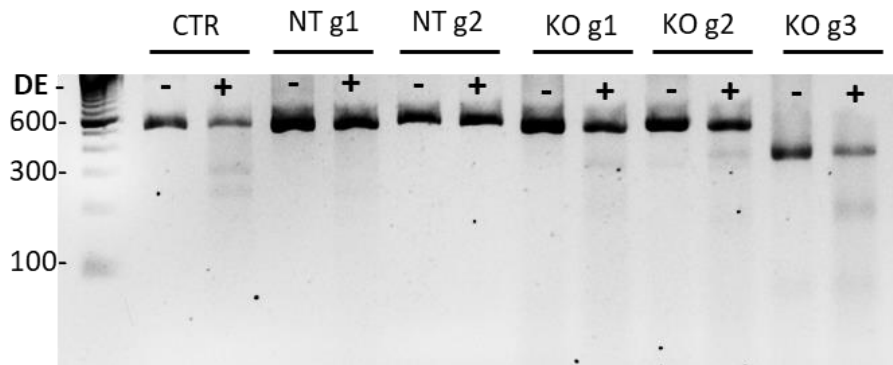


Figure 3.8 - Gel image from **UP007** sorted cells, 72 hours after transfection. CTR: positive control, NT: Non-target, KO: knockout, DE: Digestion enzyme treatment.

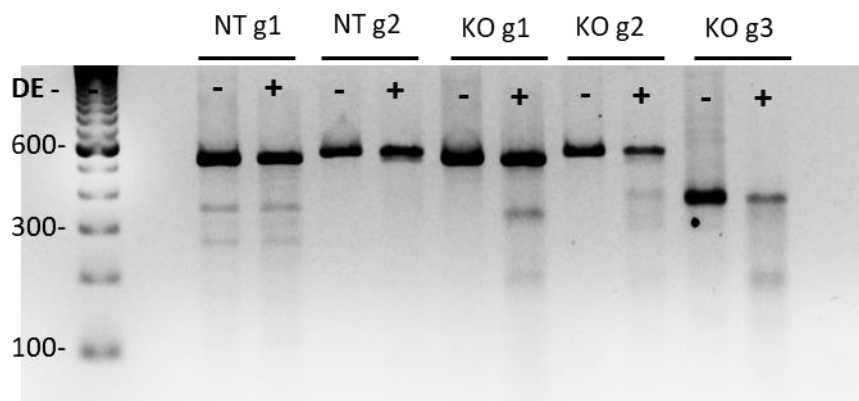


Figure 3.9 – Gel image from **UP029** sorted cells, 72 hours after transfection. CTR: positive control, NT: Non-target, KO: knockout, DE: Digestion enzyme treatment.

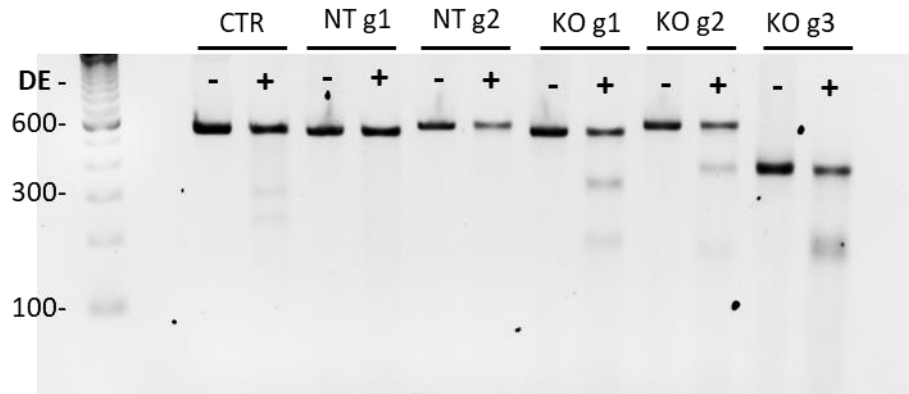


Figure 3.10 – Gel image from **CHME3** sorted cells, 72 hours after transfection. CTR: positive control, NT: Non-target, KO: knockout, DE: Digestion enzyme treatment.

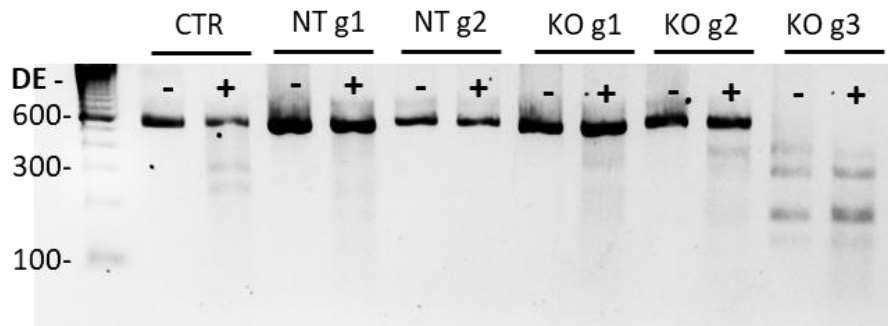


Figure 3.11 – Gel image from **THP1** sorted cells, 72 hours after transfection. CTR: positive control, NT: Non-target, KO: knockout, DE: Digestion enzyme treatment.

The figures above and the **Table 3.6** show the editing efficiency according to each cell line. NT population was amplified, showing that no genome editing was performed in this region.

Table 3.6 – Summary of editing efficiency of 5 cell lines.

	CHME3	THP1	UP007	UP029	U87
Cav1 NT G1	0%	0%	0%	0%	0%
Cav1 NT G2	0%	0%	0%	0%	0%
Cav1 KO G1	19.8%	1.3%	4.1%	4.0%	23%
Cav1 KO G2	14.7%	2.5%	4.8%	6.3%	21%
Cav1 KO G3	19.7%	11.1%	15.9%	20.1%	0%

THP1 is the hardest cell line to be genetically modified, displaying lower values of genetic editing efficiency, 1.3%, 2.5% and 11.1% (g1, g2 and g3, respectively). The U87 was the only cell line that did not display any edition with g3, meaning that each cell was cut only with one of the guides and not with both guides simultaneously. Nevertheless, the U87 together with CHME3 were the cell lines that obtained the highest genomic editing efficiency.

3.4.2 CRISPR-Cas9 clone characterization

All clones were expanded from one single cell that did not show Cav1 protein expression by dot blot. The respective clones for controls (NT) were also expanded. After reaching a T25 flask, Cav1 expression was confirmed by WB, proliferation was followed by 10 days using the MTT assay and the genomic DNA was amplified following the procedures described by Canver and colleges (Canver et al. 2014).

Cav1 protein expression by WB

Even after the Cas9 cut the DNA guided by the crRNA, the indels or mutations may not have efficiently disrupted the protein. A dot blot was performed as described by Estep *et al.* (Estep et al. 2016) in order to do an earlier selection of clones (Cav1 KO) using a small amount of protein (1/3 of one well from a 96-well plate) and to not expand clones that are expressing Cav1.

Table 3.7 – Number of transfected clones analysed by Dot Blot and WB, per cell line. *confirmed by PCR

Number of clones			
	Dot Blot		WB
	Total of clones analyzed	Cav1 negative	Cav1 negative
CHME3	17	4	4
THP1	3	3*	3*
UP007	11	4	4
UP029	10	2	2
U87	9	3	3
KOLF2 AAVS1 mCherry	83	10	10

Not all single cells generated clones after seeding them at low density. It was observed that some cells did not survive as a single cell. Nevertheless, at least two clones for each cell line were successfully generated (**Table 3.7**). Since the objective of the dot blot was to pre-select clones that do not express Cav1 protein, the technique was only performed in clones that were isolated from the population Cav1 KO and not from the Cav1 NT. All clones generated from the Cav1 NT population were expanded, analysed by WB and frozen as described in **Chapter 2 - 2.1.2**. For all cell lines, except THP1, it was possible to include or exclude clones for the Cav1 protein expression by WB.

Representative WB are categorised in **Figure 3.12** from cell lines U87, UP007, UP029, CHME3 and KOLF2, showing a KO of Cav1 at protein level.



Figure 3.12 – Representative Cav1 protein levels of NT and KO clones from U87 (a), UP007 (b), UP029 (c), CHME3 (d) and KOLF2 (e) cell lines. GAPDH was used as a control.

The THP1 cell line expresses low Cav1 protein levels as monocyte and should increase its levels after differentiation into macrophages (Y. Y. Fu et al. 2012). To analyse this cell line, the obtained clones were differentiated into macrophages with PMA and the Cav1 expression was performed by measuring the mRNA levels by PCR, since the protein levels were not good enough to classify the clones as a Cav1 KO. The PCR products were run into 2% agarose gel (**Figure 3.13**). Clones 1, 2 and 3 did not express Cav1 mRNA levels after macrophages differentiation.

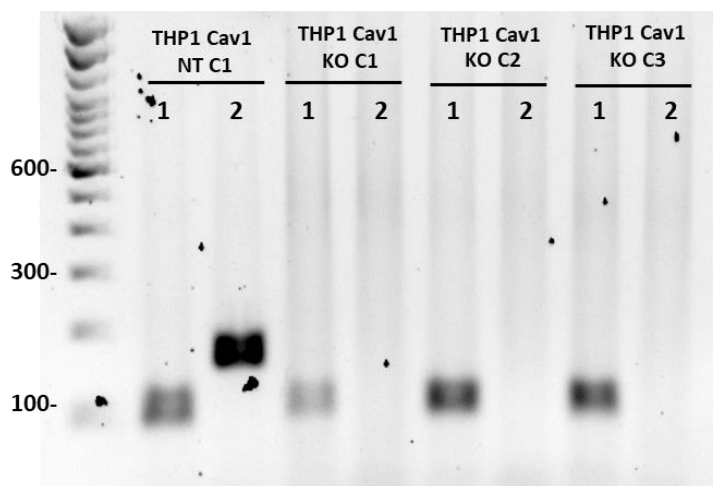


Figure 3.13 – PCR products of THP1 clones run into 2% agarose gel. 1-GAPDH, 2- Cav1.

Screening CRISPR-Cas9 clones for predicted deletions

Four set of primers were designed to target three different genome editing events in each clone. A PCR reaction was performed using different pairs of primers targeting four regions, as described in **Section 3.3.4**. After amplification the PCR products were run into 2% gel agarose. The amplification of the regions G1 of 749 bp, G2 of 460 bp and ND of 247 bp, indicates that no genetic editing was performed.

The predicted deletion of U87 clones is represented in **Figure 3.14**. The control clones, U87 Cav1 NT C1 and C2, showed an amplification of regions from G1, G2 and ND zones. Both U87 Cav1 KO clones analysed (C6 and C8) did not present a PCR product correspondent to the G1 region but generated the expected PCR product correspondent to the G2. No alterations were observed for zone D (2.4 kbp is too large to be efficiently

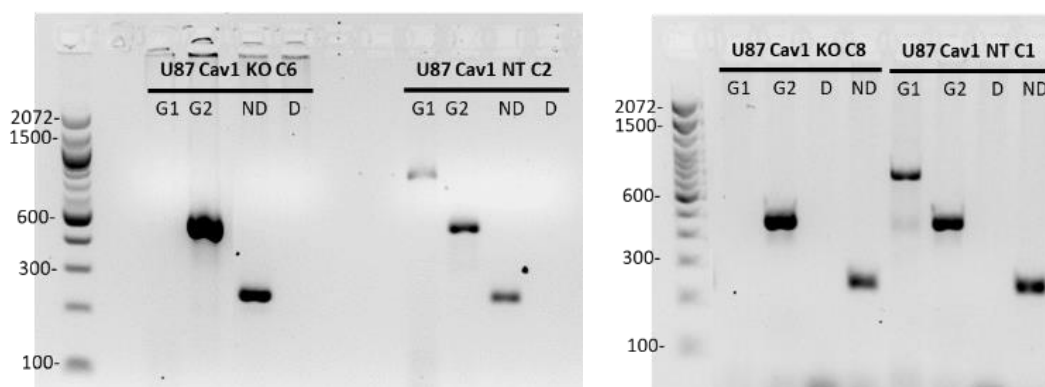


Figure 3.14 - PCR amplification products of U87 Cav1 NT C1 and C2, U87 Cav1 KO C6 and KO C8.

amplified by PCR), showing that the cells did not suffer any genomic alteration in this zone.

With regards to the UP007 clones (**Figure 3.15**), Cav1 NT analysis showed an amplification of the region from G1, G2 and ND. Cav1 KO C1 did not display any mutation detectable by PCR, however, the protein levels are disrupted, as confirmed by WB. All other clones (Cav1 KO C3, C5 and C11) showed an amplified band in the D zone, indicating that they suffered a cut between exon 1 and 2. In Cav1 KO C5 regions of G1 and G2 are efficiently deleted. Cav1 KO clone 3 and 11 have G1 deleted, however, G2 is conserved.

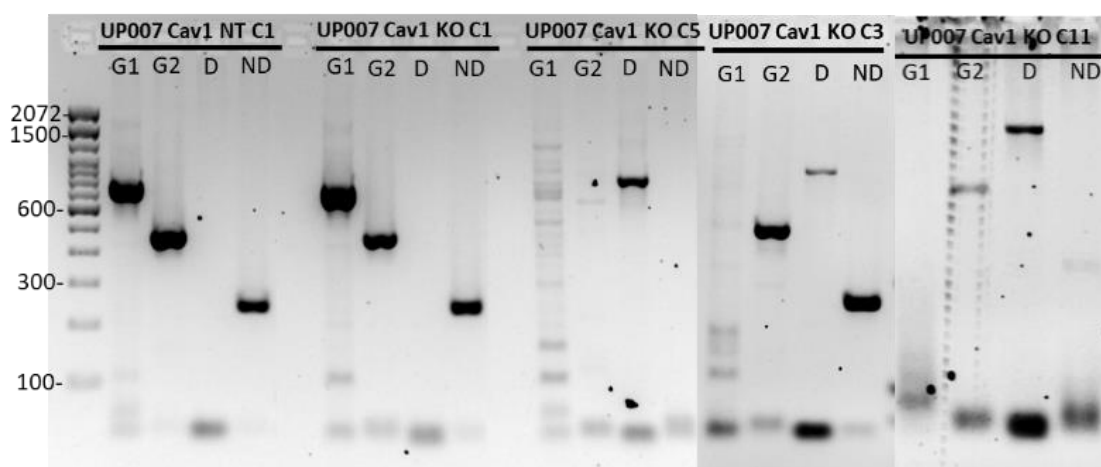


Figure 3.15 - PCR amplification products of UP007 Cav1 NT C1 and Cav1 KO C1, C5, KO C3 and KO C11. Note: UP007 Cav1 KO C3 and C11 were run in different gels.

Clones obtained from the UP029 cell line are represented in **Figure 3.16**. UP029 Cav1 NT C1 showed an amplification of the region from G1, G2 and ND. UP029 Cav1 KO C5 and C7 contain both G1 and G2 deleted. The region between G1 and G2 seems to be conserved since D amplicon was not efficiently amplified.

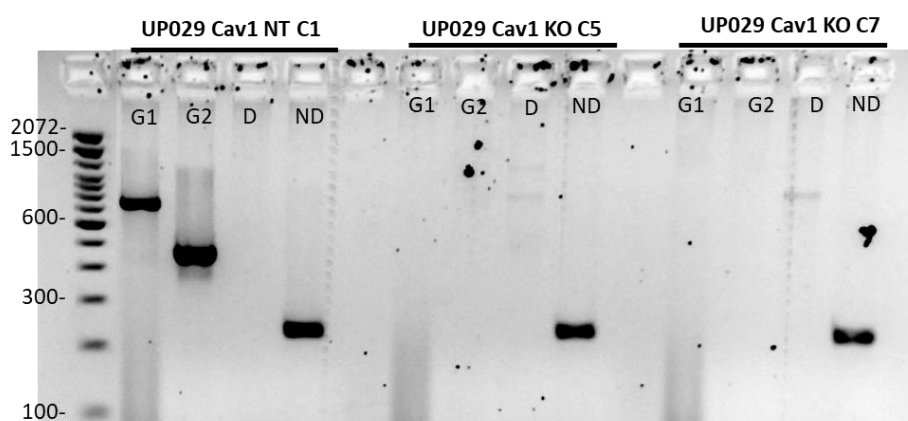


Figure 3.16 - PCR amplification products of UP029 Cav1 NT C1, UP029 Cav1 KO C5 and KO C7.

The **Figure 3.17** shows the PCR products from the analysed clones of CHME3 cell line. As expected, Cav1 NT C1 presented amplification of G1, G2, and ND zone. For the Cav1 KO clones, C6 and C9 showed an indel event in the zone of crRNA g1. C4 had an indel in the zone of crRNA g2, since no PCR product was amplified using the set of primers to target these regions. For the Cav1 KO C17, both regions G1 and G2 were efficiently amplified, however, a product of around 800 bp was amplified for the D zone as well. A deletion of roughly 1.6 kbp is expected for this clone, between the region cut by crRNA g1 and crRNA g2.

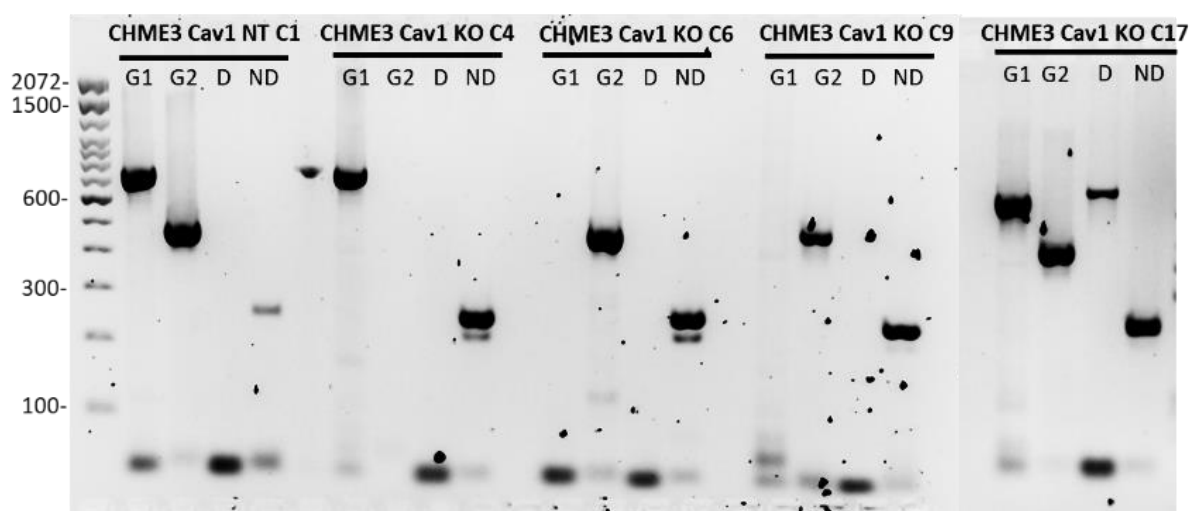


Figure 3.17 – PCR amplification products of CHME3 Cav1 NT C1, CHME3 Cav1 KO C4, KO C6, KO C9 and KO C17. Note: C17 was run in a different gel.

Regarding the THP1 (**Figure 3.18**), only Cav1 KO C1 showed a genetic mutation target by G1 (cut done by crRNA g1). For Cav1 KO C2 and C3, Cav1 expression seems to be disrupted (analysis by PCR), however, the genomic alterations should be minimal and not possible to detect with this method.

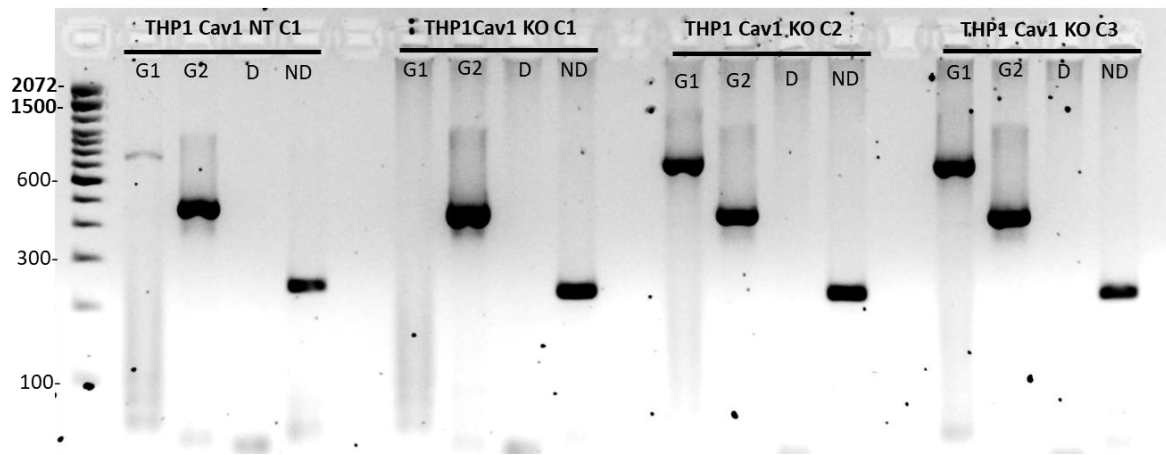


Figure 3.18 - PCR amplification products of THP1 Cav1 NT C1, THP1 Cav1 KO C1, KO C2 and KO C3.

For the iPSC line used, the Kolf2 cells, all Cav1 NT clones (C1, C2, C3 and C4) showed a PCR amplification product of the regions for the G1, G2 and ND (**Figure 3.19**). The Cav1 KO C1 and C2 did not reveal an amplification for the region correspondent to the G1. Also, Cav1 KO C6 and C8 did not amplify the region correspondent to the G2. Amplifications of the region D were not observed in any of the clones analysed.

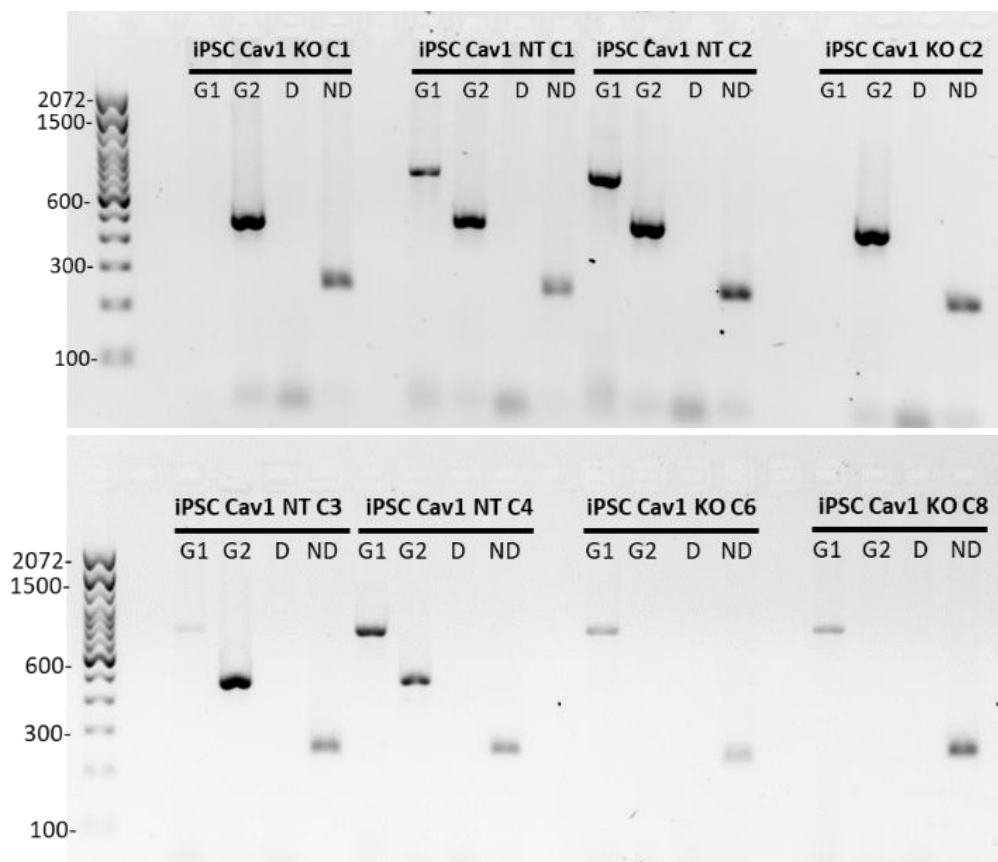


Figure 3.19 - PCR amplification products of iPSC-Kolf2 Cav1 NT C1, C2, C3, C4 and Kolf2 Cav1 KO C1, C2, C6 and C8.

Cellular proliferation

The cellular proliferation of U87, UP007, UP029, CHME3 and THP1 was studied in order to exclude clones that showed alterations in terms of proliferation, compared with the WT cell line (**Figure 3.20**).

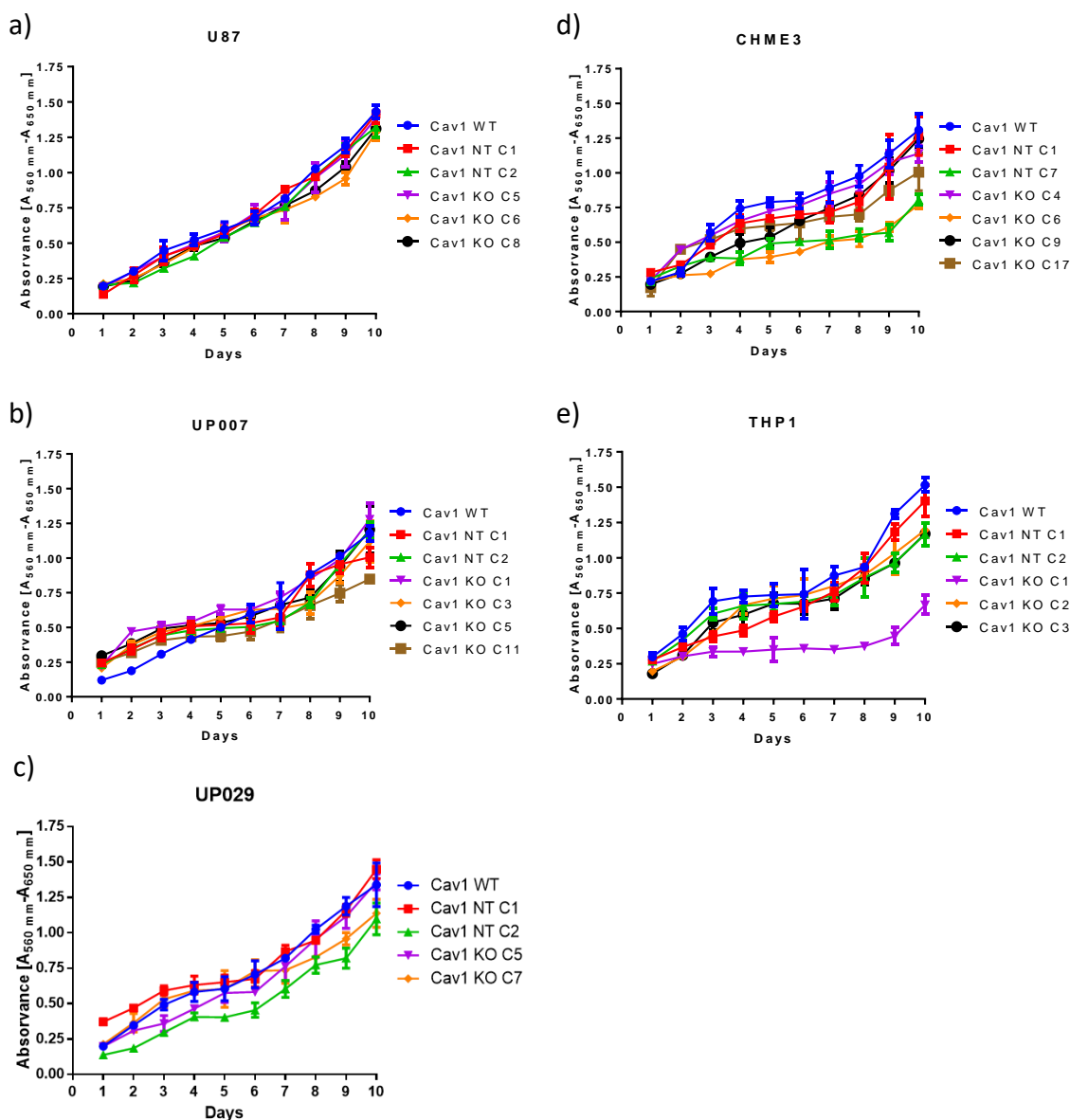


Figure 3.20 – Proliferation of U87 (a), UP007 (b), UP029 (c), CHME3 (d) and THP1 (e). Different clones, as well as WT, were seeded into a 96-well plate and followed for 10 days, using the MTT proliferation assay.

Clones of CHME3 Cav1 NT C7, CHME3 Cav1 KO C7 and THP1 Cav1 KO C1 showed a slowdown in their proliferation rate. The remaining clones analysed revealed similar proliferation patterns.

3.5 Discussion

There are three main formats of the CRISPR-Cas9 system: DNA-vector, IVT of the Cas9 mRNA and gRNA, and the conjugation of Cas9 protein with synthetic sgRNA to form the ribonucleoprotein (RNP) complex previously to transfection (Liang et al. 2015). The DNA-vector approach, Cas9 mRNA and gRNA delivered into the cells are transcribed in the nucleus, then translated in the cytoplasm, where the RNP complex will form to return to the nucleus for gene editing. On the other hand, transfection of Cas9 mRNA and gRNA starts with the translation of the Cas9 protein to form the RNP complex in the cytoplasm, entering then into the nucleus to engineer the genome. Both DNA and RNA approaches use cellular transcription and translation machinery to generate functional Cas9-sgRNA complexes within the cell before any genome editing occurs. In these cases, the Cas9 protein expression needs more time to occur (peak >12 hours) which results in a significant delay before the editing takes place.

New technologies have become available in the market, for instance, Cas9 protein and sgRNA format can be purchased already prepared and only needs ca. 1 hour to be complexed prior to transfection, presenting more consistency and less variability once this technique does not rely on cellular transcription and translation machinery to generate functional systems. Comparing the DNA-vector and RNP technologies, DNA-vectors take about 7-14 days for the preparation of plasmid and DNA purification while the RNP approach is less time consuming requiring ca. 1 hour. Furthermore after delivery, the RNP complex is available to cleave the target DNA without the need to be transcribed or translated, reducing the chances of sgRNA degradation and off-targets effects (Liang et al. 2015; Kouranova et al. 2016). Additionally, these RNP complexes can be chemically modified in order to protect against cell-mediated degradation and immunological response and thereby increase the editing efficiency.

Another way to improve the CRISPR-Cas9 efficiency is to choose the optimal delivery system. Mainly, the CRISPR system delivery can be undertaken using a lipid-based transfection or electroporation. Other techniques, such as microinjection or viral vectors, can be used as well, however they require specialised equipment and practices. Microinjection is mostly used for generation of animal models and the viral vectors used

to generate *in vitro* models, however the latter can elicit immune responses (Lino et al. 2018). Lipotransfection can be used in almost all cell lines, however the approach can be less efficient in some cell lines, particularly, cells that grown in suspension or in primary cell cultures. Furthermore, the lipofection reagents are toxic for cells, and the quantity of DNA that is transfected is restricted by the amount of reagent that the cell can tolerate. The second delivery approach, electroporation, together with specialized solutions (e.g. nucleofection solution) and using the correct voltage, allows the CRISPR system to rapidly reach the nucleus with low toxicity for cells. Additionally, the amount of RNA to be transfected is independent of the transfection solution. This system can be used in all types of cells, showing excellent results even with cells are that generally recognised as hard to transfect (Hendel et al. 2015).

The first approach this project adopted to KO Cav1 in the cell lines was the DNA-vector method described in APPENDIX I - CRISPR-Cas9 vector approach. Our laboratory has some experience in gene editing with this approach achieving good results to target other genes in other cell lines. Based on this, three different gRNAs were selected for use with this method. After testing all gRNAs in U87, UP007, UP029 and CHME3 cell lines, one clone Cav1 KO for U87 cells was generated (**Supplementary figure I.7** - U87 sequence 46, clone 3). For the remaining cell lines, all clones that survived and proliferated had some level of Cav1 expression by WB analysis, showing disappointing results. After this unsuccessful approach, the RNP complex method was designed and delivered by electroporation using a nucleofection solution. In adoption of this approach we considered all of its characteristics such as the high efficiency even for cell lines hard to edit, more control of the sgRNA and Cas9 concentration, efficiency to deliver the system, less prone to gRNA degradation and fewer off-target effects.

The comparison of transfection efficiencies of both techniques showed a considerable difference, with the RNPs method achieving outstanding results. As seen in **Supplementary table I.3**, 4.4% was the highest transfection efficiency achieved with the plasmid methodology (CHME3_sq46), compared to the lowest transfection efficiency of 90% registered with the RNP methodology (UP029_Cav1 NT), as seen in **Table 3.5**. A transfection efficiency of 99% was registered with the U87 cell line. Based on these results, it was possible to deduct which of the techniques would have a better editing

efficiency. During the first attempt to delete Cav1, after studying the editing efficiency by DNA cleavage analysis, no bands or faint bands were obtained for all cell lines transfected, resulting on the low efficiency and justifying the only clone obtained for Cav1 KO (as seen in **Supplementary figure I.6** and **Supplementary figure I.7**). Using the RNPs, it was possible to increase the editing efficiency and it was possible to identify cleavage products for the two gRNA used, across all cell lines analysed. Furthermore, since both sgRNA were delivered together, it was possible to identify the genetic editing of some cells with dual sgRNA (described as g3 in **Table 3.6**). Hendel *et al* demonstrated an increase of editing efficiency when a dual-guide system is used, compared with a single-guide system (Hendel et al. 2015). The cell lines UP007, UP029 and THP1 showed a higher efficiency, and CHME3 got a similar efficiency compared with g1. To notice that for the U87 cell line, the dual guide did not produce genomic edition. Nevertheless, DNA disruptions with one of the guides was enough to create efficient disturbs in the levels of the Cav1 protein.

The efficiency of editing was not investigated for iPSC because it was the last cell line to be genetically manipulated. Since the RNP system used was the same as the one previously applied to the remaining cell lines, it was expected to be able to disrupt the Cav1 function in this cell line just as efficiently. For this reason, we started the clone selection immediately after the nucleofection.

Considering **Table 3.7**, all clones pre-selected by dot blot, also showed no Cav1 expression by WB. Taking into consideration these results, it is possible to conclude that the dot blot shows enough sensitivity and specificity to select clones that were efficiently edited with loss of protein expression.

Due to the nature of CRISPR-Cas9 that can lead to incomplete target ablation and non-control of the NHEJ recombination, this technique requires individual clone isolation. However, the single-cell clone isolation will sacrifice some important characteristics of the main cell line, such as the cell line heterogeneity, so it will capture only a subset of the diversity present within the starting cell population, and may select certain genetic alterations that the cell can carry. To ensure that the results obtained were not an outcome of the clonal artefact, the experiments described in the next chapters include at least two different clones, except for microglia, which include three clones. In order

to select the clones, the proliferation was accessed via an MTT proliferation assay. As shown in **Figure 3.20**, clones UP007 Cav1 KO C11, CHME3 Cav1 NT C7, CHME3 Cav1 KO C6 and THP1 Cav1 KO C1 were excluded due to the abnormal decrease of proliferation probably due to the indels created. Particularly for the clone CHME3 Cav1 NT C7, the loss in proliferation was not expected because no genomic editing was performed. Nevertheless, the cell which originated this clone could have a different proliferative rate compared with the main population. Another explanation for this behaviour is that challenging a single cell to proliferate to form a clonal population constituted with millions of cells can represent a significant selective pressure, which could enrich specific genetic or epigenetic alterations that can affect the proliferation rate.

To **summarise**, Cav1 was successfully deleted in all cell lines using the CRISPR-Cas9 RNP approach. The DNA-Plasmid approach was not able to edit this gene for the cell lines tested. The sgRNA, which targeted the first or the second exon, disrupted the Cav1 gene. The dot-blot pre-selection was shown to be an efficient method to select the edited clones, saving precious time and reagents.

CHAPTER 4 –
IMPACT OF CAVEOLIN-1 KNOCKOUT UPON
CHME3 PHENOTYPE

4.1 Introduction

Microglia are the main myeloid cells in the brain, representing the first line of immune defence in the CNS. These cells are highly dynamic and in addition to immune functions, microglia serve other crucial functions, such as regulation of the synapse architecture and neurogenesis (Parkhurst et al. 2013; Zhou et al. 2019). These cells present a high plasticity, responding promptly to environmental alterations. Under healthy conditions, microglia cells are in a resting stage and present a highly ramified structure. In pathologic conditions microglia become activated to deal with pathogens or other structures that may endanger the CNS, changing their form and becoming rounded or amoeboid in morphology. Chronic and/or inappropriate microglia activation is common to several neurological disorders, which raises the importance of studies on the regulatory mechanisms of microglia activation.

In the exploration of microglia function a variety of *in vivo* and *in vitro* experimental models have been used. Due to ease of access, microglia have been extensively explored using rodent primary cell lines or murine immortalized cell lines, like BV2 cells (Blasi et al. 1990). However, Seok and colleagues showed animal models of acute inflammatory stresses can be a poor reflection of human disease, explained by different evolutionary paths, complexity of disease and distinct molecular mechanisms involved (Junhee Seok et al. 2013). It is not surprising that human cell based models are considered the standard to study human neurological diseases. However, using human microglial cells has challenges not least the availability of primary sources with obtained from aborted foetal tissue, biopsies from epileptic or tumour patients, and post-mortem brain tissue.

Nevertheless, human microglia cell lines have been established such as the HMO6 cell line and the recently commercial available HMC3 or CHME3 (Nagai et al. 2001; Janabi et al. 1995). It is believed that HMC3 and CHME3 are the same cell line sharing the same original reference of Janibe and collaborators (Dello Russo et al. 2018). The cell line was established in France by the laboratory of Professor Mark Tardieu in 1995, using SV40-dependent immortalization of human microglial cells.

To the best of our knowledge, the published studies with CHME3 cells are almost exclusively based on pro-inflammatory related stimuli, such as LPS, IL-1 α , IFN γ , TNF- α ,

beta amyloid proteins and viruses-related infection (Janabi et al. 1995; Ambrosius et al. 2017; Heaton et al. 2010; Dello Russo et al. 2018; Lindberg et al. 2005). The direct effect of anti-inflammatory stimuli is less well studied.

The function of Cav1 in immune cells, particularly in human microglia, has been little studied. Studies with murine macrophages and microglia suggest that Cav1 is involved in pro-inflammatory response, important for the increase in proinflammatory response after spinal cord injury or microbial contact (Shin 2007; X. M. Wang et al. 2006; Tsai et al. 2011; Niesman et al. 2013). A Cav1 role in the anti-inflammatory response has shown that induction of Cav1 in HK-2 cells leads to the suppression of TGF- β signalling in a fibrosis context, in a renal cell fibrosis context (Ito et al. 2004). On the other hand, Shivshankar and colleagues demonstrated upon Cav1 KO an accumulation of arginase 1-positive macrophages after mice myocardium infarction by promotion of an anti-inflammatory phenotype (Shivshankar et al. 2014).

4.2 Aim

The work described in this chapter aimed to understand the immune regulatory role of Cav1 in CHME3 microglia cells to form a basis for future GBM-based studies. CHME3 Cav1 NT and CHME3 Cav1 KO cells were used to study the impact of Cav1 in cellular migration, phagocytosis, response to TMZ, and pro-inflammatory and anti-inflammatory phenotype after the treatment with well established stimulus.

4.3 Methods

4.3.1 General methods

CHME3 Cav1 NT and CHME3 Cav1 KO cells were used during this Chapter. These cells were cultured following the protocols described in **Chapter 2**, section **2.2 - Cell culture maintenance**. At least three different clones for each Cav1 NT and KO were used during the experiments. The microglia markers IBA1 and TMEM119 were analysed by IF as described in section **2.4 - Immunofluorescence Staining**. The protocols described in **2.11- Transwell migration and invasion assay** and **2.9 - Phagocytosis assay** was used to study cell migration and phagocytosis, respectively. CHME3 cells were polarized towards pro-inflammatory or anti-inflammatory phenotypes following the stimulation protocols in **2.5 - Microglia and Macrophages polarization**. Non-stimulated cells were used as a control. To examine the role of Cav1 upon activation of CHME3 cells: (i) a panel of immune-related 'reporter' genes was studied by qRT-PCR (**2.7 - qRT-PCR**); (ii) protein levels of STAT1, NF- κ B p65, STAT3 and STAT6 were explored by WB (**2.8 - Western Blot**), and (iii) soluble products secreted into the media by these cells were examined by cytokine array (**2.10 - Cytokine array**).

4.3.2 TMZ chemosensitivity

In the context of GBM, the chemosensitivity of microglia to TMZ was accessed incubating CHME3 Cav1 NT and CHME3 Cav1 KO cells with different concentrations of TMZ for 72 hours. Microglia cells were seeded at a density of 5,000 cells/cm² into a 96-well plate. Cells were allowed to adhere overnight, at 37°C in a 5% CO₂-humidified atmosphere. On the following day the media was renewed, and the cells treated with 0 μ M, 100 μ M, 250 μ M, 500 μ M, and 1,000 μ M of TMZ, and returned to the incubator for an additional 72 hours. Media without cells was used to calculate the background. The viability was accessed using CyQUANT Direct Cell Proliferation Assay Kit, following the manufacturer's instructions. Briefly, 100 μ l of CyQUANT reagent was added to each well containing 100 μ l of media and incubated for 1 hour and 30 minutes at 37°C with 5% CO₂. After the incubation, the fluorescence at an excitation of 508nm and emission of 527nm was measured with a FLUOstar OPTIMA plate reader (BMG LABTECH Ltd).

4.4 Results

4.4.1 CHME3 cells expressed pan-microglial markers after Cav1 KO

In 1995, upon CHME3 establishment, Janabi *et al* demonstrated these microglial cells expressed CD68 and CD11b markers (Janabi et al. 1995). Later, in 2012, Etemad *et al*, using HMC3 showed the expression of IBA1 by these cells (Etemad et al. 2012). Using CHME3 cells, this thesis used the expression of the IBA1 marker and also the TMEM119 marker, recently identified to distinguish microglia from macrophages.

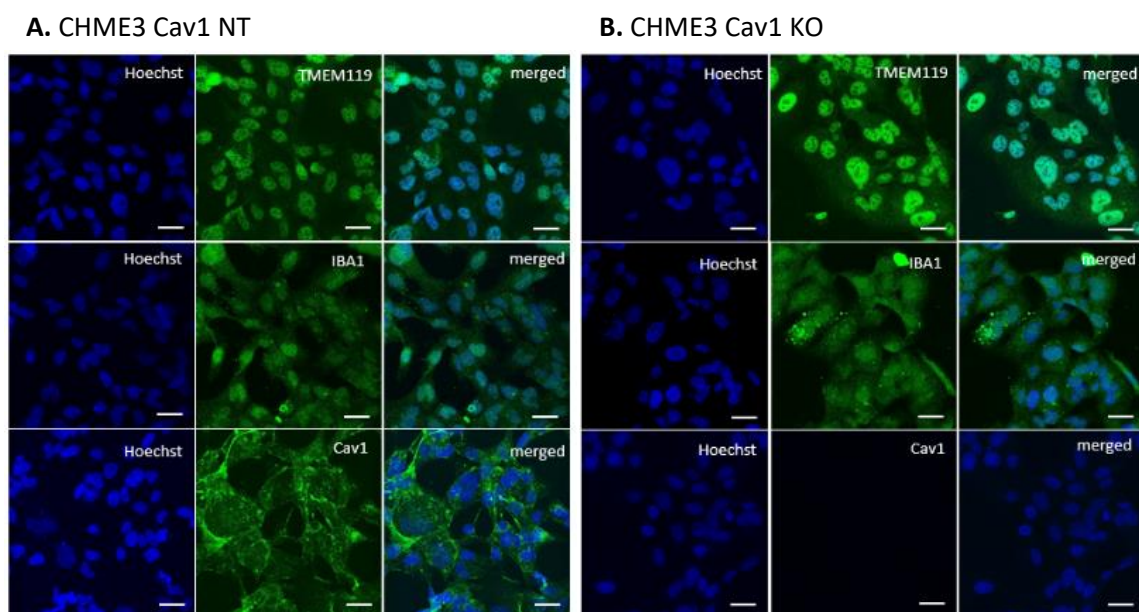


Figure 4.1 – Microglial TMEM119 and IBA1 markers and Cav1 expression. Representative images of the immunofluorescence staining of TMEM119, IBA1 and Cav1 of CHME3 Cav1 NT (A.) and CHME3 Cav1 KO cells (B.). Cells were grown for 48 hours before fixing, labelling with respective antibody, and imaging by confocal microscopy. Scale bar: 10 μ m.

CHME3 microglia cells expressed the microglial markers TMEM119 and IBA1, as seen on the left panel **Figure 4.1**. This microglia cell line expresses Cav1 which was suppressed after CRISPR-Cas9 Cav1 KO (right panel-B). The loss of Cav1 did not affect the expression of TMEM119 and IBA1.

4.4.2 CHME3 cells lack phagocytic ability irrespective of status

The impact of Cav1 status and cellular activation status (pro-inflammatory – ‘M1’ or anti-inflammatory - ‘M2’) upon microglia phagocytosis of pHrodo™ Red *E. coli* BioParticles is illustrated in **Figure 4.2**. Particles without cells were used as a negative control and particles intubated in live imaging solution pH 4 were used as a positive control.

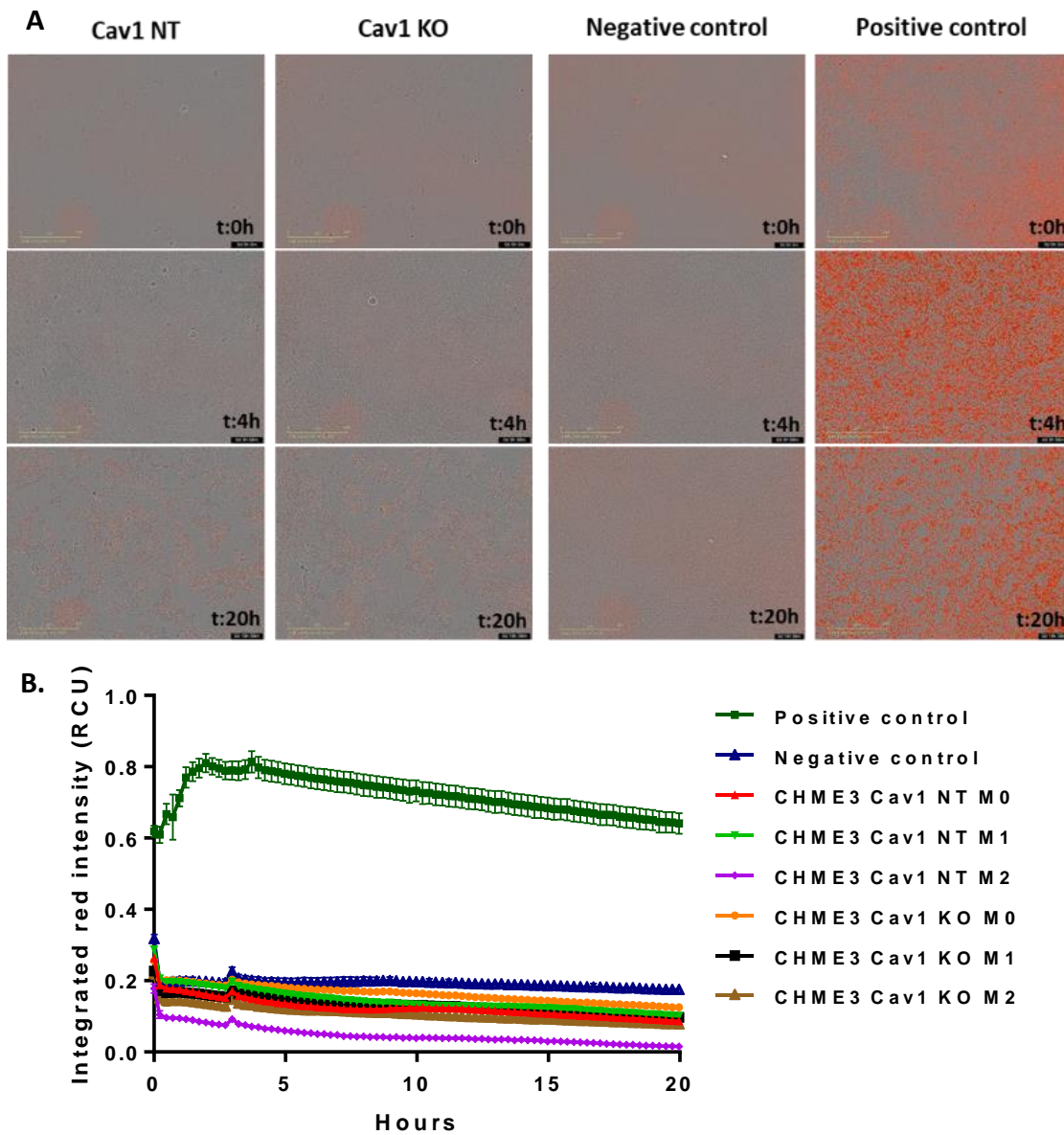


Figure 4.2 – CHME3 phagocytosis assay. **A.** Representative pictures of phagocytosis CHME3 Cav1 NT, CHME3 Cav1 KO, negative and positive control at time points 0h, 4h and 20h. **B.** Integrated red intensity for each condition. CHME3 Cav1 NT and CHME3 Cav1 KO were seeded into a 96-well plate and left overnight to adhere. On the following day, cells were treated with LPS and IFN- γ or with IL-4 and IL-13 for 48 hours, to activate the cells towards a pro-inflammatory M1 or anti-inflammatory M2 phenotype. Untreated cells were used as a control (M0). After the activation, media was exchanged by 90 μ l of live imaging solution and 10 μ l of the resuspended pHrodo *E. coli* bioparticles (50 μ g/ml) and incubated from an additional 20 hours and images taken every 20 minutes, using the Incucyte. Cells without particles were used to calculate the background, particles without cells were used as a negative control and particles intubated in live imaging solution pH 4 were used as a positive control. Mean \pm SEM. N:3 independent experiments. RCU: red calibrated units. Scale bar: 200 μ m.

As seen in **Figure 4.2**, CHME3 cells were not phagocytically active toward pHRodo *E. coli* BioParticles. Even after pro-inflammatory ‘M1’ or anti-inflammatory ‘M2’ microglial activation, independently of the Cav1 status, these cells did not increase the phagocytosis of these particles, showing an integrated intensity lower than the negative control and close to the background (blue line).

4.4.3 Cav1 important for microglial CHME3 Transwell migration

The impact of Cav1 upon microglia single cell migration was studied using a Transwell system with 8 μ m pores.

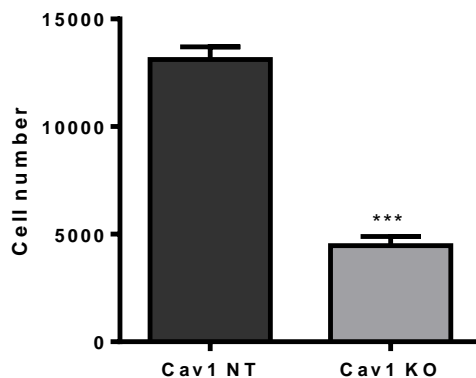


Figure 4.3 – Impact of Cav1 upon Transwell CHME3 migration. Microglia cells CHME3 Cav1 NT and CHME3 Cav1 KO were seeded into the upper chamber in media without FBS. Medium with FBS was used as a chemoattractant in the lower chamber. The cells were allowed to migrate for 16 hours. Mean of 3 different clones NT and KO \pm SEM. *** p <0.001 when compared to Cav1 NT cells, using an unpaired t -test.

The single cell migration was in response to FBS, with CHME3 cells which expressed Cav1 showing a migration over 16 hrs of 13,114 \pm 594 cells. Upon Cav1 KO, the cellular migration decreased significantly to 4,465 \pm 427 cells, as observed in **Figure 4.3**.

4.4.4 Cav1 promotes microglia CHME3 sensitivity to TMZ

Within the context of GBM, microglia cells are subjected to TMZ within the tumour environment. Here the effect of TMZ on this immune cell population was studied in CHME3 Cav1 NT and CHME3 Cav1 KO treated with concentration-range of TMZ for three days. The drug sensitivity was assessed using CyQuant assay.

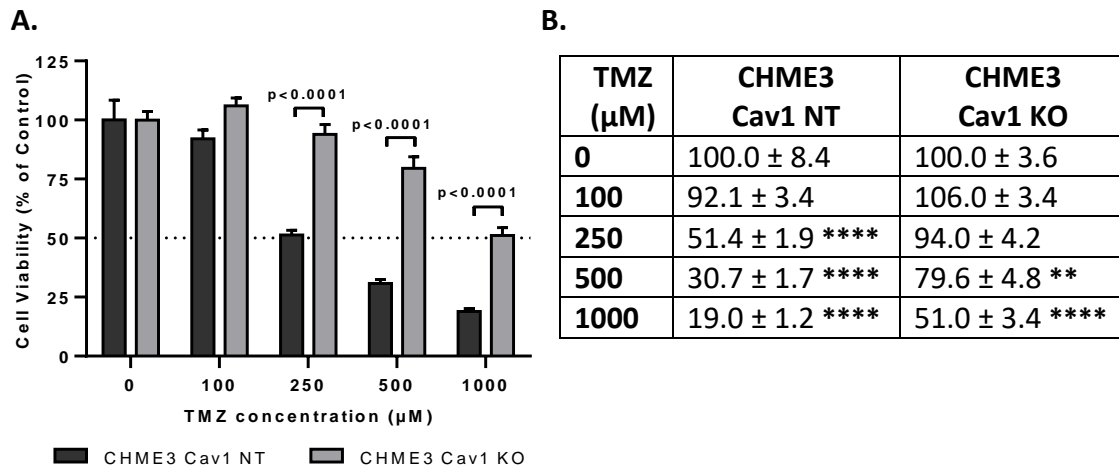


Figure 4.4 – Impact of Cav1 in microglia sensitivity to TMZ. CHME3 Cav1 NT and CHME3 Cav1 KO cells were seeded into 96-well plates and incubated overnight to let the cells adhere. On the following day, the medium was renewed, microglial cells were treated with different concentrations of TMZ and returned to the incubator for an additional 3 days. **A.** Cell viability graph of microglial Cav1 positive (NT) and Cav1 KO cells. **B.** Cell viability table, representing the cellular viability mean % ± SEM. N: 3 independent experiments. ** $p \leq 0.01$, **** $p \leq 0.0001$ compared with respective untreated cells (0 µM), Sidak's multiple comparison test.

After the three days treatment with TMZ, CHME3 Cav1 NT were significantly more sensitive, showing an IC₅₀ close to 250 µM, compared to CHME3 Cav1 KO, which showed a resistance three times higher of roughly 1,000 µM, as seen in **Figure 4.4**. At low concentrations of TMZ (100 µM) there was a trend for increased cellular proliferation on CHME3 Cav1 KO cells, increasing around 6% the cell viability.

4.4.5 Impact of Cav1 upon CHME3 phenotype in response to pro-/anti-inflammatory stimuli

In response to an inflammatory stimulus microglia coordinate a global activation or repression of gene expression, posttranscriptional regulation, and epigenetic alterations. This aspect of the work first investigated the role of Cav1 upon the microglia activation, by examining the protein expression of STAT1, STAT3, STAT6 and NF- κ B p65, the well-established regulators of inflammatory pathways. CHME3 Cav1 NT and CHME3 Cav1 KO were polarized towards pro-inflammatory (LPS and IFN- γ) or anti-inflammatory (IL-4 and IL-13) phenotype, for 48 hours. Unstimulated cells were used as control.

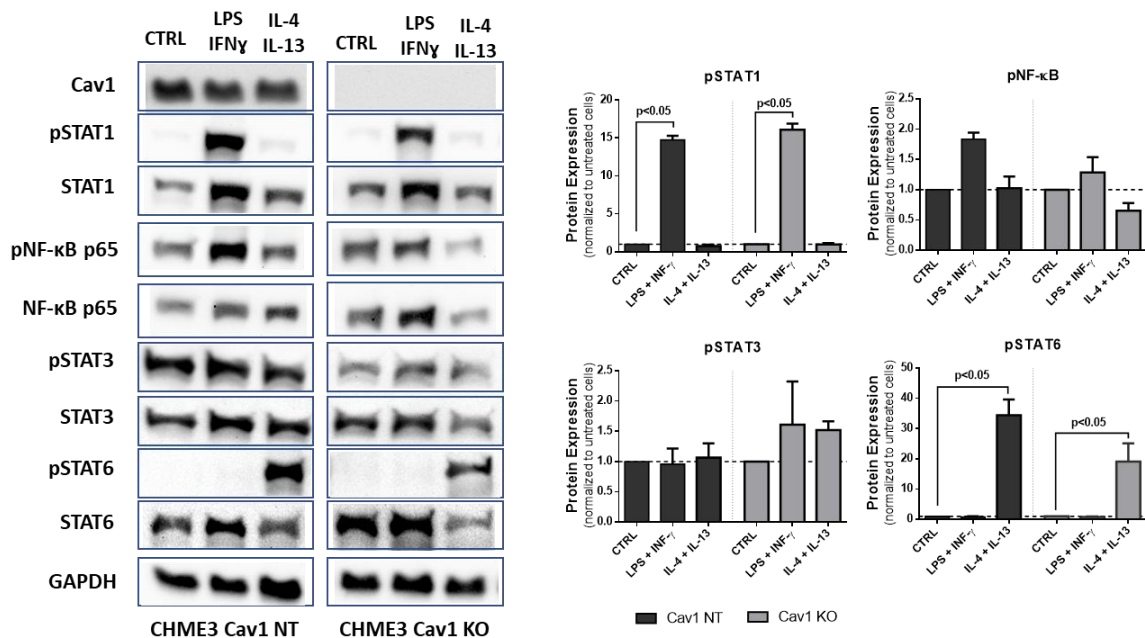


Figure 4.5 – Role of Cav1 in protein expression. **A.** Representative membranes for protein expression of Cav1, Stat1, Stat3, Stat6, NF- κ B p65 and GAPDH, of unstimulated (CTRL), pro-inflammatory phenotype (LPS + IFN- γ) and anti-inflammatory phenotype (IL-4 + IL-13) of CHME3 NT and CHME3 Cav1 KO cells. **B.** Western blot quantification. Protein expression was normalized against the respective untreated cells. Bars represent mean \pm SEM. N=3 independent experiments. Mann-Witney test.

As seen in **Figure 4.5**, the ‘CHME3 Cav1 NT’ cells showed similar Cav1 expression in unstimulated (CTRL), pro-inflammatory (LPS + IFN- γ) and anti-inflammatory (IL-4 + IL-13) phenotype. As expected, ‘CHME3 Cav1 KO’ cells did not express Cav1, even after pro-inflammatory and anti-inflammatory stimulus. The pSTAT1 and pSTAT6, well characterized pro-inflammatory and anti-inflammatory markers, respectively, showed a significant activation after LPS plus IFN- γ (pro-inflammatory stimuli) and IL-4 plus IL-13

(anti-inflammatory stimuli), respectively. Importantly these responses were evident independently of the Cav1 status (+ve NT and -ve KO). The pNF- κ B p65 can be induced by viral and bacterial infections (LPS), necrotic cell products, oxidative stress and pro-inflammatory cytokines (Taniguchi and Karin 2018). The 'CHME3 Cav1 NT' cells presented a slightly greater pNF- κ B p65 under a pro-inflammatory phenotype compared to untreated cells, whereas in the Cav1 deplete cells 'CHME3 Cav1 KO' this response was much weaker. The pSTAT3 is correlated with the anti-inflammatory status, however no real differences in expression of this protein was seen upon any of the activation stimuli or with respect to Cav1 status.

Next we studied the downstream signalling involved in immune activation, with examination of mRNA by qRT-PCR of pro-inflammatory (IL-1 β , IL-6, IL-12, CXCL10 and TNF- α) and anti-inflammatory (TGF- β , IL-10, CCL22, CD200R, CD206 and CD163) genes in the CHME3 cells.

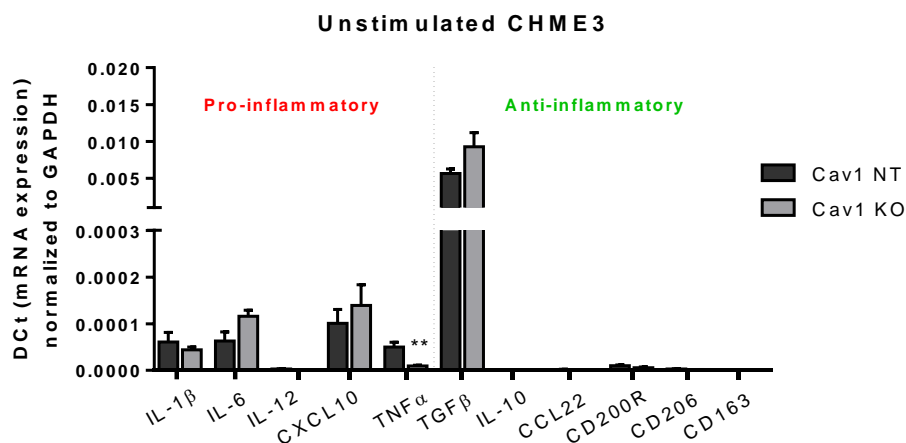


Figure 4.6 – Basal expression of the pro-inflammatory and anti-inflammatory related genes by CHME3 Cav1 NT (black) and CHME3 Cav1 KO (grey) cells. Bars represent the mean \pm SEM of 3 independent experiments. **: $p < 0.01$ when compared to Cav1 NT cells. Sidak's multiple comparison test.

Figure 4.6 shows mRNA in basal unstimulated cells with the gene products segregated by pro- or anti-inflammatory pathways. At this basal level, microglia cells that were cultured in standard culture conditions, without interference of any external stimulus, presented noticeable levels of IL-1 β , IL-6, CXCL10, TNF- α and TGF- β , independently of the Cav1 status; noting TNF- α where some difference is seen. IL-12 expression levels

were almost not perceptible, as well as the anti-inflammatory genes, IL-10, CCL22, CD200R, CD206 and CD163. This demonstrates a picture where CHME3 even under basal conditions show a more pro-inflammatory phenotype.

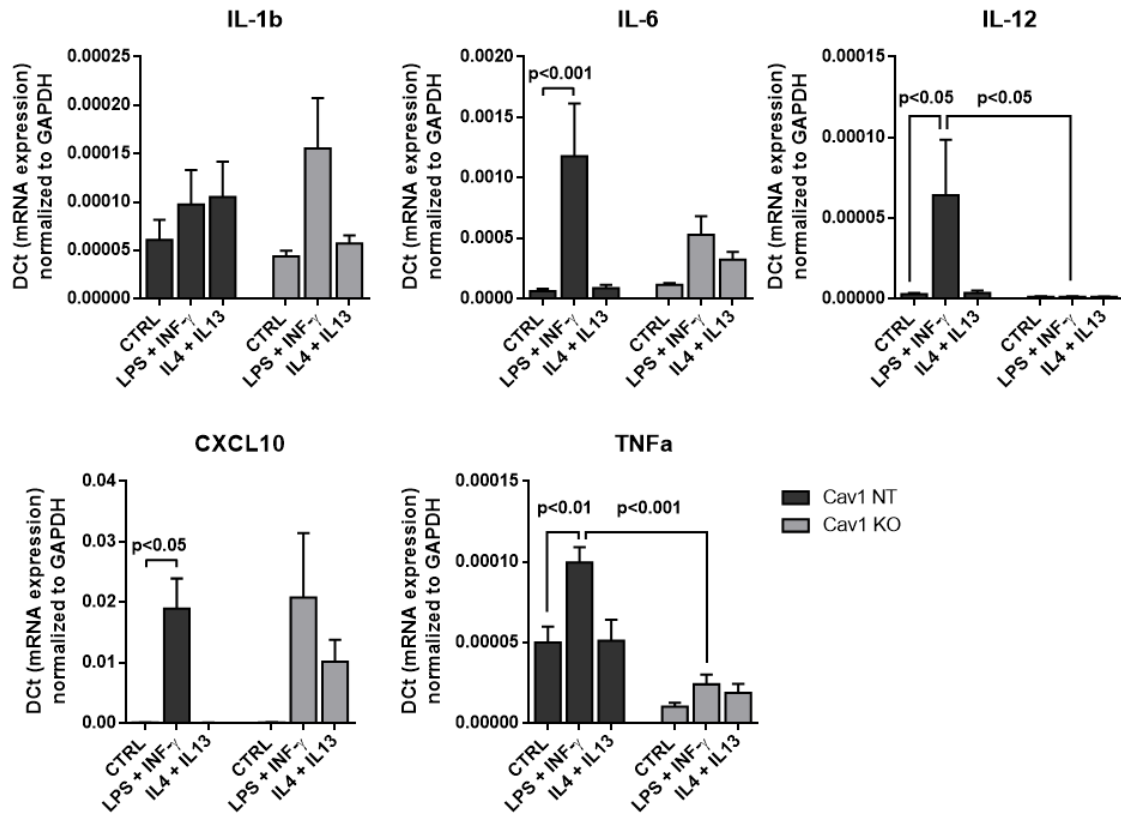


Figure 4.7 – Pro-inflammatory related marker analysis by qRT-PCR. IL-1β, IL-6, IL-12, CXCL10 and TNF-α expression by CHME3 Cav1 NT (black) or CHME3 Cav1 KO (grey). Cells were polarized towards pro-inflammatory (LPS and IFN-γ) or anti-inflammatory (IL-4 and IL-13), for 48 hours. Unstimulated cells were used as control (CTRL). The expression was normalized to HKG (GAPDH). Bars represent mean ± SEM. N=3 independent experiments. Sidak's multiple comparison test.

Figure 4.7 shows the impact of external pro-inflammatory or anti-inflammatory stimuli upon pro-inflammatory markers:

The 'CHME3 Cav1 NT' cells (**black bars**) expressing Cav1 showed under LPS/IFN-γ stimulation a significantly increased production of mRNA compared to control for IL-6, IL-12, CXCL10 and TNF-α. Of note, under anti-inflammatory stimulus (IL-4/IL-13) in these cells did not change the gene expression of these markers.

The loss Cav1 (**grey bars**) generated a statistically significant decrease of IL-12 and TNF-α compared with the Cav1 +ve cells. The levels of IL-1β, IL-6 and CXCL10 remaining

similar between Cav1 +ve and -ve cells. TNF- α is of note in that in the Cav1 -ve cells its expression is repressed compared to the respective Cav1+ve cells even in the control untreated cell populations.

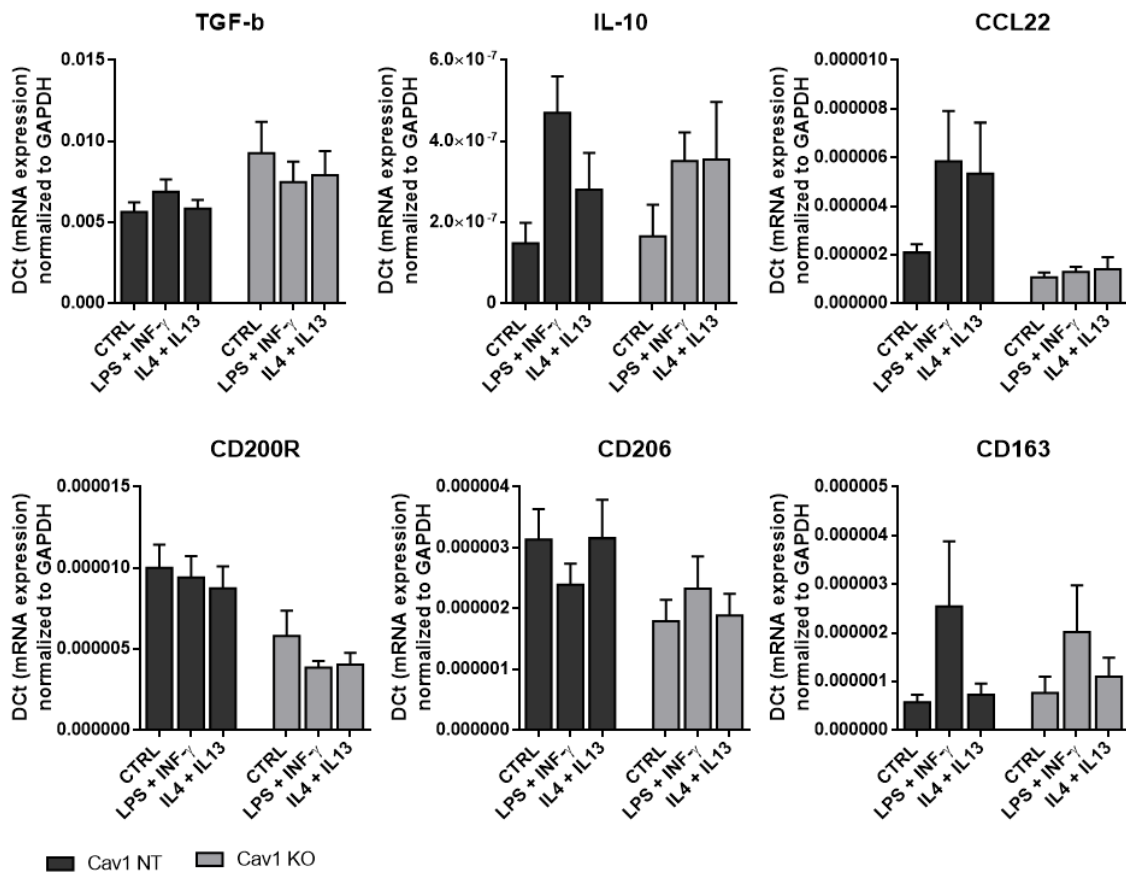


Figure 4.8 – Anti-inflammatory related markers analysis by qRT-PCR. TGF- β , IL-10, CCL22, CD200R, CD206 and CD163 expression by CHME3 Cav1 NT (black) or CHME3 Cav1 KO (grey). Cells were polarized towards pro-inflammatory (LPS and IFN- γ) or anti-inflammatory (IL-4 and IL-13), for 48 hours. Unstimulated cells were used as control (CTRL). The expression was normalized to HKG (GAPDH). Bars represent mean \pm SEM. N=3 independent experiments. Sidak’s multiple comparison test.

Figure 4.8 shows the impact of external pro-inflammatory or anti-inflammatory stimuli upon anti-inflammatory markers:

‘CHME3 Cav1 NT’ cells (**black bars**) showed under IL-4/IL-13 stimulation trends only in particular increase levels of CCL22 in the Cav1 +ve cells. The pro-inflammatory treatment did not interfere with the levels of TGF- β , CD200R and CD206, however, it showed a trend to stimulate the expression of IL-10, CCL22 and CD163.

'CHME3 Cav1 KO' cells (**grey bars**) showed under anti-inflammatory stimulation (IL-4/IL-13) a similar pattern observed in Cav1 +ve cells, excepting CCL22 which levels trended to be lower compared to microglia expressing Cav1.

Overall, the CHME3 cells appear to show a more pro-inflammatory phenotype. Upon pro-inflammatory activation, these cells showed an activation of pSTAT1 and an upregulation of IL-6, IL-12, CXCL10 and TNF- α . Under anti-inflammatory activation it was observed an activation of pSTAT6, but no significantly changes at the gene expression of the studied markers. The loss of Cav1 in microglia, did not affect the pSTAT1 under the pro-inflammatory phenotype, however led to a decrease of the levels of IL-12 and TNF- α .

4.4.6 Impact of activation and Cav1 status upon CHME3 secretome

Here the impact of Cav1 status on secreted products is explored by Cytokine Array. As in previous experiments, 'CHME3 Cav1 NT' (Cav1+ve) and 'CHME3 Cav1 KO' (Cav1-ve) cells were stimulated for 48 hours towards a pro-inflammatory phenotype (LPS/IFN- γ), or an anti-inflammatory phenotype (IL-4/IL-13). Culture supernatants were collected to evaluate the respective content using a membrane-based array, assessing 105 different cytokines, chemokines, and growth factors. A summary of the entire secretome is illustrated in **Supplementary figure VI. 2 - Appendix VI**.

The secreted products with fold-change high then 1.5 compared to unstimulated microglia released by 'CHME3 Cav1 NT' Cav1+ve cells upon pro-inflammatory stimulation are represented in **Figure 4.9-B** and in part (**grey bars**) of **Figure 4.9-C**.

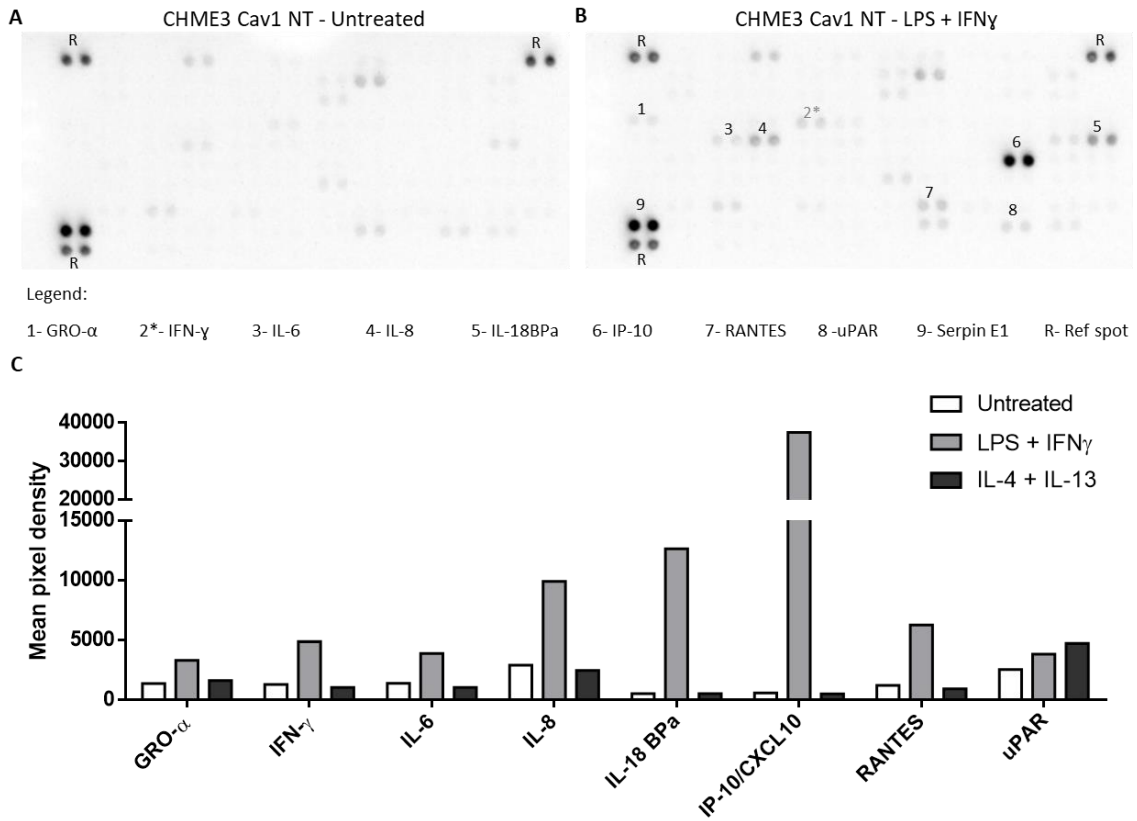


Figure 4.9 – Cytokine array of CHME3 Cav1 NT under a pro-inflammatory phenotype. CHME3 cells were stimulated with LPS and IFN- γ (B) or with IL-4 and IL-13, for 48 hours. Untreated cells were used as a control (A). C- Mean pixel density graph of the analyte with fold-change ≥ 1.5 times.

Under pro-inflammatory stimuli it was possible to identify an increase in GRO- α , IL-6, IL-8, IL-18 BPa, IP-10/CXCL10, RANTES and uPAR. The apparent increase in IFN- γ , is of course compromised by the use of this cytokine to stimulate the cells to achieve the pro-inflammatory phenotype. Stimulation using IL-4/IL-13 did not influence these cytokines, except uPAR, where treatment caused a release comparable to that of the pro-inflammatory stimulus. It was observed an elevated level of Serpin E1 in the basal level, on non-stimulated cells, that was constant on both activations.

The critical secreted products (fold-change >1.5 compared to unstimulated microglia) released by 'CHME3 Cav1 NT' Cav1+ve cells upon anti-inflammatory stimulation are represented in **Figure 4.10-B** and in part (**black bars**) of **Figure 4.10-C**.

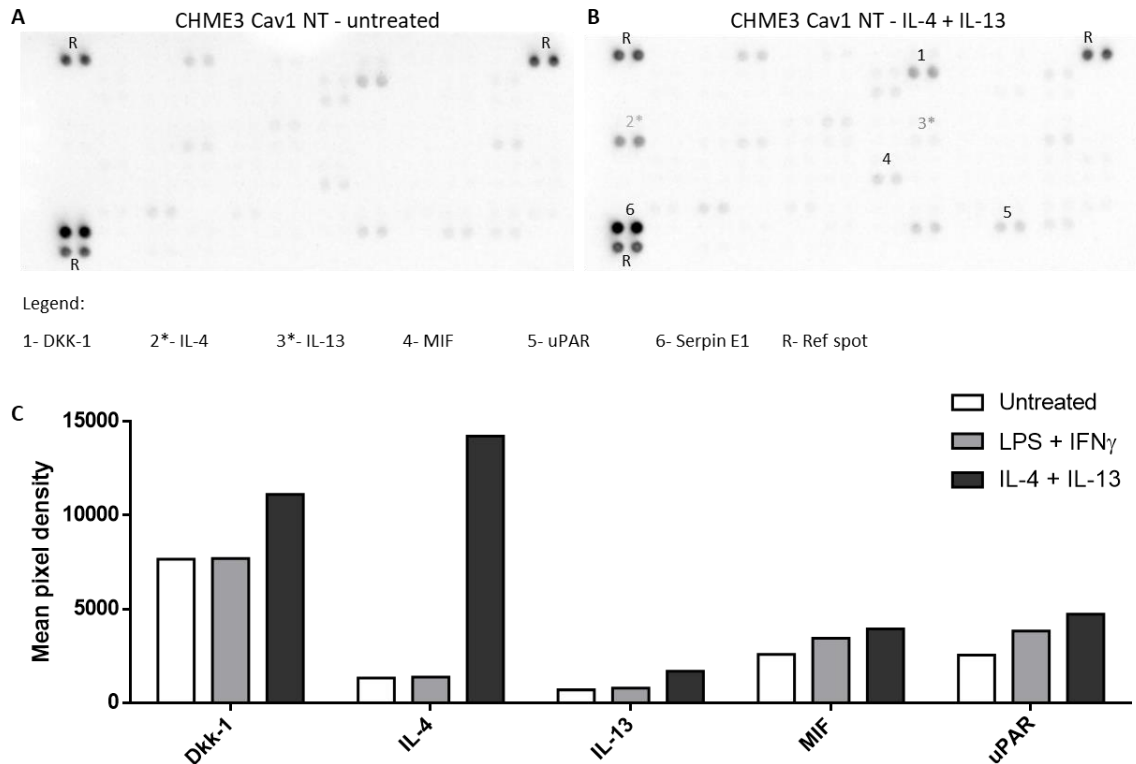


Figure 4.10 – Cytokine array of CHME3 Cav1 NT under an anti-inflammatory phenotype. CHME3 cells were stimulated with LPS and IFN- γ or with IL-4 and IL-13 (**B**), for 48 hours. Untreated cells were used as a control (**A**). **C**- Mean pixel density graph of the analyte with fold-change ≥ 1.5 times.

Under anti-inflammatory stimuli, an upregulation in the secretion of Dkk-1, MIF and uPAR were apparent compared with untreated cells. A slight increase in MIF and uPAR, was also observed under pro-inflammatory stimuli. The apparent increase in IL-4 and IL-13 is compromised by the use of these cytokines to stimulate the cells to achieve the anti-inflammatory state. The pro-inflammatory environment did not affect the secretion of Dkk-1, IL-4, and IL-13.

After loss Cav1 in CHME3 cells, the cytokine profile was evaluated using the same conditions. The secreted products released by microglia cells Cav1-ve under pro-inflammatory environment with fold-change high than 1.5 compared to untreated cells are summarized in **Figure 4.11-B** and in the part of the grey bars in the **Figure 4.11-C**.

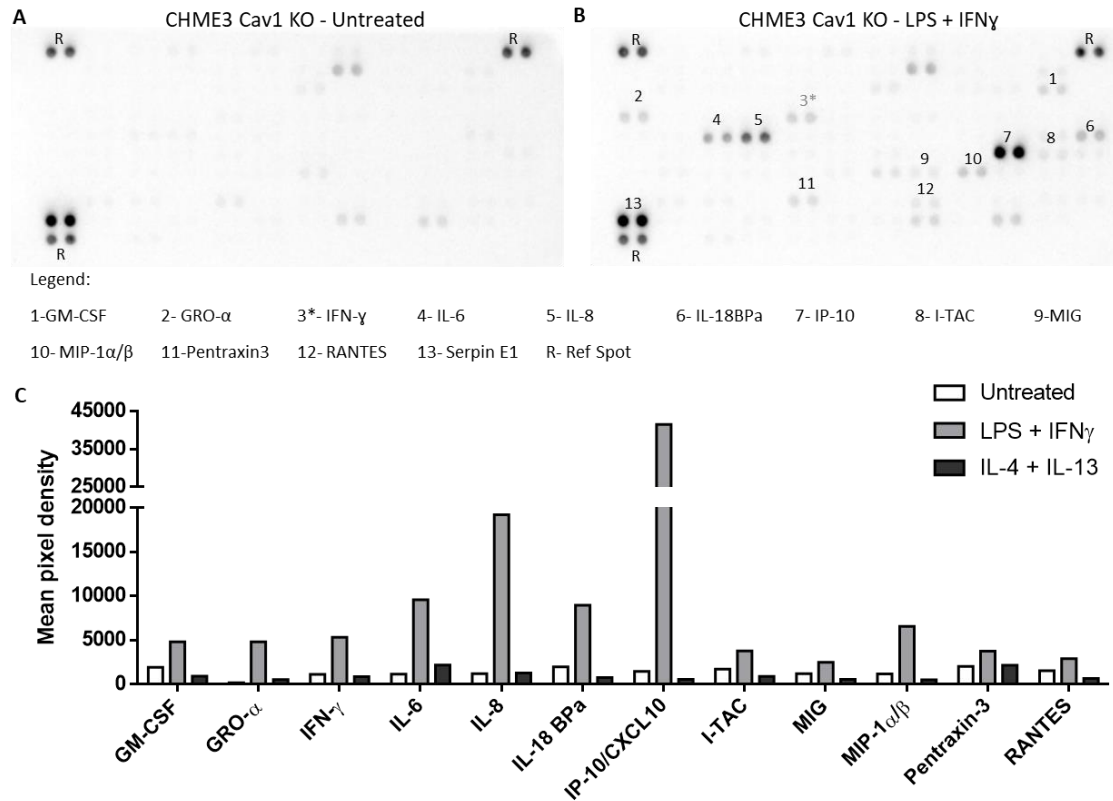


Figure 4.11 – Cytokine array of CHME3 Cav1 KO under a pro-inflammatory phenotype. CHME3 cells were stimulated with LPS and IFN- γ (B) or with IL-4 and IL-13, for 48 hours. Untreated cells were used as a control (A). C- Mean pixel density graph of the analyte with fold-change ≥ 1.5 times.

Compare to untreated cells, under pro-inflammatory stimuli (LPS/IFN- γ) it was possible to identify an increase in GM-CSF, GRO- α , IL-6, IL-8, IL-18 BPa, IP-10/CXCL10, I-TAC, MIG, MIP-1 α/β , Pentraxin-3 and RANTES. The anti-inflammatory environment (IL-4/IL-13) did not induce the production of these analytes. These microglia cells continued to secrete high levels of Serpin E1, independently of Cav1 status.

The released products by microglia cells Cav1-ve under pro-inflammatory environment with fold-change high than 1.5 compared to untreated cells are summarized in **Figure 4.12-B**.

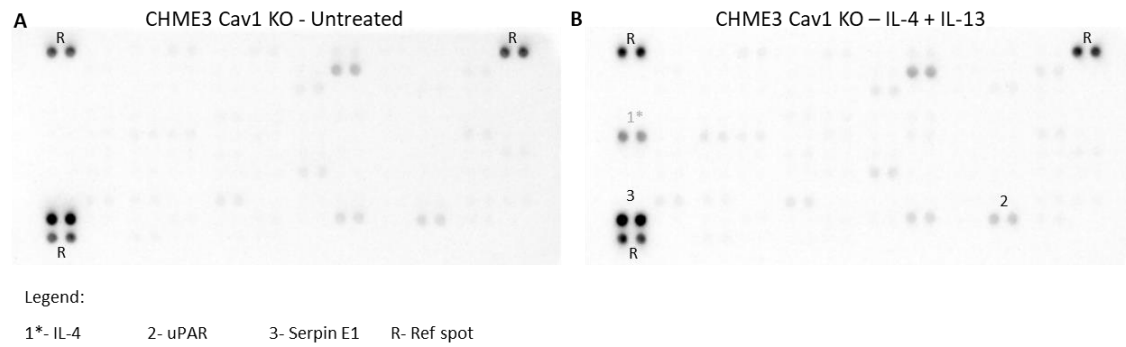


Figure 4.12 – Cytokine array of CHME3 Cav1 KO under an anti-inflammatory phenotype. CHME3 cells were stimulated with IL-4 and IL-13 (B), for 48 hours. Untreated cells were used as a control (A).

Under anti-inflammatory phenotype, microglia cells with loss of Cav1 increased the release of uPAR 1.4-times compared to untreated cells (highest increase registered). No other analyte was identified with a fold of change equal or superior to 1.5 times under this condition. The apparent increase in IL-4 is compromised by the use of this cytokine to stimulate the cells to achieve the anti-inflammatory state.

To better show the comparative impact of Cav1 status upon microglial behaviour, the cytokine profile was compared between each condition, untreated/inactivated, pro-inflammatory and anti-inflammatory phenotype. The results are shown as the analytes which presented a fold-change equal or superior to 1.5-fold compared with CHME3 Cav1+ve (NT), and presented in **Figure 4.13**.

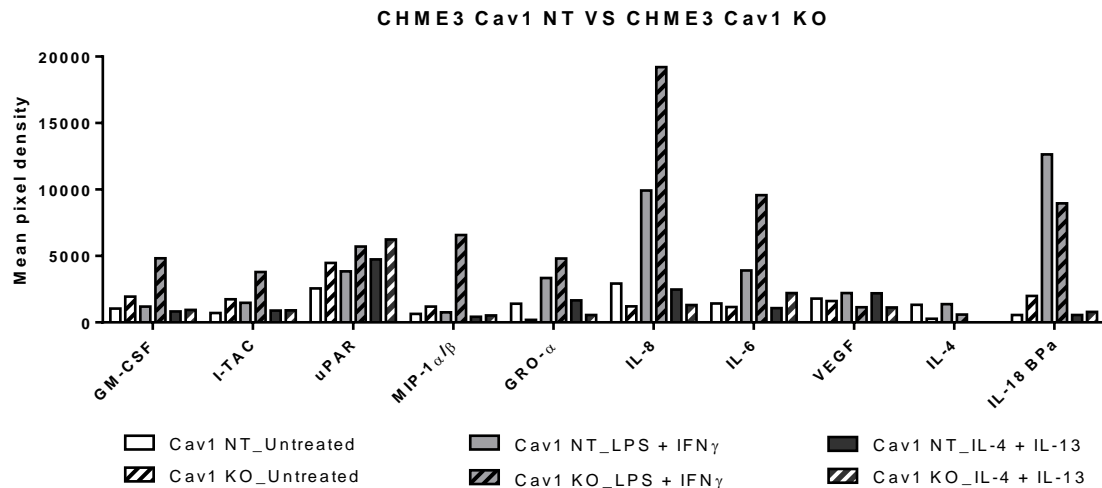


Figure 4.13 – Comparison of CHME3 Cav1 NT and CHME3 Cav1 KO. CHME3 Cav1 NT (full colour) and CHME3 Cav1 KO (colour with transversal lines) cells were stimulated with LPS and IFN- γ (light grey) or with IL-4 and IL-13 (dark grey), for 48 hours. Untreated cells were used as a control (white). Mean pixel density of the analyte with fold-change ≥ 1.5 times compared to control.

The presence of Cav1 in resulted in different secretion behaviours depending on the analyte in consideration.

With respect to:

- pro-inflammatory markers, GM-CSF, I-TAC, uPAR and MIP-1 α/β : the expression of Cav1 was associated with reduced secreted levels of these markers under both basal and pro-inflammatory state, and for UPAR and MIP-1 α/β also under the anti-inflammatory state.

With respect to:

- pro-inflammatory markers, GRO- α , IL-8 and IL-6: the expression of Cav1 was associated with increased secreted levels of these markers under basal state, but dampened to some extent the increased secreted levels of these markers upon stimulation of the cells with LPS/IFN- γ .

With respect to:

- anti-inflammatory marker IL-4 and the pro-inflammatory factor VEGF: the expression of Cav1 was associated with a higher secreted levels in basal,

proinflammatory and anti-inflammatory states (no data for IL-4 with anti-inflammatory stimulation).

With respect to:

- IL-18BP_a, which is an inhibitor of the pro-inflammatory cytokine IL-18 by binding to its receptor: the expression of Cav1 was associated with reduced secreted levels under basal conditions but increased levels in the pro-inflammatory state. Under anti-inflammatory phenotype, independently of Cav1 status, microglia released similar levels.

4.5 Discussion

The immune system in the CNS presents unique features that distinguish it from the periphery. Microglia cells are the main immune regulators in the CNS under healthy status. The immune system of other organs can be populated not only by resident macrophages, but also by circulating macrophages and other immune cells, including T-cells, B-cells, dendritic cells, and neutrophils, which can easily and rapidly access the tissues upon an inflammatory event.

The BBB is a structure highly regulated and which maintains the homeostasis of the CNS, controlling the trafficking of substances, nutrients and cells (Abbott et al. 2010). Microglia arise from the yolk sac during the embryonic development, before the BBB formation, without any contribution from foetal liver or postnatal haematopoiesis. For this reason and under physiological conditions, this is the main immune cell population in the brain (Daneman et al. 2010).

Under physiological conditions, microglia have a long lifespan, represented by a slow renewal rate compared to other monocytes-derived macrophages, 28% per year (Réu et al. 2017), however, under stress conditions, the microglia increase their proliferation (Lawson, Perry, and Gordon 1993). As a response to brain injury, auto-immune diseases or brain tumours, the BBB permeability can be modified and the presence of other immune cells, from peripheral blood migrate into the CNS to play complementary immune regulatory functions to that of the resident microglia (Abbott et al. 2010; Daneman et al. 2010).

Although microglia and macrophages have different origins and distinct markers, their function and phenotype are considered related (Guillemin 2003; Bennett et al. 2016; Dubbelaar et al. 2018; A. M. Young et al. 2019). Clearly within the CNS microglia cells need to be efficiently regulated to prevent exacerbated inflammatory responses and irreparable destruction of the brain tissue. In this context, and in contrasting to other tissue macrophages, under basal a 'healthy' environment microglia display a more downregulated phenotype (Perry and Teeling 2013) with the local environment critical to microglial regulation. Microglia establish cell-cell contact with other neuronal cells, as neurons and astrocytes, via CD200R-CD200, CX3CR1-CX3CL1, CD172a-CD47 and

CD11b-C3, which attenuate the microglial activation (Perry and Teeling 2013; Deczkowska, Amit, and Schwartz 2018). Moreover, cells of the brain release soluble regulators such as CX3CL1 or TGF- β , responsible for dampening microglia responses (Szepesi et al. 2018). The neuronal environment which regulates the microglial phenotype is unique and probably as important as any intrinsic distinction between microglia and macrophage cells. Moreover, many studies of microglia function have used non-human species, e.g rodent cell lines, which will undoubtedly show some digress from human biology, particularly when studying disease. The establishment of human microglia cell lines opened an avenue to explore this field, making possible the genetic manipulation to explore potential key genes.

From the few human microglia cell lines available, the CHME3 (or HMC3) was selected to be used in this project. Not surprisingly, this cell line has been used mainly to study pro-inflammatory related conditions, like HIV infection (Chai et al. 2017), Zika virus (Vanwalscappel, Tada, and Landau 2018), hepatitis C, Japanese encephalitis virus (Gupta et al. 2017) and inflammatory stimulation via SVCT2 via c-Src-Cav1 signalling complex (Portugal et al. 2017). Neurodegenerative disease studies have also used this cell line to study the role of microglia (Hjorth et al. 2013; Zhu et al. 2016). Some studies have now also focused on the tumour immune environment investigating the role of microglia on the support of the glioma stem cells (K. Yu 2015), tumour angiogenesis (Nijaguna et al. 2015), and tumour progression (Shen et al. 2016; Z. Li et al. 2019), and which have suggested a tumour-supportive phenotype for microglia.

The characterization of CHME3 cells has used markers such as CD68, CD11b and IBA1 to prove the microglial identity (Janabi et al. 1995; Etemad et al. 2012). Later on, Dello Russo and colleagues, using HMC3 cells, certified by ATCC (ATCC®CRL-3304), confirmed expression of IBA1, as well as that of other microglial-associated markers such as CX3CR1, CSF-1, P2PY12 and TMEM119 at mRNA level (Dello Russo et al. 2018). It is now accepted that HMC3 and CHME3 cells are the same cell line, presenting the same origin and characteristics. Corroborating these results, our CHME3 cells showed expression of both IBA1 and TMEM119.

Regarding Cav1 expression by microglia cells, and to the best of our knowledge, Portugal *et al.* was the only group reporting this protein in CHME3 cells. This group showed

internalization of the vitamin C transporter SVCT2, mediated by Cav1, triggers a proinflammatory response (Portugal et al. 2017). Studies using mouse cells, BV2 cells, showed a upregulation of Cav1 upon microglia activation, suggesting the downregulation of Cav1 to control the microglial inflammation (Niesman et al. 2013). Aiming to explore the role of Cav1 in human microglia responsiveness, our study examined microglial phagocytosis, cell migration, response to TMZ and response to pro-/anti-inflammatory stimuli. After deleting Cav1 expression, the CHME3 cells retained expression of IBA1 and TMEM119 markers, showing no impact upon the expression of pan-microglial markers.

Phagocytosis by microglia cells is essential during the brain development and homeostasis. It is involved not only in combating micro-organisms but also the clearance of apoptotic or necrotic cells, protein removal (inc. amyloid beta or neuromelanin etc.) and remodelling of neuronal connectivity by engulfment of synapses, axonal and myelin debris (Q. Li and Barres 2017). Phagocytosis is a complex process, where the uptake of particles into cells occurs by an actin dependent mechanism (Aderem and Underhill 1999). Cells must rearrange their cytoskeletal and membrane components to adhere and perform the phagocytosis, and Cav1 might be involved. Caveola have been suggested to play a role in immunity, and may be involved in pathogen-cell interaction and consecutive internalization (Feng et al. 2013). For example, the SV40 enters the cell mainly via Cav1 (Norkin 1999) and the bacteria uptake is coordinated by Cav1 as well (Gadjeva et al. 2010).

In our studies on phagocytosis in CHME3 cells using pHrodo *E. coli* bioparticles, we showed them to have a very poor phagocytic ability of these cell. The CHME3 cells were studied not only under basal status, but also upon activation towards pro-inflammatory and anti-inflammatory phenotypes; the impact of this stimulation making no difference. The maximum recommended incubation time for this assay is 4 hours, however, since no meaningful phagocytic activity was seen, the incubation time was prolonged to 20 hours. Even with this, any significant phagocytic activity by these cells was not observed. Using the same approach in iPSCs (Chapter 6) confirmed our approach was not technically flawed.

We extended the phagocytosis investigation with GFP *M. smegmatis* bacteria and with latex beads coated with fluorescently labelled rabbit IgG (Cayman's Phagocytosis Assay Kit (IgG FITC)) – these further approaches similarly showed the same poor phagocytic outcome (data not shown). Our own work therefore has shown CHME3 cells are poor phagocytes irrespective of Cav1 status and external stimulation with pro-inflammatory factors. Consistent with this Janabi and colleagues showed that immortalized microglia cells display a very low phagocytic activity in comparison with the primary cultures (Janabi et al. 1995). The cellular immortalization with SV-40 was likely to affect microglial cell behaviour and responsiveness to the environment. Infection with SV40 virus potentially resulting in alterations in the transcriptional activity of the host cells, eg. in IFN-stimulated genes (Rathi et al. 2010). To the best of our knowledge, the effect of SV-40 infection upon phagocytosis has not been studied, however, HIV-infected macrophages can present a reduced phagocytosis (Lê-Bury and Niedergang 2018) and polymorphonuclear leukocytes infected with influenza virus present a reduction of 45% in the ingestion of zymosan particles (Debets-Ossenkopp et al. 1982). Nevertheless, one study with uptake of A β ₁₋₄₂ aggregates showed that CHME3 cells are able to undertake phagocytosis in response to IFN- γ alone or IFN- γ /IL-1 β combination (Hjorth et al. 2010). Again, in our own experiments microglial treatment with IFN- γ in combination with LPS, did not affect the phagocytosis of *E. coli* bioparticles, latex beads nor indeed GFP *M. smegmatis* bacteria.

Cellular migration is another important feature of immune response. Microglia need to migrate towards an inflammation site in response to chemokines. It is a process that again depends upon co-ordinated interactions with the cell's environment (ECM and cell-cell) and involving microglia cytoskeletal rearrangement. The presence of Cav1 clearly facilitates the migration of microglia CHME3 cells, with Cav1 deletion significantly impairing migration. Niesman and collaborators showed a similar effect, using BV2 cells and siRNA technology. They showed a decrease of overall migration with the suppression of Cav1 (Niesman et al. 2013). Controversially, Fu *et al* showed the opposite results using THP1 cells, where the Cav1 overexpression inhibited the transmigration of these cells (Y. Y. Fu et al. 2012), suggesting that Cav1 role in migration should be associated with cell type and environment. Although the over-expression approach itself

can lead to off-target pathways which can impact phenotype outcome. In cancer cell models there is increasing evidence that Cav1 promotes cancer cell migration and invasion (Annabi et al. 2004; Senetta et al. 2013).

With microglia cells in the same environment of tumour cells and the role microglia may have in tumour survival, the direct effects of TMZ (first line treatment in GBM) on microglia cells was tested. Meng *et al.* investigating alterations of the glioma tumour microenvironment (TME) related to DDR (DNA damage repair) pathways (that regulate cell stress responses, tissue integrity and TME remodelling), described distinct immune phenotypes in tumours associated with DDR alterations. They reported DDR leading to overexpression of MDK (midkine) mediated by p53, and which was involved in a glioma immunosuppressive environment through promoting the anti-inflammatory phenotype in microglia (Meng et al. 2019). Given TMZ can affect DDR pathways (Yoshimoto et al. 2012), but with a focus strictly on phenotype in relation to Cav1, we investigated if Cav1 has an impact on microglia response to TMZ with respect to cell viability. We found Cav1 promotes microglia CHME3 sensitivity to TMZ, suggesting that the loss of Cav1 in microglia protects the cells from TMZ treatment.

When CNS homeostasis is disrupted, microglia cells will adopt a modified phenotype to address the new functional need. This will involve morphological change and alterations in expression of cell surface receptors and release of soluble factors (Chhor et al. 2013). The analysis of transcriptomic data from human and murine microglia identified a set of activated genes that are specific to microglia and not shared with peripheral macrophages (Butovsky et al. 2014; Hickman et al. 2013). These specific genes allow microglia cells to be regulated in a signal-specific manner, developing functional programmes. Continuous analysis of neuroinflammatory-related signalling pathways and transcription factors has identified NF- κ B/Rel, AP-1, interferon responsive factors (IRF) and STATs as master regulators of inflammatory gene expression under neuro-inflammatory conditions in microglia cells (Kaminska, Mota, and Pizzi 2016).

Taking into consideration the most important signalling pathways and transcription factors and aiming to understand the activation phenotype of CHME3 microglia cells, the analysis of protein levels of STAT1, NF- κ B p65, STAT3 and STAT6, followed by the mRNA levels of some inflammatory-related genes upregulated under pro-inflammatory

or anti-inflammatory phenotype and a cytokine array to identify the secreted products was conducted.

Under a basal status, in both CHME3 'Cav1 NT' and CHME3 'Cav1 KO' cells showed an upregulation of pNF- κ B p65 and pSTAT3 protein levels, together with increased of mRNA levels of IL-1 β , IL-6, CXCL10, TNF- α and TGF- β , suggesting that, independently of Cav1 status, these cells under standard cultured conditions are already showing a basal activation correlated with pro-inflammation.

Niesman *et al.*, using BV-2 mouse microglia cells, showed that the culture condition, free serum media vs 10% serum media, could activate the microglia cells, changing the morphology and protein expression (Niesman et al. 2013). On the other hand, Janabi and collaborators, during the CHME3 cell line establishment, showed that immortalized human microglia presented different phenotype and abilities compared to primary cells (Janabi et al. 1995), suggesting that the viral infection with SV-40 could also modify the microglial phenotype.

It is accepted that the infection of cells by virus often results in a powerful shift in the transcriptional activity of the host cellular genes, reflecting the survival strategies for both host and pathogen. Thinking about the immune population, where cells are responsible to identify and act against pathogens, the immunological reaction can be even more dramatic (Chai et al. 2017; Vanwalscappel, Tada, and Landau 2018; Gupta et al. 2017). A study with mouse embryo fibroblasts (MEFs) showed that the SV40 transformation activated the interferon pathways and pSTAT1, and upregulated the immune response-related genes (Rathi et al. 2010). Asamitsu and collaborators in human fibroblasts demonstrated a constitutive upregulation of NF- κ B in SV-40-transformed cells (Asamitsu et al. 1999). In other studies, STAT3 was evaluated after cellular transformation by oncogenes, not only SV-40, but also RAS, v-Src and EGFR, showing STAT3 constitutively activated (Garcia et al. 1997; Looyenga et al. 2012). Comparing with the protein levels presented by THP1-derived macrophages, a cell line established independently of oncovirus transformation, the phosphorylated protein levels of all proteins studied were almost undetected under basal condition (**APPENDIX III – THP1-derived macrophages**). These studies and the CHME3 obtained data suggest

that SV-40 cellular immortalization together with culture conditions seems to promote the activation of CHME3 in basal status.

The pro-inflammatory state is the best phenotype characterized in microglia. Most of the studies are related with situations where pro-inflammation is the key environment for microglia cells, as neurodegenerative diseases, strokes, viruses, or bacterial infections. The stimulation of CHME3 microglia cells with LPS and IFN- γ , which impulses cells for a pro-inflammatory phenotype, induced: the protein expression of STAT1 and NF- κ B; the mRNA expression of IL-6, IL-12, CXCL10, TNF- α and IL-10; and the secreted products GRO- α , IL-6, IL-8, IL-18 BPa, IP-10/CXCL10, RANTES and uPAR (with the exception of IL-10 and IL-18 BPa, the remaining factors are related with pro-inflammation). All the pro-inflammatory markers analysed by PCR were represented in the cytokine array. Interestingly, only levels of IL-6 and CXCL10 were identified in the supernatants. mRNA levels of IL-1 β , IL-12 and TNF- α expressed were relatively low, justifying the low levels present in the supernatant, likely below to the sensitivity of the cytokine array. Moreover, the levels of IL-6 and TNF- α were identified by Janabi *et al.* upon microglia challenge with LPS. However, it was described that all clones immortalized, including CHME3, were less responsive to LPS in comparison to primary cultures (Janabi *et al.* 1995). Observing the mRNA levels obtained in THP1-derived macrophages (**Supplementary figure III. 3**), levels of IL-1 β , IL-12 and TNF- α were considerably higher upon 48 hour treatment with LPS and IFN- γ , suggesting again the poor responsiveness to stimuli of CHME3 microglia cells. Once more, one possibility to explain this phenomenon is the SV40 infection that may modulate the signalling pathways (Butin-Israeli, Drayman, and Oppenheim 2010). The remaining factors identified by PCR and cytokine array were already identified upon microglial activation, being key elements to promote cytotoxicity (IL-1 β , IL-6, IL-8, IL-12 and TNF- α), chemoattraction and differentiation of other immune cells (IL-1 β , IL-6, IL-8, IL12, CXCL10, RANTES and GRO- α), to improve microglia migration (uPAR) and to balance the pro-inflammation (IL-10 and IL-18 BPa) (Chhor *et al.* 2013; Washington *et al.* 1996; Q. Yu *et al.* 2018; Filipovic, Jakovcevski, and Zecevic 2003).

The anti-inflammatory phenotype is the least explored in microglia. Since microglia is tightly regulated under basal state, they present a stronger anti-inflammatory

phenotype, because of the interaction with other brain cells that limits the reaction of microglia (Chhor et al. 2013). However, after infection, in order to balance pro-inflammatory signalling pathways, cells utilize a variety of mechanisms, including concurrent anti-inflammatory factors, to resolve the inflammation, re-establish the homeostasis and restore the healthy environment (Orihuela, McPherson, and Harry 2016). In the brain tumour environment, particularly in malignant gliomas, microglia present an anti-inflammatory phenotype that contributes to suppress the activation of other immune cells, and promote the tumour progression (Yin et al. 2017).

Intending to study how CHME3 cells behave under an anti-inflammatory phenotype, the microglia were stimulated with IL-4 and IL-13. After the challenge, cells increased more than 30-times the levels of STAT6, however they failed to upregulate the mRNA expression of the anti-inflammatory markers analysed. Regarding the secreted products, a slight increase of DKK-1, MIF and uPAR was identified and the remaining analytes were secreted at low levels or not secreted at all. The pSTAT3 is correlated with an anti-inflammatory status, however it is activated by IL-10R by IL-10 stimulation. Since the activation was performed with IL4 and IL-13, which interacts only with IL-4R and IL13R, this may justify the absence of STAT3 activation observed. Nevertheless, THP1-derived macrophages, were able to upregulate the pSTAT3 with IL-4 and IL-13 stimulation (**Supplementary figure III. 2**), most likely by positive feedback of IL-10 production triggered by the original stimulation. CHME3 failed to produce IL-10, which was not detected on the cytokine array, and the mRNA were relatively low. Another explanation for unsuccessful activation of STAT3 in CHME3 cells is once again the SV-40 infection. SV-40 infection can *per se* upregulate their levels, however, since the STATs analysis was not performed in the primary cells, used for the immortalization, it is hard to correlate the upregulation of STAT3 with a viral infection. Once again, comparing with THP1-derived macrophages, the anti-inflammatory challenge that was not able to induce an increase of the mRNA levels of anti-inflammatory related marker in microglia, did increase the levels of TGF- β , IL-10, CCL22, CD200R and CD206 in macrophages (**Supplementary figure III. 4**), suggesting a lack of anti-inflammatory response by CHME3 cells.

The direct effect of anti-inflammatory cytokines was not analysed in CHME3 cells (Dello Russo et al. 2018). However, levels of IL-10 (by Elisa), CD206, CD200R and CD163 (by IF) were detected in CHME3, but the increase was not observed when Hjorth and colleagues activated microglia cells with A β ₄₂ protein (Hjorth et al. 2013). Analysing all the secreted products identified (low levels), the DKK-1 is a potent inhibitor of canonical Wnt signalling, that in neurodegeneration reinforces the beneficial effect of this pathway (Caricasole et al. 2004), and is associated with tumour growth, angiogenesis and poor prognosis in gliomas (Mostofa et al. 2017). MIF and uPAR are related with pro-inflammatory events, however they have been related with tumour progression in cancer as well (Mostofa et al. 2017).

The impact of Cav1 in microglial phenotype was not thoroughly investigated, however, since it can be involved in pathway signalling, we hypothesise its involvement in microglia response to stimuli. Some studies in sepsis demonstrate that mice deficient in Cav1 were more susceptible to polymicrobial septic death than wild type mice, suggesting Cav1 as a negative regulator of eNOS via direct internalization and posterior inhibition of NF- κ B (Feng et al. 2010, 2013). Actually, upon Cav1 deletion in CHME3 cells, it was possible to notice a slight decrease of pNF- κ B upon LPS and IFN- γ challenge (no differences were observed in pSTAT1), together with a downregulation of IL-12, TNF- α and IL-6. Codrici and colleagues showed that mice Cav1^{-/-} had a reduction of pro-inflammation (Codrici et al. 2018b). On the other hand, Medina *et al.*, using another mouse model, and Shimato *et al.*, using monocytes, demonstrated that inhibiting the Cav1 protein could restore the myeloid cell function, upregulating the levels of INF- γ , TNF- α and IL-6 (Medina et al. 2006; Shimato et al. 2013). Looking at the secreted levels, the suppression of Cav1 led to increased pro-inflammatory related markers GM-CSF, I-TAC, MIP-1 α/β , IL-6 and IL-8, corroborating Medina's and Shimato's works. This contradictory result may represent some variability, since the cytokine array was only performed once in CHME3 cells and may not represent all microglial clones generated and analysed.

Regarding the impact of Cav1 on anti-inflammatory microglial phenotype, if CHME3 Cav1 NT already presented problems to achieve this status, for CHME3 Cav1 KO cells the behaviour was similar. The protein levels of pSTAT3 increased marginally with IL-4 and

IL-13 treatment. However, the levels of pSTAT6 (which were upregulated with stimuli), were slightly downregulated compared with cells that were expressing Cav1. The mRNA analysis showed that Cav1 KO cells had a comparable performance contrasted to Cav1 positive cells, with slightly lower levels of CCL22 and CD200R. Finally, from the secreted products, only uPAR showed a marginally increased. Similar results, using glucocorticoids in mouse models, showed that Cav1 can interact with anti-inflammatory receptors, but it was dispensable for the anti-inflammatory response in lung inflammation (Caratti et al. 2019).

Independently of Cav1 status, it was observed that CHME3 cells secreted elevated levels of Serpin-E1 or plasminogen activator inhibitor type 1 (PAI-1), which plays a role on the regulation of fibrinolysis, remodulation of the ECM, cell migration, and invasion of tumour cells. PAI-1 is upregulated under inflammation, promoting the migration of microglia cells and inhibiting microglial phagocytosis of zymosan particles (Jeon et al. 2012). By studying the effect of different influenza virus into immune cells, it was observed an upregulation of PAI-1 with the viral infection, suggesting an important mechanism of the antiviral response (Dittmann et al. 2015). Regarding the SV-40 large T antigen the same upregulation of the mechanism may be involved, however further experiments need to be conducted.

In **summary**, the immortalization of primary microglia cells with SV-40 large T antigen may have affected microglia's behaviour and phenotype, and led to the upregulation of Cav1 in this cell line. Because Cav1 was not studied on primary cells to generate CHME3 cell line, we do not know if the upregulation of this protein was present in the primary population or if the overexpression was a result of SV-40 large T antigen infection, as observed in other cell lines by Stergiou and collaborators (Stergiou et al. 2013). CHME3 cells, independently of Cav1 status, presented poor phagocytosis ability, some degree of activation under basal status and struggled to upregulate the anti-inflammatory markers in response to an anti-inflammatory stimulus. The presence of Cav1 in these cells seems to promote the migration, sensitivity to TMZ and upregulation of the pro-inflammatory response.

CHAPTER 5 –
GBM ENVIRONMENT AND CHME3 CAV1
KNOCKOUT

5.1 Introduction

GBM is the most common malignant primary brain tumour, despite decades of research, the new treatments tested in clinical trials are failing, and as a result the overall survival rate for these patients remains very poor. GBM presents a tremendous heterogeneity and is constituted by tumour and non-tumour cells that contribute to the formation of tumour-specialized niches (Shao et al. 2015). These niches together with the intra-tumour heterogeneity are a significant reason for the lack of success of targeted therapies. Attempts to downregulate a pathway in a distinct tumour sub-region seem to permit another pro-tumour signalling to predominate, leading to recurring drug resistance. Understanding the specialized cell-cell communication within the tumour environment will provide important mechanistic basis to identify other potential target mechanisms including those for combined therapeutics.

GBM tumours are known to be extremely immunosuppressive. Microglia and macrophages, constitute the main immune population in these tumours, and can contribute up to 50% of the tumour mass (Ransohoff and Cardona 2010). Microglia cells are the exclusive myeloid cell population in the healthy CNS, and these cells are likely to be the predominant immune cell population to interact with the tumour cells during the first steps of the tumour development. As the tumour progresses, other immune cells, mostly macrophages, cross the BBB and infiltrate the tumour. The role of microglia versus macrophages in brain tumours is still unclear, but we are beginning to see discriminatory markers, as TMEM119, can distinguish both populations and help to address the key biological questions pertinent to their distinct roles.

The role of Cav1 in tumours has been studied for several years, and the expression pattern is controversial depending on the tumour type. In GBM, Cav1 is associated with tumour progression and poorer prognosis (Pu et al. 2019; Moriconi 2019); of note - the inhibition of Cav1 in microglia seems to restore the myeloid function in the GBM (Shimato et al. 2013).

5.2 Aim

The aim of this chapter is to study the role of CHME3 cells in an in-vitro GBM tumour environment, specifically exploring the impact that Cav1 in the microglia cells may have. To explore the GBM cell-microglia cell interaction studies were performed focusing on the gene and protein expression for key genes in microglia activation, and secretome profiling for products associated with cellular proliferation, migration, and invasion.

5.3 Methods

5.3.1 General Methods

The microglia cells CHME3 Cav1 NT and CHME3 Cav1 KO, the GBM cell lines U87, UP007 and UP029, and the APC – 34D6 were used in this chapter. These cells were cultured following the protocols described in **Chapter 2, section 2.2 - Cell culture maintenance**. Human astrocytes were differentiated from APC following the protocol described in **2.2.1 - Astrocytes progenitors' cells and astrocytes differentiation**. The astrocytes were used as a control as a non-tumour cell for co-culture experiments.

CHME3 Cav1-NT (Cav1 +ve) and CHME3 Cav1-KO (Cav1 -ve) were co-cultured with GBM or astrocytes cells using Transwell systems (**2.6 – Co-culture System of GBM cell lines with CHME3**) or pre-labelled with Vybrant dyes (**2.12 – Cellular co-cultures – Vybrant™ dyes**) and co-cultured as a spheroid. Astrocytes were used as a control.

To explore the impact of the GBM co-culture environment on microglia cells, gene expression was undertaken by qRT-PCR (**2.7 – qRT-PCR**), protein expression undertaken by Western Blot (**2.8 – Western Blot**) and secretome profiling by cytokine array (**2.10 – Cytokine array**). For the influence of Cav1 status on GBM behaviour, the migration was accessed by Transwell (**2.11 – Transwell migration and invasion assay**), proliferation was performed after the co-culture in Transwell system by cell counting, and GBM invasion assessed using a 3D spheroid invasion assay described in **2.13 – Spheroid invasion assay**, and by using a confrontation assay.

Spheroid Confrontation assay

In order to investigate cell interactions, spheres were formed with GBM and Astrocytes or CHME3 (Cav1+ve or Cav1-ve) cells (500:500) with the different cell populations labelled with DiD, DiL or DiO, respectively, and following the protocol previously described in **2.12**. Additional spheres of 20,000 cells were formed, composed of astrocytes only. After 4 days of sphere formation, one sphere constituted by GBM plus astrocytes or microglia was placed together with one astrocyte sphere and tracked with epifluorescence microscope immediately upon the start of the experiment and thereafter every 24 hours for 3 days.

LightSheet microscopy

Upon invasion and confrontation assay, some spheres were fixed in 4% PFA for 1 hour at RT in a rocking plate, washed 3 times with PBS for 5 minutes at RT and counter stained with DAPI (0.5 µg/ml) for 15 minutes, followed by 3 additional washes with PBS for 5 minutes. For the invasion assay, the Matrigel was preserved as much as possible to conserve the invasive edge. Samples were embedded within 1% (w/w) agarose (low melting temperature) prepared in TAE buffer, in capillaries size 3 (~1.5 mm diameter) for the confrontation assay or in 1 ml syringes for the invasion assay. After sample preparation, the capillary or syringe was loaded, positioned in the centre of the microscope and imaged using water immersion chamber with 5x/0.1 illumination and 10x/0.5 W Plan Apo; WD = 3.7mm (water immersion) detection objectives in Zeiss Lightsheet Z.1. Data was acquired with activated pivot scan, dual-sided illumination, and online fusion. Properties of the acquired data: 0.7x zoom, 16bit, 1920x1920px image size and minimum z-stack interval (approximately 0.33 x 0.33 x 0.5 µm). Green, orange, and red fluorophores were excited using 488 nm, 561nm and 638 nm laser, respectively. Filters were used in sequential dual tracks for multi-colour images with GFP – red (beam splitter SBS LP 560; emission filters BP 505-545 and LP 660) and Dapi – orange (beam splitter SBS LP 490, emission filters BP 420-470 and BP 525-565). All image processing was executed using Arivis Vision4D software.

5.4 Results

5.4.1 Co-culture of CHME3 cells with GBM: impact on microglial proliferation and migration

To investigate the impact of the GBM cells on microglia cell proliferation, microglia cells were co-cultured with three different GBM cell lines (ratio 500:500), U87, UP007 or UP029, for 48 hours, using a Transwell 0.4 μm system, which allows for cell crosstalk by paracrine signal/soluble factors that were released into the medium; there was no direct cell-cell contact.

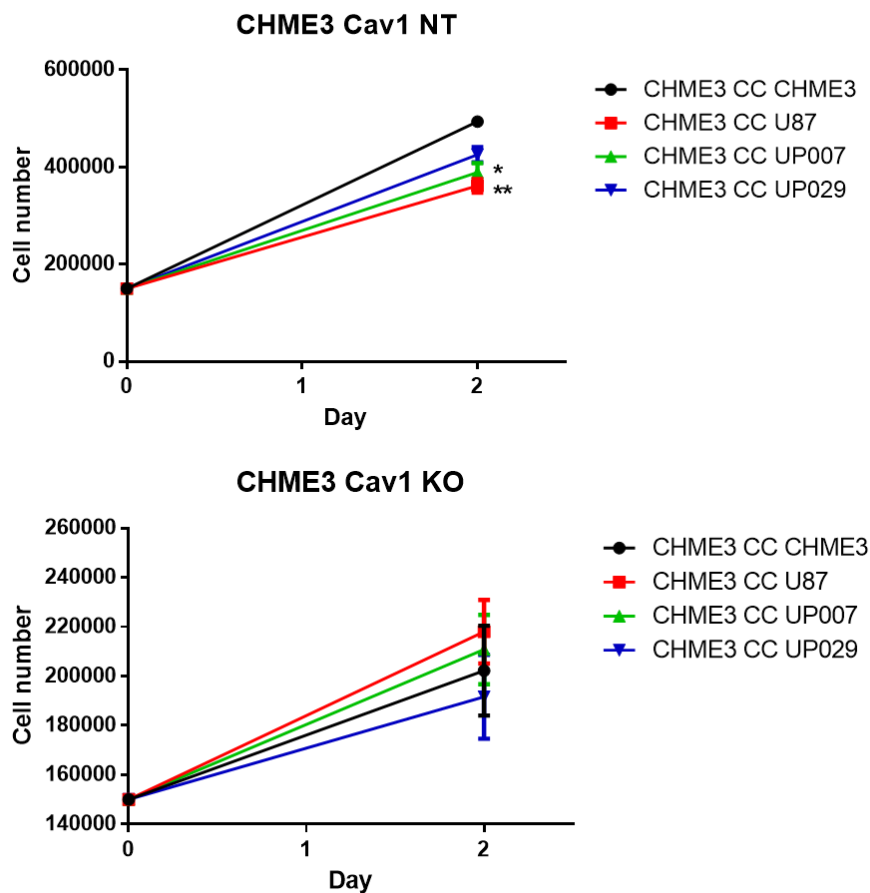


Figure 5.1 – Impact of GBM CC on microglial proliferation. 150,000 cells of CHME3 Cav1 NT or CHME3 Cav1 KO were seeded in a 6-well plate, and 150,000 cells of CHME3 Cav1 NT or CHME3 Cav1 KO (Black), U87 (red), UP007 (green) or UP029 (blue) were seeded into the insert and left to adhere for 24 hours. In the following day, the insert was placed together with the microglia cells and allowed to be in co-cultured for an additional 48 hours. After that, the cells were detached and counted using the Countess™ II FL Automated Cell Counter. Values represent the mean of 4 individual experiments \pm SEM *: $p < 0.05$; **: $p > 0.01$ when compared to CHME3 CC CHME3, Kruskal-Wallis, Dunn's multiple comparisons test.

The co-culture (CC) of CHME3 Cav1-NT (Cav1+ve) cells with each of the different GBM cells trend to reduce the proliferation of CHME3 microglia cells. The decrease in proliferation was more pronounced upon CC with U87 and UP007, $p < 0.01$ and $p < 0.05$, respectively. With Cav1 KO (Cav1-ve) microglia cells, the proliferation rate of the CHME3 was profoundly reduced by the knock-out alone compared to CHME3 Cav1 NT cells. Perhaps not surprising therefore, the impact of GBM CC on CHME3 Cav1-KO was less clear, with no meaningful significant differences observed in **Figure 5.1**.

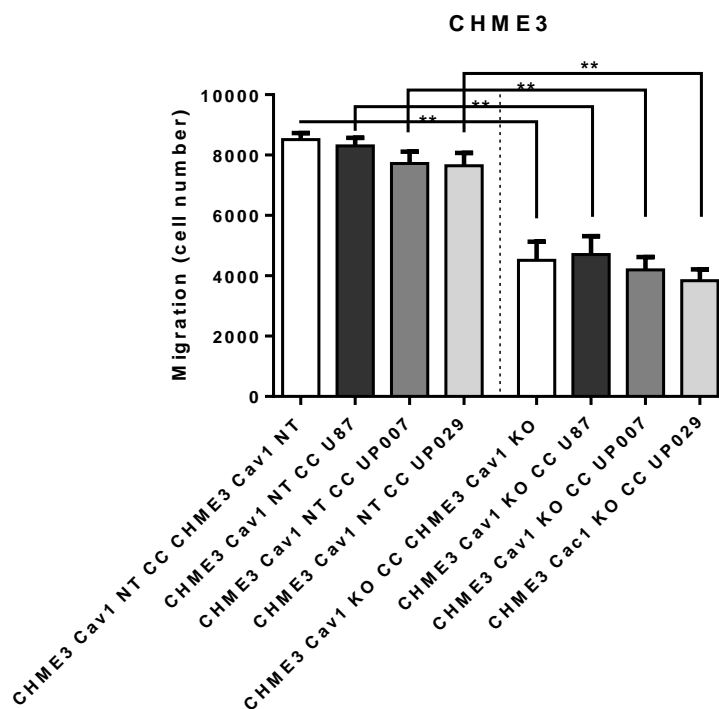


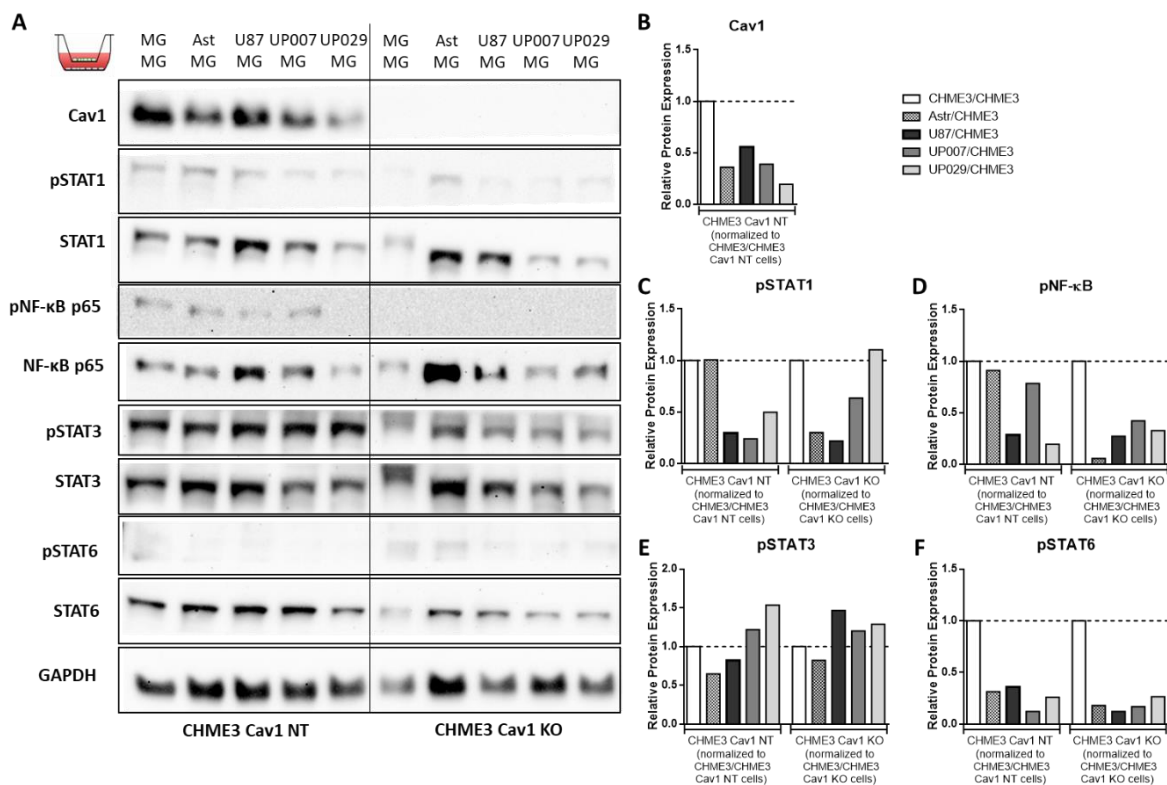
Figure 5.2 – Impact of GBM CC on microglia cell migration. CHME3 Cav1 NT and CHME3 Cav1 KO were co-cultured with U87, UP007 and UP029 for 48 hours, using a transwell system (0.4 μm). After that, using another transwell system (8 μm), microglia cells were seeded into the upper chamber in media without FBS. Medium with FBS was used as a chemoattractant in the lower chamber. The cells were allowed to migrate for 16 hours and then were counted. Mean of number of cells from 4 independent experiments \pm SEM. ** $p < 0.01$ when compared to respective Cav1 NT cells, using Mann-Whitney test.

The impact of GBM CC on the migration ability of the microglia cells was accessed after the microglia had been in CC with the GBM cell lines for 48 hours. After this, microglia were collected for a single cell migration assay using a separate Transwell system (8 μm , 16 hours).

Firstly, CHME3 Cav1 KO cells (Cav1-ve) showed approximately half the migration capacity of the corresponding CHME3 Cav1 NT cells (Cav1+ve) across all of the treatments, **Figure 5.2**. Similar results, CHME3 Cav1 NT vs CHME3 Cav1 KO, were obtained and discussed in the Chapter 4. The GBM CC itself did not affect the migration of microglial cells whether the CHME3 expressed Cav1 or not.

5.4.2 Co-culture of CHME3 cells with GBM: impact on microglial phenotype

To study the effect of GBM CC on microglia phenotype, CHME3 Cav1 NT and CHME3 Cav1 KO cells were co-cultured with GBM cells at a ratio of 1:1, using a Transwell system (0.4 μm pore). Astrocytes were used as a non-tumour cell control. Following 48 hours of co-culture CHME3 cells were harvested and assessed for the phosphorylated forms of proteins widely recognised as involved in microglia activation and for the mRNA levels of pro-inflammatory and anti-inflammatory related genes.



The CC of CHME3 Cav1-Cav1 NT cells (Cav1+ve) with U87, UP007 and UP029 cells led to an overall downregulation of pSTAT1, pNF- κ B and pSTAT6 in the microglia cells when comparing to the control of the corresponding CHME3 cells alone. pSTAT3 showed a slight increase when CHME3 Cav1 NT cells were co-cultured with UP007 and UP029 cells (**Figure 5.3**). Regarding Cav1, compared to the CHME3 control alone, it was noted that GBM's CC was associated with a trend for decreased Cav1 levels expressed by the microglial cells even when GAPDH was taken into account.

For CHME3 Cav1 KO cells (Cav1-ve), again a general downregulation of pSTAT1, pNF- κ B and pSTAT6 was observed. Not dissimilar to the CHME3-NT cells, the pSTAT3 in the CHME3-Cav1 KO (Cav1-ve) showed either no change or a slight upregulation under the GBM CC conditions. The CHME3 Cav1 KO cells appeared to present lower levels of these proteins (even with GAPDH as the reference) compared to the CHME3 cells that expressing Cav1, suggesting that Cav1 has some role in responsiveness in a GBM environment. To note: control astrocytes also downregulated the levels of pSTAT3 and pSTAT6 in CHME3 Cav1 NT (Cav1+ ve) and CHME3 Cav1 KO (Cav1-ve) cells.

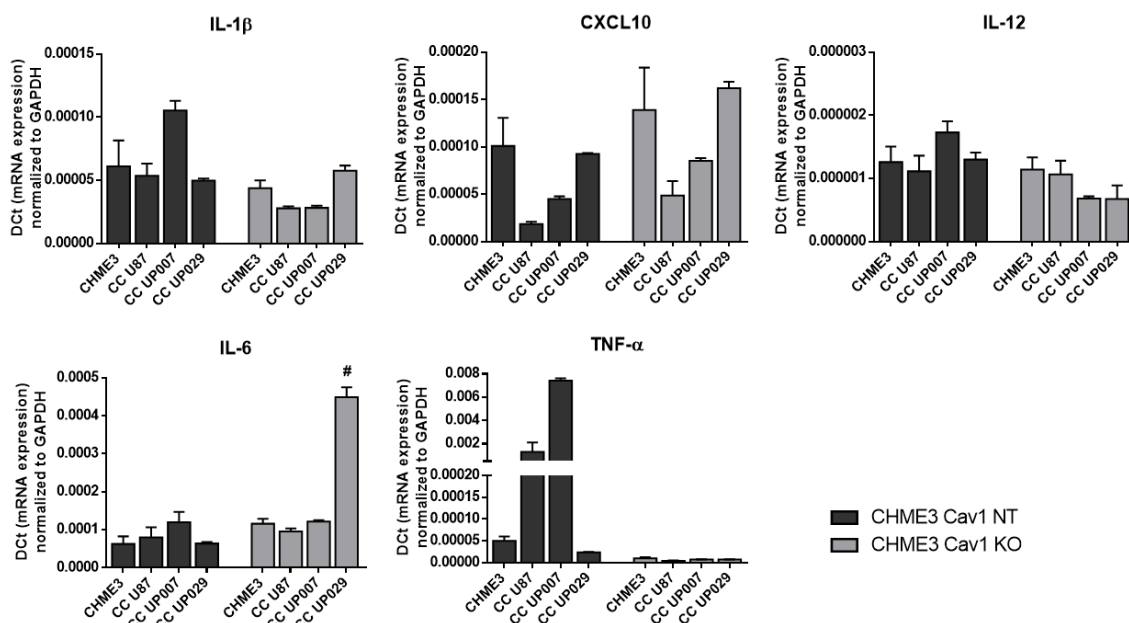


Figure 5.4 – Impact of GBM environment on CHME3 cells – Pro-inflammatory-related genes. IL-1 β , IL-6, IL-12, CXCL10 and TNF- α expression by CHME3 Cav1 NT (black) or CHME3 Cav1 KO (grey) analysed by qRT-PCR. Microglia cells were co-cultured with U87, UP007 and UP029 in a transwell system (0.4 μ m), for 48 hours. Cells without interference of GBM were used as control. Bars represent mean \pm SEM of 2 independent experiments. #: $p < 0.05$ compared to CHME3 Cav1 KO cells, Kruskal-Wallis, Dunn's multiple comparison test.

We next examined the pro-inflammatory responsiveness of CHME3 cells when in a GBM CC environment through qRT-PCR analysis of the microglia (**Figure 5.4**). We observed that CHME3 Cav1 NT (Cav1+ve) cells, CC with each of the GBM cell lines retained a consistent basal mRNA expression for IL-1 β , IL-6 and IL-12, with none of the GBM lines therefore able to stimulate the expression of the genes. However, with respect to microglia (**Figure 5.4**), the CC with U87 and UP007 led to a significant upregulation in the CHME3 Cav1 NT (Cav1+ve) cells. For CXCL10 the CC with U87 and UP007 led to a significant downregulation; UP029 elicited no alteration compared to baseline control.

For CHME3 Cav1 KO (Cav1-ve) microglia (**Figure 5.4**), mRNA levels of IL-1 β , IL-12 and TNF- α were not responsive to CC with any of the GBM cell lines. The only changes were CXCL10 which showed a slight decrease under pressure from the CC with U87 and UP007, and IL-6 which increased substantially upon CC with UP029 stress, (**Figure 5.4**)

Most profound was the near complete downregulation of TNF- α in CHME3 cells lacking Cav1 expression (CHME3 Cav1-KO).

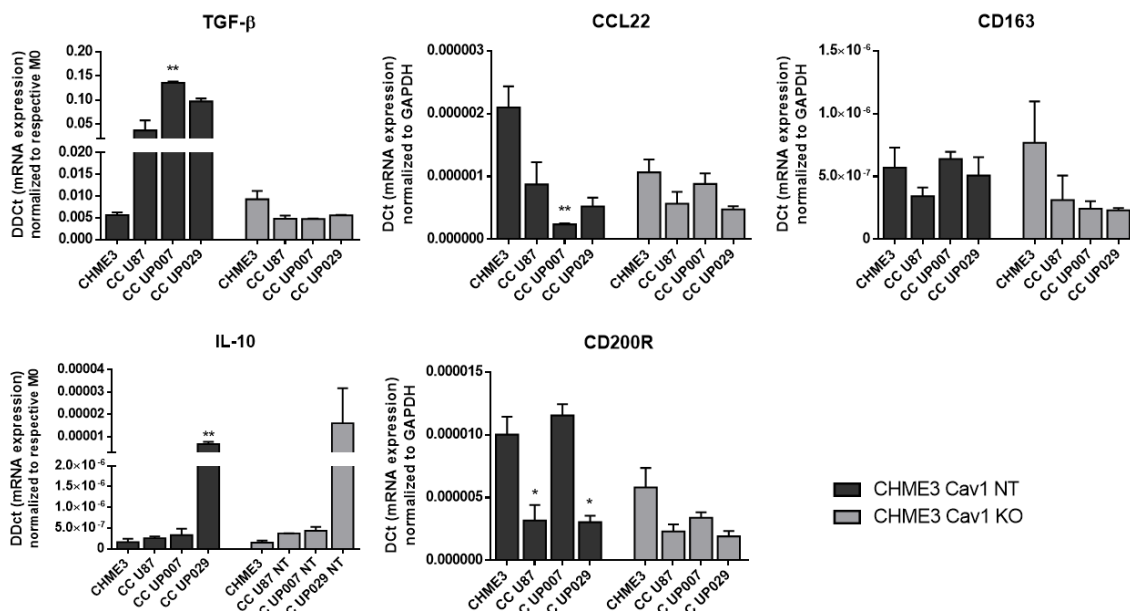


Figure 5.5 – Impact of GBM environment on CHME3 cells – Anti-inflammatory-related genes. TGF- β , IL-10, CCL22, CD200R and CD163 expression by CHME3 Cav1 NT (black) or CHME3 Cav1 KO (grey) analysed by qRT-PCR. Microglia cells were co-cultured with U87, UP007 and UP029 in a transwell system (0.4 μ m), for 48 hours. Cells without interference of GBM were used as control. Bars represent mean \pm SEM of 2 independent experiments. *: $p < 0.05$, **: $p < 0.01$ compared to CHME3 Cav1 NT cells, Kruskal-Wallis, Dunn's multiple comparison test.

With respect to the anti-inflammatory panel (**Figure 5.5**) the most significant observation is the induction of TGF- β in the CHME3 Cav1 NT (Cav1+ve) cells by all three GBM cell lines, an outcome not replicated in the corresponding Cav1-ve cells despite similar basal levels of TGF- β . The levels of CCL22 appeared suppressed by the stress of GBM CC. Thereafter varying changes were seen dependent upon the GBM cell line. An increase of IL-10 was seen with UP029 and a decrease in CD200R under U87 and UP029 CC. CD163 remained unchanged under the GBM environment.

In CHME3 Cav1 KO cells (Cav1-ve), little change was seen except for a slight increase of IL-10 that was stronger for the UP029 cells.

5.4.3 Co-culture of CHME3 cells with GBM: impact on secretome

To study the impact of the GBM environment on the secreted products released by the CHME3 microglia (either the Cav1+ve and Cav1-ve cells) we co-cultured the CHME3 cells with the GBM cell lines U87 cells for 48 hours using the Transwell system previously described, and assessed the secretome using by Cytokine Array. CHME3 'Cav1 NT' or CHME3 'Cav1 KO' cells that were cultured without influence of GBM served as control. After the completion of the co-culture, the media supernatants were collected to evaluate the respective content using a membrane based assay, evaluating 105 cytokines, chemokines and growth factors involved in immune response. A summary of the entire secretome is illustrated in **Supplementary figure VI. 2- Appendix VI**.

A secretome example from co-cultures where microglial cells Cav1+ve is, CHME3 'Cav1-NT', is shown in **Figure 5.6-B** and the secreted products with fold-change (FC) higher than 1.5 compared with microglia alone are represented in the (**grey bars**) of **Figure 5.6-C**.

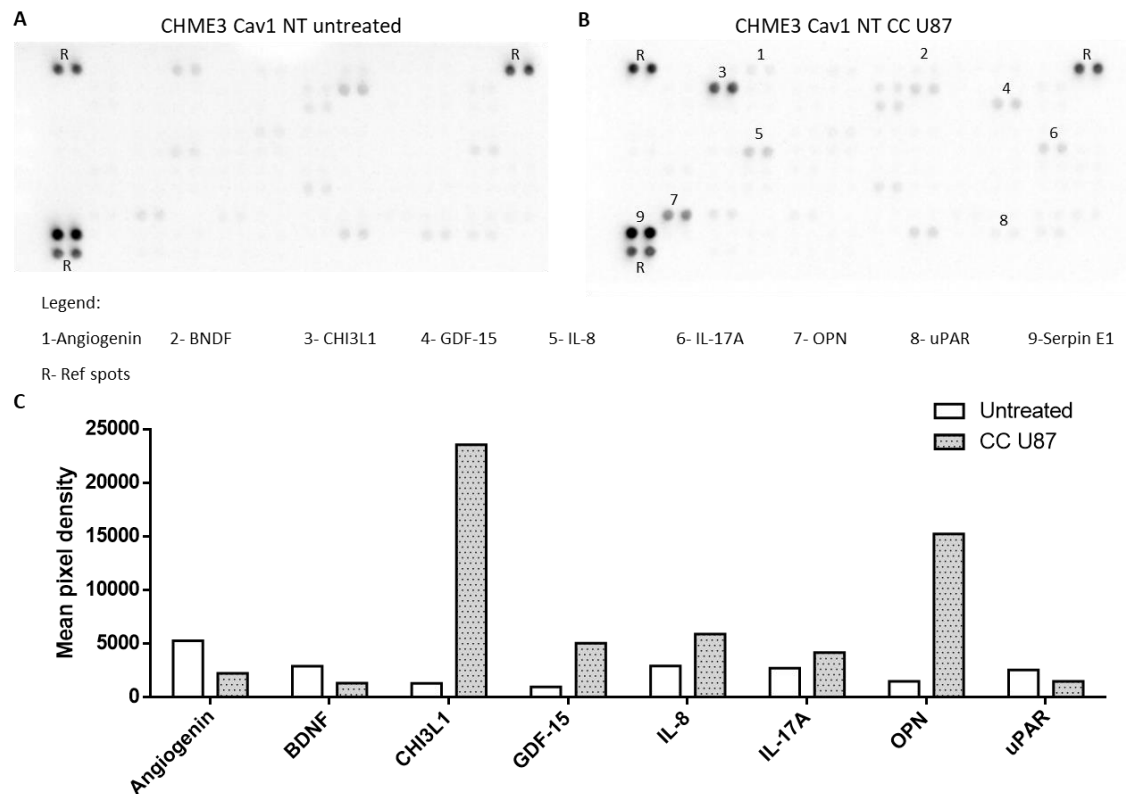


Figure 5.6 – Secretome of CHME3 Cav1 NT under GBM co-culture. CHME3 Cav1 NT were co-cultured with U87 cells for 48 hours, using a Transwell system. Supernatant collected from cells without interference of the GBM was used as a control (Untreated). The supernatants were collected for downstream analysis. Mean pixel density graph of the analyte visible on the membrane and with fold-change ≥ 1.5 times. N= 1 experiment.

Compared to CHME3 cells that were cultured without interference of GBM cells (Untreated), the CHME3 Cav1-NT / U87 co-cultured model showed a decrease in angiogenin, BDNF and uPAR and with an increase in CHI3L1, GDF-15, IL-8, IL-17A and OPN. The elevated presence of Serpin E1 (shown on the membrane only – spot 9) was previously identified in Chapter 4 and it continues to show elevated levels in this experiment (**Figure 5.6 – A and B**) suggesting that microglia cells is the major contributor for this molecule. These factors can be released for both microglia and/or U87 cells. Other factors beyond those shown in Figure 5.6 did not show alterations (co-culture conditions vs CHME 3 alone) greater than 1.5-times, however, they are described in the **Supplementary figure VI. 2-**, in **Appendix VI**.

The products released upon in co-culture of CHME3 Cav1-KO (Cav1-ve) and U87 cells are illustrated in **Figure 5.7-B** and the analytes with FC higher than 1.5 are represented in **Figure 5.7-C**.

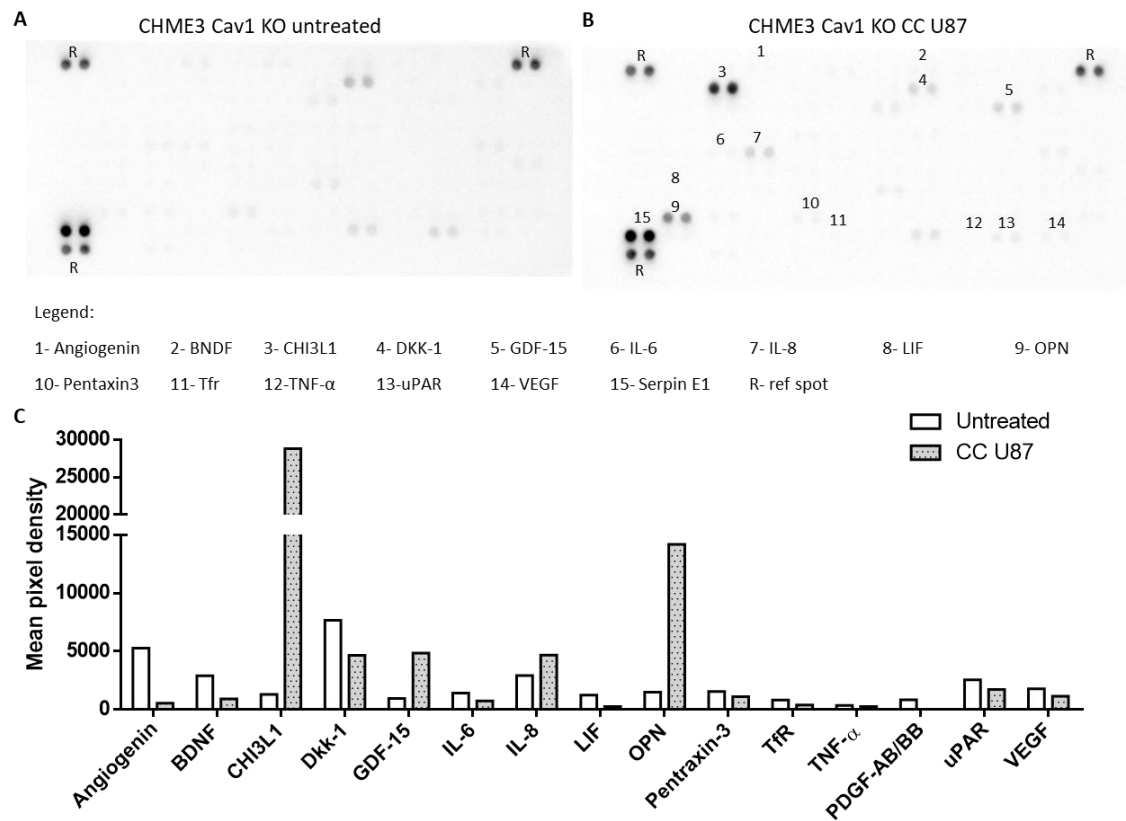


Figure 5.7 – Secretome of CHME3 Cav1 KO under GBM co-culture. CHME3 Cav1 KO were co-cultured with U87 cells for 48 hours, using a transwell system. Supernatant collected from cells without interference of the GBM was used as a control (Untreated). The supernatants were collected for downstream analysis. Mean pixel density graph of the analyte visible on the membrane and with fold-change ≥ 1.5 times. N=1 experiment.

Compared to CHME3 ‘Cav1 KO’ cells (Cav1-ve) that were cultured alone (Untreated) without influence of GBM cells, the CHME3 ‘Cav1 KO’ in co-culture with U87 cell presented lower levels of Angiogenin, BDNF, Dkk-1, IL-6, LIF, Pentraxin-3, Tfr, TNF- α , PDGF-AA/BB, uPAR and VEGF. On the other hand, the co-culture upregulated the levels of CHI3L1, GDF-15, IL-8 and OPN. Additional factor not reaching a FC or 1.5 are presented in the **Supplementary figure VI. 2- Appendix VI.**

The impact of Cav1 within the GBM environment was accessed by direct comparison between the products identified in CHME3 ‘Cav1 NT’ / U87 co-cultures (**Figure 5.8-A**) and CHME3 ‘Cav1 KO’ / U87 co-cultures (**Figure 5.8-B**). The molecules with FC higher than 1.5 are represented in **Figure 5.8-C.**

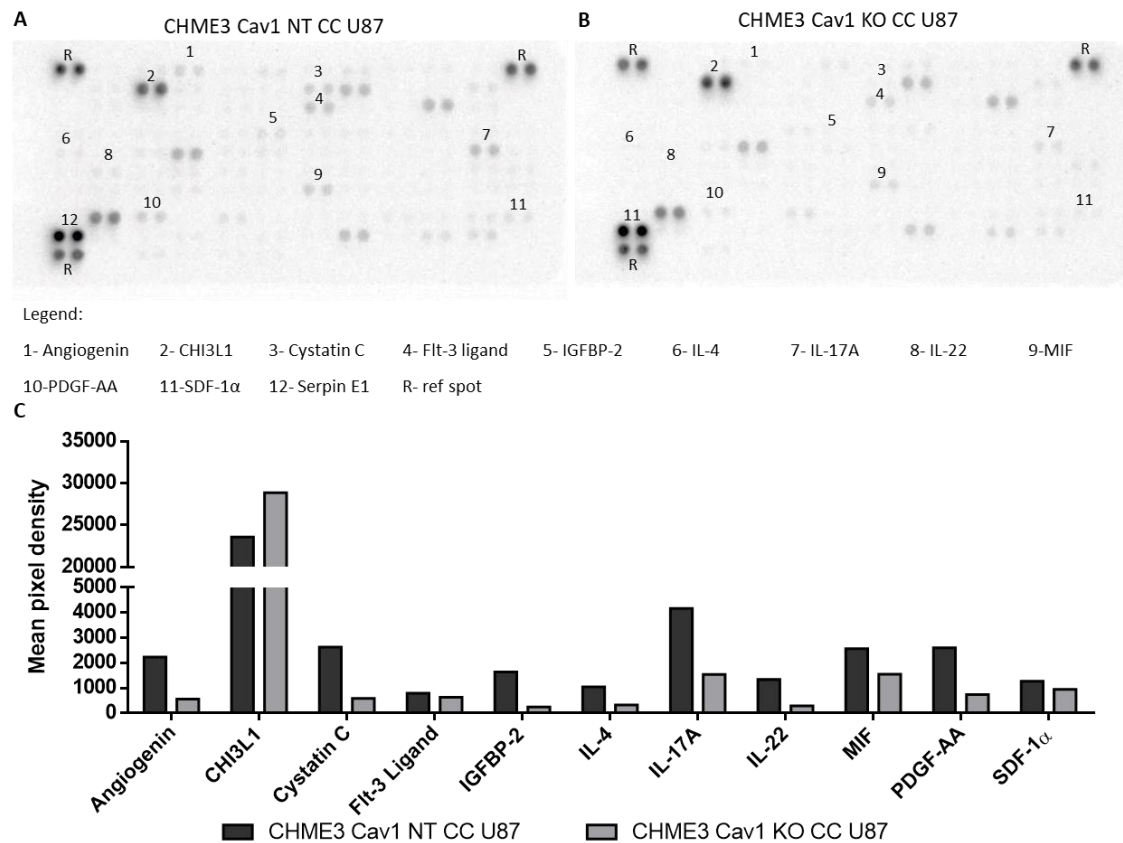


Figure 5.8 – Comparison of CHME3 Cav1 NT and CHME3 Cav1 KO under GBM co-culture. CHME3 Cav1 NT and CHME3 Cav1 KO were co-cultured with U87 cells for 48 hours, using a transwell system. The supernatant was collected for downstream analysis. Mean pixel density graph of the analyte visible on the membrane and with fold-change ≥ 1.5 times. N= 1 experiment.

Where significant differences were seen, introduction of the Cav1 deletion (CHME3 Cav1-KO) was in the main associated with reduced factors in the medium with reduced levels of angiogenin, cystatin C, Ftl-3 ligand, IGFBP-2, IL-4, IL-17A, IL-22, MIF, PDGF-AA and SDF-1 α . The only significant change in when Cav1-ve CHME3 cells were associated with increased factor presence was for CHI3L1. It is still nevertheless not easily possible to identify the basis of such changes, the Cav1 depletion could have resulted in direct effects on the microglial cell secretome, altered the microglial responsiveness to GBM cells, and/or altered the paracrine milieu of the medium such that the secretome of the GBM cells changed. A summary of all secretome is illustrated in the **Supplementary figure VI. 2- Appendix VI.**

5.4.4 Effect of CHME3 Cav1 phenotype on GBM proliferation.

The impact of Cav1 within the GBM cell itself upon the cell's invasion and migration has previously been studied in our lab using shRNA techniques and CRISPR cell lines created during the project the work showed Cav1 promotes the GBM cell invasion (Moriconi 2019). The aim of this part of the chapter is to investigate the role of Cav1 in microglial cells and the impact upon tumour progression, addressing features as tumour proliferation, migration, and invasion.

In order to investigate the impact of the Cav1 status in GBM cell proliferation, GBM cells were co-cultured with CHME3 'Cav1 NT' (Cav1 +ve) or CHME3 'Cav1 KO', (Cav1 -ve) using the Transwell system (0.4 μ m pores; 48 hours) that allows paracrine signals from both populations to regulate each other; again no direct cell-cell contact. After the incubation, GBM cells and microglia cells were trypsinized and counted.

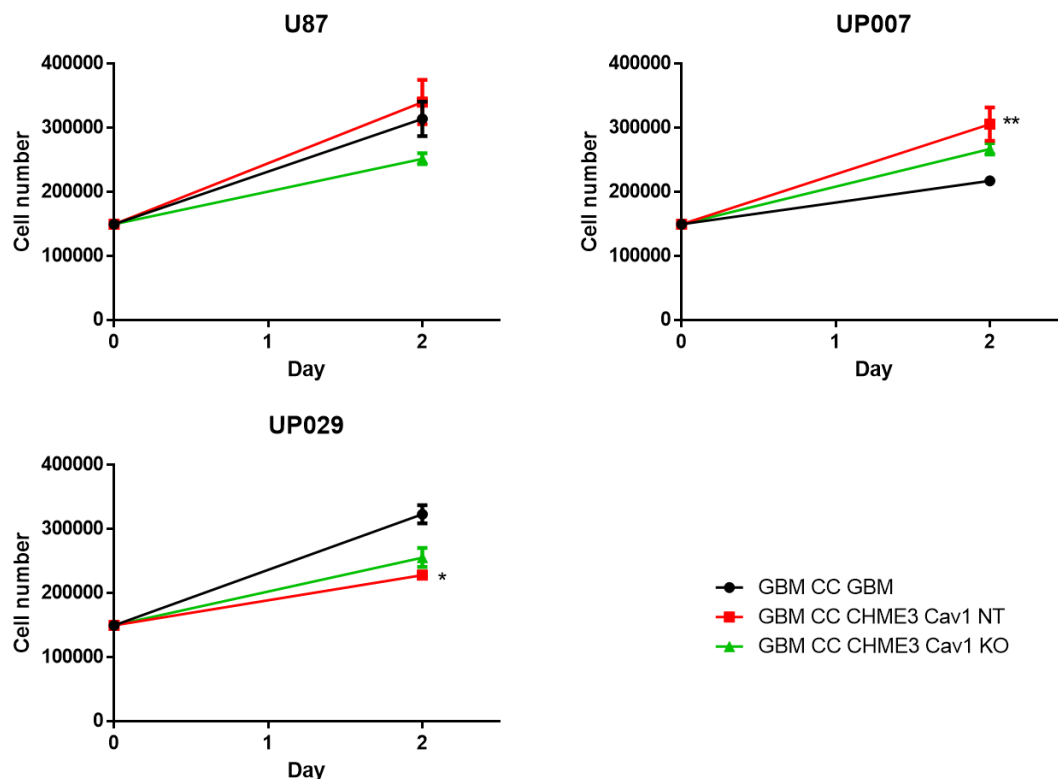


Figure 5.9 – Impact of CHME3 CC on tumour proliferation. 150,000 cells of CHME3 Cav1 NT (red) or CHME3 Cav1 KO (green), or each GBM cell line (black) were seeded into a 6-well plate, each GBM cell line tested was seeded into an insert, left to adhere for 24 hours. On the following day, the insert was placed together with microglia and tumour cells, allowing to be in CC for an additional 48 hours. After that, the cells were detached and counted using the Countess™ II FL Automated Cell Counter. Values represent the mean \pm SEM of 4 individual experiments. *: $p < 0.05$; **: $p > 0.01$ when compared to GBM CC GBM, Kruskal-Wallis, Dunn's multiple comparisons test.

The impact of microglial cells on GBM proliferation was variable and GBM cell line dependent (**Figure 5.9**) In U87 cells, CHME3 'Cav1 NT' (Cav1+ve) slightly induced the proliferation, whereas the CHME3 'Cav1 KO' (Cav1-ve) decreased U87 proliferation. For the UP007 cells, co-culture stimulated the proliferation, independently of microglia Cav1 status although the Cav1+ve microglia showed more of an effect ($p < 0.01$). In UP029 cells, the presence of microglia cells slowed down the proliferation again irrespective of microglia Cav1 status but with the CHME3 Cav1+ve cells resulting in a greater the decrease in GBM proliferation ($p < 0.05$).

5.4.5 Effect of CHME3 Cav1 phenotype on GBM migration.

The migration was assessed using the Transwell system (pore size 8 μm) within which the migration of GBM cells, U87, UP007 and UP029 was examined. These GBM cells having previously been by co-cultured in a separate Transwell system (0.4 μm pores; 48 hours) with the CHME3 cells, either Cav1+ve or Cav1-ve. Following completion of the latter incubation, the GBM cells were detached and used directly for the migration assay.

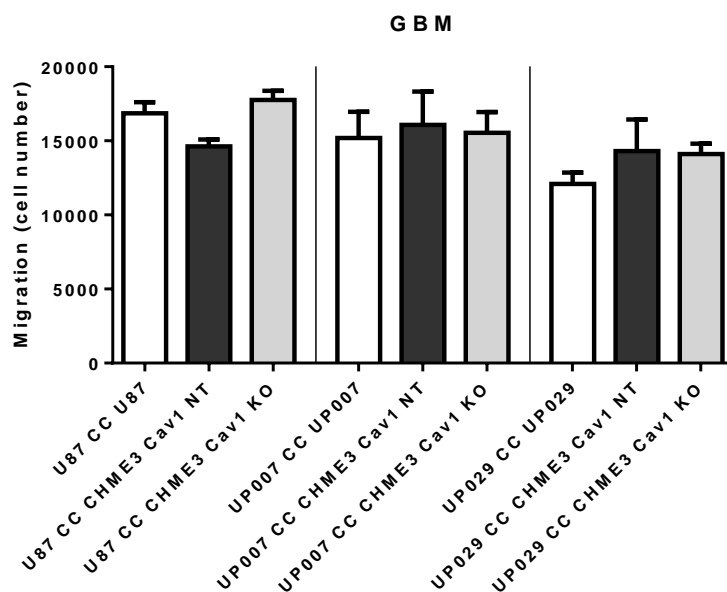


Figure 5.10 – Impact of CHME3 CC on tumour migration. 150,000 cells of CHME3 Cav1 NT (red) or CHME3 Cav1 KO (green), or GBM cell line (black) was seeded into a 6-well plate, each GBM cell line tested was seeded into an insert and left to adhere for 24 hours. On the following day, the insert was placed together with microglia and tumour cells and allowed to be in CC for an additional 48 hours. After that, the cells were collected and used into another Transwell system and left to migrate for an additional 16 hours. In the end, the number of cells that crossed the membrane was counted. Values represent the mean of cells \pm SEM of 4 individual experiments.

Figure 5.10 shows the results, with little to no differences in GBM migration observed between the GBM cells alone and the respective GBM line when co-cultured with CHME3, either Cav1+ve or Cav1-ve phenotypes

5.4.6 Effect of CHME3 Cav1 phenotype on GBM invasion

While the focus on was determining the role of microglial Cav1 status upon GBM cell invasion some initial pilot studies were undertaken comparing the impact of Cav1 knockout within the GBM cell itself. This pilot work was part of a collaboration within the laboratory (C., Neto – CRISPR-Cas9 technology).

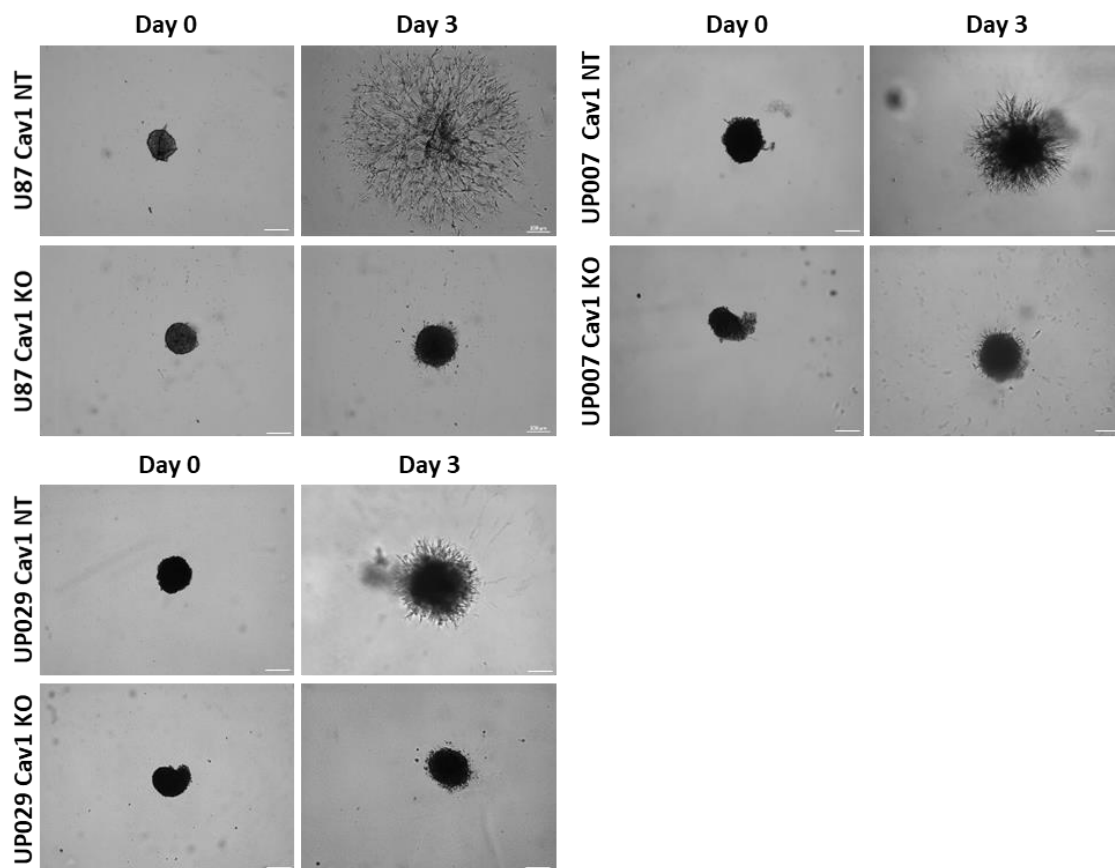


Figure 5.11 – Impact of Cav1 upon GBM spheroid invasion. Representative pictures of U87, UP007 and UP029 Cav1 NT and Cav1 KO invasion at Day 0 and 3. GBM cells were seeded into a 96-well plate, ULA and round bottom, and left to form a sphere for 4 days. After sphere formation, at day 0 in invasion, the formed spheres were embedded in Matrigel and left to invade for further 3 days. N=3 experiments. Scale bar: 200 μ M.

As can be seen from the Matrigel 3D spheroid invasion, the deletion of Cav1 in the GBM cell lines results in a uniform reduction in GBM cell invasion (**Figure 5.11**) indicative that Cav1 is a regulator of GBM cell invasion. More relevant to the question under study, the three GBM cell lines presented different extents and patterns of invasion with U87 showing the most profound and being most responsive the loss of Cav1. As a result, the cell line U87 was the main focus in the combined microglia – GBM cell invasion assay. Indeed, attempts include UP007 and UP029 cells were undertaken however, the ability for these cells to mount a sustained and reproducible invasion response in the model was poor.

Focusing on the impact of CHME3 'Cav1 NT' and CHME3 'Cav1 KO', upon U87 invasion, the spheres were formed with a ratio of 500:500. (GBM to CHME3). Astrocytes were used as a control (in combination with the GBM cells). Prior to the sphere formation, cells were differentially labelled with Vybrant dyes (DiO-green-U87, Dil-orange/red-astrocytes and DiD-red-CHME3) as described in **2.12 – Cellular co-cultures – Vybrant™ dyes**, to distinguish the different populations within the sphere. Thereafter, cells were cultured in close contact in suspension for 4 days during the sphere formation, then embedded into Matrigel (Day 0) and cultured within this matrix for a further 3 days to study the invasion. Pictures were taken in a brightfield microscope, as well as an epifluorescence microscope.

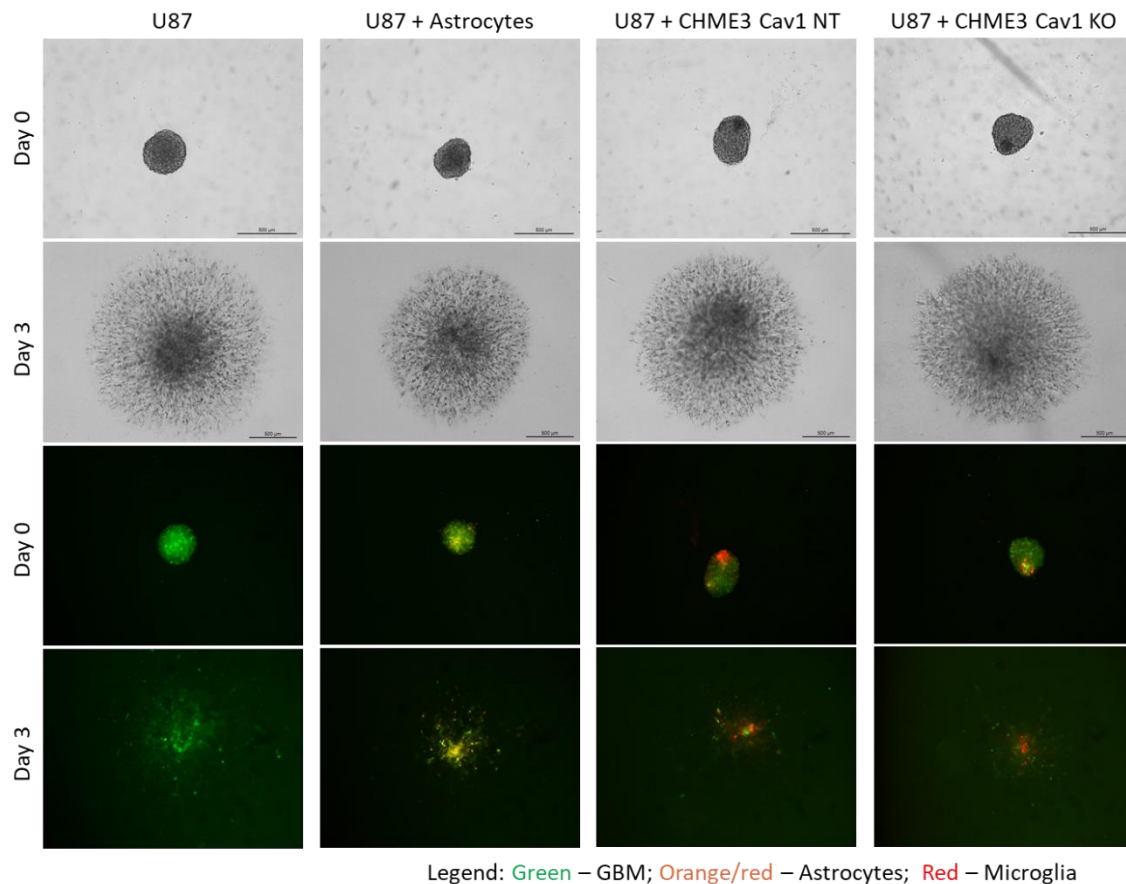


Figure 5.12 – Impact of microglia upon U87 invasion. Representative pictures of U87 invasion in CC with CHME3 Cav1 NT and CHME3 Cav1 KO. U87 cells cultured alone or cultured with astrocytes were used as a control. Prior to the sphere formation, cells were labelled with different DiO (U87-green), Dil (astrocytes-orange/red) and DID (CHME3-red). The spheres were formed in a ratio of 1:1, for 4 days. After sphere formation, around half of the media was replaced for Matrigel in a final concentration of 4 mg/ml and left to invade for an additional 3 days. N= 4 independent experiments. Scale bar: 500 μ M.

Shown in **Figure 5.12**, is the day 0 (Matrigel) and Day 3 (Matrigel) bright-field and fluorescent images for spheroid invasion. When cultured together with the U87 cells, the astrocytes and microglia cells displayed different spatial patterns within the sphere: astrocytes within the spheres showed a much more uniformly distributed pattern (Day 0, U87+Astrocyte), whereas CHME3 cells, independently of Cav1 status, displayed (day 0) a much more localised pattern tending to group together in one section of the sphere. The extent of invasion was analysed using the macro, INSIDIA run in ImageJ and the results are illustrated in **Figure 5.13**.

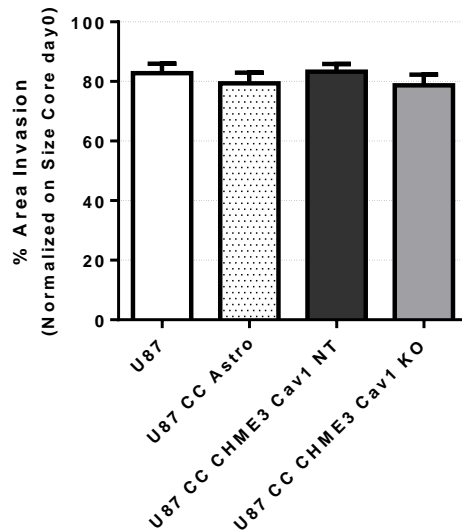


Figure 5.13 – Spheroid invasion analysis of U87 cell in CC with Astrocytes and CHME3. Area of invasion was calculated using the INSIDIA macro, and it was normalized based on the size of the core at day 0. Bars represent the mean \pm SEM. N= 4 independent experiments.

The spheroid co-culture of CHME3 cell with U87, whether the CHME3 cells expressed Cav1 (CHME3-NT) or lacked expression (CHME3-KO) made no difference.

Since microglia cells (CHME3 at least) under the conditions of this experiment did not attenuate or promote the invasion of U87 (irrespective of Cav1 status in the microglia) the distribution of CHME3 to have migrated throughout the U87 and astrocyte spheroids was assessed using lightsheet microscopy at the end of each invasion assay. Lightsheet microscopy allows high resolution image acquisition to much greater depths within large complex structures; the size of spheres was ca. 250 μm , at day 0 of invasion, and had increased ca. 1500 μm by the end of day 3.

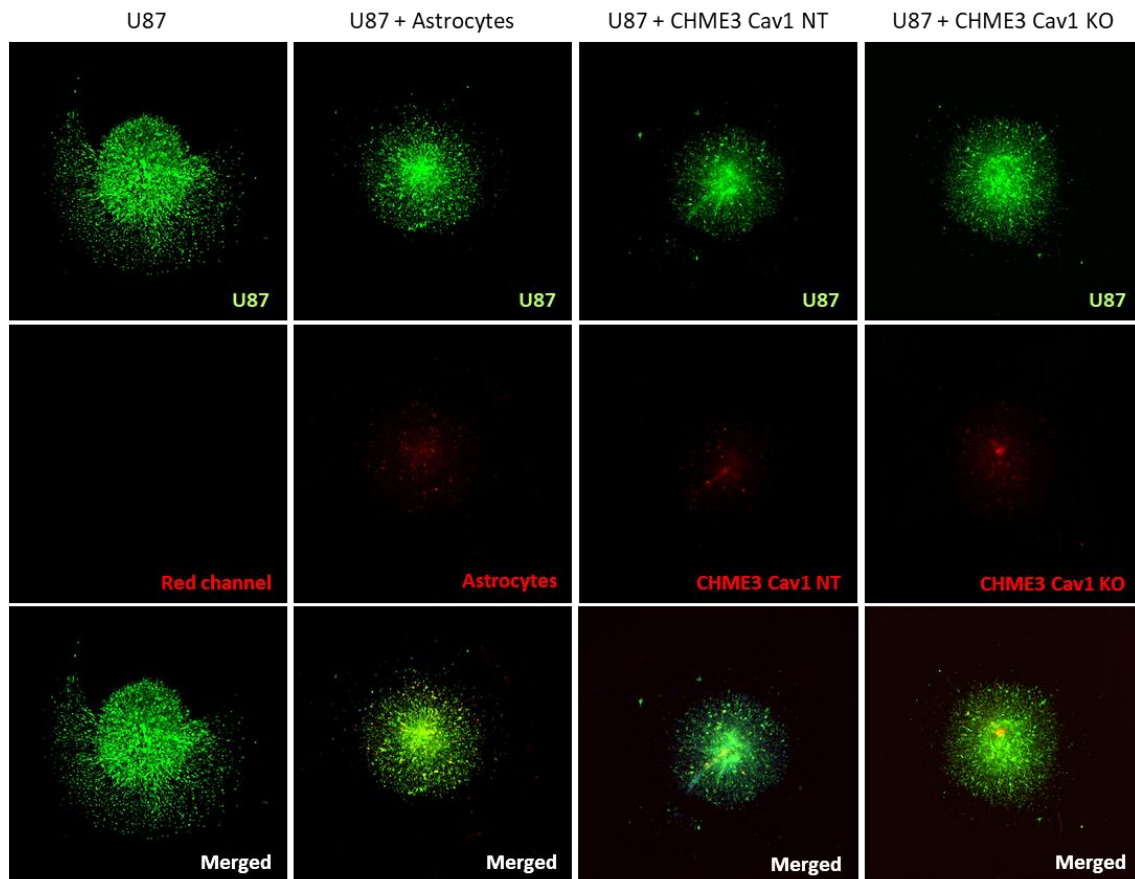


Figure 5.14 – Impact of microglia upon U87 invasion at day 3. Representative pictures of lightsheet hyperstack of U87 invasion in CC with CHME3 Cav1 NT and CHME3 Cav1 KO and Day 3 of invasion. U87 cells alone and astrocytes were used as a control. Prior to the sphere formation, cells were labelled with different DiO (U87-green), Dil (astrocytes-orange/red) and DID (CHME3-red). The spheres were formed in a ratio 1:1, for 4 days. After sphere formation, around half of the media was replaced with Matrigel in a final concentration of 4 mg/ml and left to invade for an additional 3 days. After the third day of invasion, the spheres were collected, embedded in agarose, and imaged using Zeiss Lightsheet Z.1 microscope, 10X detection objective.

Images from the lightsheet microscope (**Figure 5.14**), shows extensive U87 invasion (Green) when spheres comprised U87 cells alone. Spheres constructed from either U87/astrocytes, U87/CHME3 ‘Cav1 NT’ or U87/CHME3 ‘Cav1 KO’ all showed a slightly reduced but similar GBM invasion amongst these three experimental arms. Significantly, astrocytes and CHME3 ‘Cav1 NT’ cells were displayed a much more uniform distributed amongst the U87 spheroid, where some astrocytes and CHME3 ‘Cav1 NT’ cells were invading together with tumour cells. In contrast the CHME3 ‘Cav1 KO’ cells seemed less mobile with a significant proportion of the cells remaining after Day 3 at the initial location at day; this indicates Cav1 in the CHME3 cells has some role in their migration

and invasion. Indeed this is in agreement with differential migration of these cells in earlier Transwell experiments (**Figure 5.2**– this chapter).

We next explored how the CHME3 cells interacting with U87 within a spheroid model impacted upon the U87 cells to invade into another spheroid composed entirely of non-tumour astrocytes in what is sometimes known as a ‘confrontation assay’. Combination spheroids were formed with; U87/astrocytes; U87/CHME3-NT; U87/CHME3-KO. Separate single lineage cell spheroids were formed from U87 and astrocytes. Various combinations of spheres were placed together under floating (suspension) conditions and allowed to associate. To mimic a ‘brain tissue’ – a simplistic model the single lineage cell astrocyte spheroid was labelled RED, and used in a confrontation assay with the other combinations. Spheres were formed for 4 days, placed together in pairs and left to interact for an additional 4 days. Images were taken by brightfield and epifluorescence microscopy at day 0 and at day 4. One pair of spheres for each combination was further investigated using lightsheet microscopy in order to access in some depth the spheroids.

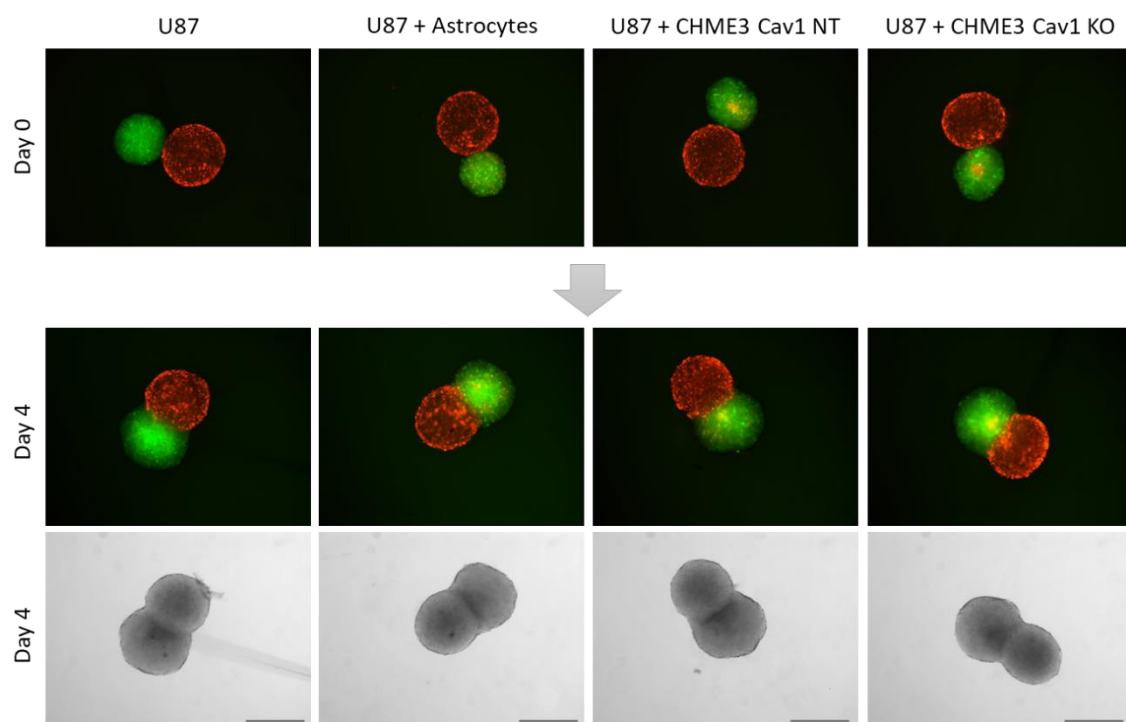


Figure 5.15 – Impact of CHME3 upon U87 invasion. U87 (green), astrocytes (red), CHME3 Cav1 NT and CHME3 Cav1 KO (orange/red) were pre-labelled to form spheroids (ratio of 500:500) for 4 days. Spheroids composed by 20,000 astrocytes were made at the same time. At day 0, one tumoral spheroid and one non-tumoral spheroid were placed together inside the same well and followed for an additional 4 days. Scale bar: 500 μ m. N= 2 experiments.

As seen in the **Figure 5.15**, all sphere combinations (exclusively U87 alone, U87/astrocytes, U87/CHME3 'Cav1 NT' and U87/ CHME3 'Cav1 KO' showed interaction in this suspension-based confrontation assay. Additional images were collected using the lightsheet microscope.

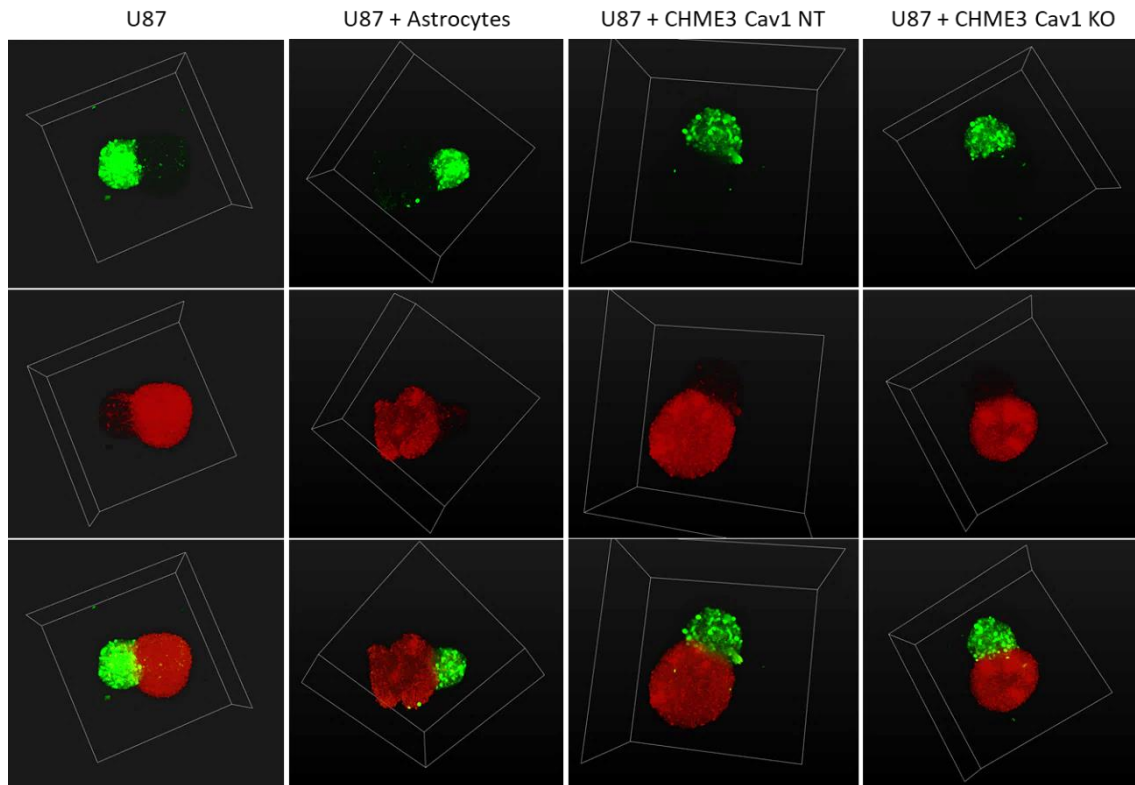


Figure 5.16 – Impact of CHME3 upon U87 invasion (Green) into Astrocyte only spheroids (RED). Z-stack of spheroid interaction and invasion at day 4, fusing lightsheet microscopy technique.

Looking into the spheres, it was possible to see that tumour cells (green) and astrocytes (red) were able to migrate into the opposite sphere, at the end of 4 days of incubation. It seems that the presence of immune cells did not affect the behaviour of the tumour cells, independently of Cav1 status.

5.5 Discussion

Tumours are composed by tumour and non-tumour cells that will be involved in co-regulation. This creates a unique tumour immune microenvironment able to modify and control the tumour behaviour and modify the tumour response to therapy. Biopsies of GBM tumour show high infiltration of both microglial and macrophages populations. In brain tumours the number of immune cells increases with tumour grade and can comprise up to half of the GBM tumour mass (Ransohoff and Cardona 2010).

Microglia and blood-derived macrophages can be distinguished via genetic lineage tracing since they arise from different populations during embryogenesis. How these two myeloid populations contribute to tumour progression is not well understood, but it seems likely that they have different functions in the tumour context since differences at chemokine and cytokine production, and in antigen presentation have been identified between microglia and macrophages (Rita et al. 2020). Microglial cells will be the first immune cells to interact with the brain tumour during the initial steps of development. Macrophages, as well as other immune cells, are attracted to the tumour during its progression when the BBB integrity is compromised. Understanding the role and key mechanisms that modulate the microglia and/or macrophage immune populations in a tumour environment may be crucial to discovering new targets and treatments for GBM.

Microglia cells are a slowly proliferating population under homeostasis conditions, but upon activation, they are able to increase their rate of proliferation significantly (Réu et al. 2017; Askew et al. 2017; Graeber, Scheithauer, and Kreutzberg 2002). Microglia can arrive to the tumour environment through their capacity to respond to a stimulus, migrate and increase their proliferative capacity once activated. CHME3 microglial cells are a highly proliferative cell line due to the immortalization process (Janabi et al. 1995), which as discussed may have implications in relating the CHME3 phenotype to the primary in-vivo cell.

In studying the impact of GBM upon microglia (CHME3) proliferation and migration we observed a reduction in microglial proliferative and migration rate, opposite to the initial expectation whereupon a 'tumour microenvironment' might activate these cells. However, during the earlier stages of glioma tumorigenesis, high levels of TGF- β are

reported and are associated with downregulation of immune cell proliferation and migration via inhibition of cell-cycle progression and stimulation of apoptosis (Joseph et al. 2013), TGF- β was upregulated in the environment created by co-culture of CHME3 with GBM cell lines.

Literature evidence indicates that the factors released by microglia are able to promote glioma proliferation, migration and invasion (Platten et al. 2003; Watters et al. 2005; Charles et al. 2011). In our co-culture experiments we no consistent effect of the CHME3 cells upon the proliferation of the GBM cell lines, with U87 and UP007 proliferation increased and UP029 reduced. This is perhaps not surprising given the genetic heterogeneity of GBM cell lines. Similarly, a consistent effect of CHME3 co-culture upon GBM cell migration response was not observed. Clearly the model was a simplistic one and comprised only a short duration (48 hours) of co-culture that may be insufficient generate a reliable 'tumour microenvironment'.

Cav1 is involved in cellular proliferation, migration and invasion (Razani, Woodman, and Lisanti 2002; Goetz et al. 2008). In microglia cells, Cav1 is correlated with actin regulation, and the disruption on actin dynamics can disturb the proliferation (Moreno-Vicente et al. 2018; Uhlemann et al. 2016). The role of Cav1 in proliferation in microglia has not previously been explored, however, it is likely to be cell line dependent. For example, the expression of Cav1 in HEK293T cells promotes the proliferation (Torres et al. 2006), and in fibroblasts, its loss accelerates the proliferation and cooperates in oncogenic transformation (Cerezo et al. 2009). CHME3 cells express high levels of Cav1, possibly due the SV40 large T antigen transformation (Stergiou et al. 2013). The deletion of Cav1 in these cells (CHME3-Cav1 KO) decreased their overall proliferation compared with Cav1+ve CHME3 cells (CHME3-Cav1 NT).

Regarding the migration, Cav1 seems to promote the migration of the CHME3 microglia with the Cav1+ve CHME3 cells showing an almost 2-fold greater migration capacity (Transwell). The impact of the Cav1 phenotype in the CHME3 did not however, impact GBM cell migration during the con-culture experiments.

Microglia and macrophages constitute a significant proportion of the GBM tumour. These immune cells in communication with the tumour cells and vice versa, will result

in variety of growth factors, chemokines and cytokines released into the cellular environment. Tumour cells can secrete cytokines as IL-6, IL-10, IL-4 and TGF- β cytokines, whose immunosuppressive properties may favour the anti-tumour immune response of microglia to dominate and thereby favour a pro-tumoral environment (Constam et al. 1992).

The microglia phenotype is a balance between pro-inflammatory and anti-inflammatory status, and due to the plasticity of these cells, they can change their transcriptome and secretome depending on the pressure created by the environment. In studies that explored the factors release into the co-culture environments, we found the STAT1, STAT6 and NF- κ B showed an overall decrease in the co-cultured GBM / microglial environment, indicative of a general downregulation of pro-inflammatory and anti-inflammatory pathways. STAT3 analysis presented a decrease upon in the U87 cocultures but a slight increase with UP007 and UP029 cells, suggesting that STAT3 pathway has a role for microglia to react to tumour environment. Ellert-Miklaszewska and colleges showed that signals from glioma cells fail to activate pro-inflammatory STAT1 and NF- κ B in rat microglia cells, inducing ERK and p38 MAPK signalling (Ellert-Miklaszewska et al. 2013). In CHME3 co-culture with astrocytes we observed a downregulation in the anti-inflammatory pathways while maintaining similar levels of pro-inflammatory pathways, suggestive of the normal cell interactions between microglia and astrocytes, that tightly regulate the immune population (Chhor et al. 2013).

The upregulation of TNF- α and TGF- β are described in the literature in the GBM context, being associated with tumour progression (Lisi et al. 2014). Nijaguna *et al.* treated microglia cells with conditioned media from different GBM cell lines, for 24 hours, and showed a downregulation of CXCL10 and TNF- α , and an upregulation of IL-1R and CD204, suggesting a pro-tumoral phenotype supported by microglia cells. However, many of the classical inflammatory-related genes and signalling pathways failed to be induced (Nijaguna et al. 2015).

The cytokine array analysis provided information on the factors secreted by the combined co-cultures of microglia and tumour cells, mimicking a simple "tumour environment, and compared with an environment comprised only by microglia cells.

Missing is the environment created only by the GBM. Nevertheless, based on these preliminary results, the 'tumour' milieu created by CHME3 and U87 cells in this system appeared to suppress angiogenin, BDNF, and uPAR, and promoted CHI3L1, GDF-15, IL-8, IL-17A and OPN. The angiogenic protein, angiogenin is implicated in glioma angiogenesis and increased malignancy (Skog et al. 2008) and together with uPAR, is involved in migration and invasion, (Yamamoto et al. 1994; Veeravalli et al. 2010). The decrease in their levels, could be correlated with the initial response of microglia cells to the tumour environment. However, to explore this observation, longer periods of co-culture should be performed. A reduction in the BDNF was observed, a protein is involved in neuroprotection in healthy brain (Branchi, Francia, and Alleva 2004) and in the reduction of intracranial glioma growth in brain tumour (Garofalo et al. 2015). The remaining analytes (CHI3L1, GDF-15, IL-8, IL-17A and OPN) oversecreted in the tumour immune environment are described in the literature and are connected with tumour proliferation, invasion and progression (Ku et al. 2011; Wurm et al. 2019; Roth et al. 2010; De La Iglesia et al. 2008; Yeung et al. 2013; Khan et al. 2017; Wei et al. 2019). The environment created by CHME3 and U878 cells is suggestive to favour the tumour progression.

Regarding the effect of Cav1 in microglia cells upon the tumour environment, to the best of our knowledge, this study was the first one conducted. The Cav1 levels in microglia cells slightly decreased in co-culture with GBM cells as well as in co-culture with astrocytes. If the environment created by astrocytes can immuno-regulate the microglia (Perry and Teeling 2013; Deczkowska, Amit, and Schwartz 2018), Cav1 may be involved in this process, suggesting that tumour cells may regulate the microglia via Cav1.

The impact of Cav1 in GBM cells was previously thoroughly investigated in our lab by Chiara Moriconi (Moriconi 2019). Cav1 is involved in GBM cell invasion and is correlated with a poor prognosis (Pu et al. 2019; Moriconi 2019). During this project, clones of CRISPR-Cas9 Cav1 KO were created for all GBM and microglia cell lines presented in our laboratory. Using a 3D spheroid invasion assay, it was confirmed that Cav1 promotes the invasion of GBM cells. But focusing on the main objective of the project, the invasion studies targeted the impact of microglia in 3D tumour invasion, taking into consideration the microglial Cav1 status. The 3D invasion investigated the capacity to invade a matrix

and to invade a mass composed by normal cells (astrocytes). In both cases, microglia seem to have no impact on the invasion, independently of Cav1 status. It is important to highlight that microglia cells (CHME3) trended to position themselves in clusters inside the spheroid, not creating a homogeneous population with tumour cells as occurred with astrocytes cells. However, Cav1 in microglia cells seems to promote their movement inside the tumour, increasing the tendency to invade and/or migrate along with tumour cells.

In **summary**, CHME3 microglia cells, independently of Cav1 status, failed to influence migration and 3D tumour invasion. The loss of Cav1 in CHME3, decreases the mobility of microglia in tumour spheroids. GBM cells suppressed the activation of microglia. In CHME3, Cav1 promotes the response of TNF- α and TGF- β to the tumour environment.

.

CHAPTER 6 –
IPSC-DERIVED MICROGLIA AND THE IMPACT
OF CAV1 KNOCKOUT

6.1 Introduction

Technical advances over the last decade allowed the development of highly efficient protocols to derive human microglia from undifferentiated cells, like HSC, ESC, or iPSC. These protocols not only generate precious cells to study a diverse range of neurological diseases, which overcomes the problems related with difficulties to access the human material, but also provide a big platform to study several genes involved in cell development, differentiation and maturation. Moreover, these techniques make genetic engineering of genes feasible, perhaps in microglial cells, allowing to understand their function in human neurodegenerative diseases, like Alzheimer's disease (Abud et al. 2017), Parkinson's disease and Huntington's diseases (Haenseler et al. 2017), other neurological injuries, like stroke spinal and cord injuries (Nagoshi and Okano 2018), and brain cancer (Stricker et al. 2013).

Cav1, which forms the caveolae, is involved in several cellular processes as vesicular transport, cell migration, cell proliferation, cell transformation and signal transduction (Niesman et al. 2013). These are important functions that can impact the normal microglia function, particularly regulating the activation and inactivation, controlling morphological and biochemical changes. Cav1 was previously identified in microglial cells from mouse cell lines in BV2 cells (Blasi et al. 1990), mouse models (Niesman et al. 2013), and human cell lines in CHME3 cells (Portugal et al. 2017). The role of Cav1 on microglia development is an avenue to be explored. Nevertheless, Fu *et al.* highlighted the importance of this protein on monocyte to macrophages differentiation through the regulation of EGR-1 transcriptional activity (Y. Y. Fu et al. 2012). On the other hand, downregulation of Cav1 in monocytes/macrophages was correlated with psoriasis, a chronic immune-mediated inflammatory skin disease (Takamura et al. 2019) and associated with the restoration of pro-inflammatory phenotype in GBMs, increasing the levels of TNF- α (Shimato et al. 2013). Niesman and colleagues studied the function of Cav1 and they observed an increase of the protein levels upon microglial activation (Niesman et al. 2013). Understanding the role of Cav1 in a specific context or disease, namely in the tumour environment, requires knowledge about their function during homeostasis and their function under physiological and healthy conditions.

6.2 Aim

The aim of this chapter is to generate human microglia cells from iPSC and explore the role of Cav1 in these cells on differentiation, maturation, activation, and phagocytosis. Kolf2 Cav1 NT and Kolf2 Cav1 KO were used to differentiate microglial cells in order to study the impact of Cav1 on activation, secretome, transcriptomic profile and on phagocytosis.

6.3 Methods

6.3.1 General methods

The iPSC Kolf2 Cav1 NT and KOLF2 Cav1 KO were used in this chapter. These cells were cultured and differentiated following the protocols described in **Chapter 2, section 2.2 - Cell culture maintenance** and summarised in **Figure 6.1**. At least three different clones of Cav1 NT and KO were used during the experiments.

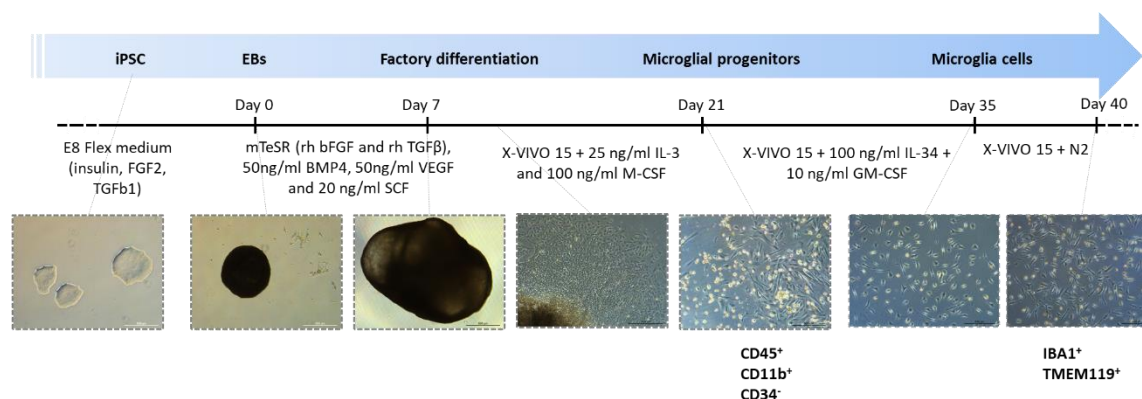


Figure 6.1 – Differentiation protocol of iPSC-derived microglia. iPSC cells were maintained in culture using E8 Flex medium. At day 0, EBs are forming using hanging-drop technique for 24 hours and kept in culture in mTeSR medium supplemented with 50 ng/ml of BMP4, 50 ng/ml of VEGF and 20 ng/ml of SCF for 7 days, for the mesodermal induction and differentiation. At day 7, the EBs are transferred into a matrigel-coated flask and cultured in X-VIVO 15 supplemented with 25 ng/ml of IL-3 and 100 ng/ml of M-CSF, for 14 days. At day 21, microglial progenitors were floating, and some cells were tested for CD45, CD11b and CD34 by FACS. The remaining cells were seeded into fibronectin-coated plates for further differentiation into microglial cells using X-VIVO 15 supplemented with 100 ng/ml of IL-34 and 10 ng/ml of GM-CSF, for an additional 14 days. At day 35 microglial cells were allowed to rest for 5 days in X-VIVO 15 media supplemented with N2. At day 40, IBA1 and TMEM119 microglial markers were evaluated by IF and the cells were used for further experiments. rh: recombinant human.

During the process of microglial differentiation, the microglial precursors were studied by FACS, using the protocol described in **2.3 - Microglia progenitor's characterization by FACS**. The microglia markers IBA1 and TMEM119, as well as Cav1 were analysed by IF as described in section **2.4 - Immunofluorescence Staining**. Microglial cells were polarized towards a pro- or anti-inflammatory phenotype following the protocol of stimulation **2.5 - Microglia and Macrophages polarization**. Non-stimulated cells were used as a control. Cav1 protein levels were studied by WB and qRT-PCR, following the protocol **2.8 – Western Blot** and **2.7 - qRT-PCR**, respectively. To understand the role of Cav1 upon activation of iPSC-MG cells, after polarization, a panel of immune-related genes were studied by qRT-PCR (**2.7 - qRT-PCR**) and the soluble factors secreted into the media by these cells were examined by cytokine array (**2.10 - Cytokine array**). The transcriptomic profile was analysed by RNA-seq. Finally, to study the phagocytosis ability, the protocol described in **2.9 - Phagocytosis assay** was used.

6.3.2 RNA-seq

For the RNA-Seq library construction, after differentiation, iPSC-MG Cav1 NT and iPSC-Cav1 KO were stimulated towards a pro-inflammatory and anti-inflammatory phenotype. Unstimulated cells were used as a control. After 48 hours of stimulation, cells were washed three times with PBS, followed by RNA extraction using AllPrep DNA/RNA/Protein Mini Kit, following the manufacturer's guidelines. RNA quantity was measured using Qubit™ RNA HS Assay Kit, with Qubit 4 fluorometer, following the manufacturer's instruction. RNA integrity number (RIN) was measured for all samples using the Bioanalyzer Agilent 2100 series.

The library preparation, RNA-sequencing, alignment, quality controls and data processing was conducted by Wales Gene Park. All libraries analysed were generated from RNA samples with RIN score ≥ 9 . 100 ng of isolated mRNA was used to construct RNA-seq libraries using NEB Ultra II directional RNA library prep kit. Libraries were sequenced on the Illumina HiSeq 4000 platform as paired-end 100 bp reads to obtain 20 to 30 M of reads per sample following the workflow illustrated on **Figure 6.2**.

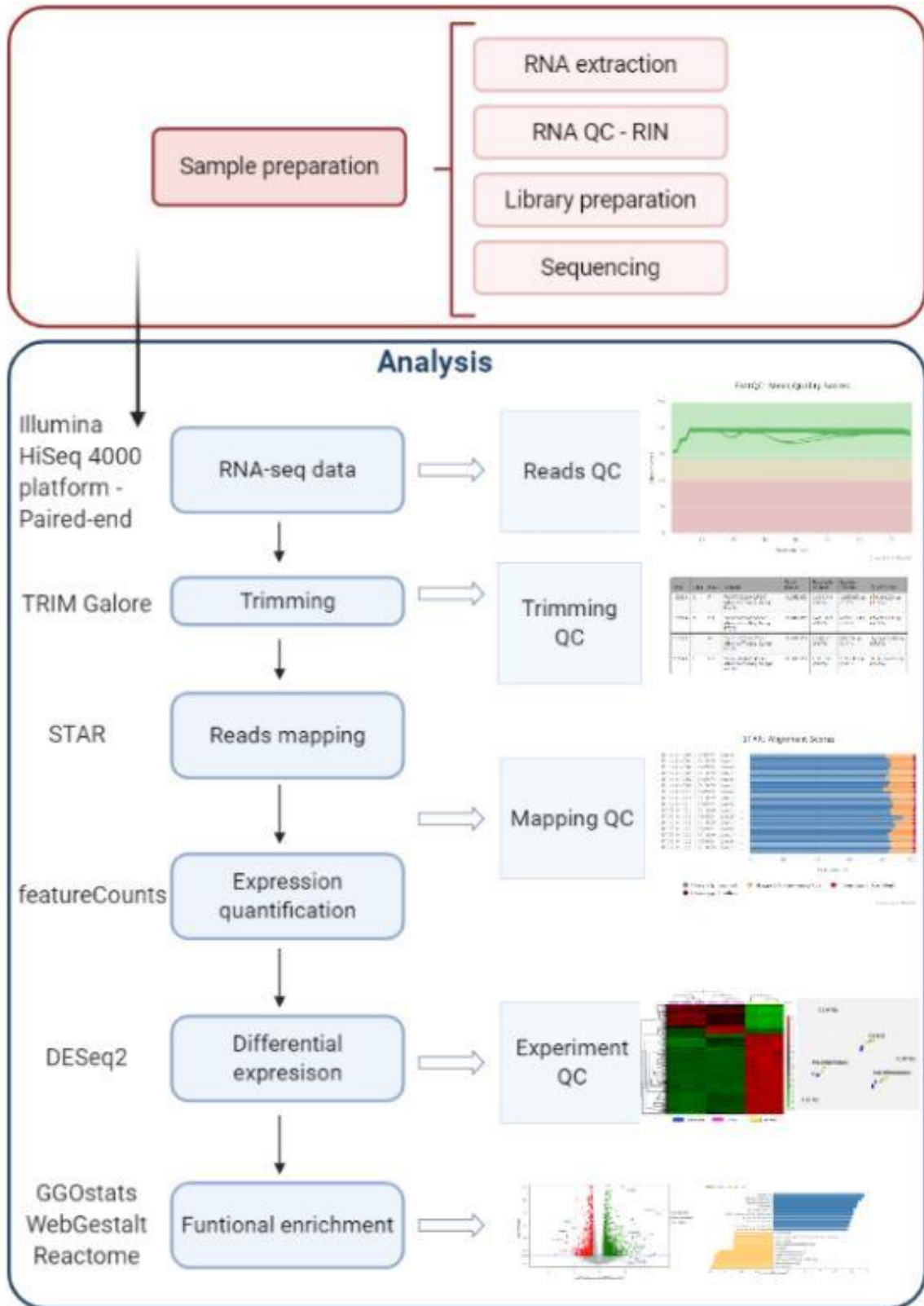


Figure 6.2 – RNA-seq workflow.

Sequenced reads were trimmed to remove adapter sequencer and poor-quality ends of reads. Trimming was performed using Trim Galore (version 0.6.4) with the default parameters in paired-end mode. The trimmed paired-end reads were aligned to the

GRCh38 no_alt_plus_hs38d1 analysis set reference using STAR (version 2.5.1b), an ultrafast universal RNA-seq aligner, following the 2-pass method (Dobin and Gingeras 2015). STAR mapping was carried out using the MultimapNMax=1 flag, whereby reads that map to more than one genomic location are treated as being unmapped, in order to exclude them from downstream analysis. QC metrics were generated using FastQC (version 0.11.2), and the summary statistics were generated using Samtools (version 0.1.19) flagstat.

Raw counts were calculated for all samples for both exons and genes using Subread featureCounts (version 1.5.1) (Yang Liao, Smyth, and Shi 2014). The featureCounts was executed with the following parameters:

- Gene-level: *featureCounts -p -s 2 --donotsort -B -t "exon" -g "gene_id" -a GENCODE*
- Transcript-level: *featureCounts -p -s 2 --donotsort -B -t "exon" -g "exon_id" -a GENCODE*
- Exon-level: *featureCounts -p -s 2 --donotsort -B -t "exon" -g "transcript_id" -a GENCODE*

The counts were generated for paired-end read fragments summarized at the exon-level and then aggregated at the transcript-level. Read fragments overlapping more than one feature were excluded from the count summaries, in order to provide stringent, but robust count data. Transcript and exon locations used in the analysis derived from the GENCODE GRCh38.p10 comprehensive gene annotation. Differentially expressed genes (DE) were identified using a DEseq2 analysis (Love, Huber, and Anders 2014) on normalised count data. The resulting p-values were corrected for multiple testing and false discovery issues using the FDR method (Benjamini and Hochberg 1995). Gene Ontology (GO) over-representation analysis (ORA) was undertaken using the GOstats bioconductor library (Falcon, Falcon, and Gentleman 2007). The resultant data was corrected for multiple testing and false discovery using the FDR method.

Further investigation using gene set enrichment analysis (GSEA) – ORA, conducted in WebGestalt (WEB-based GENE SeT Analysis Toolkit), and Reactome was performed to explore and interpret the most relevant genes (Yuxing Liao et al. 2019; Jassal et al. 2020).

6.4 Results

6.4.1 Characterization of the microglial progenitors by FACs

The microglial progenitors were differentiated from four individual clones of KOLF2 Cav1 NT and four individual clones of KOLF2 Cav1 KO. The floating progenitors were collected from day 21 onwards, stained with CD34, CD45 and CD11b and analysed by FACs. Representative gates and histograms of iPSC-MG Cav1 NT and iPSC-MG Cav1 KO are shown in **Figure 6.3.** and **Figure 6.4,** respectively.

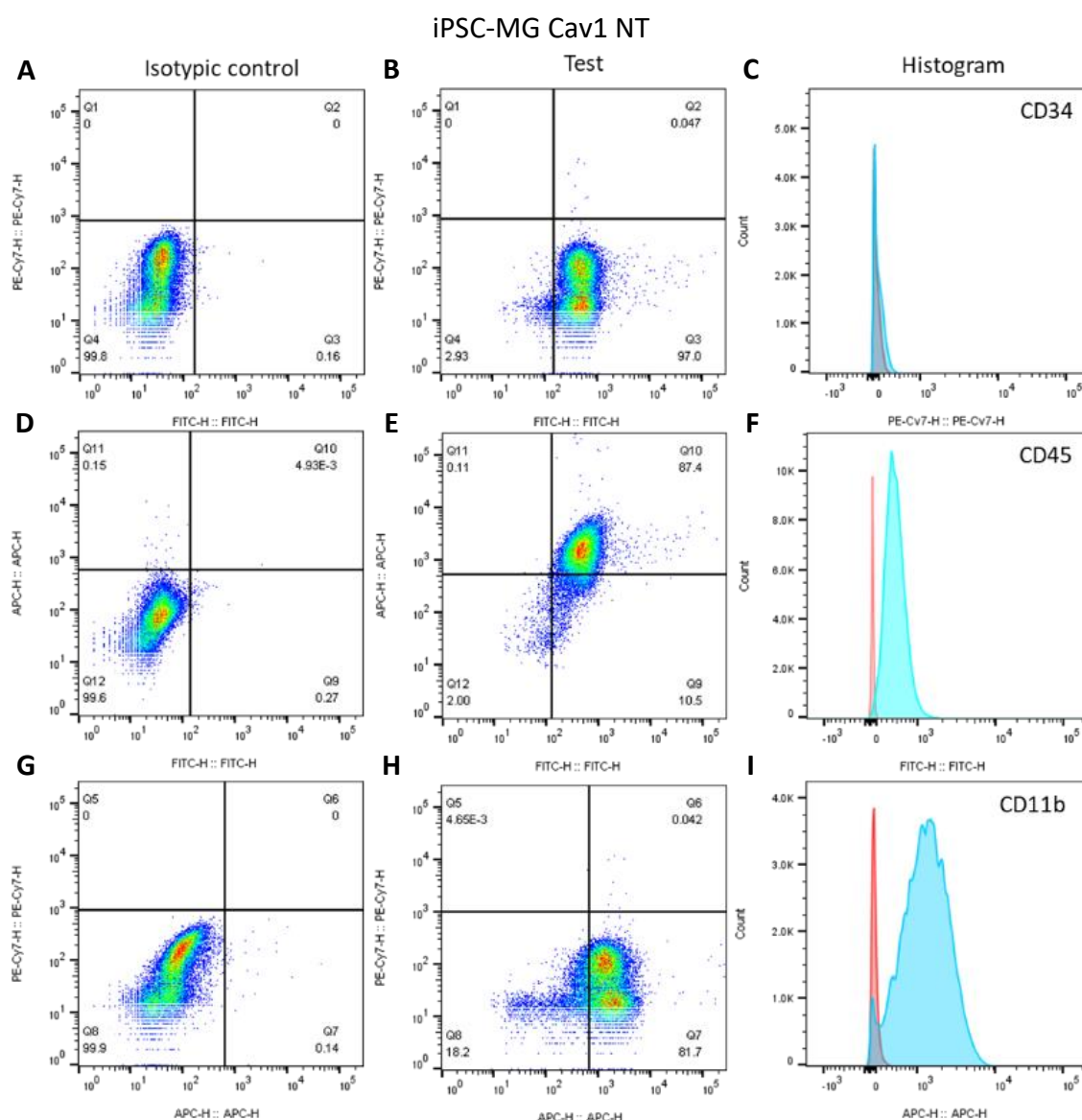


Figure 6.3 – CD34, CD45 and CD11b iPSC-derived microglial progenitors Cav1 NT population. Representative plots of FACs of iPSC-derived microglial progenitors Cav1 NT cells. Microglia progenitors were differentiated from 4 different clones of iPSC, where the floating cells were collected at day 21 or later and labelled with CD34 (PE-Cy7), CD45 (FITC) and CD11b (APC). Isotypic controls (**A, D, G**) were used as negative control. The tested population is represented in **B, E** and **H** plots. The histograms for CD14, CD45 and CD11b are represented in **C, F,** and **I,** respectively.

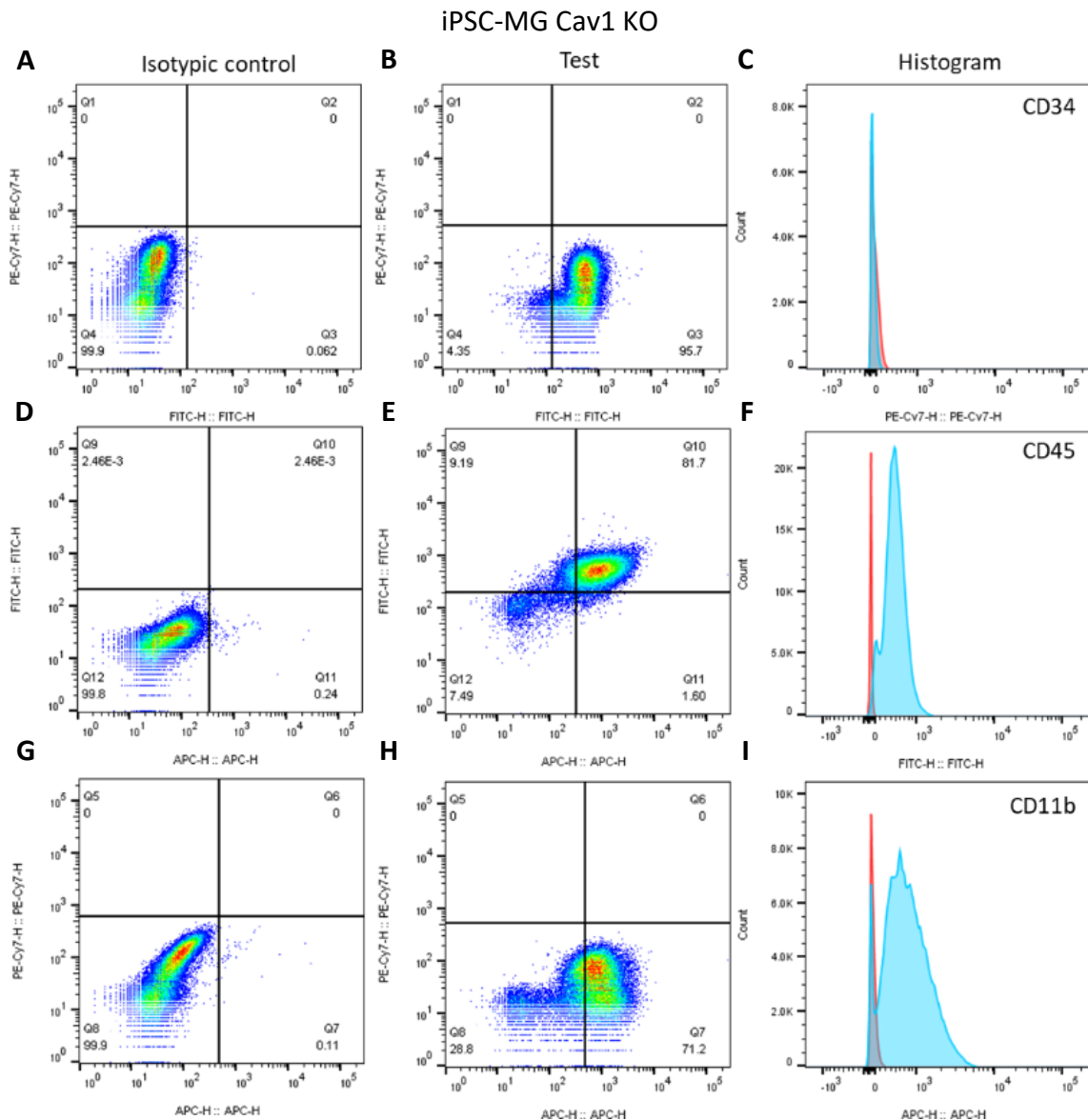


Figure 6.4 – CD34, CD45 and CD11b iPSC-derived microglial progenitors Cav1 KO population. Representative plots of FACs of iPSC-derived microglial progenitors Cav1 KO cells. Microglia progenitors were differentiated from 4 different clones of iPSC, where the floating cells were collected at day 21 or later and labelled with CD34 (PE-Cy7), CD45 (FITC) and CD11b (APC). Isotypic controls (**A**, **D**, **G**) were used as negative control. The tested population is represented in **B**, **E** and **H** plots. The histograms for CD14, CD45 and CD11b are represented on **C**, **F**, and **I**, respectively.

As seen in **Table 6.1**, the deletion of Cav1 in KOLF2 cells did not impact the differentiation of microglial progenitors from iPSC. Both iPSC-MG Cav1 NT and iPSC-MG Cav1 KO presented a high enrichment of CD11b and CD45 markers. Gate **B** and histogram **C**, for both **Figure 6.3.** and **Figure 6.4**, show that, independently of Cav1 status, these progenitors presented low levels of CD34, a HSC marker. Since it is possible to keep collecting microglial progenitors for differentiation from day 21 onwards in a

weekly basis, it was noticed that the number of CD45 and CD11b positive cells increased over time (data not shown), representing a more mature progenitor population in a longer period of time. Nevertheless, the first collected progenitors showed the lowest value of 84% of CD11b positive cells, which increased to 99.7% over time.

Table 6.1 – CD11b and CD45 positive population of iPSC-derived microglial progenitors of Cav1 NT and Cav1 KO cells. Results represent the mean \pm SD % of the parental population. Results from the total of 8 different clones (4 clones of Cav1 NT and 4 clones of Cav1 KO). N=3 independent experiments.

	iPSC-MG Cav1 NT (%)	iPSC-MG Cav1 KO (%)
CD11b	93.53 \pm 5.41	95.28 \pm 4.15
CD45	96.08 \pm 4.74	96.18 \pm 1.61
CD11b and CD45	90.97 \pm 8.16	93.17 \pm 4.53

6.4.2 Study of Cav1 in iPSC-derived microglial cells

The CRISPR-Cas9 Cav1 KO was performed on the KOLF2 level, which was investigated and discussed in **Chapter 3**. KOLF2 was previously engineered by the Nick Allen group in the safe harbour AAVS1 to express the mCherry tag. This cell line was used to perform the KO of Cav1 and respective controls. As expected, the differentiated cells are expressing mCherry, allowing to distinguish microglia cells from other cells in a co-culture context.

The study of Cav1 in differentiated microglial cells was further investigated by WB, qRT-PCR and IF. iPSC-MG Cav1 NT and iPSC-MG Cav1 KO were differentiated from the respective microglial progenitors for 14 days, with IL-34 and GM-CSF, and left to recover from the differentiation for an additional 5 days. To access the impact of the microglial activation on Cav1 expression, differentiated cells were activated towards a pro-inflammatory phenotype with LPS and IFN- γ or towards an anti-inflammatory phenotype with IL-4 and IL13, for 48 hours. The results obtained are summarized in **Figure 6.5**.

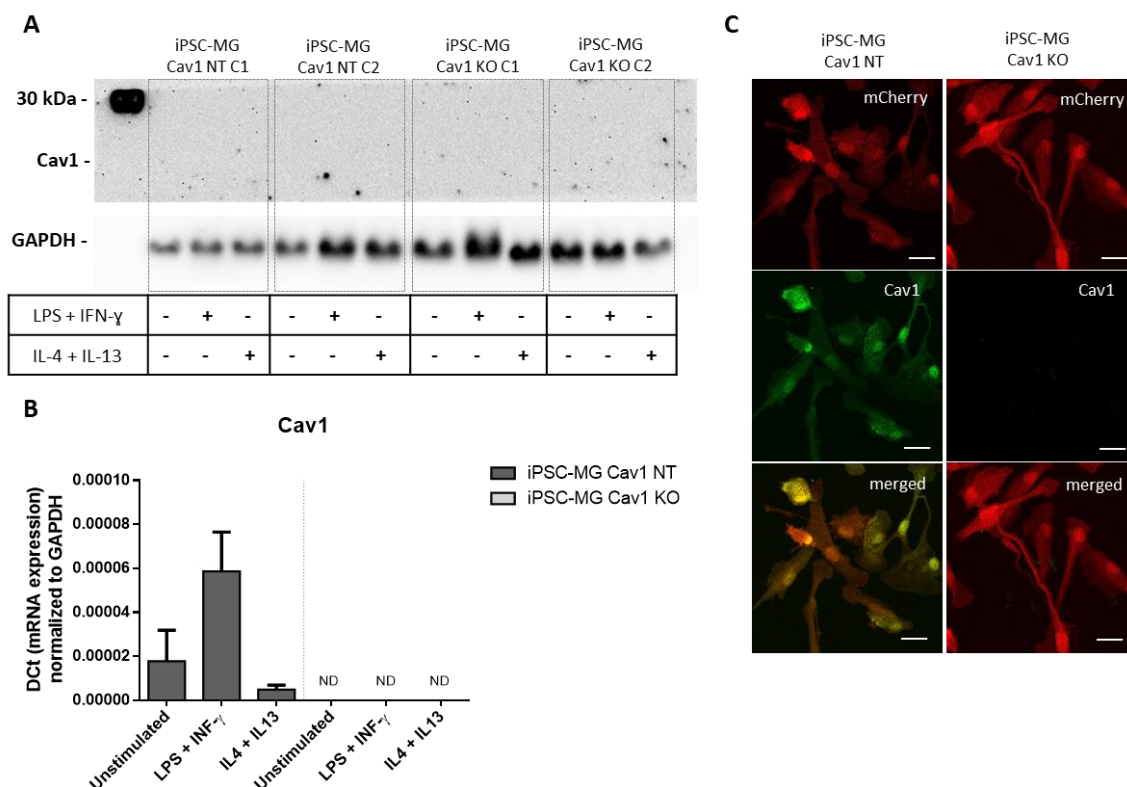


Figure 6.5 – Cav1 expression in iPSC-derived microglia cells. Microglia cells were differentiated from microglial progenitors for 14 days, with IL-34 and GM-CSF, and allowed to rest for an additional 5, followed by stimulation with LPS and IFN- γ or with IL-4 and IL-13 for further 48 hours. **A** – Representative membranes from 2 clones of Cav1 NT and other 2 clones of Cav1 KO. GAPDH was used as an internal control. **B** – Gene expression analysis by qRT-PCR. Bars represent the mean \pm SEM of the total 8 clones analysed. **C** – Representative images of the IF staining of Cav1. Cells were fixed, labelled with Cav1 antibody, and imaged by confocal microscopy. ND: not determined. Scale bar: 10 μ m.

Initially the Cav1 expression was studied by WB. But due to the low expression of Cav1 by microglia cells differentiated from KOLF2, the antibody was not sensitive enough to detect the protein expression (**Figure 6.5 – A**). Even after pro-inflammatory or anti-inflammatory activation, the Cav1 levels remained undetectable by WB. At mRNA levels, it was possible to identify low levels of Cav1 expression in iPSC-MG Cav1 NT cells in unstimulated cells, which trended to increase in pro-inflammatory phenotype and decrease in anti-inflammatory phenotype (**Figure 6.5 – B**). By using IF, it was possible to detect Cav1 expression in Cav1 NT cells (**Figure 6.5 – C**). Both iPSC-MG Cav1 NT and iPSC-MG Cav1 KO cells expressed the mCherry tag. No Cav1 mRNA or protein was detected in iPSC-MG Cav1 KO cells.

6.4.3 iPSC-MG expressed pan-microglial markers after Cav1 KO

After collection of the microglial progenitors, iPSC Cav1 NT and iPSC Cav1 KO, the cells were further differentiated with IL-34 and GM-CSF for 14 days towards a final microglia phenotype. Cells were allowed to rest from the differentiation for an additional 5 days, fixed and stained with microglial markers IBA1 and TMEM119, as observed in **Figure 6.6**.

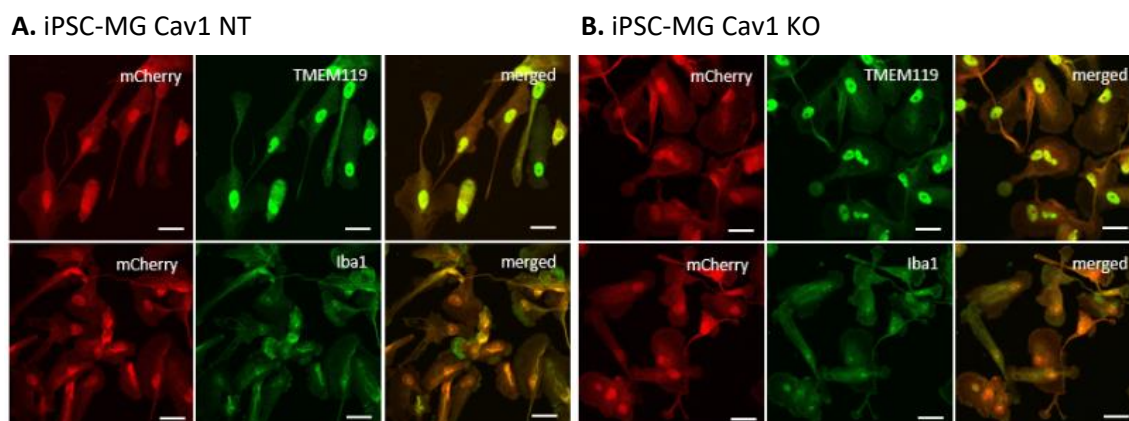


Figure 6.6 – Microglial markers and Cav1 expression. Representative images of the immunofluorescence staining of TMEM119 and IBA1 of iPSC-MG Cav1 NT (A.) and iPSC-MG Cav1 KO cells (B.). Cells were fixed, labelled with different antibodies, and imaged by confocal microscopy. Scale bar: 10 μ m.

Independently of Cav1 status, both iPSC-MG Cav1 NT and iPSC-MG Cav1 KO cells expressed the microglial markers IBA1 and TMEM119 by the end of the differentiation protocol.

6.4.4 Impact of the differentiation process on iPSC-MG

Since GM-CSF is a cytokine which is involved on the pro-inflammatory cascade and IL-34 can lead to differentiation of immunosuppressive macrophages (Foucher et al. 2013), after 14 days of differentiation, iPSC-MG Cav1 NT and iPSC-MG Cav1 KO cells were left to rest from the differentiation procedure for an additional 5 days, without interference of IL-34 and GM-CSF. To study the possible effect of the differentiation on the microglial phenotype, cells freshly differentiated were used as a comparison. After differentiation, rested and non-rested cells were further polarized towards a pro-inflammatory or anti-inflammatory phenotype and the gene expression was analysed by qRT-PCR.

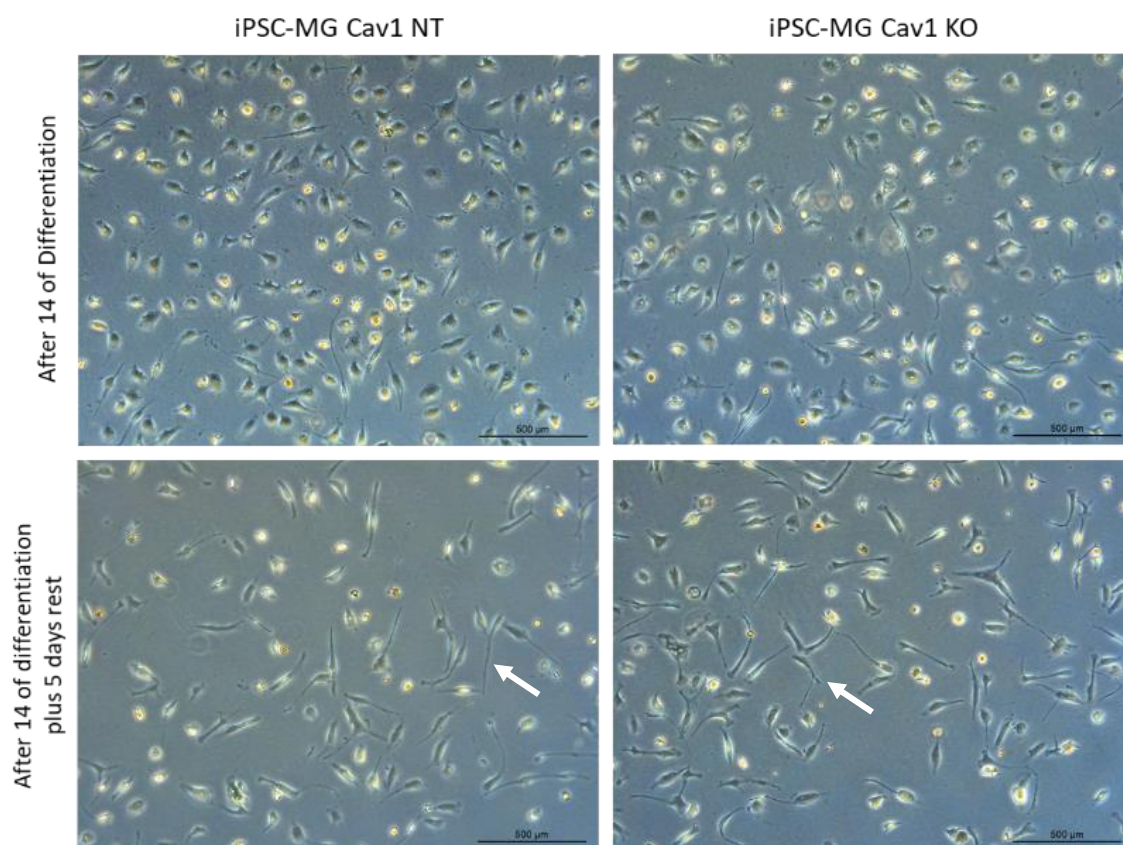


Figure 6.7 – Effect of the resting period on microglial morphology. Representative brightfield pictures of iPSC-MG Cav1 NT and iPSC-MG Cav1 KO immediately after 14 days of differentiation with IL-34 and GM-CSF, following the same protocol, plus an additional 5 days of resting without interference of IL-34 or GM-CSF factors. Microglia ramifications are signalized with white arrows. Scale bar: 500 μ M.

It was possible to observe that cells freshly differentiated showed an ameboid morphology, with few and short ramified processes, independently of Cav1 status. The 5 days of culture without the influence of IL-34 or GM-CSF, allows for a morphological adjustment, decreasing the cellular body size and increasing the quantity and size of the ramifications, as observed in **Figure 6.7** (white arrow).

In order to understand the impact of the differentiation process on the basal gene expression of the inflammatory-related markers, mRNA was extracted from cells immediately after differentiation and from cells which were allowed to rest for 5 days after differentiation. qRT-PCR was used to study of the pro-inflammatory genes, IL-1 β , IL-6, IL-12, CXCL10 and TNF- α , and the anti-inflammatory genes TGF- β , IL-10, CCL22, CD200R, CD206 and CD163. The results are represented in **Figure 6.8**.

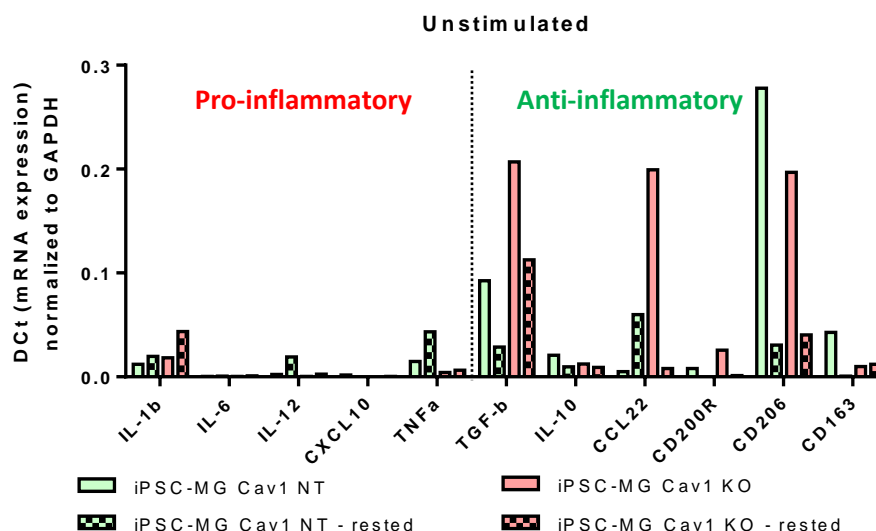


Figure 6.8 – Effect of the microglial differentiation process upon gene expression on unstimulated cells. iPSC-MG Cav1 NT (green) and iPSC-MG KO (pink) were differentiated from respective microglial precursors for 14 days. Freshly differentiated cells are represented as a full colour. Rested cells (gridded bars) were allowed to settle for additional 5 days. N= 1 experiment.

Regarding the pro-inflammatory related genes, the resting period induced slightly the increased of IL-1 β , independently of Cav1 status, and IL-12 and TNF- α , only in Cav1 NT cells. No other noticeable differences were registered for IL-6 and CXCL10. Concerning the anti-inflammatory profile, almost all the genes decreased their expression with the 5 days of resting. Independently of Cav1 status, TGF- β , CD200R and CD206 presented a major transcriptional decreased, together with IL-10 that was less notorious. CCL22 showed an increased in iPSC-MG Cav1 NT rested cells, however, iPSC-MG Cav1 KO rested cells decreased substantial their expression. CD163 Cav1 NT rested cells decreased the expression to an unnoticeable level, but the absence of Cav1 did not showed an impact on this gene.

Studying the effect of this resting period could have on the polarization state of microglia cells, freshly differentiated and rested cells, Cav1 NT and Cav1 KO cells were further stimulated for 48 hours towards a pro-inflammatory or an anti-inflammatory phenotype, with LPS and IFN- γ or with IL-4 and IL-13, respectively. After stimulation the

mRNA was extracted, the same genes panel was studied by qRT-PCR and are represented in **Figure 6.9**.

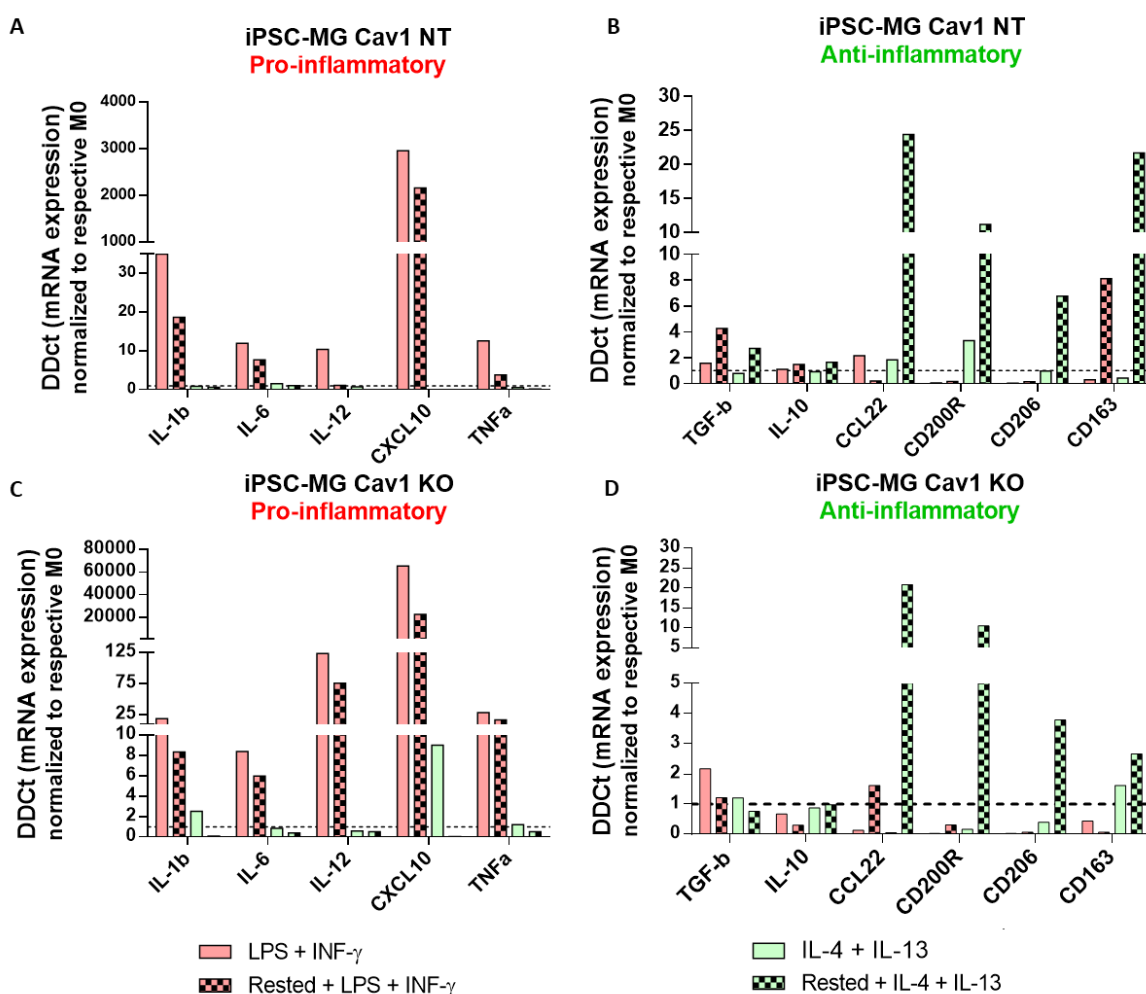


Figure 6.9 – Effect of the microglial differentiation process upon gene expression on stimulated cells. iPSC-MG Cav1 NT (**A**, **B**) and iPSC-MG Cav1 KO (**C**, **D**) were differentiated from the respective microglial precursors for 14 days. Freshly differentiated cells (full colour bars) and Rested cells (gridded bars) were polarized towards a pro-inflammatory phenotype (pink bars) with LPS plus IFN- γ or towards an anti-inflammatory phenotype (green bars) with IL-4 plus IL-13, for 48 hours. N= 1 experiment.

The differentiation and maturation process of microglia involves the use of IL-34 and GM-CSF. These cytokines can be involved with inflammatory pathways and consequently interfere with the capacity of these cells to respond to new stimulus. Regarding the pro-inflammatory response represented in graphs **A** (iPSC-MG Cav1 NT) and **C** (iPSC-MG Cav1 KO) both populations, independently of Cav1 status, were able to increase the transcriptions of all pro-inflammatory makers analysed, after 48 hours of treatment with LPS and IFN- γ . The resting period of 5 days led to a response less

exacerbated compared to fresh stimulated cells. The treatment with IL-4 and IL-13, did not impact the transcription of these markers in iPSC-MG Cav1 NT cells, however, cells where Cav1 was deleted (**C**) presented an induction of IL-1 β and CXCL10 with the anti-inflammatory treatment.

Focusing on the anti-inflammatory response, when iPSC-MG Cav1 NT (**B**) was stimulated with IL-4 and IL-13 (green bars), immediately after the differentiation, exhibited only a slightly increase of CCL22 and CD200R. However, when these cells rested for 5 days from the differentiation (green gridded bars), the gene expression of all the analysed anti-inflammatory related markers was increased with the stimulation. It was observed an increase of TGF- β , CCL22 and CD163 with treatment with LPS and IFN- γ , as well.

For the cells where Cav1 was deleted, specifically iPSC-MG Cav1 KO (**D**), the treatment with IL-4 and IL-13 only proportionated the increase of CD163 on cells stimulated right after the differentiation (green bars). However, similarly to Cav1 NT microglia cells, when iPSC-MG Cav1 KO were allowed to rest for 5 days from the differentiation (green gridded bars), they were able to respond to the stimulation, increasing the gene expression levels of CCL22, CD200R, CD206 and CD163, showing a better response to the anti-inflammatory stress compared to cells that did not rest from the differentiation. Regarding the LPS and IFN- γ treatments (pink bars), it was observed an increase of TGF- β and CCL22.

Taking these results into consideration, for further experiments the cells were allowed to recover additional 5 days from the differentiation protocol, without the interference of IL-34 and GM-CSF, recognizing that the resting stage period allows the iPSC-derived microglia to respond to pro-inflammatory as well as anti-inflammatory stimulus, representing more accurately the recognized plasticity of this population.

6.4.5 Impact of Cav1 on pro-inflammatory and anti-inflammatory gene expression by qRT-PCR

After identifying a protocol that was able to differentiate microglia from iPSC and allowed this population to respond to a pro-inflammatory and anti-inflammatory stimulus, 4 clones of KOLF2-AAVS1-mCherry-Cav1 NT and another 4 clones of KOLF2-AAVS1-mCherry-Cav1 KO were used to fully understand the impact of Cav1 deletion on microglia cells upon treatment with LPS and IFN- γ or IL-4 and IL-13, for 48 hours. The gene expression of the inflammatory-related genes was performed by qRT-PCR.

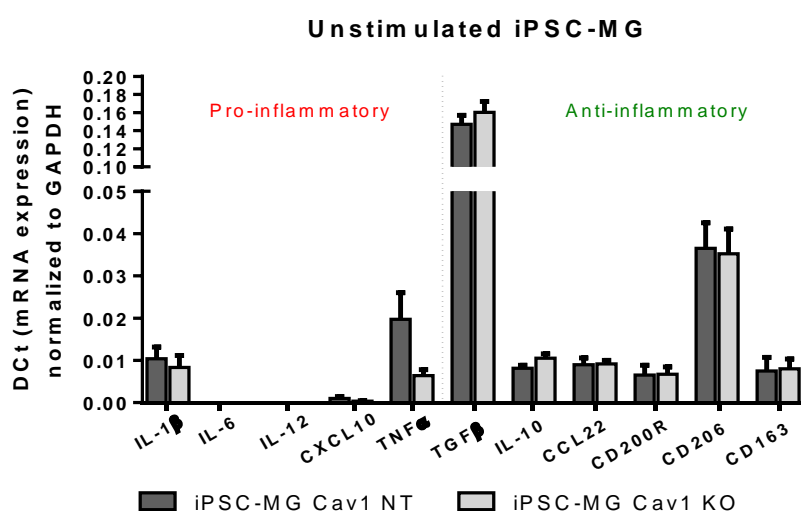


Figure 6.10 – Basal expression of the pro-inflammatory and anti-inflammatory related genes by iPSC-MG Cav1 NT (dark grey) and iPSC-MG Cav1 KO cells (light grey). Both populations were differentiated from microglial progenitors, for 14 days with IL-34 and GM-CSF and allowed to rest for an additional 5 days in medium without interference of any soluble factor. Bars represent the mean \pm SEM of 4 clones for the two independent experiments.

As for the basal state, the inflammatory-gene levels expressed by iPSC-MG Cav1 NT and iPSC-MG Cav1 are illustrated in **Figure 6.10**. The cells demonstrated similar expressions of pro-inflammatory and anti-inflammatory markers, independently of Cav1 status, with the exception of TNF- α , which showed a decrease of the expression roughly to half when Cav1 was lost. Under basal conditions, iPSC-MG almost does not express IL-6, IL-12 and CXCL10. Nevertheless, it is important to highlight the higher levels of all anti-inflammatory related genes, suggesting an intrinsic anti-inflammatory phenotype of these cells.

The **Figure 6.11** shows the expression of pro-inflammatory related genes after stimulus with LPS and IFN- γ (pro-inflammatory) as well as IL-4 and IL-13 (anti-inflammatory).

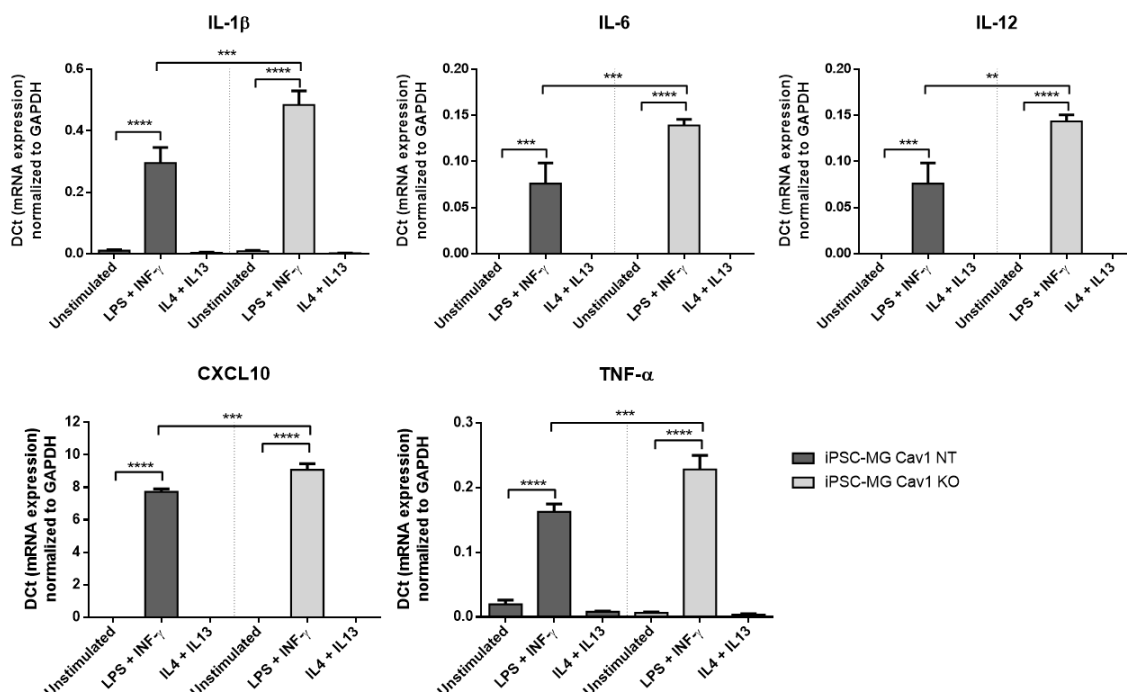


Figure 6.11 – Pro-inflammatory related genes by iPSC-MG Cav1 NT (dark grey) and iPSC-MG Cav1 KO cells (light grey). Both populations were differentiated from microglial progenitors, for 14 days with IL-34 and GM-CSF and allowed to rest for an additional 5 days in medium without interference of any soluble factor, followed by stimulation with LPS and IFN- γ for further 48 hours. Bars represent the mean \pm SEM of 4 clones for two independent experiments. **: $p < 0.01$, ***: $p < 0.001$, ****: $p < 0.0001$, Sidak's multiple comparisons test.

The pro-inflammatory activation, with LPS and IFN- γ for 48 hours, significantly induced the gene expression of all pro-inflammatory related markers analysed (IL-1 β , IL-6, IL-12, CXCL22 and TNF- α) in iPSC-MG Cav1 NT (dark grey bars) and in iPSC-MG Cav1 KO (light grey bars) populations. It is important to notice that the absence of Cav1 in these cells led to an exacerbated increase of their response ($p < 0.01$). The treatment with IL-4 and IL-13 did not change the expression of the studied genes in both populations.

Regarding the anti-inflammatory profile, the gene expression of CCL22, CD200R, TGF- β , CD206, CD163 and IL-10 upon IL-4 and IL-13 (anti-inflammatory) as well as LPS and IFN- γ (pro-inflammatory) is illustrated in **Figure 6.12**.

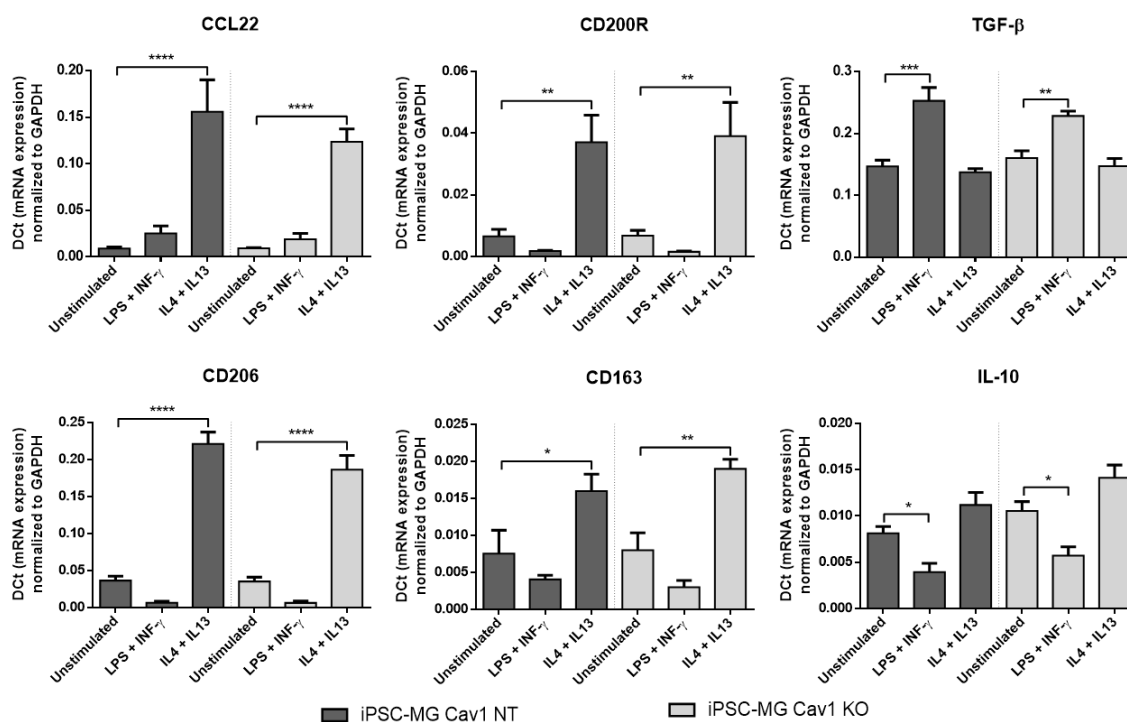


Figure 6.12 – Anti-inflammatory related genes by iPSC-MG Cav1 NT (dark grey) and iPSC-MG Cav1 KO cells (light grey). Both populations were differentiated from microglial progenitors, for 14 days with IL-34 and GM-CSF and allowed to rest for an additional 5 days in medium without interference of any soluble factor, followed by stimulation with IL-4 and IL-13 for further 48 hours. Bars represent the mean \pm SEM of 4 clones for two independent experiments. *: $p < 0.05$, **: $p < 0.01$, ***: $p < 0.001$, ****: $p < 0.0001$, Sidak's multiple comparisons test.

The treatment with anti-inflammatory cytokines, IL-4 and IL-13, induced significantly the expression of CCL22, CD206, CD200R and CD163, trending to increase the IL-10 expression as well, independently of Cav1 status. However, the deletion of Cav1 trended to marginally decrease the mRNA levels of CCL22 and CD206 and to increase of CD163 and IL-10. No alterations were observed for the expressions of CD200R and TGF- β with the same treatment in both Cav1 NT and Cav1 KO microglial populations.

The stimulation of microglia with pro-inflammatory mediators LPS and IFN- γ can impact the expression of anti-inflammatory related genes. It was observed that the decrease or increase of expression depended directly on the studied gene but were independent of the status of Cav1. The expression of CD200R, CD206, CD163 and IL-10 ($p < 0.05$)

decreased in the pro-inflammatory phenotype but increased for CCL22 and TGF- β ($p < 0.01$).

6.4.6 Impact of Cav1 on microglia activation by cytokine array

In order to access which products can be released by iPSC-MG in the different phenotypes, as well as the impact that Cav1 could have on this performance, it was performed a cytokine array to evaluate 105 cytokines, growth factors or chemokines. Microglia differentiated from KOLF2 Cav1 NT and KOLF2 Cav1 KO cells was stimulated towards a pro-inflammatory state with LPS and IFN- γ or towards an anti-inflammatory state with IL-4 and IL-13, for a period of 48 hours. Untreated cells were used as a control. A summary of the results for all secretome is illustrated in the **Supplementary figure VI. 2 – Appendix VI.**

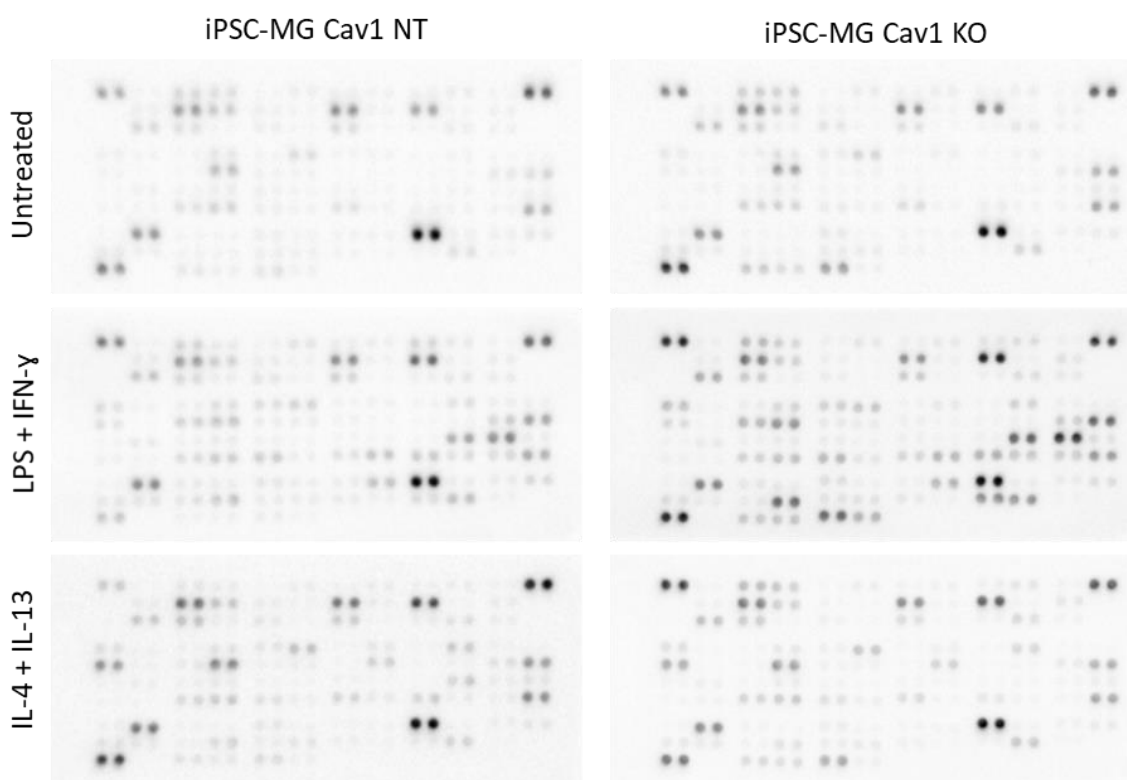


Figure 6.13 – Representative membranes from the human cytokine array. iPSC-MG Cav1 NT and iPSC-MG Cav1 KO was differentiated from KOLF2 cells, left to recover, and stimulated with LPS and IFN γ or IL-4 and IL-13, for 48 hours. Non treated cells were used as control. The supernatants were collected, centrifuged, and incubated with membrane.

The **Figure 6.14** represents the statistically significant products released by the iPSC-MG Cav1 NT cells, in response to a pro-inflammatory induction.

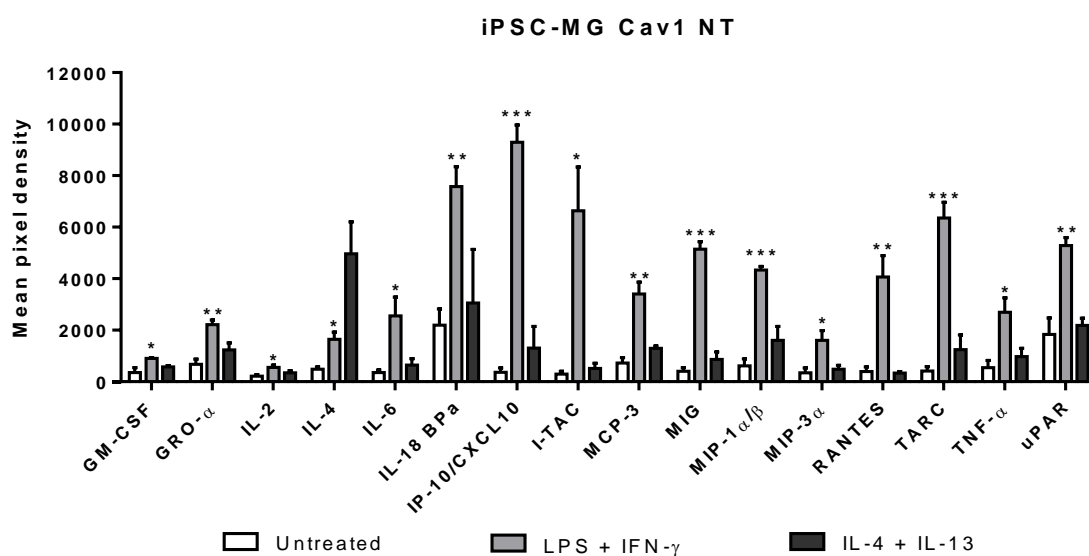


Figure 6.14 – Secreted products upon pro-inflammatory activation of iPSC-MG Cav1 NT cells. iPSC-MG Cav1 NT was differentiated from KOLF2 cells and stimulated with LPS and IFN- γ or IL-4 and IL-13, for 48 hours. Non-treated cells were used as control. The supernatants were collected, centrifuged, and incubated with membrane. Bars represent the mean \pm SEM of 3 clones. *: $p < 0.05$, **: $p < 0.01$, ***: $p < 0.001$ when compared to untreated cells, multiple t-test.

The LPS and IFN- γ treatment considerably induced the soluble forms of GM-CSF, GRO- α , IL-6, CXCL10, I-TAC (CXCL11), MCP-3, MIG (CXCL9), MIP-1 α/β (CCL3/CCL4), MIP-3 α (CCL20), Rantes (CCL5), TNF- α and uPAR, which are related with pro-inflammatory response of microglia and macrophages. It was possible to notice an increase of the anti-inflammatory related factors IL-4 and TARC (CCL17), as well as IL-2, which has essential roles on the differentiation of T-cells, and IL-18 BPa, which acts as a buffer for the inflammatory activation via IFN- γ .

The anti-inflammatory activation had no effect, or caused a slight increase, on the release of the factors mentioned previously. It is important to mention that the levels of IL-4 witnessed under the anti-inflammatory phenotype could be related with the IL-4 added to the media to stimulate these cells.

The **Figure 6.15** shows the soluble factors that showed a significant alteration, or a fold change higher than 2-times, for the anti-inflammatory response by iPSC-MG Cav1 NT.

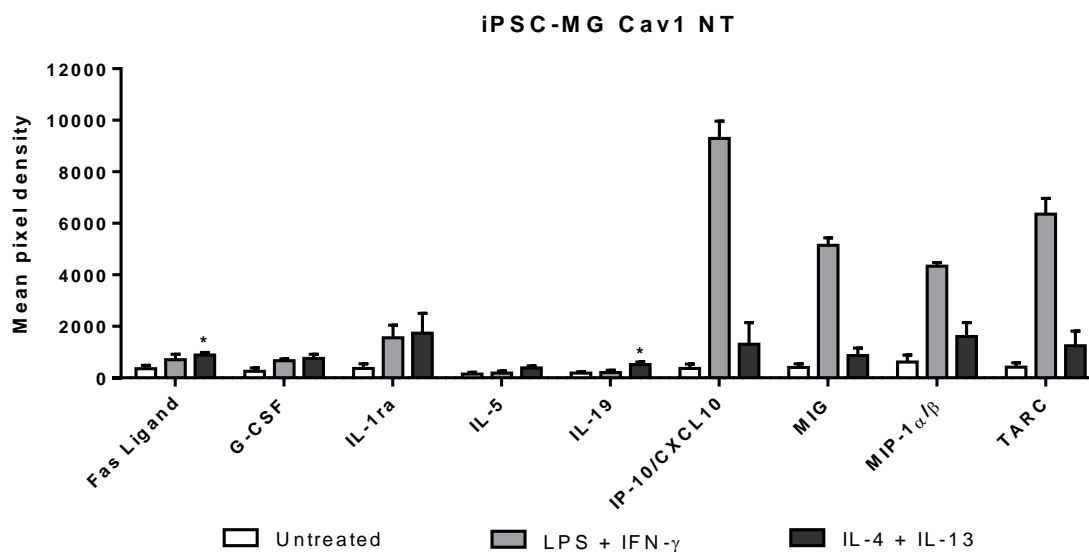


Figure 6.15 – Secreted products upon anti-inflammatory activation of iPSC-MG Cav1 NT cells. iPSC-MG Cav1 NT was differentiated from KOLF2 cells, left to rest and stimulated with LPS and IFN- γ or IL-4 and IL-13, for 48 hours. Non treated cells were used as control. The supernatants were collected, centrifuged, and incubated with membrane. Secreted products which presented FC >2. Bars represent the mean \pm SEM of 3 clones. *: $p < 0.05$ when compared to untreated cells, multiple t-test corrected.

Under an anti-inflammatory phenotype and compared to unstimulated cells, iPSC-MG boosted the anti-inflammatory related factors G-CSF, IL-1Ra, IL-19 ($p=0.04$) and TARC (CCL17), as well as the pro-inflammatory related factors Fas ligand ($p=0.03$), MIG (CXCL9) and MIP-1 α/β (CCL3/CCL4), and IL-5 which is involved in immune cell maturation. It is important to highlight that, except for the IL-19 response, the pro-inflammatory treatment induced similar response of these factors or even higher (MIG, MIP-1 α/β and TARC).

The impact of Cav1 on secretome of iPSC-MG under basal condition and upon pro-inflammatory and anti-inflammatory phenotype is resumed as a fold of change in **Table 6.2**.

Table 6.2 – The impact of Cav1 on secretome of iPSC-MG. iPSC-MG Cav1 NT and iPSC-MG Cav1 KO was differentiated from KOLF2 cells, left to rest and stimulated with LPS and IFN- γ or IL-4 and IL-13, for 48 hours. Non treated cells were used as control. The supernatants were collected, centrifuged, and incubated with membrane. The values represent the fold of change of Cav-1 KO cells normalized against Cav1 NT cells. Secreted products that are downregulated or upregulated are identified in green to yellow/red scale, respectively. Analytes with fold of difference greater than 2 or statistically significant are highlighted. *: $p < 0.05$ when compared to Cav1 NT cells, multiple t-test corrected.

Analyte	CTRL	LPS + IFN- γ	IL-4 + IL-13	Analyte	CTRL	LPS + IFN- γ	IL-4 + IL-13
IP-10/CXCL10	-1.58	1.14	-3.86	GDF-15	1.11	1.02	1.24
IL-31	-1.39	2.08	1.55	IL-1 β	1.12	1.81	1.13
Growth Hormone	-1.38	1.13	1.42	MIG/CXCL9	1.12	-1.01	-2.01
Adiponectin	-1.38	-1.03	1.35	Chitinase 3-like 1	1.13	-1.09	1.19
LIF	-1.35	-1.43	1.74	TfR	1.13	1.20	1.11
C-Reactive Protein	-1.29	-1.06	1.03	IL-3	1.13	1.15	1.30
RANTES/CCL5	-1.22	1.03	1.18	IL-22	1.15	1.33	1.19
PF4	-1.21	-1.35	1.23	RBP-4	1.16	-1.07	1.30
EGF	-1.17	1.19	1.44	MIP-3 α /CCL20	1.16	1.44	1.00
BAFF	-1.16	-1.15	1.43	TFF3	1.17	1.51	1.26
TNF- α	-1.14	1.91	1.01	IGFBP-3	1.18	1.17	1.26
Apolipoprotein A-I	-1.14	1.11	1.79	BDNF	1.18	1.18	1.22
VEGF	-1.13	-1.39	1.34	Thrombospondin-1	1.19	-1.25	1.27
IL-23	-1.13	-1.29	-1.02	IL-8	1.19	1.18	1.14
Leptin	-1.10	1.34	-1.06	EMMPRIN	1.21	1.14	1.47
IL-24	-1.09	-1.14	1.24	Serpin E1	1.22	1.27	-1.10
CD30	-1.09	1.17	1.29	Lipocalin-2	1.23	-1.03	1.13
Angiopoietin-2	-1.08	1.01	1.44	Endoglin	1.25	1.08	1.04
IL-33	-1.08	1.69	1.60	I-TAC/CXCL11	1.28	1.50	1.07
CFD/adipsin	-1.07	-1.10	1.25	ICAM-1	1.28	1.27	1.17
CD40 ligand	-1.07	-1.20	1.11	IL-6	1.29	1.57	-1.41
PDGF-AA	-1.05	1.10	-1.01	DPPIV	1.29	1.32	1.16
PDGF-AB/BB	-1.05	1.20	1.54	ENA-78	1.31	1.15	1.36
SDF-1 α	-1.04	-1.15	1.29	GRO- α	1.31	1.52	1.35
IL-19	-1.02	-1.18	1.32	MMP-9	1.31	-1.13	1.12
IL-17A	-1.02	1.28	1.30	GM-CSF	1.32	1.09	1.25
TARC	-1.01	1.43	1.55	IL-13	1.33	22.16	1.37
IL-2	1.00	1.12	1.10	MIF	1.33	1.17	1.03
Cripto-1	1.01	-1.42	1.17	IL-10	1.34	1.43	1.79
RAGE	1.01	-1.54	1.22	IL-11	1.34	1.19	1.33
Osteopontin	1.01	-1.10	1.09	Myeloperoxidase	1.37	-1.18	-1.06
IL-27	1.02	1.89	1.29	Flt-3 Ligand	1.40	1.94	1.23
ST2	1.03	-1.21	-1.01	MIP-1 α /MIP-1 β	1.41	1.08	-1.42
CD14	1.03	1.68*	1.95	Pentraxin-3	1.42	1.01	-1.09
IL-32	1.04	1.43	1.41	Vitamin D BP	1.43	1.55	1.56
IL-4	1.04	1.08	1.06	MCP-3	1.45	1.13	1.33
MIP-3 β	1.04	1.31	1.01	CD31	1.47	1.75	2.13

Angiogenin	1.05	1.36	2.36*	IGFBP-2	1.48	1.22	1.32
Relaxin-2	1.05	-1.33	1.76	uPAR	1.50	1.06	1.36
Resistin	1.06	-1.19	1.11	FGF basic	1.50	-1.22	1.33
FGF-19	1.07	-1.02	1.11	G-CSF	1.53	-1.14	-1.00
Cystatin C	1.07	-1.12	1.17	IL-1ra	1.57	1.32	1.20
VCAM-1	1.07	1.94	1.94	IL-15	1.62	3.92	1.64
C5/C5a	1.07	-1.20	1.59	IL-1 α	1.64	1.38	-1.11
SHBG	1.07	-1.48	1.04	HGF	1.67	1.13	1.16
IL-34	1.07	1.73	1.79	IFN- γ	1.70	1.08	-1.12
MCP-1	1.07	-1.01	1.24	IL-18 BP α	1.70	-1.05	1.64
IL-16	1.08	1.58	1.23	Kallikrein 3	1.72	1.16	1.03
Angiopietin-1	1.08	1.27	1.81	TIM-3	1.76	1.86	2.46
TGF- α	1.10	-1.05	1.32	IL-12 p70	1.82	1.79	1.53
M-CSF	1.10	1.58	1.14	Fas Ligand	1.98	1.05	-1.36
Dkk-1	1.11	1.15	-1.04	IL-5	2.13	-3.15	-1.13
FGF-7	1.11	-1.94	1.45				

Under basal phenotype, microglia cells where Cav1 was deleted released 1.58-times less the pro-inflammatory cytokine CXCL10 and increased the levels of 14 other analytes more than 1.5-times, where IL-5 was the most upregulated (2.13-times). The remaining analytes showed similar levels or variations lower than 1.5 times.

The pro-inflammatory phenotype allowed the microglia Cav1 KO cells to decrease the levels of IL-5 (3.15-times), FGF-7 (1.94-times) and RAGE (1.54-times) and to increase the amounts of 21 analytes more than 1.5-times. CD14 was enhanced 1.68-times ($p=0.03$) compared to Cav1 NT cells. IL-31 (2.08-times), IL-15 (3.92-times) and IL-13 (22.16-times) were the most upregulated secreted products found in the supernatant.

As for the anti-inflammatory phenotype, Cav1 KO cells reported a decrease of CXCL-10 (3.86-times) and MIG/CXCL9 (2.01-times) and an increase of 20 soluble factors superior to 1.5-times, where CD13 (2.13-times), angiogenin (2.36-times, $p=0.03$) and TIM-3 (2.46-times) showed the top improvements. The other products analysed presented similar levels or fluctuations less than 1.5 times.

In summary, iPSC-MG Cav1 KO cells showed an overall increase of secretion of inflammatory mediators, compared with cells that were able to express Cav1 protein.

6.4.7 Transcriptomic profile of activated microglia - RNA-seq

RNA-seq analysis was performed, not only under basal/inactivated stage, but also under the two main activation status, in order to explore in detail, the transcriptome of microglia cells differentiated from iPSC.

The first genes explored were the canonical genes related with microglial signature. This gene list was previously used by Abud *et al* and Haenseler *et al.* to validate the iPSC-MG (Abud *et al.* 2017; Haenseler *et al.* 2017). In independent studies, they showed an upregulation of these genes compared to macrophages and dendritic cells. Moreover, the expression of these genes was similar to foetal microglia and adult microglia.

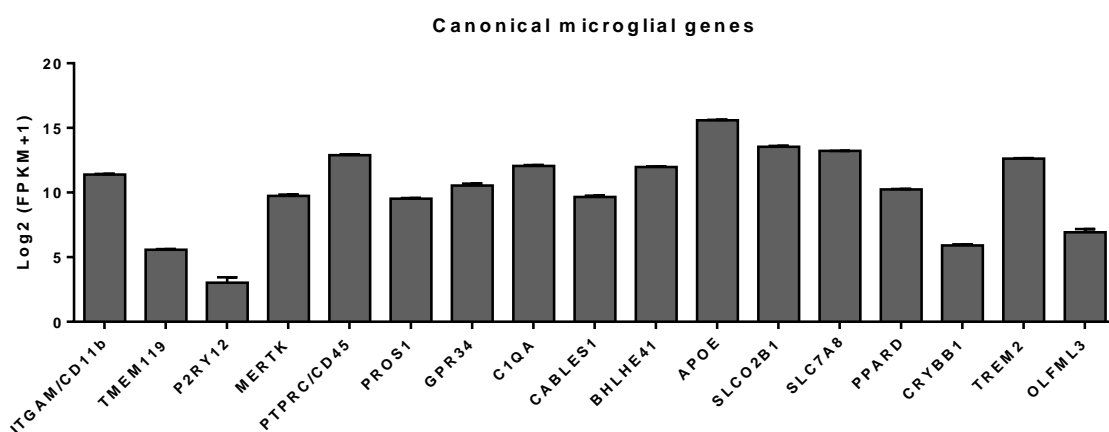


Figure 6.16 – Canonical microglial genes expressed by iPSC-MG Cav1 NT. iPSC-MG Cav1 NT was differentiated from KOLF2 cells. Bars represent microglial-specific or -enriched as [Log2 (FPKM +1)] presented as mean \pm SEM. N=3 distinct clones.

The **Figure 6.16** shows that, after differentiation, iPSC-MG Cav1 NT expressed canonical microglial genes, such as ITGAM, TMEM119, P2RY12, MERTK, PTPRC, PROS1, GPR34, C1QA, CABLES1, BHLHE41, APOE, SLCO2B1, SLC7A8, PPARD, CRYBB1, TREM2 and OLFML3. These genes are upregulated in microglia cells compared to macrophages or dendritic cells, except for PTPRC that is expected to be upregulated in macrophages and microglia, with a higher expression in macrophages.

Like in other experiments, microglia cells were differentiated from KOLF2 cells, left to recover, and further stimulated with LPS and IFN- γ or with IL-4 and IL-13, towards a pro-inflammatory or anti-inflammatory phenotype, respectively. Non stimulated cells were used as a control to access the basal state. Around 58,000 genes that could be affected

by microglial activation were evaluated, and the most relevant were used for posterior analysis.

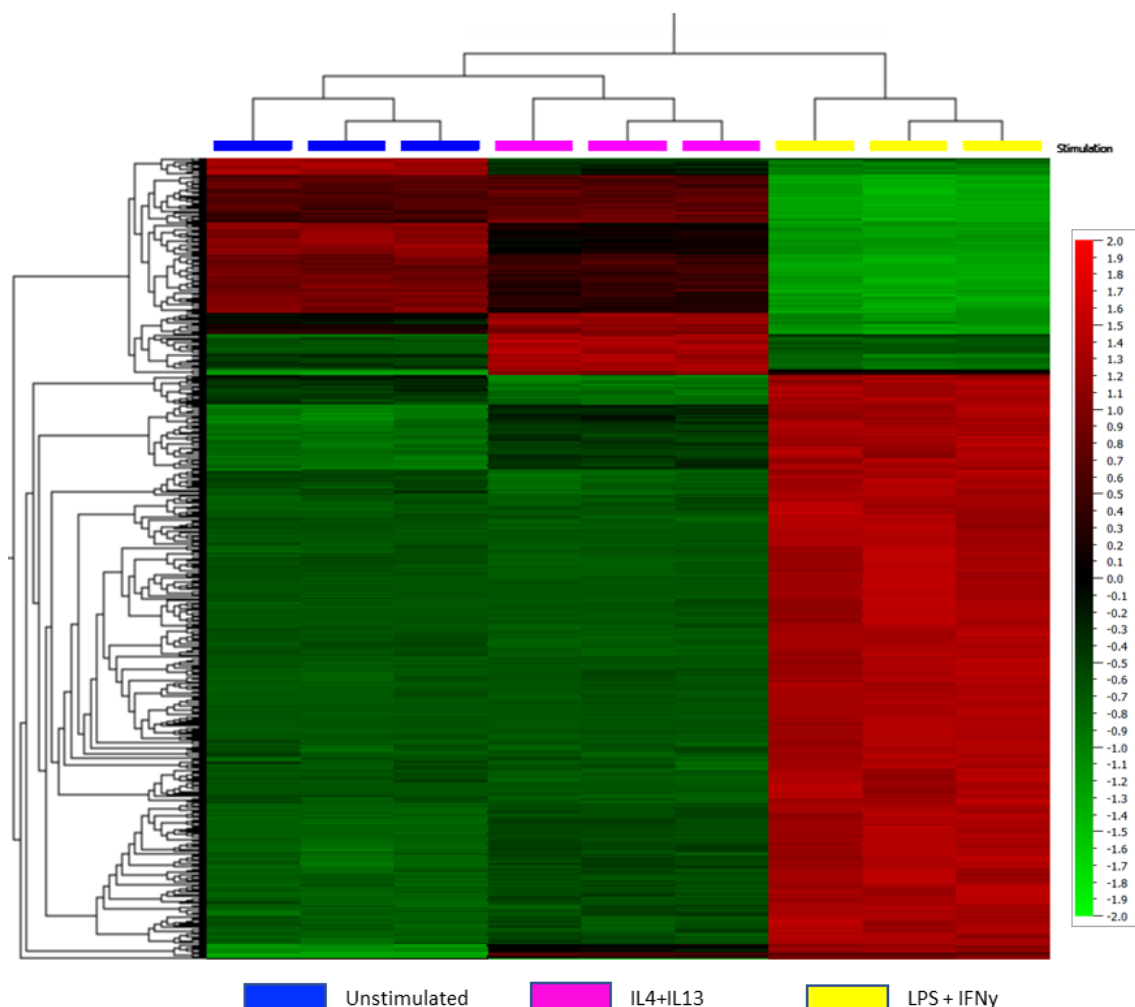


Figure 6.17 – Heatmap demonstrating the differential clustering of iPSC-MG Cav1 NT. iPSC-MG Cav1 NT were differentiated from KOLF2 cells, left to recover, and stimulated with LPS and IFN- γ (yellow) or IL-4 and IL-13 (pink), for 48 hours. Unstimulated cells were used as a control (blue). Red represents upregulated genes and green represents downregulated genes. Black represents unchanged expression. 5,000 selected genes with $p < 0.001$, multi-group comparison (F-test, ANOVA). N=3 distinct clones.

Based on normalized counts, the DE showed a gene signature associated with the microglia status and their activation phenotype (**Figure 6.17**). Hierarchical clustering based on DE genes with $p < 0.001$ showed that unstimulated and anti-inflammatory microglia are more related, which were clustering together, compared with pro-inflammatory microglia, which clustered in a different arm.

Pro-inflammatory profile of iPSC-MG Cav1 NT

Under pathological condition, microglia can be activated towards a pro-inflammatory phenotype. This phenotype will allow microglia cells to fight against pathogens or other cells that were identified as an enemy. Cells were challenged with LPS and IFN- γ in order to understand how iPSC-MG behaves under this phenotype. Using untreated cells cultured under basal conditions as control cells for comparison, it was possible to identify 1,719 upregulated and 1,772 downregulated genes (FDR<0.05 and FC>2).

The GSEA biological process analysis revealed that these genes are involved in the upregulation of 10 biological processes and in the downregulation of another 10 as seen in **Figure 6.18**. The biological processes involved in “response to virus”, “response to interferon-gamma”, “adaptive immune response”, “cell chemotaxis”, “response to type I interferon”, “positive regulation of response to external stimulus”, “response to tumour necrosis factor”, “interferon gamma production”, “positive regulation of cytokine production” and “response to molecule of bacterial origin” are significantly activated (FDR<0.05).

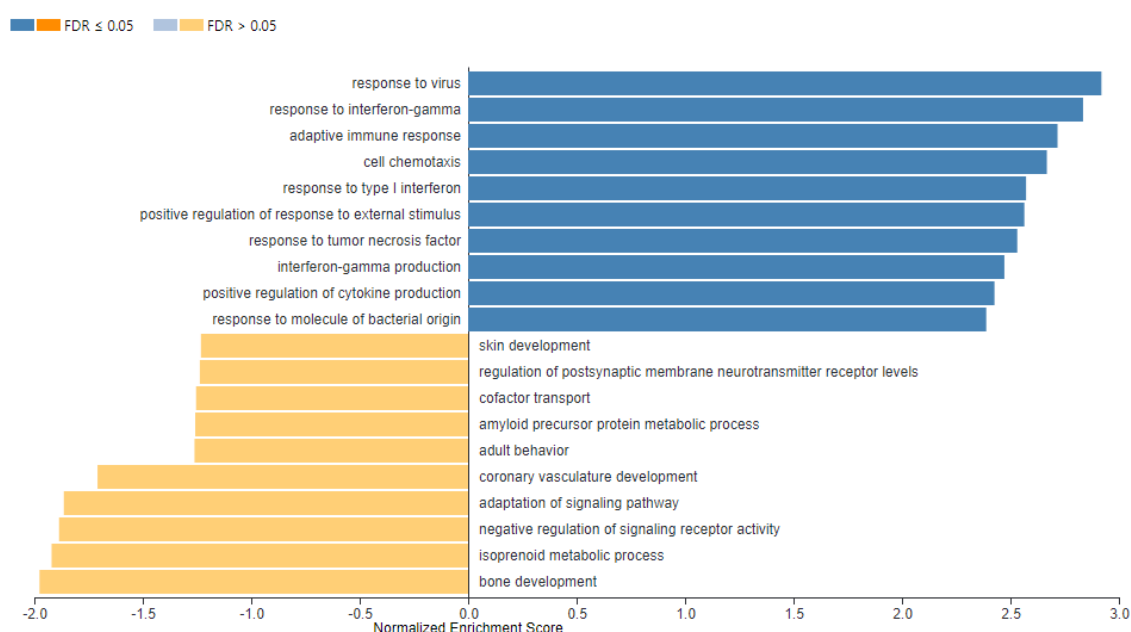


Figure 6.18 – GSEA biological process of pro-inflammatory iPSC-MG Cav1 NT. Over-representation of biological processes from 3,491 differential expressed genes, compared to untreated cells using GSEA: Gene Set Enrichment Analysis.

The GO analysis of biological processes of the differential expressed genes of iPSC-derived microglia under pro-inflammatory phenotype compared to basal iPSC-derived microglia is represented in **Figure 6.19**. Gene expression in iPSC-derived microglia under pro-inflammation was enriched in terms "adaptive immune response", "positive regulation of immune system process", "response to virus", "cytokine-mediated signalling pathway" and "response to interferon-gamma".

Focusing only on the GO analysis using "microglial cell activation" (GO:0001774), it was possible to identify an upregulation of TLR8, AIF1, TLR2 and CLU and a downregulation of TLR7 and MAPT (FDR<0.05 and FC>2). These genes are involved in the change in morphology and behaviour of a microglial cell as a result of activation

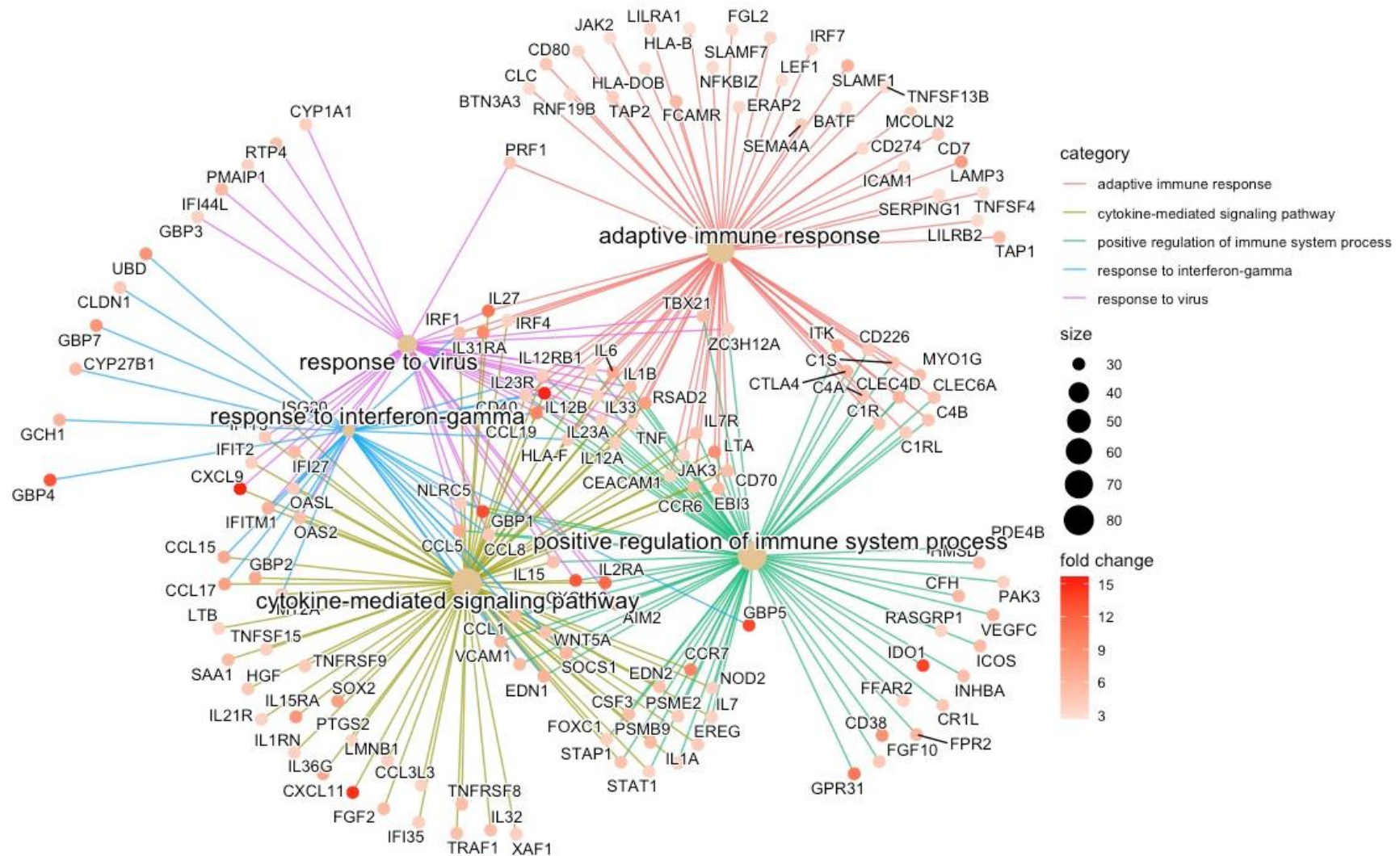


Figure 6.19 – Functional analysis of the iPSC-derived microglia under pro-inflammatory phenotype. Gene ontology analysis of biological processes (BP) for genes differentially expressed in iPSC-derived microglia under pro-inflammatory phenotype (*LPS + IFN-γ*) compared to iPSC-derived microglia unstimulated. Top 5 BP with $FDR < 0.05$ and $FC > 2$.

Anti-inflammatory profile of iPSC-MG Cav1 NT

Microglia can shift from pro-inflammatory to an anti-inflammatory phenotype in well-defined conditions, which is a crucial process for neuro-homeostasis and neuroprotection. Consequently, understanding the modulation of the microglial phenotype and the key pathways involved could be important to develop therapies, not only for neurodegenerative disorders, but also for brain tumours.

iPSC-MG cells were challenged with IL-4 and IL-13 in order to explore them under an anti-inflammatory phenotype. Using untreated cells cultured under basal conditions as control cells for comparison, it was possible to identify 318 upregulated genes and 188 downregulated genes (FDR<0.05 and FC>2). The top 10 upregulated and downregulated biological processes, where these genes are involved, were analysed with a GSEA biological process and are represented in **Figure 6.20**.

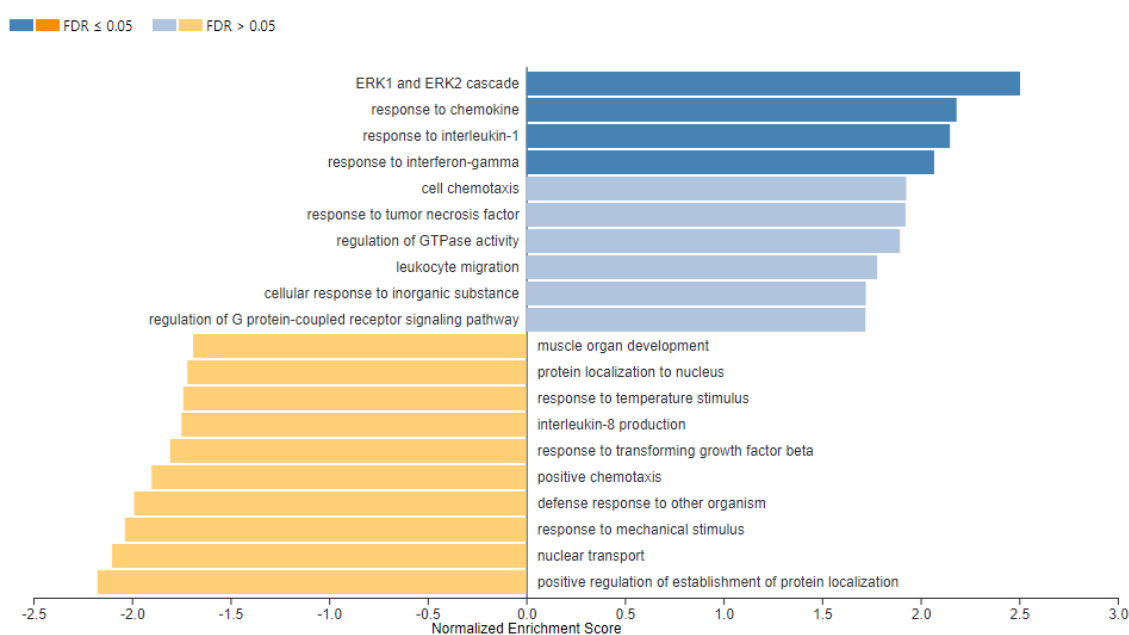


Figure 6.20 – GSEA biological process of anti-inflammatory iPSC-MG Cav1 NT. Over-representation of biological processes from 506 differential expressed genes, compared to untreated cells using GSEA.

Biological processes involved in “ERK1 and ERK2 cascade”, “response to chemokines”, “response to interleukine-1” and “response to interferon-gamma” are significantly activated (FDR<0.05). The remaining biological processes involved presented an FDR >0.05.

The GO analysis of biological processes of the differentially expressed genes of iPSC-derived microglia under the anti-inflammatory phenotype compared to basal iPSC-derived microglia is represented in **Figure 6.21**. Gene expression in iPSC-derived microglia under anti-inflammation was enriched in terms “ERK1 and ERK2 cascade”, “regulation of ERK1 and ERK2 cascade”, “positive regulation of ERK1 and ERK2 cascade”, and “G protein-coupled receptor signalling pathway”.

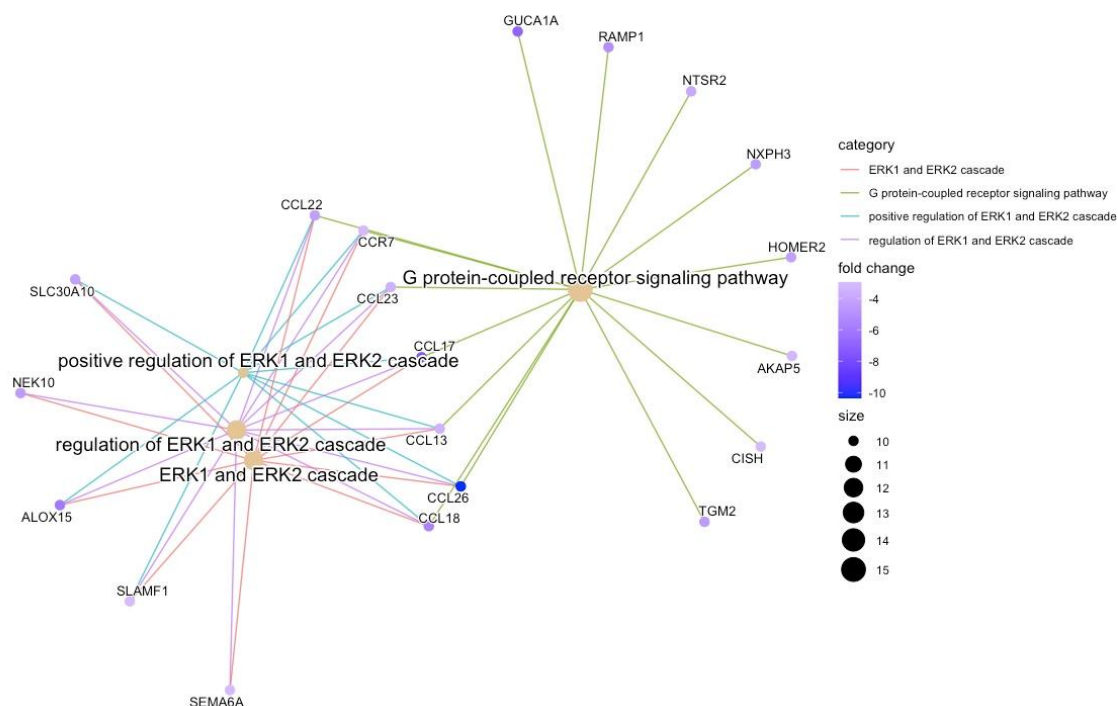


Figure 6.21 – Functional analysis of the iPSC-derived microglia under anti-inflammatory phenotype. Gene ontology analysis of biological processes for genes differentially expressed in iPSC-derived microglia under anti-inflammatory phenotype (IL-4 + IL-13) compared to iPSC-derived microglia unstimulated. BP with $FDR < 0.05$ and $FC > 1.5$.

Regarding the GO analysis using “microglial cell activation” (GO:0001774), it was possible to identify an upregulation of JUN and TRPV1 and a downregulation of TLR8, TLR7, TLR2 and TLR6 ($FDR < 0.05$ and $FC > 2$). These genes are involved in the change in morphology and behaviour of a microglial cell as a result of activation.

Microglial key genes during homeostasis and activation

The CNS is a highly vulnerable tissue which is protected with bone from the exterior and with the BBB from the interior. In addition, it is an organ with immune privileges that self-regulates its immunological components. Since it is a very delicate organ, the microglia need to be tightly regulated, otherwise an exacerbated and/or uncontrolled immune response could be destructive to the tissue.

The overlap of upregulated and downregulated genes in pro-inflammatory and anti-inflammatory phenotype was identified in order to understand the key genes and biological processes involved in microglial activation and regulation/homeostasis, as observed in **Figure 6.22**.

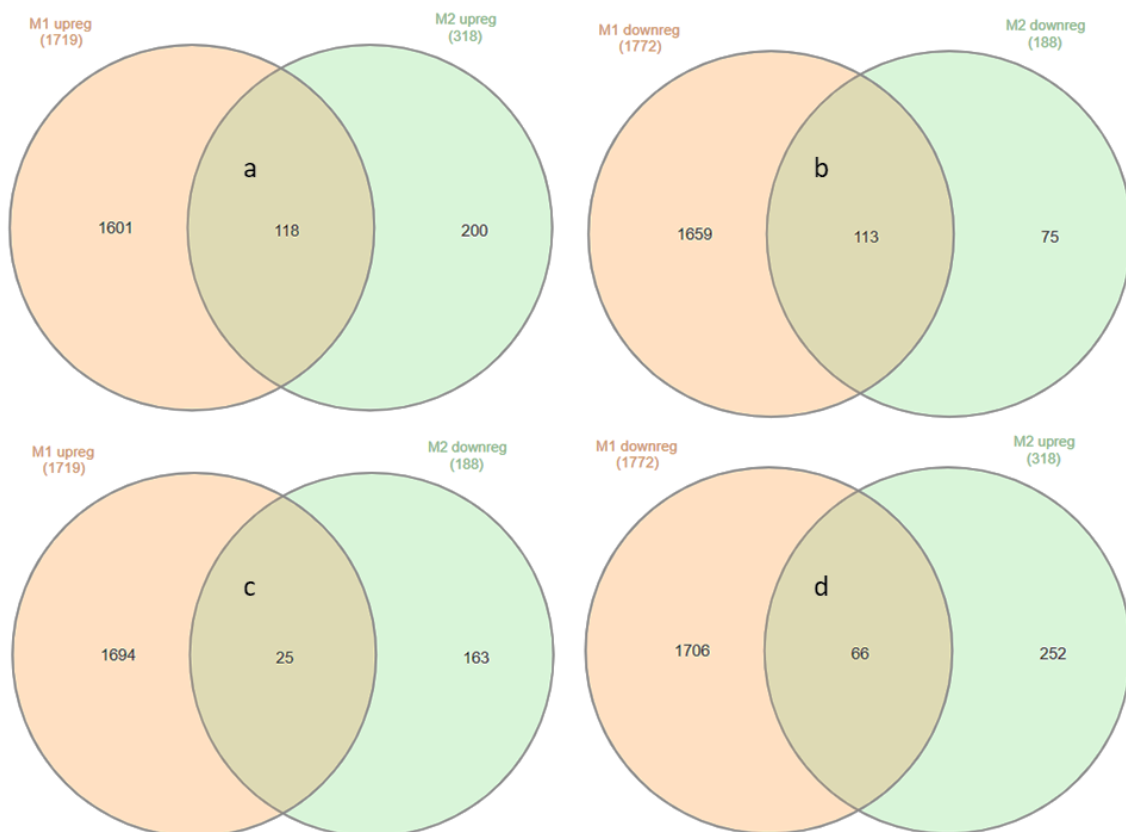


Figure 6.22 – Microglial key genes involved in activation and homeostasis. From the significantly ($FDR < 0.05$ and $FC > 2$) upregulated and downregulated genes in pro-inflammatory (M1 - LPS + IFN- γ) or in anti-inflammatory (M2 - IL-4 + IL-13) phenotype were identified the common genes in **a)** upregulated in M1 and M2, **b)** downregulated in M1 and M2, **c)** upregulated in M1 and downregulated in M2 and **d)** downregulated in M1 and upregulated in M2.

When the iPSC-MG is activated in pro-inflammatory (M1) or anti-inflammatory (M2) phenotype, 118 common genes were overexpressed **(a)** and 113 other genes were downregulated **(b)**.

Independently of the microglial status, 118 genes need to be upregulated and are involved in biological processes as “response to chemokine”, “response to interferon-gamma”, “lymphocyte mediated immunity”, “adaptative immune response”, “ERK1 and ERK2 cascade”, “cell chemotaxis”, “leukocyte cell-cell adhesion”, “T cell activation” and “positive regulation of cell adhesion” **(Figure 6.23)**.

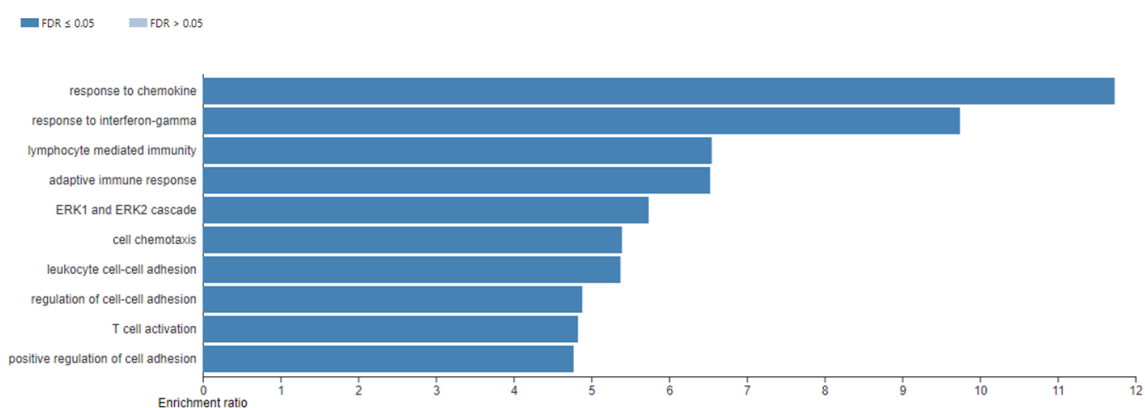


Figure 6.23 – ORA of biological processes of the common genes upregulated in pro-inflammatory and anti-inflammatory microglial phenotype.

Upon pro-inflammatory and anti-inflammatory microglial activation 113 genes were downregulated. These are mainly involved in the biological process such as “receptor complex”, “external side of the plasma membrane”, “extracellular matrix” and “cell surface”, as seen in **Figure 6.24**. The remaining biological processes presented an FDR higher than 0.05.

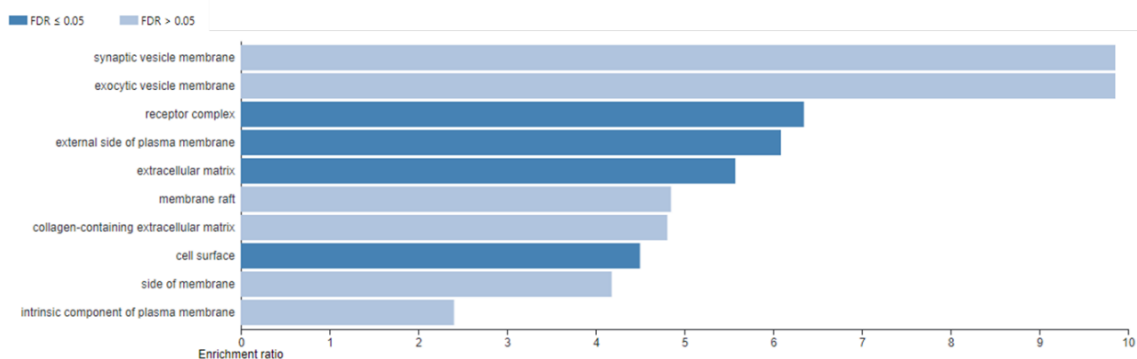


Figure 6.24 – ORA of biological process of the common genes downregulated in pro-inflammatory and anti-inflammatory microglial phenotype.

When iPSC-MG cells are in pro-inflammatory phenotype, 25 genes were identified as upregulated. These are the same genes that microglia downregulated in anti-inflammatory phenotype, suggesting that they can be key genes for pro-inflammatory immune response. These genes were involved in some biological processes; however, they presented an FDR higher than 0.05 (**Figure 6.25**).

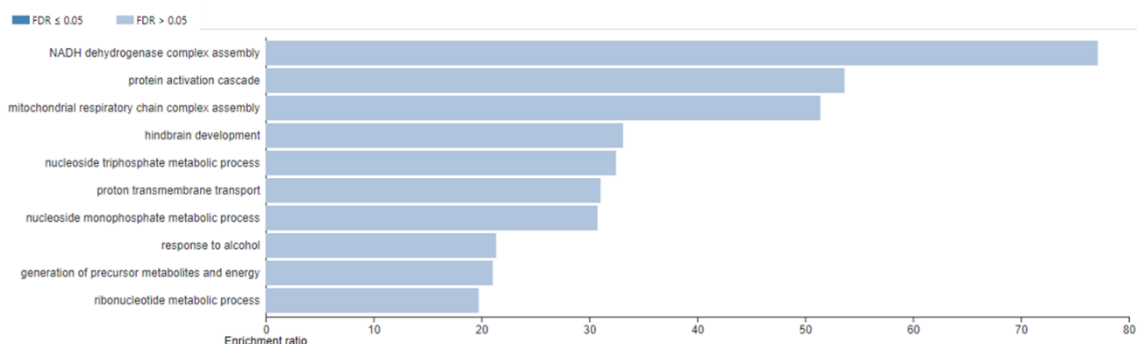


Figure 6.25 – ORA of biological process of the common genes upregulated in pro-inflammatory and downregulated in anti-inflammatory microglial phenotype.

Under an anti-inflammatory phenotype, microglia overexpressed 66 genes that overlapped the downregulated genes under a pro-inflammatory phenotype. They can be key genes involved in the anti-inflammatory response and are involved in the “regulation of inflammatory response”. The remaining biological processes presented an FDR higher than 0.05, therefore, the ORA can be misleading and a bigger sample is required to confirm these results (**Figure 6.26**).

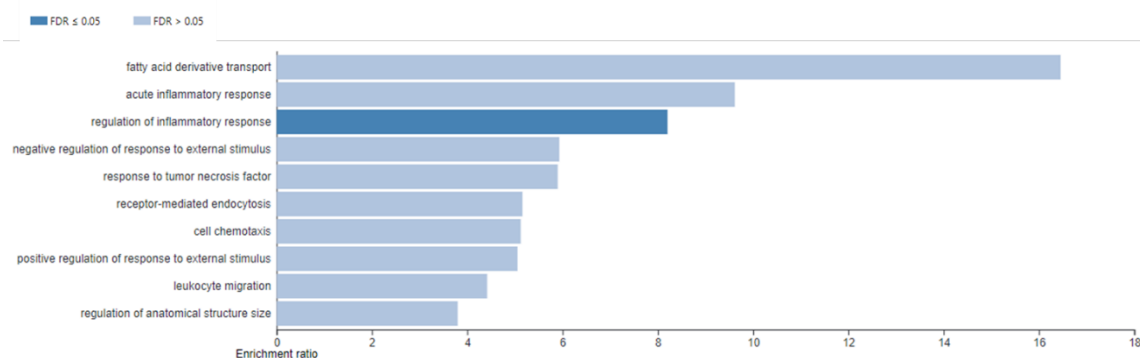


Figure 6.26 – ORA of biological process of the common genes downregulated in pro-inflammatory and upregulated in anti-inflammatory microglial phenotype.

6.4.8 Impact of Cav1 upon the transcriptomic profile – RNA-seq

Cav1 are specialized membrane microdomains involved in diverse functions, such as cholesterol homeostasis, signal transduction, cell morphology, cell migration and vesicular trafficking (Harris et al. 2002). Alterations on the metabolic state and morphology are key functions for microglial activation and Cav1 may have a role on that. Harris *et al*, in 2002 correlated the Cav1 with immune cells based on cell type, state of activation and/or maturation. Previously, in **Chapter 4**, it was demonstrated that CHME3 cell line expresses high levels of Cav1 and their role on the microglia behaviour was significantly explored.

With the objective of exploring in detail the role of Cav1 in microglia cells, iPSC-MG Cav1 KO were stimulated towards a pro-inflammatory (LPS and IFN- γ) and an anti-inflammatory (IL-4 and IL-13) phenotype and analysed by RNA-seq. Untreated cells and iPSC-Cav1 NT were used as a control.

The principal component analysis (PCA) showed a high correlation between the three biological replicates from each phenotype (control, pro-inflammatory and anti-inflammatory) and Cav1 status as seen in **Figure 6.27**.

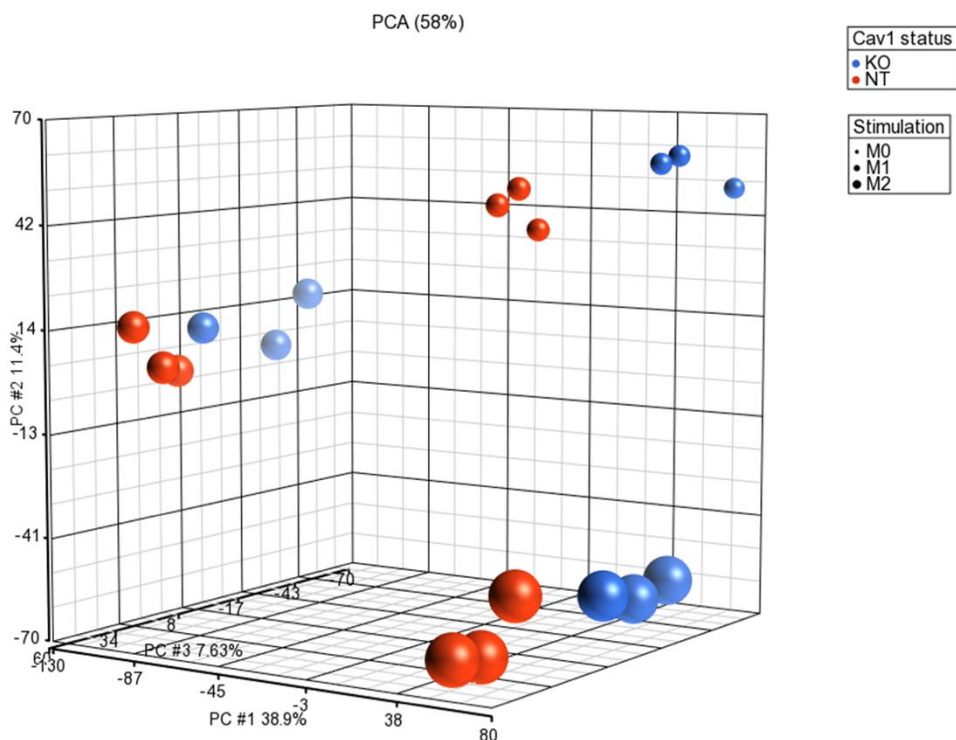


Figure 6.27 – PCA analysis of iPSC-MG Cav1 NT (Cav1 +ve) and iPSC-MG Cav1 KO. Both cells were stimulated towards a pro-inflammatory (M1: LPS and IFN- γ) and an anti-inflammatory (M2: IL-4 and IL-13) phenotype and analysed by RNA-seq. Untreated cells (M0) and iPSC-MG Cav1 NT were used as control.

Analysing the PCA plot and taking into consideration the Cav1 status, it is possible to observe a higher distance when microglia cells are under the basal or anti-inflammatory phenotype, suggesting a higher impact of Cav1 on these states.

Basal/unstimulated cells

In a simplistic approach, basal or unstimulated cells should represent the microglia under a healthy environment. Comparative with iPSC-MG Cav1 KO cells, and without interacting with any stimulus or other cell type, the presence of Cav1 in microglia led to a significant overexpression of 27 genes and to a downregulation of another 3, as seen in **Figure 6.28**. The main GSEA - biological process involved is “ERK1 and ERK2 cascade”, and on the reactome is “signalling by interleukin” highlighted, where the genes LIF, SPRY4, DUSP4, CCL4, CCL4L1, IRAK2, PTX3 and TNF have a role.

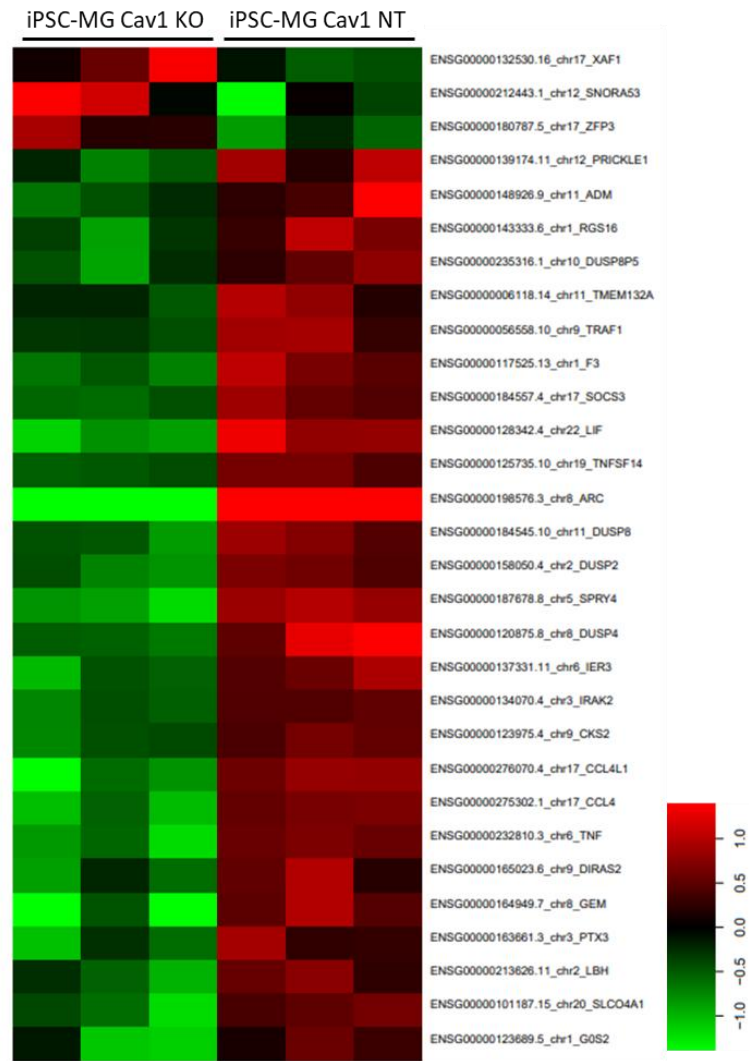


Figure 6.28 – Heatmap demonstrating the impact of Cav1 status on microglial basal phenotype. iPSC-MG Cav1 NT and iPSC-MG Cav1 KO were differentiated from KOLF2 cells and left to recover for an additional 5 days. Cells were cultured in standard conditions without the interference of any stimulus. Red represents upregulated genes and green represents downregulated genes. Black represents unchanged expression. Genes presented an $FDR < 0.05$ and $FC > 2$, multi-group comparison (F-test, ANOVA). $N = 3$ clones.

All the genes with the respective q-value are illustrated in the **Appendix VII – RNA-seq (Supplementary table VII.1)**.

Pro-inflammatory phenotype

Under a pro-inflammatory phenotype, Cav1 positive microglia significantly overexpressed 9 genes and downregulated another 3, as observed in the heatmap in **Figure 6.29**. The chemokines CXCL3 and CXCL2 are involved in the main biological processes of “response to molecule of bacterial origin”, “cellular response to biotic stimulus” and “leukocyte migration”. Regarding the reactome analysis, “signal transduction”, “metabolism of proteins” and “pro-translational protein modification” are overrepresented, where FSTL1 and IL-33 are involved.

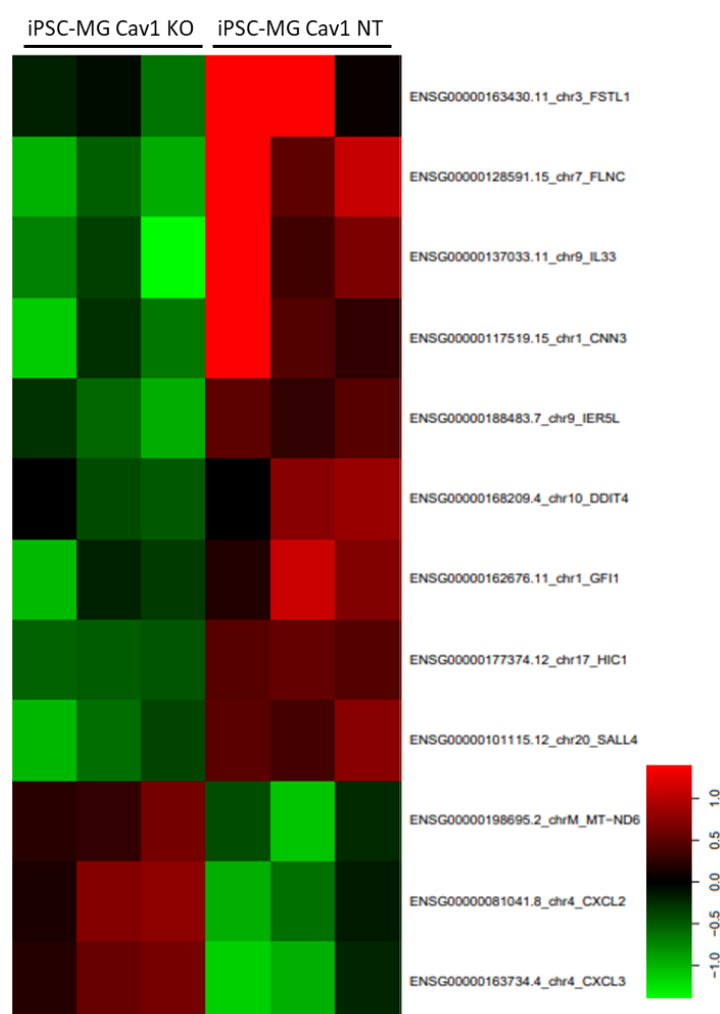


Figure 6.29 – Heatmap demonstrating the impact of Cav1 status on microglial pro-inflammatory phenotype. iPSC-MG Cav1 NT and iPSC-MG Cav1 KO were differentiated from KOLF2 cells, left to recover, and stimulated with LPS and IFN- γ , for 48 hours. Red represents upregulated genes and green represents downregulated genes. Black represents unchanged expression. Genes presented an $FDR < 0.05$ and $FC > 2$, multi-group comparison (F-test, ANOVA). $N = 3$ clones.

All the genes with the respective significance (q-value) are illustrated in the **Appendix VII – RNA-seq (Supplementary table VII.2)**.

Anti-inflammatory phenotype

The Cav1 status showed the biggest difference in terms of differential gene expression under an anti-inflammatory phenotype. Cav1 positive cells significantly overexpressed 36 genes and downregulated another 2, as observed in **Figure 6.30**.

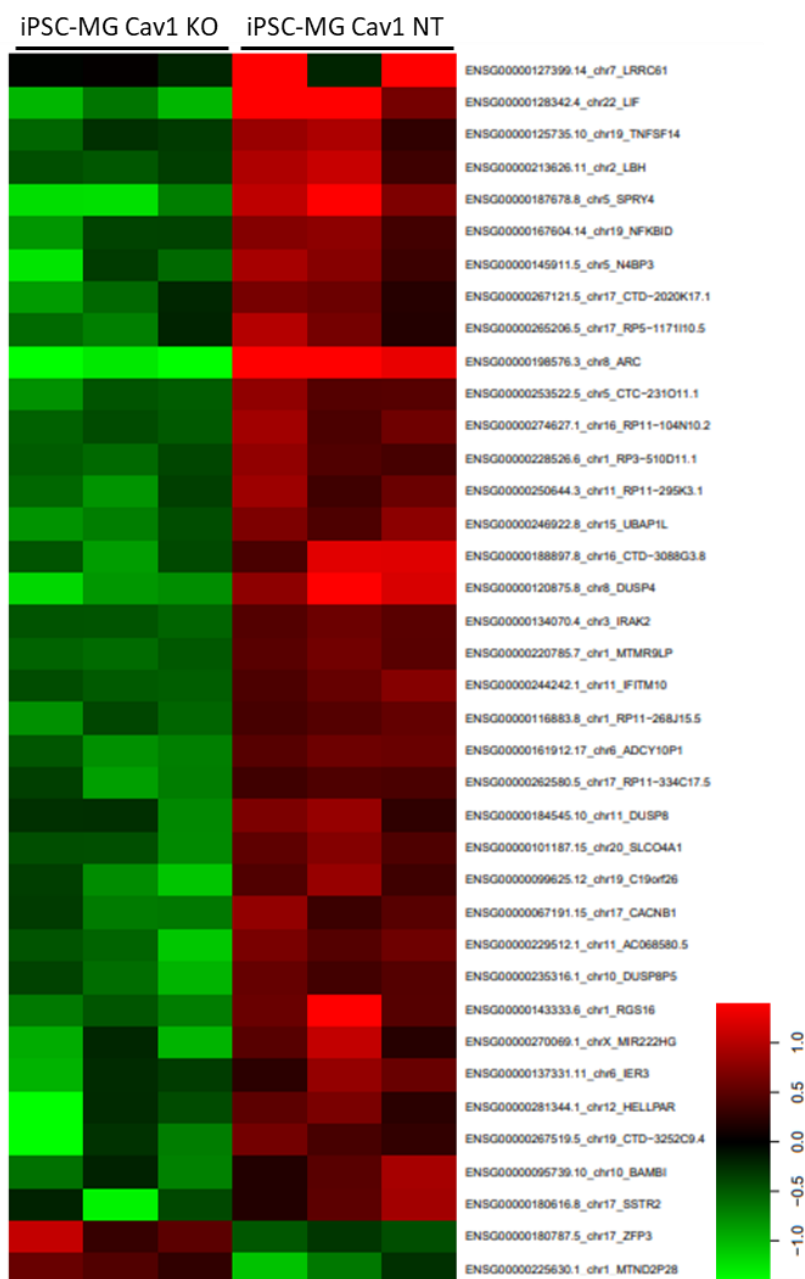


Figure 6.30 – Heatmap demonstrating the impact of Cav1 status on microglial anti-inflammatory phenotype. iPSC-MG Cav1 NT and iPSC-MG Cav1 KO were differentiated from KOLF2 cells and stimulated with IL-4 and IL-13, for 48 hours. Red represents upregulated genes and green represents downregulated genes. Black represents unchanged expression. Genes presented an $FDR < 0.05$ and $FC > 2$, multi-group comparison (F-test, ANOVA). $N = 3$ clones.

The GSEA of biological processes overrepresented LIF, DUSP8 and SPRY4, which are involved in “ERK1 and ERK2 cascade”, and IRAK2 and NFKBID, which are involved in “inflammatory response”. Regarding the ORA, the reactome highlighted the genes LIF, TNFSF14 and DUSP4, which are involved in pathways related with “signalling of interleukins”, “immune system” and “cytokine signalling in immune system”.

All the genes with the respective significance (q-value) are illustrated in the **Appendix VII – RNA-seq (Supplementary table VII.3)**.

6.4.9 Phagocytic ability on iPSC-derived microglia activation: the impact of Cav1

In order to evaluate the phagocytic ability of microglia cells derived from iPSC as well as the impact of Cav1 on that, microglia was differentiated from KOLF2 Cav1 NT and KOLF2 Cav1 KO cells, following the protocol described in **Figure 6.1**. Furthermore, to investigate if the activation phenotype influences phagocytosis, the differentiated microglia was further stimulated towards a pro-inflammatory phenotype, with LPS and IFN- γ , or towards an anti-inflammatory phenotype, with IL-4 and IL-13, for 48 hours. After these treatments, the pH-sensitive pHrodo green *E. coli* bioparticles were added and images were taken every 20 minutes for 4 hours.

The phagocytosis of green bioparticles by iPSC-MG Cav1 NT and iPSC-MG Cav1 KO is described in **Figure 6.31**.

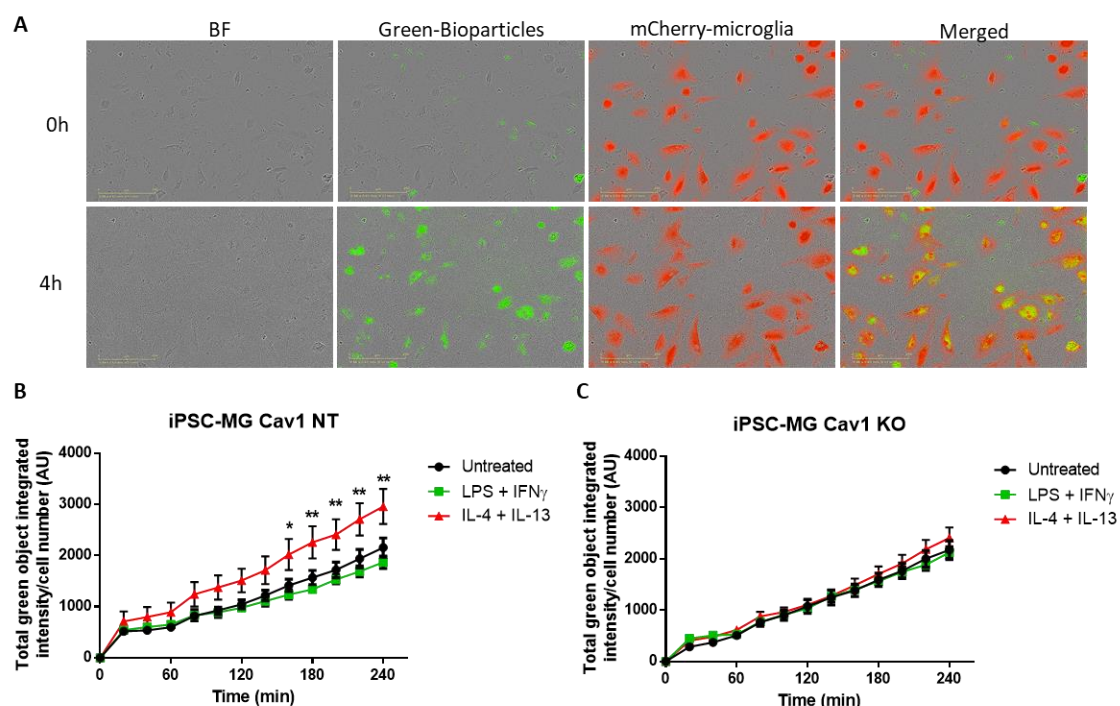


Figure 6.31 – Phagocytic ability of iPSC-MG Cav1 NT and iPSC-MG Cav1 KO. Both populations were differentiated from microglial progenitors, for 14 days with IL-34 and GM-CSF and allowed to rest for an additional 5 days in medium without interference of any soluble factor, followed by stimulation with LPS and IFN- γ (green) or with IL-4 and IL-13 (red) for further 48 hours. Untreated cells (black) were used as control. After stimulation pHrodo green *e. coli* bioparticles were added and imaged every 20 minutes for 4 hours, using the Incucyte microscope. **A.** Representative pictures immediately after the bioparticles were added and after 4 hours. **B and C.** Phagocytic capacity over time of iPSC-MG Cav1 NT and iPSC-MG Cav1 KO, respectively. Bars represent the mean of integrated intensity normalized to the number of cells \pm SEM of 4 clones from two independent experiments. *: $p < 0.05$, **: $P < 0.01$ when compared to untreated cells, two-way Anova, Dunnett's multiple comparisons test. Scale bar: 200 μ M.

Independently of Cav1 status and activation phenotype, these cells were able to engulf the bioparticles. In **Figure 6.31 – A** it is possible to observe a representative picture of iPSC-MG at the time points of 0 and 4 hours. Over time, microglia were able to phagocytose the bioparticles, which became green with the decrease of pH inside of the phagosome. Regarding the quantification analysis, it was possible to observe that the iPSC-MG Cav1 NT (**Figure 6.31 – B**), when stimulated towards a pro-inflammatory phenotype, trended to slow down the phagocytosis slightly, however, these cells showed a significant increase of the ability to phagocytose these bioparticles in an anti-inflammatory phenotype. This improvement was more evident after 140 minutes upon incubation. As for the iPSC-MG Cav1 KO (**Figure 6.31 – C**), these cells presented a performance similar to untreated cells, as well as cells that were previously activated in the direction of a pro-inflammatory or anti-inflammatory state.

The impact of Cav1 was further investigated in different microglial phenotypes and it is described in **Figure 6.32**.

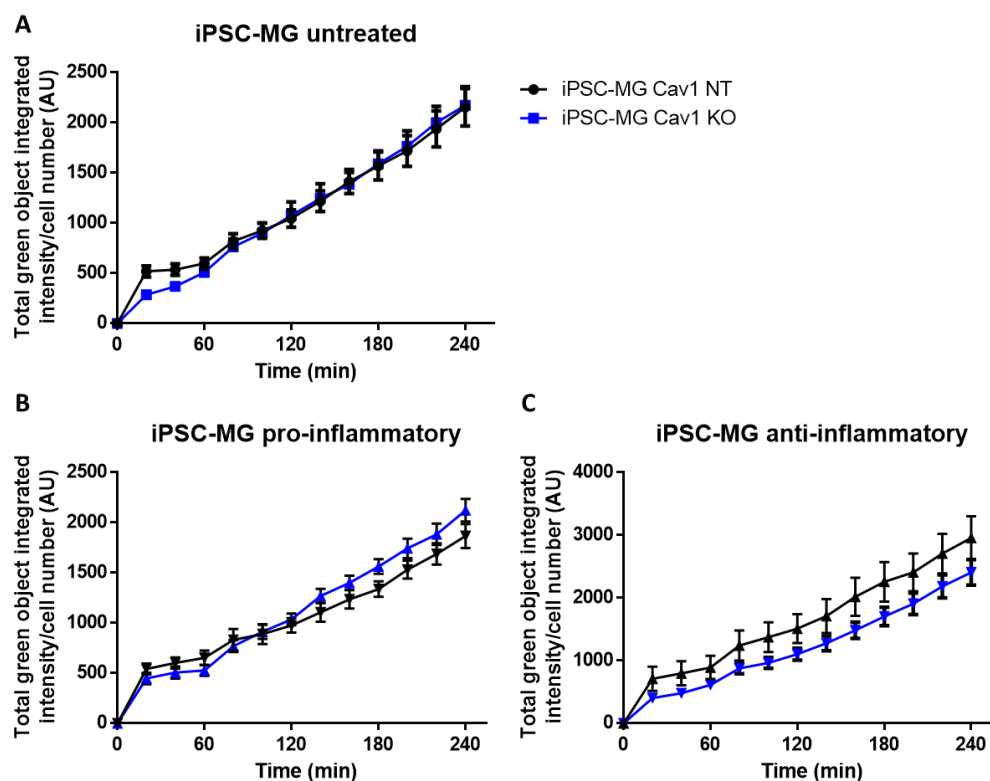


Figure 6.32 – Impact of Cav1 upon Phagocytic ability of microglia cells. iPSC-MG Cav1 NT (black) and iPSC-MG Cav1 KO (blue) were differentiated from microglia progenitors, for 14 days with IL-34 and GM-CSF and allowed to rest for an additional 5 days in medium without interference of any soluble factor, followed by stimulation with LPS and IFN- γ (B) or with IL-4 and IL-13 (B) for further 48 hours. Untreated cells (A) were used as control. After stimulation pHrodo green *e. coli* bioparticles were added and imaged every 20 minutes for 4 hours, using the Incucyte microscope. Bars represent the mean \pm SEM of 4 clones in two independent experiments.

Untreated cells, both Cav1 NT and Cav1 KO, presented a similar increase of phagocytosis over time (**Figure 6.32 - A**). For the pro-inflammatory phenotype (**Figure 6.32 - B**), compared with the Cav1 NT cells, Cav1 KO microglia cells exhibited a reduced ability up to 80 minutes of incubation, however, they recovered the phagocytic ability after 2 hours of incubation. Under an anti-inflammatory phenotype (**Figure 6.32 - C**), the presence on Cav1 on microglia cells trended to boost the engulfment of these bioparticles.

6.5 Discussion

Over the last years, with the iPSC technology, it is easier for researchers to access a big range of human differentiated cells, including the microglia population. Haenseler and collaborators compared different well-defined serum free protocols to obtain microglia cells, studying thoroughly each one. In 2017, they published a highly efficient protocol which recapitulates the development of microglia *in vitro*, where cells express key human microglial-specific markers, upregulated homeostatic pathways, and downregulated pathogen-response pathways, exhibiting a transcriptional profile similar to the foetal human microglia. Moreover, the differentiated cells presented a phagocytic capability and adopted a highly dynamic ramified microglia-like morphology. Upon pro-inflammatory activation, they display an activated morphology, shortening the ramified processes and enlarging their body, releasing a battery of microglia-relevant factors (Haenseler et al. 2017).

The well-defined serum free protocol described by Haenseler et al. 2017 was used to recapitulate the *in vivo* yolk sac-derived microglia development using human iPSC. However, a resting step was introduced in the last step of differentiation in the protocol to allow the microglia to recover from the differentiation process. The protocol started with the generation of EBs with a well-defined size, treated with BMP4 to induce the mesoderm, VEGF to induce the endothelial precursors and SCF to induce the hematopoietic precursors. At this stage it was already possible to see the development of cysts and yolk-sac-like structures. To promote the myeloid differentiation, the EBs were seeded into a Matrigel-coated flask and treated with XVIVO-15 media supplemented with IL-3 and M-CSF. Like Haenseler described, at this point the EBs were adherent, the stromal cells started to arise from the cysts and embryonic-like microglial precursors emerged into the supernatant as a uniform population of large and round cells. The literature indicates that these precursors are MYB-independent and RUNX1- and PU.1-dependent, as the foetal microglia during the *in vivo* development (Wilgenburg et al. 2013; Buchrieser, James, and Moore 2017). Cells were expressing high levels of CD11b and CD45 (microglial/macrophages markers) and low levels of CD34 (HSC marker), indicating that the differentiation was driven in the right direction and

confirming the haematopoietic commitment. The floating microglia precursors were collected for final differentiation into microglia cells (iPSC-MG), showing similar morphological features as obtained by Haenseler and colleagues and upregulating the microglial markers TMEM119 and Iba1 (Haenseler et al. 2017).

The canonical microglial-related genes were further investigated by RNA-seq, showing that the iPSC-MG obtained in this project was expressing ITGAM (also known as CD11b), P2RY12, MERTK, PRPCR, PROS1, GPR34, C1QA, CABLES1, BHLHE41, APOE, SLCO2B1, SLC7A8, PPARC, CRYBB1, TREM2 and OLFML3. This panel of genes allows to differentiate microglia from peripheral blood macrophages and macrophage-resident tissues (Muffat et al. 2016).

To the best of our knowledge, the role of Cav1 in iPSC-MG was never investigated. After differentiation, it was not possible to detect the Cav1 using WB, therefore their quantities were investigated at mRNA levels. At mRNA levels it was possible to identify Cav1 expression, which increased in a pro-inflammatory phenotype and decreased in an anti-inflammatory phenotype, suggesting already a possible involvement in microglia response to different stimulus. The levels of mRNA were confirmed in the RNA-seq data, where the number of reads was low as well. Interestingly, even with low levels of expression, it was possible to detect Cav1 protein by IF.

Klf2 cells expressed great levels of Cav1 before the differentiation into microglia, however, Cav1 dramatically decreased during this process. In order to investigate when this change happened, Cav1 protein levels were evaluated in microglial precursor cells, showing at this time point undetectable levels by WB (data not shown). This suggests an involvement of Cav1 during the differentiation, where its levels decreased between the EBs formation and the IL-3 and M-CSF treatment for differentiation (between day 0 and 21). However, further investigation is needed to determine the right time point.

During the murine development, at the mRNA level, Cav1 was detected on embryonic day (E) 7, downregulated by E11, upregulated by E15, and remained elevated until E20. As for the protein, it was detectable by E10, then undetectable at E11, upregulated at E13, and remaining elevated up to E20 (Sohn, Brick, and Tuan 2016). Although this data is from whole mouse embryos that represent more than the microglia population, it was

possible to identify a fluctuation in Cav1 during the murine development. Cav1 during development has been associated with negative regulation of TGF- β and FGF2 (Razani et al. 2001; Razani, Woodman, and Lisanti 2002), signal transduction of BMP (Nohe et al. 2005) and crypto-1 specification of mesoderm and endoderm (Bianco et al. 2008; Cheng et al. 2003), suggesting that Cav1 might need to be downregulated during the development/differentiation.

Most of the studies using iPSC-MG are stimulating the microglia with LPS and/or IFN- γ or focusing on the role of microglia in neurodegenerative diseases, where the chronic pro-inflammatory response is involved. The GBM tumour environment is known to be immunosuppressive and for this reason it is extremely important to understand the anti-inflammatory response by the iPSC-MG. Because these cells are differentiated from iPSC using a defined cocktail of cytokines and interleukins, there was a concern about the effect that they could have on the activation status in microglia cells upon differentiation. IL-34 contributes to the development and maintenance of specific myeloid cell subsets in a tissue-specific manner: Langerhans cells in the skin, and microglia in the brain, however it is correlated with anti-inflammatory response in some tumours (Baghdadi et al. 2018; Franzè et al. 2020). GM-CSF is involved not only on differentiation, but also on survival, proliferation, maturation and functional activation of immune cells, initiating the transcription of the pro-inflammatory signalling pathways PI3K-Akt, ERK1/2, JAK2/STAT5 and NF- κ B (Metcalf 2008; Bhattacharya et al. 2015).

For this reason, in our protocol, differentiated cells were allowed to recover from the differentiation to avoid the possible activation that these could present. Analysing the mRNA of pro-inflammatory and anti-inflammatory genes, it was possible to observe that these cells presented higher levels of anti-inflammatory related genes right after the differentiation. It was also observed that in the recovery period without interference of IL-34 and GM-CSF, microglia were able to downregulate their anti-inflammatory genes. This was visible in the morphological characteristics as well, where rested cells started to increase the number of ramifications and shrinking their cellular bodies, confirming the degree of activation on freshly differentiated cells. Moreover, rested microglia responded better to anti-inflammatory activation, showing an increase of anti-inflammatory genes upon treatment with IL-4 and IL-13, suggesting that the

differentiation procedure led to microglial activation, and that cells must reach an inactivated phenotype before a stimulation, particularly important for an anti-inflammatory response.

Microglia, as other immune cells, are characterized by the ability to respond to external stimulus, leading to activation or inactivation of specific inflammatory pathways. A higher expression of anti-inflammatory related genes was observed at basal level. The basal status cluster with anti-inflammatory activation (RNA-seq), confirming that microglia display anti-inflammatory regulation similar to the one found in a healthy brain, where microglia cells are tightly regulated by surrounding cells to prevent an exacerbated immune response and damage of the brain tissue (Perry and Teeling 2013; Deczkowska, Amit, and Schwartz 2018; Szepesi et al. 2018).

Upon activation iPSC-MG can display a pro-inflammatory or an anti-inflammatory phenotype. The treatment with LPS and IFN- γ led to an increase of all pro-inflammatory related genes analysed by PCR, and to a decrease of some anti-inflammatory related genes, as IL-10, CD200R, CD206 and CD163. For the secreted product levels, it was possible to confirm the presence of a battery of pro-inflammatory factors, as GM-CSF, GRO- α , IL-6, CXCL10, I-TAC (CXCL11), MCP-3, MIG (CXCL9), MIP-1 α/β (CCL3/CCL4), MIP-3 α (CCL20), Rantes (CCL5), TNF- α and uPAR, but also some anti-inflammatory factors or interleukins in order to prevent an uncontrolled inflammatory response, as IL-4 and IL-18 BPa. Regarding the big picture from the RNA-seq data, the pro-inflammatory activation showed that the upregulated or downregulated genes are involved on the overall immune system activation, where biological processes related with immune response are overrepresented proving the identity of the microglia cells.

For the anti-inflammatory response, and contrary to CHME3 cells, the iPSC-MG were able to respond to IL-4 and IL-13, increasing the mRNA levels of CCL22, CD200R, CD206, CD163 and IL-10, together with a slight decrease of TNF- α . Since the anti-inflammatory phenotype and the basal status were clustering together, it was expected a smaller variation in comparison with the one obtained in pro-inflammatory phenotype. Nevertheless, it was possible to identify factors related with suppression of the immune function, as GM-CSF, IL-1Ra, IL-19 and TARC (CCL17), and also the pro-inflammatory related factors Fas ligand, MIG (CXCL9) and MIP-1 α/β (CCL3/CCL4), to balance the anti-

inflammatory response. As for the reactome analysis from the DE expressed genes, it was possible to visualize an immune system deactivation, where the biological processes related with immune system are overrepresented, suggesting again a correlation of microglial identity with the immune response expected.

Low levels of Cav1 were observed in iPSC-MG, which were comparable with the levels found in human fresh microglia. Exploring the Darmanis data base from single cell RNA-seq (accession number GSE67835), in the immune population of a healthy brain, that should comprise only microglia cells, Cav1 levels were low and in some samples not detectable at all (Darmanis et al. 2015). Despite the low levels of Cav1 in the basal status, it was suggested that their levels increased with microglia activation (Niesman et al. 2013).

Under resting status, independently of Cav1 status, microglia presented a similar expression of the genes analysed by PCR. At secretome, a suppression of CXCL10 was observed in iPSC-MG Cav1 KO cells, however other factors like IL-5, IL-12, IFN- γ , IL-13 and IL-10 were more concentrated. Taking into consideration all genes analysed in RNA-seq, it was possible to see a clear cluster of Cav1 NT and Cav1 KO unstimulated cells. Looking in detail to the DE genes, it was possible to see that MAPK (ERK1/2 cascade) and signalling by interleukins were upregulated in cells able to express Cav1 under a basal status. EGFR – MAPK (ERK1/2 cascade) is involved in inflammatory response (Lu and Malemud 2019), and the inactivation of this pathway might lead to superior mRNA stability of inflammatory gene transcription (Pastore et al. 2005). Vetterkind *et al.* demonstrated that Cav1 is an upstream scaffold for ERK1/2 activation, using rat aorta cells (Vetterkind et al. 2013), suggesting that Cav1 might regulate the inflammation via ERK1/2 signalling by increasing the instability of inflammatory-related mRNA (post-transcriptional regulation).

Under a pro-inflammatory environment, upon LPS and IFN- γ treatment, Cav1 deletion in microglia led to the expression of higher levels of TNF- α , IL-6, IL-1 β , IL-12 and CXCL10, suggesting that the presence of Cav1 can regulate the pro-inflammatory response in this context. These alterations at mRNA were corroborated at supernatant levels, where TNF- α , IL-1 β , IL-12, IL-6 together with IL-31, CD14, IL-15 and IL-13 were higher in Cav1 KO cells in comparison with Cav1 NT cells. The DE analysis identified genes that are

involved in cellular response to biotic stimulus, response to molecule of bacterial origin and leukocyte migration upregulated in microglia Cav1 KO, and other genes involved in signal transduction (JAK-STAT and NF- κ B-I κ B), metabolism of proteins and post-translational protein modification were upregulated in Cav1 NT cells. JAK-STAT and NF- κ B are closely related with inflammatory response and its inhibition promotes an anti-inflammatory response (Ma et al. 2015). Lu *et al.* suggested that ERK1/2 could activate both MAPK and JAK/STAT signalling through pro-inflammatory activation (Lu and Malemud 2019). If Cav1 is a scaffold of ERK1/2 stabilizing the mRNA and regulating the inflammatory response, it is possible that in an anti-inflammatory environment it has the same role, but further studies are required to clarify this assumption.

Regarding the anti-inflammatory environment, upon IL-4 and IL-13 treatment, the effect of Cav1 was less noticeable. The mRNA levels from anti-inflammatory related markers analysed by PCR were similar in both populations, with the exception of a minor upregulation of IL-10 that led to an increase of IL-10 secretion by iPSC-MG KO Cav1. The remaining secreted products exhibited an overall overexpression, where not only the anti-inflammatory related factors were overrepresented, but also some pro-inflammatory related factors and immune response regulators, as CD31 and TIM-3. At a higher level, RNA-seq analysis identified a downregulation of DE genes in microglia Cav1 KO cells. These genes were involved in the inflammatory response, cytokine signalling in immune system and ERK1/2 cascade, suggesting an involvement of Cav1. Furthermore, from all 38 genes differential expressed when Cav1 was deleted, 13 of them were overlapping the basal status, corroborating the idea that unstimulated microglia cells reassemble some of the anti-inflammatory features. Taking into consideration the Cav1 role, the remaining 25 genes were probably the most important to react to an anti-inflammatory stimulus. Using reactome analysis, these 25 genes were involved in TGF- β signalling, and possibly were prompting the exacerbated inflammatory response upon activation, however further studies are needed to clearly understand the involvement of Cav1. TGF- β signalling has been suggested as an important regulator of T-cell proliferation, differentiation, magnitude and type of immune responses against microbes (M. O. Li et al. 2006).

Wang *et al.* highlighted the importance of Cav1 for the phosphorylation of ERK1/2 in murine macrophages, where the presence of Cav1 led to a decrease of TNF- α and IL-6 and to an increase of IL-10, upon cellular stimulation with LPS, suggesting that Cav1 targets MAPK and PI3K in immune responses (X. M. Wang *et al.* 2006). On the hand, Guo *et al.* studied pulmonary inflammation by infection with *K. pneumoniae*, and showed that Cav1 KO mice presented higher levels of IFN- γ , TNF- α , IL-1 β , IL-6 and IL-10 when compared to Cav1 WT mice, showing exacerbated levels of ERK1/2 phosphorylated (Guo *et al.* 2012). The Cav1 role in immune cells seems to be related with the stabilization of the inflammatory response, however, the function can differ depending on the immune cell type and environment/disease associated, like what happens in tumours that can assume a pro-tumoral or anti-tumoral role, depending of the tumour context.

Regarding the phagocytosis, it is an extremely important process during the neuronal development and adulthood, not only to clear the apoptotic cells, bacteria and virus, and remodelling the neuronal connectivity by engulfment of synapses, but also to remove unfolded proteins and neurotoxic molecules that can damage the brain tissue (Q. Li and Barres 2017; Janda, Boi, and Carta 2018). iPSC-MG were able to do phagocytosis of *E. coli* bioparticles, as reported by Haenseler *et al.* (Haenseler *et al.* 2017). However, under an anti-inflammatory phenotype, microglia substantially increase their phagocytosis. Under a pro-inflammatory phenotype, the capacity is similar to an unstimulated status, slightly decreasing over time.

Although the phagocytosis is generally linked to inflammation, von Bernhardt and colleges proved that the pro-inflammation could inhibit the phagocytosis (von Bernhardt *et al.* 2007), while the anti-inflammatory phenotype was able to stimulate phagocytosis, possibly via the TGF- β pathway (Koenigsknecht-Talboo and Landreth 2005). Cav1 has been suggested to have an important role to internalise some pathogens and toxins (Butin-Israeli, Drayman, and Oppenheim 2010; Norkin 1999; Orlandi and Fishman 1998). Upon KO of Cav1 in iPSC-MG it was not observed an impact on the phagocytic capacity of this cells, suggesting that the phagocytosis is dependent on other mechanisms, likely due to the low levels of Cav1 presented by the cells. Nevertheless, the increase of phagocytosis observed in Cav1 positive cells under an anti-inflammatory phenotype,

was not observed in KO cells, suggesting an involvement of Cav1 on the phagocytosis under this phenotype.

In **summary**, human microglia cells can be generated efficiently from iPSC. The additional resting step allowed microglia to recover from the differentiation process, allowing them to polarize towards both phenotypes. As freshly isolated microglia, iPSC-MG under basal status are more correlated with anti-inflammatory, expressing superior levels of anti-inflammatory markers. Upon activation, in a pro-inflammatory or an anti-inflammatory phenotype, it was possible to observe an overall activation or deactivation of the immune system, respectively, after reactome analysis of the DE genes. Moreover, iPSC-MG can do phagocytosis that increased under an anti-inflammatory phenotype.

The role of Cav1 in immune cells seems to be dependent of the cell type and immune environment. The loss of Cav1 did not affect the microglial differentiation; independent of Cav1 status, iPSC-derived microglia cells expressed the pan-microglial markers analysed. Human healthy microglia express low levels of Cav1, which can be upregulated under inflammatory response. Moreover, our results suggest Cav1 as a regulator of inflammatory response because the deletion of Cav1 in microglia cells led to an exacerbated pro-inflammatory response. Under a pro-inflammatory phenotype, Cav1 seems to promote genes related with ERK1/2 signalling that can contribute to mRNA instability and keep the immune response under control, as observed in **Figure 6.33**. Under an immunosuppressive environment, it was observed a downregulation of genes involved in TGF- β signalling pathway in Cav1 KO cells, suggesting a dependency of Cav1 via ERK1/2 as well. Microglia cells do phagocytosis independently of Cav1, however the presence of Cav1 may modulate the phagocytosis extension.

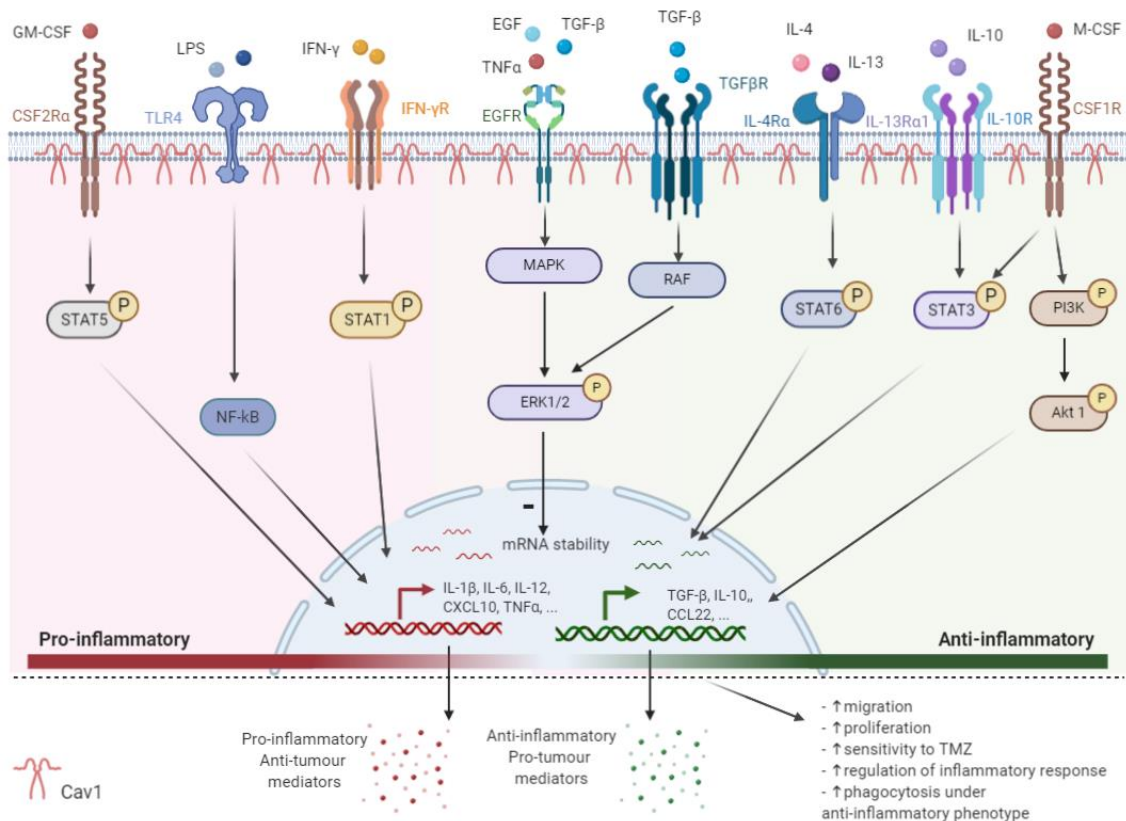


Figure 6.33 – Impact of Cav1 on microglia activation. The pro-inflammatory phenotype can be promoted with TLR4 (LPS), IFN- γ R (IFN- γ) and CSF2R α (GM-CSF) activation. This will lead to STAT1, NF- κ B and STAT5 activation, respectively, which will lead to the transcription of pro-inflammatory related genes and secretion of pro-inflammatory mediators. On the other hand, the anti-inflammatory phenotype can be promoted with IL-4R/IL-13R (IL-4 and IL-13), IL-10R (IL-10) and CSF-1R (M-CSF) activation. This will lead to STAT6, STAT3 and PI3K activation, respectively, which will lead to the transcription of anti-inflammatory related genes and secretion of anti-inflammatory mediators. The pro-inflammatory and anti-inflammatory phenotype work as a balance, where each secreted mediator can affect the other as a feedback. TGF- β and/or TNF α and activated TGF β R or EGFR, with by activation of ERK1/2 can affect the mRNA stability, controlling further the inflammatory response. Cav1 can act as a scaffold for MAPK-MEK-ERK1/2 promoting the degradation of mRNA and decrease of inflammatory response. This might also affect the migration, proliferation, sensitivity to TMZ and phagocytosis. TLR: toll like receptor; MAPK: mitogen-activated protein kinase; PI3K: phosphoinositide 3-kinases; Akt: protein kinase B.

CHAPTER 7 –
GBM AND IPSC-DERIVED MICROGLIA
ENVIRONMENT: THE ROLE OF CAV1

7.1 Introduction

Primary GBM is a malignant brain tumour with a very poor prognosis. There has been very little improvement in the effectiveness of therapies over the last 10-15 years. The tumours are constituted by a significant population of microglia and macrophages, presenting an immunosuppressive phenotype regulated by tumour cells. Understanding the GBM tumour environment is a promising avenue to establish new and effective therapies.

In vitro models have long been used to study GBM. Often these models have comprised single lineage cells, ie. the malignant astrocyte itself. Where more complex multi-lineage models have been used, they often comprise immortalised cell lines, this has been the case for microglia. Although more recently, primary dissociated microglia, and stem cell-derived microglia cultures are being used. Clearly, microglia cell lines can present some advantages however, the transformation or immortalization process can alter their phenotype (as discussed in previous chapters). Microglia cell lines and monocyte-derived models will also present a large phenotypic discrepancy from primary microglia (Melief et al. 2016), a significant concern. The poor responsiveness of an often used microglial cell line, CHME3, to external stimulus (described in Chapters 4 and 5), and as by Janabi and collaborators (Janabi et al. 1995; Dello Russo et al. 2018) reflects this concern and questions the usefulness of the recapitulated tumour model.

While primary microglia present a challenge in accessing sufficient material displaying consistent biology, this source is mostly obtained from foetal, aged and/or diseased donors, which may interfere with the microglia phenotype (Timmerman, Burm, and Bajramovic 2018). Moreover, upon dissociation, the primary microglia can modify their phenotype affecting the microglial performance (Janabi et al. 1995).

Stem cell technology holds promise for regenerative medicine and more fundamental biomedical research on human disease. It provides an unlimited availability of cells for *in vitro* purposes, addressing the supply advantages of primary cells and established cell lines. While the field is still refining how stem cell biology can be controlled at the laboratory bench, iPSC technology can generate mature microglia (Muffat et al. 2016) that resemble the primary microglia phenotype (Haenseler et al. 2017). In Chapter 6 this

work also showed reproducible microglia generation by iPSC, that were able to polarize into the two major phenotypes, pro-inflammatory and anti-inflammatory. This technology will offer a platform to better develop a GBM tumour microenvironment in the laboratory including the impact of microglia biology upon tumour cell responsiveness.

7.2 Aim

This chapter focuses on the question: What is the bi-directional influence of the tumour cells upon microglia activation; and *vice versa*. In particular what is the impact of Cav1 expression within the microglial upon this interaction. To study the role Cav1 in microglia cells, iPSC bearing a Cav1 knockout were used, (knockout before microglia differentiation). iPSC-derived microglia (Cav1 NT or Cav1 KO) were co-cultured with GBM tumour cell line models to study the gene expression within microglia and within tumour cells, as well as the combined secretome and 3D migration/invasion. Moreover, a bioinformatics-based approach was incorporated (two RNA-seq data base) to interrogate the putative role of Cav1 in immune cells within GBM tumours.

7.3 Methods

7.3.1 General methods

The iPSC Kolf2 'Cav1-NT' and Kolf2 'Cav1-KO' (iPSC-MG lines) and the GBM cell lines U87, UP007 and UP029 were used in this chapter. These cells were cultured and/or differentiated following the protocols described in **Chapter 2, 2.2 - Cell culture maintenance**.

Upon microglial differentiation, the impact of iPSC-MG 'Cav1-NT' and 'Cav1-KO' upon: spheroid GBM cell migration/invasion was analysed using the U87 cell model with invasion taking place over three days using the protocol described in **2.13 – Spheroid invasion assay**.

We went on to study how the bidirectional effects upon cell responsiveness when co-culturing the iPSC-MG lines with U87, UP007 or UP029 cells in a Transwell system (0.4 μm pore) for 48 hours, as described in **Figure 7.1**. After the co-culture, mRNA from microglia and tumour cells was extracted and isolated using the RNeasy mini Kit (Qiagen), as described in **Chapter 2, 2.7.1 – RNA isolation**, and 2.5 μg was converted into cDNA, as described in **2.7.2 – Synthesis of complementary DNA (cDNA)**. A panel of immune related genes (microglia) and another panel related to tumour invasion (GBM cells) was analysed using Taqman array. The supernatants were collected, centrifuged, and used to perform a cytokine array, as described in **2.10 – Cytokine array**. Microglial cells without interference of GBM and GBM cells without interference of microglial cells were used as controls.

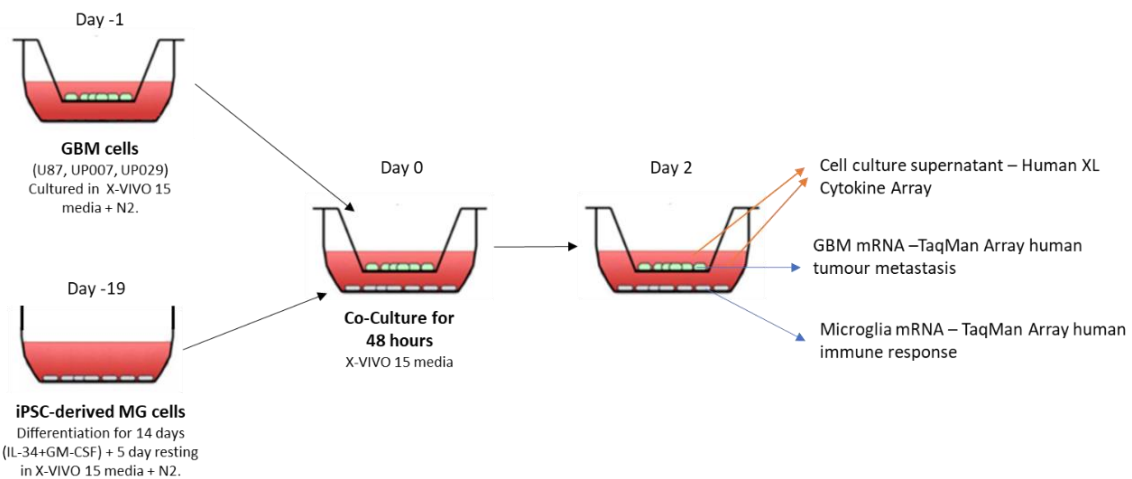


Figure 7.1 – Experimental design. iPSC-derived microglia were differentiated into 6-well plates from KOLF2 Cav1 NT or KOLF2 Cav1 KO cells for 19 days. The GBM was previously cultured gradually in X-VIVO 15 + N2 media for media transition and adaptation for 14 days. Then, the tumour cells were seeded into Transwells and left to adhere overnight. At day 0 of CC, the media was renewed, the tumour cells were placed together with microglia cells and incubated for an additional 48 hours. The supernatant was collected from the upper and lower chambers, centrifuged, and used in the Cytokine array. The GBM and microglia cells were collected, the mRNA extracted and used to perform TaqMan arrays of human tumour metastasis or human immune response, respectively.

7.3.2 TaqMan Gene Expression Array

The gene expression of genes involved in human immune response (iPSC-MG) and human tumour metastasis (U87, UP007 and UP029) were assessed by qRT-PCR using TaqMan® Gene Expression Array Plates (Applied Biosystems) containing predesigned, gene-specific primers and probes that are described in **APPENDIX VIII – TaqMan Gene expression Array plate**. Roughly 25 ng of cDNA of each sample was mixed with

TaqMan™ Fast Advanced Master Mix, in a total volume of 10 µl/well, and amplified using the QuantStudio 5, following the next protocol: UGN (Uracil-DNA glycosylase) incubation at 50°C for 1 minute plus 95°C for 20 seconds for enzymatic activation, followed by 40 cycles of 1 second at 95°C, for denaturation, plus the annealing and extension at 60°C for 20 seconds. The results obtained were analysed using the $\Delta\Delta C_t$ method.

7.3.3 Darmanis et al. scRNA-seq database

The scRNA-seq (single cell RNA-sequencing) databases GSE84465 (Darmanis et al. 2017) and GSE67835 (Darmanis et al. 2015) were downloaded. The analysed the cells were collected by Darmanis and collaborators from tumour core and surrounding tumour tissue, and foetal tissue from elective abortions and adult brain tissue from epilepsy surgeries. The RPKM expression values were analysed using Qlucore Omics Explorer to create the t-distributed stochastic neighbor embedding (tSNE) and the principal component analysis (PCA).

7.4 Results

7.4.1 Impact of iPSC-MG upon spheroid U87 invasion: Role of Cav1 status

The effect of the immune tumour environment on GBM will be an important factor for tumour invasion and progression. In order to study the impact in microglia cells of Cav1 expression and subsequent on tumour-cell invasion, iPSC-MG 'Cav1-NT' and iPSC-MG 'Cav1-KO' cells were used in a 3D spheroid model of migration/invasion with the GBM cell line, U87. Before sphere formation, U87 cells were labelled with DiO, a green fluorescent cell tracer dye. For this assay, tumour spheres were created with U87 cells and the iPSC 'Cav1-NT' or 'Cav1-KO' cells at a starting ratio of 1:1 seeding 500 cells of U87 and 500 iPSC -MG. Spheres created using only with 500 U87 cells were used as a control; we noted that iPSC-MG present a low proliferation rate in agreement with the findings of others (Haenseler et al. 2017; Darmanis et al. 2017). The spheroids were formed for 4 days. At day 0 of invasion, the spheres were imbedded in Matrigel and incubated for an additional 3 days.

The **Figure 7.2** contains the representative pictures of the impact of iPSC-MG ‘Cav1-NT’ and ‘Cav1-KO’ cells upon the spheroid invasion of U87.

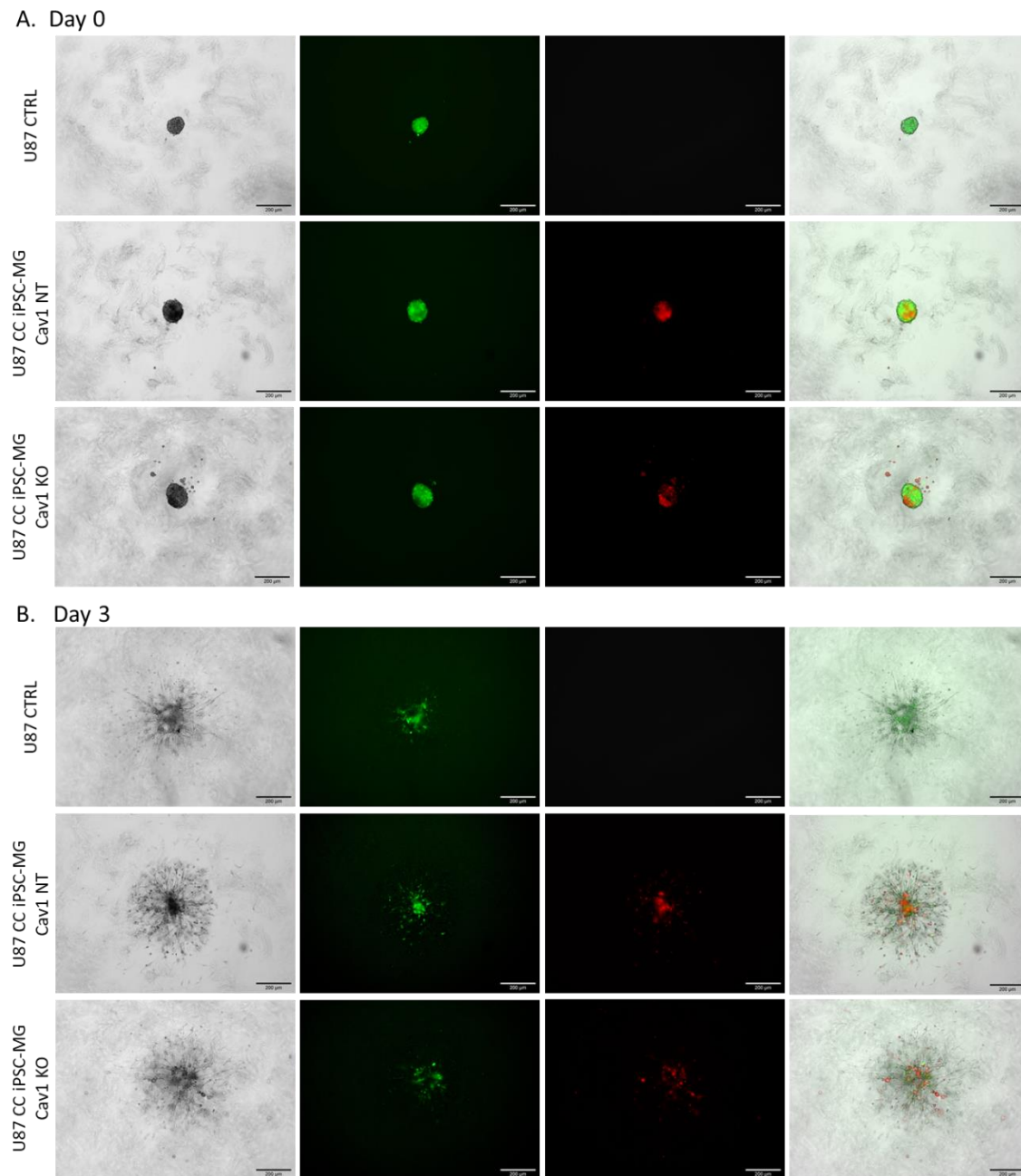


Figure 7.2 – Impact of iPSC-MG on U87 invasion. Representative pictures of U87 invasion in CC with iPSC-MG Cav1 NT and iPSC-MG Cav1 KO at day 0 (A) and day 3 (B). U87 without interference of immune cells were used as control (500 cells). Prior to the sphere formation, tumour cells were labelled with DiO (green). iPSC-MG expressed mCherry flag (red). The spheres were formed in a ratio of 500:500 cells, for 4 days. After sphere formation, around half of the media was replaced with Matrigel in a final concentration of 4 mg/ml and left to invade for an additional 3 days. The invasion was followed with an EVOS M7000 microscope, using the onstage incubator and pictures were taken every hour. N=1 independent experiment, CC performed with 2 microglial clones, three replicates per clone. Scale bar: 200 μ M.

At day 0 of the invasion protocol, the U87 cells (green) showed a homogenous distribution throughout the spheroids, while the iPSC-MG cells showed more of a localised patterning, more noticeably the 'Cav1-KO'. U87 cells were characterized by their high proliferative rate, compared with the iPSC-MG (Haenseler et al. 2017). The differences on proliferative rate (microglia vs U87) responsible for the different population densities observed by Day 0 (after the previous four days of spheroid development). Over the three days of invasion, GBM tumour cells maintained their proliferation. Regarding the invasion, the iPSC-MG cells were able to migrate along with the tumour cells, however, by Day three it was clear that the iPSC-MG 'Cav1-NT' cells showed a trend to remain closer to the spheroid core. Looking at the invasion of the GBM cells alone (Green) showed the the iPSC-MG Cav1 KO were able to promote GBM spheroid invasion by a small but statistically significant extent, **Figure 7.3**.

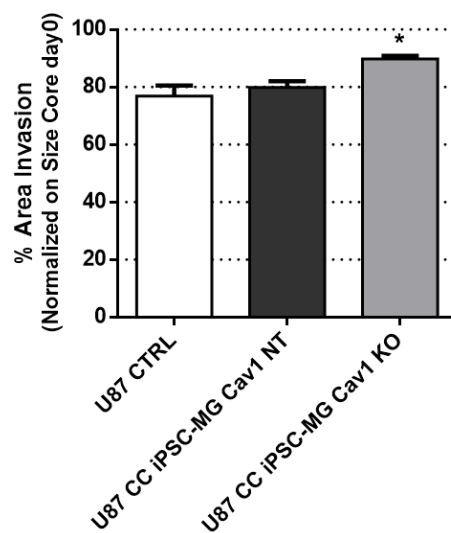


Figure 7.3 – impact of the iPSC-MG on the U87 area of invasion. The area of invasion was calculated using the INSIDIA macro, and it was normalized with the size of the core at day 0. Bars represent the mean \pm SEM. N=1 independent experiment, CC performed with 2 microglial clones, three replicates per clone. *: $p < 0.05$ compared to CTRL, Kruskal-Wallis test, followed by Dunn's multiple comparisons test.

7.4.2 Effect of the GBM cell on microglia responsiveness

Here GBM cells and iPSC-MG cells were co-cultured using a Transwell co-culture system (0.4 μ m pore) for 48 hours. This system allowed for autocrine and paracrine by diffusion of soluble factors secreted by both populations and mixing between apical and basal fluid compartments. iPSC-MG 'Cav1-KO' were included in this study the function of microglial Cav1 on the responsiveness of microglia cells to the tumour pressure and the

impact upon the GBM cells. The gene expression of 92 genes related to immune response were studied using TaqMan Gene Expression Array Plates containing predesigned primers and probes for the detection of human transcripts. The **Appendix VIII, Supplementary table VIII.1** contains the data from all the evaluated genes.

When comparing iPSC-MG 'Cav1-NT' and 'Cav1-KO' cultures without the pressure of GBM cells, we found the transcription levels of studied genes were similar (data not shown). Microglia cultured without interference of tumour cells, (the control condition), as well as microglia co-cultured with tumour cells, did not show in the microglial cell any amplification for the following genes: AGTR1, AGTR2, CCR2, CD19, CD3E, CD40L, CSF2, CYP1A2, FASLG, IFNG, IL12B, IL13, IL17A, IL2, IL3, IL4, IL5, IL9, PF4, SELE and SELP, indicating an absence of or low mRNA levels for these genes in the microglia cells (at least as detected by this assay) that was not altered by the environmental challenge.

The effect of three different tumour cell lines on microglia transcriptome followed 71 measured genes with observed upregulation, downregulation, or no effect, dependent on the tumour cell line used. The commercially available U87 cell line induced the most dramatic alterations in the microglia phenotype. The **Figure 7.4** shows the genes that presented a fold-change (FC) higher than 2-times for at least one of the GBM co-culture conditions, when compared to CTRL (respective iPSC-MG cells alone) – seen in Figure 7.4 for both the iPSC-MG 'Cav1-NT' and 'Cav1-KO' phenotypes

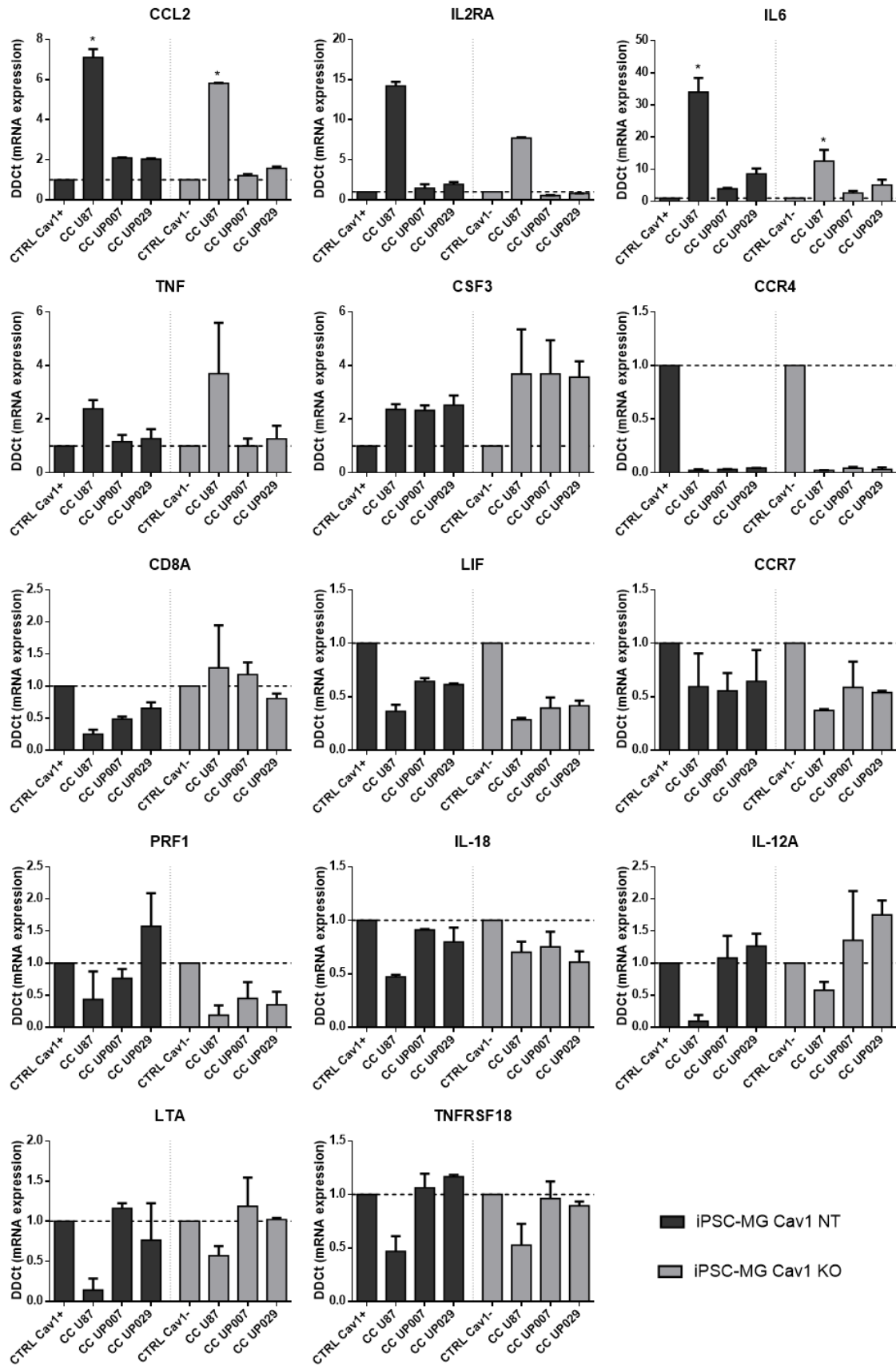


Figure 7.4 – Impact of tumour cells on the microglial immune response. iPSC-MG Cav1 NT (black) and iPSC-MG Cav1 KO (grey) were co-cultured with GBM cells in transwell systems for 48 hours. Graphs represent genes with FC > 2. $\Delta\Delta Ct$ analysis normalized to iPSC-MG Cav1 NT or iPSC-MG Cav1 KO, respectively. Mean \pm SEM from 2 microglia clones. *: p < 0.05 compared to the respective CTRL, Kruskal-Wallis test, followed by Dunn's multiple comparisons test.

With respect to the impact of U87 the following genes all showed increases in expression (mRNA) in the iPSC-MG cells when exposed to U87 GBM co-culture: CCL2 ($p < 0.05$), IL2RA, IL6, TNF α , CSF3. The pattern for these genes showed general agreement between the iPSC-MG Cav1 +ve (NT) and Cav1 -ve (KO) cells. Dependent on the gene, the impact of UP007 and UP029 did vary to some extent to that of U87. Nevertheless, the response again showed consistency between the iPSC-MG Cav1 +ve (NT) and Cav1 -ve (KO) cells. With the implication that Cav1 status may not be significant for these genes / GBM condition / outcome measure.

Independent of Cav1 status in iPSC-MG, the co-culture of microglia with three tumour cells (U87, UP007 and UP029) showed a downregulation of CCR4, LIF, CCR7 and IL18. It was observed a decrease in expression of IL-12A, LTA and TNFRSF18 in iPSC-MG Cav1 +ve (NT) and Cav1 -ve (KO) cells that were co-culture with U87 cells. The co-culture of iPSC-MG with UP007 and UP029 cells did not interfere with the expression of these last three genes.

Regarding CD8A, a downregulation of this gene was registered when iPSC-MG 'Cav1NT' was co-cultured with U87, UP007 or UP029. The loss of Cav1 seems to suppress this effect, and the tumour environment created by tumour cells did not interfere with this gene expression. Finally, looking to PRF1, Cav1 in iPSC-MG led to an upregulation of this gene with cells were co-culture with UP029, however, the loss of Cav1 downregulated PRF1 expression. The co-culture of iPSC-MG with U87 and UP029, despite Cav1 status in microglia cells, generated a decrease of PRF1 expression.

The **Figure 7.5** describes the genes where Cav1 status appears to have an impact on the responsiveness of microglia cells to the tumour environment. Specifically here there was a consistent difference for at least two of the three GBM conditions upon microglial expression and this expression showed a Cav1- status dependency.

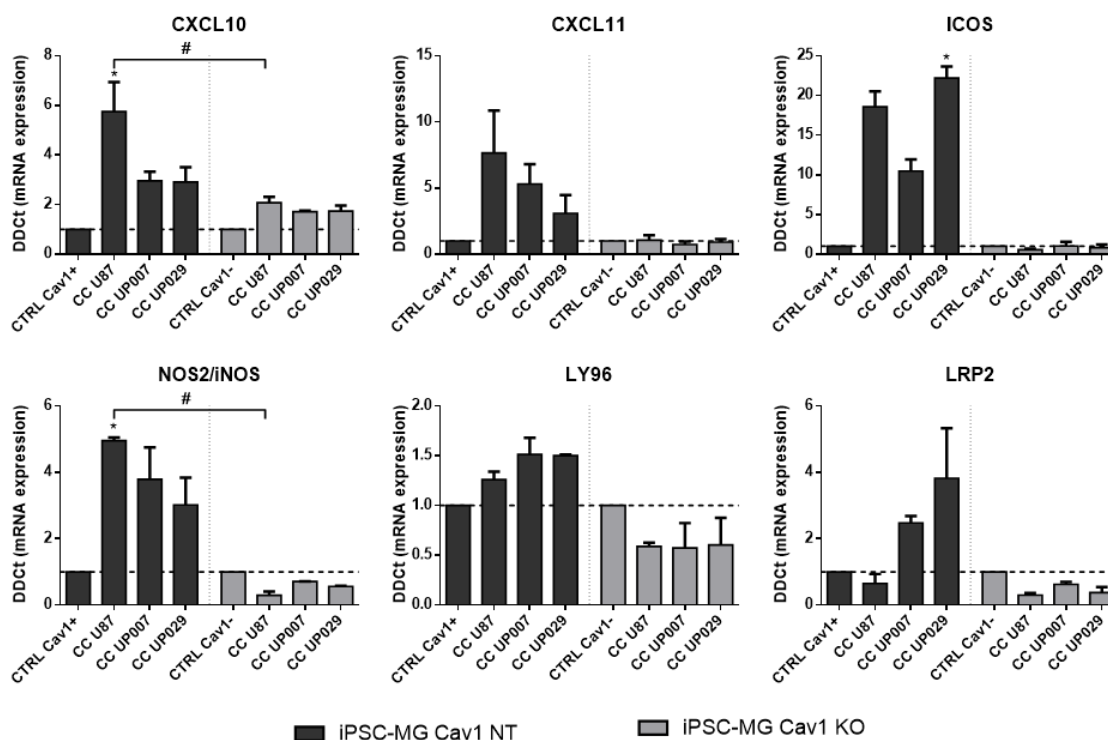


Figure 7.5 – Impact of tumour cells on the microglial immune response. iPSC-MG Cav1 NT (black) and iPSC-MG Cav1 KO (grey) were co-cultured with GBM cells in transwell systems for 48 hours. Graphs represent genes with $FC > 2$. $\Delta\Delta Ct$ analysis normalized to iPSC-MG Cav1 NT or iPSC-MG Cav1 KO, respectively. Mean \pm SEM from 2 microglia clones. *: $p < 0.05$ compared to CTRL, #: $p < 0.05$ compared to iPSC-MG Cav1 NT CC U87, Kruskal-Wallis test, followed by Dunn's multiple comparisons test.

Cav1 in microglia cells led to an increase of CXCL10, CXCL11, ICOS, iNOS and LY96 upon CC with tumour cells. The expression levels of LRP2 only increase when the co-culture was performed with UP07 and UP029. The co-culture of microglia Cav1+ve with U87 led to a slight decrease of this gene. Upon loss of Cav1 in microglia cells, the tumour environment slightly increased the expression of CXCL10 (half of the levels observed in iPSC-MG Cav1 NT). Comparing to iPSC-MG cultured without interference of GBM, similar expression levels were observed in CXCL11, ICOS, and a slight decrease was detected in the production of iNOS, LY96 and LRP2.

7.4.3 Effect of microglia on the GBM cell responsiveness

After exploration of some genes that might be involved in immune response to tumour cells, the impact of the status of Cav1 in microglia cell on the tumour transcriptome was evaluated. The tumour cells were collected from the same co-culture system, and performing a TaqMan Gene Expression Array, where 92 genes involved in tumour invasion and metastasis were analysed. The genes with FC greater than 2 compared to the respective tumour cell line cultured without interference of microglia are represented on **Figure 7.6**, **Figure 7.7** and **Figure 7.8**. All the data obtained is resumed in the **Appendix VII, Supplementary table VIII.2** and **Supplementary table VIII.3**.

The mRNA levels of CDK2A, SYK and Tmprss4 were not detected in any of the three GBM cell lines tested. DCC was not detected in UP007. KISS1R, KISS1 and LYPD3 were not noticeable in U87 cells. And finally, serpin B5 was undetectable in U87 and UP029 cells.

From the genes analysed, only 3 genes presented the same trend in all tested co-cultures. These are represented in **Figure 7.6**.

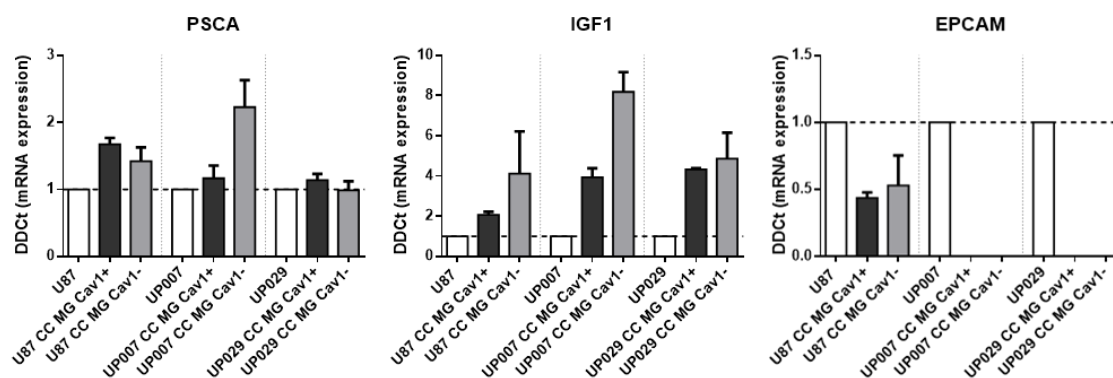


Figure 7.6 – Impact of iPSC-MG on tumour gene expression. U87, UP007 and UP029 cells were co-cultured with iPSC-MG Cav1 NT (black) or iPSC-MG Cav1 KO (grey) using transwell systems, for 48 hours. GBM cells without interference of microglia were used as control (white). mRNA from tumour cells was extracted and used to perform the TaqMan Array. Bars represent the $\Delta\Delta C_t$ analysis \pm SEM from 2 independent experiments performed with two different KOLF2 clones.

Based on the figure above (**Figure 7.6**), it is possible to observe an upregulation of IGF1 and PSCA upon co-culture of GBM cells with iPSC-MG cells, independently of Cav1 status. Regarding the EPCAM, it was registered a downregulation upon the co-culture

with microglia cells in U87. With UP007 and UP029 the levels were reduced to a level impossible to be detected using this assay.

In the **Figure 7.7** and **Figure 7.8** describe genes that change their transcription in at least one co-culture condition depending on the tumour cell line.

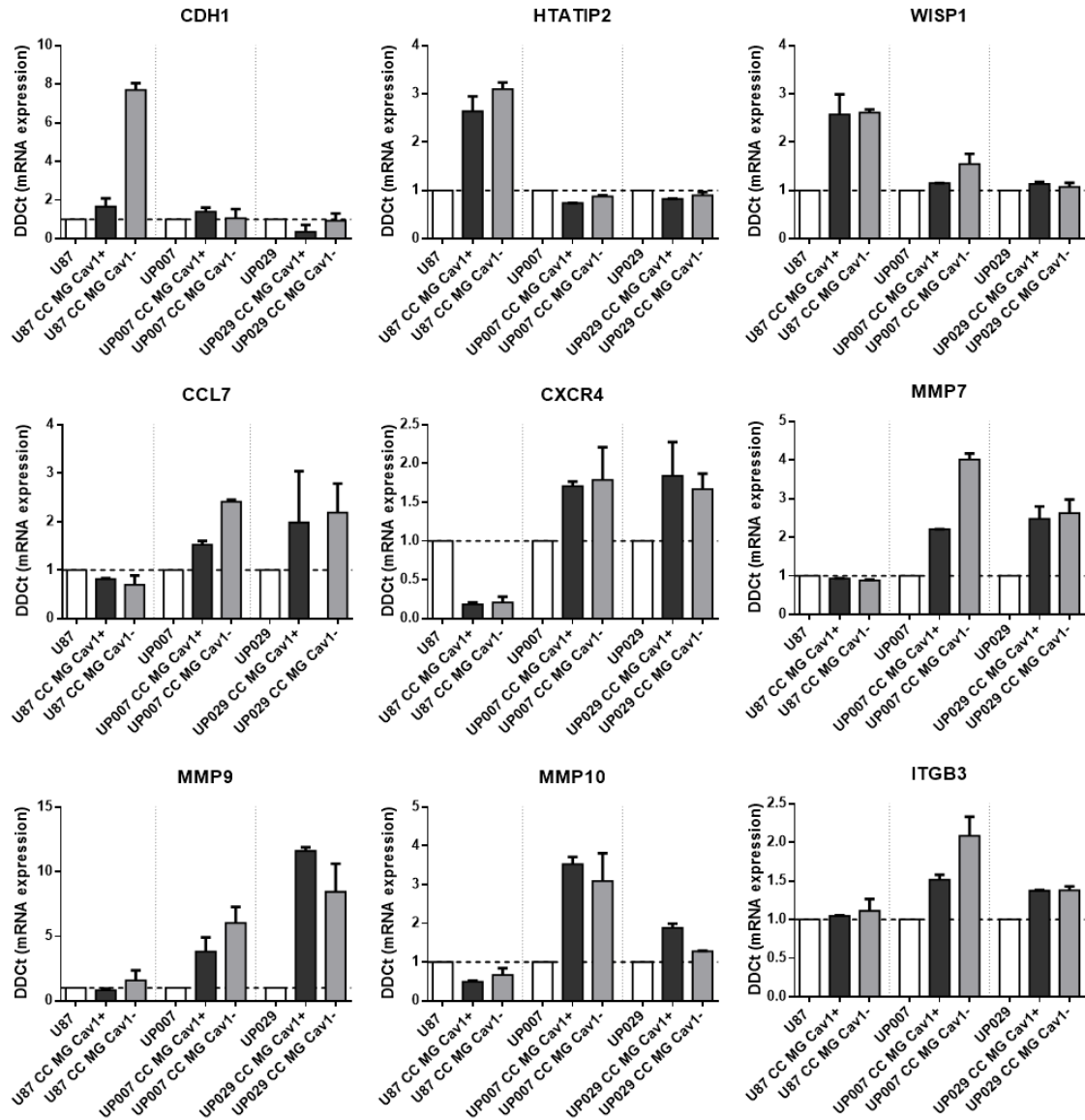


Figure 7.7 – Impact of iPSC-MG on tumour gene expression. U87, UP007 and UP029 cells were co-cultured with iPSC-MG Cav1 NT (black) or iPSC-MG Cav1 KO (grey) using transwell systems, for 48 hours. GBM cells without interference of microglia were used as control (white). mRNA from tumour cells were extracted and used to perform the TaqMan Array. Bars represent the $\Delta\Delta$ Ct analysis \pm SEM from 2 independent experiments performed with two different KOLF2 clones.

In **Figure 7.7** it is possible to observe that CDH1, HTATIP2 and WISP1 were upregulated in U87 cells when they were in co-culture with microglia cells, independent of Cav1 status of the microglia . The CDH1 upregulation was more notorious when the co-culture was performed with iPSC-MG ‘Cav1 KO’ cells. When the co-culture was performed with

UP007 or UP029 cells the expression of these genes remained roughly constant compared to the respective tumour cells that were cultured without interference of microglia (Cav1+ve and Cav1-ve).

The expression of CCL7, CXCR4, MMP7, MMP9, MMP10 and ITGB3 increased in UP007 and UP029 when co-cultured with microglia cells (Cav1+ve and Cav1-ve). This increase was more prominent for CCL7, MMP7 and ITGB3 in UP007 co-culture with iPSC-MG 'Cav1 KO' cells, compared to the co-culture performed with microglia Cav1+ve. The U87 co-culture with microglia cells did not interfere with the levels of CCL7, MMP7, MMP9 and ITGB3, however, it was able to decrease the CXCR4 and MMP10 levels, independently of Cav1 status in microglia cells.

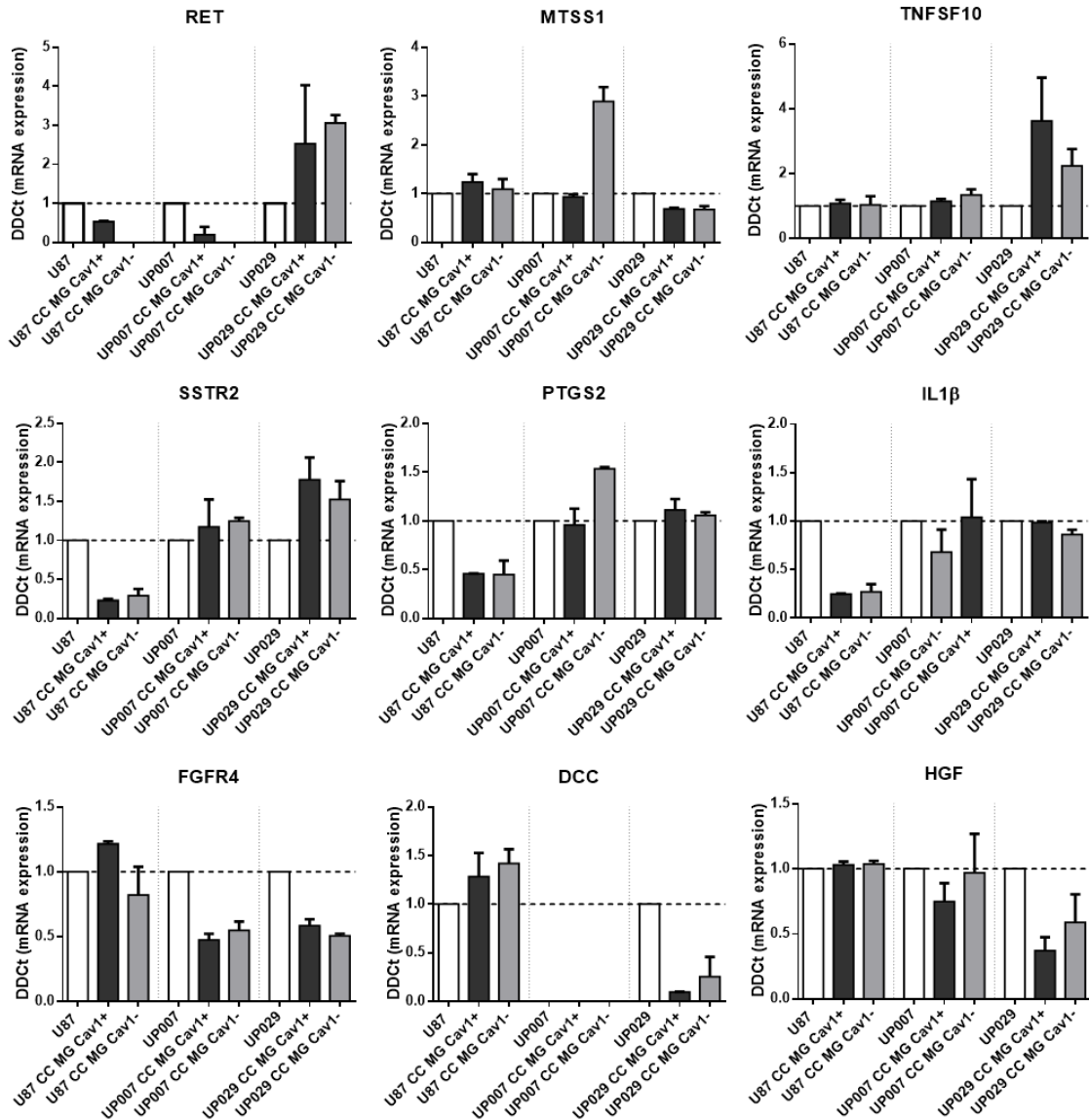


Figure 7.8 – Impact of iPSC-MG on tumour gene expression. U87, UP007 and UP029 cells were co-cultured with iPSC-MG Cav1 NT (black) or iPSC-MG Cav1 KO (grey) using transwell systems, for 48 hours. GBM cells without interference of microglia were used as control (white). mRNA from tumour cells were extracted and used to perform the TaqMan Array. Bars represent the $\Delta\Delta C_t$ analysis \pm SEM from 2 independent experiments performed with two different KOLF2 clones.

Examining the **Figure 7.8**, the gene expression pattern is less clear, and the expression seems to be dependent on the co-culture condition. Comparing to the respective tumour cell line cultured without interference of microglia cells (Cav1+ve and Cav1-ve):

- RET was upregulated with the immune environment created with UP029 cells but decreased when the co-culture was performed with U87 and UP007 cells. The levels of mRNA decreased to an unnoticeable concentration when the co-culture was performed with U87 and UP007 with iPSC-MG ‘Cav1 KO’ cells.

- MTSS1 levels increased in UP007 co-culture with iPSC-MG 'Cav1 KO', and decreased slightly in UP029 co-culture with iPSC-MG (independently of Cav1) but was not affected in the remaining conditions.
- TNFSF10 was upregulated upon UP029 co-culture with microglia (Cav1+ve and Cav1-ve) but was not affected when the co-culture was performed with the other tumour cell lines.
- The U87 co-culture with iPSC-MG (Cav1+ve and Cav1-ve) suppressed the expression levels of SSTR2, PTGS2 and IL-1 β , but the co-culture with UP007 and UP029 did not affect the expression of these genes.
- FGFR4 decreased with the co-culture was performed with UP007 and UP029 but suffered a marginal increase in U87 co-culture with iPSC-MG 'Cav1 NT'.
- DDC was promoted in U87 co-culture with iPSC-MG (Cav1+ve and Cav1-ve), not detectable in UP007 co-culture with microglia independent of Cav1 status, and decreased in UP029 co-culture, more dramatic with Cav1+ve cells.
- HGF levels decreased in UP029 co-culture with microglia (Cav1+ve and Cav1-ve), however, the co-culture U87 and UP007 with microglia (Cav1+ve and Cav1-ve) did not affect its expression.

7.4.4 Co-cultures of iPSC-MG cells with GBM: impact on secretome

Similarly to what was done in chapter 5, to study the impact that the status of Cav1 in microglia cells may have in the tumour environment, and also to study the secreted products by microglia and tumour cells, iPSC-MG 'Cav1 NT' or iPSC-MG 'Cav1 KO' were co-cultured with U87, UP007 and UP029 cells (ratio 1:1) for 48 hours, using transwell systems. Microglia cells (Cav1+ve and Cav1-ve) that were cultured without the influence of GBM were used as control. After the co-cultures, the supernatants were collected, centrifuged, and used to perform a human XL Cytokine array to evaluate 105 cytokines, chemokines and growth factors involved in immune response that may impact the tumour behaviour. The mean pixel intensity values from all the analysed analytes are described in the **Supplementary figure VI. 4**.

The secreted products present in the immune environment created only by microglia cells, or present in the tumour immune environment created by tumour and microglia cells, with a difference of at least 2-FC compared to respective control are represented in **Figure 7.9** and **Figure 7.10**.

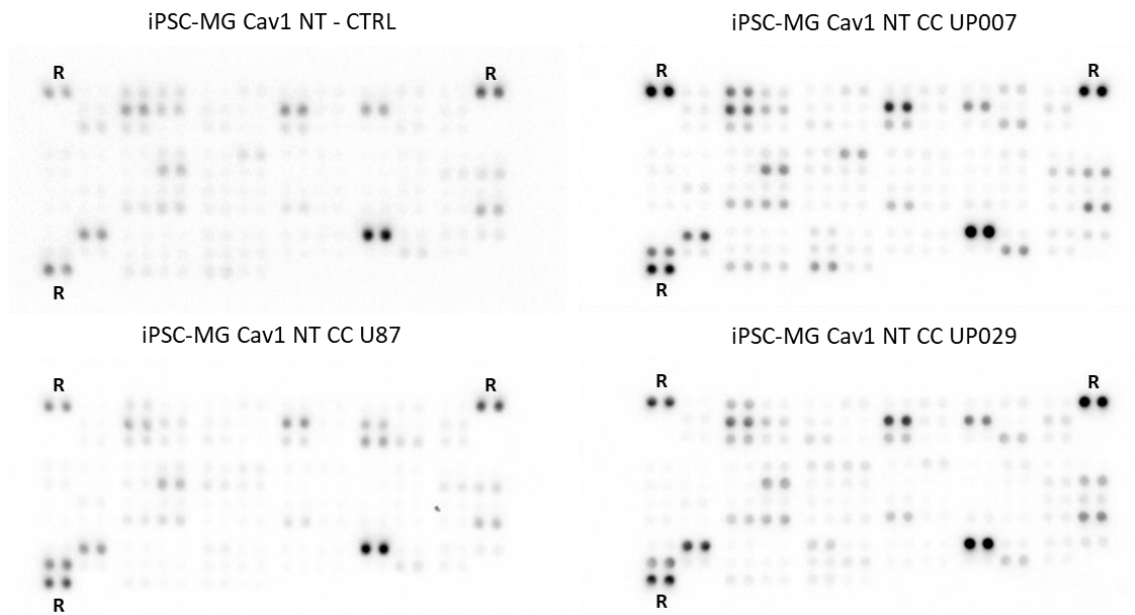


Figure 7.9 – Impact of tumour immune environment upon the secretome. U87, UP007 and UP029 tumour cells were co-cultured with iPSC-MG Cav1 NT for 48 hours using a transwell system (0.4 μ m pores). Microglia without interference of tumour cells were used as control (CTRL). The supernatants were collected, centrifuged, and incubated with cytokine array membrane. R: Reference spot.

Looking at the membranes in **Figure 7.9**, it was possible to observe a stronger overall signal produced by the tumour immune environment created by the tumour cells that were recently isolated from tumour samples, UP007 and UP029, compared with U87 cells, when they were in co-cultured with iPSC-MG Cav1 NT cells.

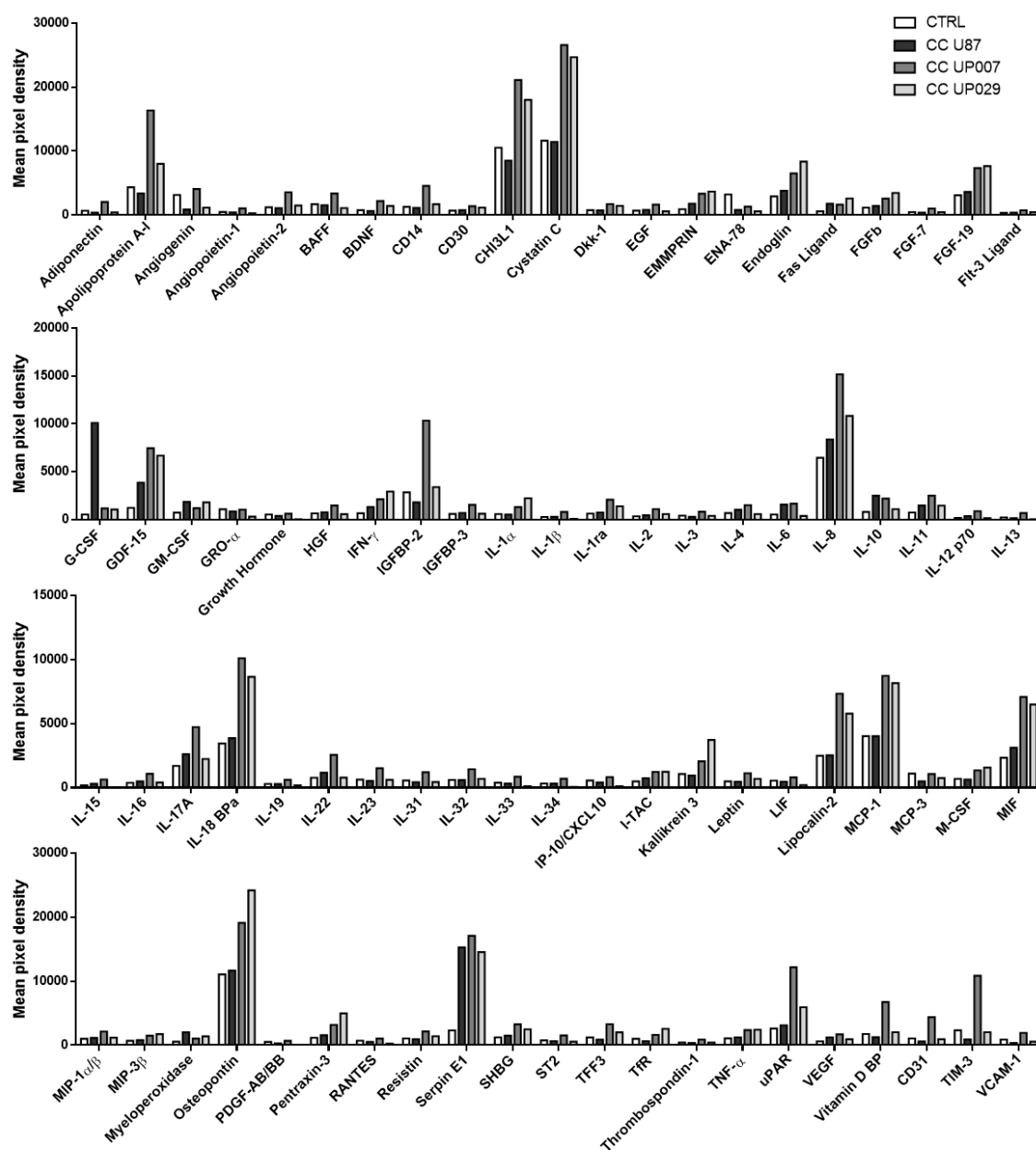


Figure 7.10 - Impact of tumour immune environment upon the secretome. Quantification of analytes which presented a FC higher than 2 in at least one CC condition, compared with the environment created only by microglia cells. U87 (black), UP007 (grey) and UP029 (light grey) tumour cells were co-cultured with iPSC-MG Cav1 NT (white) for 48 hours using a transwell system (0.4 μm pores). Bars represent the mean pixel density of 2 spots, from one experiment.

Observing the quantification of the products in **Figure 7.10**, Serpin E1 and IL-8 presented an increase of concentration in the tumour immune environment created with the three GBM cell lines tested in co-culture with microglia. CHI3L1, Cystatin C, OPN, IL-18 BPa, Lipocalin 2, MCP-1 and MIF were more concentrated in the UP007 and UP029 co-cultures with microglia, but with a marginal, or no increase was observed in U87 co-

cultures. The chemokine ENA-78 (CXCL5) decreased 4-times with U87 co-culture, 2.4-times with UP007 co-culture and 5.47-times with UP029 co-culture.

Looking at U87 co-culture with iPSC-MG 'Cav1 NT' cells independently, the co-culture condition produced an increase of 11 analytes and a decrease of another 5 with FC higher than 2-times, compared with the environment created only by microglia cells. The biggest differences were observed in G-CSF (19.5 times) and Serpin E1 (6.6-times).

The co-culture of UP029 with iPSC-MG Cav1 NT was the second condition with more alterations, with an increase of 31 factors and a decrease of another 13 factors. Serpin E1 registered an increase of 6.3-times, followed by the GDF-15 with 5.4-times. Despite of the low pixel intensity, the growth hormone decreased 22-times, PDGF-AB/BB decreased 9.1-times and IL-13 decreased 6.7-times.

The co-culture of UP029 with iPSC-MG Cav1 NT registered an increase of 71 factors and a decrease of 1 factor (ENA-78 already mentioned). From these 71 factors, Serpin E1 (7.4-times) and GDF-15 (6.1-times) were the ones with the highest differences compared to the iPSC-Cav1 NT environment.

After studying the effect of the tumour environment on microglial secretome, the effect of Cav1 in microglia cells on this tumour immune environment was analysed using iPSC-MG 'Cav1 NT' and iPSC-MG 'Cav1 KO', the membranes obtained are represented in **Figure 7.11** and the quantification of the analytes with FC greater than 2 are represented in the graphs of **Figure 7.12**.

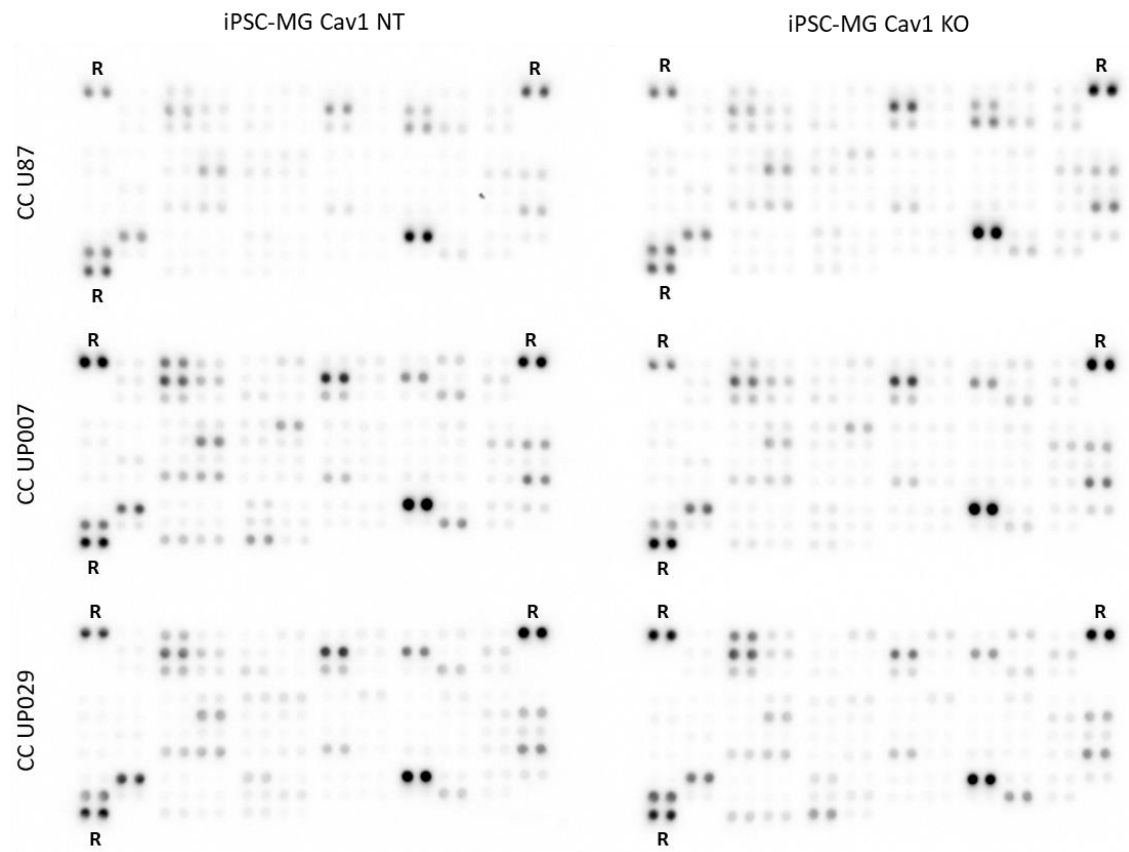


Figure 7.11 – Impact of Cav1 in microglia cell on the tumour immune secretome. U87, UP007 and UP029 tumour cells were co-cultured with iPSC-MG Cav1 NT and iPSC-MG Cav1 KO for 48 hours using a transwell system (0.4 μm pores). The supernatants were collected, centrifuged, and incubated with cytokine array membrane. R: Reference spot.

Taking into consideration the status of Cav1 in microglia cells, dependent on the tumour cell line used to perform the co-culture with microglia cells (Cav1+ve and Cav1-ve) the secretome was distinct.

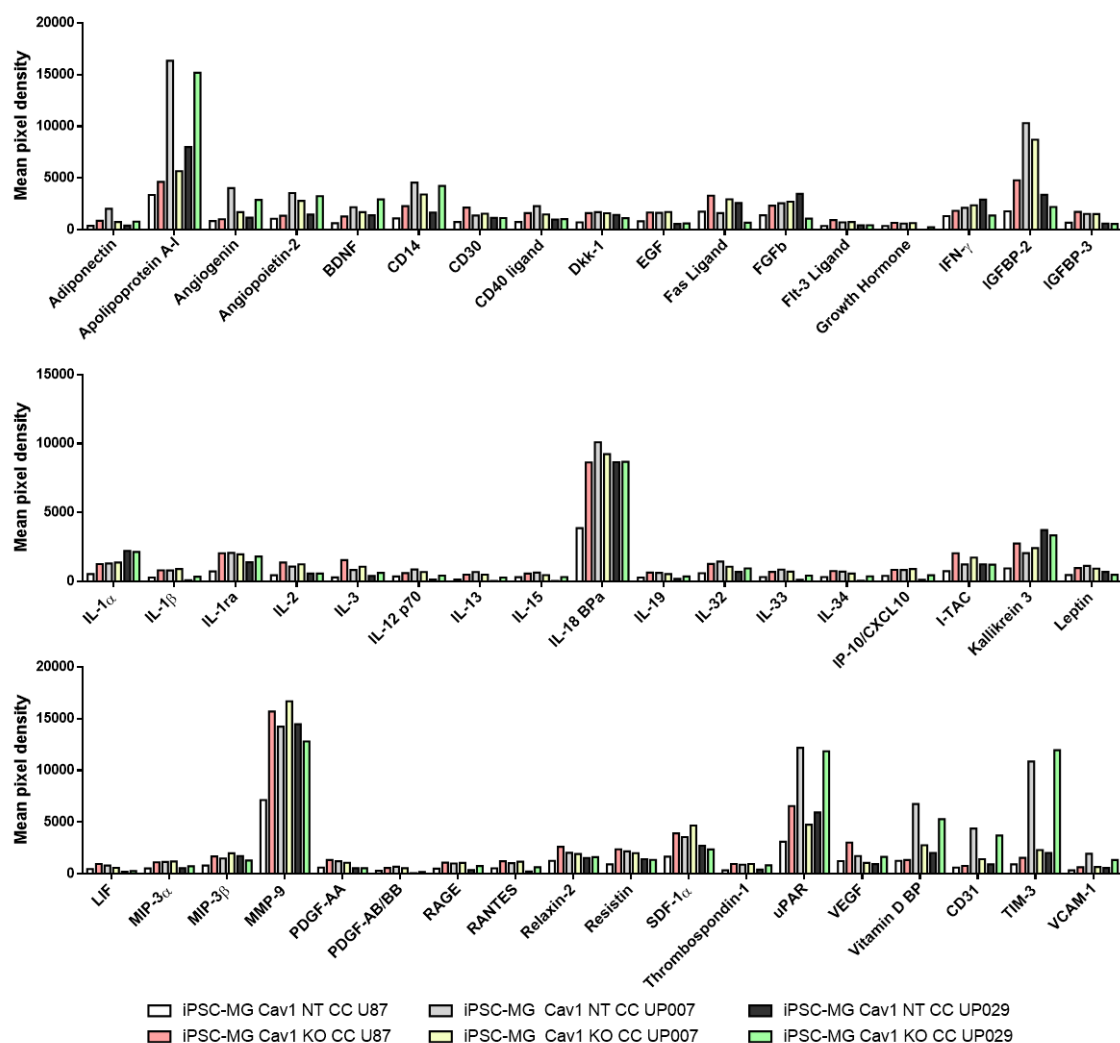


Figure 7.12 - Impact of Cav1 status in microglia cells in tumour immune environment upon the secretome. Quantification of analytes a FC higher than 2 in at least one CC condition compared to the environment created only by microglia Cav1 NT cells. Bars represent the mean pixel density of 2 spots, from one experiment.

When the co-culture was performed with U87 cells, Cav1 in microglia cells led to the upregulation of 39 factors, being IL-3 (5.3-times), IL-13 (3.4-times), IL-2 (3.1-times) and kallikrein 3 (2.9-times) the most improved, compared to the co-culture of U87 with microglia Cav1-ve.

Regarding the co-culture of UP029 with iPSC-MG ‘Cav1 NT’, the presence of Cav1 in microglia cells improved the production of 19 factors, and the most upregulated analytes were the growth hormone (10.5-times), IL-15 (10.4-times), IL-13 (8.4.times), IL-34 (7.1-times) and CXCL10 (7.1-times). On the other hand, it was observed a downregulation of FasL (3.8-times), FGFb (3.2-times) and IFN- γ (2.1-times).

As for the co-culture of UP007 cells, the presence of Cav1 in microglia cells led to an overall downregulation of the secretome, where 8 factors were identified with FC lower than 2: TIM-3 (4.7-times), CD31 (3.2-times), adiponectin (2.8-times), VCAM-1 (2.5-times), apolipoprotein A-I (2.7-times), uPAR (2.5-times), angiogenin (2.4-times) and vitamin D BP (2.4-times).

From the 53 factors identified with FC higher than 2 in at least one CC condition comparing iPSC-MG 'Cav1 NT' co-culture with GBM with iPSC-MG 'Cav1 KO' co-culture with GBM, only 4 factors presented the same trend for the co-culture with U87, UP007 and UP029 cells, namely the IL-1 β , RAGE, RANTES, and thrombospondin 1.

7.4.5 Immune population in GBM tumours: scRNA-Seq database

The latest technological advances allow for the transcriptomic analysis from one single cell. Darmanis and colleagues published two papers where the immune cell populations were analysed and were shared as online databases GSE67835 (Darmanis et al. 2015) and GSE84465 (Darmanis et al. 2017). The first study includes "healthy tissue" from adult brain collected during epilepsy surgeries and foetal tissue obtained during elective abortions (Darmanis et al. 2015). The second study includes samples from four patients diagnosed with primary GBM, where two samples from each patient were collected, one originating from the tumour core and another from the peritumoral space (cortex) immediately adjacent to the tumour core, previously demarcated by MRI (Darmanis et al. 2017). In both cases the immune cell populations were selected by FAC sorting using the CD45 marker. Other cellular populations like astrocytes, neoplastic, neurons, OPC, oligodendrocytes and vascular cells were isolated, using specific markers, but will not be included in the scope of this project. The **Figure 7.13** contains a t-distributed stochastic neighbour embedding (t-SNE) analysis from all the cells included in these studies.

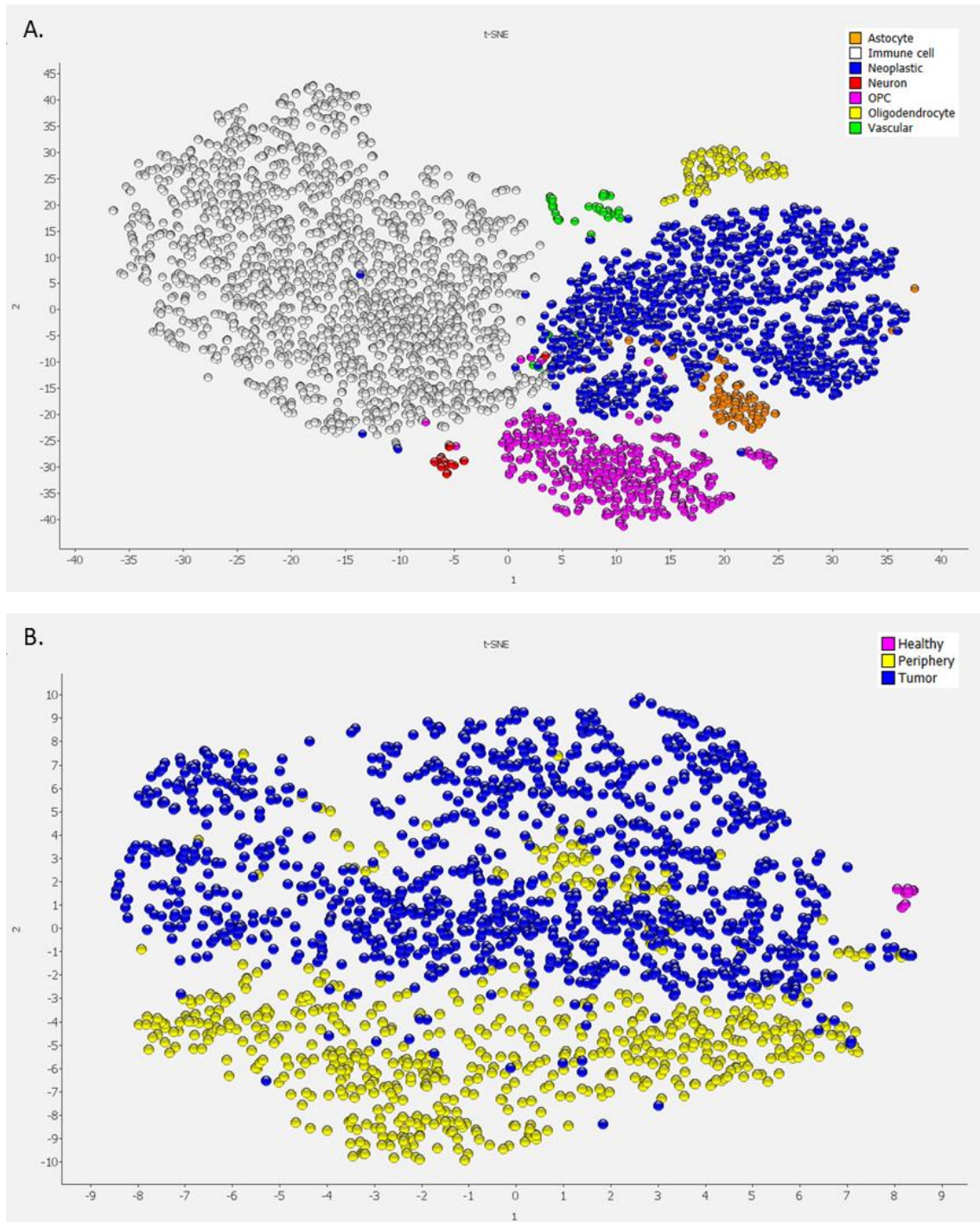


Figure 7.13 – t-SNE representation of single cells collected from four GBM samples. A. Cell clusters of 3,589 cells, coloured by cell type, using the top 200 DE genes. **B.** Immune cell population colour by localization (perplexity=50 and $q < 0.05$).

As Darmanis *et al.* showed, it is possible to distinguish seven different populations based on the transcriptomic landscape across all sequenced single cells (Darmanis *et al.* 2017). Briefly, the top 200 DE genes which presented a q -value lower than 0.05 were selected

and used to construct a distance matrix, creating a t-SNE. Based on cellular identities it is possible to identify overexpressed genes that are characteristic from each cluster.

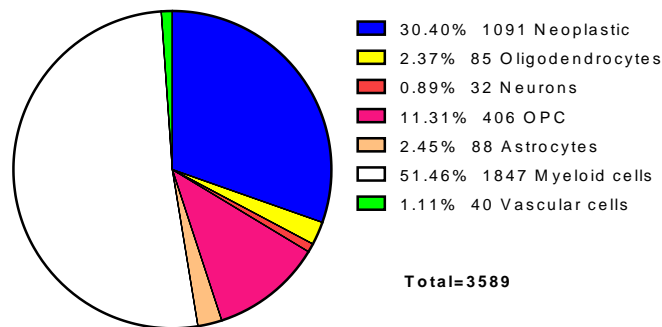


Figure 7.14 – Tumour cell distribution.

From all the cells analysed, it is possible to conclude that the immune population was the one with the highest cell count (51.36%), followed by the neoplastic or tumour cells (30.40%). Neurons were the cellular type less represented over the samples analysed. Focusing on the myeloid population, from the total 1,847 cells analysed, 1,182 were from the tumour core and the remaining 665 cells were from the periphery, explaining the high prevalence of these cells in GBM tumours.

Based on gene-expression, Darmanis and collaborators demonstrated that from the total of the myeloid population, around 95% should be classified as macrophages or microglia, and the remaining population (~4.5%) could be classified as primary dendritic cells. To better specify the identity of the myeloid population within and surrounding tumour bulk, they used a panel of established macrophage (CRIP1, S100A8, S100A9, ANXA1, and CD14) and microglia specific genes (TMEM119, P2RY12, GPR34, OLFML3, SLC2A5, SALL1, and ADORA3) validated by Bennett and colleagues (Darmanis et al. 2017; Bennett et al. 2016). The results showed that the majority of the cells within the tumour core trended to express genes characteristic of macrophages (macrophage=813, microglia=365), whereas cells from the periphery expressed genes characteristic of microglia (macrophage=85, microglia=574) (Darmanis et al. 2017).

In order to understand the role of Cav1 within this population, the expression was evaluated within macrophages and microglia cells, in the core or surrounding of the tumour, as well as in the healthy tissue.

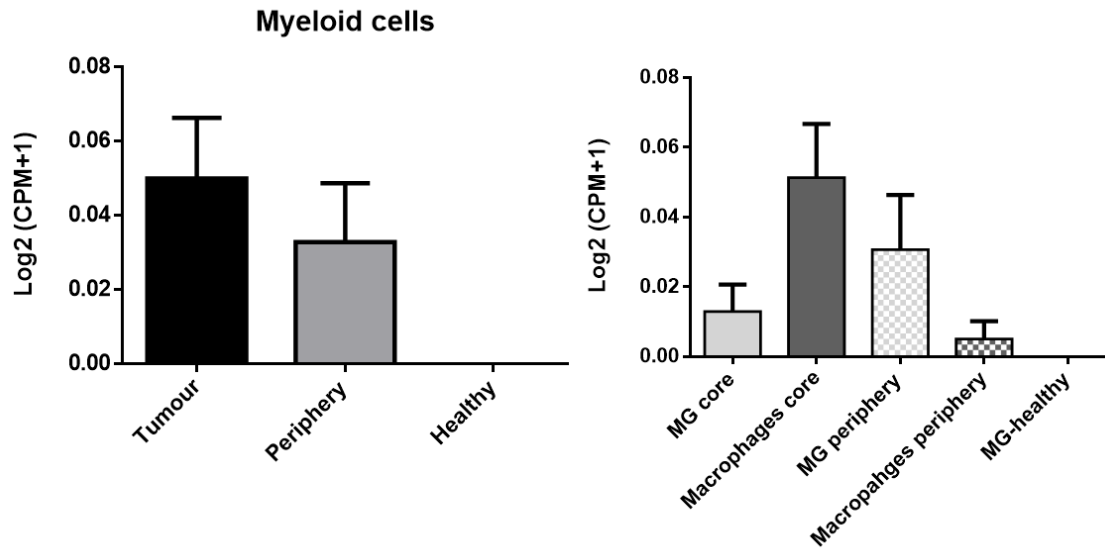


Figure 7.15 – Cav1 expression based on localization and cell type. Cav1 expression was selected from both Darmanis data bases. Macrophages and microglia were pre-selected using the list of genes validated by Bennett and colleges. Bars represent the mean $1 \pm SEM$ of Log2 of CPM (counts per million) + 1.

The **Figure 7.15** shows a low expression of Cav1 among the myeloid cells in the CNS. The microglia cells in healthy brain did not express the gene, however, myeloid cells upregulated the expression upon cellular activation, starting to increase the expression in the tumour periphery area and rich levels even higher inside the tumour core. In general, the macrophages showed the highest expression in the tumour core, while the microglia cells had a stronger expression in the periphery.

7.5 Discussion

To study the impact of microglia cells on tumour invasion requires microglia capable of answering to pro-inflammatory and anti-inflammatory stimulus. Tumours are known for their specialized microenvironments that can activate and control microglia and other immune cells. If the microglia are not fully functional, the cellular behaviour within the tumour environment might not translate the real tumour context, contributing to the unsuccess of new treatments in clinical trials.

There are different tumour models that try to comprise the immune population. However, these models mainly rely on animal cell lines and/or human cell lines, where for the other species sources, the results may be impacted due to the different complexities between animal and human diseases (Junhee Seok et al. 2013). In order to fulfil this gap, microglia derived from human iPSC was used to study the impact of microglia on the GBM invasion. iPSC-MG is able to answer to both pro-inflammatory and anti-inflammatory stimulus, as presented and discussed during the chapter 6. Therefore, the expectation was that these cells were able to react to the created tumour environment using simple models, namely a Transwell system and 3D spheres.

Using the Darmanis database to understand the importance of the myeloid population in the GBM tumour, it is possible to observe that from the analysed tumour samples more than half of the population were myeloid cells, highlighting their big importance in these tumours (Darmanis et al. 2017). Additionally, the distribution of microglia and macrophages across the tumour areas seems to be heterogeneous, where microglia are predominant in the tumour periphery and the macrophages in the tumour core. The superior number of macrophages in the tumour core is likely due to the high and immature vascularization characteristic of GBMs, which impairs the BBB and facilitates their infiltration (Prionisti et al. 2019).

Tumour spheres were successfully created with microglia cells representing the immune population of this tumour. These two populations were tracked using two different tracking systems, cell tracker dyes and mCherry tag. Regarding the first technique, it was possible to observe photobleaching of the cell trackers, which together with the decrease of the dye concentration at each cellular division, made it difficult to track the

tumour cells by the end of the third day, becoming a limitation of this study. For future projects, the GFP tag will be used to facilitate the tracking of these cells. Apart from that, since microglia cells were easily visible with the mCherry tag, it was possible to identify the tumour cells by exclusion.

As discussed previously, Cav1 may affect the microglia proliferation, phagocytosis, endocytosis, migration, and the factors released. All these properties can influence the microglia responsiveness in the tumour environment and, consequently, affect the tumour behaviour. Zhai and collaborators, showed that the ablation of microglia and macrophages could inhibit mouse glioma progression (Zhai, Heppner, and Tsirka 2011). However, the role of Cav1 in microglia or macrophages within this type of tumour remains unexplored. In our 3D spheroid model, the suppression of Cav1 promoted the tumour invasion, but no significant impact was registered in microglia cells able to express the protein. To explore the tumour invasion, this assay was only conducted once, however two different microglial clones were used. During this chapter only the 3D tumour invasion was studied. More studies of tumour proliferation, migration, invasion, and response to chemotherapeutic drugs/radiation should be conducted to further explore the role of Cav1 in microglia cells on tumour progression, using iPSC-derived microglia cells.

After seeing that Cav1 in microglia cells might influence the tumour invasion, the focus shifted to the impact of the GBM on the behaviour of microglia. iPSC-MG were able to be activated by the tumour environment, and Cav1 might have had a role on this response. Some genes studied in human inflammatory response panel were not expressed by microglia cells. From the 21 genes not detected by this assay, only IL-12 was detected in iPSC-MG cells by RNA-seq, and it was upregulated in cells upon stimulation with LPS and IFN- γ , under a pro-inflammatory environment. The other 20 genes were not detected in basal, pro-inflammatory or anti-inflammatory status, confirming the good sensibility of the TaqMan arrays. These genes may have impact on the general human inflammatory response, but not specifically in microglia.

Interestingly, the microglia gene expression suffered the highest impact when the CC was performed with U87 cells, comparing with the CC with UP007 or UP029. These cell lines were established from different patients, which may translate into different GBM

subtypes, exerting different pressure on the immune population. For the gene ontology analysis of the genes included in the TaqMan human tumour metastasis, 3 genes should be highlighted: IL-1 β , SERPINE1 and MMP3, which are involved in the regulation of the inflammatory response (GO:0050727). These genes were overexpressed in the U87 cells compared to the UP007 and UP029, under basal conditions, without the interference of immune cells. It was expected that under CC, the interplay between both populations affected the gene expression. However, since U87 cells expressed superior levels of immunoregulatory genes, this might be correlated with a greater impact observed on the microglia population upon the co-culture.

From all the changes observed on the microglial gene expression caused by the impact of the tumour immune environment, the increased of CCL2 was correlated with chemoattraction of regulatory T cells and myeloid-derived suppressor cells (Chang et al. 2016), IL-6 was related with IL-6/STAT3 pathways leading to a poor prognosis in GBM patients (Maas et al. 2020), and IL2Ra was involved in the regulation of immune tolerance by controlling regulatory T cells activity and was found upregulated in GBMs (Walentynowicz et al. 2018). As expected, the tumour immune environment seems to promote the expression of genes that can help the tumour immunosuppression and consequently tumour progression. Cav1 seems to contribute for this expression, but additional studies need to be performed to achieve more robust conclusions. Along with these genes, Cav1 in microglia seems to be mandatory to lead to the upregulation of pro-inflammatory related genes CXCL10, CXCL11, ICOS, iNOS and LRP2 as a response to the tumour cells. Suggesting that, in tumour environment context, the absence of Cav1 in microglia cells may prevent the expression of some pro-inflammatory related genes and promote the tumour invasion as an outcome.

Other genes that were related with the activation of the immune response by the chemoattraction of other immune cells, as CCR4 and CCR7, mediation of cell-cell interaction, as CD8a (Pennock et al. 2013), induction of hematopoietic differentiation, as LIF (Mathieu et al. 2012), and increase of natural killer activity and stimulation of IFN- γ production in T-helper cells, as IL-18 (Mailliard et al. 2005), tend to decrease with GBM CC, independently of Cav1 status in microglia cells, indicating that the GBM tumour environment is immunosuppressive.

As for the impact of the tumour immune environment upon the tumour gene expression, a variety of up or downregulations were observed, depending on the tumour cell line being tested. The GBM cell lines used in this project might have different mutations which might lead to these results, reflecting the huge heterogeneity of these tumours. From all the analysed genes, microglia cells trended to promote the expression of PSCA and IGF1 and suppress EPCAM. PSCA was found upregulated in tumour cells and was absent in normal brain tissue. Geiger *et al.* suggested the use of PSCA in CAR-T cell therapy for GBMs' treatment (Geiger et al. 2011). In the same context, IGF1 can regulate the immune response (Sinha et al. 2011), it can be inhibited by TNF- α , IL-1 α , and IL-6 (Lazarus, Moldawer, and Lowry 1993) and it was upregulated in GBM as well (Ho et al. 2017). The upregulation of these two genes pressured by the tumour immune environment suggests that microglia has an important role for tumour progression. On the other hand, EPCAM, which is characteristic of an epithelial phenotype (C. Rao et al. 2005; X. Chen et al. 2014), was suppressed by microglial immune environment. This suppression together with a slight increase of fibronectin suggests that microglia might be involved in the EMT of GBM cells, favouring the invasion of the tumour cells. However, other genes as N-Cadherin and vimentin need to be evaluated to study in more detail the impact of microglia on GBMs' EMT.

It is important to mention that some technical limitations from the cytokine array were taken into consideration to minimize the impact on the results between arrays. Upon the CC period, the media from both transwell compartments was collected, 1 ml was used (without dilution) to incubate with each membrane for 16 hours, and pictures of the membranes were acquired using the same exposure time. The number of iPSC-MG cells was a bit more difficult to control, since the quantity of differentiated microglia cells was dependent on the number of microglial progenitors that originated them. From the analysis of the microglia progenitors, both Cav1 NT and Cav1 KO generated similar levels of CD11b and CD45 positive cells, therefore it was expected a similar volume of differentiated cells independently of Cav1 status. After the differentiation and before the CC, iPSC-MG cells were observed under the microscope and it was not found any major difference between the cell quantities. Upon differentiation, iPSC-MG is hard to detach. To avoid activating these cells during the process, they were not detached prior

to each experiment. This problem was not observed for the CHME3, U87, UP007 and UP029 cells, where they were easily detached, counted, and seeded 24 hours before the CC. Finally, small differences of density between spots, especially in weak spots, can result in less accuracy during the analysis, especially after background subtraction.

Regarding the soluble factors present in the tumour immune environment created by GBM and microglia cells, once again, a high-level of heterogeneity was observed, depending on tumour cell line used to perform the CC. Within this environment, the factors are secreted by both populations as a result of a continuous paracrine interaction between cells. Interestingly, in this assay the CC performed with UP007 and UP029 generated an overall higher concentration of the analytes analysed. Across all the analytes analysed, some presented higher pixel density, suggesting higher concentration. Among all, CHI3L1, Cystatin, OPN, SERPINE1, CDF-15, IL-8 and uPAR were the ones overrepresented. In general, these genes were upregulated in GBM compared to non-tumour tissue and they were in the mesenchymal subtype, however, only in the proneural subtype the high expression of these genes is significantly correlated with poor survival, as observed in **APPENDIX IX – Other GBM databases**(Bowman et al. 2017). Additionally, the data produced by Darmanis *et al.* showed that these genes are expressed for both neoplastic and myeloid cells, and therefore, both populations are contributing for the production of these factors (Darmanis et al. 2017). Since these genes are correlated with a poorer survival rate and linked with the proneural subtype, this suggests a higher impact in the immune system with this subtype. However, this conclusion is based on the genes analysed, and other genes might be involved correlating the immune population with other GBM subtypes.

Although the CC with U87 cells were the one that created the biggest impact on microglia in terms of gene expression, the UP007 followed by UP029 showed the biggest impact regarding the secretome, suggesting that other mechanisms, which were not evaluated in the previous assays, are important for the tumour immune response. The cytokine profile of tumour cells was not analysed. This is a limitation of the cytokine study that it will be mitigated in the future. However, analysing the cytokine profile of microglia cells, it was possible to identify two factors that were upregulated, SERPINE1 and IL-8, and the ENA-78 that was downregulated in the tumour immune environment,

all of them created by the GBM cells. This suggests that microglia cells can be involved and are important during the process, but further studies are needed to confirm this.

As mentioned before, SERPINE1 is correlated with a poor prognosis in the proneural tumour subtype (**Supplementary figure IX. 1**), however, Sullivan and collaborators associated this gene with the mesenchymal tumour as well (Sullivan et al. 2014). IL-8 and ENA-18 are also overexpressed by mesenchymal tumours. IL-8 is mostly expressed by myeloid and vascular cells (Darmanis et al. 2017) and had no interference with the GBM's survival, but it is important to recruit other immune cells, in addition to being a potent angiogenic and proliferative factor (Sharma et al. 2018). On the other hand, ENA-78 is slightly overexpressed by GBM tumours in the mesenchymal subtype, but its high expression prolongs the overall survival rate (Bowman et al. 2017). It is mainly expressed by neoplastic, myeloid and astrocytic cells (Darmanis et al. 2017), and it is decreased in the tumour immune environment. All the information provided by these three genes suggests that the tumour immune system is associated with a poor prognosis more evident in the proneural tumour subtype, however the highest expression of these genes was observed in the mesenchymal tumours.

The effect of Cav1 in microglia cells upon tumour cells is still unknown. Human microglia cells expressed undetectable levels of Cav1, which were increased upon activation. Contrarily to macrophages, microglia upregulated Cav1 levels in the tumour periphery and downregulated it in the tumour core, suggesting different regulatory mechanism in these two populations. In the tumour environment, the absence of Cav1 seems to promote tumour invasion, but the mechanism involved was not determined. In microglia cells and in the tumour immune context, Cav1 seems to be involved with a pro-inflammatory response, which is correlated with an anti-tumoral behaviour. In tumour cells and in the tumour immune context, the absence of Cav1 in microglia tended to increase the CDH1 in U87 cells. This suggests that Cav1 in microglia is regulating some mechanism that prevents the interaction with the tumour cells, which in turn, can lead to the increase of this gene.

Cadherins play important roles during tumorigenesis, especially during the EMT where they are involved in the reduction of E-cadherin, or CDH1, and induction of N-cadherin. Dysregulation of CDH1 was associated with an aggressive phenotype in gliomas (Lewis-

Tuffin et al. 2010), but the differential expression does not seem to confer any advantage in terms of survival (Bowman et al. 2017). It is likely that other genes, not included into the Taqman array, are involved and contribute to increase the invasion of U87 cells when co-cultured with microglia unable to express Cav1.

Regarding the impact of Cav1 status in microglia on the tumour immune environment created by the CC with different GBM cell lines, once again it was observed a diverse response dependent of the tumour cell line, corroborating the results obtained in previous assays. From all the 105 evaluated factors, only four showed an increase across U87, UP007 and UP029 CC with microglia able to express Cav1, suggesting the involvement of Cav1. It was observed that the presence of Cav1 may prevent the release of pro-inflammatory interleukin IL-1 β and chemokine RANTES, as well as the inflammatory modulators thrombospondin 1 and RAGE. It is difficult to calculate which population is contributing for the concentration of each factor, but by exploring the Darmanis database it was possible to see that RAGE is mainly expressed by tumour cells, although the remaining factors were mostly expressed by myeloid cells (Darmanis et al. 2017).

Despite of the difference between the Transwell co-culture models and the 3D spheroid models, where cells are in intimate contact with each other, the analysis of the secretome profile of iPSC-Cav1 NT CC U87 vs iPSC-MG Cav1 KO CC U87 showed an overall downregulation of all the released factors suppressed by the presence of Cav1 in microglia cells. Moreover, for 37 factors the intensity increased to more than double with microglia that did not express Cav1. This observation may indicate that Cav1 in microglia acts as a suppressor for factor release, which in turn will reduce the interaction with tumour cells, decreasing the impact of microglia on the tumour invasion.

As for the co-culture with UP029 cells, the loss of Cav1 in microglia promoted the concentration of 19 factors, like the growth hormone, that may contribute for tumour growth, and IL-15 and IL-13, anti-inflammatory and immune regulator interleukins. However, for the co-culture performed with UP007 cells, the loss of Cav1 in microglia cells led to an overall decrease of the analysed factors. Together, these results suggest that Cav1 in microglia cells is not a key regulator of the immune response in the tumour context, but it might affect the tumour immune environment depending on the tumour

cells present in the environment. Nevertheless, additional studies are necessary to obtain a more robust conclusion.

In **summary**, the myeloid population is a representative population of the tumour bulk, where the macrophages are preferentially localized in the tumour core and the microglia in the periphery of the tumour. Both populations express low levels of Cav1, however, macrophages increase it in the tumour core and decrease it in the periphery, while the microglia increase it in the periphery and decrease it in the tumour core. The suppression of Cav1 seems to promote the tumour invasion possibly by the suppression of some pro-inflammatory factors, which led to an overall over-secretion of the secreted factors present in the environment. Cav1 in microglia cells does not seem to regulate the gene expression by the tumour cells. The microglia response and secretome seem to be dependent on tumour cell type, which might reflect the heterogeneous GBM environment. These results suggest that the GBM microenvironment creates pressure on the microglia, which can be modulated by Cav1. However, this protein does not seem to be a key regulator for microglia-tumour interaction.

CHAPTER 8 –
SUMMARY DISCUSSION AND
FUTURE DIRECTIONS

8.1 Summary discussion

The overall objective of this work was to explore the role of Cav1 in microglia cells and the influence that it can have in GBM tumour progression. Specifically in the GBM, Cav1 is involved in tumour invasion and associated with a shorter survival rate (Pu et al. 2019; Moriconi 2019). Microglia and macrophages are typically associated with worse prognosis and together these myeloid-derived cells can comprise of up to half of the tumour mass. Over the recent years the interest in these myeloid population has increasing as a target population for the treatment of GBM tumours. The role of Cav1 in myeloid cells is not yet clear, some studies have correlated this protein with an immune response, however, it seems to depend on the cell type and microenvironment where it is incorporated (C.-Y. Lee et al. 2017; Shimato et al. 2013; Celus et al. 2017).

To study the role of Cav1 in microglia, the correspondent gene was deleted using CRISPR-Cas9 technology. The first attempt to delete Cav1 used a technology based on plasmid vectors, and lipofectamine to deliver the system; this approach was not successful. The low transfection rates together with a lower editing efficiency resulted only in one successful Cav1 KO clone for one cell line. Changing the approach to use RNPs and a nucleofection delivery system resulted in powerful transfection rates, which provided successful Cav1 KO clones for all cell lines used. 24 hours after nucleofection, the cells were sorted as a whole population, giving them a chance to recover together from transfection, sorting and editing. This process was followed by clone isolation where the cells were seeded as a single cell using high dilution (30 cells per 96 well plate). We were aware that we could seed more than one cell per well using this method, but a careful examination 24 hours after the cell seeding procedure allowed us to exclude wells with more than one cell, which in turn allowed the correct clone selection. We tried to seed the transfected cells as a single cell using FACs, but the survival rate was minimal and most of the clones obtained were not successfully edited.

We edited Cav1 not only in microglia cells, but also GBM cell lines that were used mainly in another project in our laboratory. Due to the weak response of CHME3 cells, we tried to include the THP1 monocytic cell line to derive macrophages. However, it was a challenge to delete Cav1 in this cell line, so all the clones that survived and that were

able to be expanded were expressing Cav1 after the macrophage differentiation. Keeping the focus on microglia cells we also began the protracted process of generating microglia cells using iPSC technology (collaboration with lab of Nick Allen). We were thus able to explore the microglia and the impact of Cav1 using both CHME3 and iPSC-derived microglia.

To the best of our knowledge, Cav1 was never explored in primary human microglia cells. Since mouse and human established cell lines, BV2 (Niesman et al. 2013) and CHME3 (Portugal et al. 2017) cells respectively, are expressing Cav1, it was expected that primary human microglia cells also express the protein, and therefore, that Cav1 could have an impact on microglial functions. However, interrogating the single cell Darmanis' database (Darmanis et al. 2017, 2015), they observed Cav1 to be undetectable in healthy microglia, but upon activation, sub-populations showed increased expression of Cav1. The expression increased in the tumour periphery with slight but consistent decreases seen in the tumour core. On the other hand, macrophages, which are derived from a distinct lineage and expressed unique markers, presented the opposite pattern: highest Cav1 expression in the tumour core and a decrease in the periphery; macrophages should be absent in healthy brain tissue.

These observations raise a few questions:

Is Cav1 expression seen in the primary microglia cells or is it the result of the immortalization transformation?

If Cav1 is present in microglia, whether constitutive or induced, what effect will this expression have on phenotypic function?

The human microglia cell line CHME3 presented elevated levels of Cav1 that could be a consequence of the immortalization process. This conclusion is supported by data from primary cells and iPSC-derived microglia that do not present such elevated levels under standard conditions. Moreover, comparing the data from THP1 cells and iPSC-MG with CHME3, it appears that CHME3 cells are presenting an underlying inflammatory activation possibly through the NF- κ B and STAT3 signalling pathways which facilitate a pro-inflammatory phenotype. While the anti-inflammatory response in CHME3 seems to be affected it does not appear to be Cav1-dependent. Comparing the mRNA levels expressed by the various myeloid cells used in this project, the CHME3 produced an overall lower expression of pro-inflammatory and anti-inflammatory related markers in response to LPS and IFN- γ or IL-4 and IL-13, respectively suggesting a weaker reactivity by these cells in general.

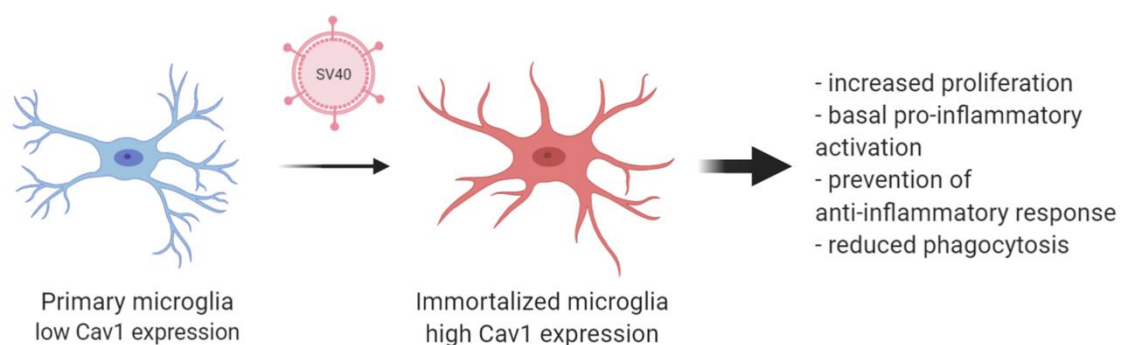


Figure 8.1 – Impact of the virus in the immortalization process on Cav1. Primary microglia present low Cav1 expression, which increases with SV40 large T antigen infection during the immortalization process, increasing their proliferation rate. The viral infection might interfere with gene transcription, activating the microglia, decreasing their ramification, enlarging their cellular body, promoting a pro-inflammatory basal activation, preventing an anti-inflammatory response, and reducing the phagocytosis.

The immunosuppressive environment predominates in GBM (Grabowski et al. 2020). The study of these tumours in model systems should incorporate microglia cell populations able to react / replicate to some extent the tumour microenvironment. The lack of responsiveness by CHME3, specially to an anti-inflammatory stimulus, added to the possible low pro-inflammatory basal activation, represents a concern in used these cells in any such model. Further, the absence of phagocytosis and low protein levels on the secretome upon the stimulation, are suggestive that CHME3 cells are 'to some extent exhausted'. Indeed the environment created by the GBM cells and CHME3 cells, did not interfere with GBM or microglia proliferation and migration/ invasion and neither did it

activate the microglial anti-inflammatory pathways (Hattermann et al. 2014; Ellert-Miklaszewska et al. 2013); only a slight increase of TGF- β was observed with GBM/CHME3 co-culture conditions. The low levels of reactivity and the exhaustive profile of these cells may be the result of the culture condition (Niesman et al. 2013) and/or the infection with SV-40 for the immortalization procedure (Janabi et al. 1995; Chai et al. 2017; Vanwalscappel, Tada, and Landau 2018; Gupta et al. 2017). However, comparison with fresh isolated and iPSC-derived microglia cells, and not with the cells that were used to establish the cell line originally. Therefore, other mechanisms might be involved.

Nevertheless, since CHME3 cells expressed relatively higher levels of Cav1, it was expected that gene deletion would show some profound effects, which could be representative of the function of Cav1 in the microglia population. The work showed Cav1 appears to be important in the CHME3 cells for migration, chemosensitivity to TMZ and transcription of pro-inflammatory genes IL-12 and TNF- α . Again, in a co-culture model there were no indications that the CHME3 Cav1 NT and CHME3 Cav1 KO had an impact upon GBM cell proliferation, migration, and invasion.

The iPSC-MG cells showed a different behaviour. With the modified Haenseler's protocol and the additional resting step after the differentiation, iPSC-MG were able to be activated towards a pro-inflammatory and an anti-inflammatory phenotype, showing an overall immune-activation or immunosuppression by differential expression (DE) gene analysis in RNA-seq. The iPSC-MG pro-inflammatory and anti-inflammatory RNA-seq database from this thesis' work will be available as an online source for others who wish to study the microglia phenotype, not only upon LPS and IFN- γ , but also upon IL-4 and IL-13 stimulation. Most of the available iPSC-MG databases focus only on the pro-inflammatory phenotype. However, analysing the gene function under the anti-inflammatory phenotype might reveal additional and important information to better understand several neurological diseases. Moreover, contrary to CHME3, the iPSC-MG cells were able to undertake phagocytosis of bioparticles, a characteristic of this immune population.

As previously mentioned, human microglia express low levels of Cav1 which seems to decrease during the development process. The impact of Cav1 on the iPSC-MG

phenotype appears to correlate a restriction of the pro-inflammatory response; a finding that contrasts to that of CHME3 where if anything Cav1 promoted a pro-inflammatory phenotype. The iPSC profile associated with Cav1 (dampening of pro-inflammatory response) was confirmed by secretome analysis; the DE analysis providing information on the genes that are involved in the inflammatory response, which might be useful for future projects. Moreover, since the iPSC-MG were phagocytic cells, it was possible to observe that the presence of Cav1 promoted the phagocytosis under the anti-inflammatory phenotype, suggesting a Cav1 involvement in microglia phagocytosis; we did not have sufficient time under COVID to study the impact of Cav1 in iPSC upon microglia cell migration, chemosensitivity to TMZ and STAT1, NF- κ B, STAT3 and STAT6 phosphorylation.

Of particular note in our data was the molecule SERPINE1. CHME3 cells secreted higher levels of SERPINE1 at the basal level when compared with iPSC-MG. However, it was only the iPSC derived microglia that responded in co-culture with GBM with increased levels of SERPINE1; a 6-fold increase in expression in the iPSC microglia cells when cultured with U87- here again there appeared no impact of Cav1 status. SERPINE1 is expressed by various cells, but in the tumour environment it is mainly expressed by vascular cells, tumour and myeloid cells (same contribution) and OPCs (marginally) as seen in the **Supplementary figure IX. 1** (Darmanis et al. 2017). SERPINE1 is associated with the mesenchymal tumour phenotype (Sullivan et al. 2014) and promotes the dispersal and migration of tumour cells, where TGF- β is a key regulator (Seker et al. 2019). SERPINE1 is the main inhibitor of both urokinase type plasminogen activator (uPA) and tissue type plasminogen activator (tPA), which converts plasminogen to plasmin. This plasmin activator/inhibitor system is involved not only in the regulation of fibrinolysis, but also in the remodulation of the ECM, cell migration and invasion, as well as in the phagocytosis of apoptotic cells (Myöhänen and Vaheri 2004; Czekay et al. 2003; Y. J. Park et al. 2008). Jeon *et al.* showed that in microglia cells the secreted levels of SERPINE1 increased after an inflammatory stimulation with LPS and IFN- γ , and that high levels of this protein promoted the microglial migration via the JAK/STAT1 pathway, however it inhibited the phagocytosis of particles (Jeon et al. 2012).

The levels of Cav1 in iPSC- MG increased in the pro-inflammatory phenotype and decreased in the anti-inflammatory phenotype. In the tumour context, it was observed an increase of Cav1 in the tumour periphery, where it should predominate a pro-inflammatory phenotype, and decreased in the tumour core, where it should prevail an immunosuppressive environment (Darmanis et al. 2017), suggesting that the suppression of Cav1 might drive to an exacerbated tumour immune environment able to promote tumour invasion. However, additional studies are needed to better understand this behaviour. Since macrophages were the main myeloid population within the tumour core, a good starting point would be to investigate the impact of Cav1 on these cells.

iPSC-MG 'Cav1 KO' presented an increase of inflammatory response to stimulus in co-culture with GBM cells, suggesting that Cav1 might act as a inhibitor of the inflammatory response in these cells. Uncontrolled microglia response to the tumour environment could lead to an increase of the inflammatory response, driven by the stimulus present in the microenvironment, able to promote tumour invasion. It would be interesting to study if the over-expression of Cav1 in iPSC-MG could prevent the microglia-tumour interaction and the inflammatory response.

Codrici *et al.* showed that Cav1 KO murine models presented higher plasmatic levels of pro-inflammatory cytokines IL-6, TNF- α and IL-12, as well as the anti-inflammatory cytokine IL-4 (Codrici et al. 2018b). One year before, Lee and collaborators showed that a downregulation of Cav1 in murine macrophages could attenuate the pro-inflammatory response induced by LPS, decreasing the pro-inflammation and increasing the IL-10 production in response to LPS (C.-Y. Lee et al. 2017). In lung cancer, the deletion of Cav1 in macrophages favours the angiogenesis via VEGFR1, MMP9 and CSF1, promoting the number and size of lung metastasis, but not affecting directly the expression of pro-inflammatory and anti-inflammatory mediators (Celus et al. 2017). Together with our results, even with the low expression presented by human cells, Cav1 in microglia cells seem to be correlated with the control of the inflammatory response. Therefore, the suppression of this protein may lead to an uncontrolled inflammatory tumour environment more permissive for invasion, but additional studies need to be conducted.

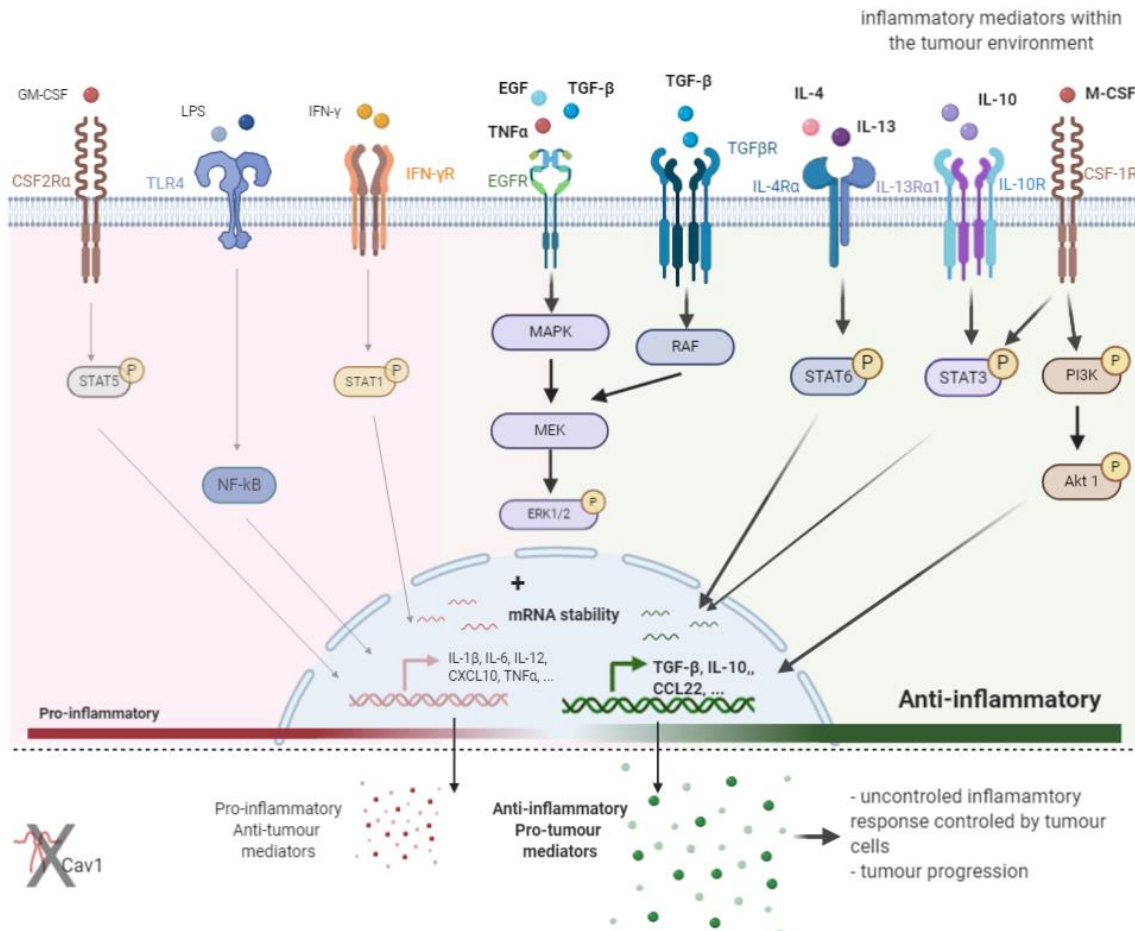


Figure 8.2 – Tumour inflammatory environment: impact of Cav1 KO in microglia cells. The immunosuppressive mediators present within the tumour niche will activate an anti-inflammatory response, where microglia cells will be able to secrete pro-tumoral mediators. This anti-inflammatory response can be modulated by Cav1, where cells not able to express the protein will not have a complete ERK1/2 pathway activation, contributing to mRNA stability exacerbating the inflammatory response and contributing to strengthen the tumour progression.

The loss of Cav1 in iPSC-derived microglia promoted the U87 tumour invasion. Contrary to what it was expected, for the tumour immune environment created by the co-culture of tumour cells with iPSC-MG-Cav1+ve in microglia cells did not induce alterations on the tumour expression of genes associated with invasion, comparatively to the environment created with microglia Cav1-ve. During this assay, we evaluated genes involved in tumour migration, invasion, and metastasis, suggesting that other genes outside of this scope might be involved. Once again, it was observed a different impact in microglia and tumour expression taking into consideration the GBM cell line, suggesting that the three tumour cell lines used in this project are heterogeneous and able to create distinct tumour immune environments, with diverse inflammatory

mediators. It would be interesting to correlate the tumour molecular profile with an immunological response.

In **summary**, CHME3 cells does not seem to be a good model to study brain tumorigenesis. iPSC-MG were shown to be a valuable method to obtain human microglia able to react to both pro-inflammatory and anti-inflammatory environments. Kolf2 progenitors proved to be a feasible cell line to be genetically engineered to study not only Cav1, but also other potential genes in microglia. Cav1 seems to be involved in microglial migration, proliferation, chemosensitivity to TMZ, phagocytosis and control of the inflammatory response. In the GBM context, the absence of Cav1 in microglia cells seems to promote the tumour invasion. Finally, similarly to tumours (Quest, Gutierrez-Pajares, and Torres 2008), Cav1 may have unique roles in immune cells for immunity and inflammation, which seem to be cell type dependent as well.

8.2 Future Directions

This project opened some doors about the role of Cav1 in microglia cells, but not all the questions were addressed. Future experiments will include a more detailed impact analysis of iPSC-MG Cav1 NT and iPSC-MG Cav1 KO upon tumour proliferation, migration and TMZ chemosensitivity, to clarify the role of microglial Cav1 on the prevention of tumour progression. Moreover, the study of 3D tumour invasion used only one focal point, at the time points D0 and D3, which could underestimate the impact of microglia on the tumour invasion. A time-lapse covering the complete invasion period, including Z-stack will be considered using the EVOS M7000 together with an onstage incubator. At the time point D3, additional images will be acquired using a lightsheet microscope to access the localization of both populations, in high resolution format.

Regarding the iPSC-MG, because Cav1 promoted microglia migration and sensitivity to TMZ in CHME3 cells, additional migration and chemosensitivity studies will be performed to evaluate the impact of Cav1 in this iPSC-MG to confirm the results using another human microglia source.

For high proliferative cell lines, such as the GBM, it is difficult to track cells for long periods with cell tracker dyes. In theory, at each cell division the dye concentration is halved. To overcome this limitation, a vector GFP-cLuc (cypridina luciferase) will be introduced into the AAVS1 safe harm in tumour cells, which will allow to track tumour cells indefinitely, not only using microscopic technologies but also cypridina luciferin substrate that can be secreted into the media by tumour cells in the presence of luciferase and be detected and quantified by bioluminescence.

Since microglia and macrophages have unique markers that make them a unique population, and because, once inside the tumour environment, they seem to express different Cav1 levels depending on the tumour location (core vs periphery), it will be interesting to investigate the role of Cav1 in macrophages and their impact in tumour progression.

There is no perfect model to study tumours, however the tumour environment can be the key for GBM tumours to be presenting the same prognosis year after year. Our group is developing a cerebral organoid model constituted by astrocytes, neurons, and oligodendrocytes. The cerebral organoid can recapitulate the multicellular complexity, with some degree of architecture, offering cell-cell interactions and autocrine/paracrine functionality, as well the influence of the matrix microenvironment. The model is formed along 40 days, where dorsomorphin, a small-molecule inhibitor of bone morphogenic protein (BMP), and SB431542, that inhibits the TGF β /activin/nodal signalling pathway, are used to prevent the spontaneous and unidirectional formation of the other germ layers such as mesoderm, which derives from the microglia, and endoderm (Pasca et al. 2015; Gabriel and Gopalakrishnan 2017). The neuronal differentiation is promoted by retinoic acid (Lancaster et al. 2017). In this model, genetically manipulated microglia can be integrated, as well as tumour cells (GFP-cLuc), to study the impact of the myeloid population on the tumour invasion, proliferation, and response to drugs (**Figure 8.3**).

Not only TMZ will be used, but also clomipramine and vincristine will be tested as well. These drugs have been previously used widely in various 2D in vitro studies using both mouse and human microglia cells in the context of GBM therapies (Leite et al. 2020).

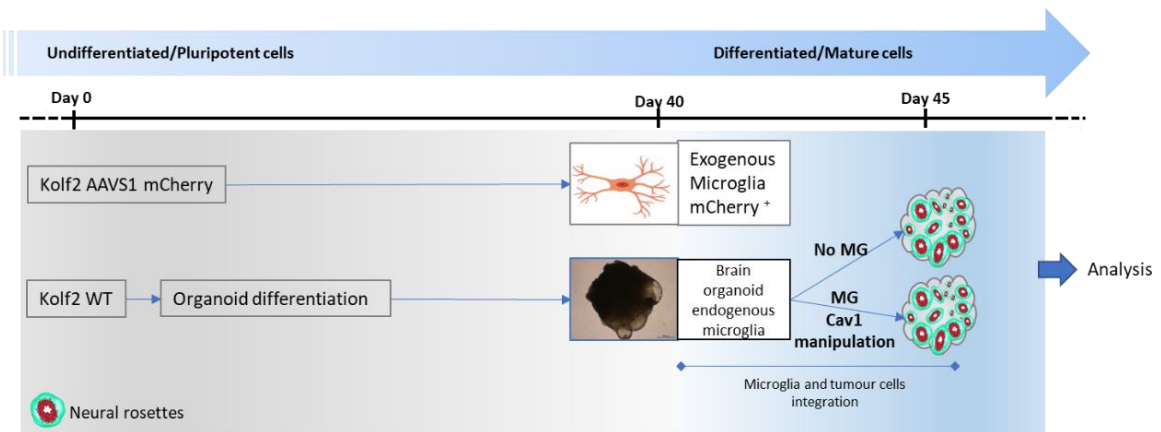


Figure 8.3 – Cerebral organoid model. The cerebral organoids are generated from Kolf2 cells, using dual SMAD inhibition to prevent the differentiation of the mesodermal and endodermal lineages, and to promote neuronal differentiation more efficiently. simultaneously, microglia are differentiated from Kolf2 AAVS1 mCherry cells, where at day 40 they will be incorporated into the organoid. The tumour cells (GFP-cLuc) can be integrated into the organoid at day 45.

U87, UP007 and UP029 cells will be the first to be tested in this model. However, in the future, blood and tumour samples will be received from patients diagnosed with primary GBM tumours. Patient-derived iPSC will be created from the peripheral blood in order to create an isogenic organoid model to study their own tumour population. The isogenic nature of such a model can facilitate a wider study of immune cell interactions and treatments including not only microglia, but also macrophage and lymphocyte populations, and novel immunotherapies such as CAR (chimeric antigen receptor) T-cell therapies. After the patient-derived iPSC creation, the cell lines will be validated together with tumour cells, aiming to be available as a resource for other future projects, internal or external to the current team.

APPENDICES

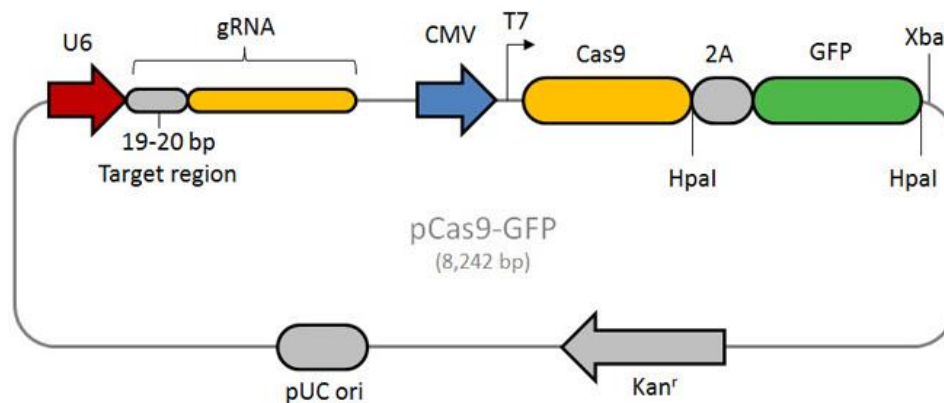
APPENDIX I - CRISPR-CAS9 VECTOR APPROACH

This section describes the CRISPR-Cas9 vector approach.

Material and Methods

sgRNA

Three different pre-designed CRISPR targets for the Cav1 gene to generate KO were purchased from Sigma-Aldrich and are described in **Supplementary figure I.1** and **Supplementary table I.1**.



Supplementary figure I.1 – Plasmid vector map (Sigma-Aldrich).

Supplementary table I.1 – sgRNA characteristics for Cav1 target.

Target ID	Vector	Exon	Target Site
HS0000173746	U6gRNA-Cas9-2A-GFP	1	TTTAGGGTCGCGGTTGACCAGG
HS0000173747	U6gRNA-Cas9-2A-GFP	1	AAACACCTCAACGATGACGTGG
HS0000173749	U6gRNA-Cas9-2A-GFP	2	CATCCCGATGGCACTCATCTGG

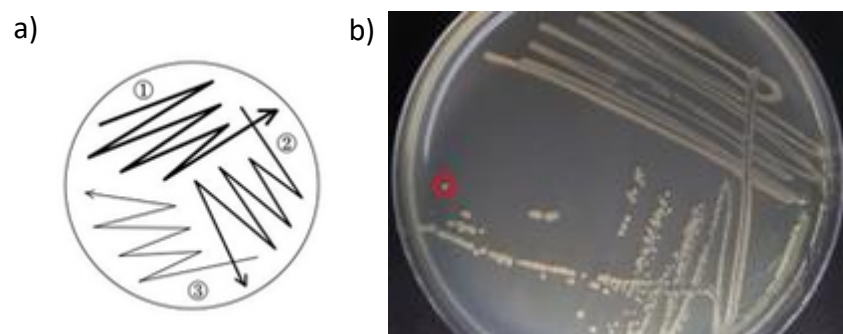
LB-agar plates

Before bacterial transformation, Luria Broth (LB)-agar plates were prepared with the respective antibiotics (50 mg/ml of Kanamycin for Cav1 sgRNA or 100 mg/ml of Ampicillin for non-target (NT) sgRNA). Briefly, LB-agar powder (Miller, Fisher Bioreagents) was dissolved in distilled water at a concentration of 37 g/L and was

autoclaved. After the autoclaving process, the medium was maintained in a water bath at 60°C, to keep the medium in a liquid state. The respective antibiotic was prepared and mixed with LB-agar medium, in sterile condition. Maintaining the sterile condition, the medium with the specific antibiotic was poured into a petri dish and allowed to dry for 30 minutes, at RT. The petri dishes were sealed with parafilm, labelled with the antibiotic's information, and stored at 4°C until used.

Bacterial transformation and amplification

Sub-cloning MAX efficiency DH5α cells (Invitrogen) were removed from the -80°C freezer and thawed on ice. The agar plates (containing the appropriate antibiotic) were taken out of 4°C to warm up to RT. 2 ng of DNA of each sgRNA was mixed into 100 µl of competent cells and incubated on ice for 30 minutes and then heat-shocked at 42°C for 45 seconds. Cells were then cooled on ice for an additional 2 minutes, and 900 µl of S.O.C. medium (Gibco) was added to the cells, before being transferred to a shaking incubator, set to 37°C and 225 RPM, for 1 hour. The plasmid pSpCas9(BB)-2A-GFP (Addgene) previously prepared without any sgRNA by Jack Sim, was used as control for NT-Cav1. For plasmid amplifications, 100 µl of this transformed cell solution, as well as, pSpCas9(BB)-2A-GFP-NT were spread on an agar plate each, as demonstrated on (**Supplementary figure I.2, a**), containing the appropriate antibiotics, using a sterile spreader. Plates were incubated upside down overnight in a 37°C incubator. The next morning, a simple colony was selected for each plate (**Supplementary figure I.2, b**).



Supplementary figure I.2 - Streaking for a single colony. a) cell transformation spread diagram. b) example of a single colony.

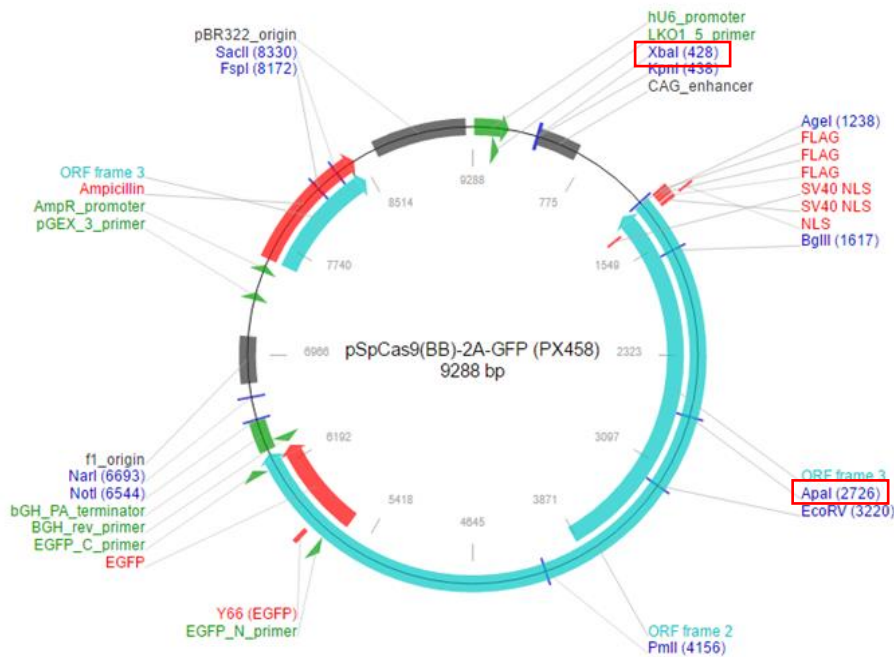
Using a toothpick, the single colony was picked and dropped into 5 ml of LB medium with the appropriate antibiotic and incubated in a shaking incubator, set to 37°C and

225 RPM, for 6 hours. After the incubation time, 1 ml of bacteria was diluted into 100 ml of LB medium and incubated overnight, at the same conditions. The remaining bacteria was used for creation of Glycerol stock (500 µl of bacteria with 500 µl of glycerol 80%) and stored at -80°C.

Plasmid isolation and Restriction Enzyme Digestion

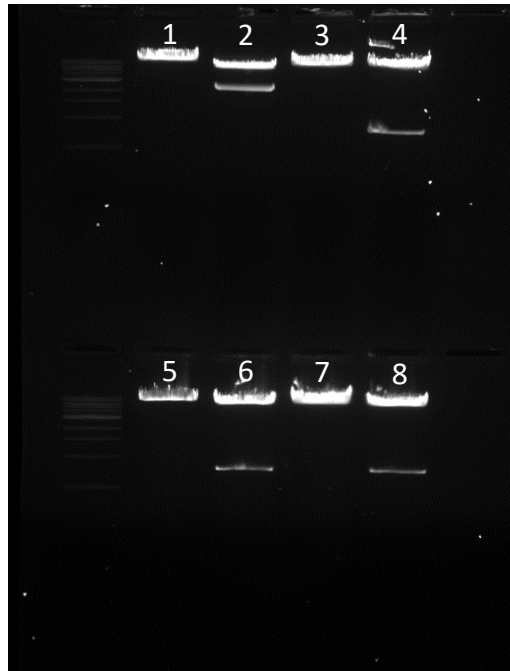
In the next morning, the bacterial culture was centrifuged at 13,000 g for 20 minutes, at 4°C, to pellet the bacteria. Plasmid DNA was then isolated from the pellet using QIAprep spin miniprep kit (Qiagen), following the manufacturer’s instructions. DNA was eluted in 30-50 µl of elution buffer. DNA concentration was measured by Genequant Pro (Hawksley).

Because all colonies that have grown under antibiotic selection carry the vector, but not all of them have the insert of target region, restriction enzyme digestion was done to verify if the generated plasmids contain the specific target region. The appropriate restriction enzymes were selected according to the plasmid (**Supplementary figure I.1** and **Supplementary figure I.3**). XbaI and HpaI were used for U6gRNA-Cas9-2A-GFP plasmid, and XbaI and ApaI were used for pSp-Cas9(BB)-2A-GFP plasmid.



Supplementary figure I.3 – pSpCas9(BB)-2A-GFP plasmid with the respective restriction enzymes (Ran et al. 2013).

The digest diagnostic was performed by Anza Restriction Enzyme Cloning System (Invitrogen) using 2 µg of bacterial DNA, following the manufactory's protocol. The DNA fragments were analysed in a 1% agarose gel, by electrophoresis.



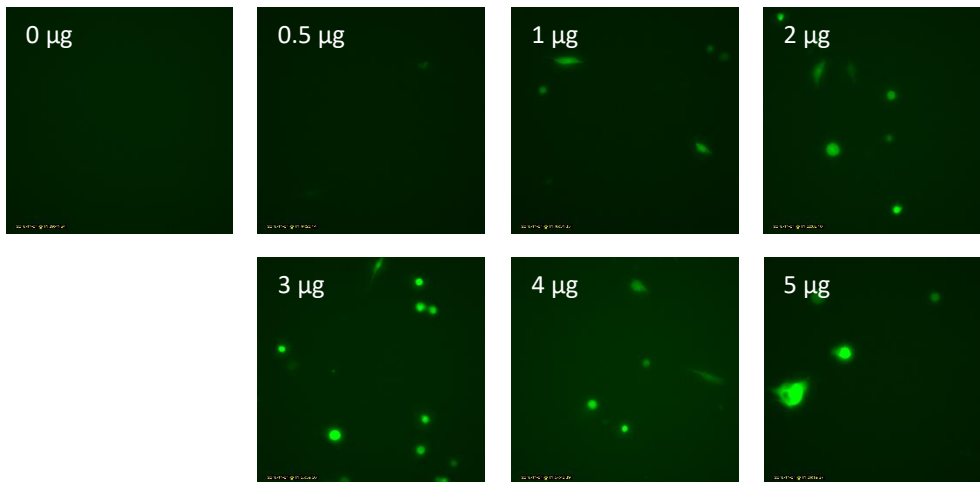
Supplementary figure I.4 - Restriction Enzymatic Digestion gel. 1 and 2 - NT sequence, 3 and 4 - Cav1 KO Sequence 46; 5 and 6 - Cav1 KO Sequence 47; 7 and 8 - Cav1 KO Sequence 49; 1, 3, 5 and 7 - one restriction site; 2, 4, 6 and 8 - two restriction sites.

When 1 restriction site was used, it was obtained a product size that corresponds to the total plasmid dimension, in this case, 9,288 bp for NT sequence (1) or 8,242 bp for the target sequences (3, 5 and 7). With the treatment of 2 enzymes for restriction it was possible to obtain 2 products for each sequence: 6,990 bp plus 2,298 bp for NT sequence (2) and 7,470 bp plus 772 bp for the target sequences (4, 6 and 8), as expected (**Supplementary figure I.4**).

Cellular transfection

Prior to cellular transfection, the quantity of DNA to be transfected was optimized by transfecting CHME3 and U87 cells with different concentrations of DNA and subsequent reagents. Several concentrations of DNA were tested: 0, 0.5, 1, 2, 3, 4 and 5 µg. After transfection, the cells were seeded into 48-well plates and followed using a Lumascop microscope for 3 days (**Supplementary figure I.5**). The transfected cells were positive

for GFP. Both cell lines presented the highest number of GFP-positive cells when using 3 μg of DNA. With superior concentrations of DNA and consequent increase of the reagents (toxic concentrations for these cell lines), the cells started to die and subsequently the GFP-positive number decreased.



Supplementary figure I.5 - Representative pictures of U87 cells transfected with different concentrations of DNA - GFP positive, at day 3.

Subsequently, CHME3 and U87MG cells were seeded at a concentration of 11,000 cell/cm² in a 6-well plate, 24 hours before the transfection at 37°C. These cells were 80-90% confluent at transfection. Cells were transfected with Lipofectamine™ 3000 reagent (Invitrogen), following the manufacturer's protocol. Briefly, cells were incubated in Opti-MEM serum free culture medium (Gibco) with pre-mixed 3 μg of DNA with 6 μl of P3000™ reagent plus 6 μl of Lipofectamine® 3000 Reagent, for 4 hours, according to the manufacturer's protocol. After 4 hours, the medium was replaced by fresh medium (DMEM with 10% FBS). After 48 hours, GFP-positive cells were sorted using the Aria flow-cytometer and plated as single cells in 96-well plates. The remaining GFP⁺ cells were collected for DNA cleavage analysis using the primers described in **Supplementary table I.2**.

Taking into consideration the gRNA that was used to transfect the cells, when the editing is successful, they are expected to sequence 46 products with 421 bp plus 183 bp, 47 products with 419 bp plus 185 bp, and 49 products with 417 bp plus 187 bp.

Supplementary table I.2 - PCR primers for PCR amplification to DNA cleavage study-

Potential cleavage site	Forward	Reverse	Product size
HS0000173746 and HS0000173747	GGCCTGCCCTAGCCCCTG	TCCCACACATCAAACCCA CAA	604 bp
HS0000173749	CTGGGAAGTCGAAGCTGCA GT	CTTTCTGCAAGTTGATGC GGA	604 bp

Cells were plated into a 96-well plate and maintained in culture at 37°C in a 5% CO₂-humidified atmosphere. The medium was renewed twice a week. When the single colonies reached the confluency, they were transferred into a 48-well plate, then a 12-well plate, followed by a 6-well plate, and finally in a T25 flask. After being in a T25 flask, two thirds of the cells were frozen, and the remaining cells were kept in culture to be used for Cav1 expression analysis by Western Blot.

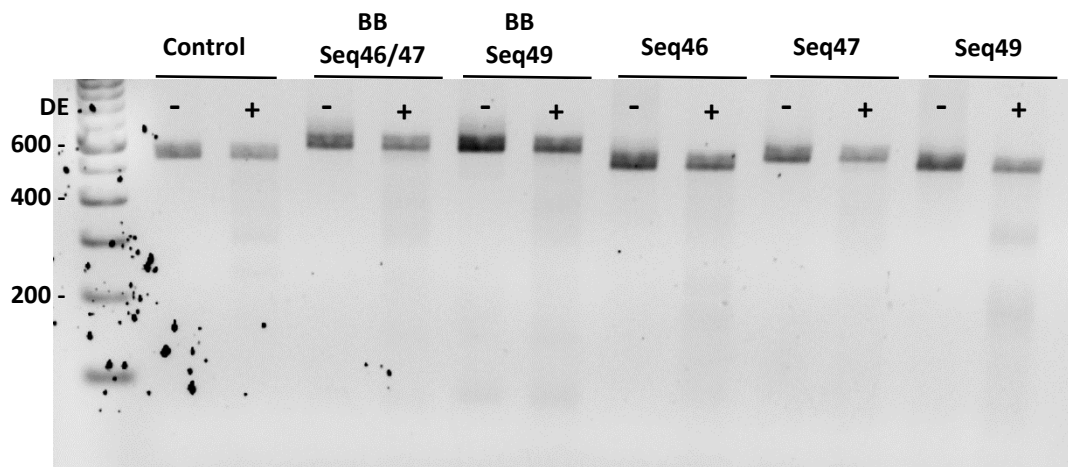
Results

Four cell lines (U87, UP007, UP029 and CHME3) were tested with this CRISPR-Cas9 plasmid approach. 72 hours after transfection, the transfected cell lines were sorted as a single cell into 96-well plates for clone selection. The efficiency of transfection is illustrated in the **Supplementary table I.3**. Potential Cav1 KO clones were generated and analysed by WB, for all the used cell lines.

Supplementary table I.3 – Transfection efficiency of each cell line and correspondent sequence. Analysis by FACs, GFP positive cells.

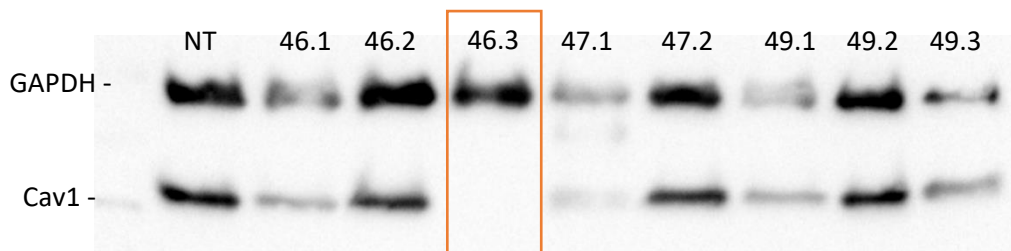
Cell Line_sequence	Transfection efficiency	Cell Line_sequence	Transfection efficiency
U87_BB	1.0%	UP007_BB	2.3%
U87_sq46	3.6%	UP007_sq46	3.6%
U87_sq47	3.3%	UP007_sq47	2.0%
U87_sq49	3.2%	UP007_sq49	1.1%
CHME3_BB	2.3%	UP029_BB	2.2%
CHME3_sq46	4.4%	UP029_sq46	3.2%
CHME3_sq47	4.0%	UP029_sq47	1.4%
CHME3_sq49	4.2%	UP029_sq49	1.8%

The **Supplementary figure I.6** shows an example of the DNA cleavage analysis for the U87 cell line after CRISPR-Cas9 plasmid transfection. There were no control cells (BB) with edited PCR products, neither with primers that target the sequence 46 and 47 or the sequence 49. When the U87 cells were transfected with plasmid that contained the sequence 46, 47 or 49, a low efficiency of edition was observed, confirmed by the faint bands from the PCR products expected around the 420 bp and 185 bp. Similar images were obtained for the other cell lines, UP007, UP029 and CHME3 (figures not shown).



Supplementary figure I.6 – Gel image from **U87** GFP⁺ sorted cells. BB: Backbone control; DE: Digestion enzyme treatment.

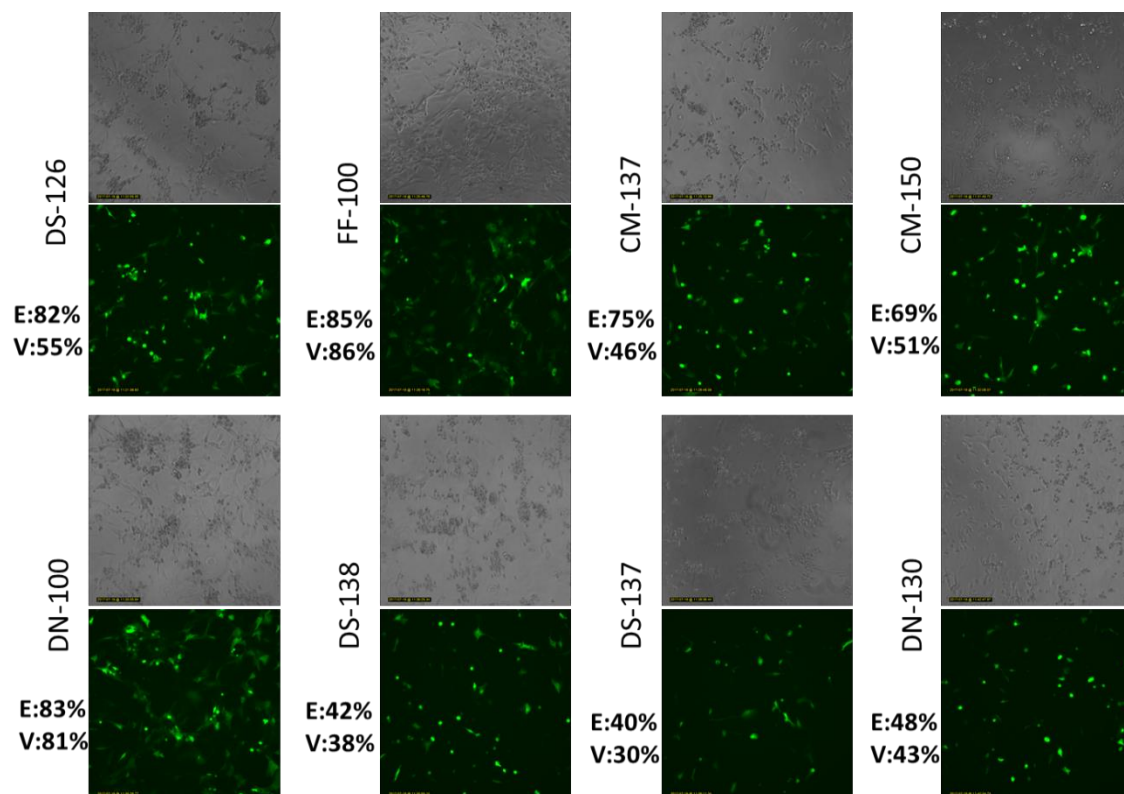
It was possible to obtain only one clone of Cav1 KO from the U87 cells with sequence 46 (U87 - clone 3), as observed in **Supplementary figure I.7**. All the remaining cell lines failed to generate Cav1 KO clones.



Supplementary figure I.7 - Cav1 protein expression by different clones obtained after DNA plasmid CRISPR-Cap9 approach in U87 cell line.

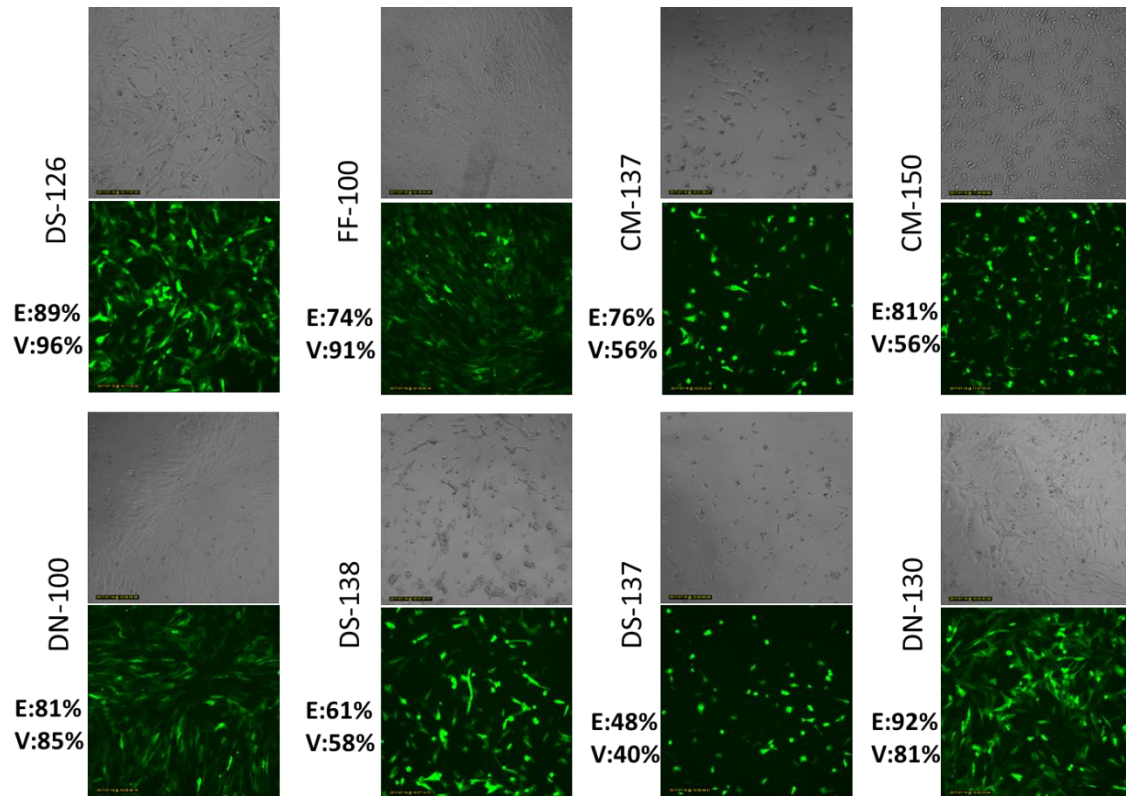
APPENDIX II - CRISPR-CAS9 RNP APPROACH OPTIMIZATION

Aiming to optimize the nucleofection for the cell lines that are not available on the Lonza database, eight different electroporation programs were tested for GFP transfection (DS-126, FF-100, CM-137, CM-150, DN-100, DS-138, DS-137 and DN-130). Per reaction, 100,000 cells (UP029) or 200,000 cells (CHME3) were resuspended into 20 μ l of Nucleofection Solution SE (Lonza) together with 4.6 μ M of GFP (same amount of RNP complex) and were electroporated. Each condition of electroporated cells and non-electroporated cells (control) was divided into 3 samples and transferred into a 48-well plate with pre-warmed medium into a culture incubator (37°C, 5% CO₂). Photos were taken after 24 hours. One well was dissociated to count the positive and negative GFP cells (editing efficiency) and the remaining two wells were analyzed for MTT viability assay to calculate the percentage of cells that survived, compared with non-electroporated cells (**Supplementary figure II. 1**). The FF-100 displayed the higher viability and transfection efficiency for CHME3, (86% and 85%, respectively), without affecting the morphology of the microglial cells.



Supplementary figure II. 1 – CHME3 nucleofection optimization. Representative photo of each different program and the respective edited efficiency (E) and viability (V).

Regarding the UP029 cell line, the programs DS-126, FF-100, DN-100 and DN-130 presented a good viability, efficiency of transfection, and did not altered the cellular morphological phenotype (**Supplementary figure II. 2**). Since DS-126 is the program recommended for U87 cell line, UP029 was electroporated using the same setting.



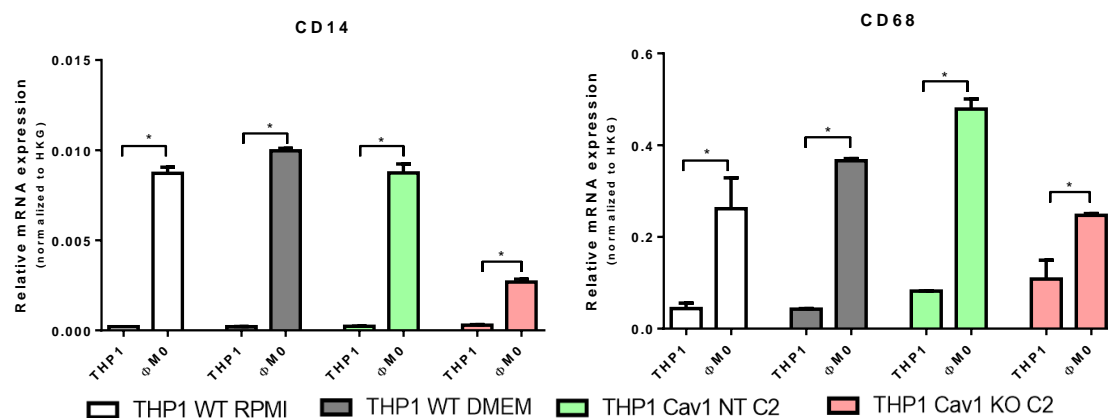
Supplementary figure II. 2 – UP029 nucleofection optimization. Representative photo of each different program and the respective edited efficiency (E) and viability (V).

APPENDIX III – THP1-DERIVED MACROPHAGES

THP1 WT, THP1 Cav1 NT C2 and THP1 Cav1 KO C2 were used for macrophages studies. THP1-derived macrophages were obtained upon differentiation with PMA for 72 hours. In the literature, the THP1 differentiation can be performed from 24 hours to 72 hours, however, Fu *et al.* (Y. Fu et al. 2012) showed that the Cav1 expression is important for macrophages differentiation and increases with longer exposure to PMA (72 hours). After differentiation, macrophages cells were allowed to rest in standard medium, without interference of PMA, for an additional 24 hours, since PMA can act as a pro-inflammatory stimulus and activate pro-inflammatory pathways. Once macrophages were obtained, the cells were polarized with standard pro-inflammatory or M1 (IFN- γ and LPS) and anti-inflammatory or M2 (IL-4 and IL-13) stimulus for 48 hours. After polarization, cells were collected for protein or mRNA analysis following the methods described in **Chapter 2, section 2.7 and 2.8.**

The medium to culture THP1 cells suggested by ECACC is the RPMI. One of the aims of this project was to study the function of macrophages in a GBM context. Since all the used GBM cell lines were grown in DMEM medium, THP1 culture condition was gradually exchanged from RPMI to DMEM and all the analysis was done in both conditions to exclude any influence of the medium composition.

The macrophages markers CD14 and CD68 were analysed by qRT-PCR in order to confirm that the cells obtained displayed macrophages features.

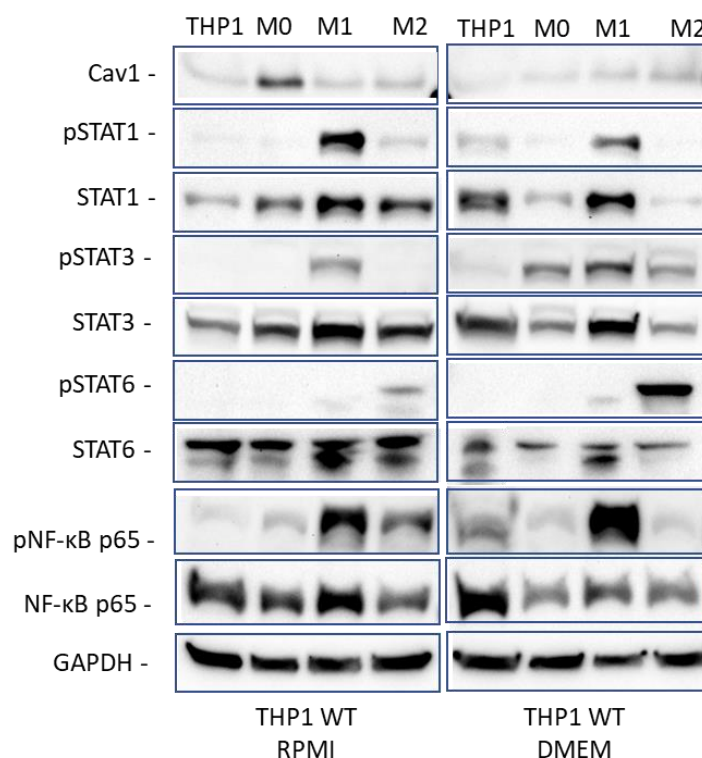


Supplementary figure III. 1 Macrophages characterization using CD14 and CD68 markers of THP1 WT cultured in RPMI (white) or DMEM (grey) medium, THP1 Cav1 NT C2 (green) or THP1 Cav1 KO C2 (red), upon 72 hours of PMA treatment. THP1 Cav1 NT and THP1 Cav1 KO were culture in DMEM based medium. Bars represent mean of relative expression (GAPDH used as housekeeping gene) \pm SEM (* $P < 0.05$, by Mann-Whitney Student's *t*-test).

The **Supplementary figure III. 1** shows a significant increase of CD14 and CD68 after PMA treatment in all THP1, WT, Cav1 NT C2 and Cav1 KO C2 cells. THP1 Cav1 KO C2 cells showed a decrease of expression of these markers compared with WT and NT, however, they showed a higher expression compared with the respective unstimulated cells. The culture of cells in RPMI or DMEM did not affect the macrophages differentiation.

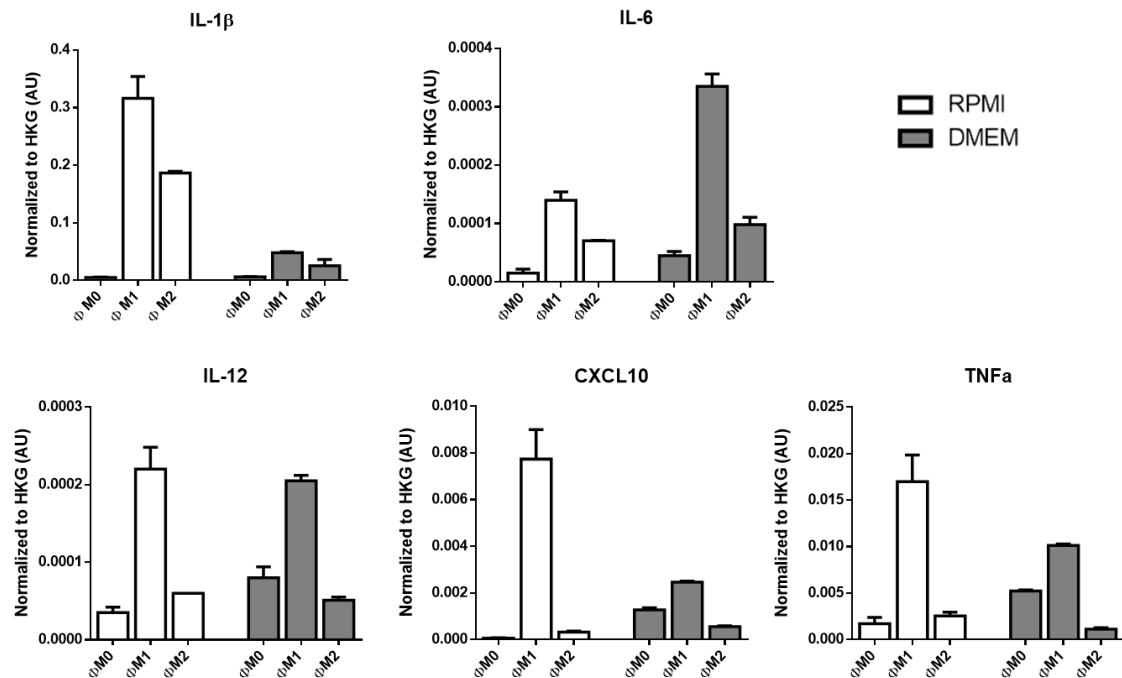
Protein and mRNA expression by THP1 WT cells when cultured in RPMI or DMEM

The culture of THP1 WT cells in RPMI seems to increase the Cav1 expression with PMA treatment, which decreases after pro-inflammatory or anti-inflammatory polarization (**Supplementary figure III. 2**). The cells cultured in DMEM did not display this increase upon PMA treatment, showing roughly the same Cav1 expression in all tested conditions. Using different medium, these macrophages were able to activate pSTAT1 and pNF- κ B p65 with pro-inflammatory polarization. The pSTAT6 activation was more pronounced for cell cultures in DMEM, as well as pSTAT3 which was active in M0, M1 and M2 phenotype (RPMI showed an activation only in M1 phenotype).



Supplementary figure III. 2 - Protein expression of Cav1, Stat1, Stat3, Stat6, NF- κ B p65 and GAPDH, of unstimulated (M0), pro-inflammatory phenotype (M1) and anti-inflammatory phenotype (M2) of THP1 WT cells cultured in RPMI (left) or DMEM (right). GAPDH was used as control.

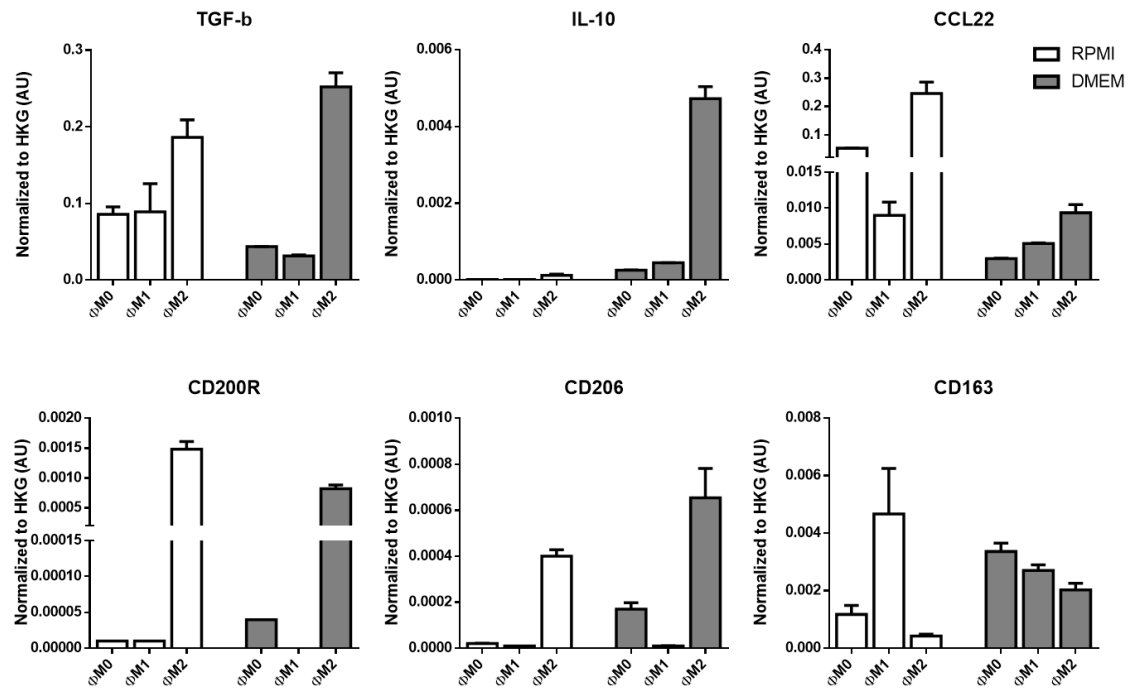
The expression of pro-inflammatory markers (anti-tumoral) by macrophages that were in the culture with RPMI and DMEM medium are represented in the **Supplementary figure III. 3**.



Supplementary figure III. 3 – Pro-inflammatory markers (M1-related) by qRT-PCR. IL-1 β , IL-6, IL-12, CXCL10 and TNF- α expression by THP1-derived macrophages were cultured in RPMI (white) or DMEM (grey). The expression was normalized to HKG GAPDH. Bars represent mean of relative expression \pm SEM. N=2 independent experiments.

The culture of THP1 cells with different mediums did not change the pattern of macrophages polarization. It was possible to observe that cells cultured in DMEM expressed a reduced amount of IL-1 β , CXCL10 and TNF- α , and an increase of the amount of IL-6, however, the pro-inflammatory stimulus increases the expression of all markers, in both RPMI and DMEM conditions.

Regarding the anti-inflammatory markers (pro-tumoral), the gene expression by THP1-derived macrophages cultured in RPMI and DMEM is represented in the **Supplementary figure III. 4**.

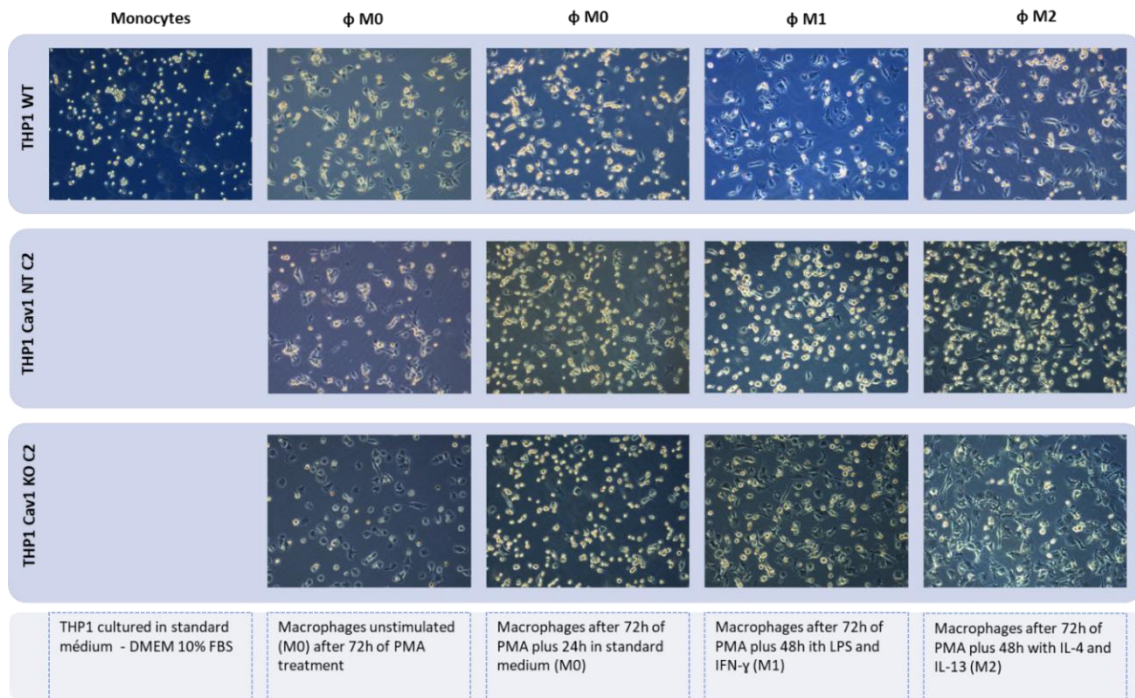


Supplementary figure III. 4 – Anti-inflammatory markers (M2-related) by qRT-PCR. TGF- β , IL-10, CCL22, CD200R, CD206 and CD163 expression by macrophages-derived from THP1 that were cultured in RPMI (white) or DMEM (grey). The expression was normalized to HKG GAPDH. Bars represent mean of relative expression \pm SEM. N=2 independent experiments.

Upon IL-4 and IL-13 stimulation, macrophages cultured in RPMI or DMEM increased the expression of TGF- β , IL-10, CD200R and CD206 at similar levels. The mRNA levels of CCL22 increased upon M2 response, however these were higher in macrophages cultured in RPMI medium. Once again, CD163 does not seem to be a good marker for THP1-derived macrophages, since its expression did not increase with M2 stimulation.

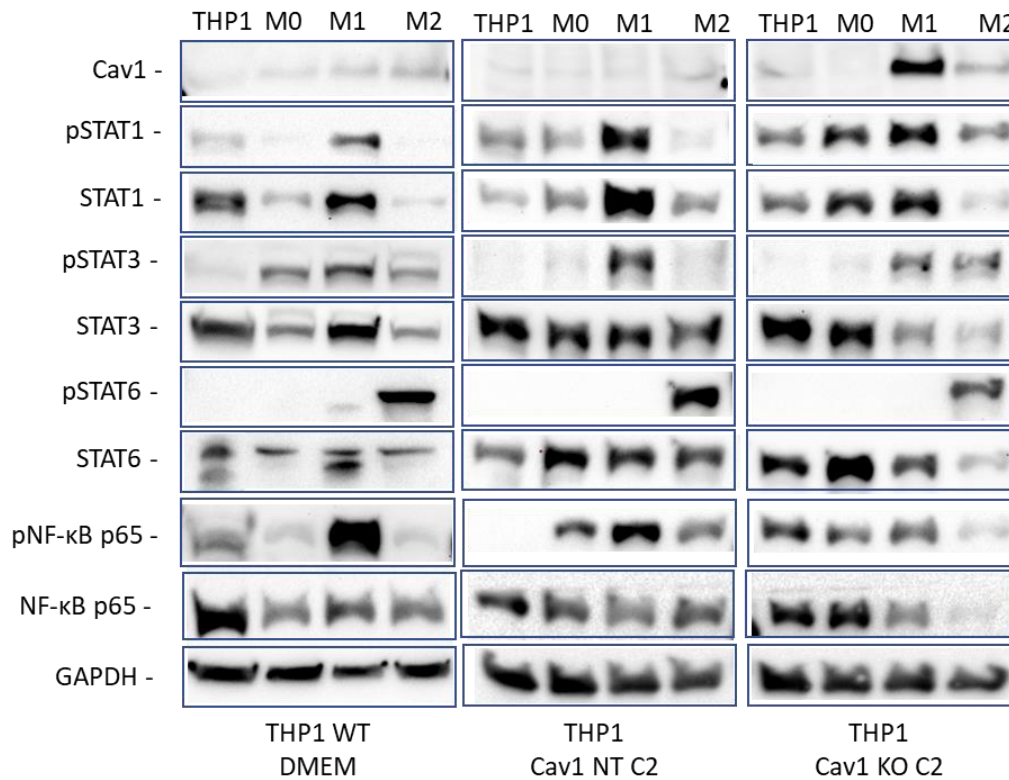
Protein and mRNA expression by THP1 WT, Cav1 NT C2 and Cav1 KO C2 cells when cultured in DMEM

The THP1 monocyte cell line grows in suspension conditions (**Supplementary figure III. 5**). Upon differentiation using the PMA protocol, macrophages become adherent and start to enlarge their cellular bodies. Resting for 24 hours from PMA cells reduces their bodies (WT, NT C2 and KO C2), remaining in adherence. With M1 and M2 polarization they elongated their bodies and resemble fibroblast-like shaped cells as mature macrophages described by Young *et al.* (D. A. Young, Lowe, and Clark 1990).



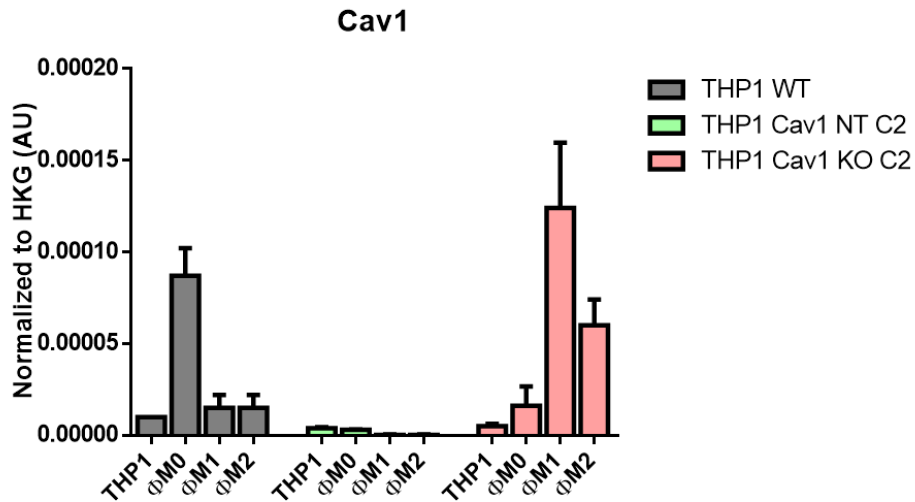
Supplementary figure III. 5– Representative photos of THP1 WT, THP1 Cav1 NT C2 and THP1 Cav1 KO C2. Pictures were taken prior to differentiation (as monocyte cells), after 72 hours of PMA treatment (macrophages cells), 24 hours in standard médium culture upon PMA differentiation, and upon 48 hours of polarization towards M1 or M2 phenotype.

With regards to the protein levels (**Supplementary figure III.6**), WT and NT C2 cells did not change the Cav1 expression. It was expected an increase of Cav1 levels in M0 at least, as described by Fu and colleges (Y. Y. Fu et al. 2012). Nevertheless, the pSTAT1 and NF-kB p65 increased with M1 activation and pSTAT6 increased with M2 activation in both WT and NT cells. The pSTAT3 expression, similarly to CHME3 microglial cells, did not increase in M2, but it was observed a slight increase in the M1 phenotype. It was detected a fluctuation in the total forms as well.



Supplementary figure III. 6 – Protein expression of Cav1, STAT1, STAT3, STAT6, NF-κB p65 and GAPDH, of unstimulated (M0), pro-inflammatory phenotype (M1) and anti-inflammatory phenotype (M2) of THP1 WT (left), THP1 Cav1 NT C2 (centre) or THP1 Cav1 KO C2 (right) cultured in DMEM.

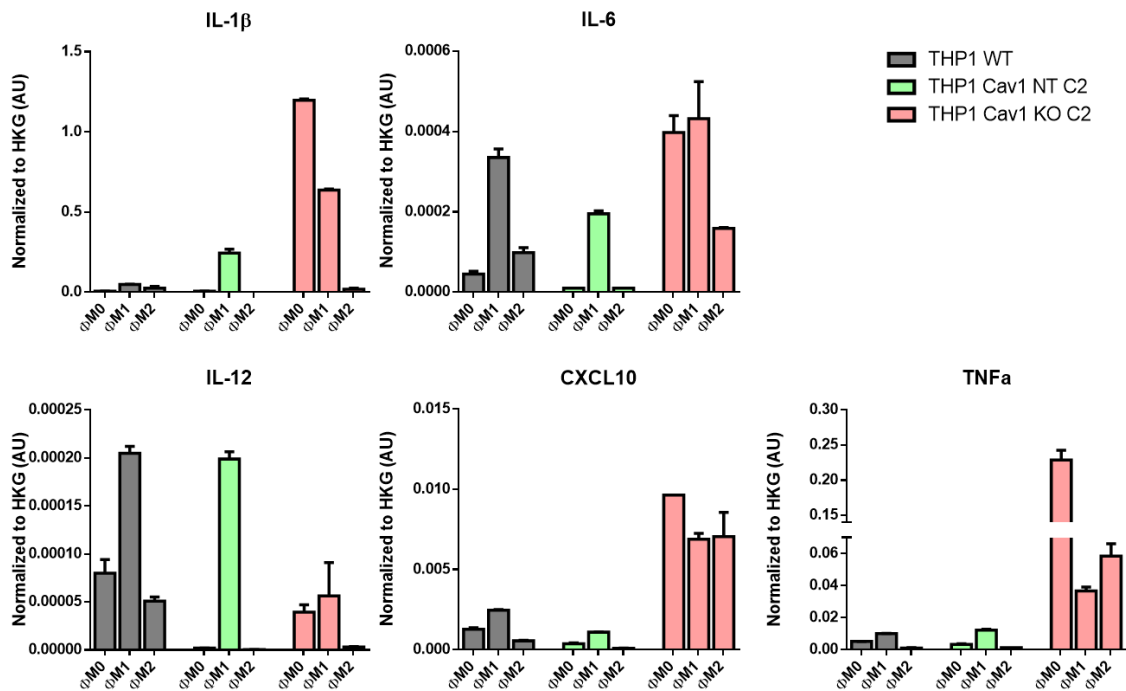
As for the THP1 Cav1 KO C2, the cells did not express Cav1 in M0, however, after polarization, the cells started to express Cav1, more intensified in M1 phenotype (**Supplementary figure III. 6**). As observed, this clone is not a Cav1 KO. During the CRISPR-Cas9 process, the indel created after DNA cut is able to increase Cav1 expression after stimulation, but further molecular studies were necessary to characterize the kind of event this clone suffered.



Supplementary figure III. 7 – mRNA expression of Cav1 by THP1 WT (grey), Cav1 NT C2 (green) or Cav1 KO C2 (red). THP1 (monocytes) and macrophages (M0, M1 and M2) were analysed. Gene expression was normalized to HKG GAPDH. Bars represent mean of relative expression \pm SEM. N=2 independent experiments.

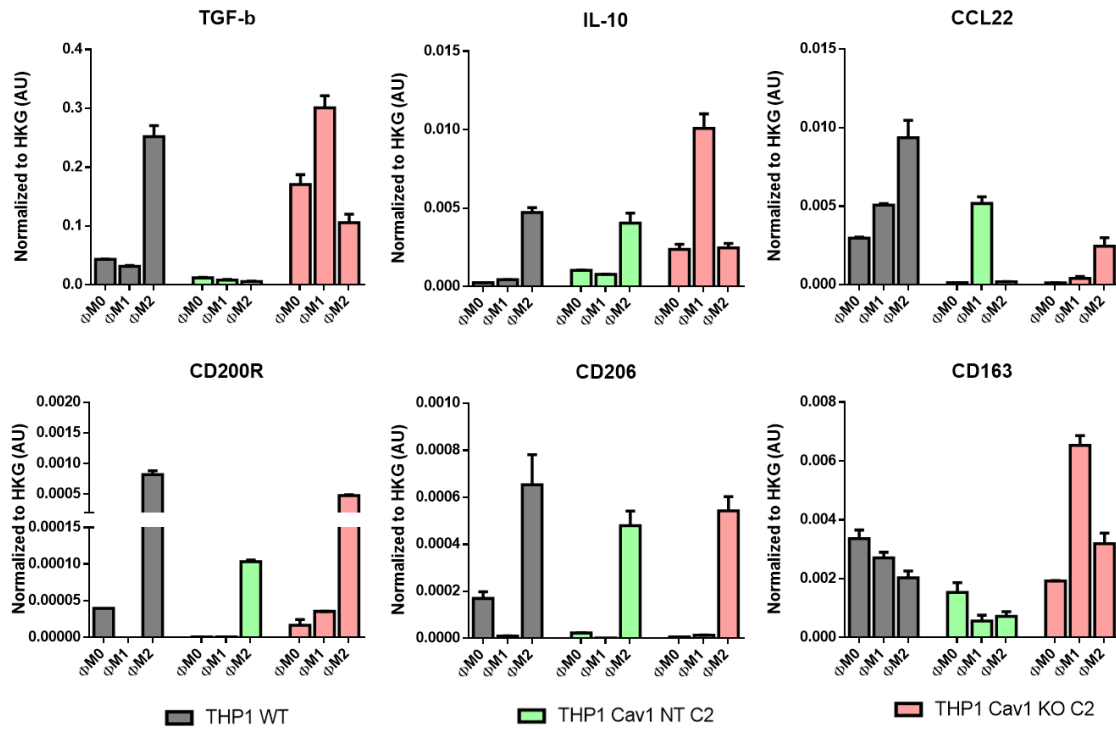
Regarding the Cav1 mRNA levels (**Supplementary figure III. 7**), the WT cells increased their expression in M0, right after differentiation, which decreased again with M1 and M2 polarizations. This fluctuation was not observed in Cav1 NT cells, which expressed low levels as monocytes and M0 phenotype and decreased to negligible levels in M1 and M2. As mentioned above, THP1 Cav1 KO C2 increased their levels after differentiation and polarization.

With regards to the pro-inflammatory markers (**Supplementary figure III. 8**), THP1 Cav1 NT C2 expressed roughly the same levels of IL-12 and TNF- α when compared with the WT cells, which decreased with M2 polarization. IL-6 and CXCL10 were slightly lower compared with the WT, nevertheless, the NT C2 cells were able to respond to M1 stimulation. On the other hand, the IL-1 β expression was intensified in M1 of THP1 Cav1 NT C2 cells, compared to the same phenotype of WT cells. Cav1 KO C2 cells, that showed Cav1 expression specially in M1 and M2 phenotype, displayed an overall increase of all markers, in all phenotypes, compared with the WT and the NT cells, with the exception of IL-1 β in M2 that sustained the repression of this cytokine expression and IL-12 which expressed lower levels.



Supplementary figure III. 8 – Pro-inflammatory markers (M1-related) by qRT-PCR. IL-1 β , IL-6, IL12, CXCL10 and TNF- α expression by THP1 WT (grey), THP1 Cav1 NT C2 (green) or THP1 Cav1 KO C2 (red). Cells were polarized towards M1 and M2 phenotype. Unstimulated cells (M0) were used as control. The expression was normalized to HKG. Bars represent mean of relative expression \pm SEM. N=2 independent experiments.

Regarding the anti-inflammatory markers expressed by THP1 cells (**Supplementary figure III. 9**), the NT C2 cells displayed an increase of IL-10, CD200R and CD206 with M2 stimulation, similarly to the WT cells. The CCL22 expression increased only in the M1 phenotype, which was unexpected, and no increase was observed for TGF- β . The CD163 expression once again was not clear and did not increase in M2 phenotype. When Cav1 was over expressed (Cav1 KO C2), the CCL22, CD200R and CD206 pattern expression was conserved, with a clear increase of M2 phenotype. However, these cells started to express a higher mRNA basal level of TGF- β , IL-10 and CD163, with the greatest increase of M1 polarization.



Supplementary figure III. 9 – Anti-inflammatory markers (M2-related) by qRT-PCR. TGF-β, IL-10 CL22, CD200R, CD206 and CD163 expression by THP1 WT (grey), THP1 Cav1 NT C2 (green) or THP1 Cav1 KO C2 (red). Cells were polarized towards M1 and M2 phenotype. Unstimulated cells (M0) were used as control. The expression was normalized to HKG. Bars represent mean of relative expression \pm SEM. N=2 independent experiments.

Overall, an overexpression of Cav1 in THP1 cells seems to lead to the overexpression of pro-inflammatory and some anti-inflammatory markers. Studies with another clone of THP1 Cav1 KO showed similar expression of Cav1 after stimulation, suggesting that the indels formed upon CRISPR-Cas9 were able to support the Cav1 expression after stimulation. THP1 Cav1 KO C1 was not used, since the cellular proliferation was reduced, and it was challenging to keep the cell in culture over time. For these reasons and because iPSC-derived microglia was introduced in this project, we decided not to carry on with this cell line for future experiments.

APPENDIX IV – SHRNA CAV1 KNOCKDOWN IN GBM CELLS

For previous projects, our laboratory created some GBM cell lines where Cav1 was knockdown via shRNA lentiviral transfection. For the first year, while CRISPR-Cas9 was in development, U87 NT, U87 Sq2, UP007 NT, UP007 Sq2, UP029 NT and UP029 Sq2 were used for preliminary results. During this period, it was evaluated the effect of Cav1 in GBM cells within an immune environment supported by CHME3 microglia cells, by spheroid invasion assay and transwell migration assay.

Methods

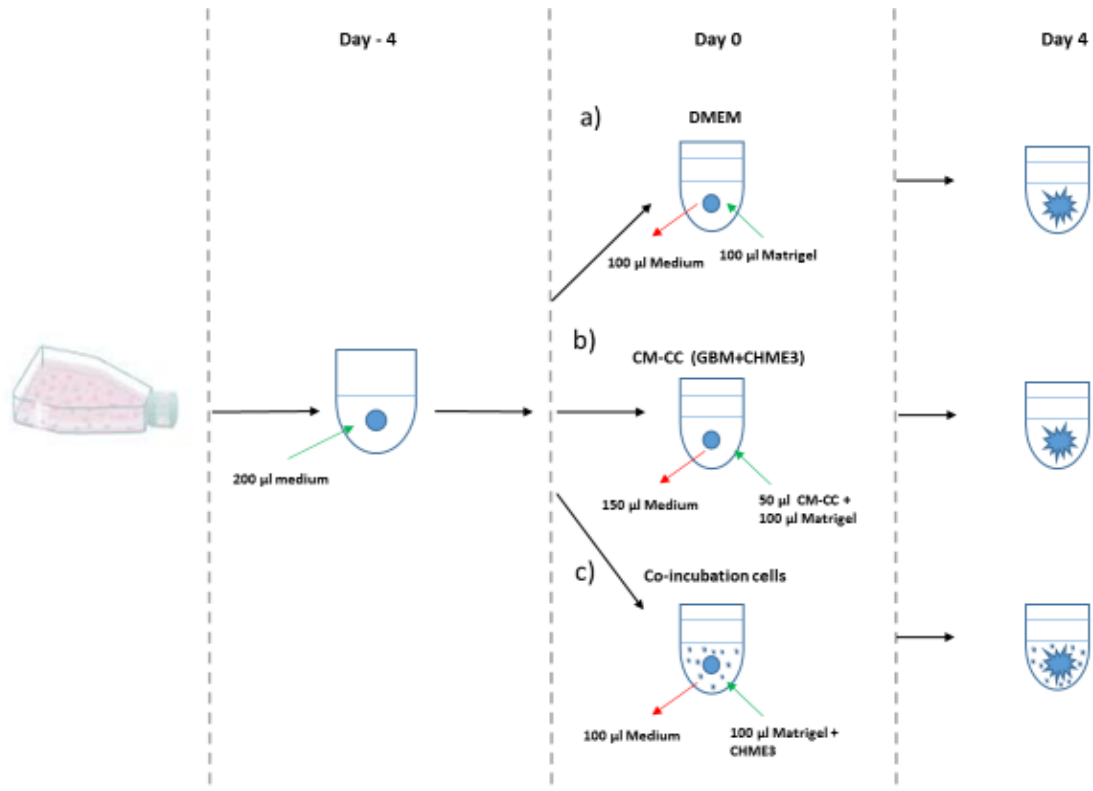
Conditioned medium

Conditioned medium (CM) from CC system (CM-CC) was collected from a transwell system, as described in **Chapter 2, section 2.3**. The CM from U87, as well as CM from CHME3 and microglia cells, was collected after 48 hours in culture in 6-well plates, at a same seeding density of 10,000 cell/cm² and used CM-CC as a control. The collected medium was then centrifuged at 1,200 RPM for 5 minutes to pellet any cell debris and the supernatant was used immediately on the following experiments.

Spheroid invasion assay

GBM cells were cultured in standard conditions without the influence of microglia. For the invasion assay (**Supplementary figure IV. 1**), GBM cells were seeded in a 96-well plate, round-bottomed and ultra-low adherence conditions, at a concentration of 1,000 cells/well for the U87 and 5,000 cell/well for UP007 and UP029. After seeding, cells were gently centrifuged at 300g, for 1 minute, and incubated for four days, at 37°C with 5% of CO₂. After sphere formation, the spheres were cultured under standard conditions, where half of the medium was replaced with Matrigel™ (4 mg/ml, growth factors reduced, Corning) **(a)**; treated with conditioned medium (CM) collected from co-culture (CC) in a transwell system of GBM with CHME3, at this condition 150 µl of medium was replaced by 50 µl of CM-CC plus 100 µl of Matrigel™ **(b)**; or around 12,000 naïve CHME3 cells were embedded into 100 µl of Matrigel and added into the well with the GBM sphere **(c)**. After the matrix was added, the plate was kept on ice for an additional 15 minutes to allow homogeneous mixture of Matrigel™ with reminiscent medium, followed by the incubation at 37°C with 5% of CO₂ to allow the polymerization of the

matrix around the spheres. After 2 hours, new medium in conditions **a)** and **c)**, or CM-CC in conditions **b)** was added to the wells or and pictures were taken immediately after and every 24 hours for an additional 3-4 days.



Supplementary figure IV. 1– Diagram with experimental conditions for invasion assay. GBM cells which were grown under adherence conditions were used to form spheres for 4 days using 96-well plates, ULA. At day 0, spheres grown without the interference of microglia were used as control **(a)**, spheres cultured with GBM-CM and CHME3- CM **(b)** or spheres cultured with microglia cells **(c)** were used to study the effect of the immune environment. After the addition of Matrigel™, the spheres were allowed to invade for 3-4 days.

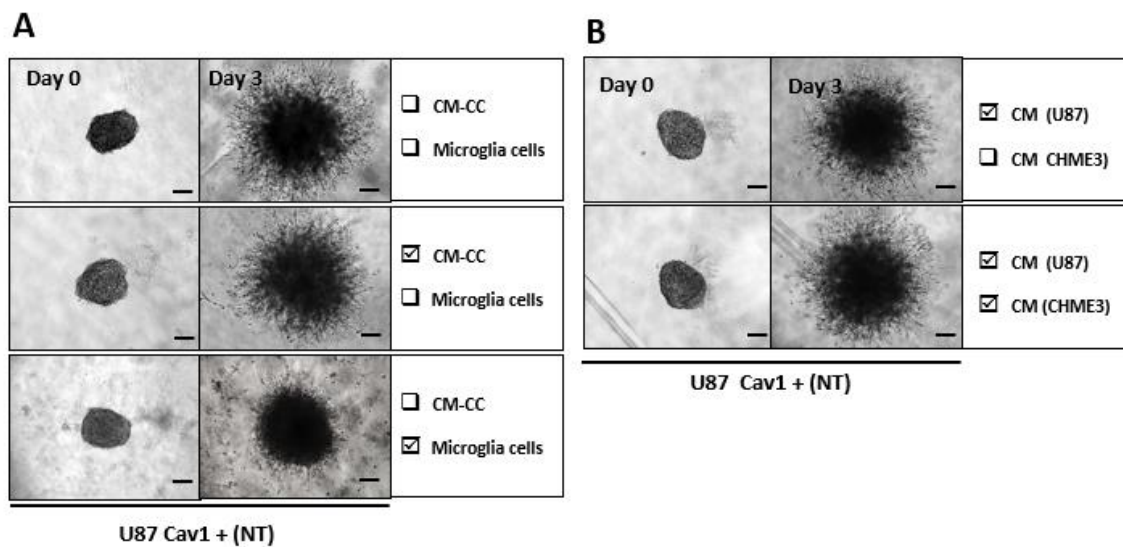
Transwell migration assay

The transwell migration assay is described in **Chapter 2, section 2.11.**

Results

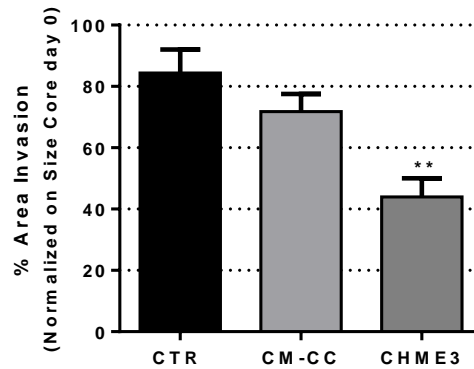
Influence of microglia on glioma invasion and migration

To address if microglia influences the glioma invasion, after sphere formation, GBM spheres were treated with CM-CC (CC of GBM with CHME3) or CHME3 cells were embedded into matrix and seeded around the sphere, allowing the direct contact microglia with the GBM cells. As a control for CM, U87 spheroids were treated with CM collected from U87 NT cells and CM collected from CHME3 cells.



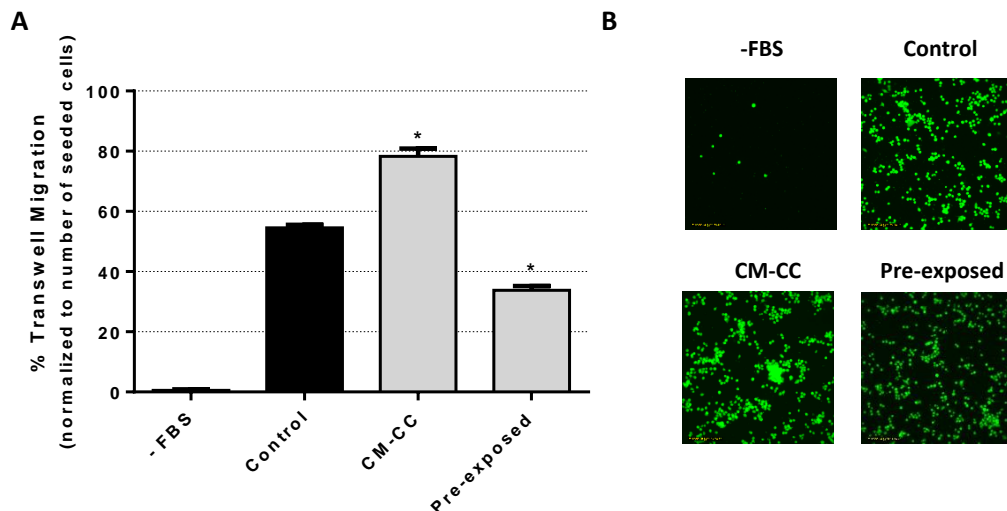
Supplementary figure IV. 2 – Impact of the microglia environment on the invasion of U87 cells. A. Representative pictures of U87 Cav1+ (NT) invasion at Day 0 and Day 3. Prior to sphere formation, U87 NT cells were cultured in standard conditions without the influence of microglia. After sphere formation, the spheres were cultured under standard conditions, treated with CM-CC of U87 NT with CHME3 in a transwell system, or naïve CHME3 were embedded into Matrigel and added into the well with the U87 sphere. **B.** After sphere formation, U87 cells were treated with CM collected from U87 NT, from CHME3 or from CC of U87 NT with CHME3, for 48 hours. N=3 experiments. Scale bar: 100 μ M.

In **Supplementary figure IV. 2**, none of the CM seem to affect the capability of U87 cells to invade, however when microglia cells were present in the same microenvironment, with predictable direct contact with these two different cell lines, the invasion capability is significantly repressed to 44% (**Supplementary figure IV. 3**).



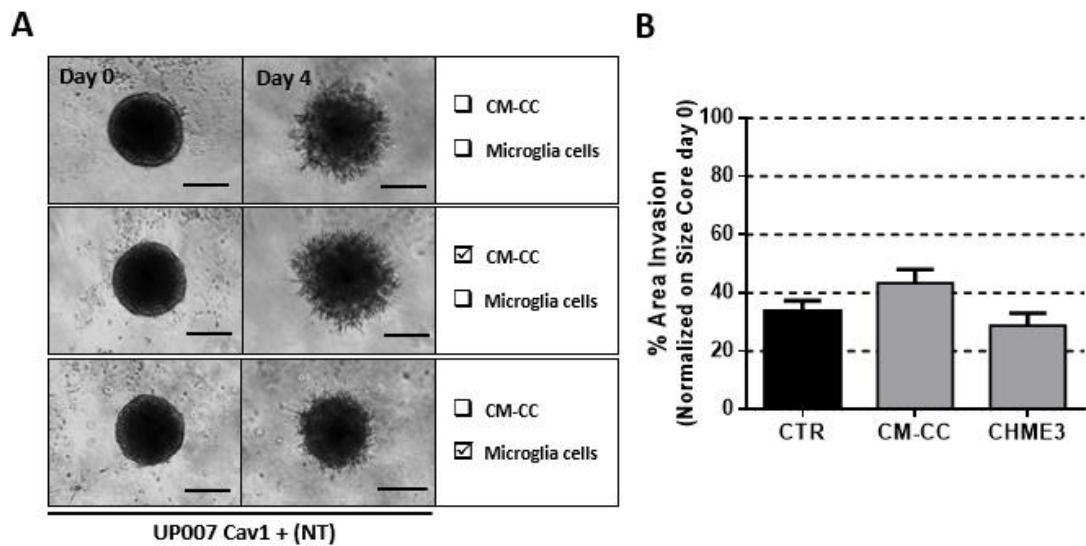
Supplementary figure IV. 3 – Impact of microglia on U87 invasion. U87 area of invasion analysed using INSIDIA Macro run into ImageJ. Mean \pm SEM, N=3 experiments. ** $p \leq 0.01$ compared with control (CTR), Turkey's multiple comparison test.

Analysing the results of migration addressed in **Supplementary figure IV. 4**, the U87 cells with normal expression of Cav1 and without the influence of microglial cells showed a migration rate of about 54%. When cells were treated with CM-CC, the single cell migration increased to 78% ($p < 0.05$). Regarding the cells that were pre-exposed to microglial cells, they significantly lost the migration capability (34%, $p < 0.05$).



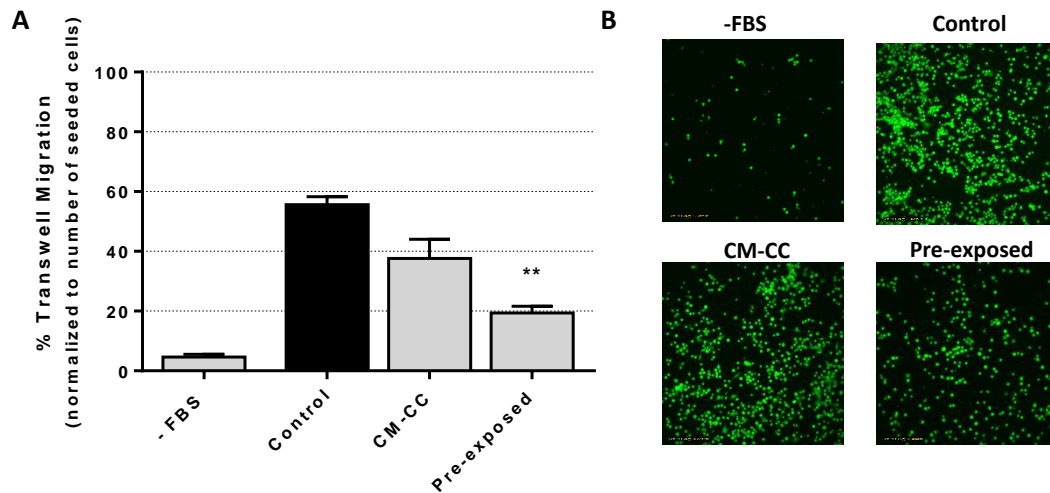
Supplementary figure IV. 4– Impact of microglia on U87 migration. Before migration, cells were cultured under standard conditions, or treated with CM-CC of U87 NT with CHME3 cultured in a transwell system, or co-cultured with CHME3 in transwell systems for 48 hours (pre-exposed). Medium without FBS was used in the lower chamber as control. **A.** graph of U87 cell migration with the respective conditions. Mean \pm SEM, N=2 experiments. $p \leq 0.05$ compared with control, Dunn's multiple comparison test. **B.** Representative pictures of cells after invasion.

Regarding the UP007 cells, this cell line seems to have the same behaviour as the U87 cells, when Cav1 is expressed.



Supplementary figure IV. 5 - Impact of microglia on invasion of UP007 cells. **A.** Representative pictures of UP007 Cav1+ (NT) invasion at Day 0 and Day 4. Prior to sphere formation, UP007 NT cells were cultured in standard conditions without the influence of microglia. After sphere formation, the spheres were cultured under standard conditions, or treated with CM-CC of UP007 NT with CHME3 cultured in a transwell system, or the naïve CHME3 cells were embedded into Matrigel and added into the well with the UP007 sphere. **B.** Area of invasion analysed using INSIDIA Macro run into ImageJ. Mean \pm SEM, N=2. Scale bar: 100 μ M.

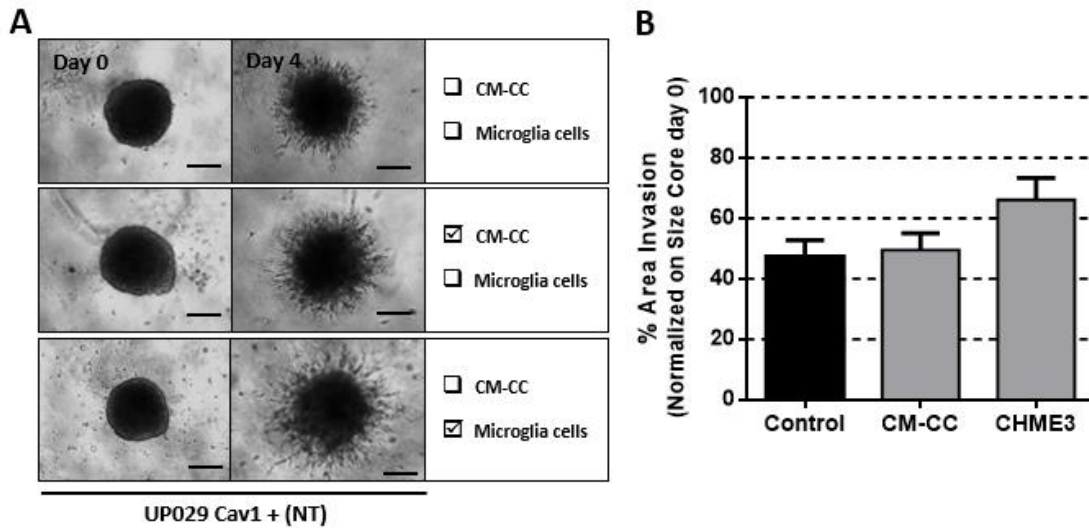
It is possible to see in **Supplementary figure IV. 5** that after 4 days in Matrigel, the CM-CC increased slightly the invasion of this GBM cell line, however, when the microglial cells were around the sphere, this environment reduced marginally the invasion. It is possible to notice diminished invasion properties of UP007 compared to U87 cells. The migration capability of this cell line is described in **Supplementary figure IV. 6**.



Supplementary figure IV. 6 – Impact of microglia on UP007 migration. Before migration, cells were cultured under standard conditions, or treated with CM-CC of UP007 NT with CHME3 cultured in a transwell system or cultured with CHME3 in transwell systems for 48 hours (pre-exposed). Medium without FBS was used as control in the lower chamber. **A.** graph of UP007 Cav1+ cell migration with the respective conditions. Mean \pm SEM. $p \leq 0.01$ compared with control, Dunn's multiple comparison test. **B.** Representative pictures of cells after invasion. N=2 experiment.

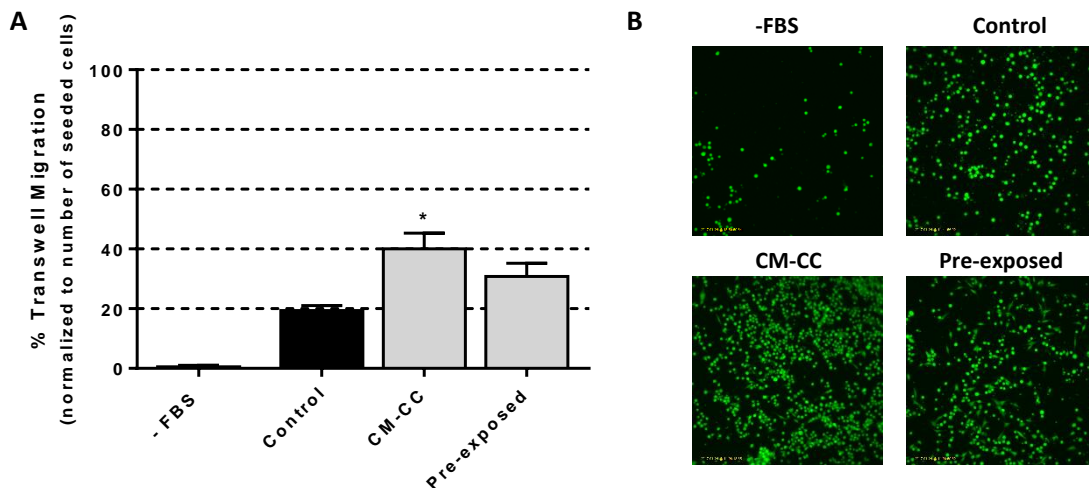
Cells that were cultured in standard conditions without pressure of microglial environment displayed a migration rate of 55%. Even without significant alterations on invasion, when UP007 NT cells were treated with CM-CC the migration rate started to decrease to 38%, furthermore, when CHME3 cells were present in the CC system, UP007 migration declined to 19% ($p < 0.01$). As observed in the invasion pictures, the results were consistent.

In what concerns the UP029 cell line, the presence of microglia seems to have an opposite effect when compared with the other two cell lines.



Supplementary figure IV. 7 – Impact of microglia on invasion of UP029 cells. **A.** Representative pictures of UP029 Cav1+ (NT) invasion at Day 0 and Day 4. Prior to sphere formation, UP029 NT cells were cultured in standard conditions without the influence of microglia. After sphere formation, the spheres were cultured under standard conditions or treated CM-CC of UP029 NT with CHME3 cultured in a transwell system or the naïve CHME3 were embedded into matrigel and added into the well with the UP029 sphere **B.** Area of invasion analysed using INSIDIA Macro run into ImageJ. Mean \pm SEM, N=2. Scale bar: 100 μ M.

The UP029 cell invasion is described in (Supplementary figure IV. 7). Compared with control, the CM-CC did not modified the invasion, however, the presence of CHME3 cells into the Matrigel led to an increase of the invasion from 47% to 66%.

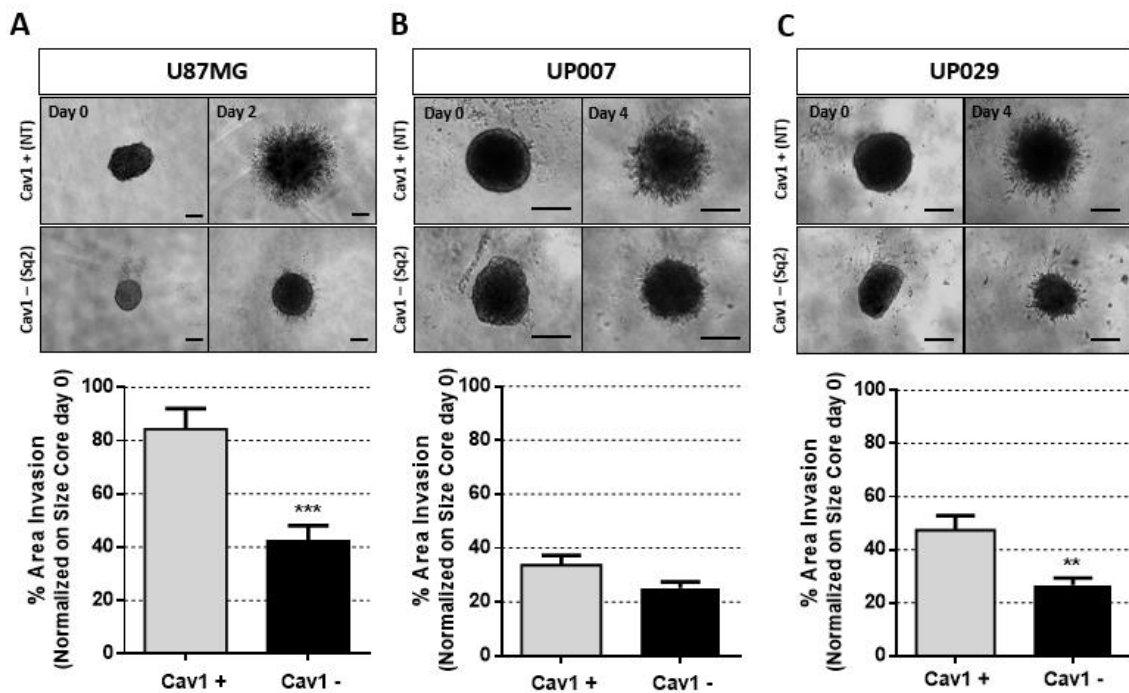


Supplementary figure IV. 8 – Impact of microglia on migration of UP029 cells. Before migration, cells were cultured under standard conditions, or treated with CM-CC of UP029 NT with CHME3 cultured in a transwell system or cultured with CHME3 in transwell systems for 48 hours (pre-exposed). Medium without FBS was used as control in the lower chamber. **A.** graph of UP029 Cav1+ cell migration with the respective conditions. Mean \pm SEM. Mean \pm SEM. $p \leq 0.05$ compared with control, Dunn's multiple comparison test. **B.** Representative pictures of cells after invasion. N=2 experiment.

Focusing on the cell migration in the **Supplementary figure IV. 8**, untreated cells displayed a migration rate of 19%, and increased to 40% when treated with CM-CC and to 31% when microglial cells were present. These results were consistent with the invasion data previously obtained. This cell line displayed the lowest migration rate. In this case the microglial environment seems to promote the invasion and migration of this cell line. Comparing the three cell lines, for the U87 and UP007, the microglial environment seems to prevent the cellular migration and invasion, however, the UP029 showed the opposite effect. It is possible that the molecular profile is different for each cell line, which can cause the different behaviour observed for this cell line.

Influence of Cav1 on glioma invasion

In previous studies in our laboratory, Chiara Moriconi demonstrated that when Cav1 was downregulated, GBM invasion was repressed in several GBM cell lines (Moriconi 2019). These experiments were done without the influence of microglial cells.



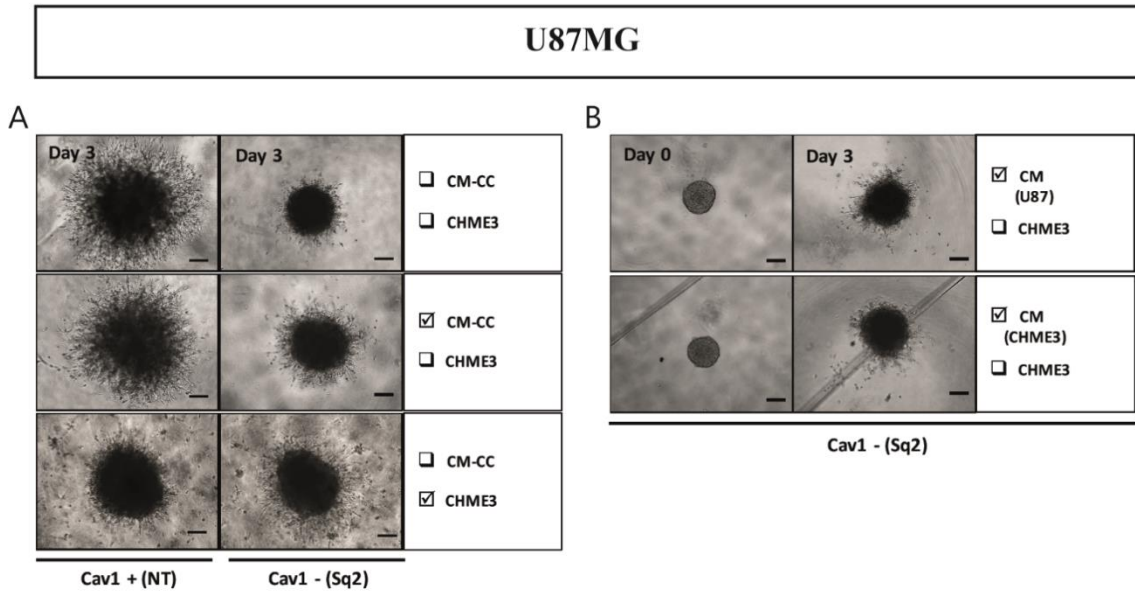
Supplementary figure IV. 9 – Influence of Cav1 knockdown on invasion of glioma cells. Representative pictures of U87 Cav1+ (NT) and U87 Cav1- (Sq2) invasion at Day 0 and Day 3 (N=3), and UP007 and UP029 Cav1+ (NT) and Cav1- (Sq2) invasion at Day 0 and Day 4 (N=2). **: P<0.01, ***: p<0.001, when compared to Cav1+ cells, Mann Whitney comparison test. Scale bar: 100 μM.

These results were consistent with Chiara's results. A decrease of GBM invasion was observed when Cav1 expression is downregulated in GBM cells (**Supplementary figure IV. 9**). When Cav1 was not present, at day 0 (timepoint to add the Matrigel) the size of the spheres was smaller in the U87 and UP029 cell lines compared with NT cells. There were no relevant effects observed in the UP007 cells.

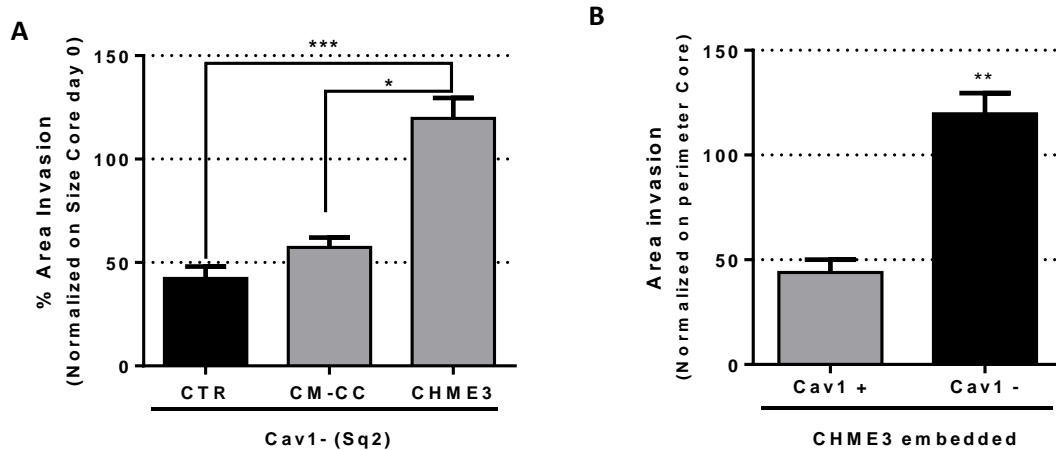
Influence of microglia and Cav1 on glioma's invasion and migration

After seeing the effect of the microglial environment on GBM cell when Cav1 is expressed, this section focuses on the effect of microglia cells upon the invasion and migration when Cav1 is downregulated.

When Cav1 was downregulated, the presence of CHME3 cells improved significantly the invasion capability of U87 cells within the environment. Compared with untreated Cav1- (Sq2), cells that were treated with CM-CC started to enhance their invasion, however, when microglia cells were present, these cells showed a significant improve of invasion capability (**Supplementary figure IV. 10** and **Supplementary figure IV. 11, A**). Considering that the cells with Cav1 downregulated have a smaller sphere size, at the end of the three days, these cells had a significantly greater invasion than the U87 Cav1+ (NT) (**Supplementary figure IV. 10** and **Supplementary figure IV. 11, B**). Therefore, the effect of the downregulation of Cav1 (that prevents the invasion) seems to be cancelled by the influence of microglial environment, which can lead to think that the factors released to the tumour milieu by the microglial cells can reactivate mechanisms involved on invasion, or activate others pathways that do not require the activation of Cav1.



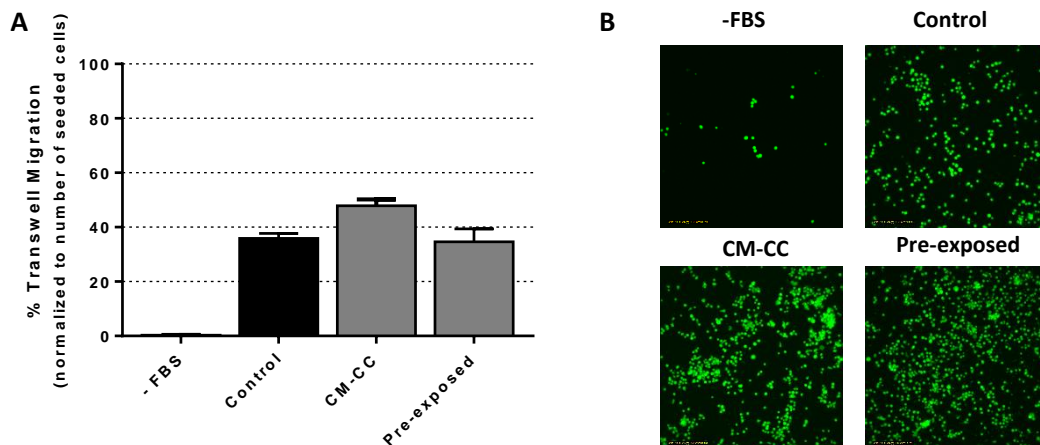
Supplementary figure IV. 10 – Impact of microglia on invasion of U87 Cav1 knockdown cells. A. Representative pictures of U87 Cav1+ (NT) and Cav1- (Sq2) invasion at Day 3. Prior to sphere formation, U87 cells were cultured in standard conditions without the influence of microglia. After sphere formation, the spheres were cultured under standard conditions or treated with CM collected from co-culture (CM-CC) in a transwell system of U87 (NT or Sq2, respectively) with CHME3, or the naïve CHME3 were embedded into Matrigel and added into the well with the U87 sphere. **B.** After sphere formation U87 (Sq2) cells were treated with CM that was in contact with U87 (Sq2), or with CHME3 for 48 hours. N=3 experiments. Scale bar: 100 μ M.



Supplementary figure IV. 11 – Impact of microglia on invasion of U87 Cav1 knockdown cells. A. U87 Cav1- (Sq2) area of invasion analysed using INSIDIA Macro run into ImageJ. $p < 0.5$; $P < 0.001$, compared to the control (CTR), Dunn's multiple comparison test. **B.** Comparison of the area of invasion between U87 Cav1+ and Cav1- with the presence of CHME3 cells. $P < 0.01$, compared to Cav1+ cells, Mann Whitney comparison test. Mean \pm SEM, N=3 experiments.

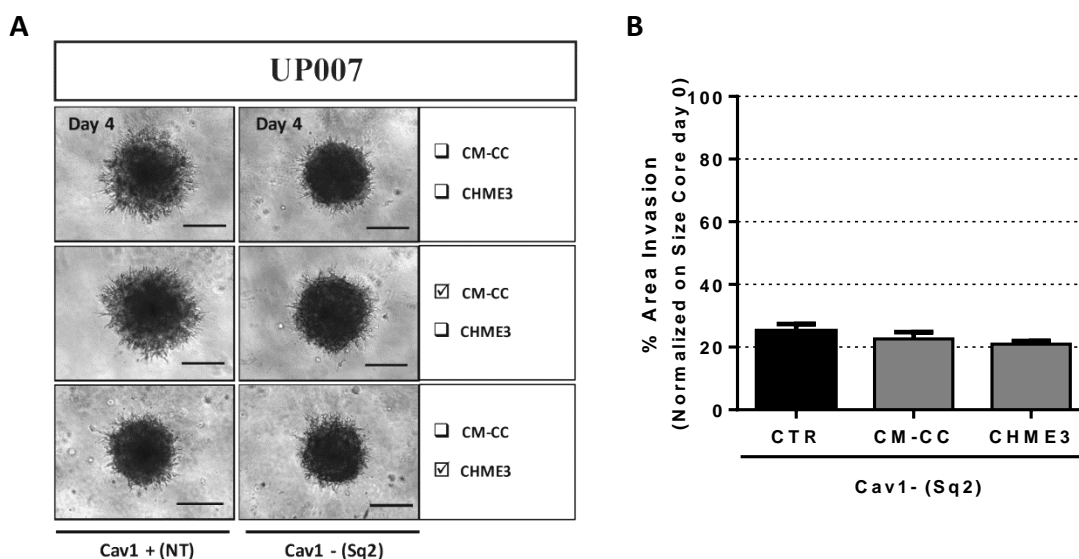
Regarding the controls of the CM, the invasion capability of CM-U87 Cav1- and CM-CHME3 cells does not seem to be affected, even with Cav1 knockdown.

Taking into consideration the single cell migration when Cav1 is downregulated (Supplementary figure IV. 12), the CM collected from the CC system improved the competence of each cell to migrate (48%). However, the presence of microglia cells improved the invasion but appears to not influence the migration, displaying almost the same migration rate as control cells (34.6% and 35.9%, pre-exposed vs control cells, respectively).



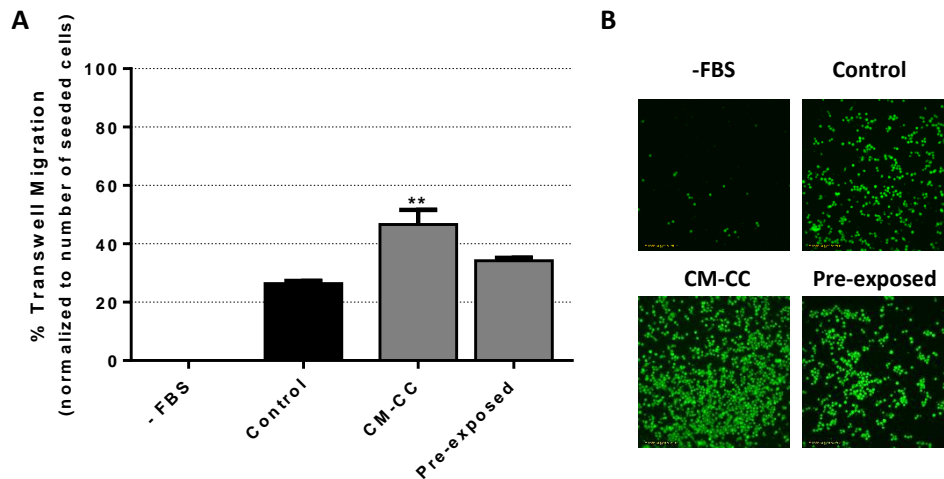
Supplementary figure IV. 12 – Impact of microglia on migration of U87 Cav1 knockdown. Before migration, cells were cultured under standard conditions (control), or treated with CM collected from co-culture (CM-CC) in a transwell system of U87 Sq2 with CHME3 or cultured with CHME3 in transwell systems for 48 hours (pre-exposed). Medium without FBS was used as control in the lower chamber. **A.** graph of U87 Sq2 cell migration with the respective conditions. **B.** Representative pictures of cells after invasion. N=3 experiments.

Regarding the UP007 cell line, the effect of microglia seems to not affect the invasion when Cav1 was knockdown. However, when compared with Cav1+ (NT) and Cav1- (Sq2) with the presence of CHME3 cells, the spheres showed the same behaviour for the invasion properties (**Supplementary figure IV. 13**).



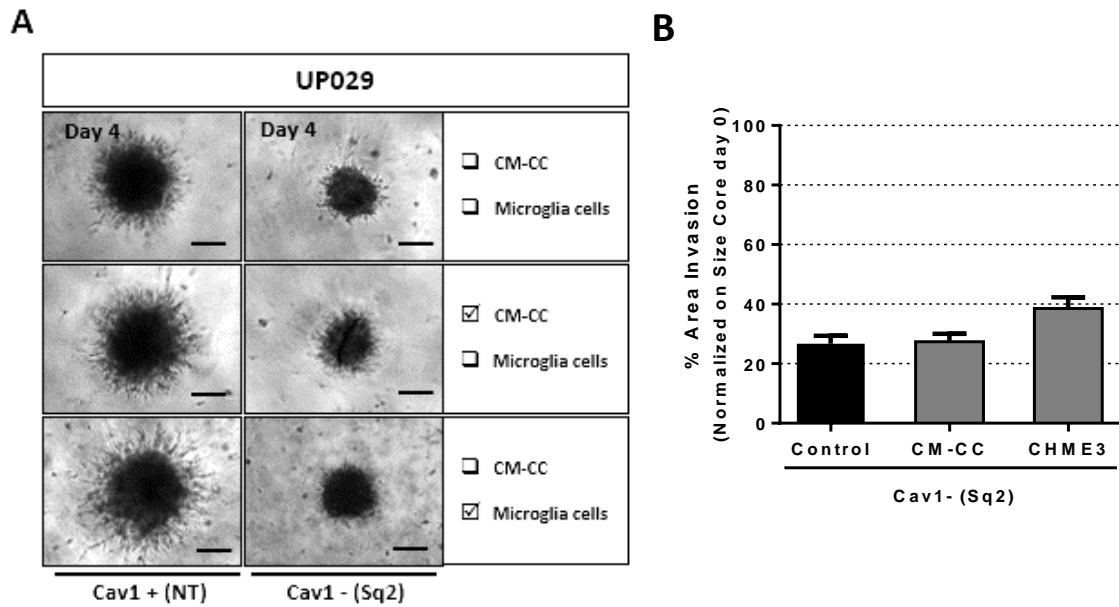
Supplementary figure IV. 13 – Impact of microglia on invasion of UP007 Cav1 knockdown cells. A. Representative pictures of UP007 Cav1+ (NT) and Cav1- (Sq2) invasion at Day 4. Prior to sphere formation, UP007 cells were cultured in standard conditions without the influence of microglia. After sphere formation, the spheres were cultured under standard conditions or treated with CM collected from co-culture (CM-CC) in a transwell system of UP007 (NT or Sq2, respectively) with CHME3, or the naïve CHME3 were embedded into Matrigel and added into the well with the UP007 sphere. N=2 experiments. Scale bar: 100 μ M.

As for the single cell migration of UP007 cells (**Supplementary figure IV. 14**), pre-exposing the tumour cells to the microglial cells increased the migration from 26.4% (Control) to 34.2%, however, the CM-CC treatment significantly improved the migration of the tumour cells to 46.6%.



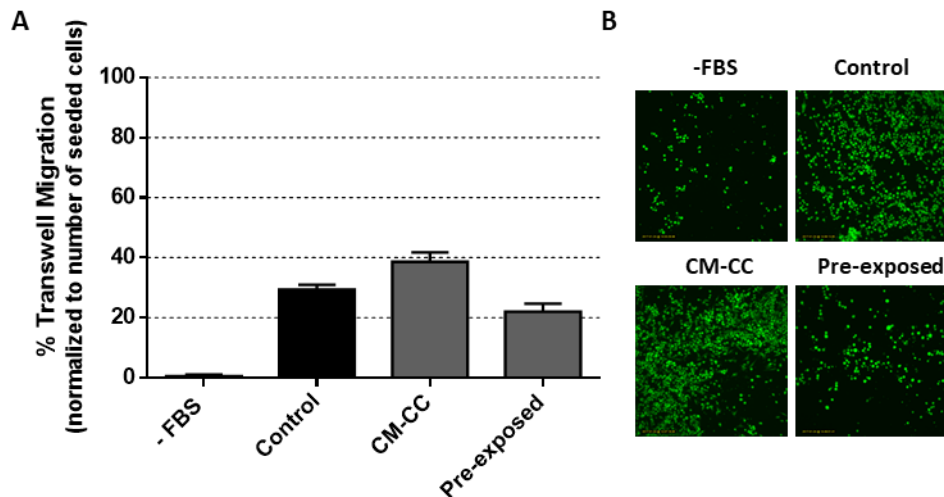
Supplementary figure IV. 14 – Impact of microglia on UP007 knockdown migration. Before migration, cells were cultured under standard conditions (control), or treated with CM collected from co-culture (CM-CC) in a transwell system of UP007 Sq2 with CHME3, or cultured with CHME3 in transwell systems for 48 hours (pre-exposed). Medium without FBS was used as control in the lower chamber. **A.** graph of UP007 Sq2 cell migration with the respective conditions. **B.** Representative pictures of cells after invasion. N=3 experiments.

The invasion of UP029 cells is described in **Supplementary figure IV. 15**. UP029 Cav1- cells showed a lower area of invasion compared with the UP029 Cav1+ for all tested conditions. Regarding the UP029 Cav1- (sq2), the treatment with CM-CC did not impact the behaviour of these cells, but the presence of CHME3 microglia increased slightly the invasion from 27% to 38.5%, as seen in **Supplementary figure IV. 15, B**.



Supplementary figure IV. 15 – Impact of microglia on invasion of UP029 Cav1 knockdown cells. A. Representative pictures of UP029 Cav1+ (NT) and Cav1- (Sq2) invasion at Day 4. Prior to sphere formation, UP029 cells were cultured in standard conditions without the influence of microglia. After sphere formation, the spheres were cultured under standard conditions or treated with CM collected from co-culture (CM-CC) in a transwell system of UP029 (NT or Sq2, respectively) with CHME3, or the naïve CHME3 were embedded into Matrigel and added into the well with the UP029 sphere. N=2 experiments. Scale bar: 100 μ M.

Regarding the ability of UP029 Cav1- to migrate, cells without interference of immune cells presented a migration ability of 29.4%, which increased to 38.6% when tumour cells were cultured with CM-CC for 48 hours, however, they showed a reduction to 22% after the tumour cells were in co-culture with microglia cells in a transwell system, as observed in **Supplementary figure IV. 16**.

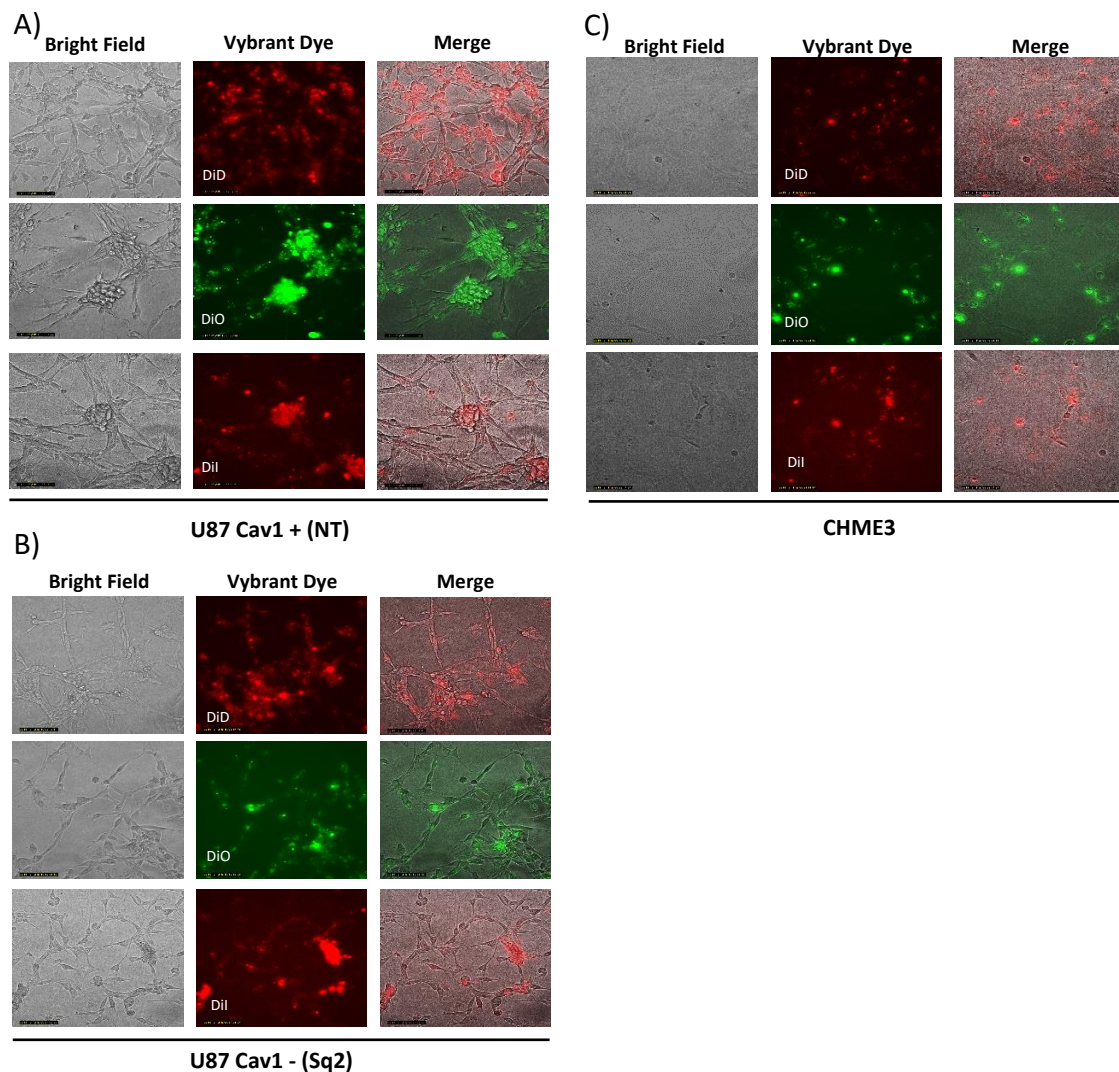


Supplementary figure IV. 16 – Impact of microglia on UP029 knockdown migration. Before migration, cells were cultured under standard conditions (control), or treated with CM collected from co-culture (CM-CC) in a transwell system of U029 Sq2 with CHME3, or cultured with CHME3 in transwell systems for 48 hours (pre-exposed). Medium without FBS was used as control in the lower chamber. **A.** graph of UP029 Sq2 cell migration with respective conditions. **B.** Representative pictures of cells after invasion. N=3 experiments.

APPENDIX V – VYBRANT™ DYES OPTIMIZATION

Incubation time optimization

To determine the optimal incubation time for CHME3 and U87 cells, Cav1+ and Cav1-, cells were incubated with three dyes for 5, 10, 15 and 20 minutes. Cells were monitored with a fluorescent microscope (Etaluma - Lumascope 620) for 8 days. Following the manufacturer's instructions, 1,000,000 cells were incubated with 5 μ l/ml of each Vybrant dye cell solution for 5, 10, 15 and 20 minutes, protected from light, at 37°C in a 5% CO₂-humidified atmosphere, followed by three PBS washing steps. After the labelling procedure, cells were seeded at a concentration of 5,000 cell/cm², in 24-well plate.

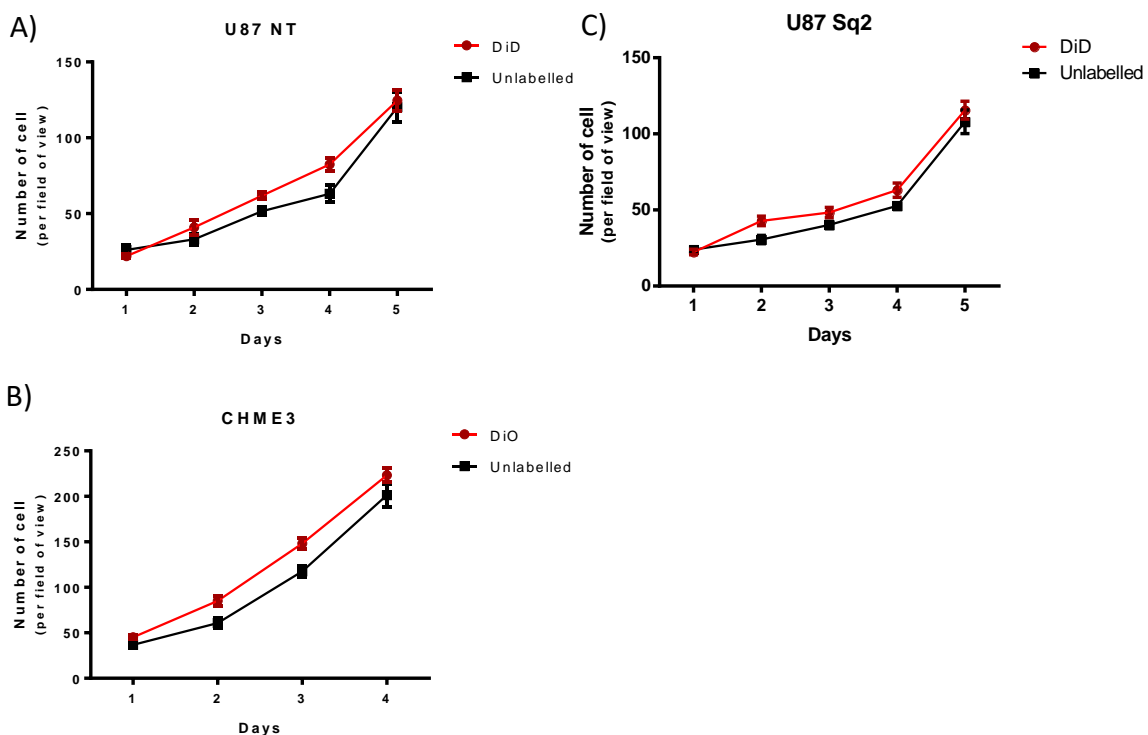


Supplementary figure V. 1 – Representative pictures at day 8, after labelling with DiD, DiO and DiI, of **A)** U87 Cav1 + (NT), **B)** U87 Cav1 - (Sq2), and **C)** CHME3. The pictures were taken using bright field and with a respective excitation laser for each dye.

The best time point for the incubation with DiO and DiD was 15 minutes, and for Dil was 20 minutes, for all cell lines tested (timepoint of pictures on **Supplementary figure V. 1**). However, Lumascope does not have the appropriate excitation laser for Dil, therefore the labelling capacity with this dye can be underestimated. In the end of the 8 days, we were able to see that all cells were labelled, and the dyes were transferred to daughter cells.

Cellular Proliferation

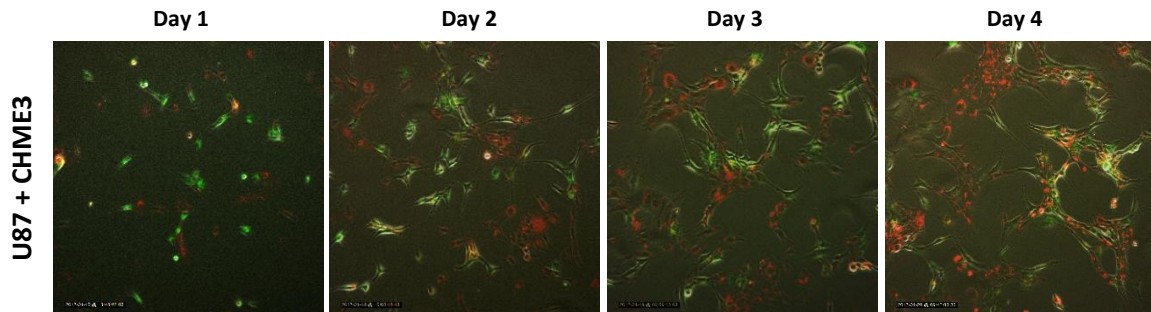
To investigate if the dyes interfere with cell proliferation, U87 Cav1+ and Cav1- cells were labelled with DiO dye, and CHME3 were labelled with DiD dye, for 15 minutes at 37°C, protected from the light. Unlabelled cells were used as control. Cells were seed at a concentration of 5,000 cell/cm², in a 12-well plate. Pictures were taken, from three different areas of the well, using an inverted microscope, every day until cells reached the confluent level. In the end, cells were manually counted with a cell counting tool in ImageJ, and the number of cells expressed by field of view.



Supplementary figure V. 2– Proliferation curves of **A)** U87 Cav1+ (NT), **B)** U87 Cav1- (Sq2) and **C)** CHME3, labelled and unlabelled cells.

Co-localization test

To verify that after labelling and mixing the cultures the dye would not diffuse to the neighbour cells in co-culture, U87 Cav1+ (NT) were pre-labelled with DiO and CHME3 with DiD, for 15 minutes, at 37°C. After PBS washes the cells were mixed at ratio 1:1, in a 12-well plate. Photos were taken every day for 4 days using a Lumascop.



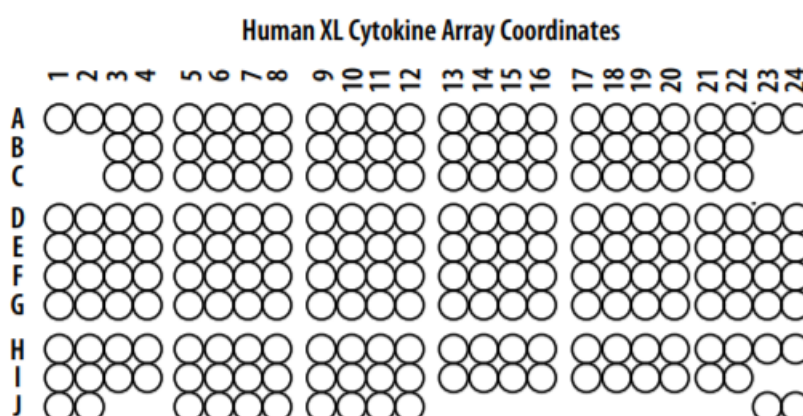
Supplementary figure V. 3 – Merged images of U87 Cav1+ (NT) with CHME3 in different days. Green-CHME3 cells; Red – U87 Cav1 (NT) cells.

During the next consecutive 4 days (**Supplementary figure V. 3**), some co-localizations started to appear but this seemed to be caused by cellular overlay. However, a review from Huysentruyt *et al.* highlighted some evidences that glioma cells can express myeloid markers, suggesting that glioma cells, especially in GBM, can form hybrid bodies by the fusion between a glioma cell with a macrophage or microglia cells, increasing the proliferative and invasive capability (Huysentruyt, Akgoc, and Seyfried 2011).

APPENDIX VI – HUMAN XL CYTOKINE ARRAY

The Human XL Cytokine Array gives the relative expression of 105 soluble human proteins that can be involved in the immune response of microglia cells and tumour environment.

In this kit, the 105 cytokines, chemokines, growth factors and reference spots are spotted in duplicate on a nitrocellulose membrane as shown on **Supplementary figure VI. 1**



Supplementary figure VI. 1 – Human XL Cytokine Array Coordinates.

The coordinates and respective soluble protein are described on the table below:

Supplementary table VI.1 – Human XL Cytokine Array Coordinates.

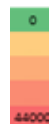
Coordinate	Analyte/Control	Coordinate	Analyte/Control
A1-A2	Reference Spots	E23-E24	IL-18 BPa
A3-A4	Adiponectin	F1-F2	IL-19
A5-A6	Apolipoprotein A-I	F3-F4	IL-22
A7-A8	Angiogenin	F5-F6	IL-23
A9-A10	Angiopoietin-1	F7-F8	IL-24
A11-A12	Angiopoietin-2	F9-F10	IL-27
A13-A14	BAFF	F11-F12	IL-31
A15-A16	BDNF	F13-F14	IL-32
A17-A18	Complement Component C5/C5a	F15-F16	IL-33
A19-A20	CD14	F17-F18	IL-34
A21-A22	CD30	F19-F20	IP-10/CXCL10
A23-A24	Reference Spots	F21-F22	I-TAC/CXCL11
B3-B4	CD40 ligand	F23-F24	Kallikrein 3
B5-B6	Chitinase 3-like 1/CHI3L1	G1-G2	Leptin

APPENDIX VI – Human XL Cytokine Array

B7-B8	Complement Factor D/CFD/adipsin	G3-G4	LIF
B9-B10	C-Reactive Protein	G5-G6	Lipocalin-2
B11-B12	Cripto-1	G7-G8	MCP-1/CCL2
B13-B14	Cystatin C	G9-G10	MCP-3/CCL7
B15-B16	Dkk-1	G11-G12	M-CSF/CSF1
B17-B18	DPPIV	G13-G14	MIF
B19-B20	EGF	G15-G16	MIG/CXCL9
B21-B22	EMMPRIN	G17-G18	MIP-1 α /MIP-1 β
C3-C4	ENA-78	G19-G20	MIP-3 α /CCL20
C5-C6	Endoglin	G21-G22	MIP-3 β /CCL19
C7-C8	Fas Ligand	G23-G24	MMP-9
C9-C10	FGF basic	H1-H2	Myeloperoxidase
C11-C12	FGF-7	H3-H4	Osteopontin/OPN
C13-C14	FGF-19	H5-H6	PDGF-AA
C15-C16	Flt-3 Ligand	H7-H8	PDGF-AB/BB
C17-C18	G-CSF	H9-H10	Pentraxin-3
C19-C20	GDF-15	H11-H12	PF4
C21-C22	GM-CSF	H13-H14	RAGE
D1-D2	GRO- α	H15-H16	RANTES/CCL5
D3-D4	Growth Hormone	H17-H18	RBP-4
D5-D6	HGF	H19-H20	Relaxin-2
D7-D8	ICAM-1	H21-H22	Resistin
D9-D10	IFN- γ	H23-H24	SDF-1 α /CXCL12
D11-D12	IGFBP-2	I1-I2	Serpin E1/PAI-I
D13-D14	IGFBP-3	I3-I4	SHBG
D15-D16	IL-1 α	I5-I6	ST2
D17-D18	IL-1 β	I7-I8	TARC/CCL17
D19-D20	IL-1ra	I9-I10	TFF3
D21-D22	IL-2	I11-I12	TfR
D23-D24	IL-3	I13-I14	TGF- α
E1-E2	IL-4	I15-I16	Thrombospondin-1
E3-E4	IL-5	I17-I18	TNF- α
E5-E6	IL-6	I19-I20	uPAR
E7-E8	IL-8	I21-I22	VEGF
E9-E10	IL-10	J1-J2	Reference Spots
E11-E12	IL-11	J5-J6	Vitamin D BP
E13-E14	IL-12 p70	J7-J8	CD31
E15-E16	IL-13	J9-J10	TIM-3
E17-E18	IL-15	J11-J12	VCAM-1
E19-E20	IL-16	J23-J24	NC
E21-E22	IL-17A		

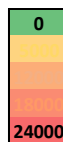
Analyte	CHME3 Cav1 NT			CHME3 Cav1 KO			CHME3 Cav1 NT CC U87	CHME3 Cav1 KO CC U87
	CTRL	LPS + IFN γ	IL4 + IL13	CTRL	LPS + IFN γ	IL4 + IL13		
Adiponectin	1628	1211	767	714	447	479	716	306
Apolipoprotein A-I	1627	1387	957	696	359	319	1592	752
Angiogenin	5280	6242	4820	1635	1205	1274	2232	559
Angiotensin-1	1204	1099	779	816	460	305	590	183
Angiotensin-2	1512	1494	1297	1611	1344	907	1165	809
BAFF	1395	1641	902	1324	888	462	704	359
BDNF	2909	2055	2118	3200	2328	1598	1322	920
Complement Component C5/C5a	1277	712	565	1796	1192	644	524	475
CD14	1264	892	587	1934	1153	653	729	440
CD30	1243	866	686	2276	1307	875	596	604
CD40 ligand	1547	1460	882	586	544	553	920	324
Chitinase 3-like 1	1305	1211	801	411	461	266	23570	28845
Complement Factor D	1427	1295	893	603	478	367	1168	535
C-Reactive Protein	1263	1194	881	752	551	406	801	323
Cripto-1	1137	1044	693	836	569	480	652	262
Cystatin C	2459	2731	1909	1635	1069	866	2628	591
Dkk-1	7671	7711	11118	9048	9074	10160	4679	4658
DPPIV	877	581	383	1608	1282	764	399	497
EGF	951	670	446	1638	1042	679	570	535
EMMPRIN	1730	2062	2035	2740	2702	2281	1368	1200
ENA-78	1523	1779	982	307	632	285	879	239
Endoglin	1265	1329	855	375	404	309	2687	2329
Fas Ligand	1236	1211	666	449	442	298	769	346
FGF basic	1250	1397	819	702	698	429	784	365
FGF-7	1217	976	721	761	508	383	588	199
FGF-19	2877	3015	2776	2364	2190	2255	3486	1999
Flt-3 Ligand	1081	928	770	1288	900	962	801	632
G-CSF	813	712	421	1489	1233	539	509	494
GDF-15	964	1152	1077	1938	1633	1419	5057	4863
GM-CSF	1038	1190	822	1940	4827	938	816	731
GRO-alpha	1403	3336	1653	197	4816	562	734	118
Growth Hormone	1065	1109	726	457	313	220	596	113
HGF	1292	1584	842	632	952	355	767	260
ICAM-1	1409	2433	843	535	1783	247	713	269
IFN-gamma	1324	4890	1075	1137	5337	897	837	655
IGFBP-2	2287	2002	2510	1040	806	711	1632	250
IGFBP-3	1250	1121	883	1147	791	593	935	429
IL-1alpha	975	1084	1158	1568	1274	935	850	715
IL-1beta	688	813	436	1271	895	432	517	320
IL-1ra	621	847	476	1492	1313	602	594	431
IL-2	912	1205	706	1837	1147	748	809	512
IL-3	446	1671	407	1844	1726	624	473	556
IL-4	1328	1379	14223	283	587	13593	1051	327
IL-5	1050	1071	778	588	512	475	606	273
IL-6	1425	3902	1078	1165	9583	2207	1166	742
IL-8	2933	9929	2480	1211	19201	1303	5904	4673
IL-10	1274	1331	911	707	940	501	839	351
IL-11	1491	1501	1394	1042	1008	968	1049	489
IL-12 p70	1038	989	763	1140	782	556	704	343
IL-13	709	791	1691	1092	617	1195	549	309
IL-15	598	1042	437	1241	956	441	436	385
IL-16	479	4282	391	1367	4312	556	442	380
IL-17A	2716	3525	2403	2751	2894	1685	4167	1533
IL-18 BPa	559	12646	554	1989	8962	785	574	629
IL-19	1107	1096	1178	162	188	1153	653	215
IL-22	1516	1426	1058	471	590	515	1341	295
IL-23	1038	1216	741	390	688	405	706	206
IL-24	1241	1363	908	705	1401	462	1102	628
IL-27	1183	1216	936	900	1092	767	781	417
IL-31	936	953	625	808	665	480	525	222
IL-32	1217	1268	980	1366	1276	797	705	454
IL-33	761	802	638	1231	873	515	526	338
IL-34	549	1066	402	1133	1318	497	348	310
IP-10/CXCL10	611	37523	531	1469	41576	576	503	419
I-TAC	708	1479	901	1745	3796	907	895	615
Kallikrein 3	833	1165	1034	2530	2483	1403	871	1235
Leptin	1336	1192	712	317	208	310	652	188
LIF	1245	1198	934	533	942	493	894	267
Lipocalin-2	1267	1174	810	532	555	389	763	262
MCP-1	1120	1087	819	446	725	364	985	397
MCP-3	954	925	714	736	710	490	537	252
M-CSF	867	1069	740	962	1060	624	554	314
MIF	2594	3454	3957	2563	2816	2972	2560	1549
MIG	779	1214	639	1223	2503	574	615	380
MIP-1alpha/MIP-1beta	639	755	432	1198	6570	528	416	335
MIP-3alpha	679	1652	510	1426	2208	642	477	455
MIP-3beta	720	757	713	1747	1458	813	658	656
MMP-9	712	675	641	1906	1332	796	648	703
Myeloperoxidase	4639	4069	2271	4276	3282	1195	1828	940
Osteopontin	1491	1413	1446	1339	1334	1779	15233	14198
PDGF-AA	3335	3678	3536	845	969	922	2600	743
PDGF-AB/BB	833	741	491	368	302	163	358	9
Pentaxin-3	1549	1731	1622	2059	3772	2177	1326	1114
PF4	776	778	616	807	535	396	387	169
RAGE	748	968	606	1015	562	457	486	294
RANTES	1243	6279	946	1554	2933	677	525	322
RBP-4	962	1272	838	1234	932	570	773	312
Relaxin-2	949	1007	915	1863	1596	892	576	550
Resistin	1070	1189	1053	1796	1428	992	1078	801
SDF-1alpha	1030	961	946	1888	1459	982	1275	950
Serpin E1	40156	40264	41596	39529	41129	42561	41392	40949
SHBG	1000	993	710	719	743	647	1811	1471
ST2	993	1066	753	331	393	266	619	37
TARC	1074	996	809	601	713	395	720	148
TFF3	727	668	449	589	446	382	471	170
TFR	829	825	840	1061	732	676	593	388
TGF-alpha	658	663	624	949	928	670	461	349
Thrombospondin-1	3817	4047	5029	4009	4418	4095	3908	2795
TNF-alpha	358	582	379	1061	758	476	402	259
uPAR	2552	3844	4749	4473	5709	6234	1484	1735
VEGF	1792	2212	2194	1611	1141	1120	1676	1152
Vitamin D BP	1124	914	877	718	978	693	857	423
CD31	760	649	459	321	367	210	430	52
TIM-3	660	550	433	554	266	316	519	132
VCAM-1	546	542	497	623	425	329	526	275

Supplementary figure VI. 2 – Secretome profile of CHME3 Cav1 NT and CHME3 Cav1 KO. CHME3 cells were stimulated with LPS and IFN- γ or with IL-4 and IL-13, or co-cultured with GBM cells in a transwell system, for 48 hours. Untreated cells were used as control. Values represent the mean of pixel density



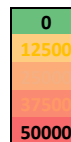
Supplementary figure VI. 3 – Secretome profile of iPSC-MG Cav1 NT and iPSC-MG Cav1 KO. iPSC-MG cells were stimulated with LPS and IFN- γ or with IL-4 and IL-13 for 48 hours. Untreated cells were used as control. Values represent the mean of pixel density.

Analyte	iPSC-MG Cav1 NT			iPSC-MG Cav1 KO		
	CTRL	LPS + IFN γ	IL4 + IL13	CTRL	LPS + IFN γ	IL4 + IL13
Adiponectin	355	638	556	258	621	751
Apolipoprotein A-I	3149	3486	2517	2764	3858	4502
Angiogenin	2196	1481	1480	2296	2018	3496
Angiotensin-1	293	473	271	317	600	491
Angiotensin-2	868	1398	767	801	1411	1106
BAFF	841	938	484	726	814	690
BDNF	622	863	698	734	1022	849
Complement Component C5/Csa	735	2033	521	787	1693	826
CD14	754	1095	647	781	1839	1261
CD30	352	579	529	322	678	682
CD40 ligand	677	1077	789	635	894	875
Chitinase 3-like 1	6628	8414	7833	7460	7740	9294
Complement Factor D	2931	3074	2701	2728	2782	3367
C-Reactive Protein	683	801	650	531	754	667
Cripto-1	304	474	390	306	334	456
Cystatin C	6843	8257	8067	7304	7357	9432
Dkk-1	413	516	628	457	591	603
DPPIV	6750	11780	9172	8709	15540	10624
EGF	345	472	402	294	563	579
EMMPRIN	562	1186	844	681	1358	1243
ENA-78	1785	3520	2420	2332	4033	3283
Endoglin	2054	2685	3310	2578	2896	3432
Fas Ligand	359	706	885	710	741	651
FGF basic	638	1495	829	959	1224	1104
FGF-7	224	402	269	249	207	391
FGF-19	1619	2848	2234	1726	2795	2476
Fit-3 Ligand	170	98	298	237	189	366
G-CSF	250	663	756	382	581	753
GDF-15	1459	1659	1502	1623	1691	1869
GM-CSF	359	902	575	475	980	717
GRO-alpha	671	2216	1239	877	3358	1668
Growth Hormone	266	221	306	193	249	434
HGF	362	475	392	604	538	454
ICAM-1	1160	1597	1125	1488	2021	1317
IFN-gamma	605	2106	997	1027	2273	893
IGFBP-2	1746	2712	3090	2582	3309	4079
IGFBP-3	275	226	350	324	264	443
IL-1alpha	511	540	859	838	745	773
IL-1beta	177	156	337	199	283	381
IL-1ra	367	1552	1734	575	2044	2087
IL-2	215	553	341	216	620	375
IL-3	223	550	266	252	632	345
IL-4	483	1648	4967	503	1787	5283
IL-5	147	185	387	313	59	343
IL-6	352	2553	641	453	4012	454
IL-8	4846	5329	5659	5756	6307	6434
IL-10	437	688	508	586	987	908
IL-11	479	622	594	643	738	791
IL-12 p70	139	275	233	254	493	355
IL-13	148	12	2114	196	267	2900
IL-15	124	54	183	201	211	300
IL-16	234	412	433	253	649	534
IL-17A	859	2619	1035	840	3341	1350
IL-18 BPa	2192	7572	3056	3732	7190	5020
IL-19	187	204	514	182	173	677
IL-22	427	515	596	491	686	708
IL-23	385	632	494	342	489	484
IL-24	727	816	835	664	713	1033
IL-27	403	458	468	410	865	605
IL-31	325	179	271	234	371	421
IL-32	401	309	382	417	444	537
IL-33	251	221	305	234	372	488
IL-34	199	253	200	213	438	358
IP-10/CXCL10	360	9295	1301	227	10605	337
I-TAC	293	6636	514	376	9973	552
Kallikrein 3	707	1154	1077	1214	1344	1105
Leptin	305	257	403	278	344	382
LIF	281	230	257	208	161	447
Lipocalin-2	1823	2330	2099	2237	2259	2379
MCP-1	2418	3358	2609	2595	3312	3245
MCP-3	724	3405	1291	1047	3834	1721
M-CSF	642	603	648	708	953	738
MIF	1653	1683	2135	2198	1969	2210
MIG	401	5141	869	451	5066	433
MIP-1alpha/MIP-1beta	616	4339	1608	868	4666	1134
MIP-3alpha	343	1603	486	399	2302	487
MIP-3beta	391	1658	542	408	2169	549
MMP-9	4489	6044	5478	5898	5331	6138
Myeloperoxidase	421	465	473	578	395	445
Osteopontin	7332	8617	7712	7404	7801	8405
PDGF-AA	382	973	461	364	1072	455
PDGF-AB/BB	305	812	263	290	975	404
Pentraxin-3	858	1493	1037	1222	1501	949
PF4	477	547	360	395	404	442
RAGE	419	634	348	423	411	425
RANTES	394	4063	333	324	4185	393
RBP-4	16798	22400	17816	19461	20861	23078
Relaxin-2	649	843	426	679	633	750
Resistin	510	751	547	538	633	606
SDF-1alpha	936	1784	842	903	1546	1089
Serpin E1	1418	1335	1233	1735	1700	1120
SHBG	772	1389	1041	827	936	1080
ST2	479	1166	471	496	961	466
TARC	417	6356	1240	414	9072	1926
TFF3	886	969	642	1035	1467	806
TFR	798	1080	842	902	1291	932
TGF-alpha	398	884	424	437	845	561
Thrombospondin-1	231	466	251	274	373	320
TNF-alpha	547	2694	976	479	5147	984
uPAR	1836	5288	2182	2745	5620	2978
VEGF	312	463	260	277	333	349
Vitamin D BP	1726	1900	1333	2475	2946	2086
CD31	1072	1734	861	1578	3041	1835
TIM-3	2982	4603	2092	5255	8577	5142
VCAM-1	533	1858	321	569	3602	624



Analyte	iPSC-MG Cav1 NT				iPSC-MG Cav1 KO			
	CTRL	CC U87	CC UP007	CC UP029	CTRL	CC U87	CC UP007	CC UP029
Adiponectin	673	391	2049	402	232	871	764	791
Apolipoprotein A-I	4349	3380	16354	8003	4263	4645	5670	15191
Angiogenin	3149	855	4050	1167	3814	1027	1715	2889
Angiotensin-1	484	408	1027	299	221	523	1105	514
Angiotensin-2	1203	1072	3555	1475	1103	1363	2800	3250
BAFF	1680	1548	3369	1082	919	2542	2535	974
BDNF	774	642	2188	1408	1006	1290	1710	2946
Complement Component C5/C5a	1366	874	2114	741	985	1672	1854	1025
CD14	1280	1113	4573	1681	925	2292	3428	4240
CD30	686	761	1399	1157	321	2154	1551	1145
CD40 ligand	1362	758	2296	990	859	1618	1494	1041
Chitinase 3-like 1	10534	8503	21119	18014	10569	10656	18583	21326
Complement Factor D	5238	3043	7431	5189	3989	3785	6821	4102
C-Reactive Protein	1183	1071	1363	1142	677	1364	1787	830
Cripto-1	593	420	1028	464	251	802	1029	480
Cystatin C	11644	11425	26579	24677	9259	22277	24601	15512
Dkk-1	768	727	1707	1448	437	1618	1605	1131
DPPiV	8967	7261	12651	14941	10706	10269	12954	11601
EGF	694	824	1634	580	308	1670	1726	620
EMMPRIN	902	1776	3327	3663	632	3430	3260	4105
ENA-78	3211	792	1318	587	4205	1227	1137	577
Endoglin	2912	3813	6503	8367	3608	5336	7411	6975
Fas Ligand	594	1757	1627	2586	821	3306	2951	687
FGF basic	1163	1410	2569	3474	1741	2337	2720	1088
FGF-7	463	387	1011	441	226	692	856	268
FGF-19	3097	3614	7342	7673	2075	6616	6819	4517
Fit-3 Ligand	340	381	727	438	148	939	756	441
G-CSF	519	10098	1173	1058	393	14763	1307	806
GDF-15	1229	3856	7454	6669	1445	5847	5613	4106
GM-CSF	728	1846	1189	1786	502	3443	1658	1386
GRO-alpha	1071	856	1034	306	1446	1708	896	359
Growth Hormone	526	378	606	24	193	667	658	248
HGF	649	756	1476	550	701	1385	1209	610
ICAM-1	2219	2277	3452	2292	1922	3707	3096	1914
IFN-gamma	657	1332	2129	2931	1224	1845	2379	1396
IGFBP-2	2846	1786	10317	3391	3320	4799	8722	2205
IGFBP-3	594	697	1545	609	203	1734	1528	583
IL-1alpha	567	532	1309	2223	818	1262	1363	2139
IL-1beta	270	286	789	75	107	810	905	345
IL-1ra	632	737	2069	1396	626	2049	1966	1800
IL-2	337	442	1086	567	187	1363	1249	563
IL-3	415	292	832	390	381	1548	1074	621
IL-4	668	1027	1507	580	771	1814	1381	929
IL-5	130	126	215	249	416	237	131	433
IL-6	530	1558	1662	381	512	2383	839	542
IL-8	6464	8380	15176	10817	8529	11271	8349	7507
IL-10	791	2492	2196	1084	330	3079	1666	853
IL-11	743	1481	2484	1452	577	1673	2012	1083
IL-12 p70	176	360	868	139	173	602	684	422
IL-13	228	144	681	34	61	496	494	286
IL-15	175	310	647	31	62	573	450	320
IL-16	378	489	1078	403	206	832	920	651
IL-17A	1709	2620	4727	2246	1014	4823	5559	2704
IL-18 BPa	3460	3869	10101	8654	6815	8648	9246	8683
IL-19	288	277	618	182	149	638	525	350
IL-22	782	1173	2571	796	550	2255	1735	766
IL-23	626	526	1523	614	455	1049	847	452
IL-24	1394	1330	2566	1772	1116	1891	1328	1002
IL-27	893	564	1040	817	301	950	832	567
IL-31	568	436	1205	449	196	809	671	478
IL-32	601	589	1439	692	425	1271	1074	946
IL-33	395	316	862	114	111	693	703	422
IL-34	325	321	711	52	78	762	570	364
IP-10/CXCL10	570	404	832	121	267	843	912	445
I-TAC	494	749	1226	1247	350	2038	1733	1215
Kallikrein 3	1069	941	2053	3731	1503	2753	2417	3342
Leptin	493	463	1131	696	347	964	925	487
LIF	557	473	808	208	226	951	599	280
Lipocalin-2	2496	2533	7340	5785	2951	4018	4541	4444
MCP-1	4029	4027	8730	8173	3161	6508	5406	6113
MCP-3	1100	494	1068	754	1091	838	809	621
M-CSF	692	644	1360	1565	690	1264	1117	1391
MIF	2343	3115	7095	6496	2447	5586	5796	7043
MIG	635	605	1196	556	458	1140	1181	809
MIP-1alpha/MIP-1beta	1005	1146	2146	1195	932	2256	1614	1544
MIP-3alpha	693	526	1157	553	459	1129	1212	743
MIP-3beta	680	802	1491	1733	438	1696	1996	1290
MMP-9	7430	7139	14237	14480	7363	15707	16686	12807
Myeloperoxidase	571	2037	1045	1391	955	3352	1857	1058
Osteopontin	11057	11656	19119	24179	10059	15381	18976	16815
PDGF-AA	620	612	1229	560	388	1340	1075	550
PDGF-AB/BB	511	284	690	56	295	573	559	182
Pentraxin-3	1174	1550	3186	4977	1590	2991	2619	3940
PF4	644	535	830	657	307	932	917	682
RAGE	650	516	1003	372	388	1093	1060	763
RANTES	713	546	1046	226	305	1233	1181	649
RBP-4	29141	34163	47149	42130	24898	44143	45133	38007
Relaxin-2	1359	1264	2041	1540	898	2620	1931	1623
Resistin	1054	932	2174	1422	582	2371	2001	1354
SDF-1alpha	1905	1668	3556	2720	1128	3922	4677	2359
Serpin E1	2304	15295	17075	14562	2603	17966	11200	21938
SHBG	1246	1499	3261	2495	1258	1834	2571	1977
ST2	770	636	1549	563	693	905	1199	607
TARC	699	556	1330	461	479	819	1048	581
TFF3	1217	881	3286	2013	1451	1312	1973	2336
TFR	1018	646	1607	2561	1221	1057	1207	2547
TGF-alpha	587	458	993	466	478	831	807	807
Thrombospondin-1	404	345	896	400	220	953	961	833
TNF-alpha	1083	1234	2366	2403	391	2127	2974	2574
uPAR	2604	3108	12184	5935	3470	6553	4757	11864
VEGF	605	1241	1717	941	154	3033	1058	1643
Vitamin D BP	1753	1266	6755	2033	4251	1336	2778	5296
CD31	1064	611	4398	933	2548	778	1430	3701
TIM-3	2327	920	10874	2032	8868	1566	2307	11957
VCAM-1	884	343	1941	570	758	645	683	1342

Supplementary figure VI. 4 – Secretome profile of iPSC-MG Cav1 NT and iPSC-MG Cav1 KO in CC with GBM cells. Microglial cells were co-cultured with GBM cells in a transwell system, for 48 hours. Cells cultured without the interference of tumour cells were used as control. Values represent the mean of pixel density



APPENDIX VII – RNA-SEQ

Supplementary table VII.1 – DE genes from the impact of Cav1 status on microglial basal phenotype.
iPSC-MG Cav1 NT and iPSC-MG Cav1 KO were differentiated from Kolf2 cells. Cells were cultured in standard conditions without the interference of any stimulus. Multi-group comparison (F-test, ANOVA). N=3 clones.

Gene	p-value	FDR – q-value	log2FC	Symbol
ENSG00000198576.3_chr8	1.39E-43	1.55E-39	3.552006	ARC
ENSG00000128342.4_chr22	1.19E-20	1.46E-17	2.002529	LIF
ENSG00000187678.8_chr5	2.78E-21	4.41E-18	1.910396	SPRY4
ENSG00000164949.7_chr8	1.98E-09	4.78E-07	1.883661	GEM
ENSG00000120875.8_chr8	2.00E-14	1.23E-11	1.771402	DUSP4
ENSG00000276070.4_chr17	7.84E-21	1.09E-17	1.696694	CCL4L1
ENSG00000275302.1_chr17	3.69E-36	2.04E-32	1.529721	CCL4
ENSG00000232810.3_chr6	1.06E-17	7.84E-15	1.501701	TNF
ENSG00000117525.13_chr1	4.94E-09	1.09E-06	1.406769	F3
ENSG00000137331.11_chr6	2.41E-19	2.67E-16	1.369379	IER3
ENSG00000184545.10_chr11	9.94E-06	1.19E-03	1.317604	DUSP8
ENSG00000158050.4_chr2	1.49E-18	1.27E-15	1.264774	DUSP2
ENSG00000148926.9_chr11	0.000897	0.038867	1.263717	ADM
ENSG00000101187.15_chr20	9.40E-12	3.47E-09	1.251305	SLCO4A1
ENSG00000139174.11_chr12	0.000232	0.014864	1.248049	PRICKLE1
ENSG00000143333.6_chr1	0.000367	0.020709	1.227241	RGS16
ENSG00000184557.4_chr17	9.68E-16	6.32E-13	1.205447	SOCS3
ENSG00000165023.6_chr9	3.78E-06	5.11E-04	1.179847	DIRAS2
ENSG00000163661.3_chr3	2.55E-07	4.42E-05	1.160806	PTX3
ENSG00000213626.11_chr2	1.20E-05	1.32E-03	1.13266	LBH
ENSG00000123689.5_chr1	0.000166	0.01175	1.100344	GOS2
ENSG00000056558.10_chr9	1.24E-11	4.43E-09	1.094243	TRAF1
ENSG00000123975.4_chr9	5.94E-13	3.14E-10	1.088176	CKS2
ENSG00000125735.10_chr19	1.31E-13	7.26E-11	1.08314	TNFSF14
ENSG00000235316.1_chr10	0.000276	0.017165	1.077677	DUSP8P5
ENSG00000134070.4_chr3	4.50E-25	1.17E-21	1.06407	IRAK2
ENSG00000006118.14_chr11	1.47E-05	1.56E-03	1.022774	TMEM132A
ENSG00000180787.5_chr17	0.000939	0.039948	-1.04017	ZFP3
ENSG00000132530.16_chr17	0.000369	0.020709	-1.15474	XAF1
ENSG00000212443.1_chr12	0.000491	0.025192	-1.4679	SNORA53

Supplementary table VII.2 – DE genes from the impact of Cav1 status on microglial pro-inflammatory phenotype. iPSC-MG Cav1 NT and iPSC-MG Cav1 KO were differentiated from Kolf2 cells and stimulated with LPS and IFN- γ , for 48 hours. Multi-group comparison (F-test, ANOVA). N=3 clones.

Gene	p-value	FDR – q-value	log2FC	Symbol
ENSG00000163430.11_chr3	0.000122	0.026652	3.785916	FSTL1
ENSG00000128591.15_chr7	0.000144	0.029271	3.009806	FLNC
ENSG00000137033.11_chr9	0.000242	0.039961	2.010051	IL33
ENSG00000117519.15_chr1	0.000152	0.029788	1.731738	CNN3
ENSG00000101115.12_chr20	9.34E-06	3.89E-03	1.420702	SALL4
ENSG00000162676.11_chr1	0.000296	0.046539	1.419719	GFI1
ENSG00000177374.12_chr17	1.04E-05	4.08E-03	1.2045	HIC1
ENSG00000188483.7_chr9	4.59E-10	8.45E-07	1.17791	IER5L
ENSG00000168209.4_chr10	0.000336	0.049212	1.027342	DDIT4
ENSG00000198695.2_chrM	3.86E-05	1.16E-02	-1.09578	MT-ND6
ENSG00000081041.8_chr4	0.00023	0.038742	-1.32297	CXCL2
ENSG00000163734.4_chr4	0.000188	0.033683	-1.41613	CXCL3

Supplementary table VII.3 – DE genes from the impact of Cav1 status on microglial anti-inflammatory phenotype. iPSC-MG Cav1 NT and iPSC-MG Cav1 KO were differentiated from Kolf2 cells and stimulated with IL-4 and IL-13, for 48 hours. Multi-group comparison (F-test, ANOVA). N=3 clones.

Gene	p-value	FDR – q-value	log2FC	Symbol
ENSG00000127399.14_chr7	6.83E-08	1.61E-05	6.704768	LRR61
ENSG00000198576.3_chr8	8.49E-41	1.08E-36	3.505175	ARC
ENSG00000128342.4_chr22	2.10E-17	3.81E-14	2.196987	LIF
ENSG00000120875.8_chr8	6.59E-15	8.37E-12	2.115187	DUSP4
ENSG00000187678.8_chr5	8.60E-20	2.73E-16	2.095312	SPRY4
ENSG00000143333.6_chr1	3.86E-05	3.27E-03	1.787447	RGS16
ENSG00000188897.8_chr16	2.81E-07	5.42E-05	1.560036	CTD-3088G3.8
ENSG00000145911.5_chr5	6.57E-05	5.02E-03	1.345089	N4BP3
ENSG00000270069.1_chrX	8.78E-05	0.006334	1.300343	MIR222HG
ENSG00000246922.8_chr15	0.000408	0.020988	1.262554	UBAP1L
ENSG00000229512.1_chr11	1.31E-12	1.24E-09	1.251761	AC068580.5
ENSG00000099625.12_chr19	4.29E-06	0.000545	1.247881	C19orf26
ENSG00000213626.11_chr2	2.66E-06	3.60E-04	1.243367	LBH
ENSG00000161912.17_chr6	1.12E-05	1.19E-03	1.196668	ADCY10P1
ENSG00000267519.5_chr19	0.000276	0.015721	1.186172	CTD-3252C9.4
ENSG00000250644.3_chr11	2.32E-08	6.54E-06	1.173407	RP11-295K3.1
ENSG00000253522.5_chr5	5.90E-09	2.14E-06	1.1614	CTC-231O11.1
ENSG00000167604.14_chr19	1.37E-12	1.24E-09	1.136233	NFKBID
ENSG00000265206.5_chr17	0.000945	0.037439	1.119901	RP5-1171I10.5
ENSG00000274627.1_chr16	1.21E-07	2.57E-05	1.119837	RP11-104N10.2
ENSG00000180616.8_chr17	0.001376	0.048269	1.114493	SSTR2
ENSG00000101187.15_chr20	4.01E-17	6.37E-14	1.090553	SLCO4A1
ENSG00000067191.15_chr17	5.97E-06	0.000708	1.088812	CACNB1
ENSG00000125735.10_chr19	6.25E-09	2.20E-06	1.086619	TNFSF14
ENSG00000235316.1_chr10	0.000215	0.013142	1.084604	DUSP8P5
ENSG00000281344.1_chr12	0.000878	0.035617	1.08081	HELLPAR
ENSG00000220785.7_chr1	0.000407	0.020988	1.069402	MTMR9LP
ENSG00000244242.1_chr11	7.50E-09	2.51E-06	1.04729	IFITM10
ENSG00000095739.10_chr10	1.05E-07	2.29E-05	1.044381	BAMBI
ENSG00000137331.11_chr6	0.000183	0.011557	1.037251	IER3
ENSG00000228526.6_chr1	3.48E-09	1.38E-06	1.036689	RP3-510D11.1
ENSG00000116883.8_chr1	0.000392	0.020644	1.032329	RP11-268J15.5
ENSG00000267121.5_chr17	0.000344	0.018362	1.018359	CTD-2020K17.1
ENSG00000262580.5_chr17	1.77E-06	2.57E-04	1.012753	RP11-334C17.5
ENSG00000184545.10_chr11	3.44E-05	0.002989	1.009391	DUSP8
ENSG00000134070.4_chr3	3.77E-26	2.39E-22	1.003496	IRAK2
ENSG00000225630.1_chr1	5.22E-10	2.47E-07	-1.05683	MTND2P28
ENSG00000180787.5_chr17	0.000104	0.00728	-1.05711	ZFP3

APPENDIX VIII – TAQMAN GENE EXPRESSION ARRAY PLATE

Supplementary table VIII.1 – TaqMan Array – Human Immune Response. Microglial cells were co-cultured with tumour cells in transwell systems for 48 hours. Cells without the interference of GBM were used as control (CTRL). Results are the mean of $\Delta\Delta Ct$ analysis \pm SD of CC with 2 microglial clones. -: not amplified

Gene	iPSC-MG Cav1 NT							iPSC-MG Cav1 KO						
	CTRL	CC U87	SD	CC UP007	SD	CC UP029	SD	CTRL	CC U87	SD	CC UP007	SD	CC UP029	SD
ACE	1.00	1.29	0.75	1.42	0.14	1.53	0.08	1.00	2.01	0.42	2.11	1.38	1.38	0.22
AGTR1	-	-	-	-	-	-	-	-	-	-	-	-	-	-
AGTR2	-	-	-	-	-	-	-	-	-	-	-	-	-	-
BAX	1.00	0.60	0.21	1.13	0.21	1.09	0.08	1.00	0.76	0.14	0.96	0.49	1.01	0.19
BCL2	1.00	1.31	0.33	1.57	0.47	1.30	0.14	1.00	0.81	0.21	1.00	0.15	1.07	0.20
BCL2L1	1.00	0.93	0.24	1.18	0.54	2.04	1.57	1.00	0.70	0.08	0.87	0.11	0.96	0.22
C3	1.00	0.66	0.06	1.24	0.33	0.95	0.05	1.00	0.61	0.29	1.49	0.19	1.22	0.65
CCL19	1.00	0.81	0.00	1.53	0.61	1.58	0.02	1.00	1.17	0.15	1.22	0.43	0.95	0.32
CCL2	1.00	7.11	0.58	2.09	0.03	2.03	0.05	1.00	5.82	0.04	1.21	0.11	1.57	0.12
CCL3	1.00	1.43	0.38	1.61	0.07	1.55	0.61	1.00	1.20	0.01	1.03	0.34	1.06	0.05
CCL5	1.00	1.15	0.35	1.06	0.12	1.18	0.13	1.00	0.73	0.14	0.82	0.05	0.87	0.14
CCR2	-	-	-	-	-	-	-	-	-	-	-	-	-	-
CCR4	1.00	0.02	0.01	0.03	0.00	0.05	0.00	1.00	0.02	0.00	0.04	0.02	0.03	0.02
CCR5	1.00	0.53	0.07	1.01	0.02	1.00	0.08	1.00	0.58	0.00	1.01	0.19	0.86	0.14
CCR7	1.00	0.59	0.44	0.55	0.24	0.64	0.41	1.00	0.37	0.02	0.59	0.34	0.54	0.02
CD19	-	-	-	-	-	-	-	-	-	-	-	-	-	-
CD28	1.00	1.58	0.21	1.24	0.26	0.94	0.27	1.00	0.91	0.40	1.37	0.74	1.09	0.01
CD34	1.00	1.70	1.41	0.62	0.26	1.66	2.35	1.00	0.34	0.14	0.00	0.00	0.11	0.10
CD38	1.00	2.35	0.51	0.96	0.20	0.88	0.09	1.00	2.08	0.42	0.65	0.27	0.61	0.17
CD3E	-	-	-	-	-	-	-	-	-	-	-	-	-	-
CD4	1.00	0.67	0.07	1.10	0.08	1.09	0.08	1.00	1.12	0.43	0.86	0.24	0.86	0.27
CD40	1.00	1.74	0.37	1.40	0.20	1.35	0.12	1.00	1.69	0.27	1.01	0.01	1.14	0.08
CD40L	-	-	-	-	-	-	-	-	-	-	-	-	-	-
CD68	1.00	0.67	0.08	1.09	0.03	1.02	0.03	1.00	0.78	0.05	0.81	0.07	0.89	0.08

APPENDIX VIII – TaqMan Gene expression Array plate

CD80	1.00	1.45	0.26	0.99	0.02	0.98	0.03	1.00	1.16	0.19	0.70	0.13	0.72	0.05
CD86	1.00	1.40	0.08	1.45	0.33	1.39	0.00	1.00	1.25	0.16	1.07	0.03	1.15	0.01
CD8A	1.00	0.25	0.10	0.48	0.06	0.65	0.13	1.00	1.28	0.94	1.18	0.26	0.81	0.11
CSF1	1.00	1.28	0.24	1.20	0.28	1.30	0.12	1.00	0.93	0.15	0.85	0.07	0.93	0.14
CSF2	-	-	-	-	-	-	-	-	-	-	-	-	-	-
CSF3	1.00	2.36	0.28	2.33	0.26	2.52	0.51	1.00	3.68	2.36	3.69	1.78	3.56	0.84
CTLA4	1.00	0.77	0.11	0.68	0.29	0.44	0.37	1.00	1.52	0.36	0.24	0.08	0.47	0.15
CXCL10	1.00	5.75	1.68	2.96	0.53	2.91	0.85	1.00	2.08	0.33	1.72	0.07	1.74	0.31
CXCL11	1.00	7.66	4.51	5.30	2.14	3.10	1.96	1.00	1.06	0.54	0.73	0.35	0.92	0.32
CXCR3	1.00	0.51	0.10	2.03	0.30	0.99	0.03	1.00	1.39	0.88	2.00	1.35	1.32	0.39
CYP7A1	1.00	1.05	0.22	1.67	0.72	1.52	0.52	1.00	0.86	0.16	1.56	0.46	1.71	0.12
CYP1A2	-	-	-	-	-	-	-	-	-	-	-	-	-	-
EDN1	1.00	1.35	0.68	2.33	1.34	1.91	1.00	1.00	0.84	0.42	1.38	0.45	1.46	0.48
FAS	1.00	0.96	0.13	0.97	0.21	1.29	0.08	1.00	0.96	0.20	0.90	0.12	0.90	0.09
FASLG	-	-	-	-	-	-	-	-	-	-	-	-	-	-
FN1	1.00	0.55	0.13	1.05	0.38	0.87	0.26	1.00	0.45	0.13	0.56	0.15	0.77	0.00
GNLY	1.00	1.03	0.18	1.43	0.10	0.80	0.46	1.00	0.62	0.02	0.59	0.15	0.87	0.28
GZMB	1.00	0.66	0.68	1.39	1.09	0.64	0.58	1.00	1.10	1.12	0.84	0.24	0.94	0.69
HLA-DRA	1.00	1.35	0.42	0.93	0.01	0.91	0.22	1.00	1.11	0.14	0.70	0.09	0.70	0.10
HLA-DRB1	1.00	0.88	0.24	0.96	0.06	1.00	0.10	1.00	0.86	0.08	0.75	0.06	0.70	0.05
HMOX1	1.00	0.57	0.06	1.19	0.11	1.03	0.01	1.00	0.69	0.07	0.92	0.03	0.89	0.05
ICAM1	1.00	1.60	0.44	1.30	0.32	1.18	0.13	1.00	2.07	0.67	1.07	0.37	1.13	0.32
ICOS	1.00	18.57	2.74	10.47	2.08	22.20	2.02	1.00	0.58	0.16	1.03	0.77	0.83	0.55
IFNG	-	-	-	-	-	-	-	-	-	-	-	-	-	-
IKBKB	1.00	0.59	0.08	0.83	0.00	0.83	0.02	1.00	0.67	0.05	0.61	0.01	0.63	0.02
IL10	1.00	1.34	0.48	1.29	0.06	1.12	0.25	1.00	1.00	0.05	0.87	0.09	0.97	0.03
IL12A	1.00	0.10	0.13	1.08	0.49	1.26	0.28	1.00	0.58	0.19	1.36	1.08	1.75	0.32
IL12B	-	-	-	-	-	-	-	-	-	-	-	-	-	-
IL13	-	-	-	-	-	-	-	-	-	-	-	-	-	-
IL15	1.00	1.08	0.45	1.62	0.10	1.53	0.28	1.00	2.33	0.17	1.95	0.07	2.70	0.10
IL17A	-	-	-	-	-	-	-	-	-	-	-	-	-	-
IL18	1.00	0.47	0.03	0.91	0.01	0.80	0.19	1.00	0.70	0.14	0.75	0.20	0.61	0.14

APPENDIX VIII – TaqMan Gene expression Array plate

IL1A	1.00	1.38	0.27	1.36	0.13	1.34	0.06	1.00	1.05	0.43	1.03	0.04	1.23	0.05
IL1B	1.00	1.39	0.52	1.13	0.17	0.96	0.25	1.00	1.80	0.89	0.94	0.05	1.00	0.07
IL2	-	-	-	-	-	-	-	-	-	-	-	-	-	-
IL2RA	1.00	14.21	0.70	1.46	0.69	1.94	0.42	1.00	7.70	0.13	0.55	0.05	0.81	0.02
IL3	-	-	-	-	-	-	-	-	-	-	-	-	-	-
IL4	-	-	-	-	-	-	-	-	-	-	-	-	-	-
IL5	-	-	-	-	-	-	-	-	-	-	-	-	-	-
IL6	1.00	34.02	6.18	3.99	0.33	8.60	2.34	1.00	12.58	4.92	2.63	0.84	5.16	2.32
IL7	1.00	1.96	1.45	2.12	0.17	1.73	0.51	1.00	1.71	0.29	0.95	0.15	0.69	0.31
IL8	1.00	0.80	0.05	0.96	0.07	1.06	0.25	1.00	0.69	0.39	1.25	0.35	1.24	0.32
IL9	-	-	-	-	-	-	-	-	-	-	-	-	-	-
LIF	1.00	0.36	0.09	0.64	0.04	0.61	0.01	1.00	0.28	0.03	0.39	0.14	0.42	0.07
LRP2	1.00	0.65	0.41	2.48	0.30	3.82	2.14	1.00	0.30	0.09	0.63	0.11	0.38	0.24
LTA	1.00	0.14	0.20	1.16	0.09	0.76	0.65	1.00	0.57	0.17	1.19	0.50	1.02	0.02
LY96	1.00	1.26	0.11	1.51	0.24	1.50	0.01	1.00	0.59	0.05	0.58	0.35	0.60	0.39
MIF	1.00	0.76	0.17	1.13	0.22	1.10	0.04	1.00	0.94	0.02	0.93	0.24	1.10	0.01
NFATC3	1.00	0.99	0.08	1.37	0.24	1.22	0.13	1.00	0.80	0.08	1.14	0.33	1.07	0.06
NFATC4	1.00	0.97	0.46	1.16	0.34	1.34	0.46	1.00	1.75	0.67	0.79	0.12	0.43	0.27
NFKB2	1.00	0.73	0.17	1.01	0.02	0.87	0.13	1.00	0.98	0.14	0.78	0.00	0.82	0.14
NOS2	1.00	4.96	0.13	3.79	1.35	3.02	1.16	1.00	0.30	0.15	0.71	0.01	0.57	0.02
PF4	-	-	-	-	-	-	-	-	-	-	-	-	-	-
PRF1	1.00	0.43	0.61	0.76	0.21	1.57	0.73	1.00	0.19	0.22	0.45	0.36	0.35	0.29
PTGS2	1.00	1.56	0.07	1.52	0.28	1.63	0.51	1.00	1.33	0.13	1.29	0.30	1.31	0.09
PTPRC	1.00	1.42	0.06	1.38	0.10	1.36	0.05	1.00	1.27	0.44	1.05	0.18	1.05	0.07
SELE	-	-	-	-	-	-	-	-	-	-	-	-	-	-
SELP	-	-	-	-	-	-	-	-	-	-	-	-	-	-
SKI	1.00	1.18	0.26	1.53	0.40	1.50	0.38	1.00	0.89	0.11	0.96	0.38	1.18	0.16
SMAD3	1.00	0.57	0.26	1.55	0.29	1.45	0.18	1.00	0.63	0.19	0.97	0.24	1.06	0.01
SMAD7	1.00	0.53	0.23	1.27	0.18	1.16	0.03	1.00	0.80	0.09	0.87	0.10	0.90	0.06
STAT3	1.00	1.04	0.09	1.26	0.15	1.14	0.06	1.00	1.30	0.33	0.91	0.16	1.01	0.06
SYK	1.00	1.00	0.06	1.48	0.40	1.13	0.09	1.00	0.75	0.02	0.99	0.02	1.09	0.09
TBX21	1.00	0.52	0.07	0.71	0.02	0.75	0.05	1.00	0.58	0.08	0.64	0.07	0.79	0.03

APPENDIX VIII – TaqMan Gene expression Array plate

TGFB1	1.00	1.20	0.31	1.73	0.27	1.22	0.13	1.00	0.74	0.10	0.89	0.05	0.94	0.04
TNF	1.00	2.39	0.45	1.16	0.36	1.28	0.49	1.00	3.70	2.68	1.00	0.39	1.27	0.70
TNFRSF18	1.00	0.47	0.20	1.06	0.19	1.17	0.03	1.00	0.53	0.28	0.96	0.23	0.90	0.06
VEGFA	1.00	0.69	0.21	0.89	0.03	0.68	0.14	1.00	0.53	0.09	0.54	0.06	0.73	0.05

APPENDIX VIII – TaqMan Gene expression Array plate

Supplementary table VIII.2 – TaqMan Array – Human Tumour Metastasis. ΔC_t values of GBM cells cultured in X-VIVO 15 plus N2 without the interference of microglia cells. Scale: red- high expression, green – low expression. HKG: 18S, GAPDH, HPRT1 and GUSB.

Target	ΔC_q			Target	ΔC_q			Target	ΔC_q			Target	ΔC_q		
	U87	UP007	UP029		U87	UP007	UP029		U87	UP007	UP029		U87	UP007	UP029
APC	5.71	4.64	5.13	FXYD5	2.03	2.61	2.89	MMP7	13.50	15.35	16.14	SET	6.64	6.80	6.62
BRMS1	5.56	5.99	6.69	GNRH1	10.64	10.30	10.45	MMP9	16.38	15.22	16.80	SMAD2	5.27	5.85	6.31
CASP8	6.89	7.61	8.11	HGF	6.13	18.67	19.34	MTA1	6.01	5.85	6.20	SMAD4	5.79	5.36	5.76
CCL7	10.21	16.07	17.88	HPSE	9.07	11.80	11.89	MTA2	4.27	4.20	4.58	SNCG	12.12	13.11	13.50
CD44	1.42	2.60	3.38	HRAS	5.70	7.18	6.73	MTSS1	6.97	15.76	15.07	SSTR2	9.71	9.92	9.87
CD82	1.88	5.80	5.78	HTATIP2	17.27	5.18	5.39	MYC	5.34	6.27	6.45	EPCAM	16.78	18.67	19.34
CDH1	19.12	17.13	16.51	IGF1	14.58	14.07	16.55	NCAM1	15.71	8.65	8.80	TCF20	6.80	6.67	6.94
CDKN2A	-	-	-	IL18	19.12	18.67	19.28	NF2	5.41	5.04	5.81	TGFB1	4.10	3.19	3.99
CEACAM1	13.17	14.72	15.62	IL1B	4.44	13.97	14.26	NME1	8.49	9.16	8.97	TGFBR2	3.70	4.28	4.32
CTBP1	9.59	8.83	8.80	ITGB3	5.23	9.65	9.63	NR4A3	11.18	8.49	8.97	TIAM1	6.47	8.94	7.79
CTNNA1	4.37	3.72	3.87	KISS1	-	15.46	15.46	PECAM1	7.90	11.37	10.46	TIMP1	1.99	2.33	2.87
CTSK	2.40	8.65	8.66	KISS1R	-	15.89	16.60	PNN	4.08	3.56	3.98	TIMP2	3.10	1.94	2.55
CXCL12	13.10	10.09	10.28	KRAS	6.48	6.63	7.10	PSCA	13.93	16.05	15.31	TIMP4	6.44	8.38	8.12
CXCR4	11.01	12.06	12.08	LAMB1	4.65	4.02	3.66	PTEN	7.28	6.89	7.55	TMPRSS4	-	-	19.34
DAPK1	19.12	6.02	7.61	LYPD3	-	15.71	16.70	PTGS2	7.48	9.65	10.38	TNFSF10	10.18	13.26	14.57
DCC	10.40	-	17.28	MCAM	6.40	4.93	5.25	RB1	6.40	4.92	5.62	TP53	6.55	4.92	5.39
EPHB2	6.27	6.08	6.68	MET	4.61	4.64	5.10	RBL1	6.09	6.48	6.60	TPBG	4.86	11.23	11.36
ERBB2	9.39	6.42	6.50	MGAT5	6.13	5.87	5.98	RBL2	5.95	6.38	6.70	TSHR	19.12	16.63	17.76
ETV4	7.92	8.30	8.17	MMP1	11.35	14.12	13.70	RET	19.12	18.67	19.31	TWIST1	8.01	19.00	19.34
FAT1	5.26	3.40	3.98	MMP10	16.44	18.67	16.37	RHOC	8.23	8.81	8.79	VEGFA	3.10	4.06	4.16
FGF2	6.39	7.19	7.83	MMP14	3.92	4.01	3.71	S100A4	9.23	8.11	8.61	VEGFC	5.89	4.77	5.87
FGFR4	16.29	8.88	8.44	MMP2	0.71	-0.63	-0.11	SERPINB5	-	17.19	-	WISP1	11.55	9.06	10.06
FN1	0.49	0.43	1.33	MMP3	4.50	8.70	9.40	SERPINE1	4.46	6.45	6.70				

APPENDIX VIII – TaqMan Gene expression Array plate

Supplementary table VIII.3 – TaqMan Array – Human Tumour Metastasis. Tumour cells were co-cultured with microglial cells in transwell systems for 48 hours. Cells without the interference of microglia were used as control (CTRL). Results are the mean of $\Delta\Delta Ct$ analysis $\pm SD$ of CC with 2 microglial clones. -: Not amplified.

Gene	U87					UP007					UP007				
	CTRL	CC iPSC-MG Cav1 NT	SD	CC iPSC-MG Cav1 KO	SD	CTRL	CC iPSC-MG Cav1 NT	SD	CC iPSC-MG Cav1 KO	SD	CTRL	CC iPSC-MG Cav1 NT	SD	CC iPSC-MG Cav1 KO	SD
APC	1.00	1.12	0.08	1.17	0.08	1.00	0.88	0.04	1.00	0.07	1.00	0.93	0.02	1.00	0.17
BRMS1	1.00	1.06	0.13	1.11	0.03	1.00	0.82	0.03	0.95	0.03	1.00	1.13	0.05	1.17	0.16
CASP8	1.00	1.01	0.02	1.03	0.17	1.00	0.83	0.08	0.95	0.16	1.00	0.97	0.11	1.04	0.02
CCL7	1.00	0.81	0.03	0.70	0.27	1.00	1.53	0.11	2.41	0.06	1.00	1.98	1.50	2.19	0.85
CD44	1.00	0.91	0.17	0.96	0.37	1.00	1.03	0.11	1.23	0.22	1.00	1.21	0.01	1.31	0.20
CD82	1.00	0.83	0.03	0.71	0.05	1.00	1.11	0.06	1.13	0.23	1.00	1.19	0.06	1.07	0.11
CDH1	1.00	1.67	0.61	7.70	0.50	1.00	1.41	0.30	1.06	0.68	1.00	0.70	0.02	0.94	0.53
CDKN2A	-	-	-	-	-	-	-	-	-	-	-	-	-	-	-
CEACAM1	1.00	0.95	0.05	0.92	0.43	1.00	1.14	0.12	1.10	0.32	1.00	1.89	0.30	1.33	0.43
CTBP1	1.00	1.24	0.09	1.20	0.16	1.00	0.95	0.09	1.02	0.28	1.00	1.04	0.12	0.93	0.08
CTNNA1	1.00	0.99	0.01	1.00	0.05	1.00	0.90	0.10	0.96	0.10	1.00	0.99	0.07	1.03	0.08
CTSK	1.00	1.39	0.10	1.30	0.12	1.00	1.14	0.11	1.39	0.23	1.00	1.23	0.09	1.13	0.11
CXCL12	1.00	1.08	0.09	1.29	0.60	1.00	0.62	0.05	0.80	0.07	1.00	0.61	0.08	0.66	0.03
CXCR4	1.00	0.18	0.03	0.21	0.10	1.00	1.71	0.08	1.79	0.59	1.00	1.84	0.62	1.67	0.28
DAPK1	1.00	-	-	-	-	1.00	0.64	0.01	0.85	0.27	1.00	0.67	0.05	0.67	0.08
DCC	1.00	1.29	0.34	1.42	0.21	-	-	-	-	-	1.00	0.10	0.00	0.26	0.29
EPCAM	1.00	0.44	0.06	0.53	0.32	1.00	-	-	-	-	1.00	-	-	-	-
EPHB2	1.00	1.07	0.07	1.10	0.18	1.00	1.02	0.03	1.17	0.21	1.00	1.07	0.01	1.13	0.12
ERBB2	1.00	1.03	0.05	1.08	0.32	1.00	0.89	0.03	0.91	0.07	1.00	0.89	0.00	0.82	0.03
ETV4	1.00	0.66	0.05	0.73	0.17	1.00	1.03	0.08	1.30	0.25	1.00	1.42	0.05	1.52	0.08
FAT1	1.00	1.19	0.09	1.37	0.05	1.00	0.99	0.15	1.27	0.27	1.00	1.18	0.04	1.33	0.24
FGF2	1.00	0.82	0.01	0.78	0.16	1.00	0.84	0.08	1.00	0.03	1.00	0.95	0.06	0.92	0.00
FGFR4	1.00	1.22	0.03	0.82	0.31	1.00	0.47	0.07	0.55	0.10	1.00	0.58	0.07	0.51	0.02
FN1	1.00	1.19	0.15	1.29	0.29	1.00	0.98	0.04	1.23	0.25	1.00	1.37	0.06	1.64	0.22
FXYD5	1.00	0.86	0.02	0.85	0.14	1.00	0.84	0.08	1.10	0.17	1.00	0.95	0.03	0.94	0.08
GNRH1	1.00	1.04	0.17	0.92	0.02	1.00	0.93	0.17	0.98	0.27	1.00	1.16	0.13	1.02	0.02
HGF	1.00	1.03	0.04	1.04	0.04	1.00	0.75	0.20	0.97	0.42	1.00	0.37	0.15	0.59	0.31

APPENDIX VIII – TaqMan Gene expression Array plate

HPSE	1.00	1.02	0.17	0.95	0.20	1.00	0.72	0.07	0.68	0.09	1.00	0.65	0.02	0.66	0.12
HRAS	1.00	0.94	0.09	0.82	0.10	1.00	0.95	0.02	0.97	0.13	1.00	0.94	0.02	0.84	0.01
HTATIP2	1.00	2.64	0.44	3.10	0.19	1.00	0.74	0.00	0.88	0.03	1.00	0.82	0.01	0.90	0.09
IGF1	1.00	2.07	0.22	4.12	2.98	1.00	3.94	0.64	8.19	1.38	1.00	4.33	0.08	4.86	1.83
IL18	1.00	1.28	0.27	1.17	0.29	1.00	1.50	0.16	1.33	0.26	1.00	0.66	0.23	1.52	0.42
IL1B	1.00	0.25	0.01	0.27	0.11	1.00	1.04	0.56	0.68	0.33	1.00	0.99	0.02	0.86	0.07
ITGB3	1.00	1.05	0.01	1.11	0.22	1.00	1.52	0.09	2.08	0.35	1.00	1.37	0.01	1.38	0.07
KISS1	-	-	-	-	-	1.00	0.73	0.13	0.54	0.12	1.00	0.53	0.04	0.58	0.20
KISS1R	-	-	-	-	-	1.00	1.02	0.11	0.73	0.25	1.00	1.11	0.18	0.98	0.26
KRAS	1.00	1.07	0.11	1.06	0.02	1.00	0.87	0.02	0.87	0.00	1.00	1.12	0.00	1.01	0.09
LAMB1	1.00	1.03	0.05	1.05	0.07	1.00	1.00	0.02	1.16	0.19	1.00	0.95	0.00	1.03	0.06
LYPD3	-	-	-	-	-	1.00	0.46	0.23	0.73	0.06	1.00	1.03	0.41	1.26	0.33
MCAM	1.00	1.10	0.01	1.29	0.06	1.00	0.80	0.05	0.98	0.16	1.00	0.96	0.01	0.97	0.03
MET	1.00	0.93	0.10	0.96	0.08	1.00	0.86	0.01	0.92	0.08	1.00	1.00	0.01	0.99	0.07
MGAT5	1.00	1.01	0.09	1.07	0.15	1.00	0.99	0.07	1.22	0.16	1.00	1.16	0.03	1.20	0.14
MMP1	1.00	1.35	0.74	1.10	0.23	1.00	1.19	0.25	1.29	0.47	1.00	1.49	0.08	1.13	0.28
MMP10	1.00	0.49	0.05	0.67	0.25	1.00	3.53	0.26	3.09	1.02	1.00	1.88	0.16	1.28	0.02
MMP14	1.00	1.34	0.03	1.20	0.14	1.00	1.19	0.03	1.36	0.40	1.00	1.31	0.03	1.32	0.03
MMP2	1.00	1.40	0.04	1.53	0.33	1.00	0.90	0.05	1.06	0.26	1.00	1.08	0.00	1.32	0.16
MMP3	1.00	0.63	0.09	0.51	0.08	1.00	1.15	0.02	1.31	0.23	1.00	1.18	0.04	1.10	0.12
MMP7	1.00	0.93	0.01	0.89	0.03	1.00	2.21	0.00	4.02	0.22	1.00	2.48	0.45	2.63	0.50
MMP9	1.00	0.83	0.18	1.58	1.10	1.00	3.82	1.54	6.03	1.77	1.00	11.60	0.42	8.45	3.07
MTA1	1.00	0.97	0.01	1.04	0.27	1.00	0.85	0.02	1.05	0.24	1.00	1.02	0.02	1.04	0.10
MTA2	1.00	1.04	0.08	1.04	0.20	1.00	0.90	0.01	1.01	0.08	1.00	0.99	0.04	1.02	0.09
MTSS1	1.00	1.24	0.23	1.09	0.29	1.00	0.93	0.08	2.89	0.42	1.00	0.69	0.04	0.67	0.10
MYC	1.00	0.67	0.03	0.72	0.22	1.00	0.98	0.24	1.10	0.23	1.00	1.07	0.19	1.06	0.12
NCAM1	1.00	0.83	0.08	3.42	3.61	1.00	0.72	0.01	0.91	0.06	1.00	0.88	0.02	0.82	0.16
NF2	1.00	0.95	0.00	1.02	0.06	1.00	0.87	0.02	0.96	0.12	1.00	1.03	0.03	1.00	0.13
NME1	1.00	0.69	0.02	0.64	0.06	1.00	1.26	0.19	1.31	0.08	1.00	1.40	0.23	1.21	0.05
NR4A3	1.00	1.02	0.06	1.00	0.18	1.00	0.82	0.02	1.01	0.22	1.00	1.25	0.01	1.27	0.13
PECAM1	1.00	1.14	0.26	1.07	0.50	1.00	1.26	0.26	1.36	0.09	1.00	1.57	0.01	1.42	0.39
PNN	1.00	1.06	0.01	1.14	0.26	1.00	0.91	0.00	1.17	0.29	1.00	1.05	0.03	1.09	0.01

APPENDIX VIII – TaqMan Gene expression Array plate

PSCA	1.00	1.68	0.13	1.42	0.29	1.00	1.17	0.27	2.23	0.57	1.00	1.14	0.13	0.99	0.19
PTEN	1.00	1.04	0.00	1.00	0.04	1.00	0.96	0.05	0.91	0.11	1.00	1.18	0.06	1.15	0.11
PTGS2	1.00	0.46	0.00	0.45	0.20	1.00	0.96	0.24	1.54	0.02	1.00	1.11	0.16	1.06	0.05
RB1	1.00	0.96	0.04	1.07	0.13	1.00	0.85	0.01	0.90	0.12	1.00	1.07	0.09	1.11	0.12
RBL1	1.00	0.92	0.04	0.97	0.14	1.00	0.85	0.03	0.90	0.15	1.00	1.01	0.04	0.94	0.03
RBL2	1.00	0.98	0.03	1.00	0.10	1.00	0.89	0.09	0.93	0.05	1.00	1.04	0.00	1.05	0.05
RET	1.00	0.53	0.03	-	-	1.00	-	-	-	-	1.00	2.53	2.12	3.06	0.29
RHOC	1.00	1.17	0.06	1.05	0.12	1.00	0.97	0.09	1.37	0.21	1.00	1.06	0.00	0.88	0.08
S100A4	1.00	1.00	0.01	0.91	0.09	1.00	0.79	0.01	0.80	0.04	1.00	0.94	0.04	0.83	0.05
SERPINB5	-	-	-	-	-	1.00	1.09	0.15	1.47	0.19	-	-	-	-	-
SERPINE1	1.00	0.72	0.00	0.73	0.07	1.00	1.09	0.10	1.41	0.36	1.00	1.30	0.06	1.25	0.04
SET	1.00	0.91	0.10	0.85	0.14	1.00	1.08	0.23	0.96	0.05	1.00	0.87	0.01	0.79	0.08
SMAD2	1.00	0.99	0.08	0.95	0.08	1.00	0.90	0.06	0.98	0.09	1.00	0.94	0.00	1.14	0.23
SMAD4	1.00	1.16	0.10	1.24	0.40	1.00	0.72	0.06	0.84	0.07	1.00	0.98	0.02	1.07	0.12
SNCG	1.00	1.17	0.05	1.06	0.10	1.00	0.97	0.09	1.20	0.10	1.00	1.41	0.25	1.16	0.13
SSTR2	1.00	0.23	0.03	0.29	0.12	1.00	1.17	0.49	1.25	0.06	1.00	1.78	0.40	1.52	0.33
SYK	-	-	-	-	-	-	-	-	-	-	-	-	-	-	-
TCF20	1.00	1.04	0.06	1.04	0.21	1.00	0.78	0.07	0.94	0.21	1.00	0.97	0.02	0.91	0.13
TGFB1	1.00	1.08	0.02	1.18	0.22	1.00	1.00	0.09	1.38	0.48	1.00	1.51	0.06	1.57	0.28
TGFBR2	1.00	1.08	0.18	1.09	0.37	1.00	0.92	0.06	1.12	0.15	1.00	0.92	0.07	0.91	0.03
TIAM1	1.00	1.05	0.01	1.00	0.15	1.00	0.60	0.07	0.71	0.13	1.00	0.61	0.06	0.68	0.04
TIMP1	1.00	0.88	0.02	0.92	0.29	1.00	0.93	0.04	1.21	0.23	1.00	1.30	0.01	1.32	0.21
TIMP2	1.00	1.10	0.04	1.14	0.14	1.00	0.83	0.02	1.06	0.04	1.00	1.04	0.03	1.04	0.09
TIMP4	1.00	1.23	0.00	1.12	0.17	1.00	0.87	0.03	1.14	0.02	1.00	1.05	0.03	1.04	0.05
TMPRSS4	-	-	-	-	-	-	-	-	-	-	-	-	-	-	-
TNFSF10	1.00	1.08	0.17	1.03	0.38	1.00	1.14	0.10	1.34	0.24	1.00	3.62	1.89	2.24	0.74
TP53	1.00	1.07	0.02	1.10	0.13	1.00	0.84	0.04	0.98	0.12	1.00	1.04	0.05	1.07	0.15
TPBG	1.00	1.06	0.13	1.17	0.49	1.00	1.45	0.29	1.64	0.33	1.00	2.17	0.59	1.65	0.53
TSHR	1.00	1.12	0.17	1.05	0.06	1.00	0.75	0.01	1.10	0.17	1.00	0.73	0.14	0.50	0.06
TWIST1	1.00	0.98	0.05	0.95	0.04	1.00	-	-	-	-	1.00	0.21	0.01	-	-
VEGFA	1.00	0.91	0.16	0.90	0.39	1.00	0.80	0.01	1.07	0.11	1.00	0.94	0.04	0.85	0.09
VEGFC	1.00	0.98	0.01	1.10	0.30	1.00	1.01	0.23	1.23	0.37	1.00	1.34	0.16	0.91	0.42

APPENDIX VIII – TaqMan Gene expression Array plate

WISP1	1.00	2.57	0.60	2.61	0.09	1.00	1.15	0.00	1.55	0.30	1.00	1.14	0.05	1.08	0.12
-------	------	------	------	------	------	------	------	------	------	------	------	------	------	------	------

Supplementary table VIII.4 – TaqMan Array – Human Immune Response details and nomenclature.

TaqMan Array – Human Immune Response (#4418718)			
Gene Symbol	Category	Group	Gene Name
18S	Molecular function unclassified	Molecular function unclassified	Eukaryotic 18S rRNA
GAPDH	Oxidoreductase	Dehydrogenase	glyceraldehyde-3-phosphate dehydrogenase
HPRT1	Transferase	Glycosyltransferase	hypoxanthine phosphoribosyltransferase 1
GUSB	Hydrolase	Galactosidase	glucuronidase, beta
IL1A	Signalling molecule	Cytokine	interleukin 1, alpha
IL1B	Signalling molecule	Cytokine	interleukin 1, beta
IL2	Signalling molecule	Cytokine	interleukin 2
IL3	Signalling molecule	Cytokine	interleukin 3 (colony-stimulating factor, multiple)
IL4	Signalling molecule	Cytokine	interleukin 4
IL5	Signalling molecule	Cytokine	interleukin 5 (colony-stimulating factor, eosinophil)
IL6	Signalling molecule	Cytokine	interleukin 6 (interferon, beta 2)
IL7	Signalling molecule	Cytokine	interleukin 7
IL8	Signalling molecule	Chemokine	interleukin 8
IL9	Signalling molecule	Cytokine	interleukin 9
IL10	Signalling molecule	Cytokine	interleukin 10
IL12A	Signalling molecule	Cytokine	interleukin 12A (natural killer cell stimulatory factor 1, cytotoxic lymphocyte maturation factor 1, p35)
IL12B	Signalling molecule	Cytokine	interleukin 12B (natural killer cell stimulatory factor 2, cytotoxic lymphocyte maturation factor 2, p40)
IL13	Signalling molecule	Cytokine	interleukin 13
IL15	Signalling molecule	Cytokine	interleukin 15
IL17A	Signalling molecule	Cytokine	interleukin 17A
IL18	Signalling molecule	Cytokine	interleukin 18 (interferon-gamma-inducing factor)
CCL3	Signalling molecule	Chemokine	chemokine (C-C motif) ligand 3
CCL19	Signalling molecule	Chemokine	chemokine (C-C motif) ligand 19
CCL2	Signalling molecule	Chemokine	chemokine (C-C motif) ligand 2
CCL5	Signalling molecule	Chemokine	chemokine (C-C motif) ligand 5
CCR2	Receptor	G-protein coupled receptor	chemokine (C-C motif) receptor 2
CCR4	Receptor	G-protein coupled receptor	chemokine (C-C motif) receptor 4

APPENDIX VIII – TaqMan Gene expression Array plate

CCR5	Receptor	G-protein coupled receptor	chemokine (C-C motif) receptor 5
CCR7	Receptor	G-protein coupled receptor	chemokine (C-C motif) receptor 7
CXCR3	Receptor	G-protein coupled receptor	chemokine (C-X-C motif) receptor 3
CXCL10	Signalling molecule	Chemokine	chemokine (C-X-C motif) ligand 10
CXCL11	Signalling molecule	Cytokine	chemokine (C-X-C motif) ligand 11
CSF1	Signalling molecule	Cytokine	colony stimulating factor 1 (macrophage)
CSF2	Signalling molecule	Cytokine	colony stimulating factor 2 (granulocyte-macrophage)
CSF3	Signalling molecule	Cytokine	colony stimulating factor 3 (granulocyte)
STAT3	Transcription factor	Other transcription factor	signal transducer and activator of transcription 3 (acute-phase response factor)
NFKB2	Transcription factor	Other transcription factor	nuclear factor of kappa light polypeptide gene enhancer in B-cells 2 (p49/p100)
IKBKB	Kinase	Protein kinase	inhibitor of kappa light polypeptide gene enhancer in B-cells, kinase beta
CD3E	Defence/immunity protein	Immunoglobulin receptor family member	CD3e molecule, epsilon (CD3-TCR complex)
CD4	Defence/immunity protein	Immunoglobulin receptor family member	CD4 molecule
CD8A	Defence/immunity protein	Immunoglobulin receptor family member	CD8a molecule
CD19	Defence/immunity protein	Immunoglobulin receptor family member	CD19 molecule
IL2RA	Receptor	Cytokine receptor	interleukin 2 receptor, alpha
CD28	Defence/immunity protein	Immunoglobulin receptor family member	CD28 molecule
CD38	Hydrolase	Glycosidase	CD38 molecule
CD40	Receptor	Cytokine receptor	CD40 molecule, TNF receptor superfamily member 5
PTPRC	Receptor	Other receptor	protein tyrosine phosphatase, receptor type, C
CD68	Molecular function unclassified	Molecular function unclassified	CD68 molecule
CD80	Signalling molecule	Membrane-bound signalling molecule	CD80 molecule
CD86	Signalling molecule	Membrane-bound signalling molecule	CD86 molecule
CTLA4	Signalling molecule	Cytokine	cytotoxic T-lymphocyte-associated protein 4
CD40LG	Signalling molecule	Cytokine	CD40 ligand

APPENDIX VIII – TaqMan Gene expression Array plate

HLA-DRA	Defence/immunity protein	Major histocompatibility complex antigen	major histocompatibility complex, class II, DR alpha
HLA-DRB1	Molecular function unclassified	Molecular function unclassified	major histocompatibility complex, class II, DR beta 1
TBX21	Transcription factor	Other transcription factor	T-box 21
TNFRSF18	Receptor	Receptor	tumour necrosis factor receptor superfamily, member 18
ICOS	Defence/immunity protein	Immunoglobulin receptor family member	inducible T-cell co-stimulator
NOS2	Synthase and synthetase	Synthase	nitric oxide synthase 2, inducible
BCL2	Miscellaneous function	Other miscellaneous function protein	B-cell CLL/lymphoma 2
BCL2L1	Miscellaneous function	Other miscellaneous function protein	BCL2-like 1
BAX	Miscellaneous function	Other miscellaneous function protein	BCL2-associated X protein
ICAM1	Cell adhesion molecule	Cam family adhesion molecule	intercellular adhesion molecule 1
SELP	Cell adhesion molecule	Other cell adhesion molecule	selectin P (granule membrane protein 140kDa, antigen CD62)
SELE	Cell adhesion molecule	Other cell adhesion molecule	selectin E
HMOX1	Oxidoreductase	Oxygenase	heme oxygenase (decycling) 1
PTGS2	Synthase and synthetase	Synthase	prostaglandin-endoperoxide synthase 2 (prostaglandin G/H synthase and cyclooxygenase)
LRP2	Molecular function unclassified	Molecular function unclassified	low density lipoprotein-related protein 2
CYP1A2	Oxidoreductase	Oxygenase	cytochrome P450, family 1, subfamily A, polypeptide 2
CYP7A1	Oxidoreductase	Oxygenase	cytochrome P450, family 7, subfamily A, polypeptide 1
IFNG	Signalling molecule	Cytokine	interferon, gamma
PRF1	Defence/immunity protein	Other defence and immunity protein	perforin 1 (pore forming protein)
GZMB	Protease	Serine protease	granzyme B (granzyme 2, cytotoxic T-lymphocyte-associated serine esterase 1)
GNLY	Defence/immunity protein	Antibacterial response protein	granulysin
FAS	Receptor	Cytokine receptor	Fas (TNF receptor superfamily, member 6)
FASLG	Signalling molecule	Cytokine	Fas ligand (TNF superfamily, member 6)
TGFB1	Signalling molecule	Cytokine	transforming growth factor, beta 1
SMAD3	Transcription factor	Other transcription factor	SMAD family member 3
SMAD7	Transcription factor	Other transcription factor	SMAD family member 7

APPENDIX VIII – TaqMan Gene expression Array plate

SKI	Transcription factor	Other transcription factor	v-ski sarcoma viral oncogene homolog (avian)
FN1	Extracellular matrix	Extracellular matrix linker protein	fibronectin 1
C3	Select regulatory molecule	Protease inhibitor	complement component 3
TNF	Signalling molecule	Cytokine	tumour necrosis factor (TNF superfamily, member 2)
LTA	Signalling molecule	Cytokine	lymphotoxin alpha (TNF superfamily, member 1)
ACE	Protease	Metalloprotease	angiotensin I converting enzyme (peptidyl-dipeptidase A) 1
VEGFA	Signalling molecule	Growth factor	vascular endothelial growth factor A
CD34	Cell adhesion molecule	Cell adhesion molecule	CD34 molecule
AGTR1	Receptor	G-protein coupled receptor	angiotensin II receptor, type 1
AGTR2	Receptor	G-protein coupled receptor	angiotensin II receptor, type 2
EDN1	Signalling molecule	Peptide hormone	endothelin 1
LIF	Signalling molecule	Cytokine	leukaemia inhibitory factor (cholinergic differentiation factor)
LY96	Miscellaneous function	Transmembrane receptor regulatory/adaptor protein	lymphocyte antigen 96
MIF	Signalling molecule	Cytokine	macrophage migration inhibitory factor (glycosylation-inhibiting factor)
NFATC3	Transcription factor	Other transcription factor	nuclear factor of activated T-cells, cytoplasmic, calcineurin-dependent 3
NFATC4	Transcription factor	Other transcription factor	nuclear factor of activated T-cells, cytoplasmic, calcineurin-dependent 4
PF4	Signalling molecule	Chemokine	platelet factor 4
SYK	Kinase	Protein kinase	spleen tyrosine kinase

Supplementary table VIII.5 – TaqMan Array – Human Tumour Metastasis details and nomenclature.

TaqMan Array – Human tumour metastasis (#4418743)			
Gene Symbol	Category	Group	Gene Name
18S	Molecular function unclassified	Molecular function unclassified	Eukaryotic 18S rRNA
GAPDH	Oxidoreductase	Dehydrogenase	glyceraldehyde-3-phosphate dehydrogenase
HPRT1	Transferase	Glycosyltransferase	hypoxanthine phosphoribosyltransferase 1
GUSB	Hydrolase	Galactosidase	glucuronidase, beta
APC	Cytoskeletal protein	Microtubule family cytoskeletal protein	adenomatous polyposis coli
BRMS1	Molecular function unclassified	Molecular function unclassified	breast cancer metastasis suppressor 1
CASP8	Protease	Cysteine protease	caspase 8, apoptosis-related cysteine peptidase
CCL7	Signalling molecule	Chemokine	chemokine (C-C motif) ligand 7
CD44	Receptor	Receptor	CD44 molecule (Indian blood group)
CD82	Signalling molecule	Membrane-bound signalling molecule	CD82 molecule
CDH1	Cell adhesion molecule	Cadherin	cadherin 1, type 1, E-cadherin (epithelial)
CDKN2A	Select regulatory molecule	Select regulatory molecule	cyclin-dependent kinase inhibitor 2A (melanoma, p16, inhibits CDK4)
CEACAM1	Cell adhesion molecule	Cam family adhesion molecule	carcinoembryonic antigen-related cell adhesion molecule 1 (biliary glycoprotein)
CTBP1	Transcription factor	Transcription cofactor	C-terminal binding protein 1
CTNNA1	Cytoskeletal protein	Actin family cytoskeletal protein	catenin (cadherin-associated protein), alpha 1, 102kDa
CTSK	Protease	Cysteine protease	cathepsin K
CXCL12	Signalling molecule	Growth factor	chemokine (C-X-C motif) ligand 12 (stromal cell-derived factor 1)
CXCR4	Receptor	G-protein coupled receptor	chemokine (C-X-C motif) receptor 4
DAPK1	Kinase	Protein kinase	death-associated protein kinase 1
DCC	Receptor	Other receptor	deleted in colorectal carcinoma
EPHB2	Receptor	Protein kinase receptor	EPH receptor B2
ERBB2	Receptor	Protein kinase receptor	v-erb-b2 erythroblastic leukaemia viral oncogene homolog 2, neuro/glioblastoma derived oncogene homolog (avian)
ETV4	Transcription factor	Other transcription factor	ets variant 4
FAT1	Cell adhesion molecule	Cadherin	FAT tumour suppressor homolog 1 (Drosophila)

APPENDIX VIII – TaqMan Gene expression Array plate

FGF2	Signalling molecule	Growth factor	fibroblast growth factor 2 (basic)
FGFR4	Receptor	Protein kinase receptor	fibroblast growth factor receptor 4
FN1	Extracellular matrix	Extracellular matrix linker protein	fibronectin 1
FXYD5	Ion channel	Ion channel	FXYD domain containing ion transport regulator 5
GNRH1	Signalling molecule	Peptide hormone	gonadotropin-releasing hormone 1 (luteinizing-releasing hormone)
HGF	Receptor	Protein kinase receptor	hepatocyte growth factor (hepapoietin A; scatter factor)
HPSE	Hydrolase	Glycosidase	heparanase
HRAS	Select regulatory molecule	G-protein	v-Ha-ras Harvey rat sarcoma viral oncogene homolog
HTATIP2	Kinase	Protein kinase	HIV-1 Tat interactive protein 2, 30kDa
IGF1	Signalling molecule	Growth factor	insulin-like growth factor 1 (somatomedin C)
IL18	Signalling molecule	Cytokine	interleukin 18 (interferon-gamma-inducing factor)
IL1B	Signalling molecule	Cytokine	interleukin 1, beta
ITGB3	Extracellular matrix	Extracellular matrix glycoprotein	integrin, beta 3 (platelet glycoprotein IIIa, antigen CD61)
KISS1	Molecular function unclassified	Molecular function unclassified	KiSS-1 metastasis-suppressor
KISS1R	Receptor	G-protein coupled receptor	KISS1 receptor
KRAS	Select regulatory molecule	G-protein	v-Ki-ras2 Kirsten rat sarcoma viral oncogene homolog
LAMB1	Extracellular matrix	Extracellular matrix linker protein	laminin, beta 1
LYPD3	Molecular function unclassified	Molecular function unclassified	LY6/PLAUR domain containing 3
MCAM	Cell adhesion molecule	Cam family adhesion molecule	melanoma cell adhesion molecule
MET	Receptor	Protein kinase receptor	met proto-oncogene (hepatocyte growth factor receptor)
MGAT5	Transferase	Glycosyltransferase	mannosyl (alpha-1,6-)-glycoprotein beta-1,6-N-acetyl-glucosaminyltransferase
MMP1	Protease	Metalloprotease	matrix metalloproteinase 1 (interstitial collagenase)
MMP10	Protease	Metalloprotease	matrix metalloproteinase 10 (stromelysin 2)
MMP14	Protease	Metalloprotease	matrix metalloproteinase 14 (membrane-inserted)
MMP2	Protease	Metalloprotease	matrix metalloproteinase 2 (gelatinase A, 72kDa gelatinase, 72kDa type IV collagenase)
MMP3	Protease	Metalloprotease	matrix metalloproteinase 3 (stromelysin 1, progelatinase)
MMP7	Protease	Metalloprotease	matrix metalloproteinase 7 (matrilysin, uterine)

APPENDIX VIII – TaqMan Gene expression Array plate

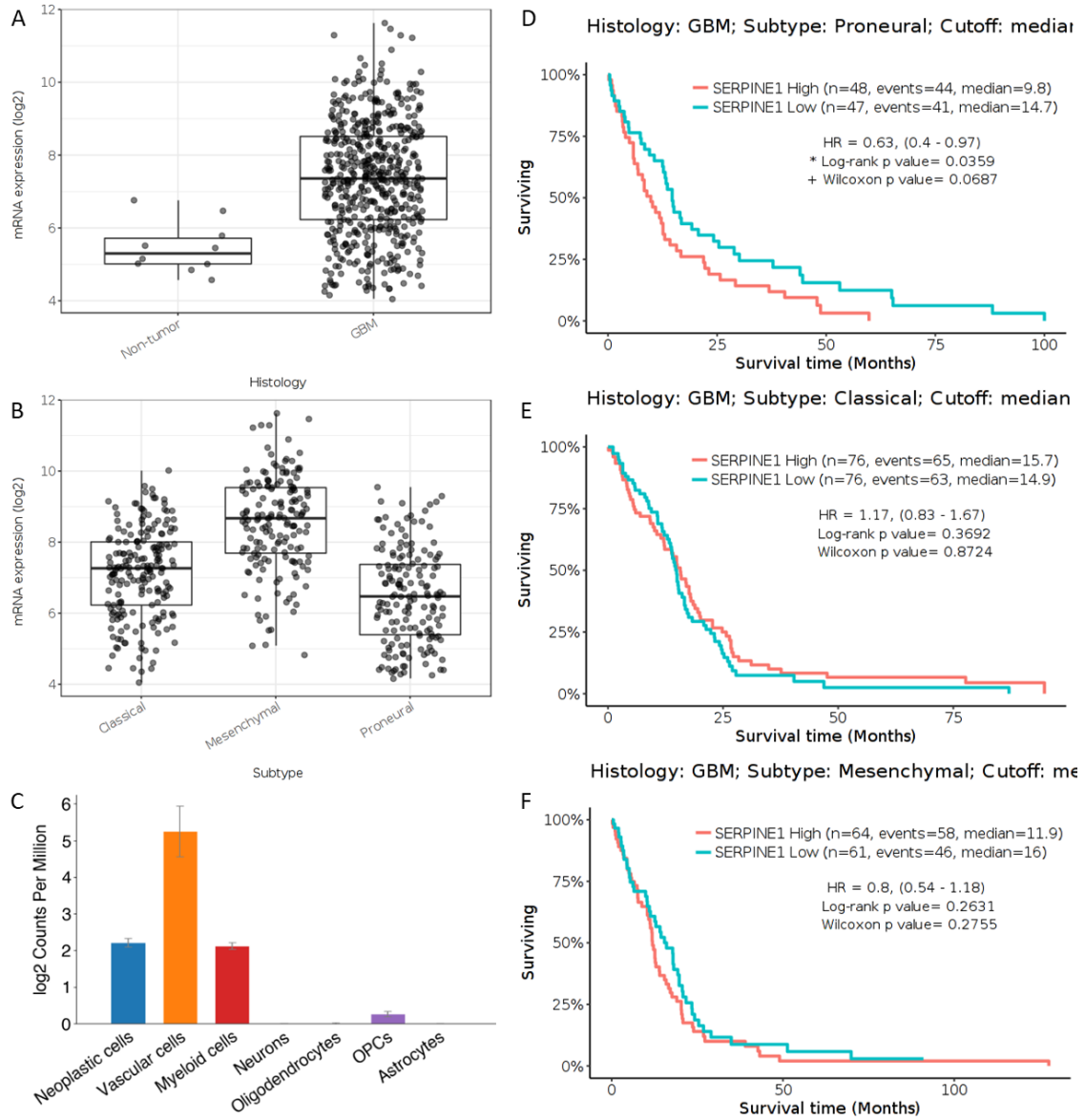
MMP9	Protease	Metalloprotease	matrix metalloproteinase 9 (gelatinase B, 92kDa gelatinase, 92kDa type IV collagenase)
MTA1	Molecular function unclassified	Molecular function unclassified	metastasis associated 1
MTA2	Transcription factor	Zinc finger transcription factor	metastasis associated 1 family, member 2
MTSS1	Molecular function unclassified	Molecular function unclassified	metastasis suppressor 1
MYC	Transcription factor	Basic helix-loop-helix transcription factor	v-myc myelocytomatosis viral oncogene homolog (avian)
NCAM1	Cell adhesion molecule	Cam family adhesion molecule	neural cell adhesion molecule 1
NF2	Cytoskeletal protein	Other cytoskeletal proteins	neurofibromin 2 (merlin)
NME1	Kinase	Nucleotide kinase	non-metastatic cells 1, protein (NM23A) expressed in
NR4A3	Transcription factor	Nuclear hormone receptor	nuclear receptor subfamily 4, group A, member 3
PECAM1	Cell adhesion molecule	Other cell adhesion molecule	platelet/endothelial cell adhesion molecule
PNN	Miscellaneous function	Miscellaneous function	pinin, desmosome associated protein
PSCA	Molecular function unclassified	Molecular function unclassified	prostate stem cell antigen
PTEN	Phosphatase	Protein phosphatase	phosphatase and tensin homolog
PTGS2	Synthase and synthetase	Synthase	prostaglandin-endoperoxide synthase 2 (prostaglandin G/H synthase and cyclooxygenase)
RB1	Transcription factor	Other transcription factor	retinoblastoma 1
RBL1	Transcription factor	Other transcription factor	retinoblastoma-like 1 (p107)
RBL2	Transcription factor	Other transcription factor	retinoblastoma-like 2 (p130)
RET	Receptor	Protein kinase receptor	ret proto-oncogene
RHOC	Select regulatory molecule	G-protein	ras homolog gene family, member C
S100A4	Select calcium binding protein	Calmodulin related protein	S100 calcium binding protein A4
SERPINB5	Select regulatory molecule	Protease inhibitor	serpin peptidase inhibitor, clade B (ovalbumin), member 5
SERPINE1	Select regulatory molecule	Protease inhibitor	serpin peptidase inhibitor, clade E (nexin, plasminogen activator inhibitor type 1), member 1
SET	Select regulatory molecule	Phosphatase modulator	SET nuclear oncogene
SMAD2	Transcription factor	Other transcription factor	SMAD family member 2
SMAD4	Transcription factor	Other transcription factor	SMAD family member 4
SNCG	Miscellaneous function	Other miscellaneous function protein	synuclein, gamma (breast cancer-specific protein 1)

APPENDIX VIII – TaqMan Gene expression Array plate

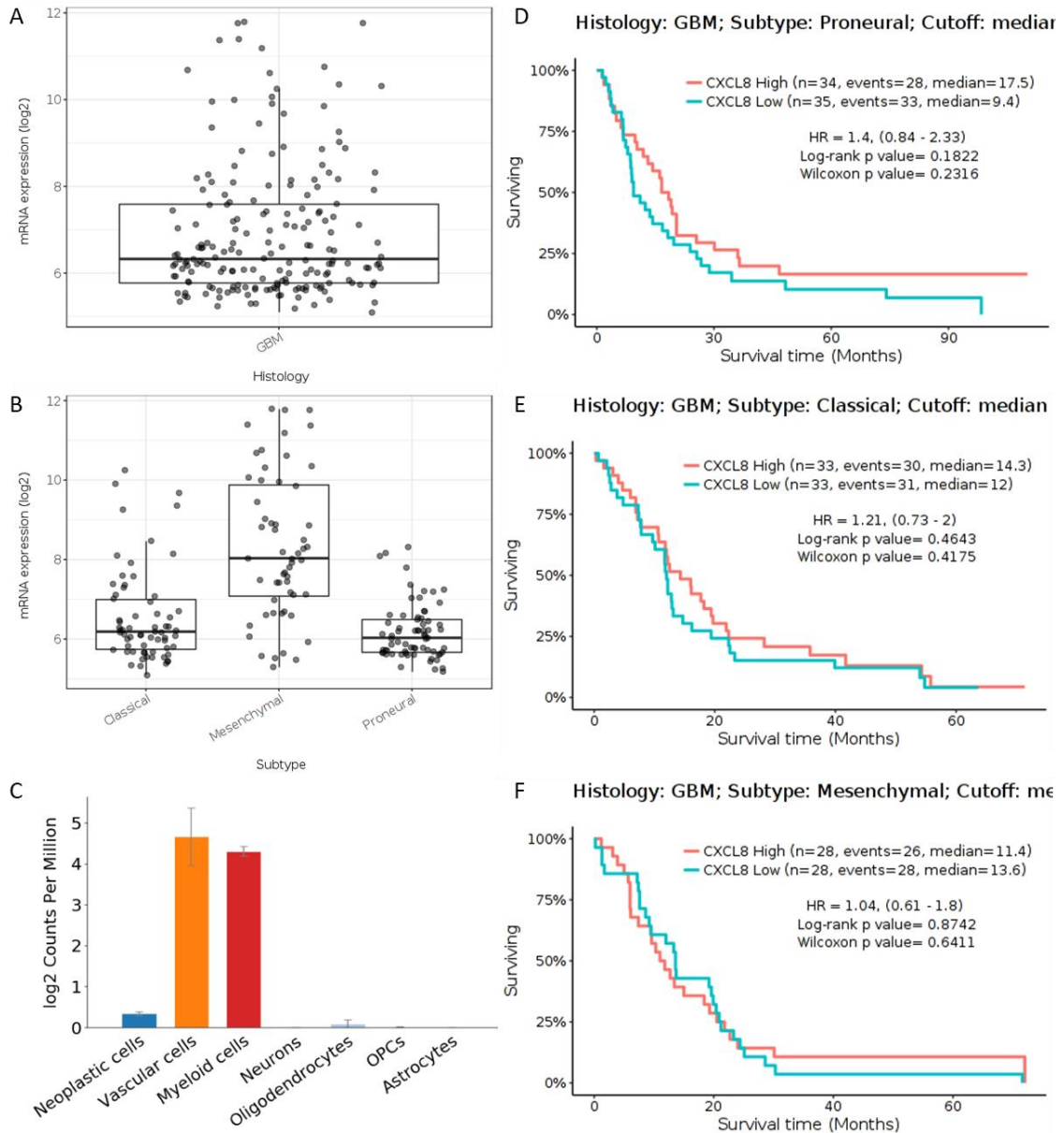
SSTR2	Receptor	G-protein coupled receptor	somatostatin receptor 2
SYK	Kinase	Protein kinase	spleen tyrosine kinase
EPCAM	Signalling molecule	Membrane-bound signalling molecule	epithelial cell adhesion molecule
TCF20	Molecular function unclassified	Molecular function unclassified	transcription factor 20 (AR1)
TGFB1	Signalling molecule	Cytokine	transforming growth factor, beta 1
TGFB2	Receptor	Cytokine receptor	transforming growth factor, beta receptor II (70/80kDa)
TIAM1	Select regulatory molecule	G-protein modulator	T-cell lymphoma invasion and metastasis 1
TIMP1	Select regulatory molecule	Protease inhibitor	TIMP metalloproteinase inhibitor 1
TIMP2	Select regulatory molecule	Protease inhibitor	TIMP metalloproteinase inhibitor 2
TIMP4	Select regulatory molecule	Protease inhibitor	TIMP metalloproteinase inhibitor 4
TMPRSS4	Protease	Serine protease	transmembrane protease, serine 4
TNFSF10	Signalling molecule	Cytokine	tumour necrosis factor (ligand) superfamily, member 10
TP53	Transcription factor	Other transcription factor	tumour protein p53
TPBG	Molecular function unclassified	Molecular function unclassified	trophoblast glycoprotein
TSHR	Receptor	G-protein coupled receptor	thyroid stimulating hormone receptor
TWIST1	Transcription factor	Basic helix-loop-helix transcription factor	twist homolog 1 (Drosophila)
VEGFA	Signalling molecule	Growth factor	vascular endothelial growth factor A
VEGFC	Signalling molecule	Growth factor	vascular endothelial growth factor C
WISP1	Signalling molecule	Growth factor	WNT1 inducible signalling pathway protein 1

APPENDIX IX – OTHER GBM DATABASES

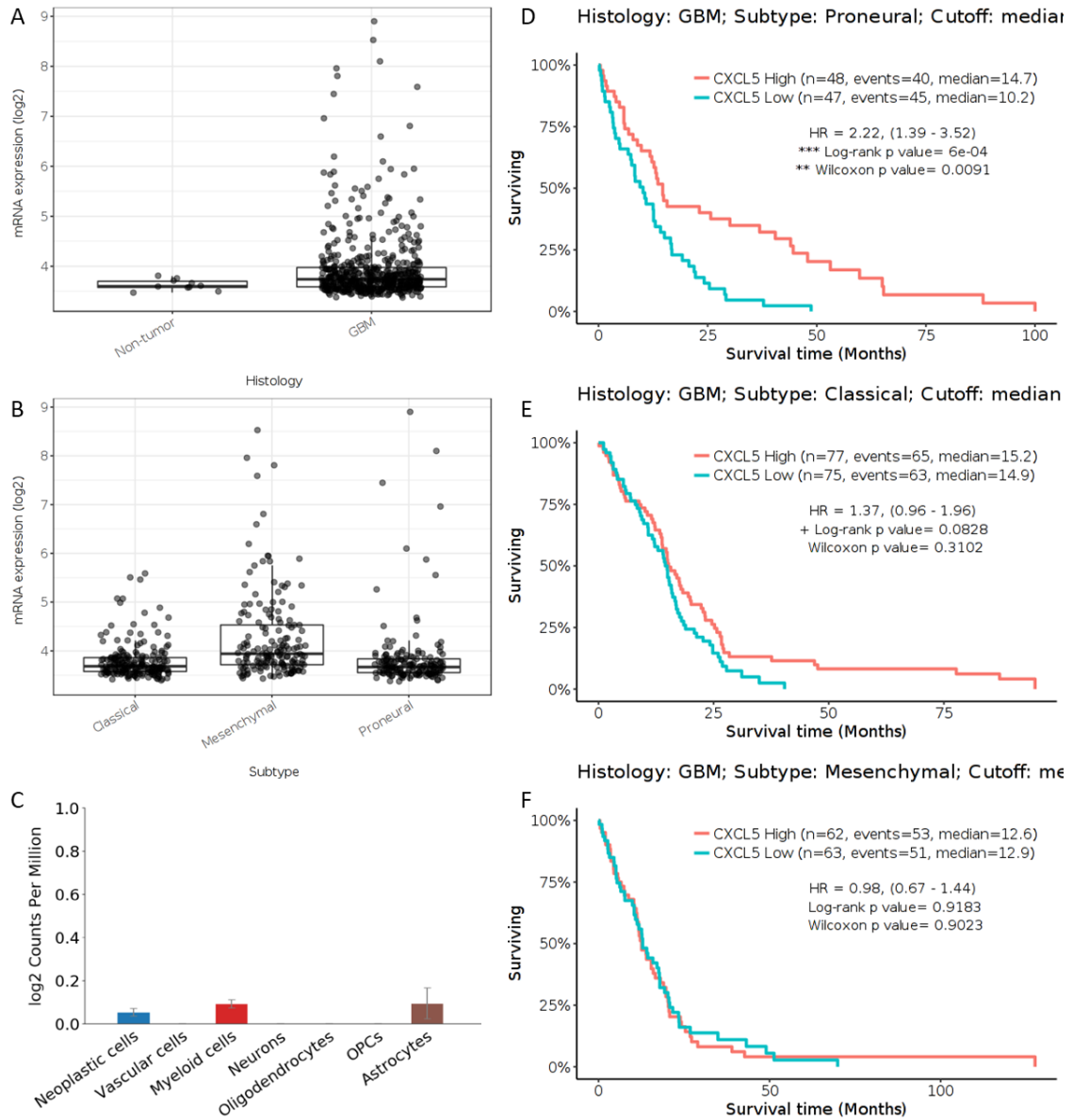
The relevant data explored from other data bases useful for discussion will be illustrated in this section.



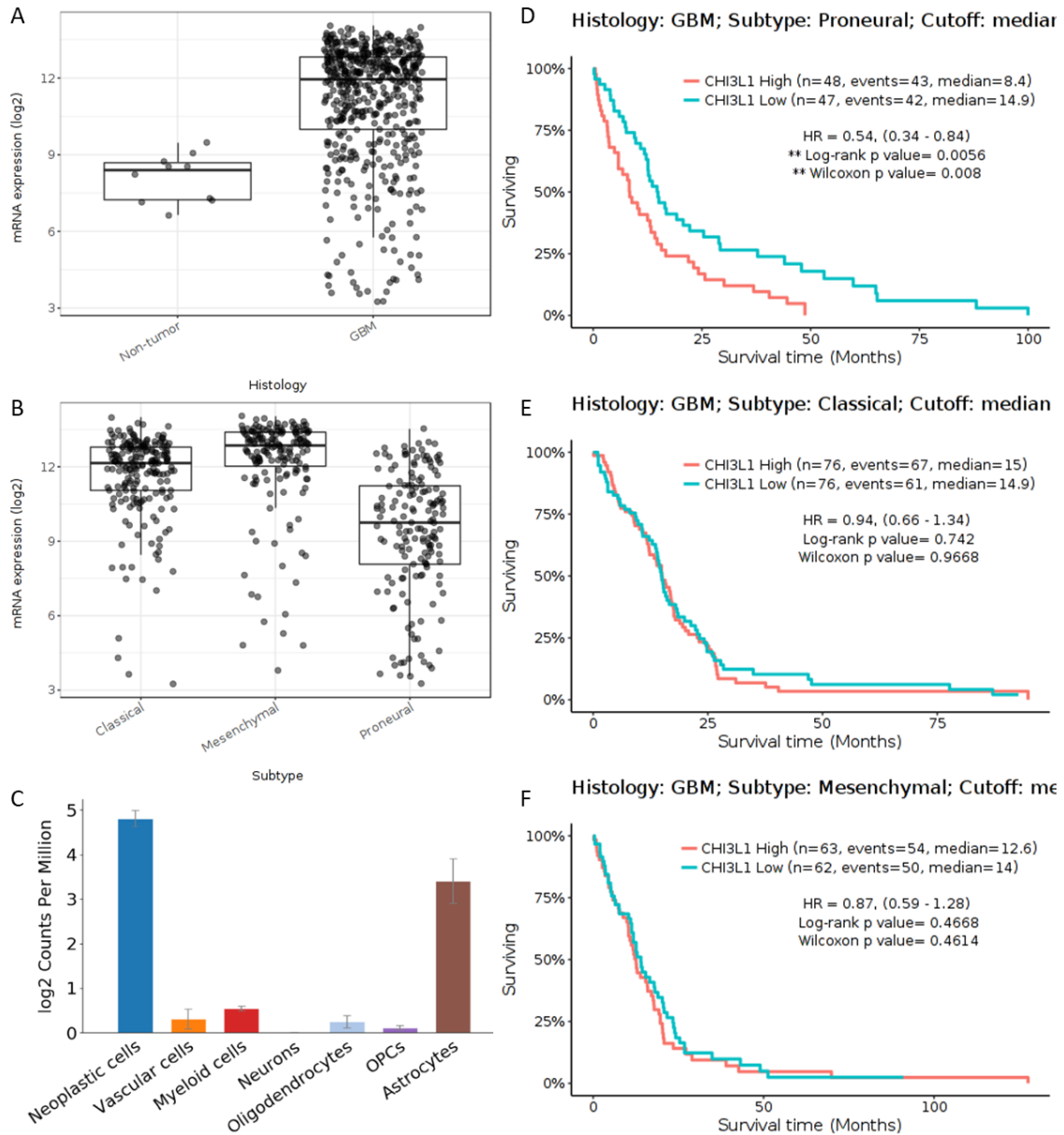
Supplementary figure IX. 1 – SERPINE1 impact on primary GBM. mRNA expression according to histology (A), tumour subtype (B) and from each cell (C-scRNA-seq (Darmanis et al. 2017)). Kaplan-Meier survival plot according to tumour subtype: Proneural (D), Classical (E) and Mesenchymal (F). Data from A, B, D, E and F extracted from GlioVis TCGA_GBM data base (Bowman et al. 2017).



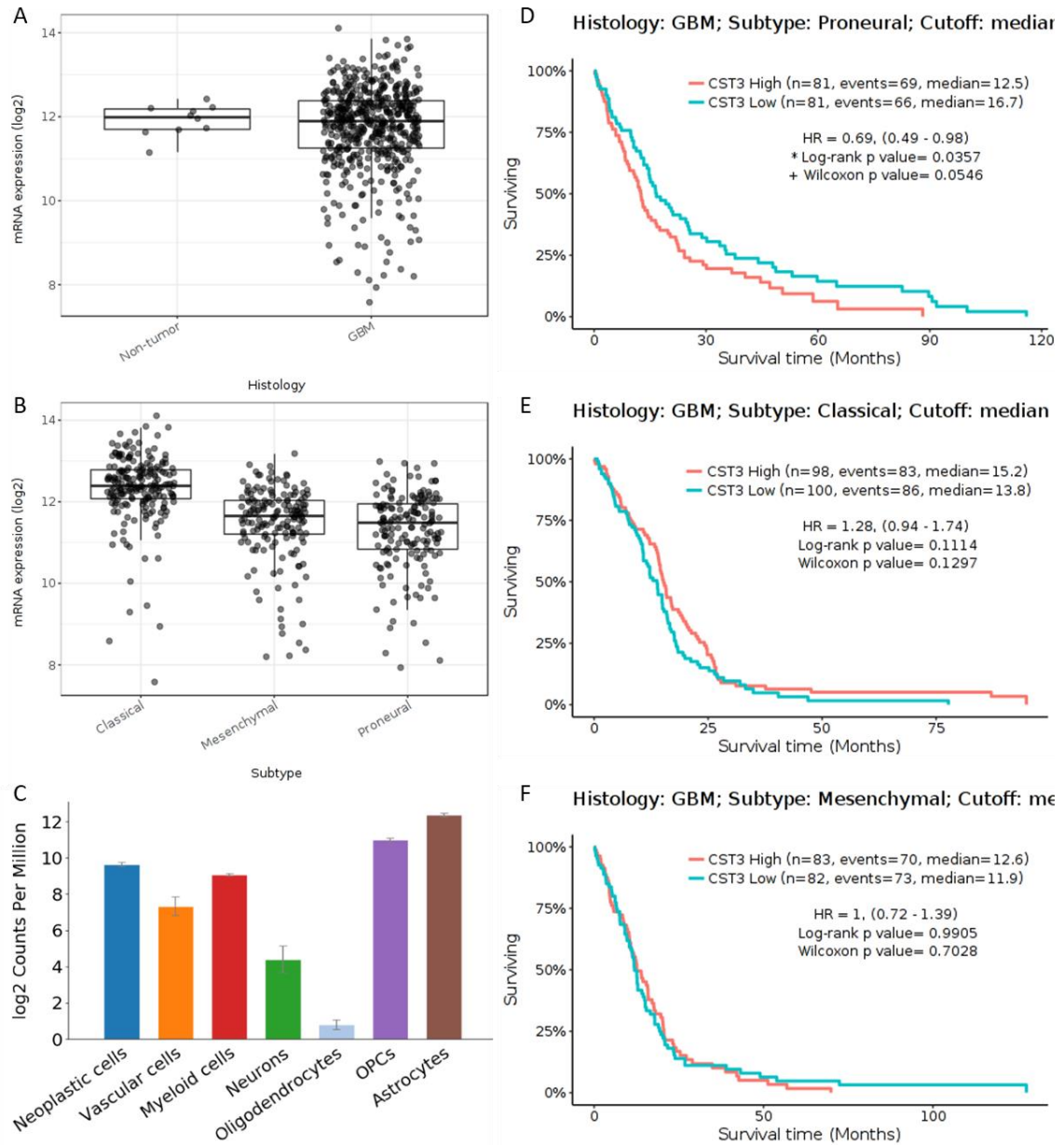
Supplementary figure IX. 2 – CXCL8 (IL8) impact on primary GBM. mRNA expression according to histology (A), tumour subtype (B) and from each cell (C-scrNA-seq (Darmanis et al. 2017)). Kaplan-Meier survival plot according to tumour subtype: Proneural (D), Classical (E) and Mesenchymal (F). Data from A, B, D, E and F extracted from GlioVis LeeY data base (Bowman et al. 2017). NOTE: TCGA_GBМ database did not include CXCL8 analysis.



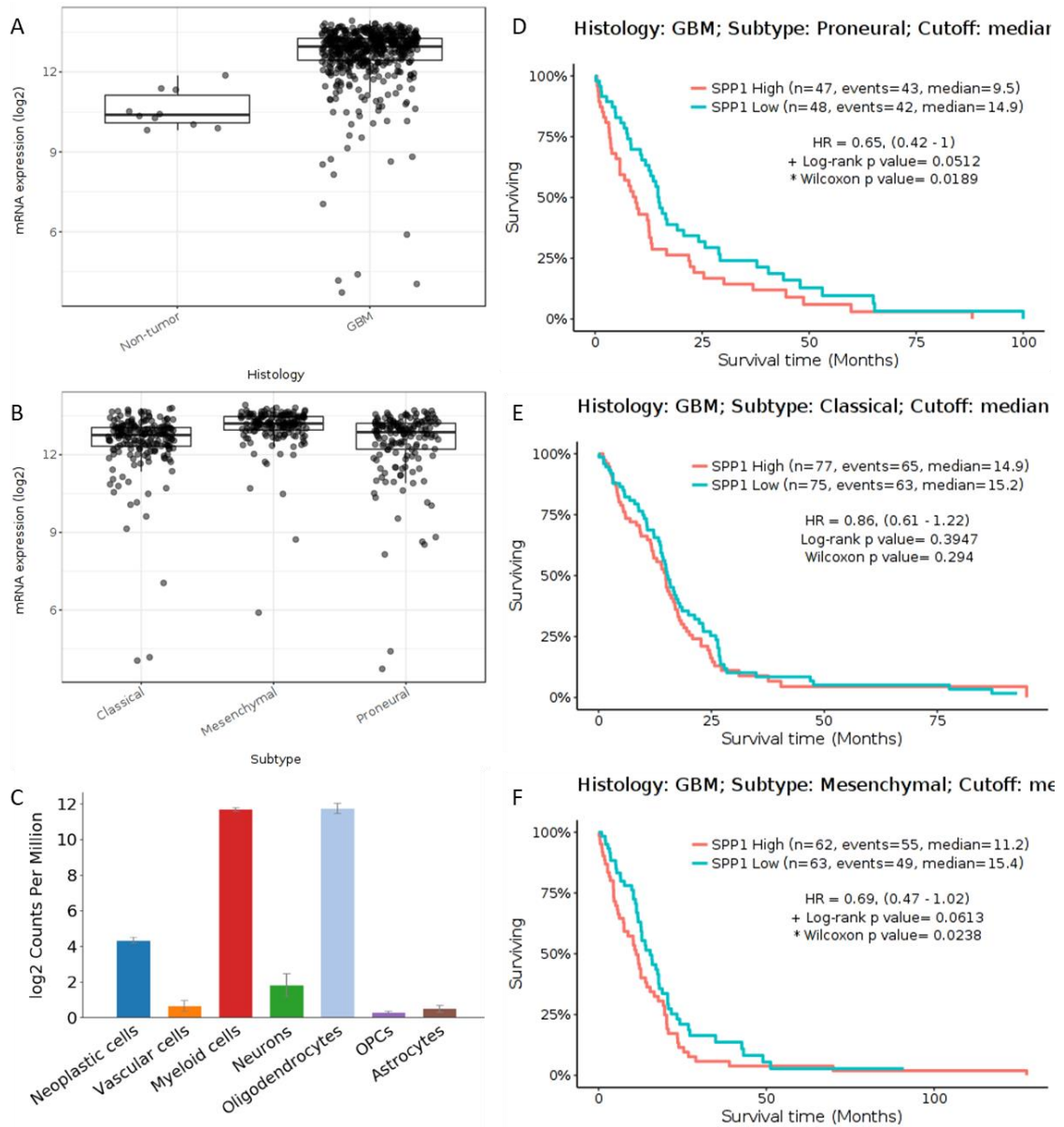
Supplementary figure IX. 3 – CXCL5 (ENA-78) impact on primary GBM. mRNA expression according to histology (A), tumour subtype (B) and from each cell (C-scRNA-seq (Darmanis et al. 2017)). Kaplan-Meier survival plot according to tumour subtype: Proneural (D), Classical (E) and Mesenchymal (F). Data from A, B, D, E and F extracted from *GlioVis* TCGA_GBMs data base (Bowman et al. 2017).



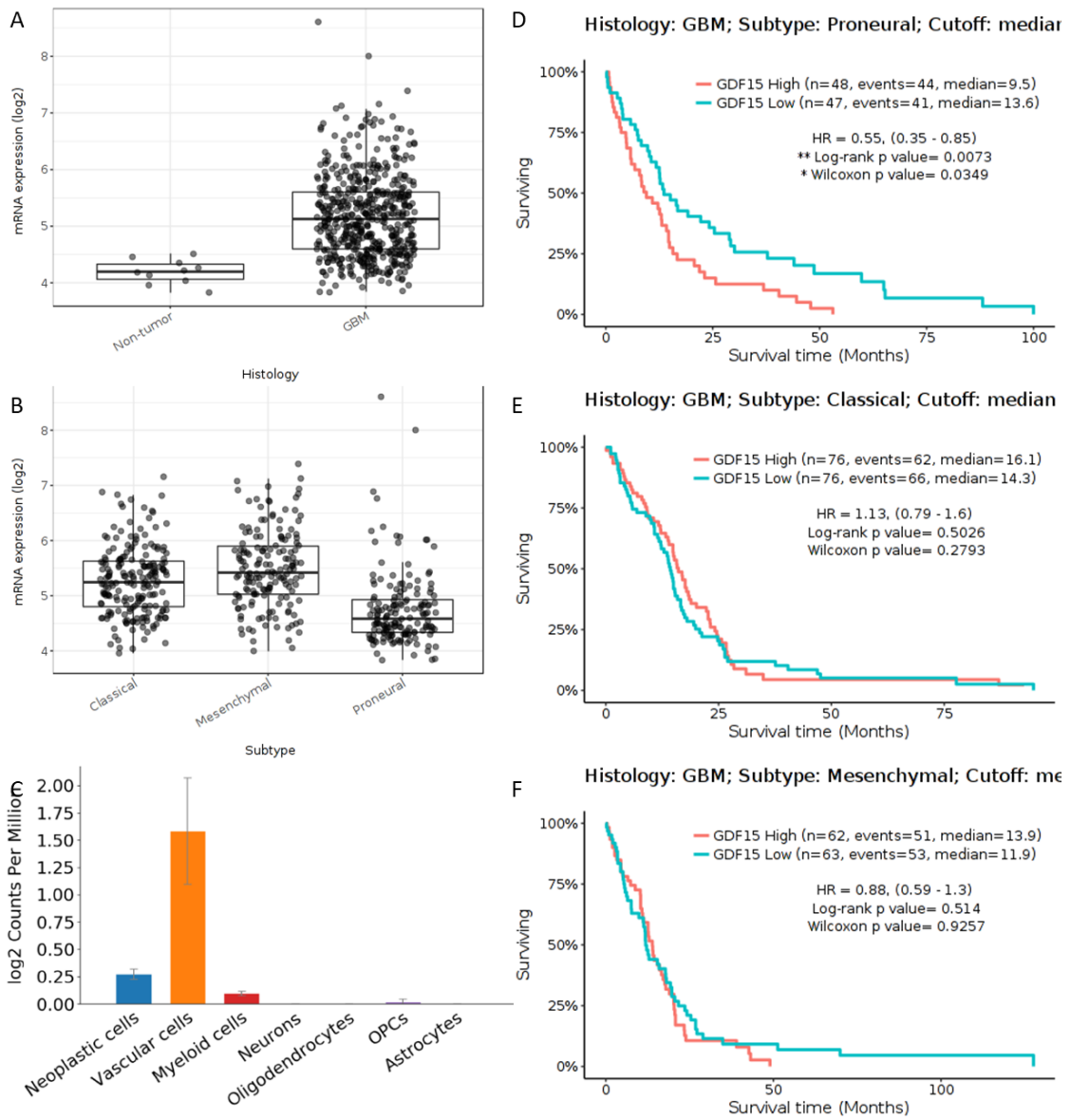
Supplementary figure IX. 4 – CHI3L1 impact on primary GBM. mRNA expression according to histology (A), tumour subtype (B) and from each cell (C-scrRNA-seq (Darmanis et al. 2017)). Kaplan-Meier survival plot according to tumour subtype: Proneural (D), Classical (E) and Mesenchymal (F). Data from A, B, D, E and F extracted from Gliovis TCGA_GBM data base (Bowman et al. 2017).



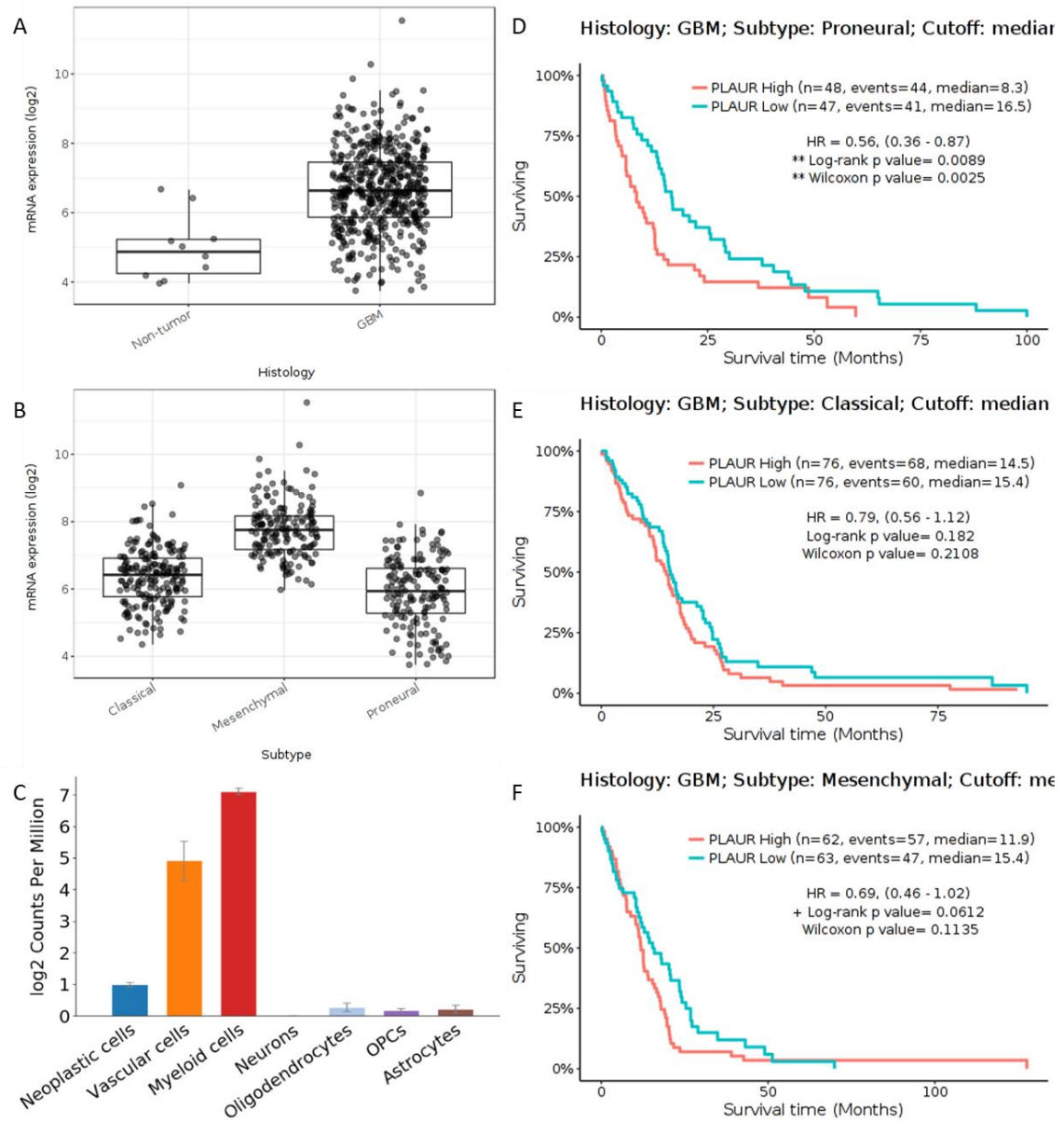
Supplementary figure IX. 5 – CST3 (Cystatin C) impact on primary GBM. mRNA expression according to histology (A), tumour subtype (B) and from each cell (C-scrNA-seq (Darmanis et al. 2017)). Kaplan-Meier survival plot according to tumour subtype: Proneural (D), Classical (E) and Mesenchymal (F). Data from A, B, D, E and F extracted from *GlioVis* TCGA_GBM data base (Bowman et al. 2017).



Supplementary figure IX. 6 – SPP1 (OPN) impact on primary GBM. mRNA expression according to histology (A), tumour subtype (B) and from each cell (C-scrRNA-seq (Darmanis et al. 2017)). Kaplan-Meier survival plot according to tumour subtype: Proneural (D), Classical (E) and Mesenchymal (F). Data from A, B, D, E and F extracted from Gliovis TCGA_GBM data base (Bowman et al. 2017).



Supplementary figure IX. 7 – GDF-15 impact on primary GBM. mRNA expression according to histology (A), tumour subtype (B) and from each cell (C-scrRNA-seq (Darmanis et al. 2017)). Kaplan-Meier survival plot according to tumour subtype: Proneural (D), Classical (E) and Mesenchymal (F). Data from A, B, D, E and F extracted from GlioVis TCGA_GBM data base (Bowman et al. 2017).



Supplementary figure IX. 8 – PLAUR (uPAR) impact on primary GBM. mRNA expression according to histology (A), tumour subtype (B) and from each cell (C-scrRNA-seq (Darmanis et al. 2017)). Kaplan-Meier survival plot according to tumour subtype: Proneural (D), Classical (E) and Mesenchymal (F). Data from A, B, D, E and F extracted from Gliovis TCGA_GBM data base (Bowman et al. 2017).

APPENDIX X– COPYRIGHT PERMISSIONS

Figure	Journal	Paper	Licence number
Figure 1.1	CA Cancer J Clin	(Meir et al. 2010)	4863310212110
Figure 1.2	Oxford University Press	(Godlewski et al. 2015)	4791880310492
Figure 1.4	Psychopharmacology	(Crews and Vetreno 2016)	¹
Figure 1.5	Nature neuroscience	(Río-Hortega 1993)	4795870336741
Figure 1.6	Nature Reviews Molecular Cell Biology	(Parton and Simons 2007)	4863680235308
Figure 1.7	Current molecular medicine	(G. Quest et al. 2013)	1047059-1

¹“This is an open access article distributed under the terms of the Creative Commons CC BY license, which permits unrestricted use, distribution, and reproduction in any medium, provided the original work is properly cited.” Not require the permission to reuse this article.

BIBLIOGRAPHY

- Abbott, N. Joan, Adjanie A.K. Patabendige, Diana E.M. Dolman, Siti R. Yusof, and David J. Begley. 2010. "Structure and Function of the Blood-Brain Barrier." *Neurobiology of Disease*. Academic Press. <https://doi.org/10.1016/j.nbd.2009.07.030>.
- Abud, Edsel M., Ricardo N. Ramirez, Eric S. Martinez, Luke M. Healy, Cecilia H.H. HH Nguyen, Sean A. Newman, Andriy V. Yeromin, et al. 2017. "IPSC-Derived Human Microglia-like Cells to Study Neurological Diseases." *Neuron* 94 (2): 278-293.e9. <https://doi.org/10.1016/j.neuron.2017.03.042>.
- Abulrob, Abedelnasser, Sabina Giuseppin, Moises F Andrade, Angela McDermid, Maria Moreno, and Danica Stanimirovic. 2004. "Interactions of EGFR and Caveolin-1 in Human Glioblastoma Cells: Evidence That Tyrosine Phosphorylation Regulates EGFR Association with Caveolae." *Oncogene* 23 (41): 6967–79. <https://doi.org/10.1038/sj.onc.1207911>.
- Aderem, Alan, and David M. Underhill. 1999. "Mechanisms of Phagocytosis in Macrophages." *Annual Review of Immunology* 17 (1): 593–623. <https://doi.org/10.1146/annurev.immunol.17.1.593>.
- Ajami, Bahareh, Jami L Bennett, Charles Krieger, Kelly M McNagny, and Fabio M V Rossi. 2011. "Infiltrating Monocytes Trigger EAE Progression, but Do Not Contribute to the Resident Microglia Pool." *Nature Neuroscience* 14 (9): 1142–49. <https://doi.org/10.1038/nn.2887>.
- Albulescu, Radu, Elena Codrici, Ionela Daniela Popescu, Simona Mihai, Georgiana Necula, Daniel Petrescu, Mihaela Teodoru, and Cristiana Pistol Tanase. 2013. "Cytokine Patterns in Brain Tumour Progression." *Mediators of Inflammation*. <https://doi.org/10.1155/2013/979748>.
- Ambrosius, Björn, Simon Faissner, Kirsten Guse, Marec von Lehe, Thomas Grunwald, Ralf Gold, Bastian Grewe, and Andrew Chan. 2017. "Teriflunomide and Monomethylfumarate Target HIV-Induced Neuroinflammation and Neurotoxicity." *Journal of Neuroinflammation* 14 (1): 51. <https://doi.org/10.1186/s12974-017->

0829-2.

- Annabi, Borhane, Sébastien Thibeault, Robert Moundjian, and Richard Béliveau. 2004. "Hyaluronan Cell Surface Binding Is Induced by Type I Collagen and Regulated by Caveolae in Glioma Cells." *Journal of Biological Chemistry* 279 (21): 21888–96. <https://doi.org/10.1074/jbc.M313694200>.
- Asamitsu, K, S Sakurada, K Mashiba, K Nakagawa, K Torikai, K Onozaki, and T Okamoto. 1999. "Alteration of the Cellular Response to Interleukin-1 by SV40 Large T Antigen in Rheumatoid Synovial Fibroblasts." *Arch Virol*. Vol. 144.
- Askew, Katharine, Kaizhen Li, Adrian Olmos-Alonso, Fernando Garcia-Moreno, Yajie Liang, Philippa Richardson, Tom Tipton, et al. 2017. "Coupled Proliferation and Apoptosis Maintain the Rapid Turnover of Microglia in the Adult Brain." *Cell Reports* 18 (2): 391–405. <https://doi.org/10.1016/j.celrep.2016.12.041>.
- Baghdadi, Muhammad, Yui Umeyama, Naoki Hama, Takuto Kobayashi, Nanumi Han, Haruka Wada, and Ken-ichiro Seino. 2018. "Interleukin-34, a Comprehensive Review." *Journal of Leukocyte Biology* 104 (5): 931–51. <https://doi.org/10.1002/JLB.MR1117-457R>.
- Barrangou, Rodolphe, and Jennifer A Doudna. 2016. "Applications of CRISPR Technologies in Research and Beyond." *Nature Biotechnology* 34 (9): 933–41. <https://doi.org/10.1038/nbt.3659>.
- Barresi, Valeria, Francesca Romana Buttarelli, Enrica Vitarelli E, Antonella Arcella, Manila Antonelli, Felice Giangaspero Md, Valeria Barresi, et al. 2009. "Caveolin-1 Expression in Diffuse Gliomas: Correlation with the Proliferation Index, Epidermal Growth Factor Receptor, P53, and 1p/19q Status." *Human Pathology* 40 (12): 1738–46. <https://doi.org/10.1016/j.humpath.2009.04.026>.
- Bauer, Daniel E, Matthew C Canver, and Stuart H Orkin. 2015. "Generation of Genomic Deletions in Mammalian Cell Lines via CRISPR/Cas9." *Journal of Visualized Experiments : JoVE*, no. 95 (January): e52118. <https://doi.org/10.3791/52118>.
- Benjamini, Yoav, and Yosef Hochberg. 1995. "Controlling the False Discovery Rate: A Practical and Powerful Approach to Multiple Testing." *Journal of the Royal*

- Statistical Society: Series B (Methodological)* 57 (1): 289–300.
<https://doi.org/10.1111/j.2517-6161.1995.tb02031.x>.
- Bennett, Mariko L, F Chris Bennett, Shane A Liddelow, Bahareh Ajami, Jennifer L Zamanian, Nathaniel B Fernhoff, Sara B Mulinyawe, et al. 2016. “New Tools for Studying Microglia in the Mouse and Human CNS.” *Proceedings of the National Academy of Sciences of the United States of America* 113 (12): E1738-46.
<https://doi.org/10.1073/pnas.1525528113>.
- Bernhardi, Rommy von, Gigliola Ramírez, Rodrigo Toro, and Jaime Eugén. 2007. “Pro-Inflammatory Conditions Promote Neuronal Damage Mediated by Amyloid Precursor Protein and Decrease Its Phagocytosis and Degradation by Microglial Cells in Culture.” *Neurobiology of Disease* 26 (1): 153–64.
<https://doi.org/10.1016/j.nbd.2006.12.006>.
- Bhattacharya, Palash, Muthusamy Thirupathi, Hatem A. Elshabrawy, Khaled Alharshawi, Prabhakaran Kumar, and Bellur S. Prabhakar. 2015. “GM-CSF: An Immune Modulatory Cytokine That Can Suppress Autoimmunity.” *Cytokine*. Academic Press. <https://doi.org/10.1016/j.cyto.2015.05.030>.
- Bianco, Caterina, Luigi Strizzi, Mario Mancino, Kazuhide Watanabe, Monica Gonzales, Shin Hamada, Ahmed Raafat, et al. 2008. “Regulation of Cripto-1 Signaling and Biological Activity by Caveolin-1 in Mammary Epithelial Cells.” *American Journal of Pathology* 172 (2): 345–57. <https://doi.org/10.2353/ajpath.2008.070696>.
- Bilican, Bilada, Andrea Serio, Sami J Barmada, Agnes Lumi Nishimura, Gareth J Sullivan, Monica Carrasco, Hemali P Phatnani, et al. 2012. “Mutant Induced Pluripotent Stem Cell Lines Recapitulate Aspects of TDP-43 Proteinopathies and Reveal Cell-Specific Vulnerability.” *Proceedings of the National Academy of Sciences of the United States of America* 109 (15): 5803–8. <https://doi.org/10.1073/pnas.1202922109>.
- Blasi, E., R. Barluzzi, V. Bocchini, R. Mazzolla, and F. Bistoni. 1990. “Immortalization of Murine Microglial Cells by a V-Raf / v-Myc Carrying Retrovirus.” *Journal of Neuroimmunology* 27 (2–3): 229–37. [https://doi.org/10.1016/0165-5728\(90\)90073-V](https://doi.org/10.1016/0165-5728(90)90073-V).

- Boettcher, Michael, and Michael T McManus. 2015. "Choosing the Right Tool for the Job: RNAi, TALEN, or CRISPR." *Molecular Cell* 58 (4): 575–85. <https://doi.org/10.1016/j.molcel.2015.04.028>.
- Bowman, Robert L., Qianghu Wang, Angel Carro, Roel G.W. Verhaak, and Massimo Squatrito. 2017. "GlioVis Data Portal for Visualization and Analysis of Brain Tumor Expression Datasets." *Neuro-Oncology* 19 (1): 139–41. <https://doi.org/10.1093/neuonc/now247>.
- Branchi, I., N. Francia, and E. Alleva. 2004. "Epigenetic Control of Neurobehavioural Plasticity: The Role of Neurotrophins." *Behavioural Pharmacology*. Lippincott Williams and Wilkins. <https://doi.org/10.1097/00008877-200409000-00006>.
- Brodbelt, Andrew, David Greenberg, Tim Winters, Matt Williams, Sally Vernon, and V. Peter Collins. 2015. "Glioblastoma in England: 2007–2011." *European Journal of Cancer* 51 (4): 533–42. <https://doi.org/10.1016/j.ejca.2014.12.014>.
- Brooks, William H., Thomas L. Roszman, and Alice S. Rogers. 1976. "Impairment of Rosette-forming T Lymphocytes in Patients with Primary Intracranial Tumors." *Cancer* 37 (4): 1869–73. [https://doi.org/10.1002/1097-0142\(197604\)37:4<1869::AID-CNCR2820370435>3.0.CO;2-Q](https://doi.org/10.1002/1097-0142(197604)37:4<1869::AID-CNCR2820370435>3.0.CO;2-Q).
- Bucci, Mariarosaria, Jean-Philippe Gratton, Radu Daniel Rudic, Lisette Acevedo, Fiorentina Roviezzo, Giuseppe Cirino, and William C. Sessa. 2000. "In Vivo Delivery of the Caveolin-1 Scaffolding Domain Inhibits Nitric Oxide Synthesis and Reduces Inflammation." *Nature Medicine* 6 (12): 1362–67. <https://doi.org/10.1038/82176>.
- Buchrieser, Julian, William James, and Michael D. Moore. 2017. "Human Induced Pluripotent Stem Cell-Derived Macrophages Share Ontogeny with MYB-Independent Tissue-Resident Macrophages." *Stem Cell Reports* 8 (2): 334–45. <https://doi.org/10.1016/j.stemcr.2016.12.020>.
- Butin-Israeli, Veronika, Nir Drayman, and Ariella Oppenheim. 2010. "Simian Virus 40 Infection Triggers a Balanced Network That Includes Apoptotic, Survival, and Stress Pathways." *Journal of Virology* 84 (7): 3431–42. <https://doi.org/10.1128/jvi.01735-09>.

- Butovsky, Oleg, Mark P. Jedrychowski, Craig S. Moore, Ron Cialic, Amanda J. Lanser, Galina Gabriely, Thomas Koeglsperger, et al. 2014. "Identification of a Unique TGF- β -Dependent Molecular and Functional Signature in Microglia." *Nature Neuroscience* 17 (1): 131–43. <https://doi.org/10.1038/nn.3599>.
- Canver, Matthew C, Daniel E Bauer, Abhishek Dass, Yvette Y Yien, Jacky Chung, Takeshi Masuda, Takahiro Maeda, Barry H Paw, and Stuart H Orkin. 2014. "Characterization of Genomic Deletion Efficiency Mediated by Clustered Regularly Interspaced Short Palindromic Repeats (CRISPR)/Cas9 Nuclease System in Mammalian Cells." *The Journal of Biological Chemistry* 289 (31): 21312–24. <https://doi.org/10.1074/jbc.M114.564625>.
- Caratti, G., T. Poolman, R. J. Hurst, L. Ince, A. Knight, K. Krakowiak, H. J. Durrington, et al. 2019. "Caveolin1 Interacts with the Glucocorticoid Receptor in the Lung but Is Dispensable for Its Anti-Inflammatory Actions in Lung Inflammation and *Trichuris Muris* Infection." *Scientific Reports* 9 (1): 1–13. <https://doi.org/10.1038/s41598-019-44963-0>.
- Caricasole, Andrea, Agata Copani, Filippo Caraci, Eleonora Aronica, Annemieke J. Rozemuller, Alessandra Caruso, Marianna Storto, Giovanni Gaviraghi, Georg C. Terstappen, and Ferdinando Nicoletti. 2004. "Induction of Dickkopf-1, a Negative Modulator of the Wnt Pathway, Is Associated with Neuronal Degeneration in Alzheimer's Brain." *Journal of Neuroscience* 24 (26): 6021–27. <https://doi.org/10.1523/JNEUROSCI.1381-04.2004>.
- Carvalho da Fonseca, Anna Carolina, Huaqing Wang, Haitao Fan, Xuebo Chen, Ian Zhang, Leying Zhang, Flavia Regina Souza Lima, and Behnam Badie. 2014. "Increased Expression of Stress Inducible Protein 1 in Glioma-Associated Microglia/Macrophages." *Journal of Neuroimmunology* 274 (1–2): 71–77. <https://doi.org/10.1016/j.jneuroim.2014.06.021>.
- Cassoni, Paola, Rebecca Senetta, Isabella Castellano, Erika Ortolan, Martino Bosco, Ivana Magnani, and Alessandro Ducati. 2007. "Caveolin-1 Expression Is Variably Displayed in Astroglial-Derived Tumors and Absent in Oligodendrogliomas: Concrete Premises for a New Reliable Diagnostic Marker in Gliomas." *The American*

Journal of Surgical Pathology 31 (5): 760–69.
<https://doi.org/10.1097/01.pas.0000213433.14740.5d>.

Celus, Ward, Giusy Di Conza, Ana Isabel Oliveira, Manuel Ehling, Bruno M Costa, Mathias Wenes, Massimiliano Mazzone, and Giusy Di Conza. 2017. “Loss of Caveolin-1 in Metastasis-Associated Macrophages Drives Lung Metastatic Growth through Increased Angiogenesis.” *Cell Reports* 21: 2842–54.
<https://doi.org/10.1016/j.celrep.2017.11.034>.

Cerezo, Ana, Marta C. Guadamillas, Jacky G. Goetz, Sara Sánchez-Perales, Eric Klein, Richard K. Assoian, and Miguel A. del Pozo. 2009. “The Absence of Caveolin-1 Increases Proliferation and Anchorage- Independent Growth by a Rac-Dependent, Erk-Independent Mechanism.” *Molecular and Cellular Biology* 29 (18): 5046–59.
<https://doi.org/10.1128/mcb.00315-09>.

Chai, Qingqing, Vladimir Jovasevic, Viacheslav Malikov, Yosef Sabo, Scott Morham, Derek Walsh, and Mojgan H. Naghavi. 2017. “HIV-1 Counteracts an Innate Restriction by Amyloid Precursor Protein Resulting in Neurodegeneration.” *Nature Communications* 8 (1). <https://doi.org/10.1038/s41467-017-01795-8>.

Chang, Alan L., Jason Miska, Derek A. Wainwright, Mahua Dey, Claudia V. Rivetta, Dou Yu, Deepak Kanojia, et al. 2016. “CCL2 Produced by the Glioma Microenvironment Is Essential for the Recruitment of Regulatory t Cells and Myeloid-Derived Suppressor Cells.” *Cancer Research* 76 (19): 5671–82.
<https://doi.org/10.1158/0008-5472.CAN-16-0144>.

Charles, Nikki A., Eric C. Holland, Richard Gilbertson, Rainer Glass, and Helmut Kettenmann. 2011. “The Brain Tumor Microenvironment.” *Glia* 59 (8): 1169–80.
<https://doi.org/10.1002/glia.21136>.

Chen, Xin, Wei Yuan Ma, Shang Chen Xu, Yu Liang, Yi Bing Fu, Bo Pang, Tao Xin, et al. 2014. “The Overexpression of Epithelial Cell Adhesion Molecule (EpCAM) in Glioma.” *Journal of Neuro-Oncology* 119 (1): 39–47.
<https://doi.org/10.1007/s11060-014-1459-5>.

Chen, Zhihong, and Dolores Hambarzumyan. 2018. “Immune Microenvironment in

- Glioblastoma Subtypes.” *Frontiers in Immunology* 9 (May): 1004. <https://doi.org/10.3389/fimmu.2018.01004>.
- Cheng, Simon K., Felix Olale, James T. Bennett, Ali H. Brivanlou, and Alexander F. Schier. 2003. “EGF-CFC Proteins Are Essential Coreceptors for the TGF- β Signals VG1 and GDF1.” *Genes and Development* 17 (1): 31–36. <https://doi.org/10.1101/gad.1041203>.
- Chhor, Vibol, Tifenn Le Charpentier, Sophie Lebon, Marie Virgine Oré, Idoia Lara Celador, Julien Josserand, Vincent Degos, et al. 2013. “Characterization of Phenotype Markers and Neuronotoxic Potential of Polarised Primary Microglia In Vitro.” *Brain, Behavior, and Immunity* 32 (August): 70–85. <https://doi.org/10.1016/j.bbi.2013.02.005>.
- Chiu, Tsung-Lang, Chih-Wen Peng, and Mei-Jan Wang. 2011. “Enhanced Anti-Glioblastoma Activity of Microglia by AAV2-Mediated IL-12 through TRAIL and Phagocytosis in Vitro.” *Oncology Reports* 25 (5): 1373–80. <https://doi.org/10.3892/or.2011.1213>.
- Chongsathidkiet, Pakawat, Christina Jackson, Shohei Koyama, Franziska Loebel, Xiuyu Cui, S. Harrison Farber, Karolina Woroniecka, et al. 2018. “Sequestration of T Cells in Bone Marrow in the Setting of Glioblastoma and Other Intracranial Tumors.” *Nature Medicine* 24 (9): 1459–68. <https://doi.org/10.1038/s41591-018-0135-2>.
- Choudhury, Amit, David L. Marks, Kirsty M. Proctor, Gwyn W. Gould, and Richard E. Pagano. 2006. “Regulation of Caveolar Endocytosis by Syntaxin 6-Dependent Delivery of Membrane Components to the Cell Surface.” *Nature Cell Biology* 8 (4): 317–28. <https://doi.org/10.1038/ncb1380>.
- Codrici, Elena, Lucian Albuлесcu, Ionela Daniela Popescu, Simona Mihai, Ana-Maria Enciu, Radu Albuлесcu, Cristiana Tanase, and Mihail E. Hinescu. 2018a. “Caveolin-1-Knockout Mouse as a Model of Inflammatory Diseases.” *Journal of Immunology Research*, 1–10. <https://doi.org/10.1155/2018/2498576>.
- Codrici, Elena, Lucian Albuлесcu, Ionela Daniela Popescu, Simona Mihai, Ana Maria Enciu, Radu Albuлесcu, Cristiana Tanase, and Mihail E. Hinescu. 2018b. “Caveolin-1-

- Knockout Mouse as a Model of Inflammatory Diseases." *Journal of Immunology Research* 2018: 1–10. <https://doi.org/10.1155/2018/2498576>.
- Cong, Le, and Feng Zhang. 2015. "Genome Engineering Using CRISPR-Cas9 System." In *Chromosomal Mutagenesis. Methods in Molecular Biology*, 197–217. Humana Press, New York, NY. https://doi.org/10.1007/978-1-4939-1862-1_10.
- Coniglio, Salvatore J, Eliseo Eugenin, Kostantin Dobrenis, E Richard Stanley, Brian L West, Marc H Symons, and Jeffrey E Segall. 2012. "Microglial Stimulation of Glioblastoma Invasion Involves Epidermal Growth Factor Receptor (EGFR) and Colony Stimulating Factor 1 Receptor (CSF-1R) Signaling." *Molecular Medicine (Cambridge, Mass.)* 18: 519–27. <https://doi.org/10.2119/molmed.2011.00217>.
- Constam, D B, J Philipp, U V Malipiero, P ten Dijke, M Schachner, and A Fontana. 1992. "Differential Expression of Transforming Growth Factor-Beta 1, -Beta 2, and -Beta 3 by Glioblastoma Cells, Astrocytes, and Microglia." *Journal of Immunology (Baltimore, Md. : 1950)* 148 (5): 1404–10. <http://www.ncbi.nlm.nih.gov/pubmed/1538124>.
- Cosset, Erika C., Julien Godet, Natacha Entz-Werlé, Eric Guérin, Dominique Guenot, Sébastien Froelich, Dominique Bonnet, et al. 2012. "Involvement of the TGFβ Pathway in the Regulation of α 5β 1 Integrins by Caveolin-1 in Human Glioblastoma." *International Journal of Cancer* 131 (3): 601–11. <https://doi.org/10.1002/ijc.26415>.
- Crews, Fulton T., and Ryan P. Vetreno. 2016. "Mechanisms of Neuroimmune Gene Induction in Alcoholism." *Psychopharmacology* 233 (9): 1543–57. <https://doi.org/10.1007/s00213-015-3906-1>.
- Crocetti, Emanuele, Annalisa Trama, Charles Stiller, Adele Caldarella, Riccardo Soffiotti, Jana Jaal, Damien C Weber, Umberto Ricardi, Jerzy Slowinski, and Alba Brandes. 2012. "Epidemiology of Glial and Non-Glial Brain Tumours in Europe." *European Journal of Cancer* 48 (10): 1532–42. <https://doi.org/10.1016/j.ejca.2011.12.013>.
- Crusz, Shanthini M., and Frances R. Balkwill. 2015. "Inflammation and Cancer: Advances and New Agents." *Nature Reviews Clinical Oncology* 12 (10): 584–96.

<https://doi.org/10.1038/nrclinonc.2015.105>.

- Czekay, Ralf Peter, Kathleen Aertgeerts, Scott A. Curriden, and David J. Loskutoff. 2003. "Plasminogen Activator Inhibitor-1 Detaches Cells from Extracellular Matrices by Inactivating Integrins." *Journal of Cell Biology* 160 (5): 781–91. <https://doi.org/10.1083/jcb.200208117>.
- Daneman, Richard, Lu Zhou, Amanuel A Kebede, and Ben A Barres. 2010. "Pericytes Are Required for Blood-Brain Barrier Integrity during Embryogenesis." *Nature*. <https://doi.org/10.1038/nature09513>.
- Darmanis, Spyros, Steven A. Sloan, Ye Zhang, Martin Enge, Christine Caneda, Lawrence M. Shuer, Melanie G. Hayden Gephart, Ben A. Barres, and Stephen R. Quake. 2015. "A Survey of Human Brain Transcriptome Diversity at the Single Cell Level." *Proceedings of the National Academy of Sciences of the United States of America* 112 (23): 7285–90. <https://doi.org/10.1073/pnas.1507125112>.
- Darmanis, Spyros, Steven A Sloan, Derek Croote, Marco Mignardi, Sophia Chernikova, Peyman Samghababi, Ye Zhang, et al. 2017. "Single-Cell RNA-Seq Analysis of Infiltrating Neoplastic Cells at the Migrating Front of Human Glioblastoma." *Cell Reports* 21 (5): 1399–1410. <https://doi.org/10.1016/j.celrep.2017.10.030>.
- Debets-Ossenkopp, Y., E. L. Mills, W. C. van Dijk, H. A. Verbrugh, and J. Verhoef. 1982. "Effect of Influenza Viras on Phagocytic Cells." *European Journal of Clinical Microbiology* 1 (3): 171–77. <https://doi.org/10.1007/BF02019619>.
- Deczkowska, Aleksandra, Ido Amit, and Michal Schwartz. 2018. "Microglial Immune Checkpoint Mechanisms." *Nature Neuroscience* 21 (6): 779–86. <https://doi.org/10.1038/s41593-018-0145-x>.
- Deltcheva, Elitza, Krzysztof Chylinski, Cynthia M. Sharma, Karine Gonzales, Yanjie Chao, Zaid A. Pirzada, Maria R. Eckert, Jörg Vogel, and Emmanuelle Charpentier. 2011. "CRISPR RNA Maturation by Trans-Encoded Small RNA and Host Factor RNase III." *Nature* 471 (7340): 602–7. <https://doi.org/10.1038/nature09886>.
- Dietzen, D. J., W. R. Hastings, and D. M. Lublin. 1995. "Caveolin Is Palmitoylated on Multiple Cysteine Residues. Palmitoylation Is Not Necessary for Localization of

- Caveolin to Caveolae." *Journal of Biological Chemistry* 270 (12): 6838–42. <https://doi.org/10.1074/jbc.270.12.6838>.
- Dittmann, Meike, Hans-Heinrich Hoffmann, Margaret A. Scull, Rachel H. Gilmore, Kierstin L. Bell, Michael Ciancanelli, Sam J. Wilson, et al. 2015. "A Serpin Shapes the Extracellular Environment to Prevent Influenza A Virus Maturation." *Cell* 160 (4): 631–43. <https://doi.org/10.1016/j.cell.2015.01.040>.
- Dobin, Alexander, and Thomas R. Gingeras. 2015. "Mapping RNA-Seq Reads with STAR." *Current Protocols in Bioinformatics* 51 (1): 11.14.1-11.14.19. <https://doi.org/10.1002/0471250953.bi1114s51>.
- Douvaras, Panagiotis, Bruce Sun, Minghui Wang, Ilya Kruglikov, Gregory Lallo, Matthew Zimmer, Cecile Terrenoire, et al. 2017. "Directed Differentiation of Human Pluripotent Stem Cells to Microglia." *Stem Cell Reports* 8 (6): 1516–24. <https://doi.org/10.1016/j.stemcr.2017.04.023>.
- Dubbelaar, Marissa L., Laura Kracht, Bart J.L. Eggen, and Erik W.G.M. Boddeke. 2018. "The Kaleidoscope of Microglial Phenotypes." *Frontiers in Immunology*. NLM (Medline). <https://doi.org/10.3389/fimmu.2018.01753>.
- Ellert-Miklaszewska, Aleksandra, Michal Dabrowski, Maciej Lipko, Marcin Sliwa, Marta Maleszewska, and Bozena Kaminska. 2013. "Molecular Definition of the Pro-Tumorigenic Phenotype of Glioma-Activated Microglia." *Glia* 61 (7): 1178–90. <https://doi.org/10.1002/glia.22510>.
- Engelman, Jeffrey A., Xiao Lan Zhang, Ferruccio Galbiati, and Michael P. Lisanti. 1998. "Chromosomal Localization, Genomic Organization, and Developmental Expression of the Murine Caveolin Gene Family (Cav-1, -2, and -3) Cav-1 and Cav-2 Genes Map to a Known Tumor Suppressor Locus (6-A2/7q31)." *FEBS Letters* 429 (3): 330–36. [https://doi.org/10.1016/S0014-5793\(98\)00619-X](https://doi.org/10.1016/S0014-5793(98)00619-X).
- Estep, Jason A., Erin L. Sternburg, Gissell A. Sanchez, and Fedor V. Karginov. 2016. "Immunoblot Screening of CRISPR/Cas9-Mediated Gene Knockouts without Selection." *BMC Molecular Biology* 17 (1): 9. <https://doi.org/10.1186/s12867-016-0061-0>.

- Etemad, Samar, Rasheeda Mohd Zamin, Marc J. Ruitenber, and Luis Filgueira. 2012. "A Novel in Vitro Human Microglia Model: Characterization of Human Monocyte-Derived Microglia." *Journal of Neuroscience Methods* 209 (1): 79–89. <https://doi.org/10.1016/J.JNEUMETH.2012.05.025>.
- Falcon, S., S. Falcon, and R. Gentleman. 2007. "Using GOstats to Test Gene Lists for GO Term Association." *BIOINFORMATICS*. <http://citeseerx.ist.psu.edu/viewdoc/summary?doi=10.1.1.207.646>.
- Feng, Hong, Ling Guo, Zhiqing Song, Dan Wang, Weisi Fu, Jingyan Han, Zhenyu Li, Bin Huang, and Xiang-An Li. 2010. "Caveolin-1 Protects against Sepsis through Modulating Inflammatory Response, Alleviating Bacterial Burden and Suppressing Thymocyte Apoptosis." *The Journal of Biological Chemistry* 285 (33): 25154–25160. <https://doi.org/10.1074/jbc.M110.116897>.
- Feng, Hong, Wen Guo, Junqing Han, and Xiang-An Li. 2013. "Role of Caveolin-1 and Caveolae Signaling in Endotoxemia and Sepsis." *Life Sciences* 93 (1): 1–6. <https://doi.org/10.1016/j.lfs.2013.05.016>.
- Filatova, Alina, Till Acker, and Boyan K Garvalov. 2013. "The Cancer Stem Cell Niche(s): The Crosstalk between Glioma Stem Cells and Their Microenvironment." *Biochimica et Biophysica Acta* 1830 (2): 2496–2508. <https://doi.org/10.1016/j.bbagen.2012.10.008>.
- Filipovic, R., I. Jakovcevski, and N. Zecevic. 2003. "GRO- α and CXCR2 in the Human Fetal Brain and Multiple Sclerosis Lesions." *Developmental Neuroscience* 25 (2–4): 279–90. <https://doi.org/10.1159/000072275>.
- Foucher, Etienne D., Simon Blanchard, Laurence Preisser, Erwan Garo, Norbert Ifrah, Philippe Guardiola, Yves Delneste, and Pascale Jeannin. 2013. "IL-34 Induces the Differentiation of Human Monocytes into Immunosuppressive Macrophages. Antagonistic Effects of GM-CSF and IFN γ ." Edited by Serge Nataf. *PLoS ONE* 8 (2): e56045. <https://doi.org/10.1371/journal.pone.0056045>.
- Franzè, Eleonora, Carmine Stolfi, Edoardo Troncone, Patrizio Scarozza, and Giovanni Monteleone. 2020. "Role of Interleukin-34 in Cancer." *Cancers* 12 (1): 252.

<https://doi.org/10.3390/cancers12010252>.

Fridolfsson, Heidi N, David M Roth, Paul A Insel, and Hemal H Patel. 2014. "Regulation of Intracellular Signaling and Function by Caveolin." *FASEB Journal: Official Publication of the Federation of American Societies for Experimental Biology* 28 (9): 3823–31. <https://doi.org/10.1096/fj.14-252320>.

Fu, Y., X.-L. Moore, M. K. S. Lee, M. A. Fernandez-Rojo, M.-O. Parat, R. G. Parton, P. J. Meikle, D. Sviridov, and J. P. F. Chin-Dusting. 2012. "Caveolin-1 Plays a Critical Role in the Differentiation of Monocytes into Macrophages." *Arteriosclerosis, Thrombosis, and Vascular Biology* 32 (9): e117–25. <https://doi.org/10.1161/ATVBAHA.112.254151>.

Fu, Y. Yi, X.-L. Xiao-Lei Moore, Man K. S. Lee, M. A. Fernandez-Rojo, M.-O. Marie-Odile M.-O. Parat, Robert G. Parton, Peter J. Meikle, et al. 2012. "Caveolin-1 Plays a Critical Role in the Differentiation of Monocytes into Macrophages." *Arteriosclerosis, Thrombosis, and Vascular Biology* 32 (9): e117–25. <https://doi.org/10.1161/ATVBAHA.112.254151>.

G. Quest, A., L. Lobos-Gonzalez, S. Nunez, C. Sanhueza, J.-G. Fernandez, A. Aguirre, D. Rodriguez, L. Leyton, and V. Torres. 2013. "The Caveolin-1 Connection to Cell Death and Survival." *Current Molecular Medicine* 13 (2): 266–81. <https://doi.org/10.2174/1566524011313020004>.

Gabriel, Elke, and Jay Gopalakrishnan. 2017. "Generation of Ipsc-Derived Human Brain Organoids to Model Early Neurodevelopmental Disorders." *Journal of Visualized Experiments* 122 (e55372): 1–8. <https://doi.org/10.3791/55372>.

Gadjeva, Mihaela, Catherine Paradis-Bleau, Gregory P. Priebe, Raina Fichorova, and Gerald B. Pier. 2010. "Caveolin-1 Modifies the Immunity to Pseudomonas Aeruginosa ." *The Journal of Immunology* 184 (1): 296–302. <https://doi.org/10.4049/jimmunol.0900604>.

Gaj, Thomas, Charles A Gersbach, Carlos F Barbas, and III. 2013. "ZFN, TALEN, and CRISPR/Cas-Based Methods for Genome Engineering." *Trends in Biotechnology* 31 (7): 397–405. <https://doi.org/10.1016/j.tibtech.2013.04.004>.

- Garcia, Roy, Chao Lan Yu, Anne Hudnall, Robyn Catlett, Kristie L. Nelson, Thomas Smithgall, Donald J. Fujita, Stephen P. Ethier, and Richard Jove. 1997. "Constitutive Activation of Stat3 in Fibroblasts Transformed by Diverse Oncoproteins and in Breast Carcinoma Cells." *Cell Growth and Differentiation* 8 (12): 1267–76.
- Garofalo, Stefano, Giuseppina D'Alessandro, Giuseppina Chece, Frederic Brau, Laura Maggi, Alessandro Rosa, Alessandra Porzia, et al. 2015. "Enriched Environment Reduces Glioma Growth through Immune and Non-Immune Mechanisms in Mice." *Nature Communications* 6. <https://doi.org/10.1038/ncomms7623>.
- Geiger, K. D., S. Hendruschk, E. P. Rieber, A. Morgenroth, B. Weigle, T. Juratli, V. Senner, G. Schackert, and A. Temme. 2011. "The Prostate Stem Cell Antigen Represents a Novel Glioma-Associated Antigen." *Oncology Reports* 26 (1): 13–21. <https://doi.org/10.3892/or.2011.1265>.
- Ginhoux, Florent, and Sonia Garel. 2018. "The Mysterious Origins of Microglia." *Nature Neuroscience* 21 (7): 897–99. <https://doi.org/10.1038/s41593-018-0176-3>.
- Ginhoux, Florent, Melanie Greter, Marylene Leboeuf, Sayan Nandi, Peter See, Solen Gokhan, Mark F. Mehler, et al. 2010. "Fate Mapping Analysis Reveals That Adult Microglia Derive from Primitive Macrophages." *Science* 330 (6005): 841–45. <https://doi.org/10.1126/science.1194637>.
- Godlewski, Jakub, Anna M. Krichevsky, Mark D. Johnson, E. Antonio Chiocca, and Agnieszka Bronisz. 2015. "Belonging to a Network—MicroRNAs, Extracellular Vesicles, and the Glioblastoma Microenvironment." *Neuro-Oncology* 17 (5): 652–62. <https://doi.org/10.1093/neuonc/nou292>.
- Goetz, Jacky G., Patrick Lajoie, Sam M. Wiseman, and Ivan R. Nabi. 2008. "Caveolin-1 in Tumor Progression: The Good, the Bad and the Ugly." *Cancer and Metastasis Reviews* 27 (4): 715–35. <https://doi.org/10.1007/s10555-008-9160-9>.
- Goswami, S, A Gupta, and S K Sharma. 1998. "Interleukin-6-Mediated Autocrine Growth Promotion in Human Glioblastoma Multiforme Cell Line U87MG." *J.Neurochem.* 71: 1837–45.
- Grabowski, Matthew M., Eric W. Sankey, Katherine J. Ryan, Pakawat Chongsathidkiet,

- Selena J. Lorrey, Daniel S. Wilkinson, and Peter E. Fecci. 2020. "Immune Suppression in Gliomas." *Journal of Neuro-Oncology*, June, 1–10. <https://doi.org/10.1007/s11060-020-03483-y>.
- Graeber, Manuel B., Bernd W. Scheithauer, and Georg W. Kreutzberg. 2002. "Microglia in Brain Tumors." *GLIA*. John Wiley & Sons, Ltd. <https://doi.org/10.1002/glia.10147>.
- Guillemin, G. J. 2003. "Microglia, Macrophages, Perivascular Macrophages, and Pericytes: A Review of Function and Identification." *Journal of Leukocyte Biology* 75 (3): 388–97. <https://doi.org/10.1189/jlb.0303114>.
- Guo, Qiang, Nan Shen, Kefei Yuan, Jiaxin Li, Hong Wu, Yong Zeng, John Fox, et al. 2012. "Caveolin-1 Plays a Critical Role in Host Immunity against *Klebsiella Pneumoniae* by Regulating STAT5 and Akt Activity." *European Journal of Immunology* 42 (6): 1500–1511. <https://doi.org/10.1002/eji.201142051>.
- Gupta, Manoj Kumar, Santosh Kumar Behera, Budheswar Dehury, and Namita Mahapatra. 2017. "Identification and Characterization of Differentially Expressed Genes from Human Microglial Cell Samples Infected with Japanese Encephalitis Virus." *Journal of Vector Borne Diseases*.
- Haenseler, Walther, Stephen N Sansom, Julian Buchrieser, Sarah E Newey, Craig S Moore, Francesca J Nicholls, Satyan Chintawar, et al. 2017. "A Highly Efficient Human Pluripotent Stem Cell Microglia Model Displays a Neuronal-Co-Culture-Specific Expression Profile and Inflammatory Response." *Stem Cell Reports* 8 (6): 1727–42. <https://doi.org/10.1016/j.stemcr.2017.05.017>.
- Hambardzumyan, Dolores, David H. Gutmann, and Helmut Kettenmann. 2015. "The Role of Microglia and Macrophages in Glioma Maintenance and Progression." *Nature Neuroscience* 19 (1): 20–27. <https://doi.org/10.1038/nn.4185>.
- Hao, Chunhai, Ian F Parney, Wilson H Roa, Joan Turner, Kenneth C Petruk, and David a Ramsay. 2002. "Cytokine and Cytokine Receptor mRNA Expression in Human Glioblastomas: Evidence of Th1, Th2 and Th3 Cytokine Dysregulation." *Acta Neuropathologica* 103 (2): 171–78. <https://doi.org/10.1007/s004010100448>.
- Harris, James, Dirk Werling, Jayne C Hope, Geraldine Taylor, and Chris J Howard. 2002.

- “Caveolae and Caveolin in Immune Cells: Distribution and Functions.” *Trends in Immunology* 23 (3): 158–64. [https://doi.org/10.1016/S1471-4906\(01\)02161-5](https://doi.org/10.1016/S1471-4906(01)02161-5).
- Hattermann, Kirsten, Susanne Sebens, Ole Helm, Anne Dorothee Schmitt, Rolf Mentlein, H. Maximilian Mehdorn, and Janka Held-Feindt. 2014. “Chemokine Expression Profile of Freshly Isolated Human Glioblastoma-Associated Macrophages/Microglia.” *Oncology Reports* 32 (1): 270–76.
- Heaton, R. K., D. B. Clifford, D. R. Franklin, S. P. Woods, C. Ake, F. Vaida, R. J. Ellis, et al. 2010. “HIV-Associated Neurocognitive Disorders Persist in the Era of Potent Antiretroviral Therapy: Charter Study.” *Neurology* 75 (23): 2087–96. <https://doi.org/10.1212/WNL.0b013e318200d727>.
- Heddleston, John M, Masahiro Hitomi, Monica Venere, William A Flavahan, Kenneth Yan, Youngmi Kim, Sana Minhas, Jeremy N Rich, and Anita B Hjelmeland. 2013. “Glioma Stem Cell Maintenance: The Role of the Microenvironment.” *Curr Pharm Des* 17 (23): 2386–2401.
- Hendel, Ayal, Rasmus O. Bak, Joseph T. Clark, Andrew B. Kennedy, Daniel E. Ryan, Subhadeep Roy, Israel Steinfeld, et al. 2015. “Chemically Modified Guide RNAs Enhance CRISPR-Cas Genome Editing in Human Primary Cells.” *Nature Biotechnology* 33 (9): 985–89. <https://doi.org/10.1038/nbt.3290>.
- Hickman, Suzanne E., Nathan D. Kingery, Toshiro K. Ohsumi, Mark L. Borowsky, Li Chong Wang, Terry K. Means, and Joseph El Khoury. 2013. “The Microglial Sensome Revealed by Direct RNA Sequencing.” *Nature Neuroscience* 16 (12): 1896–1905. <https://doi.org/10.1038/nn.3554>.
- Hjorth, Erik, Dan Frenkel, Howard Weiner, and Marianne Schultzberg. 2010. “Effects of Immunomodulatory Substances on Phagocytosis of Abeta(1-42) by Human Microglia.” *International Journal of Alzheimer’s Disease* 2010 (May). <https://doi.org/10.4061/2010/798424>.
- Hjorth, Erik, Mingqin Zhu, Veronica Cortés Toro, Inger Vedin, Jan Palmblad, Tommy Cederholm, Yvonne Freund-Levi, et al. 2013. “Omega-3 Fatty Acids Enhance Phagocytosis of Alzheimer’s Disease-Related Amyloid-B42 by Human Microglia and

- Decrease Inflammatory Markers.” *Journal of Alzheimer’s Disease* 35 (4): 697–713. <https://doi.org/10.3233/JAD-130131>.
- Ho, Kuo Hao, Peng Hsu Chen, Edward Hsi, Chwen Ming Shih, Wei Chiao Chang, Chia Hsiung Cheng, Cheng Wei Lin, and Ku Chung Chen. 2017. “Identification of IGF-1-Enhanced Cytokine Expressions Targeted by MiR-181d in Glioblastomas via an Integrative MiRNA/MRNA Regulatory Network Analysis.” *Scientific Reports* 7 (1): 1–13. <https://doi.org/10.1038/s41598-017-00826-0>.
- Hough, Soren H, Ayokunmi Ajetunmobi, Leigh Brody, Neil Humphryes-Kirilov, and Edward Perello. 2016. “Desktop Genetics.” *Personalized Medicine* 13 (6): 517–21. <https://doi.org/10.2217/pme-2016-0068>.
- Huysentruyt, Leanne C, Zeynep Akgoc, and Thomas N Seyfried. 2011. “Hypothesis: Are Neoplastic Macrophages/Microglia Present in Glioblastoma Multiforme?” *ASN Neuro* 3 (4): 183–93. <https://doi.org/10.1042/AN20110011>.
- Ito, Takafumi, John D. Williams, Donald J. Fraser, and Aled O. Phillips. 2004. “Hyaluronan Regulates Transforming Growth Factor-B1 Receptor Compartmentalization.” *Journal of Biological Chemistry* 279 (24): 25326–32. <https://doi.org/10.1074/jbc.M403135200>.
- Itoh, Yoshifumi. 2006. “MT1-MMP: A Key Regulator of Cell Migration in Tissue.” *IUBMB Life (International Union of Biochemistry and Molecular Biology: Life)* 58 (10): 589–96. <https://doi.org/10.1080/15216540600962818>.
- Janabi, Nazila, Sylviane Peudener, Bénédicte Héron, Kim Heng Ng, and Marc Tardieu. 1995. “Establishment of Human Microglial Cell Lines after Transfection of Primary Cultures of Embryonic Microglial Cells with the SV40 Large T Antigen.” *Neuroscience Letters* 195 (2): 105–8. [https://doi.org/10.1016/0304-3940\(94\)11792-H](https://doi.org/10.1016/0304-3940(94)11792-H).
- Janda, Elzbieta, Laura Boi, and Anna R. Carta. 2018. “Microglial Phagocytosis and Its Regulation: A Therapeutic Target in Parkinson’s Disease?” *Frontiers in Molecular Neuroscience* 11 (144): 1–8. <https://doi.org/10.3389/fnmol.2018.00144>.
- Jassal, Bijay, Lisa Matthews, Guilherme Viteri, Chuqiao Gong, Pascual Lorente, Antonio

- Fabregat, Konstantinos Sidiropoulos, et al. 2020. "The Reactome Pathway Knowledgebase." *Nucleic Acids Research* 48. <https://doi.org/10.1093/nar/gkz1031>.
- Jeon, Hyejin, Jong-Heon Kim, Jae-Hong Kim, Won-Ha Lee, Myung-Shik Lee, and Kyoungho Suk. 2012. "Plasminogen Activator Inhibitor Type 1 Regulates Microglial Motility and Phagocytic Activity." *Journal of Neuroinflammation* 9 (June): 149. <https://doi.org/10.1186/1742-2094-9-149>.
- Joseph, Justin V., Veerakumar Balasubramanian, Annemiek Walenkamp, and Frank A.E. Kruyt. 2013. "TGF- β as a Therapeutic Target in High Grade Gliomas-Promises and Challenges." *Biochemical Pharmacology*. Elsevier Inc. <https://doi.org/10.1016/j.bcp.2012.11.005>.
- Junhee Seok, H. Shaw Warren, G. Cuenca Alex, N. Mindrinos Michael, V. Baker Henry, Weihong Xu, Daniel R. Richards, et al. 2013. "Genomic Responses in Mouse Models Poorly Mimic Human Inflammatory Diseases." *Proceedings of the National Academy of Sciences of the United States of America* 110 (9): 3507–12. <https://doi.org/10.1073/pnas.1222878110>.
- Junttila, Ilkka S, Kiyoshi Mizukami, Harold Dickensheets, Martin Meier-Schellersheim, Hidehiro Yamane, Raymond P Donnelly, and William E Paul. 2008. "Tuning Sensitivity to IL-4 and IL-13: Differential Expression of IL-4R α , IL-13R α 1, and Gammac Regulates Relative Cytokine Sensitivity." *The Journal of Experimental Medicine* 205 (11): 2595–2608. <https://doi.org/10.1084/jem.20080452>.
- Kaminska, Bozena, Mariana Mota, and Marina Pizzi. 2016. "Signal Transduction and Epigenetic Mechanisms in the Control of Microglia Activation during Neuroinflammation." *Biochimica et Biophysica Acta - Molecular Basis of Disease* 1862 (3): 339–51. <https://doi.org/10.1016/j.bbadis.2015.10.026>.
- Khan, Md Shamsuddin Sultan, Muhammad Asif, Mohammed Khadeer Ahamed Basheer, Cheng Wei Kang, Fouad Saleh Al-Suede, Oon Chern Ein, Jing Tang, Aman Shah Abdul Majid, and Amin Malik Shah Abdul Majid. 2017. "Treatment of Novel IL17A Inhibitor in Glioblastoma Implementing 3rd Generation Co-Culture Cell Line and Patient-Derived Tumor Model." *European Journal of Pharmacology* 803 (May): 24–38.

<https://doi.org/10.1016/j.ejphar.2017.03.031>.

Kierdorf, Katrin, Daniel Erny, Tobias Goldmann, Victor Sander, Christian Schulz, Elisa Gomez Perdiguero, Peter Wieghofer, et al. 2013. "Microglia Emerge from Erythromyeloid Precursors via Pu.1-and Irf8-Dependent Pathways." *Nature Neuroscience* 16 (3): 273–80. <https://doi.org/10.1038/nn.3318>.

Koenigsknecht-Talboo, Jessica, and Gary E. Landreth. 2005. "Microglial Phagocytosis Induced by Fibrillar β -Amyloid and IgGs Are Differentially Regulated by Proinflammatory Cytokines." *Journal of Neuroscience* 25 (36): 8240–49. <https://doi.org/10.1523/JNEUROSCI.1808-05.2005>.

Komohara, Y, K Ohnishi, J Kuratsu, and M Takeya. 2008. "Possible Involvement of the M2 Anti-Inflammatory Macrophage Phenotype in Growth of Human Gliomas." *Journal of Pathology* 215 (April): 15–24. <https://doi.org/10.1002/path>.

Korkaya, Hasan, Suling Liu, and Max S Wicha. 2011. "Regulation of Cancer Stem Cells by Cytokine Networks: Attacking Cancer 's Inflammatory Roots." *Clinical Cancer Research* 17 (19): 6125–29. <https://doi.org/10.1158/1078-0432.CCR-10-2743>.

Kouranova, Evguenia, Kevin Forbes, Guojun Zhao, Joe Warren, Angela Bartels, Yumei Wu, and Xiaoxia Cui. 2016. "CRISPRs for Optimal Targeting: Delivery of CRISPR Components as DNA, RNA, and Protein into Cultured Cells and Single-Cell Embryos." *Human Gene Therapy* 27 (6): 464–75. <https://doi.org/10.1089/hum.2016.009>.

Krencik, Robert, and Su-Chun Zhang. 2011. "Directed Differentiation of Functional Astroglial Subtypes from Human Pluripotent Stem Cells." *Nature Protocols* 6 (11): 1710–17. <https://doi.org/10.1038/nprot.2011.405>.

Ku, Bo Mi, Yeon Kyung Lee, Jinhyun Ryu, Joo Yeon Jeong, Jungil Choi, Keyoung Mi Eun, Hye Young Shin, et al. 2011. "CHI3L1 (YKL-40) Is Expressed in Human Gliomas and Regulates the Invasion, Growth and Survival of Glioma Cells." *International Journal of Cancer* 128 (6): 1316–26. <https://doi.org/10.1002/ijc.25466>.

Kumar, Lekha Dinesh, and Alan R. Clarke. 2007. "Gene Manipulation through the Use of Small Interfering RNA (SiRNA): From in Vitro to in Vivo Applications." *Advanced*

- Drug Delivery Reviews* 59 (2–3): 87–100.
<https://doi.org/10.1016/J.ADDR.2007.03.009>.
- La Iglesia, Núria De, Genevieve Konopka, Kah Leong Lim, Catherine L. Nutt, Jacqueline F. Bromberg, David A. Frank, Paul S. Mischel, David N. Louis, and Azad Bonni. 2008. “Deregulation of a STAT3-Interleukin 8 Signaling Pathway Promotes Human Glioblastoma Cell Proliferation and Invasiveness.” *Journal of Neuroscience* 28 (23): 5870–78. <https://doi.org/10.1523/JNEUROSCI.5385-07.2008>.
- Lancaster, Madeline A., Nina S. Corsini, Simone Wolfinger, E. Hilary Gustafson, Alex W. Phillips, Thomas R. Burkard, Tomoki Otani, Frederick J. Livesey, and Juergen A. Knoblich. 2017. “Guided Self-Organization and Cortical Plate Formation in Human Brain Organoids.” *Nature Biotechnology* 35 (7): 659–66. <https://doi.org/10.1038/nbt.3906>.
- Lander, Eric S., Lauren M. Linton, Bruce Birren, Chad Nusbaum, Michael C. Zody, Jennifer Baldwin, Keri Devon, et al. 2001. “Initial Sequencing and Analysis of the Human Genome.” *Nature* 409 (6822): 860–921. <https://doi.org/10.1038/35057062>.
- Landskron, Glauben, Marjorie De la Fuente, Peti Thuwajit, Chanitra Thuwajit, Marcela A Hermoso, Glauben Landskron, Marjorie De la Fuente, Peti Thuwajit, Chanitra Thuwajit, and Marcela A. Hermoso. 2014. “Chronic Inflammation and Cytokines in the Tumor Microenvironment.” *Journal of Immunology Research* 2014: 149185. <https://doi.org/10.1155/2014/149185>.
- Lawson, L. J., V. H. Perry, and S. Gordon. 1993. “Microglial Responses to Physiological Change: Osmotic Stress Elevates DNA Synthesis of Neurohypophyseal Microglia.” *Neuroscience* 56 (4): 929–38. [https://doi.org/10.1016/0306-4522\(93\)90139-7](https://doi.org/10.1016/0306-4522(93)90139-7).
- Lazarus, D. D., L. L. Moldawer, and S. F. Lowry. 1993. “Insulin-like Growth Factor-1 Activity Is Inhibited by Interleukin-1 α , Tumor Necrosis Factor- α , and Interleukin-6.” *Lymphokine and Cytokine Research* 12 (4): 219–23. <https://europepmc.org/article/med/8218594>.
- Lê-Bury, Gabrielle, and Florence Niedergang. 2018. “Defective Phagocytic Properties of HIV-Infected Macrophages: How Might They Be Implicated in the Development of

- Invasive Salmonella Typhimurium?" *Frontiers in Immunology*. Frontiers Media S.A. <https://doi.org/10.3389/fimmu.2018.00531>.
- Lee, Chih-Yuan, Ting-Yu Lai, Meng-Kun Tsai, Yung-Chi Chang, Yu-Hsin Ho, I-Shing Yu, Tzu-Wen Yeh, et al. 2017. "The Ubiquitin Ligase ZNRF1 Promotes Caveolin-1 Ubiquitination and Degradation to Modulate Inflammation." *Nature Communications* 8 (June): 15502. <https://doi.org/10.1038/ncomms15502>.
- Lee, Hojin, and Alexander Y. Tsygankov. 2010. "C-Cbl Regulates Glioma Invasion through Matrix Metalloproteinase 2." *Journal of Cellular Biochemistry* 111: 1169–78. <https://doi.org/10.1002/jcb.22839>.
- Leite, Diana M., Barbara Zvar Baskovic, Prospero Civita, Catia Neto, Mark Gumbleton, and Geoffrey J. Pilkington. 2020. "A Human Co-culture Cell Model Incorporating Microglia Supports Glioblastoma Growth and Migration, and Confers Resistance to Cytotoxics." *The FASEB Journal* 34 (1): 1710–27. <https://doi.org/10.1096/fj.201901858RR>.
- Lewis-Tuffin, Laura J., Fausto Rodriguez, Caterina Giannini, Bernd Scheithauer, Brian M. Necela, Jann N. Sarkaria, and Panos Z. Anastasiadis. 2010. "Misregulated E-Cadherin Expression Associated with an Aggressive Brain Tumor Phenotype." Edited by Kurt Anderson. *PLoS ONE* 5 (10): e13665. <https://doi.org/10.1371/journal.pone.0013665>.
- Li, Ming O., Yisong Y. Wan, Shomyseh Sanjabi, Anna-Karin L. Robertson, and Richard A. Flavell. 2006. "Transforming Growth Factor- β Regulation of Immune Responses." *Annual Review of Immunology* 24 (1): 99–146. <https://doi.org/10.1146/annurev.immunol.24.021605.090737>.
- Li, Qingyun, and Ben A. Barres. 2017. "Microglia and Macrophages in Brain Homeostasis and Disease." *Nature Reviews Immunology*, no. 18 (November): 225–42. <https://doi.org/10.1038/nri.2017.125>.
- Li, Zhenzhe, Jixing Zhang, Hongshan Zheng, Chenlong Li, Jinsheng Xiong, Weiliang Wang, Hongbo Bao, Hua Jin, and Peng Liang. 2019. "Modulating LncRNA SNHG15/CDK6/MiR-627 Circuit by Palbociclib, Overcomes Temozolomide

- Resistance and Reduces M2-Polarization of Glioma Associated Microglia in Glioblastoma Multiforme.” *Journal of Experimental & Clinical Cancer Research* 38 (1): 380. <https://doi.org/10.1186/s13046-019-1371-0>.
- Liang, Xiquan, Jason Potter, Shantanu Kumar, Yanfei Zou, Rene Quintanilla, Mahalakshmi Sridharan, Jason Carte, et al. 2015. “Rapid and Highly Efficient Mammalian Cell Engineering via Cas9 Protein Transfection.” *Journal of Biotechnology* 208: 44–53. <https://doi.org/10.1016/j.jbiotec.2015.04.024>.
- Liao, Yang, Gordon K Smyth, and Wei Shi. 2014. “FeatureCounts: An Efficient General Purpose Program for Assigning Sequence Reads to Genomic Features.” *Bioinformatics* 30 (7): 923–30. <https://doi.org/10.1093/bioinformatics/btt656>.
- Liao, Yuxing, Jing Wang, Eric J Jaehnig, Zhiao Shi, and Bing Zhang. 2019. “WebGestalt 2019: Gene Set Analysis Toolkit with Revamped UIs and APIs.” *Nucleic Acids Research* 47: 199–205. <https://doi.org/10.1093/nar/gkz401>.
- Lindberg, Catharina, Erik Hjorth, Claes Post, Bengt Winblad, and Marianne Schultzberg. 2005. “Cytokine Production by a Human Microglial Cell Line: Effects of Bamyloid and α -Melanocyte-Stimulating Hormone.” *Neurotoxicity Research* 8 (3–4): 267–76. <https://doi.org/10.1007/BF03033980>.
- Lino, Christopher A., Jason C. Harper, James P. Carney, and Jerilyn A. Timlin. 2018. “Delivering Crispr: A Review of the Challenges and Approaches.” *Drug Delivery*. Taylor and Francis Ltd. <https://doi.org/10.1080/10717544.2018.1474964>.
- Lisi, Lucia, Egidio Stigliano, Libero Lauriola, Pierluigi Navarra, and Cinzia Dello Russo. 2014. “Proinflammatory-Activated Glioma Cells Induce a Switch in Microglial Polarization and Activation Status, from a Predominant M2b Phenotype to a Mixture of M1 and M2a/B Polarized Cells.” *ASN Neuro* 6 (3): 171–83. <https://doi.org/10.1042/AN20130045>.
- Looyenga, Brendan D., Danielle Hutchings, Irene Cherni, Chris Kingsley, Glen J. Weiss, and Jeffrey P. MacKeigan. 2012. “STAT3 Is Activated by JAK2 Independent of Key Oncogenic Driver Mutations in Non-Small Cell Lung Carcinoma.” Edited by Juri G. Gelovani. *PLoS ONE* 7 (2): e30820. <https://doi.org/10.1371/journal.pone.0030820>.

- Louis, David N., Arie Perry, Guido Reifenberger, Andreas von Deimling, Dominique Figarella-Branger, Webster K. Cavenee, Hiroko Ohgaki, Otmar D. Wiestler, Paul Kleihues, and David W. Ellison. 2016. "The 2016 World Health Organization Classification of Tumors of the Central Nervous System: A Summary." *Acta Neuropathologica* 131 (6): 803–20. <https://doi.org/10.1007/s00401-016-1545-1>.
- Love, Michael I., Wolfgang Huber, and Simon Anders. 2014. "Moderated Estimation of Fold Change and Dispersion for RNA-Seq Data with DESeq2." *Genome Biology* 15 (12): 550. <https://doi.org/10.1186/s13059-014-0550-8>.
- Lu, Nathan, and Charles J. Malemud. 2019. "Extracellular Signal-Regulated Kinase: A Regulator of Cell Growth, Inflammation, Chondrocyte and Bone Cell Receptor-Mediated Gene Expression." *International Journal of Molecular Sciences* 20 (15): 1–18. <https://doi.org/10.3390/ijms20153792>.
- Lund, Maria E., Joyce To, Bronwyn A. O'Brien, and Sheila Donnelly. 2016. "The Choice of Phorbol 12-Myristate 13-Acetate Differentiation Protocol Influences the Response of THP-1 Macrophages to a pro-Inflammatory Stimulus." *Journal of Immunological Methods* 430 (March): 64–70. <https://doi.org/10.1016/J.JIM.2016.01.012>.
- Ma, Chunfang, Yin Wang, Lei Dong, Minjing Li, and Wanru Cai. 2015. "Anti-Inflammatory Effect of Resveratrol through the Suppression of NF-KB and JAK/STAT Signaling Pathways." *Acta Biochimica et Biophysica Sinica* 47 (3): 207–13. <https://doi.org/10.1093/abbs/gmu135>.
- Maas, Sybren L.N., Erik R. Abels, Lieke L. Van De Haar, Xuan Zhang, Liza Morsett, Srinjoy Sil, Joana Guedes, et al. 2020. "Glioblastoma Hijacks Microglial Gene Expression to Support Tumor Growth." *Journal of Neuroinflammation* 17 (1): 120. <https://doi.org/10.1186/s12974-020-01797-2>.
- Mailliard, Robbie B., Sean M. Alber, Hongmei Shen, Simon C. Watkins, John M. Kirkwood, Ronald B. Herberman, and Pawel Kalinski. 2005. "IL-18-Induced CD83+CCR7+ NK Helper Cells." *Journal of Experimental Medicine* 202 (7): 941–53. <https://doi.org/10.1084/jem.20050128>.
- Markovic, D S, K Vinnakota, S Chirasani, M Synowitz, H Ragueta, K Stock, M Sliwa, et al.

2009. "Gliomas Induce and Exploit Microglial MT1-MMP Expression for Tumor Expansion." *Proceedings of the National Academy of Sciences of the United States of America* 106 (30): 12530–35. <https://doi.org/10.1073/pnas.0804273106>.
- Martin, Sophie, Erika C. Cosset, Jérôme Terrand, Anne Maglott, Ken Takeda, and Monique Dontenwill. 2009. "Caveolin-1 Regulates Glioblastoma Aggressiveness through the Control of A5 β 1 Integrin Expression and Modulates Glioblastoma Responsiveness to SJ749, an A5 β 1 Integrin Antagonist." *Biochimica et Biophysica Acta - Molecular Cell Research* 1793 (2): 354–67. <https://doi.org/10.1016/j.bbamcr.2008.09.019>.
- Mathieu, Marie Emmanuelle, Claire Saucourt, Virginie Mournetas, Xavier Gauthereau, Nadine Thézé, Vincent Praloran, Pierre Thiébaud, and Hélène Bœuf. 2012. "LIF-Dependent Signaling: New Pieces in the Lego." *Stem Cell Reviews and Reports*. Springer. <https://doi.org/10.1007/s12015-011-9261-7>.
- Maugeri-saccà, Marcello, Simona Di Martino, and Ruggero De Maria. 2013. "Biological and Clinical Implications of Cancer Stem Cells in Primary Brain Tumors." *Frontiers in Oncology* 3 (January): 1–10. <https://doi.org/10.3389/fonc.2013.00006>.
- Medina, Freddy A., Cecilia J. De Almeida, Elliott Dew, Jiangwei Li, Gloria Bonuccelli, Terence M. Williams, Alex W. Cohen, et al. 2006. "Caveolin-1-Deficient Mice Show Defects in Innate Immunity and Inflammatory Immune Response during Salmonella Enterica Serovar Typhimurium Infection." *Infection and Immunity* 74 (12): 6665–74. <https://doi.org/10.1128/IAI.00949-06>.
- Meir, Erwin G Van, Costas G Hadjipanayis, Andrew D Norden, and Hui-kuo Shu. 2010. "Exciting New Advances in Neuro-Oncology The Avenue to a Cure for Malignant Glioma." *Cancer Journal for Clinicians* 60 (3): 166–93. <https://doi.org/10.3322/caac.20069>.
- Melief, J., M. A. M. Sneeboer, M. Litjens, P. R. Ormel, S. J. M. C. Palmén, I. Huitinga, R. S. Kahn, E. M. Hol, and L. D. de Witte. 2016. "Characterizing Primary Human Microglia: A Comparative Study with Myeloid Subsets and Culture Models." *Glia* 64 (11): 1857–68. <https://doi.org/10.1002/glia.23023>.

- Meng, Xiangqi, Chunbin Duan, Hengyuan Pang, Qun Chen, Bo Han, Caijun Zha, Magafurov Dinislam, et al. 2019. "DNA Damage Repair Alterations Modulate M2 Polarization of Microglia to Remodel the Tumor Microenvironment via the P53-Mediated MDK Expression in Glioma." *EBioMedicine* 41 (March): 185–99. <https://doi.org/10.1016/j.ebiom.2019.01.067>.
- Metcalf, Donald. 2008. "Hematopoietic Cytokines." *Blood*. The American Society of Hematology. <https://doi.org/10.1182/blood-2007-03-079681>.
- Molinaro, Annette M., Jennie W. Taylor, John K. Wiencke, and Margaret R. Wrensch. 2019. "Genetic and Molecular Epidemiology of Adult Diffuse Glioma." *Nature Reviews Neurology*. Nature Publishing Group. <https://doi.org/10.1038/s41582-019-0220-2>.
- Monier, Solange, Dennis J. Dietzen, W.Randall Hastings, Douglas M. Lublin, and Teymuras V. Kurzchalia. 1996. "Oligomerization of VIP21-Caveolin in Vitro Is Stabilized by Long Chain Fatty Acylation or Cholesterol." *FEBS Letters* 388 (2–3): 143–49. [https://doi.org/10.1016/0014-5793\(96\)00519-4](https://doi.org/10.1016/0014-5793(96)00519-4).
- Monier, Solange, Robert G Parton, Frank Vogel, Joachim Behlke, Annemarie Henske, and Teymuras V Kurzchalia. 1995. "VIP21-Caveolin, a Membrane Protein Constituent of the Caveolar Coat, Oligomerizes In Vivo and In Vitro." *Molecular Biology of the Cell*. Vol. 6.
- Moreno-Vicente, Roberto, Dácil María Pavón, Inés Martín-Padura, Mauro Català-Montoro, Alberto Díez-Sánchez, Antonio Quílez-Álvarez, Juan Antonio López, et al. 2018. "Caveolin-1 Modulates Mechanotransduction Responses to Substrate Stiffness through Actin-Dependent Control of YAP." *Cell Reports* 25 (6): 1622–1635.e6. <https://doi.org/10.1016/j.celrep.2018.10.024>.
- Moriconi, Chiara. 2019. "Caveolin-1: A Mediator of Glioblastoma Cell Invasion and an Independent Negative Biomarker of Glioblastoma Patient Survival." Cardiff: Cardiff University.
- Moriconi, Chiara, Valentina Palmieri, Riccardo Di Santo, Giusy Tornillo, Massimiliano Papi, Geoff Pilkington, Marco De Spirito, and Mark Gumbleton. 2017. "INSIDIA: A

- Fiji Macro Delivering High-Throughput and High-Content Spheroid Invasion Analysis." *Biotechnology Journal* 12 (10): 1700140. <https://doi.org/10.1002/biot.201700140>.
- Mostofa, A. G.M., Surendra R. Punganuru, Hanumantha Rao Madala, Mohammad Al-Obaide, and Kalkunte S. Srivenugopal. 2017. "The Process and Regulatory Components of Inflammation in Brain Oncogenesis." *Biomolecules*. MDPI AG. <https://doi.org/10.3390/biom7020034>.
- Muffat, Julien, Yun Li, Bingbing Yuan, Maisam Mitalipova, Attya Omer, Sean Corcoran, Grisilda Bakiasi, et al. 2016. "Efficient Derivation of Microglia-like Cells from Human Pluripotent Stem Cells." *Nature Medicine* 22 (11): 1358–67. <https://doi.org/10.1038/nm.4189>.
- Murata, Masayuki, Johan Peränen, Rupert Schreiner, Felix Wieland, Teymuraz V. Kurzchalia, and Kai Simons. 1995. "VIP21/Caveolin Is a Cholesterol-Binding Protein." *Proceedings of the National Academy of Sciences of the United States of America* 92 (22): 10339–43. <https://doi.org/10.1073/pnas.92.22.10339>.
- Myöhänen, H., and A. Vaheri. 2004. "Regulation and Interactions in the Activation of Cell-Associated Plasminogen." *Cellular and Molecular Life Sciences*. Cell Mol Life Sci. <https://doi.org/10.1007/s00018-004-4230-9>.
- Nagai, A., E. Nakagawa, K. Hatori, H. B. Choi, J. G. McLarnon, M. A. Lee, and S. U. Kim. 2001. "Generation and Characterization of Immortalized Human Microglial Cell Lines: Expression of Cytokines and Chemokines." *Neurobiology of Disease* 8 (6): 1057–68. <https://doi.org/10.1006/nbdi.2001.0437>.
- Nagoshi, Narihito, and Hideyuki Okano. 2018. "iPSC-Derived Neural Precursor Cells: Potential for Cell Transplantation Therapy in Spinal Cord Injury." *Cellular and Molecular Life Sciences* 75 (6): 989–1000. <https://doi.org/10.1007/s00018-017-2676-9>.
- Niesman, Ingrid R., Nathan Zemke, Heidi N. Fridolfsson, Kristofer J. Haushalter, Karen Levy, Anna Grove, Rosalie Schnoor, et al. 2013. "Caveolin Isoform Switching as a Molecular, Structural, and Metabolic Regulator of Microglia." *Molecular and*

- Cellular Neuroscience* 56: 283–97. <https://doi.org/10.1016/j.mcn.2013.07.002>.
- Nifterik, Krista a Van, Jaap Van den Berg, Ben J Slotman, M Vincent M Lafleur, Peter Sminia, and Lukas J a Stalpers. 2012. “Valproic Acid Sensitizes Human Glioma Cells for Temozolomide and γ -Radiation.” *Journal of Neuro-Oncology* 107 (1): 61–67. <https://doi.org/10.1007/s11060-011-0725-z>.
- Nijaguna, Mamatha Bangalore, Vikas Patil, Serge Urbach, Shivayogi D. Shwetha, Kotha Sravani, Alangar S. Hegde, Bangalore A. Chandramouli, et al. 2015. “Glioblastoma-Derived Macrophage Colony-Stimulating Factor (MCSF) Induces Microglial Release of Insulin-like Growth Factor-Binding Protein 1 (IGFBP1) to Promote Angiogenesis.” *Journal of Biological Chemistry* 290 (38): 23401–15. <https://doi.org/10.1074/jbc.M115.664037>.
- Nohe, Anja, Eleonora Keating, T. Michael Underhill, Petra Knaus, and Nils O. Petersen. 2005. “Dynamics and Interaction of Caveolin-1 Isoforms with BMP-Receptors.” *Journal of Cell Science* 118 (3): 643–50. <https://doi.org/10.1242/jcs.01402>.
- Norkin, Leonard C. 1999. “Simian Virus 40 Infection via MHC Class I Molecules and Caveolae.” *Immunological Reviews* 168 (1): 13–22. <https://doi.org/10.1111/j.1600-065X.1999.tb01279.x>.
- Ohgaki, Hiroko, and Paul Kleihues. 2013. “The Definition of Primary and Secondary Glioblastoma.” *Clinical Cancer Research: An Official Journal of the American Association for Cancer Research* 19 (4): 764–72. <https://doi.org/10.1158/1078-0432.CCR-12-3002>.
- Omuro, Antonio. 2013. “Glioblastoma and Other Malignant Gliomas.” *Jama* 310 (17): 1842. <https://doi.org/10.1001/jama.2013.280319>.
- Omuro, Antonio, and Lisa M DeAngelis. 2013. “Glioblastoma and Other Malignant Gliomas: A Clinical Review.” *JAMA: The Journal of the American Medical Association* 310 (17): 1842–50. <https://doi.org/10.1001/jama.2013.280319>.
- Orihuela, Ruben, Christopher A McPherson, and Gaylia Jean Harry. 2016. “Microglial M1/M2 Polarization and Metabolic States.” *British Journal of Pharmacology* 173 (4): 649–65. <https://doi.org/10.1111/bph.13139>.

- Orlandi, Palmer A., and Peter H. Fishman. 1998. "Filipin-Dependent Inhibition of Cholera Toxin: Evidence for Toxin Internalization and Activation through Caveolae-like Domains." *Journal of Cell Biology* 141 (4): 905–15. <https://doi.org/10.1083/jcb.141.4.905>.
- Ostrom, Quinn T., Gino Cioffi, Haley Gittleman, Nirav Patil, Kristin Waite, Carol Kruchko, and Jill S. Barnholtz-Sloan. 2019. "CBTRUS Statistical Report: Primary Brain and Other Central Nervous System Tumors Diagnosed in the United States in 2012-2016." *Neuro-Oncology*. Oxford University Press. <https://doi.org/10.1093/neuonc/noz150>.
- Palade, George E. 1953. "Fine Structure of Blood Capillaries." *Journal of Applied Physics* 24: 1424–1953. <https://doi.org/doi:10.1161/01.RES.27.3.482>.
- Palumbo, Silvia, Luigi Pirtoli, Paolo Tini, Gabriele Cevenini, Francesco Calderaro, Marzia Toscano, Clelia Miracco, and Sergio Comincini. 2012. "Different Involvement of Autophagy in Human Malignant Glioma Cell Lines Undergoing Irradiation and Temozolomide Combined Treatments." *Journal of Cellular Biochemistry* 113 (7): 2308–18. <https://doi.org/10.1002/jcb.24102>.
- Pandya, Hetal, Michael J. Shen, David M. Ichikawa, Andrea B. Sedlock, Yong Choi, Kory R. Johnson, Gloria Kim, et al. 2017. "Differentiation of Human and Murine Induced Pluripotent Stem Cells to Microglia-like Cells." *Nature Neuroscience* 20 (5): 753–59. <https://doi.org/10.1038/nn.4534>.
- Park, Deric M, and Jeremy N Rich. 2009. "Biology of Glioma Cancer Stem Cells." *Molecules and Cells* 28 (1): 7–12. <https://doi.org/10.1007/s10059-009-0111-2>.
- Park, Young Jun, Gang Liu, Emmanuel F. Lorne, Xia Zhao, Jing Wang, Yuko Tsuruta, Jaroslaw Zmijewski, and Edward Abraham. 2008. "PAI-1 Inhibits Neutrophil Efferocytosis." *Proceedings of the National Academy of Sciences of the United States of America* 105 (33): 11784–89. <https://doi.org/10.1073/pnas.0801394105>.
- Parkhurst, Christopher N., Guang Yang, Ipe Ninan, Jeffrey N. Savas, John R. Yates, Juan J. Lafaille, Barbara L. Hempstead, Dan R. Littman, and Wen Biao Gan. 2013. "Microglia Promote Learning-Dependent Synapse Formation through Brain-

- Derived Neurotrophic Factor.” *Cell* 155 (7): 1596–1609. <https://doi.org/10.1016/j.cell.2013.11.030>.
- Parton, Robert G., and Kai Simons. 2007. “The Multiple Faces of Caveolae.” *Nature Reviews Molecular Cell Biology*. Nature Publishing Group. <https://doi.org/10.1038/nrm2122>.
- Pasca, Anca M., Steven A. Sloan, Laura E. Clarke, Yuan Tian, Christopher D. Makinson, Nina Huber, Chul Hoon Kim, et al. 2015. “Functional Cortical Neurons and Astrocytes from Human Pluripotent Stem Cells in 3D Culture.” *Nature Methods* 12 (7): 671–78. <https://doi.org/10.1038/nmeth.3415>.
- Pastore, Saveria, Francesca Mascia, Feliciana Mariotti, Cristina Dattilo, Valentina Mariani, and Giampiero Girolomoni. 2005. “ERK1/2 Regulates Epidermal Chemokine Expression and Skin Inflammation.” *The Journal of Immunology* 174 (8): 5047–56. <https://doi.org/10.4049/jimmunol.174.8.5047>.
- Pennock, Nathan D., Jason T. White, Eric W. Cross, Elizabeth E. Cheney, Beth A. Tamburini, and Ross M. Kedl. 2013. “T Cell Responses: Naïve to Memory and Everything in Between.” *American Journal of Physiology - Advances in Physiology Education* 37 (4): 273–83. <https://doi.org/10.1152/advan.00066.2013>.
- Perry, V. Hugh, and Jessica Teeling. 2013. “Microglia and Macrophages of the Central Nervous System: The Contribution of Microglia Priming and Systemic Inflammation to Chronic Neurodegeneration.” *Seminars in Immunopathology*. Springer. <https://doi.org/10.1007/s00281-013-0382-8>.
- Piperi, Christina, Marios S Themistocleous, George a Papavassiliou, Elena Farmaki, Georgia Levidou, Penelope Korkolopoulou, Christos Adamopoulos, and Athanasios G Papavassiliou. 2010. “High Incidence of MGMT and RARbeta Promoter Methylation in Primary Glioblastomas: Association with Histopathological Characteristics, Inflammatory Mediators and Clinical Outcome.” *Molecular Medicine* 16 (1–2): 1–9. <https://doi.org/10.2119/molmed.2009.00140>.
- Platten, Michael, Alexandra Kretz, Ulrike Naumann, Steffen Aulwurm, Kensuke Egashira, Stefan Isenmann, and Michael Weller. 2003. “Monocyte Chemoattractant Protein-

- 1 Increases Microglial Infiltration and Aggressiveness of Gliomas.” *Annals of Neurology* 54: 388–92. <https://doi.org/10.1002/ana.10679>.
- Pol, Albert, Sally Martin, Manuel A. Fernández, Mercedes Ingelmo-Torres, Charles Ferguson, Carlos Enrich, and Robert G. Parton. 2005. “Cholesterol and Fatty Acids Regulate Dynamic Caveolin Trafficking through the Golgi Complex and between the Cell Surface and Lipid Bodies.” *Molecular Biology of the Cell* 16 (4): 2091–2105. <https://doi.org/10.1091/mbc.E04-08-0737>.
- Portugal, Camila C, Renato Socodato, Teresa Canedo, Cátia M Silva, Tânia Martins, Vivian S M Coreixas, Erick C Loiola, et al. 2017. “Caveolin-1-Mediated Internalization of the Vitamin C Transporter SVCT2 in Microglia Triggers an Inflammatory Phenotype.” *Science Signaling* 10 (472): eaal2005. <https://doi.org/10.1126/scisignal.aal2005>.
- Prionisti, Ioanna, Léo H. Bühler, Paul R. Walker, and Renaud B. Jolivet. 2019. “Harnessing Microglia and Macrophages for the Treatment of Glioblastoma.” *Frontiers in Pharmacology*. Frontiers Media S.A. <https://doi.org/10.3389/fphar.2019.00506>.
- Province, Paula, Alexis Bashinski Shaefer, Benjamin Mccullough, and Hassan M Fathallah-shaykh. 2010. “Anti-Angiogenesis, Gene Therapy , and Immunotherapy in Malignant Gliomas.” In *Tumors of the Central Nervous System - Primary and Secondary*, 177–221. <http://dx.doi.org/10.5772/58320>.
- Pu, Wenjun, Zeyad D. Nassar, Samira Khabbazi, Nan Xie, Kerrie-Ann McMahon, Robert G. Parton, Gregory J. Riggins, Jonathan M. Harris, and Marie-Odile Parat. 2019. “Correlation of the Invasive Potential of Glioblastoma and Expression of Caveola-Forming Proteins Caveolin-1 and CAVIN1.” *Journal of Neuro-Oncology*, April, 1–14. <https://doi.org/10.1007/s11060-019-03161-8>.
- Pyonteck, Stephanie M, Leila Akkari, Alberto J Schuhmacher, Robert L Bowman, Lisa Sevenich, Daniela F Quail, Oakley C Olson, et al. 2013. “CSF-1R Inhibition Alters Macrophage Polarization and Blocks Glioma Progression.” *Nature Medicine* 19 (10): 1264–72. <https://doi.org/10.1038/nm.3337>.
- Qian, Bin-Zhi, and Jeffrey W. Pollard. 2010. “Macrophage Diversity Enhances Tumor Progression and Metastasis.” *Cell* 141 (1): 39–51.

<https://doi.org/10.1016/j.cell.2010.03.014>.

Quann, Kevin, Donna M. Gonzales, Isabelle Mercier, Chenguang Wang, Federica Sotgia, Richard G. Pestell, Michael P. Lisanti, and Jean Francois Jasmin. 2013. "Caveolin-1 Is a Negative Regulator of Tumor Growth in Glioblastoma and Modulates Chemosensitivity to Temozolomide." *Cell Cycle* 12 (10): 1510–20. <https://doi.org/10.4161/cc.24497>.

Quest, Andrew F. G., Jorge L. Gutierrez-Pajares, and Vicente A. Torres. 2008. "Caveolin-1: An Ambiguous Partner in Cell Signalling and Cancer." *Journal of Cellular and Molecular Medicine* 12 (4): 1130–50. <https://doi.org/10.1111/j.1582-4934.2008.00331.x>.

Ramírez, Cristina M., Miriam González, Mario Díaz, Rafael Alonso, Isidre Ferrer, Gabriel Santpere, Berta Puig, Gundela Meyer, and Raquel Marin. 2009. "VDAC and ER α Interaction in Caveolae from Human Cortex Is Altered in Alzheimer's Disease." *Molecular and Cellular Neuroscience* 42 (3): 172–83. <https://doi.org/10.1016/j.mcn.2009.07.001>.

Ran, F Ann, Patrick D Hsu, Jason Wright, Vineeta Agarwala, David A Scott, and Feng Zhang. 2013. "Genome Engineering Using the CRISPR-Cas9 System." *Nat. Protocols* 8 (11): 2281–2308. <https://doi.org/10.1038/nprot.2013.143> <http://www.nature.com/nprot/journal/v8/n11/abs/nprot.2013.143.html#supplementary-information>.

Ransohoff, Richard M., and Astrid E. Cardona. 2010. "The Myeloid Cells of the Central Nervous System Parenchyma." *Nature* 468 (7321): 253–62. <https://doi.org/10.1038/nature09615>.

Rao, Chandra, David Chianese, Gerald Doyle, M. Miller, Thomas Russell, Renouard Sanders, and Leon Terstappen. 2005. "Expression of Epithelial Cell Adhesion Molecule in Carcinoma Cells Present in Blood and Primary and Metastatic Tumors." *International Journal of Oncology* 27 (1): 49–57. <https://doi.org/10.3892/ijo.27.1.49>.

Rao, Donald D., John S. Vorhies, Neil Senzer, and John Nemunaitis. 2009. "SiRNA vs.

- ShRNA: Similarities and Differences." *Advanced Drug Delivery Reviews* 61 (9): 746–59. <https://doi.org/10.1016/J.ADDR.2009.04.004>.
- Rathi, Abhilasha V., Paul G. Cantalupo, Saumendra N. Sarkar, and James M. Pipas. 2010. "Induction of Interferon-Stimulated Genes by Simian Virus 40 T Antigens." *Virology* 406 (2): 202–11. <https://doi.org/10.1016/j.virol.2010.07.018>.
- Razani, Babak, Scott E. Woodman, and Michael P. Lisanti. 2002. "Caveolae: From Cell Biology to Animal Physiology." *Pharmacological Reviews* 54 (3): 431–67.
- Razani, Babak, Xiao Lan Zhang, Markus Bitzer, Gero Von Gersdorff, Erwin P. Böttinger, and Michael P. Lisanti. 2001. "Caveolin-1 Regulates Transforming Growth Factor (TGF)- β /SMAD Signaling through an Interaction with the TGF- β Type I Receptor." *Journal of Biological Chemistry* 276 (9): 6727–38. <https://doi.org/10.1074/jbc.M008340200>.
- Redmond, Kristin J, and Minesh Mehta. 2015. "Stereotactic Radiosurgery for Glioblastoma." *Cureus* 7 (12): e413. <https://doi.org/10.7759/cureus.413>.
- Réu, Pedro, Azadeh Khosravi, Samuel Bernard, Jeff E. Mold, Mehran Salehpour, Kanar Alkass, Shira Perl, et al. 2017. "The Lifespan and Turnover of Microglia in the Human Brain." *Cell Reports* 20 (4): 779–84. <https://doi.org/10.1016/j.celrep.2017.07.004>.
- Río-Hortega, Pio del. 1919a. "El 'Tercer' Elemento" de Los Centros Nerviosos: Poder Fagocitario y Movilidad de La Microglia." *Bol Soc Esp Biol*, no. 9: 154–66.
- . 1919b. "El 'Tercer Elemento' de Los Centros Nerviosos. III. Naturaleza Probable de La Microglía." *Bol Soc Esp Biol*, no. 9: 109–20.
- . 1919c. "El Tercer Elemento de Los Centros Nerviosos. I. La Microglia En Estado nor-Mal. II. Intervencion de La Microglia En Los Procesos Patologicos. III. Naturaleza Probable de La Microglia." *Bol Soc Esp Biol* 9: 69–120.
- . 1919d. "'Tercer Elemento' de Los Centros Nerviosos. II. Intervencion de La Microglia En Los Procesos Patologicos (Cellulas En Bastocito y Cuerpos Granulo-Adiposos)." *Bol Soc Esp Biol* 9: 91–103.
- . 1993. "Art and Artifice in the Science of Histology." *Histopathology* 22 (6): 515–

25. <https://doi.org/10.1111/j.1365-2559.1993.tb00171.x>.
- Rita, Ana, Pombo Antunes, Isabelle Scheyltjens, Johnny Duerinck, Bart Neyns, Kiavash Movahedi, Jo A Van Ginderachter, et al. 2020. "Understanding the Glioblastoma Immune Microenvironment as Basis for the Development of New Immunotherapeutic Strategies." *ELife* 9 (February). <https://doi.org/10.7554/eLife.52176>.
- Roth, Patrick, Markus Junker, Isabel Tritschler, Michel Mittelbronn, Yvonne Dombrowski, Samuel N. Breit, Ghazaleh Tabatabai, Wolfgang Wick, Michael Weller, and Jörg Wischhusen. 2010. "GDF-15 Contributes to Proliferation and Immune Escape of Malignant Gliomas." *Clinical Cancer Research* 16 (15): 3851–59. <https://doi.org/10.1158/1078-0432.CCR-10-0705>.
- Russo, Cinzia Dello, Natalia Cappoli, Isabella Coletta, Daniele Mezzogori, Fabiola Paciello, Giacomo Pozzoli, Pierluigi Navarra, and Alessandra Battaglia. 2018. "The Human Microglial HMC3 Cell Line: Where Do We Stand? A Systematic Literature Review." *Journal of Neuroinflammation* 15 (1): 259. <https://doi.org/10.1186/s12974-018-1288-0>.
- Sahaj, Erik. 2005. "Mechanisms of Cancer Cell Invasion." *Current Opinion in Genetics & Development* 15 (1): 87–96. <https://doi.org/10.1016/j.gde.2004.12.002>.
- Scherer, Philipp E., Zhao Lan Tang, Miyoung Chun, Massimo Sargiacomo, Harvey F. Lodish, and Michael P. Lisanti. 1995. "Caveolin Isoforms Differ in Their N-Terminal Protein Sequence and Subcellular Distribution: Identification and Epitope Mapping of an Isoform-Specific Monoclonal Antibody Probe." *Journal of Biological Chemistry* 270 (27): 16395–401. <https://doi.org/10.1074/jbc.270.27.16395>.
- Schettters, Sjoerd T.T., Diego Gomez-Nicola, Juan J. Garcia-Vallejo, and Yvette Van Kooyk. 2018. "Neuroinflammation: Microglia and T Cells Get Ready to Tango." *Frontiers in Immunology* 8 (JAN): 1905. <https://doi.org/10.3389/fimmu.2017.01905>.
- Schulz, Christian, Elisa Gomez Perdiguero, Laurent Chorro, Heather Szabo-Rogers, Nicolas Cagnard, Katrin Kierdorf, Marco Prinz, et al. 2012. "A Lineage of Myeloid Cells Independent of Myb and Hematopoietic Stem Cells." *Science* 335 (6077): 86–

90. <https://doi.org/10.1126/science.1219179>.
- Seker, Fidan, Ahmet Cingoz, İlknur Sur-Erdem, Nazli Erguder, Alp Erkent, Firat Uyulur, Myvizhi Esai Selvan, et al. 2019. "Identification of SERPINE1 as a Regulator of Glioblastoma Cell Dispersal with Transcriptome Profiling." *Cancers* 11 (11). <https://doi.org/10.3390/cancers11111651>.
- Senetta, Rebecca, Giulia Stella, Ernesto Pozzi, Niccolo Sturli, Daniela Massi, and Paola Cassoni. 2013. "Caveolin-1 as a Promoter of Tumour Spreading: When, How, Where and Why." *Journal of Cellular and Molecular Medicine* 17 (3): 325–36. <https://doi.org/10.1111/jcmm.12030>.
- Serio, Andrea, Bilada Bilican, Sami J Barmada, Dale Michael Ando, Chen Zhao, Rick Siller, Karen Burr, et al. 2013. "Astrocyte Pathology and the Absence of Non-Cell Autonomy in an Induced Pluripotent Stem Cell Model of TDP-43 Proteinopathy." *Proceedings of the National Academy of Sciences of the United States of America* 110 (12): 4697–4702. <https://doi.org/10.1073/pnas.1300398110>.
- Shao, Bin, Xiawei Wei, Min Luo, Jiayun Yu, Aiping Tong, Xuelei Ma, Tinghong Ye, et al. 2015. "Inhibition of A20 Expression in Tumor Microenvironment Exerts Anti-Tumor Effect through Inducing Myeloid-Derived Suppressor Cells Apoptosis." *Scientific Reports* 5 (November): 16437. <https://doi.org/10.1038/srep16437>.
- Sharma, Ira, Avninder Singh, Fouzia Siraj, and Sunita Saxena. 2018. "IL-8/CXCR1/2 Signalling Promotes Tumor Cell Proliferation, Invasion and Vascular Mimicry in Glioblastoma." *Journal of Biomedical Science* 25 (1): 62. <https://doi.org/10.1186/s12929-018-0464-y>.
- Shen, Xianli, Miguel A Burguillos, Ahmed M Osman, Jeroen Frijhoff, Alejandro Carrillo-Jiménez, Sachie Kanatani, Martin Augsten, et al. 2016. "Glioma-Induced Inhibition of Caspase-3 in Microglia Promotes a Tumor-Supportive Phenotype." *Nature Immunology*, no. September. <https://doi.org/10.1038/ni.3545>.
- Shimato, Shinji, Lisa M. Anderson, Martin Asslaber, Jeffrey N. Bruce, Peter Canoll, David E. Anderson, and Richard C. E. Anderson. 2013. "Inhibition of Caveolin-1 Restores Myeloid Cell Function in Human Glioblastoma." Edited by James Bradley Elder. *PLoS*

- ONE* 8 (10): 1–8. <https://doi.org/10.1371/journal.pone.0077397>.
- Shin, Taekyun. 2007. “Increases in the Phosphorylated Form of Caveolin-1 in the Spinal Cord of Rats with Clip Compression Injury.” *Brain Research* 1141 (April): 228–34. <https://doi.org/10.1016/j.brainres.2007.01.009>.
- Shivshankar, Pooja, Ganesh V. Halade, Cheresa Calhoun, Gladys P. Escobar, Ali J. Mehr, Fabio Jimenez, Cindy Martinez, et al. 2014. “Caveolin-1 Deletion Exacerbates Cardiac Interstitial Fibrosis by Promoting M2 Macrophage Activation in Mice after Myocardial Infarction.” *Current Therapeutic Research - Clinical and Experimental* 76 (November): 84–93. <https://doi.org/10.1016/j.yjmcc.2014.07.020>.
- Sierra, Amanda, Rosa C. Paolicelli, and Helmut Kettenmann. 2019. “Cien Años de Microglía: Milestones in a Century of Microglial Research.” *Trends in Neurosciences*, October. <https://doi.org/10.1016/j.tins.2019.09.004>.
- Sinha, Sanchari, Nitin Koul, Deobrat Dixit, Vivek Sharma, and Ellora Sen. 2011. “IGF-1 Induced HIF-1 α -TLR9 Cross Talk Regulates Inflammatory Responses in Glioma.” *Cellular Signalling* 23 (11): 1869–75. <https://doi.org/10.1016/j.cellsig.2011.06.024>.
- Skog, Johan, Tom Würdinger, Sjoerd van Rijn, Dimphna H. Meijer, Laura Gainche, William T. Curry, Bob S. Carter, Anna M. Krichevsky, and Xandra O. Breakefield. 2008. “Glioblastoma Microvesicles Transport RNA and Proteins That Promote Tumour Growth and Provide Diagnostic Biomarkers.” *Nature Cell Biology* 10 (12): 1470–76. <https://doi.org/10.1038/ncb1800>.
- Soeda, A, M Park, D Lee, A Mintz, R D McKay, J Engh, T Iwama, et al. 2009. “Hypoxia Promotes Expansion of the CD133-Positive Glioma Stem Cells through Activation of HIF-1 A.” *Oncogene* 28 (45): 3949–59. <https://doi.org/10.1038/onc.2009.252>.
- Sohn, Jihee, Rachel M. Brick, and Rocky S. Tuan. 2016. “From Embryonic Development to Human Diseases: The Functional Role of Caveolae/Caveolin.” *Birth Defects Research Part C: Embryo* 108 (1): 45–64. <https://doi.org/10.1002/bdrc.21121>.
- Sotgia, Federica, Ubaldo E Martinez-Outschoorn, Anthony Howell, Richard G Pestell, Stephanos Pavlides, and Michael P Lisanti. 2012. “Caveolin-1 and Cancer Metabolism in the Tumor Microenvironment: Markers, Models, and Mechanisms.”

- Annu. Rev. Pathol. Mech. Dis* 7: 423–67. <https://doi.org/10.1146/annurev-pathol-011811-120856>.
- Stergiou, Lilli, Manuel Bauer, Waltraud Mair, Damaris Bausch-Fluck, Nir Drayman, Bernd Wollscheid, Ariella Oppenheim, and Lucas Pelkmans. 2013. “Integrin-Mediated Signaling Induced by Simian Virus 40 Leads to Transient Uncoupling of Cortical Actin and the Plasma Membrane.” Edited by Ludger Johannes. *PLoS ONE* 8 (2): e55799. <https://doi.org/10.1371/journal.pone.0055799>.
- Stricker, Stefan H., Andrew Feber, Pär G. Engström, Helena Carén, Kathreena M. Kurian, Yasuhiro Takashima, Colin Watts, et al. 2013. “Widespread Resetting of DNA Methylation in Glioblastoma-Initiating Cells Suppresses Malignant Cellular Behavior in a Lineage-Dependent Manner.” *Genes and Development* 27 (6): 654–69. <https://doi.org/10.1101/gad.212662.112>.
- Stupp, R. 2005. “Radiotherapy plus Concomitant and Adjuvant Temozolomide for Glioblastoma.” *N Engl J Med* 352: 987–96. <http://dx.doi.org/10.1056/NEJMoa043330>.
- Sullivan, James P., Brian V. Nahed, Marissa W. Madden, Samantha M. Oliveira, Simeon Springer, Deepak Bhere, Andrew S. Chi, et al. 2014. “Brain Tumor Cells in Circulation Are Enriched for Mesenchymal Gene Expression.” *Cancer Discovery* 4 (11): 1299–1309. <https://doi.org/10.1158/2159-8290.CD-14-0471>.
- Suzumura, A, M Sawada, H Yamamoto, and T Marunouchi. 1993. “Transforming Growth Factor-Beta Suppresses Activation and Proliferation of Microglia in Vitro.” *Journal of Immunology (Baltimore, Md. : 1950)* 151: 2150–58.
- Sze, Chun-I, Wan-Pei Su, Ming-Fu Chiang, Chen-Yu Lu, Yu-An Chen, and Nan-Shan Chang. 2013. “Assessing Current Therapeutic Approaches to Decode Potential Resistance Mechanisms in Glioblastomas.” *Frontiers in Oncology* 3 (March): 59. <https://doi.org/10.3389/fonc.2013.00059>.
- Szepesi, Zsuzsanna, Oscar Manouchehrian, Sara Bachiller, and Tomas Deierborg. 2018. “Bidirectional Microglia–Neuron Communication in Health and Disease.” *Frontiers in Cellular Neuroscience*. Frontiers Media S.A.

<https://doi.org/10.3389/fncel.2018.00323>.

Taetle, R., J. Oval, M. Smedsrud, C. Davis, and B. Gansbacher. 1991. "Analysis of Granulocyte-Macrophage Colony-Stimulating Factor Action in Differentiating Myeloid Leukemia Cells: Treatment with DMSO May Reveal a Common Pathway for Growth Factor Gene Regulation." *Experimental Hematology*.

Takamura, Naoko, Yukie Yamaguchi, Yuko Watanabe, Miho Asami, Noriko Komitsu, and Michiko Aihara. 2019. "Downregulated Caveolin-1 Expression in Circulating Monocytes May Contribute to the Pathogenesis of Psoriasis." *Scientific Reports* 9 (1): 1–12. <https://doi.org/10.1038/s41598-018-36767-5>.

Takata, Kazuyuki, Tatsuya Kozaki, Christopher Zhe Wei Lee, Morgane Sonia Thion, Masayuki Otsuka, Shawn Lim, Kagistia Hana Utami, et al. 2017. "Induced-Pluripotent-Stem-Cell-Derived Primitive Macrophages Provide a Platform for Modeling Tissue-Resident Macrophage Differentiation and Function." *Immunity* 47 (1): 183-198.e6. <https://doi.org/10.1016/j.immuni.2017.06.017>.

Taniguchi, Koji, and Michael Karin. 2018. "NF- κ B, Inflammation, Immunity and Cancer: Coming of Age." *Nature Reviews Immunology*, January, 1–16. <https://doi.org/10.1038/nri.2017.142>.

Teo, Wan Yee, Karthik Sekar, Pratap Seshachalam, Jianhe Shen, Wing Yuk Chow, Ching C. Lau, Hee Kyoung Yang, et al. 2019. "Relevance of a TCGA-Derived Glioblastoma Subtype Gene-Classifer among Patient Populations." *Scientific Reports* 9 (1): 1–10. <https://doi.org/10.1038/s41598-019-43173-y>.

Thakkar, Jigisha P, Therese A Dolecek, Craig Horbinski, Quinn T Ostrom, Donita D Lightner, Jill S Barnholtz-Sloan, and John L Villano. 2014. "Epidemiologic and Molecular Prognostic Review of Glioblastoma." *Cancer Epidemiology, Biomarkers & Prevention: A Publication of the American Association for Cancer Research, Cosponsored by the American Society of Preventive Oncology* 23 (10): 1985–96. <https://doi.org/10.1158/1055-9965.EPI-14-0275>.

Timmerman, Raissa, Saskia M. Burm, and Jeffrey J. Bajramovic. 2018. "An Overview of in Vitro Methods to Study Microglia." *Frontiers in Cellular Neuroscience* 12

(August): 242. <https://doi.org/10.3389/fncel.2018.00242>.

Torres, Vicente A., Julio C. Tapia, Diego A. Rodríguez, Mario Párraga, Pamela Lisboa, Margarita Montoya, Lisette Leyton, and Andrew F.G. Quest. 2006. "Caveolin-1 Controls Cell Proliferation and Cell Death by Suppressing Expression of the Inhibitor of Apoptosis Protein Survivin." *Journal of Cell Science* 119 (9): 1812–23. <https://doi.org/10.1242/jcs.02894>.

Tsai, Tsung-Huang, Shu-Fen Chen, Tai-Yu Huang, Chun-Fu Tzeng, Ann-Shyn Chiang, Yu Ru Kou, Tzong-Shyuan Lee, and Song-Kun Shyue. 2011. "Impaired Cd14 and Cd36 Expression, Bacterial Clearance, and Toll-Like Receptor 4-Myd88 Signaling in Caveolin-1-Deleted Macrophages and Mice." *Shock* 35 (1): 92–99. <https://doi.org/10.1097/SHK.0b013e3181ea45ca>.

Uhlemann, Ria, Karen Gertz, Wolfgang Boehmerle, Tobias Schwarz, Christiane Nolte, Dorette Freyer, Helmut Kettenmann, Matthias Endres, and Golo Kronenberg. 2016. "Actin Dynamics Shape Microglia Effector Functions." *Brain Structure and Function* 221 (5): 2717–34. <https://doi.org/10.1007/s00429-015-1067-y>.

Vanwalscappel, Bénédicte, Takuya Tada, and Nathaniel R. Landau. 2018. "Toll-like Receptor Agonist R848 Blocks Zika Virus Replication by Inducing the Antiviral Protein Viperin." *Virology* 522 (September): 199–208. <https://doi.org/10.1016/j.virol.2018.07.014>.

Veeravalli, Krishna Kumar, Chandramu Chetty, Shivani Ponnala, Christopher S. Gondi, Sajani S. Lakka, Daniel Fassett, Jeffrey D. Klopfenstein, Dzung H. Dinh, Meena Gujrati, and Jasti S. Rao. 2010. "MMP-9, UPAR and Cathepsin B Silencing Downregulate Integrins in Human Glioma Xenograft Cells In Vitro and In Vivo in Nude Mice." Edited by Nils Cordes. *PLoS ONE* 5 (7): e11583. <https://doi.org/10.1371/journal.pone.0011583>.

Verhaak, Roel G W, Katherine A Hoadley, Elizabeth Purdom, Victoria Wang, Matthew D Wilkerson, C Ryan Miller, Li Ding, et al. 2010. "An Integrated Genomic Analysis Identifies Clinically Relevant Subtypes of Glioblastoma Characterized by Abnormalities in PDGFRA, IDH1, EGFR and NF1." *Cancer Cell* 17 (1): 1–25.

<https://doi.org/10.1016/j.ccr.2009.12.020>.An.

Vetterkind, Susanne, Ransom H. Poythress, Qian Qian Lin, and Kathleen G. Morgan. 2013. "Hierarchical Scaffolding of an ERK1/2 Activation Pathway." *Cell Communication and Signaling* 11 (1): 1–16. <https://doi.org/10.1186/1478-811X-11-65>.

Virgintino, D, D Robertson, M Errede, V Benaglio, U Tauer, L Roncali, and M Bertossi. 2002. "Expression of Caveolin-1 in Human Brain Microvessels." *Neuroscience* 115 (1): 145–52. [https://doi.org/10.1016/S0306-4522\(02\)00374-3](https://doi.org/10.1016/S0306-4522(02)00374-3).

Vleeschouwer, Steven De, Isabel Spencer Lopes, Jan L Ceuppens, and Stefaan W Van Gool. 2007. "Persistent IL-10 Production Is Required for Glioma Growth Suppressive Activity by Th1-Directed Effector Cells after Stimulation with Tumor Lysate-Loaded Dendritic Cells." *Journal of Neurooncology* 84 (2): 131–40. <https://doi.org/10.1007/s11060-007-9362-y>.

Walentynowicz, Kacper A., Natalia Ochocka, Maria Pasierbinska, Kamil Wojnicki, Karolina Stepniak, Jakub Mieczkowski, Iwona A. Ciechomska, and Bozena Kaminska. 2018. "In Search for Reliable Markers of Glioma-Induced Polarization of Microglia." *Frontiers in Immunology* 9 (1329): 1–13. <https://doi.org/10.3389/fimmu.2018.01329>.

Wang, Xiao Mei, Hong Pyo Kim, Ruiping Song, and Augustine M K Choi. 2006. "Caveolin-1 Confers Antiinflammatory Effects in Murine Macrophages via the MKK3/P38 MAPK Pathway." *American Journal of Respiratory Cell and Molecular Biology* 34 (4): 434–42. <https://doi.org/10.1165/rcmb.2005-0376OC>.

Wang, Zhiyu, Neng Wang, Pengxi Liu, Fu Peng, Hailin Tang, Qianjun Chen, Rui Xu, et al. 2015. "Caveolin-1, a Stress-Related Oncotarget, in Drug Resistance." *Oncotarget* 6 (35): 37135–50. www.impactjournals.com/oncotarget.

Washington, R.A., B. Becher, R. Balabanov, J. Antel, and P. Dore-Duffy. 1996. "Expression of the Activation Marker Urokinase Plasminogen-activator Receptor in Cultured Human Central Nervous System Microglia." *Journal of Neuroscience Research* 45 (4): 392–99. [https://doi.org/10.1002/\(SICI\)1097-4547\(19960815\)45:4<392::AID-](https://doi.org/10.1002/(SICI)1097-4547(19960815)45:4<392::AID-)

JNR8>3.0.CO;2-4.

- Watters, Jyoti J, Jill M Schartner, Behnam Badie, and Brain Tumors. 2005. "Mini-Review Microglia Function in Brain Tumors." *Journal of Neuroscience Research* 81: 447–55. <https://doi.org/10.1002/jnr.20485>.
- Wei, Jun, Konrad Gabrusiewicz, and Amy Heimberger. 2013. "The Controversial Role of Microglia in Malignant Gliomas." *Clinical and Developmental Immunology* 2013: 1–12. <https://doi.org/10.1155/2013/285246>.
- Wei, Jun, Anantha Marisetty, Brett Schrand, Konrad Gabrusiewicz, Yuuri Hashimoto, Martina Ott, Zacharia Grami, et al. 2019. "Osteopontin Mediates Glioblastoma-Associated Macrophage Infiltration and Is a Potential Therapeutic Target." *Journal of Clinical Investigation* 129 (1): 137–49. <https://doi.org/10.1172/JCI121266>.
- Wesolowska, A, A Kwiatkowska, L Slomnicki, M Dembinski, A Master, M Sliwa, K Franciszkiewicz, S Chouaib, and B Kaminska. 2008. "Microglia-Derived TGF- β as an Important Regulator of Glioblastoma Invasion—an Inhibition of TGF- β -Dependent Effects by ShRNA against Human TGF- β Type II Receptor." *Oncogene* 27: 918–30. <https://doi.org/10.1038/sj.onc.1210683>.
- Wick, Wolfgang, Michael Platten, and Michael Weller. 2001. "Glioma Cell Invasion: Regulation of Metalloproteinase Activity by TGF- β β β ." *Journal of Neuro-Oncology* 53: 177–85.
- Wilgenburg, Bonnie van, Cathy Browne, Jane Vowles, and Sally A. Cowley. 2013. "Efficient, Long Term Production of Monocyte-Derived Macrophages from Human Pluripotent Stem Cells under Partly-Defined and Fully-Defined Conditions." Edited by Dimas Tadeu Covas. *PLoS ONE* 8 (8): e71098. <https://doi.org/10.1371/journal.pone.0071098>.
- Woroniccka, Karolina, Pakawat Chongsathidkiet, Kristen Rhodin, Hanna Kemeny, Cosette Dechant, S. Harrison Farber, Aladine A. Elsamadicy, et al. 2018. "T-Cell Exhaustion Signatures Vary with Tumor Type and Are Severe in Glioblastoma." *Clinical Cancer Research* 24 (17): 4175–86. <https://doi.org/10.1158/1078-0432.CCR-17-1846>.

- Woroniecka, Karolina I., Kristen E. Rhodin, Pakawat Chongsathidkiet, Kristin A. Keith, and Peter E. Fecci. 2018. "T-Cell Dysfunction in Glioblastoma: Applying a New Framework." *Clinical Cancer Research*. American Association for Cancer Research Inc. <https://doi.org/10.1158/1078-0432.CCR-18-0047>.
- Wu, Duoqiao, Leying Zhuo, and Xiangdong Wang. 2016. "Metabolic Reprogramming of Carcinoma-Associated Fibroblasts and Its Impact on Metabolic Heterogeneity of Tumors." *Seminars in Cell and Developmental Biology*, 1–7. <https://doi.org/10.1016/j.semcdb.2016.11.003>.
- Wurm, Julian, Simon P. Behringer, Vidhya M. Ravi, Kevin Joseph, Nicolas Neidert, Julian P. Maier, Roberto Doria-Medina, et al. 2019. "Astrogliosis Releases Pro-Oncogenic Chitinase 3-like 1 Causing Mapk Signaling in Glioblastoma." *Cancers* 11 (10). <https://doi.org/10.3390/cancers11101437>.
- Yamamoto, M, R Sawaya, S Mohanam, V H Rao, J M Bruner, G L Nicolson, and J S Rao. 1994. "Expression and Localization of Urokinase-Type Plasminogen Activator Receptor in Human Gliomas." *Cancer Research* 54 (18): 5016–20. <http://www.ncbi.nlm.nih.gov/pubmed/8069869>.
- Yeung, Y T, K L McDonald, T Grewal, and L Munoz. 2013. "Interleukins in Glioblastoma Pathophysiology: Implications for Therapy." *British Journal of Pharmacology* 168 (3): 591–606. <https://doi.org/10.1111/bph.12008>.
- Yin, Jie, Katherine L. Valin, Michael L. Dixon, and Jianmei W. Leavenworth. 2017. "The Role of Microglia and Macrophages in CNS Homeostasis, Autoimmunity, and Cancer." *Journal of Immunology Research* 2017 (December): 1–12. <https://doi.org/10.1155/2017/5150678>.
- Yoshimoto, Koji, Masahiro Mizoguchi, Nobuhiro Hata, Hideki Murata, Ryusuke Hatae, Toshiyuki Amano, Akira Nakamizo, and Tomio Sasaki. 2012. "Complex DNA Repair Pathways as Possible Therapeutic Targets to Overcome Temozolomide Resistance in Glioblastoma." *Frontiers in Oncology* 2. <https://doi.org/10.3389/fonc.2012.00186>.
- Young, Adam MH, Natsuhiko Kumasaka, Fiona Calvert, Timothy R. Hammond, Andrew

- Knights, Nikolaos Panousis, Jeremy Schwartzentruber, et al. 2019. "A Map of Transcriptional Heterogeneity and Regulatory Variation in Human Microglia." *BioRxiv*, December, 2019.12.20.874099. <https://doi.org/10.1101/2019.12.20.874099>.
- Young, D A, L D Lowe, and S C Clark. 1990. "Comparison of the Effects of IL-3, Granulocyte-Macrophage Colony-Stimulating Factor, and Macrophage Colony-Stimulating Factor in Supporting Monocyte Differentiation in Culture. Analysis of Macrophage Antibody-Dependent Cellular Cytotoxicity." *Journal of Immunology (Baltimore, Md. : 1950)* 145 (2): 607–15. <http://www.ncbi.nlm.nih.gov/pubmed/2142182>.
- Yu, Kenny. 2015. "Cancer Stem Cells and Tumour Associated Macrophages in Glioblastoma Multiforme."
- Yu, Qian, Da-Li Tian, Ye Tian, Xi-Tong Zhao, and Xue-Ying Yang. 2018. "Elevation of the Chemokine Pair CXCL10/CXCR3 Initiates Sequential Glial Activation and Crosstalk During the Development of Bimodal Inflammatory Pain after Spinal Cord Ischemia Reperfusion." *Cellular Physiology and Biochemistry* 49 (6): 2214–28. <https://doi.org/10.1159/000493825>.
- Zhai, Haiyan, Frank L. Heppner, and Stella E. Tsirka. 2011. "Microglia/Macrophages Promote Glioma Progression." *GLIA* 59 (3): 472–85. <https://doi.org/10.1002/glia.21117>.
- Zhang, F., Y. Wen, and X. Guo. 2014. "CRISPR/Cas9 for Genome Editing: Progress, Implications and Challenges." *Human Molecular Genetics* 23 (R1): R40–46. <https://doi.org/10.1093/hmg/ddu125>.
- Zhang, Jing, Susobhan Sarkar, Rowena Cua, Yan Zhou, Walter Hader, and V. Wee Yong. 2012. "A Dialog between Glioma and Microglia That Promotes Tumor Invasiveness through the CCL2/CCR2/Interleukin-6 Axis." *Carcinogenesis* 33 (2): 312–19. <https://doi.org/10.1093/carcin/bgr289>.
- Zhou, Li Jun, Jiyun Peng, Ya Nan Xu, Wei Jie Zeng, Jun Zhang, Xiao Wei, Chun Lin Mai, et al. 2019. "Microglia Are Indispensable for Synaptic Plasticity in the Spinal Dorsal

Horn and Chronic Pain.” *Cell Reports* 27 (13): 3844-3859.e6.
<https://doi.org/10.1016/j.celrep.2019.05.087>.

Zhu, Mingqin, Xiuzhe Wang, Erik Hjorth, Romain A. Colas, Lisa Schroeder, Ann Charlotte Granholm, Charles N. Serhan, and Marianne Schultzberg. 2016. “Pro-Resolving Lipid Mediators Improve Neuronal Survival and Increase A β 42 Phagocytosis.” *Molecular Neurobiology* 53 (4): 2733–49. <https://doi.org/10.1007/s12035-015-9544-0>.

Zulch, K.J. 1986. *Brain Tumors: Their Biology and Pathology*. 3rd ed. Springer-Verlag.